

VOLUME 75

MAY 13, 1971

NUMBER 10

JPCA_x

THE JOURNAL OF

PHYSICAL

CHEMISTRY

PUBLISHED BIWEEKLY BY THE AMERICAN CHEMICAL SOCIETY

THE JOURNAL OF
PHYSICAL
CHEMISTRY

Volume 75

MAY—AUGUST 1971

PAGES 1333—2710

BRYCE CRAWFORD, JR., *Editor*

STEPHEN PRAGER, *Associate Editor*

ROBERT W. CARR, JR., FREDERIC A. VAN-CATLEDGE, *Assistant Editors*

EDITORIAL BOARD

A. O. ALLEN
R. BERSOHN
J. R. BOLTON
S. BRUNAUER
M. FIXMAN
H. S. FRANK
J. R. HUIZENGA

M. KASHA
W. J. KAUZMANN
W. R. KRIGBAUM
R. A. MARCUS
W. J. MOORE
J. A. POPE
B. S. RABINOVITCH

H. REISS
S. A. RICE
R. E. RICHARDS
F. S. ROWLAND
R. L. SCOTT
R. SEIFERT

CHARLES R. BERTSCH, *Manager, Editorial Production*

AMERICAN CHEMICAL SOCIETY

FREDERICK T. WALL, *Executive Director*

BOOKS AND JOURNALS DIVISION

JOSEPH H. KUNEY

Head, Business Operations Department

JOHN K. CRUM
Director (Acting)

RUTH REYNARD
Assistant to the Director

THE JOURNAL OF PHYSICAL CHEMISTRY

BRYCE CRAWFORD, Jr., *Editor*

STEPHEN PRAGER, *Associate Editor*

ROBERT W. CARR, Jr., FREDERIC A. VAN CATLEDGE, *Assistant Editors*

EDITORIAL BOARD: A. O. ALLEN (1970-1974), R. BERSOHN (1967-1971), J. R. BOLTON (1971-1975), S. BRUNAUER (1967-1971), M. FIXMAN (1970-1974), H. S. FRANK (1970-1974), J. R. HUIZENGA (1969-1973), M. KASHA (1967-1971), W. J. KAUZMANN (1969-1973), W. R. KRIGBAUM (1969-1973), R. A. MARCUS (1968-1972), W. J. MOORE (1969-1973), J. A. POPLE (1971-1975), B. S. RABINOVITCH (1971-1975), H. REISS (1970-1974), S. A. RICE (1969-1975), R. E. RICHARDS (1967-1971), F. S. ROWLAND (1968-1972), R. L. SCOTT (1968-1972), R. SEIFERT (1968-1972)

CHARLES R. BERTSCH, *Manager, Editorial Production*

AMERICAN CHEMICAL SOCIETY, 1155 Sixteenth St., N.W., Washington, D. C. 20036

FREDERICK T. WALL, *Executive Director*

Books and Journals Division

JOHN K. CRUM, *Director (Acting)*

JOSEPH H. KUNEY, *Head, Business Operations Department*

RUTH REYNARD, *Assistant to the Director*

©Copyright, 1971, by the American Chemical Society. Published biweekly by the American Chemical Society at 20th and Northampton Sts., Easton, Pa. 18042. Second-class postage paid at Easton, Pa.

All manuscripts should be sent to *The Journal of Physical Chemistry*, Department of Chemistry, University of Minnesota, Minneapolis, Minn. 55455.

Additions and Corrections are published once yearly in the final issue. See Volume 74, Number 26 for the proper form.

Extensive or unusual alterations in an article after it has been set in type are made at the author's expense, and it is understood that by requesting such alterations the author agrees to defray the cost thereof.

The American Chemical Society and the Editor of *The Journal of Physical Chemistry* assume no responsibility for the statements and opinions advanced by contributors.

Correspondence regarding accepted copy, proofs, and reprints should be directed to Editorial Production Office, American Chemical Society, 20th and Northampton Sts., Easton, Pa. 18042. Manager: CHARLES R. BERTSCH. Assistant Editor: EDWARD A. BORGER. Editorial Assistant: EVELYN J. UHLER.

Advertising Office: Century Communications Corporation, 142 East Avenue, Norwalk, Conn. 06851.

Business and Subscription Information

Remittances and orders for subscriptions and for single copies,

notices of changes of address and new professional connections, and claims for missing numbers should be sent to the Subscription Service Department, American Chemical Society, 1155 Sixteenth St., N.W., Washington, D. C. 20036. Allow 4 weeks for changes of address. Please include an old address label with the notification.

Claims for missing numbers will not be allowed (1) if received more than sixty days from date of issue, (2) if loss was due to failure of notice of change of address to be received before the date specified in the preceding paragraph, or (3) if the reason for the claim is "missing from files."

Subscription rates (1971): members of the American Chemical Society, \$20.00 for 1 year; to nonmembers, \$40.00 for 1 year. Those interested in becoming members should write to the Admissions Department, American Chemical Society, 1155 Sixteenth St., N.W., Washington, D. C. 20036. Postage to Canada and countries in the Pan-American Union, \$4.00; all other countries, \$5.00. Single copies for current year: \$2.00. Rates for back issues from Volume 56 to date are available from the Special Issues Sales Department, 1155 Sixteenth St., N.W., Washington, D. C. 20036.

This publication and the other ACS periodical publications are now available on microfilm. For information write to: MICROFILM, Special Issues Sales Department, 1155 Sixteenth St., N.W., Washington, D. C. 20036.



*The Editors join with his former students and
research associates in dedicating this issue of
The Journal of Physical Chemistry to*

George B. Kistiakowsky

on the occasion of his seventieth birthday year.

Hand in hand we come
To lay this book in your lap.
Say you're surprised?
Say you like it?
Say it's just what you wanted?
Because it's yours—
Because we love you.

From the book WINNIE-THE-POOH by A.
A. Milne. Copyright 1926 by E. P. Dutton
& Co., Inc. Renewal copyright 1954 by A.
A. Milne. Reprinted with permission of E.
P. Dutton & Co., Inc., publishers.

GEORGE BOGDAN KISTIAKOWSKY

It is a privilege and a great pleasure as well to have been asked to write about George B. Kistiakowsky, Abbott and James Lawrence Professor of Chemistry at Harvard, Vice President of the National Academy of Sciences, former Special Assistant for Science and Technology to the President of the United States, and holder of many other titles. This pleasure comes not only from the distinction of his scientific accomplishments and the importance of his many public services, past, present, and future, but also from his outstanding qualities of character and leadership and his tremendous personality. The fund of stories about him is almost inexhaustible, as we all know, because he is courageous, adventurous, original, intuitive, witty, often extremely gay, always ready to enjoy life and to defend what he believes in. His presence enlivens any meeting and banishes dullness.

But a selection has to be made, and much as I should like to write about him as a unique, admired, and fascinating personality, my duty here is to give a brief sketch of his major scientific activities and some idea of how he is contributing to the relations of science with the larger public interests.

Kistiakowsky's scientific career began in Berlin where, because of time taken out by several years of hair-raising adventures in the Russian revolution, he hurried his formal education—three years altogether for the bachelor's and doctor's degrees. He was a student of Bodenstein, who started him on his life-long interest in chemical kinetics and photochemistry. Although his research career has been marked by unusual versatility, the elucidation of the elementary molecular steps and the nature of the intermediates involved in reactions have remained at the core of his studies.

In 1926 he joined forces with Hugh Taylor at Princeton. In that very active center of research in kinetics, he widened his interests to include much work on catalysis and adsorption, besides several classical papers and a book on photochemistry. Very typically, with W. T. Richards, he engaged in a pioneer investigation of the use of ultrasonic dispersion as a tool for measuring fast reaction rates.

The next step careerwise was his appointment at Harvard in 1930, which marked the beginning of a period of teaching, research, and leadership at that institution which has lasted for 40 years so far.

Kinetics continued, but landmarks were made in other fields as well. Let us mention the study and analysis of the rotational fine structure of the ultraviolet spectrum of formaldehyde, carried out with G. H. Dieke of Johns Hopkins, a "first" which stood unrivaled for a long time. The program of precise heats of hydrogenation of unsaturated hydrocarbons was a bold, large-scale operation pushed through with great experimental skill and success, at just the critical time to contribute to the swirling discussions on the significance of resonance energies. Also timely were his development of other thermodynamic measurements—low-temperature and higher-temperature heat capacities and equilibrium constants for gases. These were crucial in settling the then very controversial question of the existence of substantial barriers to internal rotation about single bonds.

Kistiakowsky and his group developed the techniques and made the measurements on the heat capacity of ethane and on the heat of reaction and equilibrium constant for the hydrogenation of ethylene to ethane. They then pointed out that this information was incompatible with free internal rotation in ethane but could be made consistent if the internal rotation were hindered by a substantial potential barrier.

Kistiakowsky would be the first to protest that these accomplishments were carried through in collaboration with very able students and postdoctoral fellows, and indeed the success and loyalty of his former associates testify to the attraction he has had for good students and postdoctorals, the wise choice of problems, and the skill and insight he has provided. They would all acknowledge the influence he has had not only on their scientific careers but on their whole lives. They remember fondly the pleasant and relaxed give and take of his daily coffee breaks, where his willingness to exchange views on all subjects—from science and politics to sports and practical jokes—was put to lively test and was much appreciated. During the era of the barrier problem, I had an especially good view of his method of working with students. He was really involved. Emotions were sometimes high and sometimes very low, as days were marked by success or by setbacks. On the latter days, it was sometimes wiser to take a long detour around the corridors to avoid contact, but then there would be the time when sleeves were rolled up, the difficulties analyzed and cured in person, sometimes with glass-blowing torch in hand. A small but typical example of his exceptional experimental skills: there was a time when only he could make the delicate quartz spiral for a special type of pressure gauge, until he finally was able to teach a professional glass-blower how to do it. Thus besides providing the problems, the plan of action, the critical analysis, and interpretation of the data, his involvement in the research projects of his group often goes much further. His knowledge of machine shop and other techniques provide a classic illustration of the physical chemist's need to be able to handle a vast range of skills from plumbing to advanced mathematics and subtle thermodynamic reasoning—and to enjoy them all. It is a rare blend of intuition and analysis together with technical resourcefulness which permits Kistiakowsky to see new experimental approaches and to follow them through to a successful conclusion.

World War II arrived and all this changed. President Conant of Harvard was one of the organizers of the National Defense Research Committee which mobilized civilian scientists to meet the desperate threat posed by the German and later Japanese tides of conquest. Kistiakowsky volunteered and was assigned by Conant to work on explosives, a subject he knew only as the victim of a fair number of laboratory accidents. He very quickly found that American military science, in this as in most areas, was essentially nonexistent, that the establishment did not welcome academic assistance from amateurs, and that bureaucratic in-fighting over privileges and status often took precedence over patriotism. In one large area of explosives research not one single scientific report was turned up from the previous 20 years.

German submarines were soon sinking American ships within sight of the American coasts with practically complete impunity, opposed only by obsolete World War I weapons.

Kistiakowsky set up the Explosives Research Laboratory on the grounds of the Bureau of Mines near Pittsburgh; soon he became chief of the Explosives Division of the National Defense Research Committee. Under contracts from this organization, there were developed greatly improved methods for making explosives more powerful than TNT, new types of propellants, specialized explosives, shaped charges, etc. Also important, a great deal was learned about the theory of detonation and shock waves, the names of Kirkwood and von Neumann entering prominently here. In all this activity, Kistiakowsky's leadership was extremely important. He made decisions, followed them up with vigor, entered into the frequently necessary combats with even, let us face it, a certain relish, and generally emerged victorious with a successful program, such as the conversion of the Navy to more powerful explosives. This surely had a part, along with the work of other civilian scientists in radar, operations analysis, underwater sound, etc., in finally turning the tide against the German submarine offensive, which at one time was sinking three ships a day and came within inches of isolating Britain. Later he was made head of the explosives division at Los Alamos and put to work the newly acquired basic knowledge on the design and construction of the atomic bomb.

On his return to Harvard, a double task faced him. One was to rehabilitate himself as a teacher and academic scientist; the other was to serve as Department Chairman during a critical period. He succeeded admirably at both. In research he began his program in the application of shock tubes to chemical problems. This applied war-time techniques to provide new and very powerful means of studying kinetic processes. The theory of shock and detonation waves permits tubes to be designed which can subject molecules to an almost instantaneous rise in temperature of thousands of degrees. Many processes were studied under these hitherto unobtainable conditions. An area where he and his group have made very valuable contributions is that of measurement techniques whereby the instantaneous density, pressure, temperature, and chemical composition in the exceedingly narrow shock front and reaction zone can be determined. He introduced, for example, the method of absorption of soft X-rays to measure density, and the time-of-flight mass spectrometer to measure composition. One by-product of the shock tube has been a definite discrimination among the several rival values proposed for the heat of dissociation of nitrogen. Another recent discovery is the importance of relatively stable conjugated ions, particularly cyclic $C_3H_3^+$, in the mechanism of the oxidation of acetylene.

He also began several projects with mass spectrometers. One was a series of studies of the very complicated system of reactions in active nitrogen, the classic problem of the Lewis-Raleigh afterglow, on which he and his students have shed much light. The other main application of this type of tool was to the coupling of a time-of-flight mass spectrometer to a shock tube so that time scans could be made on reaction mixtures subjected to sudden intense heating.

An area in which he has made and continues to make landmark contributions is that of the kinetics of free radicals.

To mention a few high points: Gomer and Kistiakowsky made a classic study of the absolute rate of recombination of two methyl radicals, which has served as a basis for determining the rates of other radical reactions. He has initiated a whole series of studies of the behavior of methylene radicals, an initially most puzzling species because of the fact, at first unsuspected, that they can exist in either a singlet or a triplet state (as demonstrated by Herzberg). Various ways of preparing CH_2 , its addition to double bonds, insertion in CH bonds, addition to CO, etc., have been investigated.

As evidence of the breadth of his interests, a series of careful studies on the kinetics of enzyme reactions should be mentioned. These showed, for example, that an enzyme could have more than one active site. Earlier, his program of precise thermal measurements had included the denaturation of a protein and an antibody-antigen reaction.

It is difficult to include everything of importance in this short survey, but there should not be omitted his very early entry into chemical applications of nuclear magnetic resonance spectroscopy with his student H. S. Gutowsky and collaborators Pake and Purcell.

Science was rolling along impressively in the Gibbs Laboratory when once more a national crisis demanded Kistiakowsky's time. Sputnik aroused a government which had almost completely excluded scientists from its councils. The dormant President's Science Advisory Committee was upgraded under Killian, with Kistiakowsky as a member and ultimately full-time Science Advisor to President Eisenhower. The history of this operation is not yet completely in the public domain but many developments in the relationship of science and government were born in that era, which was also notable for the confidence the President then had in his Science advisor.

Harvard finally got Kistiakowsky back, but not yet all of his attention. He has remained in too much demand on questions of large public policy, at first on various government committees, then as Vice President of the National Academy of Sciences, in which his influence has strengthened greatly that body's capacity for dealing with the interaction of science and the public interest. This work continues very actively today. For example, he has been closely identified with the formation of the Academy's Committee on Science and Public Policy, under whose aegis a number of landmark reports have been issued, and he has also been active in the initiation and operation of the new Report Review Committee, which provides a review mechanism for the growing number and increasingly important body of Academy and Research Council reports. Both these innovations have increased the impact and the responsibility of the Academy with respect to the relation of science to national affairs. Thus, the report, "Growth of World Population," is an illustration of an important document sponsored by the Committee on Science and Public Policy which is believed to have been influential in guiding government policy toward the provision of assistance in population control to foreign countries.

In science, despite these time-consuming outside duties, he has continued to do work that makes its mark. Thus the several studies on the intersystem crossing of excited benzene at very low pressures produced controversies, much further work by others in both theory and experiment,

and have greatly helped clarify an area of importance.

This rapid and limited survey of a truly notable career, still going strong of course, should not be ended without some remarks about his courage, both physical and moral. I have seen him steadfast and imperturbable with shells exploding around him (a ship chose the field in which he was setting up tests for its target during gunnery practice). I have also seen him steadfast when figurative bomb-shells

were bursting about him after he had refused to consult further with the military, on account of his opposition to the Vietnam War. In both situations lesser men were either running in panic for cover or staying snug and safe in sheltered positions.

E. Bright Wilson
February 19, 1971

Biographical Notes

Abbott and James Lawrence Professor of Chemistry and Faculty Associate of the Institute of Politics, Harvard University, Professor Kistiakowsky was born in Kiev, Russia, in 1900. His father was a professor of international law there, and he attended private schools in Moscow and Kiev. During the Russian revolution (1918–1920), he was a soldier in the anti-Communist White Russian Army. After defeat, he spent most of a year in Turkey and the Balkans and then entered the University of Berlin. Studying under Max Bodenstein, he achieved the Doctor of Philosophy degree. He worked as Professor Bodenstein's assistant for a year and then came to the United States as an International Education Board Fellow at Princeton University, working under Professor H. S. Taylor. He became an assistant professor at Princeton and taught there for 2 years. In 1930, he joined the Harvard faculty, where he has held office since. He became Professor of Chemistry in 1938.

His knowledge of explosions was put to work on defense problems during World War II. He became Chief of the Explosives Division of the National Defense Research Committee. He established and ran the Explosives Research Laboratory at Bruceton, Pa., and helped establish a second laboratory, for underwater explosives research, at Woods Hole, Mass. In 1944, he became chief of the explosives division of the Los Alamos Laboratory of the Manhattan Project, and there he designed the arrangement of conventional explosives necessary to detonate the atomic bomb. For his service, he received the President's Medal for Merit.

He was one of the original members (1957–1964) of the President's Science Advisory Committee (PSAC) and was Chairman of that body from 1959 to 1961. He was a member of the

United States delegation at technical talks with the Soviets in Geneva during 1948 on ways of reducing the danger of surprise nuclear attack. From 1953 to 1958, he was a member of the Ballistic Missiles Advisory Committee of the Air Force and Defense Department. From 1959 to 1961, he was Special Assistant to President Eisenhower for Science and Technology. In 1961–1965, he was appointed the first chairman of the Committee on Science and Public Policy of the National Academy of Sciences which is advisory to the U. S. Government and Congress on national problems involving scientific research.

Professor Kistiakowsky is a director of the Itek Corporation. In 1965, he was elected to the vice presidency of the National Academy of Sciences.

Professor Kistiakowsky holds the King's Medal of the United Kingdom for Services in the Cause of Freedom, the Exceptional Service Award of the U. S. Air Force, the Presidential Medal of Freedom, and the National Medal of Science.

His scientific honors include the Nichols, the Willard Gibbs, and the Richards Medals, the Joseph Priestley Award, membership in the National Academy of Sciences, Foreign membership in the Royal Society, honorary Fellowship in the Chemical Society of London, the American Chemical Society's Charles Lathrop Parsons Award for outstanding public service, the George Ledlie Prize (Harvard's top faculty award) for 1961, and honorary degrees from Harvard, Oxford, Princeton, University of Pennsylvania, Carnegie Institute of Technology, Case Institute of Technology, Williams College, and Columbia University. In September 1967, he received the Peter Debye Award in Physical Chemistry sponsored by the Humble Oil Co.

Publications of George Bogdan Kistiakowsky

BOOKS

"Photochemical Processes," American Chemical Society Monograph No. 43, The Chemical Catalog Co., Inc., New York, N. Y., 1927.

ARTICLES

"The Photochemical Decomposition of Chlorine Monoxide," (with M. Bodenstein), *Z. Phys. Chem.*, **116**, 371 (1925).

"Decomposition of Ozone in Red Light," *Z. Phys. Chem.*, **117**, 337 (1925).

"The Ionization Potentials of Nitrogen and Hydrogen on Iron and Other Metals," *J. Phys. Chem.*, **30**, 1356 (1926).

"Contact Catalysis and Activation of Gases by Adsorption," (with H. S. Taylor), *Z. Phys. Chem.*, **125**, 341 (1927).

"Heats of Adsorption on Poisoned and Heat-Treated Catalysts," (with E. W. Florsdorf and H. S. Taylor), *J. Amer. Chem. Soc.*, **49**, 2200 (1927).

"Methanol Catalysts, I," (with H. S. Taylor), *J. Amer. Chem. Soc.*, **49**, 2468 (1927).

"Activation of Gases by Adsorption," *Proc. Nat. Acad. Sci. U. S.*, **13**, 1 (1927).

"Contact Catalysis on Metals," *Metallwirtschaft*, **7**, 676 (1928).

"Temperature Coefficients of Some Photochemical Reactions," *Proc. Nat. Acad. Sci. U. S.*, **15**, 194 (1929).

"Budde Effect in Bromine and Chlorine," *J. Amer. Chem. Soc.*, **51**, 1395 (1929).

"Photochemical Decomposition of Nitrosyl Chloride," *J. Amer. Chem. Soc.*, **52**, 102 (1930).

- "Platinum Black Catalysts. I. Physical Properties and Catalytic Activity," (with G. B. Taylor and J. H. Perry), *J. Phys. Chem.*, **34**, 748 (1930).
- "Platinum Black Catalysts. II. Heats of Adsorption," *J. Phys. Chem.*, **34**, 799 (1930).
- "Hydrogenation over Metallic Cesium," (with D. G. Hill), *J. Amer. Chem. Soc.*, **52**, 892 (1930).
- "The Photochemical Hydrogen-Oxygen Reaction," *J. Amer. Chem. Soc.*, **52**, 1868 (1930).
- "The Photochemical Oxygen-Carbon Monoxide Reaction," (with W. F. Jackson), *J. Amer. Chem. Soc.*, **52**, 3741 (1930).
- "Heats of Adsorption on Catalytically Active Surfaces," (with E. W. Florsdorf), *J. Phys. Chem.*, **34**, 1907 (1930).
- "Gaseous Oxidations. I. Homogeneous Uncatalyzed Reaction between Oxygen and Acetylene," (with S. Lenher), *J. Amer. Chem. Soc.*, **52**, 3785 (1930).
- "An Attempt to Measure the Velocity of Dissociation of Nitrogen Tetroxide by the Method of Sound Waves," (with W. T. Richards), *J. Amer. Chem. Soc.*, **52**, 4661 (1930).
- "Kinetics of Acetylene-Oxygen Reaction," (with R. Spence), *J. Amer. Chem. Soc.*, **52**, 4837 (1930).
- "The Ultraviolet Absorption Spectrum of Acetylene," *Phys. Rev.*, **37**, 276 (1931).
- "Kinetics of a Thermal *cis-trans* Isomerization," (with M. Nelles), *Z. Phys. Chem. Bodenstein-Festband*, 369 (1931).
- "The Reactivity of Activated Atoms," (with P. E. Millington), *Z. Phys. Chem., Abt. B.*, **13**, 1556 (1931).
- "Kinetics of the Hydrogen Chloride and Phosgene Combination as a Problem of Modern Photochemistry," *Z. Angew. Chem.*, **44**, 602 (1931).
- "Rates of Atomic Reactions," *Chem. Rev.*, **10**, 91 (1932).
- "A High-Powered Source of Continuous Ultraviolet Spectrum," *Rev. Sci. Instrum.*, **2**, 549 (1931).
- "Absorption Spectra in Solution at Low Temperatures," (with L. B. Arnold, Jr.), *J. Amer. Chem. Soc.*, **54**, 1713 (1932).
- "Photochemical Decomposition of Ammonia," (with E. O. Wiig), *J. Amer. Chem. Soc.*, **54**, 1806 (1932).
- "Kinetics of a Thermal *cis-trans* Isomerization. II.," (with M. Nelles), *J. Amer. Chem. Soc.*, **54**, 2208 (1932).
- "The Rotational Structure of the Ultraviolet Absorption Bands of Formaldehyde," (with G. H. Dieke), *Proc. Nat. Acad. Sci. U. S.*, **18**, 367 (1932).
- "The Heat of Sublimation of Carbon," (with W. E. Vaughan), *Phys. Rev.*, **40**, 457 (1932).
- "An Apparatus for Quantum Yields of Gas Reactions by Actinometry," (with G. S. Forbes and L. J. Heidt), *J. Amer. Chem. Soc.*, **54**, 3246 (1932).
- "The Resonance Fluorescence of Benzene," (with M. Nelles), *Phys. Rev.*, **41**, 595 (1932).
- "Anomalous Decomposition of Ozone in the Presence of Chlorine," (with L. J. Heidt and G. S. Forbes), *J. Amer. Chem. Soc.*, **55**, 223 (1933).
- "The Thermal Decomposition of Ethylene Iodide," (with L. B. Arnold, Jr.), *J. Chem. Phys.*, **1**, 166 (1933).
- "The Thermal Dissociation of Cyanogen into Cyanide Radicals," (with H. Gershinowitz), *J. Chem. Phys.*, **1**, 432 (1933).
- "The Thermal Decomposition of Tertiary Butyl and Tertiary Amyl Alcohols. Homogeneous Unimolecular Reactions," (with R. F. Schultz), *J. Amer. Chem. Soc.*, **56**, 395 (1934).
- "Kinetics of the Thermal Isomerization of Cyclopropane," (with T. S. Chambers), *J. Amer. Chem. Soc.*, **56**, 399 (1934).
- "Kinetics of Thermal *cis-trans* Isomerization. III.," (with W. R. Smith), *J. Amer. Chem. Soc.*, **56**, 638 (1934).
- "The Structure of the Ultraviolet Absorption Spectrum of Formaldehyde. I.," (with G. H. Dieke), *Phys. Rev.*, **45**, 4 (1934).
- "The Photochemical Decomposition of Ketene," (with W. F. Ross), *J. Amer. Chem. Soc.*, **56**, 1112 (1934).
- "Heats of Organic Reactions. I. Apparatus and the Heat of Hydrogenation of Ethylene," (with H. Romeyn, Jr., J. R. Ruhoff, H. A. Smith, and W. E. Vaughan), *J. Amer. Chem. Soc.*, **57**, 65 (1935).
- "Kinetics of Thermal *cis-trans* Isomerization. IV.," (with W. R. Smith), *J. Amer. Chem. Soc.*, **57**, 269 (1935).
- "The Photochemical Hydrogen-Oxygen Reaction," (with H. A. Smith), *J. Amer. Chem. Soc.*, **57**, 835 (1935).
- "Heats of Organic Reactions. II. Hydrogenation of Some Simpler Olefinic Hydrocarbons," (with J. R. Ruhoff, H. A. Smith, and W. E. Vaughan), *J. Amer. Chem. Soc.*, **57**, 876 (1935).
- "Gaseous Unimolecular Reactions," *Chem. Rev.*, **17**, 47 (1935).
- "The Thermal Equilibrium between Ethylene Iodide, Ethylene, and Iodine," (with G. R. Cuthbertson), *J. Chem. Phys.*, **3**, 631 (1935).
- "Photochemical Formation and Reactions of Radicals and Atoms," *Cold Spring Harbor Symp. Quant. Biol.*, **3**, 44 (1935).
- "Thermal Decomposition of Tertiary Butyl and Tertiary Amyl Chlorides, Gaseous Homogeneous Molecular Reactions," (with D. Brearley and C. H. Stauffer), *J. Amer. Chem. Soc.*, **58**, 43 (1936).
- "Kinetics of Some Diels-Alder Reactions," *J. Amer. Chem. Soc.*, **58**, 123 (1936).
- "Heats of Organic Reactions. III. Hydrogenation of Some Higher Olefins," (with J. R. Ruhoff, H. A. Smith, and W. E. Vaughan), *J. Amer. Chem. Soc.*, **58**, 137 (1936).
- "Heats of Organic Reactions. IV. Hydrogenations of Some Dienes and Benzene," *J. Amer. Chem. Soc.*, **58**, 146 (1936).
- "Resonance Fluorescence of Benzene. II.," (with G. R. Cuthbertson), *J. Chem. Phys.*, **4**, 9 (1936).
- "Kinetics of Thermal *cis-trans* Isomerization. V.," (with W. R. Smith), *J. Amer. Chem. Soc.*, **58**, 766 (1936).
- "The Kinetics of Racemization of 2,2'-Diamino-6,6'-dimethylbiphenyl," (with W. R. Smith), *J. Amer. Chem. Soc.*, **58**, 1043 (1936).
- "Kinetics of Polymerization of Cyclopentadiene," (with W. H. Mears), *J. Amer. Chem. Soc.*, **58**, 1060 (1936).
- "Kinetics of Thermal *cis-trans* Isomerization. VI.," (with W. R. Smith), *J. Amer. Chem. Soc.*, **58**, 2428 (1936).
- "Kinetics of Gaseous Addition of Halogen Acids to Isobutene," (with C. H. Stauffer), *J. Amer. Chem. Soc.*, **59**, 165 (1937).
- "Thermal Decomposition of Gaseous Hydrogen Peroxide," (with S. L. Rosenberg), *J. Amer. Chem. Soc.*, **59**, 422 (1937).
- "Some Aspects of Investigations of Molecular Structure of Organic Compounds," *J. Phys. Chem.*, **41**, 175 (1937).
- "Heats of Organic Reactions. V. Heats of Hydrogenation of Various Hydrocarbons," (with M. A. Dolliver, T. L. Gresham, and W. E. Vaughan), *J. Amer. Chem. Soc.*, **59**, 831 (1937).
- "Energy Changes Involved in Addition Reactions of Unsaturated Hydrocarbons," (with J. B. Conant), *Chem. Rev.*, **20**, 181 (1937).
- "Studies in Gaseous Polymerizations," (with J. B. Harkness and W. H. Mears), *J. Chem. Phys.*, **5**, 682 (1937).
- "The Gaseous Equilibrium of 1,2-Diiodobutane, Butene-1, and Iodine," (with J. E. Cline), *J. Chem. Phys.*, **5**, 990 (1937).
- "The Low-Temperature Heat Capacity of Gaseous Ethane," (with F. Nazmi), *J. Chem. Phys.*, **6**, 18 (1938).
- "Heats of Organic Reactions. VI. Heats of Hydrogenation of Some Oxygen-Containing Compounds," (with M. A. Dolliver, T. L. Gresham, E. A. Smith, and W. E. Vaughan), *J. Amer. Chem. Soc.*, **60**, 440 (1938).
- "Internal Free Rotation in Hydrocarbons," (with E. B. Wilson, Jr.), *J. Amer. Chem. Soc.*, **60**, 494 (1938).
- "Hindered Internal Rotation of Ethane," (with J. R. Lacher and F. Stitt), *J. Chem. Phys.*, **6**, 407 (1938).
- "Internal Rotation of Propane and Propylene; the Origin of the Internal Restricting Potentials," (with J. R. Lacher and W. W. Ransom), *J. Chem. Phys.*, **6**, 900 (1938).
- "Heats of Organic Reactions. VII. Addition of Halogens to Olefins," (with J. B. Conn and E. A. Smith), *J. Amer. Chem. Soc.*, **60**, 2764 (1938).
- "Bromination of Trimethylethylene," (with J. B. Conn and E. A. Smith), *J. Amer. Chem. Soc.*, **61**, 216 (1939).
- "Gaseous Heat Capacities. I. The Method and the Heat Capacities of C₂H₆ and C₂D₆," (with W. W. Rice), *J. Chem. Phys.*, **7**, 281 (1939).
- "The Low-Temperature Gaseous Heat Capacities of C₂H₆ and C₂D₆," (with J. R. Lacher and F. Stitt), *J. Chem. Phys.*, **7**, 289 (1939).
- "Heats of Organic Reactions. VIII. Further Hydrogenations, Including Those of Some Acetylenes," (with J. B. Conn and E. A. Smith), *J. Amer. Chem. Soc.*, **61**, 1868 (1939).
- "The Polymerization of Gaseous Butadiene," (with W. W.

- Ransom), *J. Chem. Phys.*, **7**, 725 (1939).
- "Entropy and Heat Capacity of Propylene," (with B. L. Crawford, W. W. Rice, A. J. Wells, and E. B. Wilson, Jr.), *J. Amer. Chem. Soc.*, **61**, 2980 (1939).
- "Gaseous Heat Capacities. II," (with W. W. Rice), *J. Chem. Phys.*, **8**, 601 (1940).
- "Heats of Organic Reactions. IX. A New Calorimeter and the Denaturation of Methemoglobin by Alkali," (with J. B. Conn and R. M. Roberts), *J. Amer. Chem. Soc.*, **62**, 1895 (1940).
- "Low-Temperature Gaseous Heat Capacities of Certain C₃ Hydrocarbons," (with J. R. Lacher and W. W. Ransom), *J. Chem. Phys.*, **8**, 970 (1940).
- "Synthesis of Radioactive Lactic Acid," (with R. D. Cramer), *J. Biol. Chem.*, **137**, 549 (1941).
- "The Heat of an Antibody-Antigen Reaction," (with W. C. Boyd, J. B. Conn, D. C. Gregg, and R. M. Roberts), *J. Biol. Chem.*, **139**, 787 (1941).
- "Heats of Organic Reactions. XI. The Denaturation of Pesin by Alkali," (with J. B. Conn, D. C. Gregg, and R. M. Roberts), *J. Amer. Chem. Soc.*, **63**, 2080 (1941).
- "Ethylene-Ethane and Propylene-Propane Equilibria," (with A. G. Nickle), *J. Chem. Phys.*, **10**, 78, 146 (1942).
- "The Photochemical Decomposition of Cyclic Ketones," (with S. W. Benson), *J. Amer. Chem. Soc.*, **64**, 80 (1942).
- "The Carbon-Hydrogen Bond Strengths in Methane and Ethane," (with H. G. Andersen and E. R. Van Artsdalen), *J. Chem. Phys.*, **10**, 305 (1942).
- "Heats of Organic Reactions. XIII. Heats of Hydrolysis of Some Acid Anhydrides," (with J. B. Conn, R. M. Roberts, and E. A. Smith), *J. Amer. Chem. Soc.*, **64**, 1747 (1942).
- "Use of Deuterium as a Tracer in the Claisen Rearrangement," (with R. L. Tichenor), *J. Amer. Chem. Soc.*, **64**, 2302 (1942).
- "The Activation Energy of the Reaction CH₃ + HBr = CH₄ + Br and the Carbon-Hydrogen Bond Strength in Methane," (with H. C. Andersen), *J. Chem. Phys.*, **11**, 6 (1943).
- "The Radioactive Exchange and Adsorption of MeBr with Several Inorganic Bromides," (with J. R. Van Wazer), *J. Amer. Chem. Soc.*, **65**, 1829 (1943).
- "Bromination of Hydrocarbons. I. Photochemical and Thermal Bromination of CH₄ and CH₃Br. C-H Bond Strength in CH₄," *J. Chem. Phys.*, **12**, 469 (1944).
- "Radioactive Studies. I. Analytical Procedure for Measurement of Long-Lived Radioactive Sulfur, S₃₅, with a Lauritzen Electrode and Comparison of Electrode with Special Geiger Counter," (with F. C. Henriques, Jr., C. Margnetti, and W. C. Sneider), *Ind. Eng. Chem., Anal. Ed.*, **18**, 349 (1946).
- "Inhibition of Urease," (with J. F. Ambrose and A. G. Kridl), *J. Amer. Chem. Soc.*, **71**, 1898 (1949).
- "Anomalous Temperature Effects in the Hydrolysis of Urea by Urease," (with R. Lumry), *J. Amer. Chem. Soc.*, **71**, 1006 (1949).
- "The Relative Efficiencies of Various Surfaces for the Recombination of Hydrogen Atoms," (with S. Katz and R. F. Steiner), *J. Amer. Chem. Soc.*, **71**, 2258 (1949).
- "Structural Investigations by Means of Nuclear Magnetism. I. Rigid Crystal Lattices," (with H. S. Gutowsky, G. E. Pake, and E. M. Purcell), *J. Chem. Phys.*, **17**, 972 (1949).
- "On the Theory of Odors," *Science*, **112**, 154 (1950).
- "Inhibition of Urease by Sulfur Compounds," (with J. F. Ambrose and A. G. Kridl), *J. Amer. Chem. Soc.*, **72**, 317 (1950).
- "Photochemical Decomposition of Ketene. II," (with N. W. Rosenberg), *J. Amer. Chem. Soc.*, **72**, 321 (1950).
- "The Nature of Thermochemistry," (with W. T. Grubb), *J. Amer. Chem. Soc.*, **72**, 419 (1950).
- "Specificity of Urease Action," (with W. H. R. Shaw), *J. Amer. Chem. Soc.*, **72**, 634 (1950).
- "Gaseous Detonations. I. Stationary Waves in Hydrogen-Oxygen Mixtures," (with D. J. Berets and E. F. Greene), *J. Amer. Chem. Soc.*, **72**, 1080 (1950).
- "Gaseous Detonations. II. Initiation by Shock Waves," *J. Amer. Chem. Soc.*, **72**, 1086 (1950).
- "Specificity of Urease Action—a Correction," (with W. H. R. Shaw), *J. Amer. Chem. Soc.*, **72**, 2817 (1950).
- "Inhibition of Urease by Silver Ions," (with J. F. Ambrose and A. G. Kridl), *J. Amer. Chem. Soc.*, **73**, 1232 (1951).
- "Rate Constant of Ethane Formation from Methyl Radicals," (with R. Gomer), *J. Chem. Phys.*, **19**, 85 (1951).
- "High Intensity Source for Molecular Beam. II. Experimental," (with W. P. Slichter), *Rev. Sci. Instrum.*, **22**, 328 (1951).
- "The Heat of Dissociation of Nitrogen," (with H. T. Knight and M. Malin), *J. Amer. Chem. Soc.*, **73**, 2972 (1951).
- "Initiation of Detonation in Gases," *Ind. Eng. Chem.*, **43**, 2794 (1951).
- "Photochemical Decomposition of Ketene. III," (with W. L. Marshall), *J. Amer. Chem. Soc.*, **74**, 88 (1952).
- "Ethane-Ethylene and Propane Equilibria," (with A. G. Nickle), *Discuss. Faraday Soc.*, No. 10, 175 (1951).
- "Density Measurements in Gaseous Detonation Waves," *J. Chem. Phys.*, **19**, 1611 (1951).
- "The Kinetics of Coordinate-Bond Formation," (with D. Garvin), *J. Chem. Phys.*, **20**, 105 (1952).
- "Gaseous Detonations. III. Dissociation Energies of Nitrogen and Carbon Monoxide," (with H. T. Knight and M. Malin), *J. Chem. Phys.*, **20**, 876 (1952).
- "Gaseous Detonations. IV. The Acetylene-Oxygen Mixtures," *J. Chem. Phys.*, **20**, 884 (1952).
- "The Effects of Electrolytes on Urease Activity," (with P. C. Manglesdorf, A. J. Rosenberg, and W. H. R. Shaw), *J. Amer. Chem. Soc.*, **74**, 5015 (1952).
- "The Kinetics of Urea Hydrolysis by Urease," (with A. J. Rosenberg), *J. Amer. Chem. Soc.*, **74**, 5020 (1952).
- "Gaseous Detonations. V. Nonsteady Waves in CO-O₂," (with H. T. Knight and M. Malin), *J. Chem. Phys.*, **20**, 994 (1952).
- "On the Mechanism of the Inhibition of Urease," (with W. H. R. Shaw), *J. Amer. Chem. Soc.*, **75**, 886 (1953).
- "Training Scientists Today," *Chem. Eng. Progr.*, **49**, 216, (April 1953).
- "Ureolytic Activity of Urease at pH 8.9," (with W. H. R. Shaw), *J. Amer. Chem. Soc.*, **75**, 2751 (1953).
- "Rate of Association of Methyl Radicals," (with E. K. Roberts), *J. Chem. Phys.*, **21**, 1637 (1953).
- "Primary Photochemical Process in Bromine," (with J. C. Sternberg), *J. Chem. Phys.*, **21**, 2218 (1953).
- "The Temperature Pattern Method in the Study of Fast Chemical Reactions," (with D. Garvin and V. P. Guinn), *Discuss. Faraday Soc.*, **17**, 32 (1954).
- "The Reaction Zone in Gaseous Detonations," (with P. H. Kydd), *J. Chem. Phys.*, **22**, 1940 (1954).
- "Gaseous Detonations. VI. The Rarefaction Wave," (with P. H. Kydd), *J. Chem. Phys.*, **23**, 271 (1955).
- "The Kinetics of Coordinate Bond Formation. II," (with R. Williams), *J. Chem. Phys.*, **23**, 334 (1955).
- "Gaseous Detonations. VII. A Study of Thermodynamic Equilibration in Acetylene-Oxygen Waves," (with W. G. Zinman), *J. Chem. Phys.*, **23**, 1889 (1955).
- Book Review: "Diffusion and Heat Exchange in Chemical Kinetics," by D. A. Frank-Kamenetskii, *Science*, **123**, 67 (1956).
- "Stability of Ethylidene Radicals," (with B. H. Mahan), *J. Chem. Phys.*, **24**, 922 (1956).
- "The Kinetics of Ester Hydrolysis by Liver Esterase," (with P. C. Manglesdorf, Jr.), *J. Amer. Chem. Soc.*, **78**, 2964 (1956).
- "Gaseous Detonations. VIII. Two-Stage Detonations in Acetylene-Oxygen Mixtures," (with P. Manglesdorf), *J. Chem. Phys.*, **25**, 516 (1956).
- "Mass Spectrometric Study of the Kinetics of Nitrogen Afterglow," (with W. A. Chupka and J. Berkowitz), *J. Chem. Phys.*, **25**, 457 (1956).
- "Kinetics of the Urease-Catalyzed Hydrolysis of Urea at pH 4.3," (with W. E. Thompson), *J. Amer. Chem. Soc.*, **78**, 4821 (1956).
- "The Rate and Mechanism of Some Reactions of Methylene," (with K. Sauer), *J. Amer. Chem. Soc.*, **78**, 5699 (1956).
- "The Photolysis of Methyl Ketene," (with B. H. Mahan), *J. Amer. Chem. Soc.*, **79**, 2412 (1957).
- "Stoss und Detonationswellen," *Chimia*, **11**, 124 (1957).
- "Reactions of Methylene. I. Ethylene, Propane, Cyclopropane, and n-Butane," (with H. M. Frey), *J. Amer. Chem. Soc.*, **79**, 6373 (1957).

- "A Mass Spectrometric Study of Flash Photochemical Reactions. I," (with P. H. Kydd), *J. Amer. Chem. Soc.*, **79**, 4825 (1957).
- "Lewis-Rayleigh Nitrogen Afterglow," (with P. Warneck), *J. Chem. Phys.*, **27**, 1417 (1957).
- "Reactions of Methylene. 2. Ketene and Carbon Dioxide," (with K. Sauer), *J. Amer. Chem. Soc.*, **80**, 1066 (1958).
- "Kinetics of Ester Hydrolysis by Horse Liver Esterase. II," (with N. C. Craig), *J. Amer. Chem. Soc.*, **80**, 1574 (1958).
- "Reactions of Nitrogen Atoms. II. H₂, CO, NH₃, NO, and NO₂," (with G. G. Volpi), *J. Chem. Phys.*, **28**, 665 (1958).
- "Reactions of Methylene. III. Addition to Carbon Monoxide," (with T. B. Wilson), *J. Amer. Chem. Soc.*, **80**, 2934 (1958).
- "Gaseous Detonations. X. Study of Reaction Zones," (with J. P. Chesick), *J. Chem. Phys.*, **28**, 956 (1958).
- "Gaseous Detonations. XI. Double Waves," (with M. Cher), *J. Chem. Phys.*, **29**, 506 (1958).
- "On the Mechanism of the Lewis-Rayleigh Nitrogen Afterglow," (with K. D. Bayes), *J. Chem. Phys.*, **29**, 949 (1958).
- "Gaseous Detonations. XII. Rotational Temperatures of the Hydroxyl Free Radicals," (with F. D. Tabbutt), *J. Chem. Phys.*, **30**, 577 (1959).
- "Kinetics of Coordinate Bond Formation. III. Method of Temperature Patterns and the Reaction NH₃ + BF₃," (with F. T. Smith), *J. Chem. Phys.*, **31**, 621 (1959).
- "Reactions of Methylene. IV. Propylene and Cyclopropane," (with J. N. Butler), *J. Amer. Chem. Soc.*, **82**, 759 (1960).
- "On the Mechanism of the Lewis-Rayleigh Nitrogen Afterglow," (with K. D. Bayes), *J. Chem. Phys.*, **32**, 992 (1960).
- "Reactions of Methylene. IV. Propylene and Cyclopropane," (with J. N. Butler), *J. Amer. Chem. Soc.*, **82**, 759 (1960).
- "Kinetics of Coordinate Bond Formation. V. Kinetics of the Reaction P(CH₃)₃ + BF₃," (with C. E. Klots), *J. Chem. Phys.*, **34**, 715 (1961).
- "Reactions of Methylene. V. The Effect of Inert Gases on the Reaction with Cyclopropane," (with J. N. Butler), *J. Amer. Chem. Soc.*, **83**, 1324 (1961).
- "Thermal Dissociation Rate of Hydrogen," (with W. C. Gardiner, Jr.), *J. Chem. Phys.*, **35**, 1765 (1961).
- "Gaseous Detonations. XIII. Rotational and Vibrational Distributions of OH Radicals," (with R. K. Lyon), *J. Chem. Phys.*, **35**, 995 (1961).
- "Gaseous Detonations. XIV. The CH Radical in Acetylene-Oxygen Detonations," (with R. K. Lyon), *J. Chem. Phys.*, **34**, 1069 (1961).
- "Gaseous Detonations. XV. Expansion Waves in Gaseous Detonations," (with H. Miyama and P. Kydd), *J. Chem. Phys.*, **34**, 2038 (1961).
- "Shock Wave Studies by Mass Spectrometry. I. Thermal Decomposition of Nitrous Oxide," (with J. N. Bradley), *J. Chem. Phys.*, **35**, 256 (1961).
- "Shock Wave Studies by Mass Spectrometry. II. Polymerization and Oxidation of Acetylene," (with J. N. Bradley), *J. Chem. Phys.*, **35**, 264 (1961).
- "The Enzymic Kinetics of Carbonic Anhydrase from Bovine and Human Erythrocytes," (with H. DeVoe), *J. Amer. Chem. Soc.*, **83**, 274 (1961).
- "Isolation and Properties of Pig Liver Esterase," (with A. J. Adler), *J. Biol. Chem.*, **236**, 3240 (1961).
- "Density Measurements in Reflected Shock Waves," (with W. C. Gardiner, Jr.), *J. Chem. Phys.*, **34**, 1080 (1961).
- "Kinetics of Coordinate Bond Formation. IV. Kinetic Isotope Effect in the Reaction NH₃ + BF₃," (with C. E. Klots), *J. Chem. Phys.*, **34**, 712 (1961).
- "National Policy for Science," *Chem. Eng. News*, **40**, 120 (Jan 22, 1962).
- "Kinetics of Pig Liver Esterase Catalysis," (with A. J. Adler), *J. Amer. Chem. Soc.*, **84**, 695 (1962).
- "Emission of Vacuum Ultraviolet Radiation from the Acetylene-Oxygen and the Methane-Oxygen Reactions in Shock Waves," (with L. W. Richards), *J. Chem. Phys.*, **36**, 1707 (1962).
- "Ionization Accompanying the Acetylene-Oxygen Reaction in Shock Waves," (with C. W. Hand), *J. Chem. Phys.*, **37**, 1239 (1962).
- "Centenary Lecture, The Mechanism of Oxidation of Acetylene at Very High Temperatures," *Proc. Chem. Soc.*, 289 (1962).
- "The Reactions of Methylene. VI. The Addition of Methylene to Hydrogen and Methane," (with J. A. Bell), *J. Amer. Chem. Soc.*, **84**, 3417 (1962).
- "The Scientific Endeavor Introduction," *Proc. Nat. Acad. Sci. U. S.*, **50**, 1193 (1963).
- "The Photolysis of Methylketene. II," (with D. P. Chong), *J. Phys. Chem.*, **68**, 1793 (1964).
- "Mechanism of Chemi-Ionization in Hydrocarbon Oxidations," (with J. V. Michael), *J. Chem. Phys.*, **40**, 1447 (1964).
- "A Synthesis of C₃H₃ + ?," (with G. P. Glass), *J. Chem. Phys.*, **40**, 1448 (1964).
- "Mechanism of the Acetylene-Oxygen Reaction in Shock Waves," (with G. P. Glass, J. V. Michael, and H. Niki), *J. Chem. Phys.*, **42**, 608 (1965).
- "The Oxidation Reactions of Acetylene and Methane," (with G. P. Glass, J. V. Michael, and H. Niki), "Tenth Symposium on Combustion," The Combustion Institute, 1965, pp 513-522.
- "Effects of Pressure on Fluorescence and Intersystem Crossing in Benzene Vapor," (with C. S. Parmenter), *J. Chem. Phys.*, **42**, 2942 (1965).
- "Thermal Decomposition of Acetylene in Shock Waves," (with I. D. Gay, J. V. Michael, and H. Niki), *J. Chem. Phys.*, **43**, 1720 (1965).
- "Pyrolysis and Oxidation of Formaldehyde in Shock Waves," (with I. D. Gay, G. P. Glass, and H. Niki), *J. Chem. Phys.*, **43**, 4017 (1965).
- "The Photolysis of Ketene in the Presence of *trans*-2-Butene," (with R. W. Carr, Jr.), *J. Phys. Chem.*, **70**, 118 (1966).
- "Photochemical Decomposition of Diazoethane," (with C. L. Kibby), *J. Phys. Chem.*, **70**, 126 (1966).
- "Reactions of Metal Carbonyls with Active Nitrogen," (with W. R. Brennen), *J. Chem. Phys.*, **44**, 2694 (1966).
- "Acetylene-Oxygen Reaction in Shock Waves. Origins of CH* and CO*," (with J. B. Homer), *J. Chem. Phys.*, **45**, 1359 (1966).
- "Pyrolysis of Ethylene in Shock Waves," (with I. D. Gay, R. D. Kern, and H. Niki), *J. Chem. Phys.*, **45**, 2371 (1966).
- "Photolysis of Ketene in the Presence of Carbon Monoxide," (with B. A. DeGraff), *J. Phys. Chem.*, **71**, 3984 (1967).
- "The Photolysis of Ketene in the Presence of Carbon Monoxide," (with B. A. DeGraff), *J. Phys. Chem.*, **71**, 1553 (1967).
- "Acetylene-Oxygen Reaction in Shock Waves. Origin of CO₂," (with J. B. Homer), *J. Chem. Phys.*, **46**, 4213 (1967).
- "Ethylene-Oxygen Reaction in Shock Waves," (with I. D. Gay, G. P. Glass, and R. D. Kern), *J. Chem. Phys.*, **47**, 313 (1967).
- "Oxidation and Pyrolysis of Ethylene in Shock Waves," (with J. B. Homer), *J. Chem. Phys.*, **47**, 5290 (1967).
- "Photolysis of Ketene by 2139-Å Radiation," (with T. A. Walter), *J. Phys. Chem.*, **72**, 3952 (1968).
- "Pressure Dependence of Benzene Fluorescence," (with E. M. Anderson), *J. Chem. Phys.*, **48**, 4787 (1968).
- "Isotopic Exchange between Oxygen and Carbon Monoxide in Shock Waves," (with S. H. Garnett and B. V. O'Grady), *J. Chem. Phys.*, **51**, 84 (1969).
- "Fluorescence and Intersystem Crossing of Benzene-*h₆*, -*d₆*, and -*1,4-d₂*," (with E. M. Anderson), *J. Chem. Phys.*, **51**, 182 (1969).
- "The Reaction of Active Nitrogen with Acetylene. I," (with C. A. Arrington, Jr., and O. O. Bernardini), *Proc. Roy. Soc., Ser. A*, **310**, 161 (1969).
- "Reaction of Carbon Dioxide with Atomic Oxygen and the Dissociation of Carbon Dioxide in Shock Waves," (with T. C. Clark and S. H. Garnett), *J. Chem. Phys.*, **51**, 2885 (1969).
- "The Limitation of Strategic Arms," (with G. W. Rathjens), *Sci. Amer.*, **222** (1970).
- "Exchange Reaction of ¹⁸O Atoms with CO₂ and with SO₂ in Shock Waves," (with T. C. Clark and S. H. Garnett), *J. Chem. Phys.*, **52**, 4692 (1970).
- "Oxidation of Carbon Monoxide by Oxygen in Shock Waves," (with A. M. Dean), *J. Chem. Phys.*, **53**, 830 (1970).
- "Reactions of Methyl Radicals Produced by the Pyrolysis of Azomethane or Ethane in Reflected Shock Waves," (with T. C. Clark and T. P. J. Izod), *J. Chem. Phys.*, **54**, 1295 (1971).
- "Effect of Organic Impurities on the Observed Activation Energy of CO₂ Dissociation," (with T. C. Clark and A. M. Dean), *J. Chem. Phys.*, **54**, 1726 (1971).

THE JOURNAL OF PHYSICAL CHEMISTRY

Volume 75, Number 10 May 13, 1971

This collection of papers is given by former participants in George Kistiakowsky's research program in the Gibbs Laboratory as a representative offering from all past and present Gibbsians. We are extremely grateful for the opportunity of having worked in such a stimulating environment and hope in this way to show our appreciation to George for his invaluable contributions to our lives, to chemistry, and to the cause of science. The names of the Kistiakowsky students are printed in italics in the by-lines and a author index.

R. W. C.

A Comparison of RRK and RRKM Theories for Thermal Unimolecular Processes David M. Golden, Richard K. Solly, and Sidney W. Benson	1333
Proton Magnetic Resonance Spectra of Molten Alkali Metal Acetate Solutions of Polyhydric Alcohols and Phenols Louis L. Burton, S. Sherer, and E. R. VanArtsdalen	1338
Hidden Degeneracy and the Vibration of Larger Molecules Walter F. Edgell	1343
An <i>Ab Initio</i> LCAO-MO-SCF Study of the Phosphoryl Fluoride Molecule, OPF_3 Ilyas Absar and John R. Van Wazer	1360
Energy Transfer in Thermal Isocyanide Isomerization. Noble Gases in the Ethyl Isocyanide System S. P. Pavlou and B. S. Rabinovitch	1366
Studies of the Chymotrypsinogen Family of Proteins. XV. pH and Temperature Dependence of the α -Chymotryptic Hydrolysis of <i>N</i> -Acetyl-L-tryptophan Ethyl Ester Shyamala Rajender, Rufus Lumry, and Moon Han	1375
Studies of the Chymotrypsinogen Family of Proteins. XVI. Enthalpy-Entropy Compensation Phenomenon of α -Chymotrypsin and the Temperature of Minimum Sensitivity Rufus Lumry and Shyamala Rajender	1387
Nuclear Magnetic Resonance Spectral Interpretation by Pattern Recognition B. R. Kowalski and C. A. Reilly	1402
Chemistry of Barium Released at High Altitudes N. W. Rosenberg and G. T. Best	1412
Difference Chromatography of Sea Water Paul C. Mangelsdorf, Jr., and T. Roger S. Wilson	1418
Dynamics of the Reactions of O_2^+ with H_2 and D_2 M. H. Chiang, E. A. Gislason, B. H. Mahan, C. W. Tsao, and A. S. Werner	1426
The Thermal Unimolecular Decomposition of 1,1,2-Trimethylcyclobutane A. T. Cocks and H. M. Frey	1437
Circular Dichroism of Chlorophyll and Related Molecules Calculated Using a Point Monopole Model for the Electronic Transitions Kenneth D. Philipson, S. Chang Tsai, and Kenneth Sauer	1440
Liquid Crystal-Isotropic Phase Equilibria in the System Poly- γ -benzyl- α ,L-glutamate-Dimethylformamide Elizabeth L. Wee and Wilmer G. Miller	1446
Thermodynamics of cis-trans Isomerizations. II. The 1-Chloro-2-fluoroethylenes, 1,2-Difluorocyclopropanes, and Related Molecules Norman C. Craig, Lawrence G. Piper, and Vicki L. Wheeler	1453
Photoionization Mass Spectrometric Study of XeF_2 , XeF_4 , and XeF_6 J. Berkowitz, W. A. Chupka, P. M. Guyon, J. H. Holloway, and R. Spohr	1461
Predissociation and Dissociation Energy of HBr^+ Michael J. Haugh and Kyle D. Bayes	1472
Selective Solvation of Ions by Water in Propylene Carbonate David R. Cogley, James N. Butler, and Ernest Grunwald	1477
Equilibrium Distributions of Some Octane and Nonane Isomers Richard K. Lyon	1486

RADIATION CHEMISTRY

ADVANCES IN CHEMISTRY SERIES NOS. 81 AND 82

Seventy-seven papers and 34 abstracts from the International Conference on Radiation Chemistry at Argonne National Laboratories, chaired by Edwin J. Hart. Includes review and research papers from 12 countries besides U.S., Canada, and England, including 8 from U.S.S.R. and two other East European countries.

Volume I groups papers on radiation in aqueous media, radiation of biological systems, dosimetry, and one plenary lecture.

Volume II has papers on radiation of gases, of solids, and of organic liquids, plus three plenary lectures.

No. 81 Radiation Chemistry—I

616 pages with index

No. 82 Radiation Chemistry—II

558 pages with index

Each \$16.00

Ordered together \$30.00

Cloth (1968)

Set of L.C. cards free with library orders.

Other books in the ADVANCES IN CHEMISTRY SERIES in physical and colloid chemistry include:

No. 68 Mössbauer Effect and its Application in Chemistry. Ten papers that will familiarize chemists with Mössbauer spectroscopy as an analytical tool, for studying chemical bonding, crystal structure, electron density, magnetism, and other properties. 178 pages

Cloth (1967) \$8.00

No. 67 Equilibrium Concepts in Natural Water Systems. Sixteen papers represent the collaboration of aquatic chemists, analytical chemists, geologists, oceanographers, limnologists, and sanitary engineers, working with simplified models to produce fruitful generalizations and valuable insights into the factors that control the chemistry of natural systems. 344 pages

Cloth (1967) \$11.00

No. 64 Regenerative EMF Cells. Seventeen papers survey current progress and research on regenerative systems for converting and storing electrical energy. Principal emphasis is on thermally regenerative systems, but chemical and photochemical systems are considered. 309 pages

Cloth (1967) \$11.00

No. 63 Ordered Fluids and Liquid Crystals. Twenty-two studies on characterization, properties, and occurrence of these phenomena in many substances such as tristearin, p-azoxyanisole, mono- and di-hydric alcohols, phospholipids and polypeptides. 332 pages

Cloth (1967) \$11.50

No. 58 Ion-Molecule Reactions In the Gas Phase. Eighteen papers survey spectrometric and other methods for producing and studying ion-molecule reactions, such as pulsed sources for studying thermal ions, reactions in flames and electrical discharges. 336 pages

Cloth (1966) \$10.50

No. 54 Advanced Propellant Chemistry. Primarily directed to the search for new oxidizers; 26 papers survey oxygen-containing oxidizers, fuels and binders, fluorine systems including oxygen difluoride and difluoramines and liquid systems. 290 pages

Cloth (1966) \$10.50

No. 47 Fuel Cell Systems. Developments in theory, performance, construction, and new systems for the energy converter that is proving itself in military and space uses. 360 pages

Cloth (1965) \$10.50

No. 43 Contact Angle, Wettability, and Adhesion. Twenty-six papers on theoretical and practical approaches to wettability and adhesion; with summary of the surface chemical studies of W. A. Zisman, the 1963 Kendall Award winner. 389 pages

Cloth (1964) \$10.50

No. 40 Mass Spectral Correlations. By Fred W. McLafferty. Over 4000 spectral listed by mass/charge ratios of fragment ions with the most probable original structures for each. 117 pages

Paper (1963) \$6.00

No. 33 Solid Surfaces and the Gas-Solid Interface. Thirty-seven papers from the Kendall Award Symposium honoring Stephen Brunauer. Theory and techniques for studying surface phenomena. 489 pages

Cloth (1961) \$12.00

No. 31 Critical Solution Temperatures. By Alfred W. Francis. CST answers the question, "Do two liquids mix?" and is widely used for screening solvents. Over 6000 systems are included, 70% with a hydrocarbon as one component; nearly 1100 non-hydrocarbon solvents are listed. 246 pages

Cloth (1961) \$8.00

No. 29 Physical Properties of Chemical Compounds—III. By Robert R. Dreisbach. Supplements earlier volumes with properties of 434 aliphatic compounds and 22 miscellaneous compounds and elements. Index to volumes I, II, and III. 489 pages

Cloth (1961) \$10.00

No. 25 Physical Functions of Hydrocolloids. Papers on natural gums, gelatin pectins and related polysaccharides, and theoretical and functional aspects of hydrocolloids, emulsions, foams, and dispersions. Strong food industry emphasis. 103 pages

Paper (1960) \$5.00

No. 22 Physical Properties of Chemical Compounds—II. By Robert R. Dreisbach. Properties of 476 alkanes, haloalkanes, alkenes, haloalkenes, diolefins, and alkynes. 491 pages

Cloth (1959) \$10.00

No. 18 Thermodynamic Properties of the Elements. By D. R. Stull and G. C. Sinke. Tabulated values of heat capacity, heat content, entropy, and free energy function of solid, liquid, and gas states of first 92 elements in range of 298° to 3000°K. Some auxiliary data frequently included. 489 pages

Cloth (1956) \$8.00

No. 15 Physical Properties of Chemical Compounds. By Robert R. Dreisbach. Tables of parameters for calculating physical properties of 511 organic cyclic compounds. 536 pages

Cloth (1955) \$10.00

All books postpaid in U.S. and Canada; plus 30 cents in PUAS and elsewhere.

Order from: SPECIAL ISSUES SALES,
AMERICAN CHEMICAL SOCIETY
1155 SIXTEENTH ST., N.W.
WASHINGTON, D.C. 20036

Single-Pulse Shock Tube Studies of Hydrocarbon Pyrolysis. II. The Pyrolysis of Ethane <i>J. N. Bradley and M. A. Frend</i>	1492
Ignition of Aromatic Hydrocarbon-Oxygen Mixtures by Shock Waves <i>Hajime Miyama</i>	1501
Initiation Rate for Shock-Heated Hydrogen-Oxygen-Carbon Monoxide-Argon Mixtures as Determined by OH Induction Time Measurements <i>W. C. Gardiner, Jr., M. McFarland, K. Morinaga, T. Takeyama, and B. F. Walker</i>	1504
Calculations of the Optical Properties of 1-Methyluracil Crystal by an All-Order Classical Oscillator Theory <i>Howard DeVoe</i>	1509
Circular Dichroism Studies of Lysine-Rich Histone f-1-Deoxyribonucleic Acid Complexes. Effect of Salts and Dioxane upon Conformation <i>Alice J. Adler and Gerald D. Fasman</i>	1516
Reformulation of the Quasiequilibrium Theory of Ionic Fragmentation <i>Cornelius E. Klots</i>	1526
Mass Spectrum of Isocyanic Acid <i>Denis J. Bogan and Clifford W. Hand</i>	1532
Methylene Reaction Rates. Quantum Yields in the Diazomethane-Propane Photolysis System: Effects of Photolysis Time, Reactant Ratios, and Added Gases <i>Jerry A. Bell</i>	1537
Expressions for Multiple Perturbation Energies <i>D. P. Chong</i>	1549
The Nitrogen Afterglow and the Rate of Recombination of Nitrogen Atoms in the Presence of Nitrogen, Argon, and Helium <i>W. Brennen and Edward C. Shane</i>	1552
The Absorption Spectrum of Benzene Vapor near 2537 Å <i>G. H. Atkinson and C. S. Parmenter</i>	1564
Single Vibronic Level Fluorescence. IV. Its Application to the Analysis of Resonance Fluorescence from Benzene Excited by the 2537-Å Mercury Line <i>G. H. Atkinson, C. S. Parmenter, and M. W. Schuyler</i>	1572
Absolute Rate Constants for the Reactions of Hydrogen Atoms with Olefins <i>J. A. Cowfer, D. G. Keil, J. V. Michael, and C. Yeh</i>	1584
The Use of Tubular Flow Reactors for Kinetic Studies over Extended Pressure Ranges <i>Robert V. Poirier and Robert W. Carr, Jr.</i>	1593
Mass Spectrometric Studies of Rate Constants for Addition Reactions of Hydrogen and of Deuterium Atoms with Olefins in a Discharge-Flow System at 300°K <i>E. E. Daby, H. Niki, and B. Weinstock</i>	1601
Numerical Quadrature Methods in the Analysis of Reaction Kinetic Experiments <i>Ian D. Gay</i>	1610
The Rate of Exchange of Hydrogen and Deuterium behind Reflected Shock Waves. Dynamic Analysis by Time-of-Flight Mass Spectrometry <i>R. D. Kern and G. G. Nika</i>	1615

COMMUNICATIONS TO THE EDITOR

Vibrational Relaxation of Hydrogen Chloride by Chlorine Atoms and Chlorine Molecules <i>Norman C. Craig and C. Bradley Moore</i>	1622
---	------

AUTHOR INDEX

- Absar, I., 1360
 Adler, A. J., 1516
 Atkinson, G. H., 1564, 1572

Bayes, K. D., 1472
Bell, J. A., 1537
Benson, S. W., 1333
Berkowitz, J., 1461
 Best, G. T., 1412
 Bogan, D. J., 1532
Bradley, J. N., 1492
Brennen, W., 1552
 Burton, L. L., 1338
Butler, J. N., 1477

 Carr, R. W., Jr., 1593
 Chiang, M. H., 1426
 Chong, D. P., 1549
Chupka, W. A., 1461

 Cocks, A. T., 1437
 Cogley, D. R., 1477
 Cowfer, J. A., 1584
Craig, N. C., 1453, 1622

 Daby, E. E., 1601
DeVoe, H., 1509

Edgell, W. F., 1343

 Fasman, G. D., 1516
 Friend, M. A., 1492
Frey, H. M., 1437

Gardiner, W. C., Jr., 1504
 Gay, I. D., 1610
 Gislason, E. A., 1426
 Golden, D. M., 1333
 Grunwald, E., 1477

 Guyon, P. M., 1461

 Han, M., 1375
Hand, C. W., 1532
 Haugh, M. J., 1472
 Holloway, J. H., 1461

 Keil, D. G., 1584
Kern, R. D., 1615
Klots, C. E., 1526
 Kowalski, B. R., 1402

Lumry, R., 1375, 1387
Lyon, R. K., 1486

Mahan, B. H., 1426
Mangelsdorf, P. C., Jr., 1418
 McFarland, M., 1504
Michael, J. V., 1584
Miller, W. G., 1446

Miyama, H., 1501
 Moore, C. B., 1622
 Morinaga, K., 1504

 Nika, G. G., 1615
Niki, H., 1601

Parmenter, C. S., 1564, 1572
 Pavlou, S. P., 1366
 Philipson, K. D., 1440
 Piper, L. G., 1453
 Poirier, R. V., 1593

Rabinovitch, B. S., 1366
 Rajender, S., 1375, 1387
Reilly, C. A., 1402
Rosenberg, N. W., 1412

Sauer, K., 1440
 Schuyler, M. W., 1572

 Shane, E. C., 1552
 Sherer, S., 1338
 Solly, R. K., 1333
 Spohr, R., 1461

 Takeyama, T., 1504
 Tsai, S. C., 1440
 Tsao, C. W., 1426

VanArtsdalen, E. R., 1338
Van Wazer, J. R., 1360

 Walker, B. F., 1504
 Wee, E. L., 1446
 Weinstock, B., 1601
 Werner, A. S., 1426
 Wheeler, V. L., 1453
 Wilson, T. R. S., 1418

 Yeh, C., 1584

A Comparison of RRK and RRKM Theories for Thermal Unimolecular Processes¹

by David M. Golden,* Richard K. Solly, and Sidney W. Benson

Department of Thermochemistry and Chemical Kinetics, Stanford Research Institute,
Menlo Park, California 94025 (Received December 14, 1970)

Publication costs borne completely by The Journal of Physical Chemistry

It is shown that in prescribed temperature regions the Kassel integral of RRK theory gives values of k/k_∞ in good agreement with values computed from RRKM theory for a number of widely different thermal unimolecular processes. The parameter s is uniquely defined as $C_{\text{vib}}(T)/R$.

Introduction

The application of transition state theory to gas phase chemical kinetics, combined with rapidly increasing experiences with various types of chemical reactions, has progressed to the point where the activation parameters, and thus the rates, for many elementary chemical reactions can be estimated fairly accurately. This state of affairs is very useful to the chemist who may be trying to understand the mechanism of a chemical process consisting of many such elementary reactions.

Often some of these elementary processes are unimolecular, or the reverse (*i.e.*, radical combination), and as such can be pressure dependent. It is useful to be able to predict simply the degree of such dependence. This kind of prediction has often been made by using the Rice-Ramsperger-Kassel (RRK)² theory incorporating an estimated empirical parameter, s , the "number of effective oscillators." Benson³ has suggested $s \equiv C_{\text{vib}}/R$.

Recent publications^{4a,b} have claimed, based on the more accurate modification of RRK theory by Marcus (RRKM), that s was too complicated a function of the complexity of the species, the frequency pattern, and the temperature to be estimated in any simple way. It was suggested that only application of RRKM theory is appropriate.

Lamenting both the fact that simple use of tables of the "Kassel integral" would not suffice to predict k/k_∞ , and the necessity of using the costly (in both

time and money) procedure involved with use of RRKM theory, it was decided to compare RRKM and RRK ($s \equiv C_{\text{vib}}/R$) for a number of different thermal unimolecular processes.

Table I^a

A	Parameter		Model no.
	E	S	
H	H	H	1
H	H	L	2
L	H	H	3
L	H	L	4
H	L	H	5
H	L	L	6
L	L	H	7
L	L	L	8

^a The definitions of H and L might be

	Log A	E	S
H ≥	15.5	50	25
L ≤	13.5	20	15

(1) This work was supported in part by Contract NAS 7-472, with the National Aeronautics and Space Administration, Ames Research Center, Moffett Field, Calif.

(2) L. S. Kassel, "Kinetics of Homogeneous Gas Reactions," Reinhold, New York, N. Y., 1932.

(3) S. W. Benson, "Thermochemical Kinetics," Wiley, New York, N. Y., 1968.

(4) (a) D. W. Plazcek, B. S. Rabinovitch, G. Z. Whitten, and E. Tschuikow-Roux, *J. Chem. Phys.*, **43**, 4071 (1965); (b) E. Tschuikow-Roux, *J. Phys. Chem.*, **73**, 3891 (1969).

Experimental Section

Procedure. a. RRKM. The procedures of Rabinovitch and coworkers⁵ have been followed. The program, used with a CDC 6400 computer, was kindly supplied by Professor Rabinovitch. Moments of inertia products for reacting molecules and activated

complexes were calculated with the use of a program kindly provided by Dr. L. H. Scharpen of Hewlett-Packard Corp. Frequency assignments for reacting molecules were taken from the literature where available. Otherwise, frequencies were assigned by analogy. Hindered rotors were treated as torsions. The

Table II: Calculated Falloff Data ($k/k_{\infty}(T)$) for Models 1-8

1. HHH $n\text{-C}_4\text{H}_{10} \rightarrow 2\text{C}_2\text{H}_5$ $\log k_{\infty} = 18.2 - 81.7/\theta^a$								
P^b	$k/k_{\infty}(300)$		$k/k_{\infty}(600)$		$k/k_{\infty}(900)$		$k/k_{\infty}(1200)$	
	M^c	$K(s=7)^d$	M	$K(s=16)$	M	$K(s=23)$	M	$K(s=27)$
10^3	1.0	0.55	1.0	(-1) 0.97	9.9	(-1) 9.4	8.7	(-1) 8.1
10^1	1.0	0.078	9.9	(-1) 7.0	7.9	(-1) 5.5	3.5	(-1) 2.9
10^{-1}	1.0	0.0033	8.1	(-1) 2.3	2.6	(-1) 1.3	4.0	(-2) 3.9
10^{-3}	9.3	(-1) ^e 0.0067	2.8	(-1) 0.30	2.6	(-2) 1.4	1.8	(-3) 2.3
k_{∞}	3.4×10^{-42}		2.4×10^{-12}		2.1×10^{-2}		1.9×10^3	
2. HHL $\text{C}_2\text{H}_6 \rightarrow 2\text{CH}_3$ $\log k_{\infty} = 18.3 - 90.6/\theta$								
P	$k/k_{\infty}(300)$		$k/k_{\infty}(600)$		$k/k_{\infty}(900)$		$k/k_{\infty}(1200)$	
	M	$K(s=2)$	M	$K(s=7)$	M	$K(s=10)$	M	$K(s=13)$
10^3	1.0	8.7×10^{-6}	9.1	(-1) 1.1	6.0	(-1) 1.9	2.9	(-1) 1.4
10^1	0.84	8.7×10^{-8}	3.3	(-1) 0.051	9.0	(-2) 1.5	2.2	(-2) t.0
10^{-1}	0.20	8.7×10^{-12}	2.1	(-2) 0.011	3.0	(-3) 5.2	5.2	(-4) 3.4
10^{-3}	8.5×10^{-3}	8.7×10^{-12}	4.3	(-4) 0.016	4.7	(-5) 1.1	7.0	(-6) 7.3
k_{∞}	6.78×10^{-48}		2.36×10^{-16}		2.19×10^{-4}		6.95×10^1	
3. LHH $\text{PhCO} \rightarrow \text{Ph} \cdot + \text{CO}$ $\log k_{\infty} = 14.6 - 28.6/\theta$								
P	$k/k_{\infty}(300)$		$k/k_{\infty}(600)$		$k/k_{\infty}(900)$		$k/k_{\infty}(1200)$	
	M	$K(s=10)$	M	$K(s=19)$	M	$K(s=24)$	M	$K(s=27)$
10^3	1.0	0.96	9.7	(-1) 9.4	6.9	(-1) 9.4	2.9	(-1) 2.9
10^1	9.9	(-1) 5.4	5.4	(-1) 4.4	9.5	(-2) 9.7	1.2	(-2) 1.3
10^{-1}	6.9	(-1) 0.89	6.5	(-2) 5.8	3.0	(-3) 3.7	1.9	(-4) 2.1
10^{-3}	9.6	(-2) 0.39	2.0	(-3) 2.9	4.5	(-5) 7.1	2.1	(-6) 2.4
k_{∞}	5.6×10^{-7}		1.4×10^6		4.3×10^7		2.3×10^9	
4. LHL $\text{CH}_3\text{NHNH}_2 \rightarrow \text{NH}_3 + \text{CH}_2=\text{NH}$ $\log k_{\infty} = 13.2 - 53.9/\theta$								
P	$k/k_{\infty}(300)$		$k/k_{\infty}(600)$		$k/k_{\infty}(900)$		$k/k_{\infty}(1200)$	
	M	$K(s=4)$	M	$K(s=9)$	M	$K(s=13)$	M	$K(s=15)$
10^3	1.0	0.87	1.0	0.99	1.0	0.99	9.8	(-1) 9.7
10^1	1.0	0.18	9.9	(-1) 8.0	9.0	(-1) 7.6	6.4	(-1) 5.5
10^{-1}	9.8	(-1) 0.056	7.3	(-1) 2.2	3.2	(-1) 2.0	9.9	(-2) 8.2
10^{-3}	4.2	(-2) 0.0076	1.1	(-1) 0.16	2.0	(-2) 1.6	3.4	(-3) 4.1
k_{∞}	8.7×10^{-27}		3.5×10^{-7}		1.2		2.3×10^3	
5. HLH $\text{tert-BuO} \rightarrow (\text{CH}_3)_2\text{CO} + \text{CH}_3$ $\log k_{\infty} = 15.5 - 16.9/\theta$								
P	$k/k_{\infty}(300)$		$k/k_{\infty}(600)$		$k/k_{\infty}(900)$		$k/k_{\infty}(1200)$	
	M	$K(s=9)$	M	$K(s=18)$	M	$K(s=23)$	M	$K(s=27)$
10^3	8.0	(-1) 4.6	1.5	(-1) 1.5	1.5	(-2) 1.6	2.2	(-3) 2.1
10^1	1.5	(-1) 0.49	4.4	(-3) 6.2	2.0	(-4) 2.3	2.3	(-5) 2.1
10^{-1}	3.3	(-3) 1.8	5.5	(-5) 12	2.1	(-6) 2.5	2.4	(-7) 2.2
10^{-3}	3.4	(-5) 3.5	5.6	(-7) 17	2.1	(-8) 2.6	2.4	(-9) 2.2
k_{∞}	2.2×10^3		2.1×10^9		2.3×10^{11}		2.5×10^{12}	

Table II (Continued)

6. HLL CH ₃ CO → CH ₃ + CO log k_{∞} = 14.5 - 21.5/ θ												
P	$k/k_{\infty}(300)$			$k/k_{\infty}(600)$			$k/k_{\infty}(900)$			$k/k_{\infty}(1200)$		
	M	K (s = 2)		M	K (s = 6)		M	K (s = 8)		M	K (s = 9)	
10 ³	4.6	(-1)	0.031	1.5	(-1)	1.1	5.1	(-2)	6.1	1.9	(-2)	2.5
10 ¹	1.2	(-2)	0.0031	2.5	(-3)	3.2	6.8	(-4)	16	2.3	(-4)	4.7
10 ⁻¹	1.3	(-4)	0.0031	2.5	(-5)	5.0	6.8	(-6)	24	2.3	(-6)	6.1
10 ⁻³	1.3	(-6)	0.0031	2.5	(-7)	5.9	6.8	(-8)	29	2.3	(-8)	6.9
k_{∞}	8.3 × 10 ⁻²			4.2 × 10 ⁶			1.7 × 10 ⁹			3.5 × 10 ¹⁰		

7. LLH n-hexyl → sec-hexyl log k_{∞} = 10.0 - 13.5/ θ												
P	$k/k_{\infty}(300)$			$k/k_{\infty}(600)$			$k/k_{\infty}(900)$			$k/k_{\infty}(1200)$		
	M	K (s = 12)		M	K (s = 25)		M	K (s = 33)		M	K (s = 39)	
10 ³	1.0		1.0	1.0		1.0	1.0		1.0	9.9	(-1)	9.9
10 ¹	1.0		1.0	9.8	(-1)	9.7	8.3	(-1)	8.2	5.4	(-1)	5.4
10 ⁻¹	9.7	(-1)	8.4	4.9	(-1)	4.7	9.1	(-2)	9.2	1.7	(-2)	1.7
10 ⁻³	4.1	(-1)	2.5	2.6	(-2)	3.1	1.3	(-3)	1.4	1.9	(-4)	1.8
k_{∞}	1.3			1.3 × 10 ⁶			5.8 × 10 ⁶			3.8 × 10 ⁷		

8. LLL cyclobutane → butadiene log k_{∞} = 12.8 - 32.1/ θ												
P	$k/k_{\infty}(300)$			$k/k_{\infty}(600)$			$k/k_{\infty}(900)$			$k/k_{\infty}(1200)$		
	M	K (s = 4)		M	K (s = 11)		M	K (s = 15)		M	K (s = 18)	
10 ³	1.0		0.72	1.0		0.98	9.8	(-1)	9.5	9.0	(-1)	8.5
10 ¹	9.9	(-1)	0.83	8.6	(-1)	6.3	5.3	(-1)	4.2	2.4	(-1)	2.0
10 ⁻¹	61	(-2)	0.19	2.0	(-1)	1.1	4.2	(-2)	4.1	8.6	(-3)	9.2
10 ⁻³	180	(-4)	0.23	3.9	(-3)	5.8	6.2	(-4)	14	1.1	(-4)	1.8
k_{∞}	1.5 × 10 ⁻¹¹			1.2 × 10 ⁴			9.7 × 10 ⁴			8.4 × 10 ⁵		

^a At $\langle T \rangle = 900^{\circ}\text{K}$, units sec^{-1} , $\theta = 2.3 RT$ kcal/mol. ^b Torr. ^c $k/k_{\infty}(T)$ as computed from RRKM theory. ^d $k/k_{\infty}(T)$ as computed from RRK theory ($s \equiv C_{\text{vib}}(T)/R$). ^e (-1) signifies multiplication by 10^{-1} for entries in both columns M and K .

frequencies of the activated complex were assigned by appropriate adjustments in those of the reacting species as described in the Appendix.

The total entropy of the reacting species was computed, and frequencies were assigned with an eye toward agreement with known values. The entropy of the activated complex was adjusted to yield known or expected A factors [$\log A = \log (ekT_m/h) + (\Delta S_{\ddagger}^{\ddagger}/2.3 R)$]. T_m = mean temperature in experiment.

b. RRK. A program for evaluating the Kassel integral for given values of $B \equiv E/RT$ (E = Arrhenius activation energy),^{6a} $D \equiv \log (A/\omega)$ (ω = collision frequency), and s was obtained from Dr. G. Emanuel of the Aerospace Corp.^{6b} This program was modified to accept exactly the same input data as the RRKM program (*i.e.*, frequencies, moments of inertia, collision diameters, etc.), from which it computed values of B and D , as defined above, and $s \equiv C_{\text{vib}}/R$. Thus, regardless of the reality of the models, they are identical.

c. Test Species. In order to cover the widest possible range of model systems, we envisaged the eight possibilities for high (H) and low (L) values of kinetic

parameters, shown in Table I. As will be seen, not all the models chosen are perfect examples of models 1–8, but, although it was not necessary, a preference for working with real reactions was expressed.

Results

Table II shows the results for eight prototype reactions at 300, 600, 900, and 1200°K, and at pressures of 10³, 10¹, 10⁻¹, and 10⁻³ Torr. (The values of ω , the collision frequency, vary slightly from model to model as a result of slight changes in mass and collision diameter.)

Discussion

The results in Table II show that the computed values for k/k_{∞} are very similar whether RRK or RRKM

(5) B. S. Rabinovitch and D. W. Setser, *Advan. Photochem.*, **3**, 1 (1964).

(6) (a) The usual definition of B is E_0/RT where E_0 is the activation energy of 0°K. We prefer to use the above definition since the value of the Kassel integral at infinite pressure is $k_{\infty} = Ae^{-B}$. If B is E_0/RT , then A cannot be the usual Arrhenius A factor defined as $A = k_{\infty}e^{E_0/RT}$, but must be redefined as $A_0 = k_{\infty}e^{E_0/RT}$. This use of A and E_{∞} , instead of A_0 and E_0 , makes insignificant differences in the values of k/k_{∞} . (b) G. Emanuel, Air Force Report No. SAMSOTR-69-36, Aerospace Report No. TR-0200(4240-20)-5.

Table III:^a Calculated Falloff Data [$k/k_{\infty}(T)$] for Example from Ref 3

1. $\text{CH}_4 \rightarrow \text{CH}_3 + \text{H}$ (Model 2 of ref 3)
 $k_{\infty}(2500) = 15.5 - 107.2/\theta$

P, Torr	$k/k_{\infty}(1000)$		$k/k_{\infty}(1500)$		$k/k_{\infty}(2500)$		$k/k_{\infty}(4000)$	
	M	K(s = 5)	M	K(s = 8)	M	K(s = 8)	M	K(s = 9)
10 ⁸	1	1	1	0.99	1	1	9.9 (-1)	9.8
10 ⁶	1	0.96	9.8 (-1)	9.2	8.6 (-1)	8.3	5.6 (-1)	5.3
10 ⁴	8.8 (-1)	4.2	6.3 (-1)	3.2	2.2 (-1)	2.0	4.7 (-2)	4.9
10 ²	2.2 (-1)	0.29	7.4 (-2)	2.0	1.0 (-2)	1.0	1.1 (-3)	1.3
1	4.6 (-3)	0.60	1.2 (-3)	0.41	1.3 (-4)	2.3	1.2 (-5)	2.1
k_{∞}	1.7×10^{-8}		8.7×10^{-1}		1.4×10^8		4.8×10^9	

2. $\text{CF}_3\text{H} \rightarrow \text{CF}_2 + \text{HF}$ (Model 2 of ref 3)
 $\log k_{\infty}(1400) = 14.66 - 71.99/\theta$

P, Torr	$k/k_{\infty}(600)$		$k/k_{\infty}(1000)$		$k/k_{\infty}(1400)$		$k/k_{\infty}(1800)$		$k/k_{\infty}(2200)$	
	M	K(s = 5)	M	K(s = 7)	M	K(s = 8)	M	K(s = 8)	M	K(s = 9)
10 ⁸	1	1	1	1	1	1	1	1	1	1
10 ⁶	1	1	1	1	9.9 (-1)	9.8	9.5 (-1)	9.4	8.9 (-1)	8.6
10 ⁴	9.9 (-1)	8.0	8.7 (-1)	7.6	6.3 (-1)	5.9	4.1 (-1)	3.5	2.5 (-1)	2.0
10 ²	6.7 (-1)	1.5	2.6 (-1)	1.5	8.9 (-2)	7.7	3.2 (-2)	2.5	1.3 (-2)	0.96
1	6.9 (-2)	0.52	1.2 (-2)	0.72	2.6 (-3)	2.9	7.0 (-4)	6.6	2.3 (-4)	2.0
k_{∞}	4.1×10^{-12}		8.9×10^{-2}		2.6×10^8		8.4×10^6		3.4×10^7	

^a Nomenclature identical with Table II.

theory is used, as long as the rate constant itself is in a measurable range. Thus, for values of $k > 10^{-4} \text{ sec}^{-1}$ ($k = [(k/k_{\infty}) \times k_{\infty}]$), the values of k/k_{∞} computed by the two methods usually agree to within a factor of 2 or 3. This is more than enough accuracy to justify use of RRK, particularly for predictive purposes. Conversely, if one is using measurements of k in the falloff

region to obtain high-pressure Arrhenius parameters, an error of a factor of 2 or 3 will lead to an error of ca. 1 kcal/mol in the activation energy for a process whose A factor is known.

The only exception in Table II is the value for acetyl at 300°K, where the value of $s = 2$ is probably the problem. This could lead to a generalization about

Table IV: Molecular Parameters Used

	1. $n\text{-C}_4\text{H}_{10}$		2. C_2H_6		3. PhCO							
	Molecule	Complex	Molecule	Complex	Molecule	Complex						
Frequencies, cm^{-1} , and regeneracies	2950 (6) 2870 (4) 1460 (6) 1370 (3) 1280 (3) 1170 (2) 1030 (2) 960 (2) 820 (2) 730 (1) 431 (1) 271 (1) 210 (2) 102 (1)	2950 (6) 2870 (4) 1460 (6) 1370 (3) 1280 (3) 1180 (1) 1030 (2) 952 (1) 803 (1) 730 (1) 109 (2) 32 (2)	2974 (2) 2950 (2) 2915 (2) 1469 (2) 1460 (2) 1370 (1) 1370 (1) 1190 (2) 995 (1) 822 (2) 260 (1)	2960 (6) 1436 (6) 95 (2) 66 (2)	3060 (5) 1700 (1) 1600 (3) 1483 (1) 1260 (3) 1160 (2) 1035 (3) 940 (3) 785 (3) 655 (2) 440 (3) 350 (2) 154 (1) 80 (1)	3060 (5) 1950 (1) 1600 (3) 1483 (1) 1290 (2) 1160 (2) 1035 (3) 940 (3) 785 (3) 655 (1) 440 (3) 310 (1) 175 (2) 80 (1)						
$I_A I_B I_C (\text{g cm}^2)^3 \times 10^{120}$	2.01×10^8		1.56×10^7		1.85×10^4		3.28×10^5		5.83×10^7		1.17×10^8	
$\pi I_{ri} (\text{g cm}^2) \times 10^{40a}$			9.16×10^3				2.92				3.00×10^1	
$\pi \sigma_{ir}^b$			27				3				3	
Sigma ^c	2		2		6		6		1		1	
Collision diameter, Å	6.0		2		5.0		6		1		8.0	

^a Product of reduced moments of inertia for internal rotors (internal symmetry = "foldness" of the rotor). ^b Product of internal isomers.

values of $s < 5$ or 6, but the problem really does not arise that much in molecules of chemical interest at the usual pyrolysis temperatures. In several of the model cases presented here, the reverse reaction is susceptible to study under conditions where the unimolecular process is not. Data on these systems (*i.e.*, $\text{CH}_3 + \text{CH}_3$; $\text{C}_2\text{H}_5 + \text{C}_2\text{H}_5$) show that the RRKM formulation predicts more closely the correct pressure dependence.⁷ This in no way detracts from the simple notion presented here, to wit: RRK theory may be used to estimate pressure dependence of thermal unimolecular processes in the "measurable" range.

In ref 3 and 4 the authors have defined values of s in terms of the vibrational energy content, and they have shown that these values are generally lower than s_k , the value of s from a best fit of the Kassel integral. However, s may also be defined as C_{vib}/R , and this value of s is close to s_k , so much so that it serves to make s a known input parameter. The fact that C_{vib}/R , at the temperature T , is not the same as E_{vib}/RT is not surprising for nonclassical oscillators.

It is not the intention here to prove by analytical means that C_{vib}/R is a better definition of s than E_{vib}/RT . Clearly these are the same in the classical limit. Given that C_{vib}/R turns out to work better as a definition for the Kassel integral, one is tempted to offer as an explanation the fact that, whereas the energy is a measure of the average number of "effective oscillators" from 0 to $T^\circ\text{K}$, the heat capacity at T measures the number of oscillators at this temperature.

The examples of ref 3 have been recomputed here as

well. The RRKM calculations agree fairly well with those tabulated therein; the small differences probably being due to the fact that the collision diameters used in this work are probably slightly different than those in ref 3.

Table III illustrates the fact that even in the cases originally used to substantiate the claim of complexity of s , the RRK method is adequate for predicting k/k_∞ as long as $k \gtrsim 10^{-4}$.

It is, therefore, concluded that use of RRK theory through the readily available tabulated values of the Kassel integral^{6b} is justified for thermally activated systems in most practical cases. The value of $s \equiv C_{\text{vib}}/R$ can be obtained from tabulated or estimated² heat capacities by subtracting the contribution of translation and rotation, *viz.*

$$C_p - R = C_v$$

$$C_{\text{vib}} = C_v - [(3/2)R]_{\text{trans}} - [(3/2)R]_{\text{rot}}$$

$$s \equiv \frac{C_{\text{vib}}}{R} = \frac{C_p - 4R}{R} = \frac{C_p - 8}{2}$$

It is certainly no harder to estimate A factors than to estimate the geometry and frequency assignment for the activated complex which is required by RRKM theory.

Appendix

Standard Parameters and Frequencies. The actual molecular structure parameters and frequencies used as input for the computations are shown in Table IV.

4. CH_2NHNH_7		5. <i>tert</i> -BuO		6. CH_3CO		7. <i>n</i> -hexyl		8. cyclobutene	
Molecule	Complex	Molecule	Complex	Molecule	Complex	Molecule	Complex	Molecule	Complex
		2980 (6)	2980 (6)	2900 (3)	2900 (3)	2940 (7)	2920 (12)	3080 (2)	3300 (6)
3300 (2)	3293 (3)	2900 (3)	2900 (3)	1714 (1)	1900 (1)	2870 (6)	2200 (1)	2950 (4)	1320 (12)
3000 (2)	2890 (2)	1465 (6)	1465 (6)	1400 (3)	1400 (3)	1460 (7)	1462 (7)	1566 (1)	660 (5)
2800 (2)	2250 (2)	1350 (4)	1350 (4)	1109 (1)	450 (2)	1360 (4)	1376 (2)	1430 (2)	
1500 (4)	1600 (1)	1220 (2)	1220 (2)	900 (2)	256 (1)	1303 (3)	1270 (8)	1250 (4)	
1250 (3)	1350 (2)	1106 (2)	1106 (1)	512 (1)		1250 (3)	1040 (3)	1090 (3)	
1050 (3)	1140 (5)	1013 (3)	1013 (2)	150 (1)		1160 (2)	940 (5)	986 (1)	
850 (2)	821 (2)	919 (1)	919 (1)			1040 (4)	890 (2)	840 (4)	
447 (1)	700 (2)	748 (1)	530 (2)			890 (3)	800 (3)	640 (2)	
315 (1)	300 (1)	450 (3)	450 (1)			760 (3)	575 (2)	325 (1)	
257 (1)		350 (2)	350 (2)			474 (1)	420 (2)		
		250 (3)	225 (2)			336 (2)	300 (2)		
			200 (2)			212 (2)	212 (1)		
						132 (2)			
						94 (1)			
						61 (1)			
1.97×10^6	7.06×15^6	5.60×10^6	1.20×10^7	7.99×10^4	3.25×10^6	2.95×10^7	2.42×10^7	5.68×10^6	5.68×10^6
			5.15		3.34				
			3		3				
0.5	0.5	3	1	1	1	1	1	2	2
	4.0		5.0		5.0		6.0		4.0

rotation symmetry numbers. ^c Sigma = σ/n , where σ is the symmetry number for *external* rotation and n is the number of optical

Some of these frequencies are averages from the careful vibrational assignment. Sources are: Model 1, n -C₄H₁₀ and complex (ref 8); Model 2, C₂H₆ and complex (ref 7); Model 3, PhCO and complex (ref 9); Model 4, CH₃NHNH₂ (ref 10) and the complex from this work using the four-center transition state of Benson (ref 2); Model 5, *tert*-BuO this work, using *tert*-BuOH as a model (ref 11) and complex (this work, reducing the four deformations destined to become external rotations of products to 50%, changing the CH₃ torsion to a free rotation and using the C-C stretch as the reaction coordinate.); Model 6, acetyl (this work, using acetaldehyde as a model) (ref 12), and complex (this work, reducing the three deformations destined to become external rotations of products to 50%, changing the CH₃ torsion to a free rotation and using the C-C stretch as the reaction coordinate); Model 7, n -hexyl and complex were assigned in this work, the n -hexyl from simple

modifications to the assignment for n -hexane (ref 13), and the complex using methyl-cyclopentane as a basis (ref 14); Model 8, cyclobutene and complex (ref 15).

- (7) E. V. Waage and B. S. Rabinovitch, *Int. J. Chem. Kinet.*, in press.
- (8) G. Z. Whitten and B. S. Rabinovitch, *J. Phys. Chem.*, **69**, 4348 (1965).
- (9) R. K. Solly and S. W. Benson, *J. Amer. Chem. Soc.*, in press.
- (10) J. R. Durig, W. C. Harris, and D. W. Wertz, *J. Chem. Phys.*, **50**, 1449 (1969).
- (11) E. J. Beynon and J. J. McKetta, *J. Phys. Chem.*, **67**, 2761 (1963).
- (12) (a) J. C. Evans and H. J. Bernstein, *Can. J. Chem.*, **34**, 1083 (1956); (b) K. S. Pitzer and W. Weltner, *J. Amer. Chem. Soc.*, **71**, 2842 (1949).
- (13) J. H. Schachtschneider and R. G. Snyder, *Spectrochim. Acta*, **19**, 117 (1963).
- (14) D. W. Scott, W. T. Berg, and J. P. McCullough, *J. Phys. Chem.*, **64**, 906 (1960).
- (15) C. S. Elliott and H. M. Frey, *Trans. Faraday Soc.*, **62**, 895 (1966).

Proton Magnetic Resonance Spectra of Molten Alkali Metal Acetate

Solutions of Polyhydric Alcohols and Phenols

by Louis L. Burton, S. Sherer, and E. R. VanArtsdalen*

Department of Chemistry, University of Alabama, University, Alabama 35486 (Received January 6, 1971)

Publication costs assisted by the University of Alabama

Molten sodium-cesium-rubidium acetate eutectic has been demonstrated to be a suitable fused salt solvent for study of solutions of polyhydric alcohols and phenols between 100 and 150°. Results of nmr investigations are reported which demonstrate strong solute-solvent interaction in these solutions. A pronounced downfield shift of OH is interpreted as indicating hydrogen bonding and exchange. Aromatic diols and triols show stronger interaction than the polyhydric alcohols. Phloroglucinol in acetate melt between 130 and 150° shows but a single, sharp peak somewhat downfield from the customary C-H peaks, indicating rapid exchange of all hydrogens.

Considerable research has been directed toward heterogeneous reactions in fused salts.¹ While simple molten salts have advantageous properties, such as thermal stability, low vapor pressure, wide liquid ranges, and high conductivity, their use as solvents for homogeneous organic studies has been limited by their generally high melting points and frequently poor solubility characteristics. Several recent studies have investigated reactions of organic compounds in molten salt solvents, such as quaternary alkylammonium salts^{2,3} and alkali metal thiocyanates⁴ and acetates.⁵

Phenols, polyhydric alcohols, and some amino compounds were found to be soluble in molten alkali metal

acetates at 190 to 240°. ^{5b} Although molten alkali metal nitrates and thiocyanates have been reported to be neutral to phenolic indicators,^{4a,6} the phenols and

- (1) W. Sundermeyer, *Angew. Chem., Int. Ed. Engl.*, **4**, 222 (1965).
- (2) J. E. Gordon, *J. Amer. Chem. Soc.*, **86**, 4492 (1964).
- (3) (a) J. E. Gordon, *ibid.*, **87**, 1499 (1965); (b) J. E. Gordon, *ibid.*, **87**, 4347 (1965).
- (4) (a) T. I. Crowell and P. Hillery, *J. Org. Chem.*, **30**, 1339 (1965); (b) P. Hillery, Ph.D. Thesis, University of Virginia, Charlottesville, Va., 1968; (c) K. Stewart, M.S. Thesis, University of Virginia, Charlottesville, Va., 1968.
- (5) (a) L. L. Burton and T. I. Crowell, *J. Amer. Chem. Soc.*, **90**, 5940 (1968); (b) L. L. Burton, Ph.D. Thesis, University of Virginia, Charlottesville, Va., 1968.

several amino compounds dissociated in molten alkali metal acetates to give the color characteristic of their anions. Alcohols with α -hydrogens dehydrated to olefins. Pentaerythritol, 2-hydroxymethyl-2-methyl-1,3-propanediol, and 2,2'-dihydroxymethyl-1-butanol reacted to give methanol, water, and unsaturated aldehydes. Based in kinetic studies, a mechanism involving the alkoxide was proposed.⁵

A spectroscopic technique to study the solution directly would have aided in investigating the solvated reagent, possible reaction intermediates, and the fused salt, itself. Although most spectroscopic methods require special equipment or are even unsuitable for application to molten salt solutions,⁷ pmr spectra with the Varian A-60 have been reported of pentaerythritol in molten alkali metal thiocyanate at 130°^{4a} and *p*-nitrophenol in molten tetra-*n*-pentylammonium bromide at 107°.^{3b} Therefore, it was decided to make a more detailed study of pmr spectra of a series of polyhydroxy compounds in molten acetates with the expectation that data so obtained would assist in interpreting reactions and structures of these solutions.

The low-melting sodium-cesium-rubidium acetate eutectic (30.5:55.5:14.0 mol %, mp 95°)⁸ was found to be suitable for pmr studies at 100 to 150° and unless otherwise specified is the acetate melt employed in studies described in this paper. Spectra were recorded of phenols and polyhydric alcohols in this fused salt and certain other solvents to investigate solvated species. Suitable high-temperature reference and lock signals were tested.

To avoid dehydration in the fused salts, alcohols without α -hydrogens were used exclusively; consequently there was no vicinal coupling for conformational analysis by the Karplus equation.

Experimental Section

Chemicals. Commercial phenols and polyhydric alcohols were obtained from Eastman Kodak Co. Purity was checked by melting point. *cis*- and *trans*-2,2,4,4-tetramethyl-1,3-cyclobutanediol was obtained as a 1 + 1 mixture, and the isomers were separated as diformate esters or by acid cleavage of the *trans* isomer.⁹ Rubidium and cesium acetates (K & K, 99.9%) and sodium acetate (Baker Analyzed reagent) were oven-dried at 110–120° for 6 hr prior to preparation of the eutectic mixture, then stored in a desiccator until used. Pains were taken to prevent contamination by moisture in preparing solutions. Acetic acid-*d*₄ and deuterium oxide from Mallinckrodt Nuclear Co., dimethyl sulfoxide-*d*₆ from New England Nuclear Co., deuteriochloroform from Columbia Organic Chemicals, Inc., and spectral grade pyridine from Eastman Co. were used as solvents. Also acetic acid-*d*₄ was used to prepare alkali metal acetate-*d*₃ by exchange or reaction with sodium hydroxide.

Nuclear Magnetic Resonance Spectroscopy. Spectra

were run on a Varian HA-100 spectrometer with variable temperature probe. Temperature calibration was made by the chemical shift difference of the two peaks in neat ethylene glycol.¹⁰ Solutions were 15% by weight or, if solubility was less than 15%, a saturated solution was used.

Samples in fused salt were preheated before placing in the probe at 130 or 150° to ensure homogeneity and rapid thermal equilibration. The alkali metal acetate singlet was satisfactory both as a lock and reference for most solutes. When the solvent peak interfered with the solute spectrum, deuterated acetate salt and *p*-dichlorobenzene were used in a coaxial sample tube. Although this aromatic lock signal was advantageous for recording alkyl spectra, it gave a weaker signal than the alkali metal acetate or a coaxial sample tube with ethylene glycol. However, this technique does permit pmr studies to be made in aprotic molten salts at 100–150°.

Since little or no coupling was observed in the spectra of fused salt solutions, only a first-order analysis was required. For comparison with chemical shifts relative to TMS, an offset of 2.40 or 7.05 ppm was used with the alkali metal acetate and *p*-dichlorobenzene locks, respectively. (Relative to TMS in a coaxial sample tube the aqueous alkali metal acetate peak at 25° is 2.40 ppm downfield. Relative to the molten alkali metal acetate peak *p*-dichlorobenzene in a coaxial sample tube at 100–150° is 7.05 ppm downfield.)

Samples in other solvents were prepared in concentrations similar to the fused salt solutions and run at 27° with an internal capillary of TMS as lock and reference, unless specified otherwise.

Results and Discussion

Chemical shifts of nmr spectra of several polyhydric alcohols in fused alkali metal acetate solution are shown in Table I. These shifts are comparable with values in other solvents, as may be seen from data for the same compounds in Table II which were obtained with a coaxial sample tube containing pure TMS as reference. Corrections have not been made for differences in volume magnetic susceptibility of the solvents,¹¹ because data are not available for dimethyl sulfoxide or the fused salt.

(6) B. J. Brough, D. H. Kerridge, and M. Moseley, *J. Chem. Soc. A*, 1556 (1966).

(7) (a) J. K. Wilmshurst, *J. Chem. Phys.*, **39**, 2545 (1963); (b) J. K. Wilmshurst, *ibid.*, **39**, 1779 (1963).

(8) G. C. Diogenov and G. S. Sergeva, *Zh. Neorg. Khim.*, **9**, 1499 (1964); *Chem. Abstr.*, **61**, 5005b (1964).

(9) (a) H. R. Hasek, E. U. Elam, J. C. Martin, and R. G. Nations, *J. Org. Chem.*, **26**, 700 (1961); (b) R. H. Hasek, R. D. Clark, and J. H. Chaudet, *ibid.*, **26**, 3130 (1961).

(10) "Variable Temperature Accessory with V-6040 Controller," Varian Publication Number 87-202-006, Palo Alto, Calif., pp 4–10.

(11) J. A. Pople, W. G. Schneider, and J. J. Bernstein, "High Resolution Nuclear Magnetic Resonance," McGraw-Hill, New York, N. Y., 1959, pp 80–82.

Table I: Chemical Shift of Polyhydric Alcohols in Fused Alkali Metal Acetate at 130° Relative to $\delta = 2.40$ for Molten Acetate

	δ_{CH_2} or			$\delta_{\text{CH}_2} - \delta_{\text{CH}}$
	δ_{OH}	δ_{CH}	δ_{CH_3}	
Pentaerythritol	6.00	4.01		
2-Amino-2-hydroxymethyl-1,3-propanediol	5.06	3.98		
2-Hydroxymethyl-2-methyl-1,3-propanediol	5.85	3.99	1.41	2.58
2-Amino-2-methyl-1,3-propanediol	4.75	3.90	1.58	2.32
2,2-Dimethyl-1,3-propanediol	5.87	3.88	1.42	2.46
<i>cis</i> -2,2,4,4-Tetramethyl-1,3-cyclobutanediol (13.5%)	6.46	3.84	1.63, 1.53	2.21, 2.31
<i>trans</i> -2,2,4,4-Tetramethyl-1,3-cyclobutanediol (15.6%)	5.91	4.03	1.59	2.44

Table II: Chemical Shift of Polyhydric Alcohols at 27° Relative to $\delta = 0.00$ for Neat TMS in a Coaxial Sample Tube

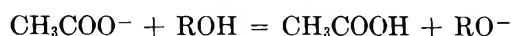
Solute	Solvent	δ_{CH_2} or			$\delta_{\text{CH}_2} - \delta_{\text{CH}_3}$ or $\delta_{\text{CH}} - \delta_{\text{CH}_3}$
		δ_{OH}	δ_{CH}	δ_{CH_3}	
Pentaerythritol	D ₂ O	5.19	4.05		
2-Amino-2-hydroxymethyl-1,3-propanediol	D ₂ O	5.24	3.99		
2-Hydroxymethyl-2-methyl-1,3-propanediol	D ₂ O	5.24	3.96	1.34	2.62
2-Amino-2-methyl-1,3-propanediol	D ₂ O	5.22	3.90	1.49	2.41
2,2-Dimethyl-1,3-propanediol	D ₂ O	5.20	3.82	1.35	2.47
	DMSO	4.65	3.52	1.13	2.39
	C ₆ H ₅ N	5.61	3.51	0.98	2.53
	CD ₃ COOD	10.04	3.53	0.96	2.57
<i>cis</i> -2,2,4,4-Tetramethyl-1,3-cyclobutanediol	D ₂ O	5.18	3.87	1.56, 1.45	2.31, 2.42
	DMSO	4.82	3.50	1.35, 1.21	2.15, 2.29
	C ₆ H ₅ N	5.68	3.44	1.22, 1.02	2.22, 2.42
	CD ₃ COOD	10.26	3.50	1.20, 1.12	2.30, 2.38
<i>trans</i> -2,2,4,4-Tetramethyl-1,3-cyclobutanediol	D ₂ O	5.16	4.00	1.47	2.53
	DMSO	4.86	3.69	1.30	2.39
	C ₆ H ₅ N	5.65	3.65	1.12	2.53
	CD ₃ COOD	10.30	3.66	1.13	2.53

In a strict sense, comparison of spectra in different solvents can be made without corrections for volume magnetic susceptibility only if an internal reference has been used. Rather than add another solute, such as Tier's salt (sodium 2,2-dimethyl-2-silapentane-5-sulfonate) to each solution, the methyl peak in each polyhydric alcohol is taken as reference for that solute and ($\delta_{\text{CH}_2} - \delta_{\text{CH}_3}$) or ($\delta_{\text{CH}} - \delta_{\text{CH}_3}$) is listed in Tables I and II. This comparison shows that the methylene and methine protons in each polyhydric alcohol exhibit comparable shifts in acetate melts and in aqueous solution as well as conventional organic solvents. Indeed, the methylene and methine proton shifts in D₂O and the acetate melt are almost identical in all cases studied. Thus, the hydrocarbon structure of the solvated species in the fused salt solution must not be distorted greatly by the strong electrostatic forces expected in the ionic melt.

The two methyl peaks observed for *cis*-2,2,4,4-tetramethyl-1,3-cyclobutanediol (but the single peak for its *trans* isomer) are in agreement with previous work^{9a} although the authors did not specify the solvent.

A solution of acetic acid in the acetate melt showed a broad peak at about $\delta = 8.2$, well downfield from the

OH absorption by these polyhydric alcohols. However, their OH peaks, with exception of the two amino derivatives are shifted significantly downfield in acetate melt compared with the corresponding compounds in the common solvents, heavy water and dimethyl sulfide. Presumably this results from hydrogen bonding or rapid exchange with the solvent



This is in agreement with earlier studies of weak acid indicators, such as 2,4-dinitroaniline, and the proposed mechanism for the trimethylolethane reaction at 200°.⁵

Upfield shifts for hydrogen-bonded protons are caused by increased temperature;¹² in fact, this shift in neat ethylene glycol is used routinely for temperature calibration of the Varian variable temperature controller.¹⁰ We determined this shift for ethylene glycol in molten alkali metal acetate. This change is less pronounced in fused salt solution, although the peaks are more widely separated with the OH absorption farther downfield

(12) Reference 11, pp 98-100.

in the fused salt, indicating solute-solvent interaction. The sample was a glass below 90° and some discoloration was observed at 150°; however, in the range 100–150° the change in chemical shift in Hertz between the methylene and hydroxyl peaks, Δ , was linear and is represented by

$$\Delta = 234 + 0.76(150 - T)$$

where the temperature, T , is in degrees Celsius and the average deviation of individual experimental points was less than 1 Hz. This is to be compared with

$$\Delta = 37 + 0.99(150 - T)$$

for neat ethylene glycol.¹⁰ Upfield shifts with increasing temperature also were observed for the other polyhydric alcohols in fused alkali metal acetate. Comparison of data for 2,2-dimethyl-1,3-propanediol in Tables I and III shows an upfield shift of the OH peak of about 0.5 Hz per degree between 130 and 150°.

Table III: Variation of Chemical Shift with Concentration of 2,2-Dimethyl-1,3-propanediol in Deuteriochloroform at 27° and Molten Alkali Metal Acetate at 130°

Solvent	Wt % solute	δ_{OH}	δ_{CH_2}	δ_{CH_3}	$\delta_{\text{OH}} - \delta_{\text{CH}_3}$
Na, Rb, Cs/C ₂ H ₃ O ₂	17.2	5.89	3.87	1.41	4.47
	12.2	6.05	3.86	1.41	4.64
	8.2	6.15	3.86	1.40	4.75
DCCl ₃	21.0	4.31	3.41	0.87	3.44
	14.6	4.15	3.41	0.87	3.28
	10.5	3.96	3.42	0.87	3.09

The effect of concentration on the chemical shift has been used to study hydrogen-bonded protons.¹³ In an inert solvent decreased solute-solute intermolecular hydrogen bonding causes an upfield shift on dilution; for a donor solvent with solute-solvent hydrogen-bonding, a downfield shift occurs. Table III contains chemical shift data obtained for 2,2-dimethyl-1,3-propanediol at several concentrations in deuteriochloroform at 27° and in fused alkali metal acetate at 130°, confirming that the polyhydric alcohol is hydrogen bonded with the alkali metal acetate solvent.

The external *p*-dichlorobenzene reference made possible pmr studies in aprotic molten salts with the HA-100. For comparison, the spectra of pentaerythritol (15% by weight) in alkali metal acetate, nitrate, and thiocyanate at 130° are summarized in Table IV. The lithium-potassium nitrate (56:46 mol %, mp 125°) and sodium-potassium thiocyanate (70:30 mol %, mp 123.5°) eutectics¹⁴ were used.¹⁵ Since magnetic susceptibility data are not available, corrections have not been made; however, the downfield shift of the methylene protons is probably caused by increased diamagnetic susceptibility and the upfield shift of the

Table IV: Chemical Shift of Pentaerythritol in Molten Alkali Metal Salt Eutectics at 130°

Solvent	δ_{OH}	δ_{CH_2}
Na, Cs, Rb/C ₂ H ₃ O ₂	6.00	4.01
Na, K/SCN	4.62	4.81
Li, K/NO ₃	4.47	4.21

hydroxyl protons by decreased solute-solvent hydrogen bonding. The variation in observed chemical shift for pentaerythritol in these three low-melting salt solutions is greater than that observed for 2,2-dimethyl-1,3-propanediol in the common nmr solvents—chloroform, dimethyl sulfoxide, and water (Table II).

Pmr spectra were obtained for solutions of five benzenediols and -triols in molten acetate melts and chemical shift data are presented in Table V. In all cases

Table V: Chemical Shift of Phenols in Fused Alkali Metal Acetate at 150° Relative to $\delta = 2.40$ for Molten Acetate

	δ_{OH}	δ_{CH}
Hydroquinone (1,4-benzenediol)	10.58	7.26
Resorcinol (1,3-benzenediol)	10.99	7.50 ^a 6.99 6.87 ^b
Pyrocatecol (1,2-benzenediol)	11.30	7.38 7.14
Pyrogallol (1,2,3-benzenetriol)	10.20	6.96
Phloroglucinol (1,3,5-benzenetriol)	One peak at 7.56	

^a Triplet, coupling 8 Hz ($J_{4,5} = J_{5,6}$); assigned to C₅. ^b Doublet, coupling 8 Hz; assigned to C₄ and C₆.

integrated areas under the peaks corresponded to the correct number of protons. Only in the case of resorcinol was spin-spin coupling observed. Our assignments for ring protons of resorcinol in the fused eutectic appear to be in reasonable agreement with data in other solvents.^{16,17} It is interesting that with pyrocatecol we observed two peaks, apparently corresponding to the two protons each at positions 3, 6 and 4, 5, respectively, although they are more or less completely unresolved in spectra reported elsewhere.^{16,18} Ring pro-

(13) Reference 11, Chapter 15.

(14) R. A. Bailey and G. J. Janz in "Chemistry of Non-Aqueous Solvents," J. J. Lagowski, Ed., Academic Press, New York, N. Y., 1966, p 293.

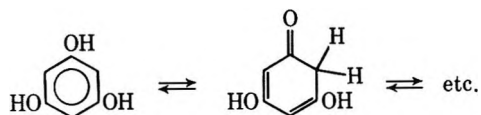
(15) Although we experienced no difficulty, great care should be exercised in using fused nitrates as solvents for organic compounds. Preliminary tests were always made with small quantities behind safety shields. In fact, in a small DTA test of pentaerythritol in the nitrate eutectic we detected no evidence of chemical reaction to well above 250°.

(16) J. C. Schug and J. C. Deck, *J. Chem. Phys.*, **37**, 2618 (1962).

(17) H. B. Evans, A. R. Tarpley, and J. H. Goldstein, *J. Phys. Chem.*, **72**, 2552 (1968).

tions appear slightly farther downfield in the melt eutectic than in conventional solvents. Generally in other solvents the OH peak of phenols appears upfield from the ring proton peak or peaks. This is reversed in molten acetate solution and the far downfield shift of the hydroxyl proton bespeaks very strong hydrogen bonding and exchange between solute and solvent in these systems, confirming previous experiments with phenolic indicators such as alizarin.^{4a,6} Although the reference signal was not specified, a similar downfield shift of 2 ppm has been reported for *p*-nitrophenol in molten quaternary ammonium bromide.^{3b} If the solutions were not degassed, there was a tendency for some reaction to occur very slowly with resorcinol and more rapidly with pyrogallol which we attribute to oxygen. Under these conditions the OH peaks degraded and tended to move upfield. The OH peaks were quite dependent on concentration, but ring proton peaks were almost independent of concentration.

The single peak exhibited by phloroglucinol is interpreted as resulting from rapid equilibration of the type



perhaps involving the anion and the relatively stable dianion.¹⁹ However, the pmr spectrum did not correspond to that of the dianion salt at room temperature.

The fused salt solution was bright red-orange, suggesting the presence of a highly conjugated or resonance-stabilized species.

The absence of observable spin-spin coupling in the cases of pyrocatecol and pyrogallol is intriguing. One previous report of pyrocatecol¹⁸ not only shows no coupling, but, as noted previously, merely a single sharp ring proton peak. We can only suggest that somewhat poorer resolution with these two compounds at 150° prevented our distinguishing coupling which, as shown by Schug and Deck,¹⁶ is not too obvious.

This study confirms the basic properties of molten alkali metal acetates toward weak organic acids previously reported.^{5a} In the polyhydric alcohol and phenol solutions studied the solvated species are hydrogen bonded with the solvent; however, no pronounced effect was detected of electrostatic forces from the fused salt solvent, assumed to be an ionic melt.

Work is in progress to obtain magnetic susceptibility (and density) data for correcting chemical shifts of molten salt solutions, and to explore pmr spectra in further detail for these and similar systems.

Acknowledgment. This study was supported in part by a grant from the Research Grants Committee of the University of Alabama.

(18) High Resolution NMR Spectra Catalog, Vol. I, Spectrum Number 124, Varian Associates, 1962.

(19) R. J. Highet and T. J. Batterham, *J. Org. Chem.*, **29**, 475 (1964).

Hidden Degeneracy and the Vibration of Larger Molecules

by **Walter F. Edgell**

Department of Chemistry, Purdue University, West Lafayette, Indiana 47901 (Received December 29, 1970)

Publication costs assisted by the Advanced Research Projects Agency and the National Science Foundation

The vibration of larger molecules is characterized by the presence of hidden degeneracy. This degeneracy is associated with the presence of symmetry not contained in the point group M of the molecule and results from the existence of localization in the modes of vibration. The symmetry for a set of localized vibrations is described by a permutation group G and the selection rules, degeneracy of the frequencies, number of modes of a given type, transformation properties of the components of the dipole moment vector and polarizability tensor, etc., are obtained from it. An example of the application of the method is given.

Introduction

Investigations of the infrared and Raman spectra of polyatomic molecules for long have been characterized by the use of theoretical analysis of the molecular vibrations. The principles of vibrational analysis described in the popular works of Herzberg¹ and Wilson, Decius, and Cross² are in excellent accord with the experiment when applied to the spectra of moderate-sized molecules. In this scheme, the determination of the number and degeneracies of the vibrations and of the selection rules, the potential energy characterization and frequency computation, and the intensity treatments are all carried out with the aid of group theory using the group formed from the symmetry operations of the point group of the molecule. However, numerous discrepancies are found between the expectations of theory and the observations when this same scheme is applied to larger molecules. Experiment does not wait for theory; the methods of dealing with the spectra of such larger molecules are outlined in the works of Bellamy³ and Rao.⁴ In this paper, the group theory and its base are extended to deal with the common types of observations for somewhat larger molecules.

Let us start by asking what characterizes a larger molecule from a smaller one. In a typical small molecule, the symmetry operations of the point group move atoms to equivalent atoms. As molecules become larger, these same operations develop a new feature—they move the atoms from one functional group (CH₃, CO, C₆H₅, NO₂, etc.) to those of an equivalent group. Now, two kinds of transport phenomena are involved: the transportation of atom to atom within a functional group and the transportation of one functional group to another. These are different kinds of operations in the abstract sense. The applicability of both kinds of transport operations to a molecule is regarded here as a primary characteristic which may be possessed by a larger molecule.

It has been said, on occasion, that all atoms move in every vibration of a molecule. While this may be the case for small molecules, it certainly cannot be the

situation in larger ones. If it were true, group frequencies would not exist.⁵ Yet the existence of frequencies associated with the presence of functional groups in a molecule is the second dominant fact about the vibration of larger molecules.^{3,4}

Theory

Hidden Degeneracy. The vibrational potential energy for a molecule can be written in terms of the normal coordinates as

$$V = \sum_i \lambda_i Q_i^2 + \sum_{k\alpha} \lambda_k Q_{k\alpha}^2 \quad (1)$$

where $\lambda_i = (2\pi\omega_i)^2$ is the square of the i th circular frequency and the first sum is over the nondegenerate coordinates. The second sum is over the degenerate coordinates— $Q_{k\alpha}$ being the α th normal coordinate corresponding to the k th frequency. The potential energy must be invariant to any symmetry operation R of the point group M of the molecule. This requires that

$$\begin{aligned} RQ_i &= \pm Q_i \\ RQ_{k\alpha} &= \sum_{\beta} R_{\alpha\beta} Q_{k\beta} \end{aligned} \quad (2)$$

with the $R_{\alpha\beta}$ being the elements of a unitary matrix. This is well known. But consider now the converse. Suppose one has a set of coordinates Q which reduce the vibrational potential energy to the form of eq 1 and transform like eq 2 under all the operations of some group M . It is further supposed that they reduce the kinetic energy to a sum of squares in the \dot{Q} . One finds that the potential (and kinetic) energy is invariant to

(1) G. Herzberg, "Infrared and Raman Spectra," Van Nostrand, Princeton, N. J., 1945.

(2) E. B. Wilson, Jr., J. Decius, and P. Cross, "Molecular Vibrations," McGraw-Hill, New York, N. Y., 1955.

(3) L. J. Bellamy, "The Infrared Spectra of Complex Molecules," Wiley, New York, N. Y., 1954.

(4) C. R. Rao, "Chemical Applications of Infrared Spectroscopy," Academic Press, New York, N. Y., 1963.

(5) For an excellent discussion of the theoretical basis for group frequencies, see W. King and B. Crawford, Jr., *J. Mol. Spectrosc.*, **5**, 421 (1960).

the operations of M not only when each λ is unique, *i.e.*, when $\lambda_m \neq \lambda_n$, but also, in fact, when $\lambda_m = \lambda_n$ for some of the λ of eq 1. This means that there is no requirement that each frequency called for by the point group M of the molecule be unique. It is an experimental fact, however, that $\lambda_m \neq \lambda_n$ for small molecules except in rare instances referred to as accidental degeneracy.

To illustrate what occurs for larger molecules, let us suppose that the only symmetry element apparent in CH_3Cl were one plane of symmetry. Treating the molecule on the basis of the C_s group, instead of C_{3v} , leads to normal coordinates which satisfy eq 1 and 2 with nine λ_i . This would compare with the six λ_i found experimentally and one would appear to have a case of "accidental" degeneracy. Of course, the missing degeneracy in the treatment under C_s is due to the symmetry present in CH_3Cl but missing in the group C_s .

Finding fewer frequencies than predicted from the point group M of the molecule is a common event with larger molecules. Its occurrence in this case, however, is no accident, but results from the fact that not all the symmetry present in the vibrations is displayed by M . A fundamental problem for larger molecules then is to locate the symmetry missing in M . And since the missing degeneracy for larger molecules is no accident, it seems preferable to use the term hidden degeneracy in place of accidental degeneracy.

Localization. The vibrational spectra of many larger molecules exhibit certain characteristic frequencies associated with the presence of functional groups.^{3,4} These are characteristic since they occur at or near the same frequency irrespective of the molecule in which the group is present. This implies that the force constants associated with the bonds and angles of that structural unit make the dominant contribution to the potential energy of the vibration in question. It also implies that only the atoms of that structural unit undergo major displacements during the vibration, while the atoms in the remainder of the molecule move very little, if at all. Thus, vibrations of larger molecules tend to group themselves into specific types which are related to the deformation of the constituent structural units of which the molecule is built.

It is seen that the existence of group frequencies implies the localization of motion in such vibrations. This localization involves an exclusion of some parts of the molecule from deformation in the vibration, but this is not the only kind of vibratory motion which involves exclusion. Suppose the motions in the vibrations of a functional group are confined to the atoms of that group. Then, since all vibrations of the molecule must be orthogonal, there must be other vibrations in which the functional group moves as a rigid unit. These are the "framework" vibrations. The point is that such framework vibrations also involve exclusions in an ab-

stract sense since they do not involve the distortion of the functional group in question. Both kinds of exclusions enter the vibrational analysis in a similar way, and it is convenient to define localization to include both.

A vibration is said to be localized when the number of coordinates required for the description of its kinetic and potential energies is less than the number of coordinates required for the kinetic and potential energies describing all the vibrations of the molecule.

Let q be the set of coordinates which span the whole vibrational domain. In terms of them, the potential and kinetic energies are $V(q)$ and $T(\dot{q})$, respectively. Designate by q_i the subset of the coordinates which participate in the i th group of localized vibrational modes. It follows from the definition that there are terms in $V(q)$ and $T(\dot{q})$ which do not involve the q_i . Such terms have no connection with and exert no influence on the modes of vibration in the i th group, and consequently they can be ignored in treating it. Since only the truncated potential and kinetic energies

$$\begin{aligned} V_{\text{eff}} &= V(q_i) \\ T_{\text{eff}} &= T(\dot{q}_i) \end{aligned} \quad (3)$$

are effective for this i th group of modes, localization is seen to be a basis for factoring the kinetic and potential energies of the molecule. The frequencies and normal coordinates for the modes of this group of localized vibrations may be obtained from the solution of the secular equation

$$|\mathbf{V}_{\text{eff}} - \mathbf{T}_{\text{eff}}E| = 0 \quad (4)$$

or from the computational equivalents designed for computer use. Here \mathbf{V}_{eff} and \mathbf{T}_{eff} are the matrices of the coefficients of the coordinates in $V(q_i)$ and $T(\dot{q}_i)$. One, of course, would like to say something about the number of frequencies to be expected, the degeneracy of each frequency, selection rules, polarization of Raman lines, etc. These are not to be sought from the symmetry expressed by the point group M of the molecule but, in fact, they are the consequences of the symmetry contained in the truncated potential and kinetic energies V_{eff} and T_{eff} . But how is this latter symmetry to be expressed? One notes that a number of operations which *permute* identical atoms involved in the i th group of localized vibrations leave its V_{eff} and T_{eff} invariant. These operations form a group G , and it is this group G which provides the answers we seek for this group of modes. Since there is a separate V_{eff} and T_{eff} for each group of localized vibrations, there is a separate (and generally different) G for each such group.

Permutation Operations and Groups. In this section, we consider an example of a permutation operation, how they arise for a molecule, and place G and M in perspective. The kinetic and potential energy ex-

pressions which contain the full quota of terms permitted by M , none of which are negligible, are very restrictive for a larger molecule. For a molecule with such energy expressions, all the vibrations would follow the full consequences of M ; no group or framework modes would exist. As cross terms drop out of these expressions or become small enough to be treated as perturbations, V and T become more general. This increased generality leads to symmetry not present in the kinetic and potential energy expressions associated with M . For example, consider a methyl group in a molecule for which the point group M is C_1 . Suppose that the kinetic and potential energies were invariant under the operation σ^m which carries *only* the atoms of the methyl group through a plane of symmetry localized in this group, all other atoms being unchanged. This represents symmetry in V and T that is not contained in M . It is symmetry which is pertinent to vibrations localized in the methyl group. The operation σ^m is an element of the group G which leaves invariant V_{eff} and T_{eff} for the vibrations localized in this CH_3 moiety. It is worthwhile noting that while σ^m is a permutation operation for the molecule it is not a covering operation of M .

In a larger molecule, a number of permutation operations exist which exchange equivalent atoms. These operations form a group P . Now, P has many subgroups including M and C_1 . Not all operations of P will leave T and V invariant for a given molecule. Therefore, P and some of its subgroups are not useful for treating the vibrations. The group G for a given group of localized modes of the molecule is that subgroup of P which contains all the elements of P which leave the corresponding V_{eff} and T_{eff} invariant.

Localized Modes from One Moiety. Vibrations tend to be localized in the functional groups of a larger molecule, e.g., OH, C=O, NH_2 , CH_3 , C_6H_5 , etc., or in coupled functional groups of which the isopropyl and *tert*-butyl groups are examples. The former case is considered in this section and the latter in the next one.⁶

To apply group theory to the vibrations of a given system, one classically asks the question, "What group is to be associated with this system?" For a small molecule, the answer to such a question is straightforward—the point group corresponding to the molecular geometry. For a larger molecule, V_{eff} and T_{eff} not only depend upon the geometry of the moiety but also upon the nature of its immediate environment, and since these features may vary with the molecule of which the moiety is a part, there is no unique answer to the question put in that way. This does not mean that theory cannot be developed for larger molecules, but it does mean that its basic relation with experiment will differ from the classical one enjoyed by small molecules. The question which can be asked of theory for larger molecules is not that which is asked for smaller molecules. It is, "What are the group theoretical conse-

quences of a given V_{eff} and T_{eff} for the moiety?" One may then compare the answers of theory for the several possible forms which V_{eff} and T_{eff} may take for the moiety in the molecule with the experimental results. The experiment is destined to serve as the arbiter between the several possibilities, and it is apparent that the experiment will naturally be concerned with the interaction of a moiety with its environment in the molecule.

Let us now inquire about the details of V_{eff} and T_{eff} . In a mode localized in a functional group of a real molecule, there will be some relatively small displacements of atoms outside the moiety. The energies of the molecule may be written as

$$\begin{aligned} V &= \sum_r V(q_r) + \sum_{r>r'} V'(q_r, q_{r'}) \\ T &= \sum_r T(\dot{q}_r) + \sum_{r>r'} T'(\dot{q}_r, \dot{q}_{r'}) \end{aligned} \quad (5)$$

in a set of coordinates relevant to the distortion of the various moieties and to the displacements of the framework modes. Here $V(q_r)$ and $T(\dot{q}_r)$ are the terms associated with the distortion of the r th moiety or framework and V' and T' are the interaction terms. The k th coordinate which enters the subsets of eq 5 has the value

$$q_k = \sum_n \mathbf{s}_{kn} \cdot \boldsymbol{\tau}_n \quad (6)$$

in the i th mode of vibration when the normal coordinate $Q_i = 1$. Here $\boldsymbol{\tau}_n$ is the displacement of the n th atom in this mode (when $Q_i = 1$), the \mathbf{s}_{kn} are the vectors introduced by Wilson,² and the sum is over all the atoms. The potential and kinetic energies generated by this vibration localized in the m th moiety (when $Q_i = 1$) are

$$\begin{aligned} V &= V(q_m) + \sum_r V(q_r) + \sum_{r>r'} V'(q_r, q_{r'}) \\ T &= T(\dot{q}_m) + \sum_r T(\dot{q}_r) + \sum_{r>r'} T'(\dot{q}_r, \dot{q}_{r'}) \end{aligned} \quad (7)$$

where the primed sums are over all moieties and frameworks but the m th. Because of the localization, the leading term is dominant in each expression and the remaining terms are small or zero (many $q_k = 0$). The effective kinetic and potential energies for this vibration contains, in the subset q_i , just those coordinates which have not vanished in eq 7. They can be written as

$$\begin{aligned} V_{\text{eff}} &= V(q_m) + V(q_m, q_r) = V_m + V_r \\ T_{\text{eff}} &= T(\dot{q}_m) + T(\dot{q}_m, \dot{q}_r) = T_m + T_r \end{aligned} \quad (8)$$

where the dominant contribution to the energies in the vibration comes from the V_m and T_m terms in V and T and the remaining small contribution comes from that

(6) The word moiety is used in this paper to mean that part of the molecule in which one or more localized vibrations occur. It sometimes includes several functional groups.

part of the remainder of V and T which is contained in V_r and T_r . Of course, eq 8 apply just as well if there are several localized vibrations in the m th set. Then q_m spans the dominant coordinates of all the several vibrations.

A given moiety is basically the same in each molecule of which it is a part. Therefore, V_m can be thought of as composed of two parts—an inherent part, V_n , plus the terms V_s which represent the effect of the site. Of course, such a partition is arbitrary; we place in V_s , here, only that part of V_m which distorts the inherent symmetry of the moiety. The same partition is made for T_m .

The full consequences of symmetry in localized modes are to be obtained from V_{eff} and T_{eff} as given by eq 8. However, in practice, an excellent approximation can be obtained by truncating them to V_m and T_m and, in some cases, to V_n and T_n .

As an example, let us consider a single methyl group in a larger molecule. This moiety is inherently trigonal and the group G corresponding to $V_{\text{eff}} = V_n$, $T_{\text{eff}} = T_n$ is C_{3v}^m whose operations are the permutations: E^m , C_3^m , $(C_3^m)^2$, σ_{v1}^m , σ_{v2}^m , σ_{v3}^m . When the CH_3 moiety is in a molecule where the site terms make a contribution to V_{eff} and T_{eff} , the permutation group G will be C_s^m when there is one unique CH unit and C_1^m when each CH unit is unique.

Localized Modes from Coupled Functional Groups. Coupling between several functional groups produces vibrations in which the atoms of each functional group move in a significant manner.⁷ Equations 8 apply to this case also since the molecular moiety, m , by definition, includes the groups which are coupled. Both the effective kinetic and potential energies can be written in the form

$$V_{\text{eff}} = \sum_g V_g + V_c \quad (9)$$

where V_g is that portion of the potential energy which depends upon the relevant coordinates of the group g ; the sum is over all coupled groups; and V_c is the potential energy coupling the groups. V_{eff} can be written in this form exactly if the contributions from V_r are included in V_g and V_c . In practice, it is convenient to drop from V_g and V_c those terms from V_r which have a small effect on the frequencies.

G is the group of permutation operations which leave V_{eff} (and T_{eff}) invariant, in the form given by eq 9. It is dependent upon V_c as well as upon the V_g . Several special cases appear depending upon the nature of V_c . To develop these, one may introduce the coordinates q_{ig} which reduce V_g and T_g to the diagonal form. Then eq 9 becomes

$$V_{\text{eff}} = \sum_{g,i} \lambda_{ig} q_{ig}^2 + 2 \sum_{g>g'} \sum_{i,i'} \lambda_{ig,i'g'} q_{ig} q_{i'g'} \quad (10)$$

The size of the terms in the second sum of this equation, and hence their contribution to a vibrational spectrum,

depends upon a number of factors. First in importance is the inherent tendency of the vibrations of a particular functional group to couple with those of another group. Of almost equal importance is the relative positions of the functional groups in the molecule and whether other atoms intervene, how many, their kind, etc. Several cases arise depending upon the size of the coupling terms in (10). A trivial case occurs when the coupling terms are vanishingly small. Then each functional group becomes a moiety in the sense that the word is used here (see footnote 6) and the considerations of the last section apply to each one. The other cases are dealt with separately below.

First Case. In the first case that we consider, the potential (and kinetic) energy takes the form

$$V_{\text{eff}} = \sum_{g,i} \lambda_{ig} q_{ig}^2 + 2 \sum_{g>g'} \sum_i \lambda_{ig,i'g'} q_{ig} q_{i'g'} \quad (11)$$

where it has been assumed further that all the functional groups of the moiety are equivalent. Equation 11 may be obtained from (10) by dropping the terms involving $\lambda_{it'}$.⁸ Equation 11 obviously holds when all the $\lambda_{it'}$ are vanishingly small. There is another important situation, in addition, where (11) applies. When the effects of the coupling terms may be treated by perturbation theory, eq 11 gives the vibrational frequencies through the first order.⁹ Then the $\lambda_{it'}$ terms make a second, or higher, order correction to the frequencies. Thus the results of this section are exact for the cases when $\lambda_{it'} = 0$ and are correct through the first order when the $\lambda_{it'}$ terms may be treated by perturbation theory.

Let L be the group of local operations which leave the V_g and T_g for a particular functional group invariant. Because the groups are identical, the operations of L also leave V_g and T_g for each group invariant when they are applied to it. We now show that the operations of L , when applied to all the functional groups in turn, also leaves V_c and hence V_{eff} invariant. Consider the term $\lambda_{ig,i'g'} q_{ig} q_{i'g'}$, where q_{ig} transforms by a non-degenerate irreducible representation of L . Then $q_{i'g'}$ transforms by the same irreducible representation and the product $q_{ig} q_{i'g'}$ is unchanged by the transformation. When the coordinate $q_{\alpha g}$ transforms by an irreducible representation of order greater than one

$$L q_{\alpha g} = \sum_{\beta} L_{\alpha\beta} q_{\beta g} \quad (12)$$

where the $L_{\alpha\beta}$ are the members of the irreducible representation, *i.e.*, of the matrix which is the repre-

(7) When this is not true, the vibrations fall into the category of the previous section.

(8) Since the functional groups are equivalent, the identification of them by g and g' in the subscript of λ is no longer relevant and hence is dropped.

(9) W. F. Edgell, Paper No. 16, Sixty-First Session, Iowa Academy of Science (Inorganic and Physical Chemistry Section), April 1949; see also W. F. Edgell and T. R. Reithof, *J. Phys. Chem.*, **56**, 326 (1952).

sentation. Such a coordinate enters V_c in (11) as part of the collection of terms

$$\lambda_{\alpha\alpha} \sum_{\alpha} Q_{\alpha\sigma} Q_{\alpha\sigma'}$$

Under an operation of L , considered applied in turn to all groups, the above terms become

$$\lambda_{\alpha\alpha} \sum_{\alpha} \sum_{\beta, \beta'} L_{\alpha\beta} L_{\alpha\beta'} Q_{\beta\sigma} Q_{\beta'\sigma'} = \lambda_{\alpha\alpha} \sum_{\beta, \beta'} Q_{\beta\sigma} Q_{\beta'\sigma'} \sum_{\alpha} L_{\alpha\beta} L_{\alpha\beta'} = \lambda_{\alpha\alpha} \sum_{\alpha} Q_{\alpha\sigma} Q_{\alpha\sigma'}$$

since the sum over α in the second line is the Kronecker $\delta_{\beta\beta'}$ and the sum of the coordinate product over β is the same as the sum over α . Hence these terms of V_c also are unchanged by an operation of L . Thus, any operation of L leaves V_c as well as each V_{σ} unchanged and hence leaves V_{eff} (and T_{eff}) invariant. The character of an operation of L should be emphasized. It is not an operation (like σ_v) which is applied to all the atoms of m . Instead it is an operation for m which consists of applying the same local operation at each of the functional groups of which m is composed.

There is symmetry in V_{eff} (and T_{eff}) associated with the permutation of the groups. Let I_k be an interchange operation which carries the functional group g to the group h . Its effect upon the coordinate q_{ig} is $I_k q_{ig} = q_{ih}$. This same operation carries the group g' to the group h' and $I_k q_{ig'} = q_{ih'}$. I_k specifies how each functional group of the moiety is moved. We see that the operation I_k transforms the collection of terms from V_c

$$\lambda_{ii} \sum_{g>g'} q_{ig} q_{ig'}$$

into

$$\lambda_{ii} \sum_{g>g'} (I_k q_{ig}) (I_k q_{ig'}) = \lambda_{ii} \sum_{h>h'} q_{ih} q_{ih'}$$

and we see that I_k leaves V_{eff} (and T_{eff}) unchanged. The interchange operations which leave V_{eff} (and T_{eff}) invariant for the moiety m form a group I .

The following properties of the operations of L and I are important.

1. All of the interchange operations of I which carry a given functional group into a specific second group also carry a given atom in the first group into the same atom of the second group. Thus each atom of a functional group finds one (and only one) atom in each of the other functional groups into which it is carried by the interchange operations. This condition is necessary to what follows and serves to define specifically what an interchange operation accomplishes.

2. An operation of the local group L carries atoms from one position to another within the same functional group; it never carries an atom from one functional group to one of another functional group. An operation of L always leaves V_{eff} (and T_{eff}) unchanged; it does not contain elements which change V_c and T_c while leaving V_{σ} and T_{σ} unchanged.

Note that the result of performing the operation I_k followed by L_j also does not change V_{eff} and T_{eff} . This pair of operations is designated by $L_j I_k$ in the standard manner. The operations L_j and I_k commute, i.e., $L_j I_k = I_k L_j$. This follows from the fact that the exchanges that result from the two kinds of symmetry present in the problem have been separated, the one into the operations of L and the other into those of I . As a result of these two properties the symmetry group G for this case is the direct product group

$$G = L \times I$$

These points may be illustrated by several examples. Consider two equivalent, coupled methyl groups at an angle to each other in a larger molecule such that a plane of reflection σ^i carries the atoms of one CH_3 group into those of the other. The operations of the interchange group are the unity operation $I_1 = E^i$ and the interchange $I_2 = \sigma^i$. These form a permutation group which is isomorphic to the point group C_s and which we designate by the symbol C_s^i . For the particular spatial arrangement of the methyl groups and what it implies, it is most probable that the effective energies would be invariant to the operations $L_1 = E^i$ and $L_2 = \sigma^i$ performed at each methyl group. L is also isomorphic to the point group C_s and it is given the symbol C_s^i . The symmetry group for the localized vibrations in such a case would be $G = C_s^i \times C_s^i$, which is isomorphic to the point group C_{2v} . Suppose, however, that the site of each methyl group did not destroy its inherent trigonal symmetry and that this was also maintained in the interaction between the groups. Then, the consequences of these conditions are found with $L = C_{3v}^i$ and $G = C_{3v}^i \times C_s^i$.¹⁰

As a second illustration consider three equivalent, coupled methyl groups in a larger molecule the atoms of which are transformed into each other by the operations of the point group C_{3v} applied to these atoms alone. It will further be supposed that the operations of C_{3v} are not necessarily the elements of the point group M of the molecule. The most natural site terms and coupling expected from such a conformation would lead to $L = C_s^i$, $I = C_{3v}^i$, and $G = C_s^i \times C_{3v}^i$. A word about the operations of C_{3v}^i is in order. The operations $I_1 = E^i$, $I_2 = C_3^i$, $I_3 = (C_3^i)^2$ are straightforward and move CH_3 groups in the same manner as the corresponding operations of C_{3v} . The operations σ_{v1}^i , σ_{v2}^i , and σ_{v3}^i are not like the operations σ_{v1} , σ_{v2} , and σ_{v3} of C_{3v} . The interchange operation σ_{v1}^i leaves all the atoms of methyl group 1 unchanged; it moves the atoms of methyl group 2 to those of methyl group 3 in the same way that C_3^i does; and it moves the atoms of methyl group 3 to those of methyl group 2 in the same

(10) Although this group is isomorphic to the point group D_{3h} , it does not have the transformation properties for M_x , α_{2z} , etc., listed in the standard tables for D_{3h} . The relevant transformation properties for such quantities are considered in a later section of this paper.

way that $(C_3^t)^2$ does. The operations σ_{o2}^t and σ_{o3}^t transport atoms in a similar manner, differing only in which functional group the atoms are unchanged.

Other conditions are possible for three methyl groups in this conformation. When the site terms do not destroy the trigonal character of the methyl groups and this is maintained by the coupling terms, the group theoretical consequences are obtained through $G = C_{3v}^t \times C_{3v}^t$.

Second Case. In this section, we again consider localized vibrations in a moiety consisting of several of the same functional groups which are coupled. However, the case is now considered where the environment of all the functional groups is not the same. Since each functional group is inherently the same, each localized frequency which would occur for it, in the absence of coupling would be nearly degenerate to the corresponding frequency from each of the other groups. The effective energies are written in the form

$$V_{\text{eff}} = \sum_{q,i} \lambda_{iq} q_{iq}^2 + 2 \sum_{q>q'} \sum_i \lambda_{iq, iq'} q_{iq} q_{iq'} \quad (13)$$

for the second case. The group theoretical consequences apply to those cases where the energies take the form of eq 13 either because terms are missing in V and T or they are small enough to make the perturbation treatment effective in this form.

The results are similar to those for the first case in that the consequences of the permutation symmetry for the modes localized in such a moiety are expressed in the group

$$G = L \times I$$

One recalls that the operations of L are restricted to those local operations which leave eq 13 invariant when applied at *each* functional group. What equivalence still remains between the functional groups in eq 13 is expressed in terms of a group I of interchange operations.

An illustration will be found in the case of three coupled methyl groups in the same conformation as the previous example. It will be supposed, however, that now the environment of these groups is such that only two of the three are equivalent. The most natural expectation for L is C_s^t and I is now C_s^t to give $G = C_s^t \times C_s^t$. Note that the operation σ^t does *nothing* to the odd CH_3 group while exchanging the two equivalent groups. The group theoretical consequences for the other possibilities for the three methyl groups which fall into this general category are to be obtained from $C_{3v}^t \times C_s^t$ and $C_1^t \times C_s^t$.

When none of the three methyl groups are equivalent, G may be $C_{3v}^t \times C_1^t$, $C_s^t \times C_1^t$, and $C_1^t \times C_1^t$ depending upon the form which eq 13 takes.

Third Case. Here the situation is considered where the coupling terms in eq 10 are too large to be treated by the perturbation procedure. Then eq 10 itself

must be used. It is invariant to the operations of the permutation group $G = C^m$, where C^m is some point group suggested by the part of the molecule relevant to the localized motions and the mechanism of coupling. C^m is almost always a subgroup of the direct product group $L \times I$ which would apply if eq 11 or 13 could be used. This means that while C^m itself is often not a direct product group, each of its operations are then expressible as an operation of L followed by one of I (or *vice versa*).

For the first illustration, consider the earlier case of two methyl groups. The geometry of these functional groups is expressed by C_{2v}^m , and if no other part of the larger molecule intrudes through the coupling mechanism, $G = C_{2v}^m$. This is the same group as $G = L \times I = C_s^t \times C_s^t$ and the group theoretical consequences are the same whether eq 10 or 11 is used, *i.e.*, whether the interaction terms are large or small.

We return to the case of the three equivalent, coupled methyl groups for the second example. When the coupling terms of eq 10 are too large to be treated by perturbation theory, a normal candidate for G is the group C_{3v}^m . This is a subgroup of $G = C_{3v}^t \times C_{3v}^t$ and $G = C_s^t \times C_{3v}^t$. The differences in the expectations between the former group and either of the two latter ones results from the differences in the effective kinetic and potential energies for the modes localized in this moiety. Which case occurs in nature for a specific molecule depends upon the nature of the interactions in that molecule.

Representations. In applying the results developed above, one will be concerned with how sets of coordinates, the set of dipole moment components, and the set of polarizability components transform under the operations of G . The matrix of the transformation of a set under an operation G_i is called the representation $\Gamma(G_i)$. The properties and uses of these quantities in vibrational theory are well known for the 32 point groups.² Some properties of the representations of the direct product group, which are of use to us, will be cited here briefly.

Every operation of the direct product group $G = L \times I$ is two-dimensional in nature. One part of it, the L_j , gives the prescription for how the atoms are to be transformed at a local functional group; the other part of it, the I_k , gives the prescription for how the atoms are to be moved from one functional group to another. Both levels of the bilevel operation are required to specify how the atoms at any group are transformed. Neither level does the work of the other. This is to be contrasted with the rotations, reflections, etc., of the point groups, where the operations are unilevel.

Consider now the effect of an operation $G_i = L_j I_k$ of the group $G = L \times I$ upon one of the sets above. The representation of G_i generated by the basis set is

$$\Gamma(G_i) = \Gamma(L_j) \times \Gamma(I_k) \quad (14)$$

The matrix $\Gamma(L_j)$ describes the transformation of that part of the basis set which belongs to a functional group (any one of the functional groups) under the operation L_j .¹¹ The matrix $\Gamma(I_k)$ describes the permutation of the functional groups—each functional group being considered a single abstract entity. It can be shown that whenever the representations of L_j and I_k are irreducible, the direct product matrix is an irreducible representation of G_i .¹² Thus

$$\Gamma^{(a)}(G_i) = \Gamma^{(b)}(L_j) \times \Gamma^{(c)}(I_k) \quad (15)$$

where a is the irreducible representation of G_i which arises from the b and c irreducible representations of L_j and I_k , respectively. The elements of the direct product matrix are given by the elements of the component matrices through

$$\Gamma^{(a)}(G_i)_{\alpha m, \alpha' m'} = \sum_{\alpha', m'} \Gamma^{(b)}(L_j)_{\alpha \alpha'} \Gamma^{(c)}(I_k)_{m m'} \quad (16)$$

It follows at once that the characters obey

$$\chi^{(a)}(G_i) = \chi^{(b)}(L_j) \chi^{(c)}(I_k) \quad (17)$$

and the orders of the three groups are related by $h(G) = h(L)h(I)$.

We proceed now to develop a useful way to write the standard decomposition formula for a reducible representation of G_i . In terms of the usual group theoretical meaning

$$\Gamma(G_i) = \sum_a n^{(a)} \Gamma^{(a)}(G_i) \quad (18)$$

with

$$n^{(a)} = \frac{1}{h(G)} \sum_i \chi(G_i) \chi^{(a)}(G_i) \quad (19)$$

Using eq 16 and the order relation, it is readily seen that

$$n^{(a)} = n^{(b)} n^{(c)} \quad (20)$$

with

$$n^{(b)} = \frac{1}{h(L)} \sum_j \chi(L_j) \chi^{(b)}(L_j) \quad (21)$$

$$n^{(c)} = \frac{1}{h(I)} \sum_k \chi(I_k) \chi^{(c)}(I_k)$$

It will be convenient to introduce the symbol $S^{(c)}$ for $\Gamma^{(c)}(I_k)$, where $S^{(c)}$ stands for the usual letter designation (A' , B_{2u} , etc.) of the irreducible representations, and $s^{(b)}$ for $\Gamma^{(b)}(L_j)$, where $s^{(b)}$ stands for the usual letter designations (a' , b_{2u} , etc.), the lower case being used to distinguish the local from the interchange representations. Expression 18 can be written through eq 14 with

$$\Gamma(L_j) = \sum_b n^{(b)} s^{(b)}$$

$$\Gamma(I_k) = \sum_c n^{(c)} S^{(c)} \quad (22)$$

to give

$$\Gamma(G_i) = \sum_{b,c} n^{(a)} s^{(b)} S^{(c)} \quad (23)$$

Here $s^{(b)} S^{(c)}$ stands for $\Gamma^{(b)}(L_j) \times \Gamma^{(c)}(I_k)$. The use of the symbol $s^{(b)} S^{(c)}$ for the a th irreducible representation of G has the advantage that it exposes at once both its local and interchange symmetry behavior. Further, it is more convenient to form eq 23 from 22 through the use of (14) than to work through the properties of the group G .

Distribution of Frequencies among Symmetry Types and Frequency Degeneracy. When the group G is isomorphic to a standard point group, the distribution of frequencies among the symmetry types is accomplished by well-known methods.² It often happens that there are several equivalent moieties present in the molecule. Then, this part of the frequency spectrum looks just like that of the single moiety but the degeneracy of each frequency is now that of the frequency for the single moiety multiplied by the number of the equivalent moieties.

Now consider the moiety which consists of several functional groups where the G is isomorphic to a standard point group. Every operation of G which does not move a particular functional group to another is also a symmetry operation for that functional group. The character of the localized vibrations (in G) for the operation G_i is given by

$$\chi(G_i) = n_o \sum_{\gamma} n^{(\gamma)} \chi^{(\gamma)}(G_i) \quad (24)$$

where $\chi^{(\gamma)}(G_i)$ is the character of the operation G_i for the γ irreducible representation of the local group, $n^{(\gamma)}$ is the number of localized vibrations of symmetry type γ which occur in one functional group, and n_o is the number of functional groups of the moiety which are not moved by G_i . The standard reduction formula for a reducible representation gives the frequency distribution. As an example, consider the CH_3 stretching frequencies of the three equivalent, coupled methyl groups of the earlier illustration where G was C_{3v}^m . Suppose further that V_o and T_o for each methyl group is invariant to the operations of C_{3v}^l . There are two symmetry operations of C_{3v}^m which are also symmetry operations of C_{3v}^l , namely E^m and σ_v^m . There is one CH_3 stretching frequency of local symmetry type a_1 and one of type e in the vibration of a single CH_3 group. Therefore, $n^{(a_1)} = n^{(e)} = 1$, $\chi^{(a_1)}(E^m) = \chi^{(a_1)}(\sigma_v^m) = 1$, $\chi^{(e)}(E^m) = 2$, $\chi^{(e)}(\sigma_v^m) = 0$ and with n_o being 3 and 1 for E^m and σ_v^m , respectively, one obtains $\chi(E^m) = 9$ and $\chi(\sigma_v^m) = 1$. Reduction on C_{3v}^m shows the distribution: $2A_1 + A_2 + 3E$.

(11) More properly, it describes the transformation in the abstract functional group which represents all the functional groups in the moiety.

(12) M. Tinkham, "Group Theory and Quantum Mechanics," McGraw-Hill, New York, N. Y., 1964, Chapter 3.

This procedure is also useful for correlation purposes to relate vibrations in G with those in the local functional group. In such a usage eq 24 reduces to $\chi(G_i) = n_p \chi^{(\nu)}(G_i)$.

Let us now take up the case where $G = L \times I$. The best way to compute the frequency distribution expected in the spectrum for such a case is with eq 23 as outlined in the previous section. The quantities $n^{(b)}$ and $n^{(c)}$ for use in eq 22 are calculated with eq 21. The character $\chi(I_k)$ is simply the number of functional groups unremoved by the interchange operation I_k . The problem of obtaining the $\chi(L_j)$ is just the standard problem of obtaining² the character of the vibrations of a small molecule—in this case the functional group. To illustrate the procedure, consider the case of the three equivalent, coupled methyl groups where $G = C_{3v}^i \times C_{3v}^i$. The character tables for the relevant groups are given in Table I.

Table I

C_i	L			I		
	E^i	σ	C_{3v}^i	E^i	$2C_3$	$3\sigma_v^i$
a'	1	1	A_1	1	1	1
a''	1	-1	A_2	1	1	-1
$\nu(\text{CH}_3)$	3	1	E	2	-1	0
$\delta(\text{CH}_3)$	3	1	$3(\text{CH}_3)$	3	0	1
$r(\text{CH}_3)$	2	0				
$t(\text{CH}_3)$	1	-1				

The upper portion of each table gives the character of the irreducible representations of L and I . Since these permutation groups are isomorphic to point groups, these characters are obtainable from the standard point group tables. The characters in the lower portion of the tables are those of the reducible representations needed to compute the frequency distribution for each type of CH_3 vibration. The line labeled $\nu(\text{CH}_3)$ in the table for L gives the character of the representation whose basis is the three CH stretching coordinates of the methyl group and, as is well known,² this is simply the number of these coordinates unchanged by the operation. The characters for the deformation (δ), rocking (r), and torsion (t) vibrations of the methyl group are also listed. The characters in the table for the interchange group I are just those for the appropriate permutation group of three objects—namely the methyl groups. The numbers entered in the last line of I are obtained in the following way. The three methyl groups form the basis of a reducible representation of the operations of this group, and, as pointed out above, these characters are simply the number of methyl groups not shifted by the interchange operation.

The computation of the frequency distribution will be illustrated for the stretching vibrations of the

methyl group. Reduction of $\nu(\text{CH}_3)$ on L by eq 21 gives the distribution formula (eq 22)

$$\Gamma(L) = 2a' + a''$$

and reduction of the representation for the collection of three methyl groups on the interchange group I by eq 21 gives the distribution formula (eq 22)

$$\Gamma(I) = A_1 + E$$

The distribution of the stretching vibrations of the three methyl groups over the different symmetry types of vibration for the group $G = L \times I$ is given by eq 18. Combining the above two component distribution expressions by eq 14 gives the stretching vibration distribution for the group G in its most useful form (eq 23)

$$\begin{aligned} \Gamma(G) &= (2a' + a'')(A_1 + E) \\ &= 2a'A_1 + 2a'E + a''A_1 + a''E \end{aligned}$$

There are two different frequencies of the $a'A_1$ type, two different frequencies of the $a'E$ type, one of the $a''A_1$ type, and one of the $a''E$ type. A vibration of the $a'A_1$ type is symmetrical to reflection through the plane at each functional group (from a') and is symmetrical to all interchanges of the methyl groups (from A_1); a vibration of type $a''A_1$ changes sign upon reflection thru the plane at each methyl group (from a'') and is symmetrical to all interchanges of the groups (from A_1), etc. Thus we see that the distribution expression in this form, *i.e.*, in the form of eq 23, exposes clearly both the symmetry of the vibration at the local functional group level and its symmetry under interchange of the functional groups—a natural way of describing the vibration.

In the same way, $\Gamma(G)$ can be obtained for each of the other kinds of vibrations of the methyl groups with the results

$$\delta(\text{CH}_3): 2a'A_1 + 2a'E + a''A_1 + a''E$$

$$r(\text{CH}_3): a'A_1 + a'E + a''A_1 + a''E$$

$$t(\text{CH}_3): a''A_1 + a''E$$

Equation 15 shows that the dimension of the a irreducible representation of G formed from the b and c irreducible representations of L and I is just the product of the dimension of b and c . Since the dimension of an irreducible representation is just the degeneracy of a vibrational frequency of that symmetry type, one obtains

$$d^{(a)} = d^{(b)}d^{(c)} \quad (25)$$

It follows from this equation that the degeneracies of the frequencies of type $a'A_1$, $a''A_1$, $a'E$, and $a''E$ are 1, 1, 2, and 2, respectively.

Normal Coordinates and Atomic Displacements. The purpose of this section is to point out the necessary rela-

tions which exist between G , on the one hand, and the form of the normal coordinates and the atom displacements, on the other. Since a G is uniquely associated with a V_{eff} and T_{eff} , these are relations between the form which the coordinates and the displacements take and the form which V_{eff} and T_{eff} has. Let us start by considering a moiety made up of several equivalent, coupled groups, and further, let q_{ig} be the i th "normal coordinate" of the g th set which reduces V_g and T_g to diagonal form. The displacement vector for the n th atom moved by the coordinates of this functional group is

$$q_{ng} = \sum_i \tau_{ng,i} q_{ig} \quad (26)$$

where $\tau_{ng,i}$ is the displacement of the n th atom in the g th set when $q_{ig} = 1$ and all other coordinates, both in this and the other sets are zero.¹³

Consider now the case where $G = L \times I$. It can be shown that the normal coordinates for this case can be written as

$$Q_{m\alpha} = \sum_g U_{mg} q_{\alpha g} \quad (27)$$

where the $q_{\alpha g}$ govern the displacements through the relation

$$q_{ng} = \sum_{\alpha} \tau_{ng,\alpha} q_{\alpha g} \quad (28)$$

The coordinate $q_{\alpha g}$ is the α th coordinate associated with the g th functional group. The $q_{\alpha g}$ specify the displacements of the atoms of the g th functional group, and the displacements for each functional group are combined, in and out-of-phase, through the relationship of eq 27, to form the displacements in the fundamental mode of vibration. Note that the $q_{\alpha g}$ determine the displacement of the atoms of the g th functional group only. This combining of certain basic displacements in each functional group to give the displacements of the fundamental is a consequence of the fact that G is a direct product group.

Of course, these coordinates show symmetry properties. The $q_{\alpha g}$ for a single functional group form the basis of a completely reduced representation of L . This means that each operation of L converts $q_{\alpha g}$ into a combination of the $q_{\alpha g}$ of the same group as given by eq 12, where the $L_{\alpha\beta}$ are the elements of the irreducible representations of L . The $Q_{m\alpha}$ form the basis of a completely reduced representation of the group I . The effect of an operation of I upon $Q_{m\alpha}$ is given by

$$IQ_{m\alpha} = \sum_{m'} I_{mm'} Q_{m'\alpha} \quad (29)$$

where the $I_{mm'}$ are the elements of the irreducible representations of I . The effect of the terms in V_c is to mix the q_{ig} as follows

$$q_{\alpha g} = \sum_i B_{\alpha i} q_{ig} \quad (30)$$

Each q_{ig} transforms as an irreducible representation of L .¹⁴ Only those q_{ig} which transform by the same row of the same irreducible representation as does $q_{\alpha g}$ are mixed by (30).

The converse of the proposition of this paragraph is also true. That is, if each normal coordinate can be written as a linear combination over the functional groups (eq 27) of coordinates $q_{\alpha g}$, each of which speaks *only* of the displacements of atoms in its functional group (eq 28), it is required that $G = L \times I$ and V_{eff} and T_{eff} take the form of eq 11.

Note the form of eq 27. The coefficients U_{mg} are governed by the interchange group I , and these coefficients do not depend explicitly upon α . Of course, normal coordinates of the m th symmetry type under I cannot be formed from some of the α because they have the wrong symmetry type under L . Which m and α can go together is specified by the distribution expression, eq 23.

The above considerations provide the recipe for forming symmetry coordinates. Let R_{mi} be the symmetry coordinate for G of type $s^{(b)}S^{(m)}$ which is formed from the i th local coordinate for each functional group, *i.e.*, from the r_{ig} . The coordinate r_{ig} is a symmetry coordinate under L of symmetry type "b" for the g th functional group. Then, in analogy with eq 27, one writes

$$R_{mi} = \sum_g U_{mg} r_{ig} \quad (27')$$

where the U_{mg} are determined by the normalizing condition and the fact that R_{mi} transforms under an operation I of the interchange group by

$$IR_{mi} = \sum_{m'} I_{mm'} R_{m'i} \quad (29')$$

In using eq 29' to determine the U_{mg} , note that r_{ig} transforms under the operation I as $Ir_{ig} = r_{ih}$ where h is the functional group into which the g th functional group is carried by I . The formation of the r_{ig} from the internal coordinates of the functional group follows the standard methods.² We take as an illustration the formation of symmetry coordinates from the CH stretching coordinates t for the three coupled methyl groups in the case where $G = C_s^t \times C_{3v}^i$. Let t_{11}, t_{21}, t_{31} , be the three CH coordinates for methyl group 1, t_{12}, t_{22}, t_{32} the coordinates for methyl group 2, and t_{13}, t_{23}, t_{33} the coordinates for methyl group 3. The coordinate associated with the unique CH in each methyl group is t_{11}, t_{12} , and t_{13} . These coordinates may be combined in the usual manner to give the symmetry coordinates under L at each methyl group. The result is

(13) The coordinates q_{ig} and q_{ig}' will sometimes move several atoms in common (by small amounts). These atoms "link" the functional groups together and are common to each of the sets.

(14) If L is not the same as the group which leaves V_g and T_g invariant, it is a subgroup of that group. As a result, it is always possible to choose the q_{ig} so that they reduce L as well as the group for V_g and T_g .

a'

$$\begin{aligned} r_{11} &= t_{11} & r_{12} &= t_{12} \\ r_{21} &= (t_{21} + t_{31})/2^{1/2} & r_{22} &= (t_{22} + t_{32})/2^{1/2} \\ & & r_{13} &= t_{13} \\ & & r_{23} &= (t_{23} + t_{33})/2^{1/2} \end{aligned}$$

 a''

$$\begin{aligned} r_{31} &= (t_{21} - t_{31})/2^{1/2} & r_{32} &= (t_{22} - t_{32})/2^{1/2} \\ & & r_{33} &= (t_{23} - t_{33})/2^{1/2} \end{aligned}$$

and the symmetry coordinates for G are readily formed. Thus

 $a'A_1$

$$\begin{aligned} R_{11} &= (r_{11} + r_{12} + r_{13})/3^{1/2} \\ R_{12} &= (r_{21} + r_{22} + r_{23})/3^{1/2} \end{aligned}$$

 $a''A_1$

$$R_{23} = (r_{31} + r_{32} + r_{33})/3^{1/2}$$

 $a''E$

$$\begin{aligned} R_{33} &= (r_{32} - r_{33})/2^{1/2} \\ R_{33'} &= (2r_{31} - r_{32} - r_{33})/6^{1/2} \end{aligned}$$

In the computational practice of this laboratory, we most often form our symmetry coordinates under G from the "normal" coordinates for the functional groups, *i.e.*, from the $q_{i\sigma}$ of eq 26, rather than from the internal symmetry coordinates $r_{i\sigma}$. Equation 27' is used with $q_{i\sigma}$ in place of $r_{i\sigma}$. Thus the symmetry coordinates for the CH stretching vibrations in the case of the three coupled methyl groups are given by the R_{mi} given above in which each $r_{i\sigma}$ is replaced by the corresponding $q_{i\sigma}$. For example

$$R_{11} = (q_{11} + q_{12} + q_{13})/3^{1/2}$$

Here q_{12} is the symmetric (a_1) CH_3 stretching "normal" coordinate from the set which diagonalizes V_σ and T_σ from methyl group 2.

Let us now take up the case where $G = C^m$. Again, the normal coordinates can be written as

$$Q_{m\alpha} = \sum_g U_{m\sigma} q_{\alpha\sigma}^m \quad (31)$$

where m indexes the irreducible representation of C^m to which it belongs. The $q_{\alpha\sigma}^m$, in this case, depend upon the m as well as α and g . The atom displacement vectors are determined by $q_{\alpha\sigma}^m$ through the expression

$$\rho_{n\sigma} = \sum_m \sum_{\alpha m i n} \tau_{n\sigma, \alpha}^m \sum_{g'} U_{g m}^{-1} U_{m g'} q_{\alpha\sigma}^m \quad (32)$$

When a specific $q_{\alpha\sigma}^m$ is nonzero while all the others are zero, atoms in all functional groups move. This results from the fact that V_c and T_c mixes the $q_{i\sigma}$ in a different way for each irreducible representation of C^m , *i.e.*

$$q_{\alpha\sigma}^m = \sum_{i m i n} B_{\alpha i}^m q_{i\sigma} \quad (33)$$

The converse of the proposition of this paragraph is also true. If the atom motions in the vibrations are governed by eq 31 and 32, then the best G is C^m and eq 10 must be used for V_{eff} and T_{eff} instead of (11).

Of course, the same considerations apply if not all the coupled groups are equivalent. Whenever $G = C^m$, either for the moiety with a single functional group or when it is more complex, the standard results² for normal coordinates apply.

Factoring the Secular Equation. When localization occurs, certain terms drop out of the potential and the kinetic energies. In computing the frequencies of vibration in such a case, one has two choices: to work directly with the truncated T and V matrices or to calculate a reduced G matrix from the elements of the full G matrix for use with the truncated V . The former is simpler, especially in this day of digital computers, and this is the form our frequency and force constant calculations have taken for some time. If one chooses a set of coordinates R_i appropriate for the description of the modes of vibration, the displacement of the n th atom may be written

$$\rho_n = \sum_i \tau_{ni} R_i$$

The elements of the matrix for twice the kinetic energy are

$$T_{ij} = \sum_n m_n \tau_{ni} \cdot \tau_{nj} \quad (34)$$

The potential energy is expressed in terms of internal coordinates as

$$2V = \sum_{q,r} k_{qr} r_q r_r$$

The elements of the matrix for twice the potential energy in terms of the R_i coordinates are

$$V_{ij} = \sum_{q,r} k_{qr} r_q r_r \quad (35)$$

where the r_{qi} are given by

$$r_{qi} = \sum_n s_{qn} \cdot \tau_{ni}$$

and the s_{qn} are the "s" vectors introduced by Wilson.² In our computer program the (truncated) T and V matrices are reduced to diagonal form by an iterative procedure. If the starting k_{qr} do not reproduce the observed frequencies, the force constants can be corrected by an iterative procedure which may be constrained by weighted least-squares methods.

The T and V matrices for a localized mode calculation would look like

m	c	c'
c	l	
c'		

Here m is the block corresponding to the coordinates dealing with the vibratory motion localized in the moiety, l is the block for the vibratory motion which distorts the parts of the molecule by which the moiety is "linked" with the rest of the molecule, and c and c' are coupling blocks whose elements are small when localization occurs. How much of V and T is to be included in l depends upon the size of the coupling terms and the accuracy requirements for the calculation. The calculations for the modes localized in the moiety are made with the blocks m , l , and c , and only these need be computed. They are the V_{eff} and T_{eff} referred to elsewhere. Thus, the localized modes are factored.

Besides giving results for the localized modes, these calculations also yield "frequencies" and "normal" coordinates for the nonlocalized or l -type motions. While such "frequencies" are irrelevant, the coordinates give an accurate description of the small amount of distortion of the moiety which enters the framework vibrations and they are useful as starting coordinates for such calculations. If one is interested in the vibrations of the molecule not localized in the moiety, including the framework modes, one may compute them from the truncated parts of V and T corresponding to the lower right-hand part of the above diagram, *i.e.*, from



and as indicated, one should use the starting coordinates described above for the l block to obtain highest accuracy.

The factoring procedure just outlined neglects the elements of c' . These must be small or localization does not occur. If needed, their contribution may be added by perturbation methods. Of course, if all modes are needed and the molecule is relatively small, one may make the calculations with the full T and V .

Suppose now that there are several coupled, equivalent groups in the molecule. Blocks in T and V like that described above for a moiety can be made for each functional group. The linking units for a group are not to include the elements of another group but some parts of T and V may be common to the l block for each group. The diagonalization of the block made up of m , l , and c for a single group produces the $q_{i\theta}$ for the vibratory motions localized in that group. These same vibratory motions occur for each of the functional groups. The $q_{i\theta}$ for the localized motions of a group may include small motions of the linking atoms. Some of these atoms may be moved by the $q_{i\theta}$ of each group, and their total motion is then obtained by summing over all groups.

Using the $q_{i\theta}$ for the localized motions, V and T take the form



shown here for three localized vibratory motions in two coupled groups. Each diagonal block corresponds to each group (V_θ , T_θ) and is itself a diagonal submatrix. The coupling terms in the c block (V_c , T_c) take the form

$$\begin{aligned} T_{i\theta, i'\theta'} &= \sum_n m_n \tau_{n\theta, i} \tau_{n\theta', i'} \\ V_{i\theta, i'\theta'} &= \sum_{q, r} k_{qr} r_{q, i\theta} r_{r, i'\theta'} \end{aligned} \quad (36)$$

The V_{eff} and T_{eff} referred to elsewhere are obtained by truncating V and T to the terms shown in the above diagrams. Diagonalization of V_{eff} and T_{eff} gives the frequencies and modes for the coupled system. It often occurs in practice that the group motions divide into types (*e.g.*, stretching and deformation) which are well separated in frequency. When this happens, the blocking of the T and V matrices may be made separately for each of such types of group motion. Note that the nature of the coupling (and hence G) may be different for each type of motion.

Eigenfunctions. The eigenfunction for a localized mode of vibration takes the usual form

$$\begin{aligned} \phi_v &= N_v \exp(-z^2/2) H_v(z) \\ z &= \omega Q / h^{1/2} \end{aligned} \quad (37)$$

where N_v is the normalizing constant, H_v is the v th Hermite polynomial, Q is the normal coordinate, and ω is the circular frequency of vibration.² We cite the equation here for completeness and to note that for equivalent coupled functional groups to which eq 37 applies, to within the differences associated with the problems of convergence in the quantum mechanical perturbation theory, eq 37 is the same as the eigenfunction arrived at by considering the coupling as a quantum perturbation. This is interesting because it suggests that coupling between functional groups can be considered as a vibrational exciton interaction.

Selection Rules for Infrared Spectra. The eigenfunction ψ_v which defines the vibrational state of the molecule is given by the product of the ϕ which specify the state of excitation of each of the modes of vibration. The transition from the state whose function is $\psi_{v'}$ to the state whose function is ψ_v can occur if one or more of the integrals

$$(M_\alpha)_{v'v} = \int \psi_v M_\alpha \psi_{v'} d\tau \quad (\alpha = X, Y, Z) \quad (38)$$

are different from zero. Here α refers to the components of the dipole moment in a molecule-fixed axis system. We consider the excitation of modes localized in the moiety. For any kind of molecule, only that part of the M_α which arises from the deformation of the molecule during vibration contributes to the value

of the integrals of (38). In the same way, only that part of the M_α which comes from the molecular distortion arising in the modes localized in the moiety contribute to the intensity of such vibrations. Just as for T and V , the coordinates which do not take part in the localized modes are set to zero in the M_α for the evaluation of the intensities of these modes. As a result, the integration over the configuration space of the non-localized modes may be performed at once. The result can be written in the form of eq 38 if we understand the ψ_ν to consist of the ϕ for the modes localized in the moiety. Symmetry requires that certain of these integrals be zero.

Some preliminary considerations are in order. The eigenfunctions ψ_ν which correspond to a degenerate state can always be formed (by linear combination) in such a way that they form the basis of completely reduced representations of G . This is automatically true for ψ_ν of a nondegenerate state. A complication, however, arises for the M_α when $G = L \times I$. Some of the operations of such a G do not correspond to "proper" or "improper" rotations performed on the moiety atoms. These operations, while they change an M_α , do not convert it into a linear combination of the M_α and so the usual method of establishing selection rules cannot be used. However, a modification of it does establish useful rules.

In such a case, some of the operations of G do correspond to "proper" or "improper" rotations; they form a subgroup of G which will be designated by G_s . An operation of G_s converts M_α into a linear combination of all the M_α , and the axes may be oriented so that the M_α form the basis of completely reduced representations of G_s . The ψ_ν which transform as irreducible representations of G whose dimension is one also transform as irreducible representations of G_s of dimension one. The ψ_ν which form the basis of an irreducible representation of G whose dimension is greater than one also form the basis of a representation of this same operation in G_s , but this representation may be reducible in G_s . In that event, it is always possible to form new ψ_ν' by taking linear combinations of the degenerate ψ_ν such that the ψ_ν' are a basis of a completely reduced representation of the operation in G_s . This representation is, at the same time, an irreducible representation of the operation in G . Therefore, the ψ_ν' are eigenfunctions for the set of vibrational states degenerate to each other which reduce the representations on G and G_s , *simultaneously*. We shall assume below that the state eigenfunctions have been chosen to have this character.

Consider first a transition from the ground state ν'' to an excited state ν' . Let R be an operation in the G_s of G . Then

$$R\psi_{\nu''} = \psi_{\nu''}$$

$$RM_\alpha = \sum_{\beta} R_{\alpha\beta}^{(i)} M_\beta \quad (39)$$

$$R\psi_{\nu'\alpha'} = \sum_{\beta'} R_{\alpha'\beta'}^{(j)} \psi_{\nu'\beta'}$$

where $R_{\alpha\beta}^{(i)}$ and $R_{\alpha'\beta'}^{(j)}$ are the components of the i th and j th irreducible representations of the operation R on G_s . Such an operation will leave the integral of eq 38 unchanged. Thus

$$(M_\alpha)_{\nu'\alpha',\nu''} = \sum_{\beta,\beta'} (R_{\alpha\beta}^{(i)} R_{\alpha'\beta'}^{(j)}) \int \psi_{\nu'\beta'} M_\beta \psi_{\nu''} d\tau$$

but this is true of each of the operations in G_s , of which there are h_s in number. Consequently

$$(M_\alpha)_{\nu'\alpha',\nu''} = \sum_{\beta,\beta'} (h_s^{-1} \sum_{\text{in } G_s} R_{\alpha\beta}^{(i)} R_{\alpha'\beta'}^{(j)}) \int \psi_{\nu'\beta'} M_\beta \psi_{\nu''} d\tau$$

The sum in the parenthesis is zero, by the great orthogonality theorem, unless $i = j$, $\alpha = \alpha'$, and $\beta = \beta'$.

This means that the transition from the ground state to the ν' states defined above is forbidden in the infrared spectrum unless some eigenfunction $\psi_{\nu'\alpha}$ transforms by the same row of the same irreducible representation in G_s as a component M_α of the dipole moment.

The transition ν'' to ν' between any two such states is forbidden in the infrared spectrum unless the species in G_s of one or more components M_α is found among the species in G_s of $\Gamma^{(j)} \times \Gamma^{(k)}$, where $\Gamma^{(j)}$ and $\Gamma^{(k)}$ refer to the species in G_s of the eigenfunctions corresponding to ν' and ν'' , respectively.

These rules can be extended to apply to all kinds of moieties by including the cases where $G = G_s$.

The above rules are reasonably definitive unless the subgroup G_s contains substantially fewer operations than G . However, there is another approach which does not suffer from such a debility and which has the additional advantage that it is particularly useful in a quantitative treatment of the intensities. The X component of the dipole moment is given by eq 40 where e_n is the effective charge on the n th atom whose X coordinate is X_n .²

$$M_x = \sum_n e_n X_n \quad (40)$$

This sum can also be achieved by summing over the atoms of the group g and over the groups to give¹⁵

$$M_x = \sum_g m_{gx} \quad m_{gx} = \sum_{\text{of } g} e_n X_n \quad (41)$$

The vector moment \mathbf{M} is

$$\mathbf{M} = \sum_\alpha \mathbf{u}_\alpha M_\alpha \quad (\alpha = X, Y, Z)$$

$$= \sum_g \mathbf{m}_g \quad (42)$$

(15) When the $q_{\alpha\sigma}$ of the several groups in the moiety move a linking atom in common, the e_n for that atom is divided equally among the groups. Although the above sum includes strictly all the groups (and framework pieces) of the molecule, only those groups which are part of the moiety contribute to the integrals below and (41) is considered limited to these in the expressions below.

While \mathbf{m}_g can be written with the molecule-fixed X , Y , and Z components as in eq 41, it is more useful to project upon x , y , z axes suitably fixed in each group. Then

$$\mathbf{m}_g = \sum_a \mathbf{a}_g m_{ga} \quad (43)$$

The orientation of the axis system in each group is chosen so that the m_{ga} reduces the group L of the local operations. The requirement that the integrals of (38) be nonzero is the same as requiring that the vector

$$\begin{aligned} (\mathbf{M})_{v'a',v''} &= \sum_\alpha \mathbf{u}_\alpha \int \psi_{v'a'} M_\alpha \psi_{v''} d\tau \\ &= \int \psi_{v'a'} \mathbf{M} \psi_{v''} d\tau \\ &= \sum_g \sum_a \mathbf{a}_g \int \psi_{v'a'} m_{ga} \psi_{v''} d\tau \end{aligned} \quad (44)$$

be nonzero.

Now consider a transition from the ground state v'' to an excited degenerate state $v'a'$ in which modes localized in the moiety are excited. The vector of (44) is unchanged when the operation $I_k L_j$ of the group $G = L \times I$ is applied to its components. The eigenfunction $\psi_{v'a'}$ transforms under L_j by an irreducible representation of L . Then

$$\begin{aligned} L_j \psi_{v''} &= \psi_{v''} \\ L_j m_{ga} &= \sum_b L_{ab}^{(g)} m_{gb} \\ L_j \psi_{v'a'} &= \sum_{b'} L_{a'b'}^{(r)} \psi_{v'b'} \end{aligned}$$

where $L_{ab}^{(g)}$ and $L_{a'b'}^{(r)}$ are the components of the g th and r th irreducible representations of L_j . With these

$$(\mathbf{M})_{v'a',v''} = \sum_g \sum_a \mathbf{a}_g \sum_{b,b'} L_{ab}^{(g)} L_{a'b'}^{(r)} \times \int (I_k \psi_{v'b'}) (I_k m_{gb}) (I_k \psi_{v''}) d\tau$$

but this same expression holds for each of the L_j operations in L , of which there are h_i . It follows that

$$(\mathbf{M})_{v'a',v''} = \sum_g \sum_a \mathbf{a}_g \sum_{b,b'} \left(h_i^{-1} \sum_j L_{ab}^{(g)} L_{a'b'}^{(r)} \right) \times \int (I_k \psi_{v'b'}) (I_k m_{gb}) (I_k \psi_{v''}) d\tau$$

One can form an interchange dipole component by

$$M_{nb} = \sum_g U_{ng} m_{gb} \quad (45)$$

which transforms under I_k as does the normal coordinate

$$Q_{nb} = \sum_g U_{ng} q_{bg}$$

Since

$$I_k q_{bg} = q_{bh}; \quad I_k m_{gb} = m_{hb}$$

where the operation I_k takes the g th group into the h th group. Then

$$\begin{aligned} I_k \psi_{v''} &= \psi_{v''} \\ I_k \psi_{v'b'} &= \sum_{m'} I_{n'm'}^{(s)} \psi_{v'm'} \end{aligned}$$

$$I_k M_{nb} = \sum_m I_{nm}^{(t)} M_{mb}$$

where $I_{n'm'}^{(s)}$ and $I_{nm}^{(t)}$ are components of the s th and t th irreducible representations of I_k . The eigenfunction $\psi_{v'b'}$ also is part of the basis set which transforms as the $I^{(s)}$ irreducible representation of the operation I_k ; it transforms by the n' th row of $I^{(s)}$. With these our vector becomes

$$\begin{aligned} (\mathbf{M})_{v'a',v''} &= \sum_n \sum_g \sum_a U_{gn}^{-1} \mathbf{a}_g \sum_{b,b'} \sum_{m,m'} \left(h_i^{-1} \sum_j L_{ab}^{(g)} L_{a'b'}^{(r)} \right) \times \\ &\quad \left(h_i^{-1} \sum_k I_{n'm'}^{(s)} I_{nm}^{(t)} \right) \int \psi_{v'm'} M_{mb} \psi_{v''} d\tau \end{aligned} \quad (46)$$

when the sum is made over the h_i identical quantities from each of the operations of the interchange group I . This vector is zero unless $g = r$, $s = t$, and $a = a'$, $n = n'$, and $b = b'$, $m = m'$.

This means that a transition from the ground state to a state $\psi_{v'a'}$ in which only modes localized in the moiety are excited, and whose species in $s^{(a)} S^{(n)}$, is forbidden in the infrared spectrum unless the species $s^{(a)}$ is the same as the one of the components m_{ga} of the local dipole moment and provided this m_{ga} generates a nonzero interchange dipole moment M_{na} whose interchange species is the same as that for $\psi_{v'a'}$, namely $S^{(n)}$.

The transition between any two such states v'' and v' is forbidden in the infrared spectrum unless one of the species of $\Gamma^{(v'')} \times \Gamma^{(v')}$ such as $s^{(a)} S^{(n)}$ contains the same local symmetry species $s^{(a)}$ as one of the components of the local dipole moment m_{ga} and provided it generates a nonzero interchange dipole moment M_{na} of interchange symmetry species $S^{(n)}$.

It would be helpful to clarify what is meant by a nonzero interchange moment. If one substitutes m_{ga} obtained from the inverse of (45) into (42), one obtains for the dipole moment

$$\mathbf{M} = \sum_{na} \mathbf{D}_{na} M_{na} \quad (47)$$

$$\mathbf{D}_{na} = \sum_g U_{gn}^{-1} \mathbf{a}_g = \sum_g U_{ng} \mathbf{a}_g$$

since U is generally an orthogonal matrix. The intermoment M_{na} is said to be zero when the vector \mathbf{D}_{na} vanishes.

The above selection rules were obtained from transitions between states of the molecule which involve changes in excitation only of the modes localized in the moiety. The same results apply to transitions involving only changes in modes localized in the framework or in another moiety. But what of transitions between states involving changes in the excitation of two modes each of which is localized in a separate moiety, or in a moiety and in the framework? When there are two separate moieties in a molecule, the dipole moment can be written as

$$M = M_1 + M_2 + M_7 \quad (48)$$

where there are no atoms common to moieties 1 and 2 or the remnant.

It is a consequence of (48) that all transitions are forbidden in the infrared spectrum which involve a simultaneous change in the state of excitation of modes in two separate moieties as long as the effective charge of the atoms in one moiety does not depend upon the displacements of the atoms in the second—a condition not inconsistent with the assumption of localization.

The same statement can be made about transitions involving the simultaneous change in the state of excitation of framework and moiety modes. This depends upon the fact that framework modes involve the translation and/or rotation of the moiety and assumes that the effective charges of the atoms of the moiety do not change with displacement.

The first selection rule can be expected to be rather well followed in spectra except when the two moieties are quite close in space. The second rule is less well founded and will probably be breached more in practice. Further, these two rules are compromised when localization is not exact. Yet it follows that combination bands involving the simultaneous excitation of a localized and a nonlocalized mode for the moiety should be infrequent and weak.

Selection Rules for Raman Spectra. In obtaining selection rules for the Raman effect, it is useful to write the polarizability tensor $\hat{\alpha}$ in dyadic form rather than as a matrix.

$$\begin{aligned} \hat{\alpha} &= \mathbf{ii}\alpha_{XX} + (\mathbf{ij} + \mathbf{ji})\alpha_{XY} + \dots \\ &= \sum_a \hat{\mathbf{a}}\alpha_a \end{aligned}$$

but the components α_a of the tensor frequently do not transform as the irreducible representations of the group even for small molecules and it is necessary to form linear combinations of them to obtain this property. Forming such combinations

$$\alpha_m = \sum_a C_{ma}\alpha_a$$

one can write

$$\begin{aligned} \hat{\alpha} &= \sum_m \hat{\mathbf{c}}_m \alpha_m \\ \hat{\mathbf{c}}_m &= \sum_a \hat{\mathbf{a}} C_{am}^{-1} \end{aligned}$$

but the same complication enters here as with the dipole moment. Only the operations of $G = L \times I$ which form the subgroup G_s transform the α_m into linear combinations of the α_m .

It follows by the same procedure used for the infrared rules that the transition from the ground state to the state $\psi_{v'm}$ in which only modes localized in the moiety are excited is forbidden in the Raman spectra unless the species of $\psi_{v'm}$ in G_s is the same as that of one of the components α_m of the polarizability tensor.

The transition v'' to v' between any two such states is forbidden in the Raman spectra unless the species in G_s of one or more of the components α_m of the polarizability tensor is found among the species in G_s of $\Gamma^{(v'')} \times \Gamma^{(v')}$.

In analogy with the dipole moment one writes

$$\hat{\alpha} = \sum_g \hat{\mathbf{a}}_g \quad (49)$$

It is convenient to use an axis system oriented to the functional group in expressing $\hat{\mathbf{a}}_g$ and to form the linear combinations α_{mg} which transform by the irreducible representations of L . Forming the interchange polarizability components

$$A_{nm} = \sum_g U_{ng} \alpha_{mg}$$

which transform like the normal coordinate Q_{nm} under the operations of I , one has

$$\hat{\alpha} = \sum_{n,m} \hat{\mathbf{c}}_{nm} A_{nm} \quad (50)$$

and A_{nm} is said to be zero if $\hat{\mathbf{c}}_{nm}$ vanishes.

Then a transition from the ground state to a state $\psi_{v'm}$ in which only modes localized in the moiety are excited, and whose species is $s^{(m)}S^{(n)}$, is forbidden in the Raman spectrum unless the species $s^{(m)}$ is the same as one of the components α_{mg} of the local polarizability tensor and provided this component α_{mg} generates a nonzero interchange component A_{nm} of species $S^{(n)}$.

The same comments about simultaneous excitation of localized modes in separate moieties or in a moiety and the framework made above for the infrared spectrum also apply to the Raman effect.

The sum of the diagonal elements of the polarizability tensor is not changed by the operations of G and hence it transforms as the completely symmetric irreducible representation. Therefore, only the completely symmetric species of G can give rise to polarized Raman lines.

An Example

As an example of the application of the theory for the vibration of larger molecules outlined in the above sections, we consider the localized modes arising from three equivalent methyl groups in the spatial conformation cited above; *i.e.*, the atoms of the methyl groups are exchanged by the operations of the point group C_{3v} . The point group M of the molecule is irrelevant. It might be any one of the 32 point groups, and we shall suppose it to be $M = C_1$. The vibrational spectrum of these localized modes is not determined alone by the details of the spatial arrangement of these three groups but is fundamentally influenced by the nature of the interaction of the methyl groups with each other and with their environment in the molecule at hand—all of which is expressed by the V_{eff} and T_{eff} for these localized modes in the particular molecule of concern. We shall not try to cover all of the possibilities here but will con-

sider several of the more likely cases to be encountered in practice as well as those which illustrate interesting points.

First Case. In this section, let us consider a molecule in which the three methyl groups are far enough removed from one another, or otherwise "insulated," so that the vibratory motions in the methyl groups do not couple with each other. Further, we consider a molecule in which the environment of each methyl group in the molecule does not disturb its inherent trigonal character. Then, each methyl group is a moiety in the sense of the word used here and $G = C_{3v}^m$. The localized vibrations may be of type a_1 , a_2 , or e of C_{3v}^m . Since there are three identical methyl moieties in the molecule, the degeneracy of these three kinds of frequencies are 3, 3, and 6, respectively. The properties of modes of vibration of these types are summarized in Table II. The transformation properties of the components of the dipole moment and polarizability tensor for modes localized in a CH_3 moiety are obtainable from the well-known C_{3v} point group table and are listed in columns 3 and 4 of Table II. Here x , y , and z refer to components along the usual axis system for a CH_3 group. It follows from these two columns that only vibrations of type a_1 or e are active in the infrared or Raman spectra. The a_1 vibrations give rise to polarized Raman bands (see column 5). The frequency distribution is given in the last column. The symbols ν , δ , r , and t stand for stretching, angle deformation, rocking, and torsion motions in the CH_3 group. To illustrate the use of this table, note that there are two CH_3 stretching frequencies in the spectrum, one of a_1 type and one of e type. Both of these frequencies may appear in the Raman and in the infrared spectrum. The a_1 Raman band is polarized; the e band is depolarized. The former is threefold degenerate; the latter is sixfold degenerate.

Table II: $(\text{CH}_3)_3$

C_{3v}^m ^a	d	\mathbf{M}	$\hat{\alpha}$	ρ	Freqs
a_1	3	M_z	$\alpha_{zz}, (\alpha_{xx} + \alpha_{yy})$	p	ν, δ
a_2	3	t
e	6	(M_x, M_y)	$(\alpha_{xx} - \alpha_{yy}, \alpha_{xy})$ $(\alpha_{yz}, \alpha_{zx})$	d	ν, δ r

^a $m = \text{CH}_3$.

Second Case. In the last section, we considered the case where the effective potential energy was just V_n , the inherent potential energy for the methyl group. In this section, we take up the case where V_{eff} is made up of V_n plus V_s . We consider specifically the case where the site effect at each methyl group results in the force resisting the distortion of one CH being different from that for the other two, which are equal. No

coupling terms between the localized modes of the three CH_3 groups are present in V_{eff} and T_{eff} for this molecule. Here also each methyl group is a moiety and $G = C_s^m$. The localized vibrations are of symmetry type a' or a'' , for which the properties listed in Table III are readily obtained. Now we see that three stretching frequencies may appear in both the infrared and Raman spectra, each of which is threefold degenerate. Two of the three Raman bands are polarized.

Table III: $(\text{CH}_3)_3$

C_s^m ^a	d	\mathbf{M}	$\hat{\alpha}$	ρ	Freqs
a'	3	M_x, M_z	$\alpha_{xx}, \alpha_{yy}, \alpha_{zz}, \alpha_{xy}$	p	$2\nu, 2\delta, r$
a''	3	M_y	α_{xy}, α_{yz}	d	ν, δ, t, r

^a $m = \text{CH}_3$.

Third Case. Let us turn now to a molecule in which motions of the three equivalent methyl groups are coupled. Consider specifically a molecule in which both site and coupling terms contribute such that $G = C_s^t \times C_{3v}^i$. We have seen above that the localized modes for this case may be of symmetry type $a'A_1, a''A_1, a'E$, or $a''E$ with degeneracies 1, 1, 2, and 2, respectively. All the operations of G do not correspond to exchanges of the atoms of these three functional groups which may be classified as "proper" or "improper" rotations. Let us see exactly how this arises in this case. To determine to which atom a particular atom of the moiety is carried by the operation $G_i = L_j I_k$, one performs the transport within the functional group prescribed by the operation L_j followed by that resulting from the transport of the functional group contained in the prescription I_k . The transport given by the prescription L_j and I_k is carried out for each atom of the moiety. The operations of G for this case are: $E^i E^i, E^i C_3^i, E^i (C_3^i)^2, E^i \sigma_{v1}^i, E^i \sigma_{v2}^i, E^i \sigma_{v3}^i, \sigma^i E^i, \sigma^i C_3^i, \sigma^i (C_3^i)^2, \sigma^i \sigma_{v1}^i, \sigma^i \sigma_{v2}^i, \sigma^i \sigma_{v3}^i$. The operation $E^i C_3^i$ accomplishes the same atom transport that is obtained by rotation by 120° about the threefold axis of the $(\text{CH}_3)_3$ moiety, and we can write $E^i C_3^i = C_3^m$. Thus $E^i C_3^i$ is a "proper" rotation. The operation $\sigma^i \sigma_{v1}^i$, when applied to an atom of methyl group 1, provides the transport within the functional group prescribed by σ^i and this is followed by the transport specified by the interchange operation σ_{v1}^i , which leaves atoms of this group alone. When $\sigma^i \sigma_{v1}^i$ is applied to an atom of methyl group 2, it provides the transport within methyl group 2 specified by σ^i . This is followed by the transport specified by the interchange operation σ_{v1}^i which carries the atoms of methyl group 2 to those of methyl group 3 in the same way that the atoms are moved between these two methyl groups by the interchange operation C_3^i . (See the discussion of L and I

Table IV: $(\text{CH}_3)_3^a$

$C_s^l \times C_{3v}^m$	d	M_n	A_{nm}	$\mathbf{M}(C_{3v}^m)$	$\hat{\alpha}(C_{3v}^m)$	ρ	Freqs
$a'A_1$	1	m_z, m_z	$\alpha_{zz}, \alpha_{yy}, \alpha_{zz}, \alpha_{zz}$	M_z	$\alpha_{zz}, \alpha_{zz} + \alpha_{yy}$	p	$2\nu, 2\delta, r$
$a''A_1$	1	ν, δ, r, t
$a'E$	2	m_x, m_x	$\alpha_{xx}, \alpha_{yy}, \alpha_{xx}, \alpha_{xx}$	M_x, M_y	$\left\{ \begin{array}{l} (\alpha_{xx} - \alpha_{yy}, \alpha_{xy}) \\ (\alpha_{yz}, \alpha_{zz}) \end{array} \right\}$	d	$2\nu, 2\delta, r$
$a''E$	2	m_y	α_{yz}, α_{yz}	M_x, M_y	$\left\{ \begin{array}{l} (\alpha_{xx} - \alpha_{yy}, \alpha_{xy}) \\ (\alpha_{yz}, \alpha_{zz}) \end{array} \right\}$	d	ν, δ, r, t

^a $G_s = C_{3v}^m$; $m = (\text{CH}_3)_3$.

operations above.) Applying $\sigma^l \sigma_{v1}^i$ to an atom of methyl group 3 accomplishes the transport within this methyl group specified by σ^l and is followed by the transport from methyl group 3 to methyl group 2 specified by σ_{v1}^i , *i.e.*, in the same way the atoms are moved by $(C_3^l)^2$. The transport of atoms accomplished by $\sigma^l \sigma_{v1}^i$ is seen to be the same as that obtained by reflection thru the "plane of symmetry" of the $(\text{CH}_3)_3$ moiety, *i.e.*, $\sigma^l \sigma_{v1}^i = \sigma_{v1}^m$. It is an "improper" rotation. Consider the operation $\sigma^l E^i$. It accomplishes the transport of atoms in methyl group 1 specified by σ^l , the transports in methyl group 2 specified by σ^l , and the transports at methyl group 3 specified by σ^l . This is neither a "proper" or an "improper" rotation. An examination of the operations of G will readily show that the subgroup consisting of the "proper" and "improper" rotations is $G_s = C_{3v}^m$, where the moiety m is $(\text{CH}_3)_3$. As pointed out in earlier sections, some selection rules in this kind of case may be obtained by finding the transformation properties of the components of the moiety dipole moment and moiety polarizability tensor under G_s . Using the correspondence between each symmetry type of G and one of G_s , one obtains the results listed in columns 5 and 6 in Table IV. All vibrations but those of symmetry type $a''A_1$ are allowed in both the infrared and Raman spectra. How good are these selection rules? Like all selection rules, the verbot is good but the allowed is not always found.

As outlined in earlier sections, selection rules can also be obtained by examining the transformation properties of the interchange dipole moment components and of the interchange polarizability tensor components, which are formed from the functional group contributions by eq 45 and 49. The formation of the interchange components is a straightforward matter. For example, the functional group dipole moment components $M_{\rho b}$ transform under the operations of L like symmetry types of this group. The $m_{\rho b}$ form the basis of a representation of the interchange group I . Reduction of this representation on I by standard methods gives the interchange components M_{nb} . Any of the methods of reduction well known for their use in forming symmetry coordinates may be used. The interchange polarizability tensor components can be formed the same way.

Some examples will be given. Following the subscript nomenclature of eq 43 and 45, the dipole moment components of methyl group 1 in the appropriate axis

system (x, y, z) of methyl group 1 are m_{1x} , m_{1y} , and m_{1z} , while polarizability tensor components include α_{xx1} , α_{yy1} , α_{zz1} , etc. Standard methods give

$$M_{nb}$$

$a'A$:

$$M_{1z} = (m_{1z} + m_{2z} + m_{3z})/3^{1/2}$$

$$M_{1x} = (m_{1x} + m_{2x} + m_{3x})/3^{1/2}$$

$a'E$:

$$M_{2z} = (m_{2z} - m_{3z})/2^{1/2}$$

$$M'_{2z} = (2m_{1z} - m_{2z} - m_{3z})/6^{1/2}$$

etc.

$$A_{nm}$$

$a'A$:

$$A_{1zz} = (\alpha_{zz1} + \alpha_{zz2} + \alpha_{zz3})/3^{1/2}$$

$$A_{2zz} = (\alpha_{zz1} + \alpha_{zz2} + \alpha_{zz3})/3^{1/2}$$

$a'E$:

$$A_{2zz} = (\alpha_{zz2} - \alpha_{zz3})/2^{1/2}$$

$$A'_{2zz} = (2\alpha_{zz1} - \alpha_{zz2} - \alpha_{zz3})/6^{1/2}$$

etc.

The fact that an interchange dipole moment component of symmetry $a'A_1$ can be formed from the m_z components of the three methyl groups, *i.e.*, M_{1z} , is indicated in the M_n column of Table IV by placing the symbol m_z in the $a'A_1$ row. The entries listed in the M_n and A_{nm} columns were obtained in this way.

One can also form the following linear combinations of symmetry type $a''A_1$

$$M_r = (m_{1z} + m_{2z} + m_{3z})/3^{1/2}$$

$$A_{r1} = (\alpha_{zv1} + \alpha_{zv2} + \alpha_{zv3})/3^{1/2}$$

$$A_{r2} = (\alpha_{zv1} + \alpha_{zv2} + \alpha_{zv3})/3^{1/2}$$

The first interchange component M_r appears in the expression for the dipole moment vector given by eq 47 as the scalar coefficient of the vector

$$\mathbf{D}_r = (\mathbf{j}_1 + \mathbf{j}_2 + \mathbf{j}_3)/3^{1/2}$$

The interchange components A_{r1} and A_{r2} appear in the expression for the polarizability dyadic given by eq 50 as the coefficients of the dyadics

$$\hat{\mathbf{c}}_{r1} = (\mathbf{i}_1\mathbf{j}_1 + \mathbf{j}_1\mathbf{i}_1 + \mathbf{i}_2\mathbf{j}_2 + \mathbf{j}_2\mathbf{i}_2 + \mathbf{i}_3\mathbf{j}_3 + \mathbf{j}_3\mathbf{i}_3)/3^{1/2}$$

$$\hat{\mathbf{c}}_{r2} = (\mathbf{j}_1\mathbf{k}_1 + \mathbf{k}_1\mathbf{j}_1 + \mathbf{j}_2\mathbf{k}_2 + \mathbf{k}_2\mathbf{j}_2 + \mathbf{j}_3\mathbf{k}_3 + \mathbf{k}_3\mathbf{j}_3)/3^{1/2}$$

Table V: $(\text{CH}_3)_3$

$C_{3v}^l \times C_{3v}^i$	d	M_n	A_{nm}	$M(C_{3v}^m)$	$\hat{\alpha}(C_{3v}^m)$	ρ	Freqs
$a_1 A_1$	1	m_z	$\alpha_{zz}, \alpha_{zz} + \alpha_{yy}$	M_Z	$\alpha_{zz}, \alpha_{zz} + \alpha_{yy}$	p	ν, δ
$a_2 A_1$	1	t
$A_1 E$	2	m_z	$\alpha_{zz}, \alpha_{zz} + \alpha_{yy}$	M_X, M_Y	$(\alpha_{zz} - \alpha_{yy}, \alpha_{zy})$ $(\alpha_{yz}, \alpha_{zz})$	d	ν, δ
$a_2 E$	2	M_X, M_Y	$(\alpha_{zz} - \alpha_{yy}, \alpha_{zy})$ $(\alpha_{yz}, \alpha_{zz})$...	t
$e A_1$	2	m_x, m_y	$\{(\alpha_{zz} - \alpha_{yy}, \alpha_{zy})\}$	M_Z	$\alpha_{zz}, \alpha_{zz} + \alpha_{yy}$	d	ν, δ, τ
$e E$	4	m_x, m_y	$\{(\alpha_{yz}, \alpha_{zz})\}$	M_X, M_Y	$(\alpha_{zz} - \alpha_{yy}, \alpha_{zy})$ $(\alpha_{yz}, \alpha_{zz})$	d	ν, δ, τ

^a $G_s = C_{3v}^m$; $m = (\text{CH}_3)_3$.

In these expressions, $\mathbf{i}_1, \mathbf{j}_1, \mathbf{k}_1$ are unit vectors in the $x, y,$ and z directions of the axis system fixed in methyl group 1; $\mathbf{i}_2, \mathbf{j}_2, \mathbf{k}_2$ are the unit vectors for methyl group 2. The z axis has been taken as the trigonal axis of the methyl group in each case. The x axis lies in the plane of symmetry of each methyl group, pointing away from the C_3 axis of the $(\text{CH}_3)_3$ moiety. The y axis is chosen to make each methyl group axis system right-handed. It is apparent by inspection that the vector \mathbf{D}_r is zero. While less obvious, the dyadics $\hat{\mathbf{c}}_{r1}$ and $\hat{\mathbf{c}}_{r2}$ are also zero, as can be shown by expressing the above vectors in a common axis system. The combinations $M_r, A_{r1},$ and A_{r2} are *redundant* interchange components since they contribute nothing to the dipole moment or polarizability dyadic. Only the nonzero interchange components have been entered in columns 3 and 4 of Table IV.

According to the selection rules derived in the above sections, a fundamental frequency of a given symmetry type may appear in the infrared spectrum when there is an interchange component M_{nb} of that symmetry type, *i.e.*, an entry in the M_n column for that symmetry type, and it may appear in the Raman spectrum when this is an entry in the A column for that symmetry type. It can be seen at once from Table IV that both methods of obtaining selection rules give the same results in this instance.

The frequency distribution of the methyl group modes in such a molecule was obtained in an earlier section and is collected in the last column of Table IV. It is seen that six stretching frequencies occur, five of

which are allowed in both infrared and Raman spectra. Two of these give polarized Raman bands (column 7).

Fourth Case. In this section, we consider the case where $G = C_{3v}^l \times C_{3v}^i$, which is interesting from a group theory point of view. It corresponds physically to the methyl group existing in a molecule where the site effects do not destroy the trigonal character of each CH_3 ($V_s = 0$) and coupling exists as required by this G . Then the expectations for the localized modes are contained in Table V.

Note the interesting point that selection rules under the subgroup $G_s = C_{3v}^m$ does not require the $a_2 E$ modes to be inactive in the infrared and Raman spectra. This is because C_{3v}^m anticipates mixing between all its E -type motions. However, $G = C_{3v}^l \times C_{3v}^i$ does not permit the $a_2 E$ -type motion to mix with the other motions of G which are also E under $G_s = C_{3v}^m$. The $a_2 E$ motions do not generate the dipole moment nor a polarizability change at the local level and hence these modes are inactive in the Raman and infrared spectra for this case.

Other Applications. The methods employed herein have application in other areas. For example, we have already applied them to vibrations in crystalline materials.

Acknowledgment. The work reported here has developed in stages in the course of projects supported by the National Science Foundation, the Advanced Research Projects Agency, and the Atomic Energy Commission. The author is grateful for the support of these agencies.

An *Ab Initio* LCAO-MO-SCF Study of the Phosphoryl Fluoride Molecule, OPF_3

by Ilyas Absar and John R. Van Wazer*

Department of Chemistry, Vanderbilt University, Nashville, Tennessee 37203 (Received December 31, 1970)

Publication costs borne completely by The Journal of Physical Chemistry

Ab initio LCAO-MO-SCF calculations have been carried out on the phosphoryl fluoride molecule, OPF_3 , using a Gaussian basis set consisting of eight s and four p atom-optimized exponents (with and without an added d exponent) to describe the phosphorus, with five s and two p atom-optimized exponents to describe the oxygen as well as each of the three fluorine atoms. In addition, a CNDO calculation has also been done for this molecule, and the resulting orbital energies have been compared to the *ab initio* values. The effect of allowing d character in this molecule is examined in detail. Three-dimensional electron-density plots are presented for the valence orbitals in a plane containing the phosphorus, the oxygen, and one of the fluorine atoms.

I. Introduction

The electronic structure of phosphoryl fluoride,¹ OPF_3 , is particularly interesting in that both the fluorine and oxygen atoms are highly electronegative with respect to the phosphorus and both have unshared pairs of electrons which may feed into the unoccupied d orbitals of the phosphorus so as to prevent unduly large charge differences between the phosphorus and either the oxygen or the fluorine atoms. A preliminary *ab initio* study² of p_π - d_π bonding in the hypothetical molecule phosphine oxide, OPH_3 , has shown that, upon adding phosphorus d atomic orbitals to the (sp) wave function, there is a clearly observable transfer of charge from the lone-pair region of the oxygen to the P-O bonding region. The main purpose of the study described herein is to discover whether or not a similar transfer occurs from the oxygen to the phosphorus as well as from the fluorine to the phosphorus when d character is allowed in the description of the phosphoryl fluoride molecule. It is also of interest to see whether or not p_π - d_π feedback is clearly recognizable in the Hartree-Fock representation of this molecule and whether it is confined to specific delocalized molecular orbitals for the P-O bond and for the P-F bond.

II. Computational Details

The *ab initio* LCAO-MO-SCF calculations using uncontracted Gaussian orbitals were carried out with the program MOSES,³ which is part of a package of computer programs for quantum-mechanical calculations put together in our group (primarily by Dr. J. H. Letcher and H. Marsmann). With the (841/52/52) basis set,⁴ which was the larger of the two used to describe the OPF_3 molecule, a linear combination of 70 atomic orbitals is employed to delineate the 25 filled molecular orbitals, thus necessitating the calculation of nearly 3×10^6 two-electron integrals and nearly 2×10^3 one-electron integrals.

When d orbitals are employed with the version of

MOSES we use, they are couched in terms of d_{z^2} , d_{y^2} , d_{x^2} , d_{xy} , d_{xz} , and d_{yz} . When these are converted to the usual spherical-harmonic representation involving five d orbitals, a 3s orbital which exhibits the same exponent as those used for the d's also results. This means that this 3s orbital should also be included in the atomic basis set when binding-energy calculations are carried out with the use of d functions.

The exponents for the phosphorus atom in the (84) Gaussian basis set were obtained in our laboratory from an atom-optimizing program⁵ and were found to be the following: 5941.5, 920.30, 221.51, 68.164, 23.685, 5.1733, 1.9202, and 0.2141 for the s type; and 48.818, 10.6798, 2.7458 and 0.2478 for the p type. In the calculation involving d character on the phosphorus, the d exponent was chosen to be 0.36 from the results of optimization in the phosphine⁶ and phosphine oxide² molecules. The energy for the phosphorus atom in the (84) basis set was found to be -340.0926 au, whereas addition of the 3s orbital having an exponent of 0.36 lowered this energy to -340.1000 au. The exponents and energies for the oxygen and fluorine atoms were taken from the literature.^{7,8}

(1) A brief report of a Slater minimum-basis set SCF study of this molecule has been given by I. H. Hillier and V. R. Saunders, *Chem. Comm.*, 1183 (1970).

(2) H. Marsmann, L. C. D. Groenweghe, L. J. Schaad, and J. R. Van Wazer, *J. Amer. Chem. Soc.*, **92**, 6107 (1970).

(3) L. M. Sachs and M. Geller, *Int. J. Quant. Chem.*, **15**, 445 (1967).

(4) The notation (*abc/ef/gh*) corresponds to the assignment a 1s, b 2p, c 3d atom-optimized Gaussian type orbital-exponents to the phosphorus, e 1s and f 2p to each of the three identical fluorine atoms, g 1s and h 2p to the oxygen atom. For the phosphorus atom alone, the notation is (*ab*), or (*abc*) when d orbitals are employed.

(5) B. Roos, C. Salez, A. Veillard, and E. Clementi, "A General Program for Calculation of Atomic SCF Orbitals by the Expansion Method," IBM Research Laboratory, San Jose, Calif.

(6) J.-B. Robert, H. Marsmann, L. J. Schaad, and J. R. Van Wazer, submitted for publication.

(7) D. R. Whitman and C. J. Hornback, *J. Chem. Phys.*, **51**, 398 (1969).

(8) C. J. Hornback, Ph.D. Thesis, Case Institute of Technology, Cleveland, Ohio, 1967.

The CNDO (complete neglect of differential overlap) program⁹ was obtained from the Quantum Chemistry Program Exchange. Planar electron-density maps were calculated by one program¹⁰ and these were converted to a three-dimensional representation by another.¹¹

In accord with the literature,¹² the C_{3v} geometry of the OPF_3 molecule was chosen to correspond to a P-O distance of 1.45 Å and a P-F distance of 1.52 Å, with the FPF angle equal to $102^\circ 30'$.

III. Results and Discussion

In a recent study¹³ of the polarizing effects¹⁴ of d orbitals, it was shown that the total energy of silane was lowered by only 0.032 au when two reasonably selected d exponents were added to a contracted (129/51) Gaussian basis set (to give a total energy close to the Hartree-Fock limit) as compared with a lowering of 0.095 au when a molecularly optimized d function was added to a Slater minimum-basis set. We interpret these findings in terms of the d function, which was added to the minimum Slater set, partially serving in the place of an s or p function badly needed to give a proper description of the molecule. In our study of phosphine oxide,² where a very small Gaussian basis set was employed to describe the phosphorus, the effect of adding a molecularly optimized d function to convert a (73/52/2) to a (731/52/2) basis set was contrasted to the effect of adding another atom-optimized p function on the phosphorus to give a (74/52/2) basis set. Although the energy lowering on adding the p orbital was 1.67 au, as compared with 0.20 au for adding the d, the larger change was seen to be due mainly to improving the description of the phosphorus inner orbitals (primarily the 1s and three 2p), whereas the d addition led to considerably larger changes in the energies and calculated electronic populations of the valence orbitals (particularly the outermost one). Because of the fact that the added p and d orbitals played such different roles in a very small, unbalanced basis-set description of phosphine oxide, we believe that interpretation of d-orbital participation given herein for a larger, better-balanced Gaussian basis set ought to lead to a reasonably meaningful picture.

The total energies calculated for phosphoryl fluoride in the (84/52/52) and (841/52/52) basis sets are presented in Table I along with the respective binding energies which have not been corrected for extra-correlation energy. The relatively large difference between the total energy in the two Gaussian basis sets reflects the fact that these basis sets are small and that (as will be shown later) the d character allowed to the phosphorus acts not only in polarizing¹⁴ the p orbitals but is also fundamentally involved in bonding.

The values of the uncorrected binding energies derived from the *ab initio* calculations exhibit the correct sign for a stable compound but are very small, much

Table I: Energies Calculated for Phosphoryl Fluoride, OPF_3

Energies	<i>ab initio</i> Gaussian		CNDO (with d)
	(82/52/52)	(821/52/52)	
Total, au	-710.0193	-710.5867	
Binding, ^a eV	-1.99	-1.25	-14.40
(experimental ^b 21.1 eV)			
Orbital, eV			
1a ₁ (P 1s)	-2185.9	-2182.5	
1e (F 1s) ^c	-720.3	-722.0	
2a ₁ (F 1s)	-720.3	-722.0	
3a ₁ (O 1s)	-560.5	-561.8	
4a ₁ (P 2s)	-213.9	-210.3	
5a ₁ (P 2p)	-155.0	-151.4	
2e (P 2p)	-155.0	-151.4	
6a ₁	-47.2	-46.9	-47.5
3e	-45.1	-43.7	-46.8
7a ₁	-36.9	-36.0	-39.7
8a ₁	-23.1	-23.1	-25.4
4e	-19.9	-20.0	-24.7
9a ₁	-18.6	-19.0	-24.6
5e	-16.6	-17.8	-23.5
6e	-16.0	-16.6	-21.6
1a ₂	-16.0	-16.0	-20.8
10a ₁	-13.0	-13.7	-18.4
7e	-11.3	-11.7	-18.4
11a ₁ (virtual)	+8.3	+9.7	-1.1

^a The value of the (uncorrected) binding energy was obtained by simply subtracting the sum of the calculated total energies of the constituent atoms from that of the molecule, using the same basis sets in the atomic and molecular calculations. ^b From $\Delta H^\circ = -476$ kcal/mol [D. D. Wagman, W. H. Evans, V. B. Parker, I. Halow, S. M. Bailey, R. H. Schum, *Nat. Bur. Stand. (U. S.) Tech. Note*, No. 270-3 (1968)] at 0°K for the formation of $\text{OPF}_3(\text{g})$ from the ground-state gaseous atoms, the binding energy was calculated using a correction of 9.1 kcal/mol for the zero-point energy [H. S. Gutowsky and A. D. Liehr, *J. Chem. Phys.*, **20**, 1652 (1952)]. ^c There is a degenerate pair of orbitals for each e symmetry.

smaller than the experimental value. This low value is probably attributable to the fact that there are three covalently bonded fluorine atoms in the molecule. For the NF_3 molecule,¹⁵ the uncorrected binding energy is positive, but this is converted to the appropriate value when the molecular extra-correlation energy¹⁶ is added.

(9) P. A. Dobosh, Program CNDO, Program 142 of the Quantum Chemistry Program Exchange, Chemistry Department, Room 204, Indiana University, Bloomington, Ind.

(10) W. E. Palke, an electron-density program modified by T. H. Dunning at the California Institute of Technology and later improved by H. Marsmann.

(11) D. L. Nelson, "Perspective Plotting of Two Dimensional Asays—PLOT3D," a computer program for a digital plotter, University of Maryland, Department of Physics and Astronomy, College Park, Md.

(12) Q. Williams, J. Sheridan, and W. Gordy, *J. Chem. Phys.*, **20**, 164 (1952).

(13) S. Rothenberg, R. H. Young, and H. F. Schaefer, *J. Amer. Chem. Soc.*, **92**, 3243 (1970).

(14) C. A. Coulson, *Nature*, **221**, 1106 (1969).

(15) M. L. Unland, J. H. Letcher, and J. R. Van Wazer, *J. Chem. Phys.*, **50**, 3214 (1969).

Even at the Hartree-Fock limit, the F_2 molecule is seen also to exhibit a positive binding energy, with stabilization of the molecule being closely accounted for by pair correlations.¹⁶ For the semiempirical CNDO calculations,¹⁷ the uncorrected binding energy is much larger than the values obtained from the *ab initio* computations. This difference must surely be attributable to the approximations involved in avoiding evaluation of the integrals rather than to differences between the basis sets used (a minimum Slater plus a single fivefold set of Slater d atomic orbitals on the phosphorus for the CNDO).

Inspection of the orbital energies shows that inclusion of the d atomic orbitals in the *ab initio* calculations has an appreciable effect on the inner-shell molecular orbitals, raising the energy of the orbital corresponding to the phosphorus "1s" by 3.4 eV while lowering the fluorine and oxygen "1s" orbital energies by 1.7 and 1.3 eV, respectively. Similarly, the energies of the phosphorus "2s" and "2p" electrons are each raised by 3.6 eV. We can interpret these results in terms of the idea developed in the study of photoelectron spectroscopy^{18,19} that, when electrons are withdrawn from a given atom, the inner-orbital binding energies increase (so that the respective orbital energies should decrease) by about the same amount for each of the inner-shell orbitals of that atom. Application of this rule to the calculated results given above indicates that, upon allowing d character to the phosphorus, the fluorine and oxygen atoms lose electrons and the phosphorus gains electrons. Note that the CNDO optimization does not involve the inner-shell orbitals.

For the valence-shell molecular orbitals, the *ab initio* calculations show essentially no change in the energies of the four orbitals $8a_1$, the $4e$ pair, and $1a_2$ upon allowing d character to the phosphorus. The valence orbitals having the higher energies (*i.e.* $10a_1$, $6e$, $5e$, and $9a_1$) are stabilized by allowing d character, whereas the other orbitals, except for the four which were not affected appreciably, are destabilized. The orbital energies calculated from the CNDO approximation are consistently large, with the difference between them and the comparable *ab initio* calculation in which a d orbital is involved [*i.e.*, the (841/52/52) basis set] being greatest for the orbitals of lesser stability. Indeed for the pair of $7e$ molecular orbitals (*i.e.*, those related to the first ionization energy of the molecule), the absolute numerical value obtained from the CNDO calculation is nearly twice as large as that from the *ab initio* computations. Another interesting result of this particular CNDO calculation is that the first virtual (*i.e.*, unfilled) orbital is computed to be slightly stable. These results again emphasize the fact that numerical values of energies of the valence-shell filled orbitals as well as those of the virtual orbitals are usually poor if they are based²⁰ on the CNDO approximation.

The calculated dipole moments and the atomic charges, obtained by subtracting the gross population for each atom (as obtained from a Mulliken population analysis²¹) from its atomic number, are shown in Table II. The dipole moment from the CNDO calculation

Table II: Calculated Dipole Moment and Atomic Changes for Phosphoryl Fluoride, OPF_3

Property	— <i>ab initio</i> Gaussian—		CNDO (with d)
	(82/52/52)	(841/52/52)	
Dipole moment, D (experimental 1.77 D)	2.05	2.00	2.29
Atomic Charges (Electrons)			
On P	+1.616	+0.628	+0.826
On O	-0.658	-0.344	-0.277
On each F	-0.320	-0.095	-0.183
Total Overlap Populations (Electrons)			
P-O	0.67	1.34	
P-F (per bond)	0.37	0.67	

was the farthest from the experimental value with the *ab initio* calculation including d atomic orbitals being the closest. In accord with the prediction made from the changes in inner-orbital energies, it is seen that, upon allowing d character, the calculated positive charge on the phosphorus atom is decreased by nearly a full electron whereas the negative charge on the oxygen and the fluorine is simultaneously decreased by nearly $1/3$ and $1/4$ of an electron, respectively. In all three calculations, it is clear that the oxygen is assigned a more negative charge than each of the fluorine atoms. Furthermore, the CNDO and (841/52/52) calculations, both of which realistically include d orbitals, are in agreement in assigning a formal charge of around +0.7 electron to the phosphorus atom and around -0.1 to -0.2 electron to each fluorine atom. Since fluorine is the most electronegative of all elements, the higher negative charge on oxygen as compared with fluorine in the phosphoryl fluoride molecule as calculated without phosphorus d character must be attributable to the

(16) C. Hollister and O. Sinanoglu, *J. Amer. Chem. Soc.*, **88**, 13 (1966). Also see G. Das and A. C. Wahl, *Phys. Rev. Lett.*, **24**, 440 (1970) for a related treatment.

(17) J. A. Pople, D. P. Santry, and G. A. Segal, *J. Chem. Phys.*, **43**, S129 (1965).

(18) K. Siegbahn, *et al.*, "ESCA—Atomic, Molecular and Solid State Structure Studied by Means of Electron Spectroscopy," Almqvist and Wiksels, Boktryckeri, Uppsala, 1967; also see "ESCA Applied to Free Molecules," North-Holland Publishing Co., Amsterdam, 1959.

(19) R. Nordberg, H. Brecht, R. G. Albridge, A. Fahlman, and J. R. Van Wazer, *Inorg. Chem.*, **9**, 2469 (1970).

(20) M. L. Unland, J. H. Letcher, I. Absar, and J. R. Van Wazer, *J. Chem. Soc. London*, in press.

(21) R. S. Mulliken, *J. Chem. Phys.*, **23**, 1833, 1841, 2338, 2343 (1955).

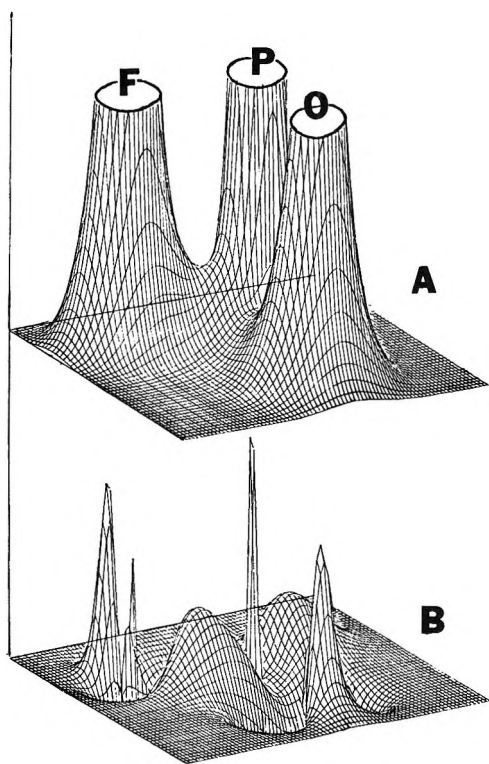


Figure 1. Electron-density maps for the plane passing through the oxygen, the phosphorus, and one of the fluorine atoms of phosphoryl fluoride, OPF_3 . The basal plane of these plots shows the molecular geometry in the F-P-O plane, with the electron density in this plane being shown vertically to this plane. (A) Total electron density for the (841/52/52) basis set and (B) an electron-density-difference map for the (841/52/52) minus the (84/52/52) basis set. The electron density (vertical scale) in (B) is magnified five times over that in (A).

dative (coordinate-covalent) bonding between the oxygen and the phosphorus. Furthermore, since the drop in negative charge due to allowing d character is large for the oxygen as well as for each of the fluorine atoms, electronic feedback from the unshared pairs to the bond with phosphorus is indicated for both fluorine and oxygen. This conclusion is supported by the approximate doubling of the substantial P-O and P-F overlap populations upon allowing d character to the phosphorus.

In Figure 1A, a relief map of the electron density of the phosphoryl fluoride molecule is shown for the plane passing through the phosphorus, the oxygen, and one of the three fluorine atoms. In the representations given in Figures 1 and 2, the electron density at any point on the plane is plotted perpendicular to that point. The unshared pairs of electrons around the fluorine and oxygen atoms are readily apparent in Figure 1A. This plot corresponds to the (841/52/52) basis set, and when d character is forbidden to the phosphorus [*i.e.*, for the (84/52/52) basis set], the resulting plot has the same general appearance. However, the relatively subtle differences in the electron density brought about by allowing d character to the phospho-

rus can be seen from a difference map such as the one shown as Figure 1B, in which the vertically plotted electron-density differences are magnified fivefold as compared to the electron densities of Figure 1A.

From Figure 1B, as well as from similar plots made for different viewing angles, it is apparent that addition of d character to the phosphorus causes a concentration of electronic charge in the neighborhood of each of the nuclei. In addition, a ring of charge is removed from around the oxygen and each of the fluorine atoms. These rings of charge deletion, the centers of which lie on the respective bond axis, represent the transfer of charge corresponding to unshared pairs on the oxygen and fluorine atoms to other parts of the molecule. These are predominantly the regions near the nuclei mentioned above, as well as a ring of increased charge around the phosphorus atom. This ring is a wobbly shaped (with a threefold axis) annulus, as indicated by the two mammilar humps on either side of the phosphorus atom in Figure 1B. Without question, the charge transfer from the oxygen to the phosphorus can be interpreted as p_π - d_π bonding. However, for the charge transfer from the fluorine to the phosphorus, the placement of the humps on either side of the phosphorus is such that it appears that some of the electrons taken from the fluorine lone-pair region by allowing d character on the phosphorus would have to be considered in terms of an increase in P-F σ as well as P-F π character. It should be noted that the terms σ and π used in this discussion refer to the charge-density maxima lying along the respective bond axis for the σ bond or on either side of the bond axis for the π bond. Of course, the usual precise mathematical definition of σ and π applies only to planar molecules.

A population analysis for the 16 valence-shell molecular orbitals is given in Table III. These values should be compared with the electron-density plots shown for these orbitals (with d character being allowed) in Figure 2. Most of these delocalized Hartree-Fock orbitals are dominated by one or two bonding functions as defined in the classical valence-bond sense. These dominant contributions are listed in the second column of Table II.

Note that the electronic populations of orbitals, $6a_1$, $7a_1$, $4e$, $6e$, and $1a_2$ are not greatly affected by allowing d character on the phosphorus. However, in the pair of $3e$ orbitals, there is some increase in the overlap of each P-F bond along with a transfer of a total of about 0.2 electron from the three fluorine atoms to the phosphorus. The most notable change in molecular orbital $8a_1$ upon allowing d character to the phosphorus is an increase in the overlap of each P-F bond from nothing to about 0.3 electron. For orbital $9a_1$, there is also a small increase in P-F overlap accompanied by a transfer of a small amount of charge from the fluorine to the phosphorus. Upon allowing d character to the phosphorus atom, the pair of $5e$ orbitals is

Table III: Electronic Populations²¹ of the Valence Orbitals^a

Orbital	Dominant contribution	Overlap population		Gross population		
		P-O	Each P-F	P	O	Each F
6a ₁	P-F σ	0.01 <i>0.01</i>	0.15 <i>0.16</i>	0.39 <i>0.45</i>	0.01 <i>0.01</i>	0.53 <i>0.51</i>
3e ^b	F lp, P-F σ	0.00 <i>0.00</i>	0.24 (0.24) ^c <i>0.16 (0.16)</i>	0.50 <i>0.34</i>	0.00 <i>0.00</i>	1.17 (1.17) <i>1.21 (1.21)</i>
7a ₁	P-O σ , O lp	0.59 <i>0.54</i>	0.00 <i>-0.01</i>	0.50 <i>0.44</i>	1.45 <i>1.49</i>	0.02 <i>0.02</i>
8a ₁	P-F σ , O lp	-0.01 <i>-0.04</i>	0.34 <i>0.00</i>	0.47 <i>0.53</i>	0.11 <i>0.12</i>	0.47 <i>0.45</i>
4e	P-F σ	-0.04 <i>-0.08</i>	0.15 (0.06) <i>0.12 (0.09)</i>	0.84 <i>0.96</i>	0.06 <i>0.12</i>	1.03 (0.69) <i>0.98 (0.33)</i>
9a ₁	P-F π , ^d F lp	-0.04 <i>-0.31</i>	0.10 <i>0.08</i>	0.35 <i>0.30</i>	0.17 <i>0.17</i>	0.49 <i>0.48</i>
5e	F lp, P-F σ	0.02 <i>0.00</i>	0.16 <i>0.00</i>	0.40 <i>0.00</i>	0.04 <i>0.02</i>	1.19 (0.65) <i>1.33 (0.70)</i>
6e	F lp	0.02 <i>0.00</i>	0.06 (0.05) <i>0.00 (-0.01)</i>	0.18 <i>0.00</i>	0.04 <i>0.00</i>	1.26 (1.01) <i>1.33 (1.08)</i>
1a ₂	F lp	0.00 <i>0.00</i>	0.00 <i>0.00</i>	0.00 <i>0.00</i>	0.00 <i>0.00</i>	0.67 <i>0.67</i>
10a ₁	O lp, F lp	0.05 <i>0.07</i>	-0.01 <i>-0.03</i>	0.20 <i>0.14</i>	1.44 <i>1.35</i>	0.12 <i>0.17</i>
7e	P-O π , O lp F lp	0.66 <i>0.34</i>	-0.05 (-0.04) <i>-0.11 (-0.09)</i>	0.56 <i>0.22</i>	3.00 <i>3.32</i>	0.14 (0.12) <i>0.15 (0.11)</i>

^a The values in regular type correspond to the (841/52/52) basis set, whereas the values in italics correspond to the (84/52/52) basis. Hence the italicized numbers give the respective numbers of electrons when d character is disallowed. ^b The charges in electron units shown for each set of e orbitals correspond to the sum of the constituent pairs of a₁ and a₂ orbitals. ^c Values are given in parentheses for the a₁ orbital of each e pair (when the charge is unequally distributed between the a₁ and a₂ orbitals) for the fluorine atom appearing in the electron-density plots of the figures. ^d See text for this usage of the " π " notation.

seen to evidence P-F overlap accompanied by an increase of the charge on the phosphorus from zero to about 0.4 electron, with this increase in charge having come from the three fluorine atoms. The same situation holds for the pair of 6e orbitals, but to a lesser extent. The effect on orbital 10a₁ is also small, corresponding to charge transfer from the fluorines to both the oxygen and the phosphorus. In the case of the pair of 7e orbitals, there is an appreciable increase in the P-O overlap accompanied by the transfer of about 0.3 electron from the oxygen to the phosphorus.

From inspection of the data given in Tables I and III as well as Figure 2, it is clear that P-O π bonding is associated with the orbital of least negative energy whereas the electronic feedback from the fluorine atoms to the phosphorus upon allowing d character to the latter shows up in orbitals which are considerably more stable (8a₁, 5e, and 3e). Likewise, as expected, the orbitals associated with the fluorine lone-pair character are somewhat more stable than those associated with the oxygen lone pair, with both of these being less stable than the orbital which accounts for much of the P-O σ bonding. Further, in spite of the fact that the P-F σ bonding is delocalized among a number of orbitals, this bond appears to involve more energy per bond than does the P-O σ bond.

From the geometries shown in Figure 2, only molecular orbital 9a₁ is seen to have at all the proper shape to

correspond to a P-F π bond. However, upon allowing d character to the phosphorus, there was only a small increase in the P-F overlap population for this orbital. The orbital (8a₁), which shows the greatest increase in P-F overlap on allowing d character to the phosphorus, clearly involves P-F σ bonding as can be seen from Figure 2. These results on the various individual orbitals are, of course, consistent with the overall electron-density-difference map of Figure 1B which shows that the ring of charge increase lying around the phosphorus atom appears to pretty much block the P-F bond axis.

In Figure 2, molecular orbitals 6a₁ and 3e in the case of the fluorine atom and orbitals 7a₁, 8a₁, and 9a₁ for the oxygen clearly exhibit a central spike of charge surrounded by a ring of charge. This observed charge geometry is clearly a distortion of the 2s atomic orbitals²² of these atoms. Likewise, the split electron-density maxima (8a₁, 4e, 9a₁, 5e, 6e, and 7e for the fluorine and 4e, 10a₁, and 7e for the oxygen) represent distortions of the 2p orbitals of these atoms.²² Figure 2 shows for the phosphorus central maxima surrounded by two more or less annular rings of charge (with the outer ring being very flat and diffuse) in orbitals 6a₁ and 8a₁. These represent distortions of the 3s atomic orbital of phosphorus.²⁰ Likewise, the split central

(22) W. T. Bordass and J. W. Linnett, *J. Chem. Educ.*, **47**, 672 (1970).

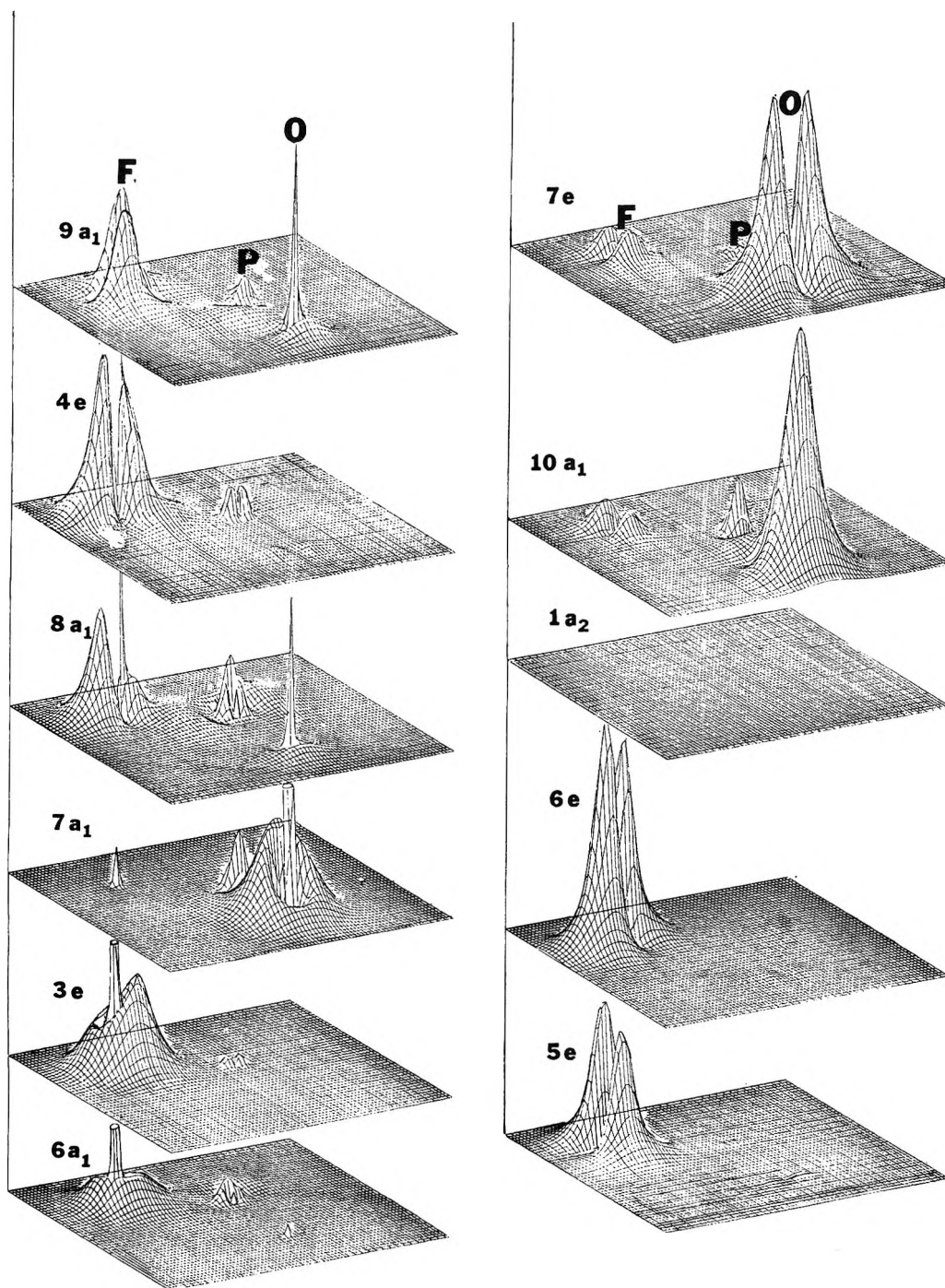


Figure 2. Electron-density maps of the valence orbitals of phosphoryl fluoride, OPF_3 , in the (841/52/52) basis set as observed in the plane determined by the oxygen, the phosphorus, and one of the fluorine atoms. The electron-density scale is the same as that used in part A of Figure 1.

hump surrounded on either side by flat diffuse humps, as seen in orbitals 3e, 7e, and particularly 4e are similar to a 3p phosphorus atomic orbital.²² As was pointed out in a previous paper,²³ electron-density plots, such as shown in Figure 2, clearly relate the shape of the molecular orbitals of the main contributing atomic orbitals of the respective atoms, and this occurs in even as complex a molecular structure as OPF_3 .

Acknowledgment. We wish to thank the National Science Foundation for support of this study, and Drs. J. H. Letcher, M. L. Unland, and H. Marsmann for some preliminary studies of phosphoryl fluoride in a localized description.

(23) J.-B. Robert, H. Marsmann, I. Absar, and J. R. Van Wazer, *J. Amer. Chem. Soc.*, in press.

Energy Transfer in Thermal Isocyanide Isomerization.

Noble Gases in the Ethyl Isocyanide System¹

by S. P. Pavlou and B. S. Rabinovitch*

Department of Chemistry, University of Washington, Seattle, Washington 98105 (Received November 12, 1970)

Publication costs assisted by the National Science Foundation

Relative collisional activation-deactivation efficiencies of added inert bath gases for the thermal unimolecular isomerization of ethyl isocyanide have been measured in the lower region of falloff just above the second-order regime at 231°. The effect of He, Ne, Ar, Kr, and Xe on the rate of isomerization was studied at 231° and at total pressures between 7×10^{-3} and 1×10^{-1} Torr; $\beta_0(\infty)$ increases monotonically from 0.27 to 0.44 with increase of atomic weight. The behavior of the experimental efficiencies as a function of the degree of falloff (reaction order) and of the dilution of substrate by bath gas is illustrated. Their relation to the predicted behavior given by calculations based on a stochastic model is discussed. The average energy $\langle \Delta E \rangle$ removed from the substrate by the bath molecules per down-transition was evaluated. The effect of structural and internal parameter changes of the substrate molecule on the process of intermolecular energy exchange is examined in the light of the data obtained in earlier work with the simpler CH_3NC homolog.

Introduction

Gas phase thermal unimolecular reactions, especially at low pressures, provide a simple and convenient technique for the study of some aspects of intermolecular energy transfer by molecules at high levels of vibrational excitation. In the second-order region the rate of reaction is the rate of activation by collision, and studies in this nonequilibrium region are uniquely advantageous.²⁻⁴

For reasons discussed previously,^{3,4} the detailed documentation of a specific reaction system and the systematic investigation of the parameters affecting the energy-transfer process is a desideratum for successful exploitation of this technique. The thermal unimolecular isomerization of isocyanides to nitriles was chosen to provide such a system.

To this time, the methyl isocyanide system has been studied in some detail. The behavior of a large number of bath gases has been investigated.^{3,4} The temperature dependence of the relative collisional efficiency of inert bath gas is also under investigation.⁵ Dilution effects⁶ and relative cross sections of inert gases⁷ have also been examined. In order to further our understanding of the nature of collisional transition probabilities, the experimental work on bath gas behavior is here extended to the next homolog, the thermal isomerization of $\text{C}_2\text{H}_5\text{NC}$ to $\text{C}_2\text{H}_5\text{CN}$. This substrate has been investigated previously in some detail by Maloney and Rabinovitch.⁸ It is one of the advantages of thermal unimolecular reaction systems that the magnitude of $\langle E^+ \rangle_0$ tends to follow classical statistical behavior and is only weakly dependent on substrate complexity.⁹ Thus the pragmatic operational test of bath molecule activation-deactivation efficiency is virtually invariant

for a homologous substrate series in which E_0 is also nearly invariant, as is the case for isocyanides.⁸ Thus the structure of the substrate molecule is significantly changed, but the low-pressure reaction parameters are scarcely altered (Table I); an internally consistent reaction series is obtained for a given deactivator, and the effects of the internal parameter changes, *i.e.*, vibration frequency pattern, internal rotation, low-frequency bending modes, and total number of vibrational modes, on the transition probabilities can be evaluated.

Our initial study in this system is of the effect of noble gases on the isomerization of $\text{C}_2\text{H}_5\text{NC}$. This paper presents a detailed description of the experimental relative collisional efficiencies and their behavior as a function of dilution and region of falloff.

Experimental Section

Materials. Ethyl isocyanide was prepared by Ma-

(1) (a) This work was supported by the National Science Foundation; (b) abstracted in part from the Ph.D. thesis of S. P. Pavlou, University of Washington, Seattle, Wash., 1970.

(2) M. Volpe and H. S. Johnston, *J. Amer. Chem. Soc.*, **78**, 3903 (1956).

(3) F. J. Fletcher, B. S. Rabinovitch, K. W. Watkins, and D. J. Locker, *J. Phys. Chem.*, **70**, 2823 (1966).

(4) S. C. Chan, B. S. Rabinovitch, J. T. Bryant, L. D. Spicer, T. Fujimoto, Y. N. Lin, and S. P. Pavlou, *ibid.*, **74**, 3160 (1970).

(5) S. C. Chan, J. T. Bryant, and B. S. Rabinovitch, *ibid.*, **74**, 2055 (1970).

(6) Y. N. Lin and B. S. Rabinovitch, *ibid.*, **72**, 1726 (1968).

(7) Y. N. Lin, S. C. Chan, and B. S. Rabinovitch, *ibid.*, **72**, 1932 (1968); S. C. Chan, J. T. Bryant, L. D. Spicer, and B. S. Rabinovitch, *ibid.*, **74**, 2058 (1970).

(8) K. M. Maloney and B. S. Rabinovitch, *ibid.*, **73**, 1652 (1969) (MR).

(9) D. W. Placzek, B. S. Rabinovitch, G. Z. Whitten, and E. Tschui-kow-Roux, *J. Chem. Phys.*, **43**, 4071 (1965).

Table I: Reaction Parameters for the CH_3NC and $\text{C}_2\text{H}_5\text{NC}$ Systems^a

	CH_3NC	$\text{C}_2\text{H}_5\text{NC}$
$A_\infty, \text{sec}^{-1}$	$10^{13.6}$	$10^{13.8}$
$E_0, \text{kcal mol}^{-1}$	37.9	37.6
$\langle E^+ \rangle_{p=0}, \text{kcal mol}^{-1}$	1.22	1.37
$\langle E^+ \rangle_{p=\infty}, \text{kcal mol}^{-1}$	2.49	4.50
n^a	4.6	6.1
s^b	3.3	4.5

^a Observed Slater n value. ^b Observed Kassel s value.

loney⁸ and was purified by gas chromatography. Analysis revealed no detectable impurities.

Helium, neon, argon, krypton, and xenon were assayed reagent grade gases from Air Reduction Co. These gases were used without further purification.

Apparatus and Procedure. Rate determinations were made in a static system. The reaction vessel was a 229-l. Pyrex sphere heated in a stirred air furnace. Pumping of the reaction vessel was by an 8-l. sec^{-1} Hughes VP-8R ion pump and a cryogenic molecular sieve sorption pump. After baking above 400° , a pumped-down pressure before each run at 231° of $<10^{-6}$ mm was obtained, as monitored by a cold cathode ion gauge and by a thermopile gauge which read down to 10^{-5} mm.

The furnace temperature was controlled by a proportional controller and was measured by using eight calibrated chromel-alumel thermocouples placed in good thermal contact with various points of the reaction vessel. During a run the temperature was constant to $\pm 0.3^\circ$; the agreement between all thermocouple readings was $\pm 0.2^\circ$. A standard temperature of 231° was used; occasionally, over the history of the work, the vessel temperature differed a little from that value.

Runs with seasoned and unseasoned vessels were performed and no difference in rate determinations was observed; seasoning between runs was therefore unnecessary except in cases where air had been admitted into the reactor. No detectable outgassing of the reaction vessel was observed on the thermopile gauge when the background pressure was monitored over time intervals corresponding to actual reaction times.

A conventional glass vacuum apparatus was used for gas handling, storage, and pressure measurements. Pumping was by an oil diffusion pump and mechanical forepump. Mercury vapor was excluded from the gas handling system and reaction vessel. Amounts of substrate and inert gas were measured in standard volumes with a glass null-point Bourdon gauge.

A reaction mixture of $\text{C}_2\text{H}_5\text{NC}$ containing $\sim 6\%$ CH_3CN as an internal analytical standard was used for kinetic runs. Because of the small initial pressure ($\sim 3 \times 10^{-4}$ mm) of $\text{C}_2\text{H}_5\text{NC}$ used (2.0×10^{-6} mol),

the whole sample was removed for analysis. Isomerization was carried to between 10 and 40% reaction.

Kinetic runs were ended by pumping the mixture through a high-conductance trap maintained at -196° .

Analysis. Unreacted $\text{C}_2\text{H}_5\text{NC}$ was quantitatively removed by passage of the sample through a AgCN column. All gas chromatographic analyses were performed on a Hewlett-Packard F & M Model 700 chromatograph equipped with a dual flame ionization detector, a Model 5771A electrometer, and a Honeywell Electrorik 19 recorder. A 12-ft, 5% tricresyl phosphate on 60–80 mesh, acid-washed Chromosorb G column was used for analyses. Calibrations of the column were made with standard mixtures of $\text{C}_2\text{H}_5\text{CN}-\text{CH}_3\text{CN}$ before and after each series of analyses. Reproducibility was achieved to within $\pm 1\%$.

Results

Rate constants for the isomerization were calculated by using both an "absolute" and an "internal standard" basis. Since in most cases reasonable reproducibility between internal and absolute values was achieved, an average value was taken. When isocyanide interference with the acetonitrile peak occurred due to inadvertent saturation of the AgCN column with isocyanide, only absolute values were used.

Corrections to the Data. *a. Temperature Correction.* All rate data were brought to a standard temperature of 231.0° with use of the energy of activation for pure $\text{C}_2\text{H}_5\text{NC}$ ⁸ at a reaction order equal to that for the inert gas kinetic run.

b. Dead Space. This amounted to 1.4% and no correction was necessary, especially since relative inert gas efficiency is desired.

c. Pump-out Time. At the conclusion of a run the pressure drop in the reaction vessel was observed as a function of time. Time correction for removal of the sample varied from 1 to 10%, depending on the total pressure, the inert gas used and the run time; it was determined quite accurately from plots of pressure *vs.* pumping time measured for each gas.

d. Heterogeneity. Increase of the rate due to wall effects occurs at pressures below 4×10^{-3} mm ($\omega = 6 \times 10^4 \text{ sec}^{-1}$) in the $\text{C}_2\text{H}_5\text{NC}$ system.⁸ It was found

Table II: Some Calculated and Pragmatic Heterogeneity Functions

$P,$ mm	$\omega,$ sec^{-1}	$\langle H(E)' \rangle^a$	$\langle H(E)' \rangle + x$
2×10^{-4}	3.2×10^3	0.21	0.74
5×10^{-4}	8.0×10^3	0.13	0.58
1.5×10^{-3}	2.4×10^4	0.04	0.33
2.5×10^{-3}	4.0×10^4	0.02	0.20
6.4×10^{-2}	1.0×10^5	0.001	0.05

^a From ref 8.

by MR⁸ that the correction for simple heterogeneity, *i.e.*, simple wall activation collisions, was not sufficient to account for the observed rate at lower pressures. Some surface catalysis appears to occur. Table II shows values for the simple wall activation correction function $\langle H(E) \rangle$ at a given homogeneous collision rate ω , as given by MR, and the pragmatic deviation at various collision rates, defined similarly as

$$[\langle H(E) \rangle + \chi] = \Delta k/k_{\text{tot}}; \quad \Delta k = k_{\text{tot}} - k_{\text{hom}}$$

where k_{hom} is the homogeneous rate constant that would prevail in the absence of any wall effects; k_{tot} is the observed rate constant having homogeneous and wall activation contributions, *plus* some additional wall-catalysis component χ . The experimental data for the noble gas series show pragmatically (Figure 1) that deviation from the theoretical falloff curves is comparable with that of the pure substrate in the same range of falloff, *i.e.*, between k/k_{∞} values of 0.032 and 0.011. Relative collisional efficiencies were calculated from rate data obtained over the homogeneous region of falloff and extending into a region, $k/k_{\infty} \geq 0.02$, where only nominal deviation due to heterogeneity occurred. The data below this region were not used for determinations of efficiencies but solely for comparative and diagnostic purposes.

Interrelation of Relative Collisional Efficiencies, β . A detailed discussion of several alternative definitions of relative collisional efficiency quantities in thermal unimolecular systems has been given previously.¹⁰ Since these ideas are central to our work and to the discussion that follows, we will briefly review and summarize some aspects of this subject.

The notation $\beta_{\omega}(D)$ employed in this paper is the same as that given by TR.¹⁰ The subscript ω indicates in terms of the collision rate—whether ∞ , 0, or intermediate falloff, ω —the region of behavior of k/k_{∞} ; the parenthetic quantity D refers to the degree of dilution of the substrate by heat bath inert gas, $\omega(\text{M})/\omega(\text{A})$.

Collisional efficiencies may be classified as “differential” or “integral” quantities. The need for recognizing and defining these arises from both experimental custom and necessity.

a. Differential. At finite dilution, the relative efficiency equals the ratio of the increments of total specific collision rate of the parent, due either to addition of more substrate, $\Delta\omega(\text{A})$, or of inert gas, $\Delta\omega(\text{M})$, required to produce a given increment in the specific reaction rate, Δk ; the meaning of this quantity is clearest when these increments are small so that the dilution is low.¹¹ Thus

$$\beta_{\omega}(D) = \Delta\omega(\text{A})/\Delta\omega(\text{M}); \quad \Delta k(\text{A}) = \Delta k(\text{M}) \quad (1)$$

A related differential quantity may also be defined as

$$\beta'_{\omega}(D) = \Delta k(\text{M})/\Delta k(\text{A}); \quad \Delta\omega(\text{A}) = \Delta\omega(\text{M}) \quad (1')$$

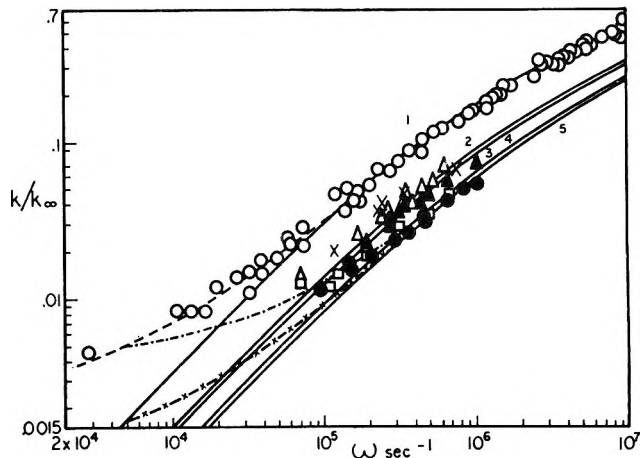


Figure 1. Plots of k/k_{∞} vs. ω for $\text{C}_2\text{H}_5\text{NC}$ at 504°K : $\text{C}_2\text{H}_5\text{NC}$, \circ ; He, \bullet ; Ne, \square ; Ar, \blacktriangle ; Kr, \times ; Xe, \triangle ; (1) RRKM 300(400) strong collider model;⁸ (2) 710 cm^{-1} P model; (3) 635 cm^{-1} P model; (4) 545 cm^{-1} EXP; and (5) 495 cm^{-1} EXP. The x-dashed curve represents the predicted dilution path for the 495 cm^{-1} EXP model; the dash-dotted line shows the predicted behavior after the correction for heterogeneity is applied.

The designations A and M which represent parent and inert gas signify strong collider and weak collider bath gas, respectively; of course, not all bath gases are weak colliders, but all noble gases are such, here.

b. Integral. At high dilution of parent in inert gas mixtures, in other than the low-pressure second-order region, it is more suitable to use an efficiency ratio which refers to total specific rates, *i.e.*, to an “integral” quantity expressed as

$$\bar{\beta}_{\omega}(D) = \omega(\text{A})/\omega(\text{Mix}); \quad k(\text{A}) = k(\text{Mix}) \quad (2)$$

or as

$$\bar{\beta}'_{\omega}(D) = k(\text{Mix})/k(\text{A}); \quad \omega(\text{A}) = \omega(\text{Mix}) \quad (2')$$

where Mix refers to the inert gas mixture of specified dilution.

The relative collisional efficiencies are functions of the order of reaction, $\phi [= 1 + d(\ln k)/d(\ln \omega)]$, of the dilution of substrate, D , and of the strength of collision which was specified by TR in terms of the reduced parameter E' , characteristic of the bath molecule for a given model of collisional transition probabilities; $E' = \langle \Delta E \rangle / \langle E^+ \rangle$, where $\langle \Delta E \rangle$ is the average energy removed per deactivating collision by the bath molecule and

(10) D. C. Tardy and B. S. Rabinovitch, *J. Chem. Phys.*, **48**, 1282 (1968) (TR).

(11) This definition of differential efficiencies reflects the conventional experimental practice of adding a finite and variable amount of bath gas to the pure substrate to give a final mixture of dilution D . This corresponds to averaging over the whole dilution range covered by the increment. A more exact definition would involve infinitesimal increments of substrate or of bath gas to an initial mixture of dilution D , but this quantity cannot be measured in practice with any precision. The fundamental significance of differential quantities becomes more obscure in studies above the second-order region.

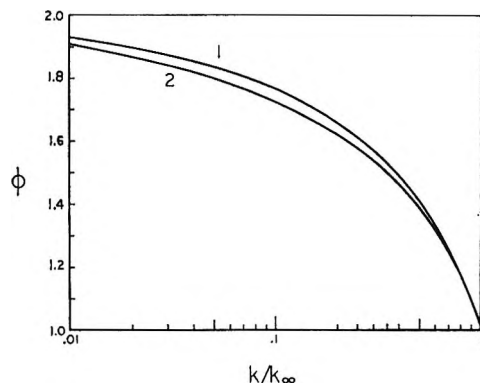


Figure 2. Calculated plots of ϕ vs. k/k_∞ for (1) $n = 4.6$ and (2) $n = 6.1$, based on the Slater function $I_n(\theta)$.

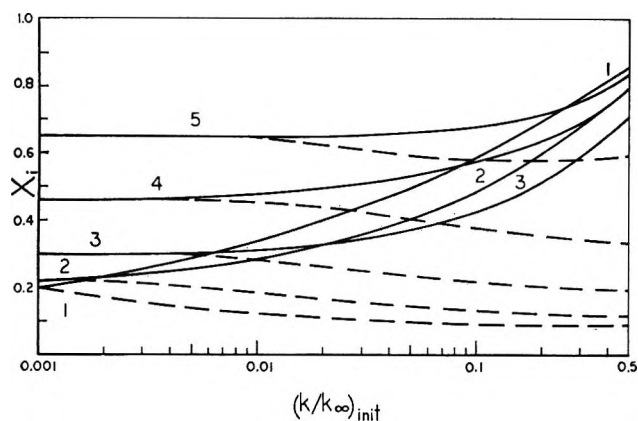


Figure 3. Calculated plots of $\beta'_\omega(D)$, $\beta_\omega(D)$, vs. $(k/k_\infty)_{\text{init}}$ for $\text{C}_2\text{H}_3\text{NC}$, 504°K, 385 cm^{-1} SL; curves 1, 2, 3, 4, and 5 correspond to $D = 200, 50, 10, 3,$ and 1, respectively.

$\langle E^+ \rangle$ is the thermodynamic equilibrium value of the average active energy possessed by the reacting molecules above the critical threshold, E_0 . A correlation of order with k/k_∞ for methyl and ethyl isocyanide (for which Slater's n is 4.6 and 6.1, respectively) is given in Figure 2.

The limiting values of all the β quantities and their general trend as a function of falloff region and dilution is given in Table III. The numerical magnitudes of the various β quantities are illustrated in terms of a typical weak collider for which $E' = 0.75$ ($\langle \Delta E \rangle = 1.03$, $\langle E^+ \rangle = 1.37 \text{ kcal mol}^{-1}$) in Figures 3–5. A maximum spread between β'_ω and β_ω and between β'_ω and β_ω occurs at high values of ϕ . All quantities converge to the same value in the second-order region at $D = \infty$. β'_ω passes through a minimum value at intermediate dilution for all values of ϕ , while β_ω increases continuously as $D \rightarrow 0$; β'_ω passes through a minimum value at intermediate dilution if k/k_∞ is less than 0.05 for $D = 0$; β_ω behaves similarly to β_ω ; however, its magnitude at low dilution is less than β_ω . Three-dimensional plots of β'_ω and β_ω vs. both D and the reference value of k/k_∞ for the pure substrate (Figure 5) show these qualitative relationships more clearly: two surfaces

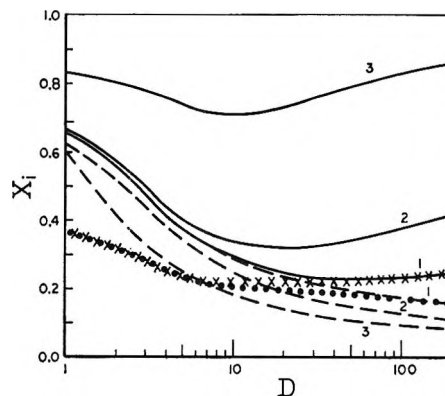


Figure 4. Calculated plots of $\beta'_\omega(D)$, $\beta_\omega(D)$, vs. D for various values of $(k/k_\infty)_{\text{init}}$. For $\text{C}_2\text{H}_3\text{NC}$, 504°K, 385 cm^{-1} SL; solid lines refer to the primed quantities and dashed lines correspond to unprimed quantities; sets 1, 2 and 3 correspond to the calculated behavior for $(k/k_\infty)_{\text{init}}$ values of 0.0025, 0.025, and 0.5, respectively. Set 1 corresponds to the low pressure limit and the behavior for $\beta_0(D), \dots$ and $\beta'_0(D)$, $\times \times \times$, is also displayed.

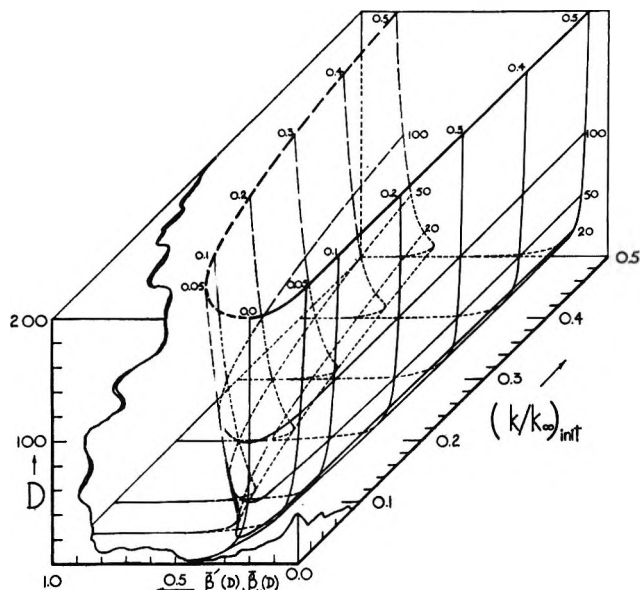


Figure 5. Calculated three-dimensional plots for $\beta'_\omega(D)$, $\beta_\omega(D)$, vs. $(k/k_\infty)_{\text{init}}$ and D , for $\text{C}_2\text{H}_3\text{NC}$; 504°K, 385 cm^{-1} SL; the dashed and solid surfaces depict the behavior of the β' and β quantities, respectively. The horizontal curves lie on various dilution planes slicing the two surfaces along all values of k/k_∞ , while the curves on vertical planes span values of the efficiencies for all dilutions on various intersecting k/k_∞ planes.

span all regions of D , from 0 to ∞ , and all regions of falloff; both surfaces converge at low values of k/k_∞ for all values of D , converge on unity for $D = 0$, at all values of k/k_∞ , and diverge at high values of k/k_∞ for all $D > 0$.

For a stronger collider, similar behavior is predicted. However, the surfaces are shallower and closer to a plane at a value of unity.

Noble Gas Falloff Data. The measured rate con-

Table III: Relationships of Relative Collisional Efficiencies at Various Regions of Falloff and Dilution

Dilution	Second order	Falloff	First order ^{b,c}
0	$\bar{\beta}'_0(0) = \bar{\beta}_0(0) = 1$ $\bar{\beta}'_0(0) = \beta_0(0)^a$	$\bar{\beta}'_\omega(0) = \bar{\beta}_\omega(0) = 1$ $\beta'_\omega(0) = \beta_\omega(0) < \beta_0(0)$	$\bar{\beta}'_\infty(0) = \bar{\beta}_\infty(0) = 1$ $\beta'_\infty(0) = \beta_\infty(0) < \beta_\omega(0)$
D	$\bar{\beta}'_0(D) = \bar{\beta}_0(D) < 1$ $\beta'_0(D) = \beta_0(D) < \beta_0(0)$	$\bar{\beta}'_\omega(D) > \bar{\beta}_\omega(D)^d$ $\beta'_\omega(D) > \beta_\omega(D)$	$\bar{\beta}'_\infty(D) = \bar{\beta}_\infty(D) > \bar{\beta}_\infty(0)$ $\beta'_\infty(D) > \beta_\infty(D), \beta_\infty(0)$
∞	$\bar{\beta}'_0(\infty) = \bar{\beta}_0(\infty) = \beta'_0(\infty)$ $= \beta_0(\infty) < \beta_0(0)$	$\bar{\beta}'_\omega(\infty) > \bar{\beta}_\omega(\infty)$ $\beta'_\omega(\infty) > \beta_\omega(\infty)$	$\bar{\beta}'_\infty(\infty) = \bar{\beta}_\infty(\infty) = 1 > \bar{\beta}_\infty(0)$ $= \beta_\infty(\infty) < \beta_\infty(D), \bar{\beta}_\infty(\infty)$

^a Magnitude less than unity, in general, and may be obtained from quasiuniversal curves given by TR and depend only on E' for a particular collisional transition probability model. ^b $\omega \rightarrow \infty$; $k/k_\infty \rightarrow 1$. ^c This region is not experimentally useful. ^d $\beta'_\omega(D_i) > \beta'_\omega(D_j) > Q < \beta'_\omega(D_k) \dots < \beta'_\omega(D_\infty)$ and $\beta_\omega(D_i) > \beta_\omega(D_j) \dots > \beta_\omega(D_\infty)$; where $i < j < k$, and Q is a minimum value. The same trend is observed for $\bar{\beta}'$ and $\bar{\beta}$ quantities; see Figure 2.

stants are summarized in the Table IV. Curves of $\log k/k_\infty$ vs. $\log \omega$ are given in Figure 1 for the pure substrate and for substrate-noble gas mixtures of increasing dilution. In practice, it was not convenient to work either at a constant or near-infinite dilution: to work at constant dilution would have meant restricting experiments to a value of D significantly lower than infinite, while to work near infinite dilution would have meant restricting rate data to a k/k_∞ range which was higher in falloff. The experiments represent a compromise. The smallest value of substrate pressure was chosen ($\sim 3 \times 10^{-4}$ mm) such that accurate analysis could be performed, while the smallest amount of bath gas added was dictated by the heterogeneity artifact described earlier and by the requirement that $k(\text{Mix})$ should be sufficiently increased so that good accuracy was possible. Thus, various amounts of inert gases were added to a constant amount of substrate such that D varied on a collision basis from approximately 20 to 260, depending somewhat on the gas. The lower range of dilution corresponds neither to an infinite value nor to effectively constant dilution. The experimental expediency thus forced on us constituted in part a modest study of the variation of β quantities with dilution.

The collision rates, ω , may be related to pressure, and the "integral" efficiencies may be expressed as

$$\bar{\beta}_\omega(D) = \omega(A)/\omega(\text{Mix}) = \frac{P(A)/[P(A,D) + P(M,D)\rho_\mu\rho_s]}{k(A) = k(\text{Mix})} \quad (3)$$

here $k(\text{Mix})$ is the specific rate constant for the mixture of dilution D ; $P(A,D)$ is the pressure of A in the mixture of dilution D , etc.; $\rho_\mu = (\mu_{AA}/\mu_{AM})^{1/2}$, $\rho_s = (s_{AM}/s_{AA})^2$, where μ is the reduced mass of the collision partners, and s_{AA} and s_{AM} are equivalent hard-sphere diameters; values of intermolecular potential parameters are given in Table V.¹² Also

$$\bar{\beta}'_\omega(D) = k(\text{Mix})/k(A); \quad P(A) = P(A,D) + P(M,D)\rho_\mu\rho_s \quad (3')$$

For the case $D = \infty$, then $P(M, \infty)\rho_\mu\rho_s \gg P(A, \infty)$, and

$$\bar{\beta}_\omega(\infty) = \lim_{D \rightarrow \infty} \bar{\beta}_\omega(D) = P(A)/P(M, \infty)\rho_\mu\rho_s; \quad k(A) = k(M) \quad (4)$$

$$\bar{\beta}'_\omega(\infty) = \lim_{D \rightarrow \infty} \bar{\beta}'_\omega(D) = k(M)/k(A); \quad P(A) = P(M, \infty)\rho_\mu\rho_s \quad (4')$$

Expressions 4 and 4' correspond directly to relations 2 and 2', respectively. Relative efficiencies on a pressure-to-pressure basis, $\bar{\beta}_p(D)$ and $\bar{\beta}'_p(D)$, and on a reduced mass-corrected basis, $\bar{\beta}_\mu(D)$ and $\bar{\beta}'_\mu(D)$, can be obtained from (3) and (3'), or from (4) and (4'), by deleting the factors ρ_s and $\rho_\mu\rho_s$, respectively. When the dilution, D , is large ($D \simeq 100$ is for all practical purposes an infinite value), then for a narrow range of dilution for a weak collider ($200 > D > 50$, in these studies), and a narrow range of falloff ($0.03 < k/k_\infty < 0.07$, in these studies), the dependence of the β quantities on D and ϕ is small and they can be averaged for all data points in this range.

Discussion

Correlation with Stochastic Calculations. The theoretical dependence of $\bar{\beta}_\omega$ and $\bar{\beta}'_\omega$ on D for He, Ne, Ar, Kr, and Xe is illustrated in Figure 6, as based on various models for the transition probability distribution function. The measured values of $\bar{\beta}'_\omega(D)$ for a given bath gas are greater than $\bar{\beta}_\omega(D)$ in agreement with the theoretical prediction for a given collisional model.

For He and Ne, the best fit was obtained for values of the average size of down jumps, $\langle \Delta E \rangle$, of 495 and 545 cm^{-1} ($\sim 1.5 \text{ kcal mol}^{-1}$), respectively, based on an exponential (EXP) model, which has been shown to be the correct qualitative form for the transition probabilities for low values of $\langle \Delta E \rangle$.⁴⁻⁷ For the heavier members of the noble gas series, the efficiencies are intermediate between strong and weak colliders, i.e., $\beta \simeq 0.4-0.5$. Then $\langle \Delta E \rangle$ is larger and the data are better fitted by a Poisson (P) model¹⁰ and values of $\langle \Delta E \rangle = 635, 710, \text{ and } 710 \text{ cm}^{-1}$ ($\sim 2 \text{ kcal mol}^{-1}$), respectively.

(12) (a) J. O. Hirschfelder, C. F. Curtiss, and R. B. Bird, "Molecular Theory of Gases and Liquids," Wiley, New York, N. Y., 1954; (b) R. A. Svehla, NASA Technical Report, R-132, 1962, p 36.

Table IV: Summary of Rate Data

D^a	$\omega,^a$ 10^6 sec^{-1}	$P(\text{Mix}),$ 10^{-2} mm	$k(\text{Mix}),^b$ 10^{-4} sec^{-1}	$\bar{\beta}'_p(D)$	$\bar{\beta}_p(D)$	$\bar{\beta}'\omega(D)$	$\bar{\beta}\omega(D)$
Helium							
18	1.00	0.765	$1.73 \pm (0.02)^c$	0.30	0.18	0.36	0.23
30	1.47	1.14	$2.61 \pm (0.02)$	0.35	0.22	0.40	0.27
31	1.49	1.16	2.39	0.32	0.19	0.37	0.24
42	2.06	1.62	$2.82 \pm (0.01)$	0.29	0.17	0.34	0.21
69	3.00	2.38	$3.60 \pm (0.00)$	0.28	0.17	0.33	0.20
72	3.54	2.81	4.23	0.29	0.18	0.34	0.22
96	4.58	3.65	$5.06 \pm (0.08)$	0.29	0.18	0.34	0.22
125	4.77	3.81	$4.94 \pm (0.03)$	0.27	0.16	0.32	0.20
138	6.75	5.40	6.46	0.29	0.17	0.33	0.21
174	8.71	6.97	$7.65 \pm (0.09)$	0.29	0.17	0.33	0.21
196	10.17	8.15	$8.08 \pm (0.08)$	0.27	0.16	0.31	0.19
Neon							
15	0.706	0.915	$1.88 \pm (0.02)$	0.29	0.17	0.47	0.34
24	1.11	1.45	$1.84 \pm (0.00)$	0.20	0.11	0.34	0.21
27	1.27	1.67	2.16	0.22	0.12	0.36	0.23
42	1.94	2.57	$2.98 \pm (0.05)$	0.22	0.12	0.37	0.24
65	3.17	4.22	$4.32 \pm (0.11)$	0.22	0.12	0.38	0.26
103	4.89	6.39	$5.18 \pm (0.09)$	0.20	0.10	0.34	0.22
176	6.96	9.31	$7.02 \pm (0.05)$	0.22	0.11	0.35	0.23
Argon							
48	1.98	2.41	$3.38 \pm (0.05)$	0.26	0.15	0.41	0.28
73	2.78	2.88	$4.22 \pm (0.00)$	0.28	0.18	0.45	0.33
42	2.79	3.40	$4.69 \pm (0.06)$	0.28	0.17	0.45	0.32
92	3.08	3.74	5.26	0.30	0.19	0.45	0.35
89	3.56	4.33	$5.90 \pm (0.13)$	0.30	0.19	0.47	0.35
90	4.43	5.39	$6.32 \pm (0.09)$	0.28	0.17	0.43	0.31
101	4.98	6.04	6.88	0.28	0.17	0.43	0.32
158	6.57	8.01	$9.23 \pm (0.27)$	0.32	0.19	0.48	0.36
258	10.25	10.60	$10.88 \pm (0.04)$	0.31	0.18	0.47	0.34
Krypton							
25	1.18	1.51	$3.04 \pm (0.02)$	0.33	0.20	0.54	0.41
53	2.44	3.15	$5.18 \pm (0.37)$	0.34	0.21	0.54	0.39
45	2.60	3.34	$5.69 \pm (0.34)$	0.34	0.23	0.57	0.42
61	3.50	4.51	$6.38 \pm (0.14)$	0.32	0.20	0.52	0.40
145	7.53	9.77	$10.61 \pm (0.17)$	0.32	0.19	0.50	0.38
Xenon							
18	0.72	0.909	$2.02 \pm (0.17)$	0.32	0.19	0.49	0.35
30	1.72	2.08	$3.82 \pm (0.05)$	0.33	0.21	0.53	0.39
50	2.66	3.25	$5.03 \pm (0.15)$	0.31	0.18	0.47	0.34
54	2.77	3.37	$5.17 \pm (0.05)$	0.31	0.19	0.49	0.37
73	3.52	4.31	$6.74 \pm (0.57)$	0.29	0.17	0.44	0.33
80	3.82	4.66	5.84	0.37	0.26	0.50	0.39
93	4.56	5.58	$7.51 \pm (0.04)$	0.33	0.21	0.50	0.39
120	5.83	7.15	$8.98 \pm (0.14)$	0.33	0.20	0.51	0.39
123	6.39	7.82	$10.37 \pm (0.23)$	0.36	0.23	0.55	0.44

^a Dilution, D , is on a collision basis, where $\omega = \omega(A,D) + \omega(M,D) = 1.59 \times 10^7 P(A,D) + 1.97 \times 10^6 [\sigma_{AM}^2 / \mu_{AM}^{1/2}] P(M,D)$; the average value of $P(A,D)$ was $3.2 (\pm 0.2) \times 10^{-4} \text{ mm}$. ^b $k_\infty = 1.56 \times 10^{-2} \text{ sec}^{-1}$. ^c Average deviation of absolute and internal standard values from mean.

A summary of the average jump sizes $\langle \Delta E \rangle$, and related probabilities, $\langle p \rangle$, for the different models used is given in Table VI.

For values of $D < 50$, the data depart from the infinite dilution curve. The situation is illustrated in particular in Figure 1 for the weakest collider He. The experimental points are in agreement with calculations based

on the stochastic model that fits the data at $D = \infty$ and lie along the S-shaped dashed curve that connects the pure substrate curve (initial value of $k/k_\infty = 1.65 \times 10^{-3}$) and the infinite dilution curve. Ne is also expected to lie close to this curve.

The effect of heterogeneity below $D = 100$ was introduced into the dilution mixture calculations at each

Table V: Various Parameters for C₂H₅NC and Noble Gases

Molecule	Å σ _a	ε/k, ^a °K	μ _{AM} ^b	σ _{AM} , ^c Å	ε _{AM} /k, ^d °K	Ω ^(2,2) *(T*, δ _{max}) ^e	ε _{AM} ²	ρ _B	ρ _μ
C ₂ H ₅ NC	5.00	400	27.5	5.00	400	1.65	41.25	1.00	1.00
He	2.58	10.2	3.7	3.79	64	0.85	12.20	0.30	2.72
Ne	2.79	36	14.8	3.90	120	0.96	14.56	0.35	1.37
Ar	3.42	124	23.2	4.21	223	1.13	20.03	0.49	1.09
Kr	3.61	190	33.2	4.30	276	1.22	22.52	0.55	0.91
Xe	4.06	229	38.8	4.53	303	1.26	25.77	0.63	0.84

^a All values same as in ref 4 except for C₂H₅NC from ref 8. ^b μ_{AM} = M_AM_M/M_A + M_M. ^c σ_{AM} = (σ_A + σ_M)/2. ^d ε_{AM}/k = [(ε_A/k)(ε_M/k)]^{1/2}. ^e δ_{max} ≠ 0 only for C₂H₅NC, for which μ = 3.93 D (A. L. McClellan, "Tables of Experimental Dipole Moments," W. H. Freeman, San Francisco, Calif., 1963) and δ_{max} = 1.12 [L. Monchick and E. A. Mason, *J. Chem. Phys.*, **35**, 1676 (1961)].

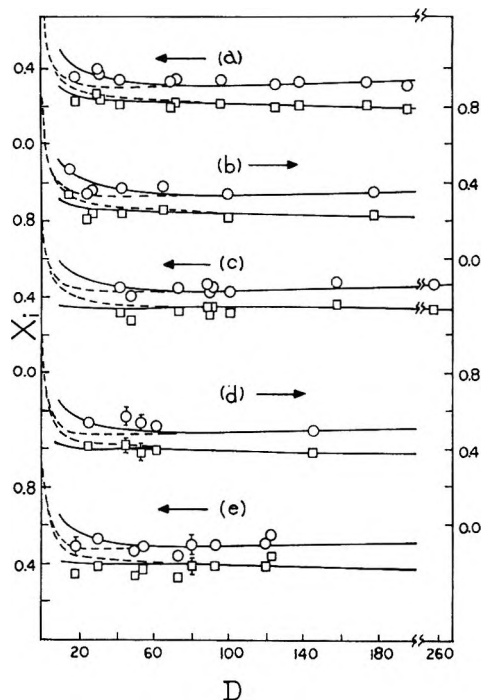


Figure 6. Experimental plots of $\bar{\beta}'_{\omega}(D)$, \circ , and $\bar{\beta}_{\omega}(D)$, \square , vs. D for: (a) He, 497 cm⁻¹ EXP; (b) Ne, 547 cm⁻¹ EXP; (c) Ar, 633 cm⁻¹ P; (d) Kr, 710 cm⁻¹ P; and (e) Xe, 710 cm⁻¹ P.

The solid curves correspond to the theoretical behavior, including a heterogeneity correction. The theoretical curves, without correction, are shown by dashed lines.

Table VI: Energy Jump Sizes and Related Probabilities in the C₂H₅NC System

Gas	Model	E' ^a	⟨ΔE⟩ _{down} , ^b cm ⁻¹	⟨ΔE⟩ _{up} , ^b cm ⁻¹	⟨p⟩ _{down}
He	EXP	1.04	495	240	0.67
Ne	EXP	1.14	545	250	0.68
Ar	P	1.32	635	440	0.75
Kr	P	1.48	710	490	0.77
Xe	P	1.48	710	490	0.77

^a E' = ⟨ΔE⟩/⟨E⁺⟩, where ⟨E⁺⟩ = 480 cm⁻¹ for C₂H₅NC at 504°K. ^b All values of ⟨ΔE⟩ were calculated for the infinite dilution curve for each gas.

effective pressure by weighting the strong-collision probability matrix, \mathbf{P}^A , by a collision fraction which includes the heterogeneity function, $\langle H(E)' \rangle + \chi$; *i.e.*, the expression of TR for the transition probability matrix corresponding to the mixture of strong and weak colliders, \mathbf{P}^{mix} , is

$$\mathbf{P}^{\text{mix}} = [(\omega(A) + \langle H(E)' \rangle + \chi)/\omega_t] \mathbf{P}^A + [\omega(M)/\omega_t] \mathbf{P}^M$$

where $\omega_t = \omega(A) + \omega(M) + \langle H(E)' \rangle + \chi$ and \mathbf{P}^M is the particular weak-collision matrix. The calculations on this basis are given by the solid lines in Figure 6 and the agreement with experiment is quite satisfactory.

Comparison with the CH₃NC System. The collisional efficiency of the noble gases in the thermal isomerization of methyl isocyanide was reported for infinite dilution in the second-order region⁴ where all β quantities have the same value (Table III). Since the experimental data for C₂H₅NC refer to a ϕ range of 1.81–1.91, extrapolation of the present high dilution integral quantities, $\bar{\beta}'_{\omega}(\infty)$ and $\bar{\beta}_{\omega}(\infty)$, to their second-order limit, $\beta_0(\infty)$, is necessary for direct comparison of the two systems. The extrapolation was made for each bath gas with use of the theoretical model that fits the data.

The $\beta_0(\infty)$ values for all noble gases in the CH₃NC and C₂H₅NC systems are gathered in Table VII. The

Table VII: Summary Values of $\beta_0(\infty)$ for the Noble Gases in the CH₃NC and C₂H₅NC Systems at 504°K

	C ₂ H ₅ NC				CH ₃ NC, β ₀ (∞) ^b
	$\bar{\beta}'_{\omega}(\infty)$	$\bar{\beta}_{\omega}(\infty)$	k(Mix)/k _∞ ^a	β ₀ (∞)	
He	0.33	0.21	0.037	0.27	0.27
Ne	0.36	0.24	0.035	0.30	0.31
Ar	0.45	0.33	0.040	0.39	0.31
Kr	0.53	0.40	0.045	0.46	0.27
Xe	0.50	0.38	0.046	0.44	0.26

^a Average value of k(Mix)/k_∞ over the range for which $\bar{\beta}'_{\omega}(D)$ and $\bar{\beta}_{\omega}(S)$ were averaged. ^b Data of ref 4 at 553.7°K corrected to 504°K according to the measured temperature dependence of β₀(∞) for He (ref 5) (all noble gases have near-equal efficiencies for CH₃NC).

latter values are close to the mean of $\bar{\beta}'_{\omega}(\infty)$ and $\bar{\beta}_{\omega}(\infty)$, as is predicted for the present region of ϕ . The efficiencies of He and Ne are very similar for both systems. Those of Ar, Kr, and Xe are distinctly higher in the C_2H_5NC system; Kr and Xe have equivalent efficiencies and the maximum (or plateau) observed for CH_3NC around Ar is shifted to Kr for the C_2H_5NC homolog. Several factors influence the observed alterations in efficiencies and suggest some difficulties in making *a priori* predictions.

1. *Size (Complexity) of the Substrate Molecule.* The equal or enhanced efficiencies for C_2H_5NC relative to those for CH_3NC are unexpected if one considers only the complexity of the two substrate molecules; C_2H_5NC is a larger heat reservoir than CH_3NC and energy removal by heat bath atoms should be less efficient if a quasistatistical energy accommodation process is involved on collision, as has been proposed.¹³

2. *Conservation of Angular Momentum Restrictions.* As was also pointed out by LR,^{13a} conservation of angular momentum restrictions influence profoundly the efficiency of energy transfer. Qualitative consideration may be made here of the relative magnitudes of the moments of inertia (Table VIII) that enter into the

Table VIII: Some Values of Moments of Inertia for the Noble Gas Systems in $\text{amu } \text{Å}^2$

	CH_3NC	C_2H_5NC
I_A	3.2	12.6
I_B	50.3	97.8
I_C	50.3	110.4
I_{A^+}	11.6	14.6
I_{B^+}	31.7	110.5
I_{C^+}	40.0	117.0
I_L^a	He	33
	Ne	155
	Ar	343
	Kr	523
	Xe	690

^a $I_L = \mu_{AM}(b^2)$. ^b The values of b used here are those of LR.

contributions to the total angular momentum \mathbf{M} from rotational angular momentum \mathbf{J} of the isocyanide molecule (I_B, I_C) and from orbital angular momentum \mathbf{L} due to relative translation of the collision partners (I_L). The more disparate these moments, the less effective is their coupling *via* the collision complex and the fewer are the possibilities for composing their sum so as to conserve the total, $M = \mathbf{J} + \mathbf{L}$, after collision and energy transfer.

For He and C_2H_5NC , these restrictions are expected to be more severe than in the CH_3NC case since the disparity between moments is larger in the former case, and He would again be expected to be less efficient for C_2H_5NC . However, for Ne, Ar, Kr, and Xe the reverse

is expected (Table VIII) since their related moment of inertia values are more comparable with the I values of C_2H_5NC . Indeed, excepting Ne, the $\beta_0(\infty)$ values in Table VII for the heavier bath gases are in accord with this expectation.

3. *Effective Number of Transition Modes of the Collision Complex.* One further consideration will assist in rationalizing the high $\beta_0(\infty)$ value for He in the ethyl case. Previously,^{13a} the molecule figure axis rotation was treated as an ineffective heat sink (*i.e.*, there is a large centrifugal effect) for transfer of internal energy from CH_3NC . There is a fourfold change between I_A and I_{A^+} (Table VIII), and this treatment accorded with an earlier successful RRKM treatment^{13b} of CH_3NC isomerization, according to which vibrational energy is not efficiently removed *via* this degree of freedom; this restriction is removed for C_2H_5NC ⁸ for which $I_A \sim I_{A^+}$. Thus LR treated energy transfer from CH_3NC into two transition modes only and excluded the methyl torsion of the collision complex (which correlates with the methyl isocyanide figure axis rotation) as inactive; the appropriate number becomes three for C_2H_5NC , with concomitant increase in energy-transfer efficiency as compared with the CH_3NC case.

Thus the observed behavior of inert bath gas efficiencies for C_2H_5NC is plausibly, although by no means rigorously, explained. A slightly low relative value for Ne may be only apparent inasmuch as the measured Ne value of CH_3NC appears to be a little high and may itself contain some error.

Figure 7 summarizes the relative collisional efficiencies of the noble gases for the two isocyanide homologs and for a number of other unimolecular systems.

The trend observed for C_2H_5NC appears similar to that for N_2O_5 .¹⁴ The data for the latter system were

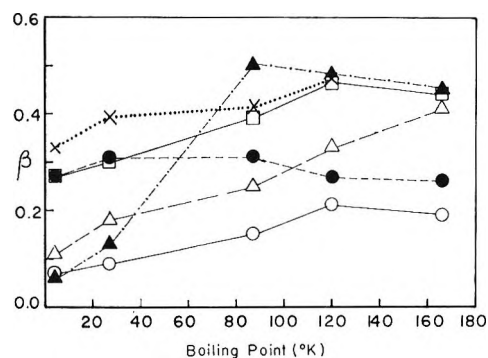


Figure 7. Plots of relative collisional efficiencies of noble gases β -quantities vs. boiling point for various unimolecular systems: CH_3NC , 504°K, ●; C_2H_5NC , 504°K, □; N_2O_5 , 223°K, ○; NO_2Cl , 546°K, △; *sec*- C_4H_9 , 300°K, ×; cyclobutanone, 296°K, ▲.

(13) (a) Y. N. Lin and B. S. Rabinovitch, *J. Phys. Chem.*, **74**, 3151 (1970) (LR); (b) F. W. Schneider and B. S. Rabinovitch, *J. Amer. Chem. Soc.*, **84**, 4215 (1962).

obtained in the second-order region but the dilutions used were between 1 and 40 (on a pressure-to-pressure basis) and the efficiencies correspond to values of $\beta_0(D)$ rather than of $\beta_0(\infty)$. In the case of Ar, D varied from 2.5 to 6 over a k/k_∞ range from 0.0025 to 0.004. With use of the quasiuniversal plots of TR for $\beta_0(\infty)$ vs. E' , a reduced-energy parameter, together with the curves given by TR for $\beta_0(\infty)$ as a function of D at various values of E' ($E' = 0.15$ for Ar at 250), the values reported by Wilson and Johnston may be lowered by $\sim 20\%$ when brought to infinite dilution. Similar corrections apply to the other members of the noble gas series; however, the basic trend reported¹⁴ would not change significantly.

For NO_2Cl , the β quantities presented in Figure 7 correspond to extrapolated $\beta_0(\infty)$ values derived¹⁰ from the original data.² The increase of efficiency with mass is more prominent throughout the series and there is no maximum or plateau between He and Xe.

In the *sec*-butyl radical¹⁵ system, the behavior of the noble gases is qualitatively similar to that of the $\text{C}_2\text{H}_5\text{-NC}$ system.

In the cyclobutanone system,¹⁶ the efficiency values for He and Ne are very low and their disparity with the values for Ar, Kr, and Xe is excessively large. The heat capacities for cyclobutanone and $\text{C}_2\text{H}_5\text{NC}$ are similar but the excess energy above the reaction threshold in the former system is much larger ($E^+ \simeq 45$ kcal

mol^{-1}). We believe that interpretation of this system is premature.

A fuller interpretation of the behavior in these systems is by no means simple. Comparison with the $\text{C}_2\text{H}_5\text{NC}$ system involves various counterbalancing factors: (1) one of these is temperature, which governs the magnitude of the thermal criterion energy, E_{th} , described by LR; collisional efficiency tends to increase at lower temperatures as E_{th} decreases; (2) a second is the excess energy, E^+ , which governs the operational definition of collisional deactivation efficiency and whose increase has been demonstrated¹⁰ to cause decrease of β ; (3) the heat capacity of the substrate molecule whose increase causes decrease of β ; (4) finally, rotational coupling and angular momentum conservation restrictions which vary from case to case.

Acknowledgment. B. S. R. wishes to acknowledge the debt of pleasure and profit which he owes to Professor G. B. Kistiakowsky in connection with his tenure as Royal Society of Canada Research Fellow and as Milton Research Fellow at Harvard University, 1946–1948. This paper reflects that stimulus and the benefits of continuing fellowship with G. B. K.

(14) H. S. Johnston, *J. Amer. Chem. Soc.*, **75**, 1567 (1953); D. J. Wilson and H. S. Johnston, *ibid.*, **75**, 5763 (1953).

(15) G. H. Kohlmaier and B. S. Rabinovitch, *J. Chem. Phys.*, **38**, 1692 (1963).

(16) N. E. Lee and E. K. C. Lee, *ibid.*, **50**, 2094 (1969).

Studies of the Chymotrypsinogen Family of Proteins. XV.

pH and Temperature Dependence of the α -Chymotryptic Hydrolysis of *N*-Acetyl-L-tryptophan Ethyl Ester

by Shyamala Rajender, Rufus Lumry,* and Moon Han

*Laboratory for Biophysical Chemistry, Department of Chemistry, University of Minnesota, Minneapolis, Minnesota 55455 (Received October 12, 1970)**Publication costs borne completely by The Journal of Physical Chemistry*

A complete grid of kinetic and thermodynamic quantities, characterizing rate and equilibrium processes for the reaction of α -chymotrypsin with *N*-acetyl-L-tryptophan ethyl ester as a function of pH, temperature, substrate, and ethanol concentrations are presented. Analysis of the data on the basis of a catenary chain mechanism revealed the following: k_2 , the first-order rate constant for acylation, exhibited a bell-shaped pH-rate profile, implicating two ionizing groups; k_{-2} was pH independent beyond pH 8.0 in the higher temperature range but showed deviations from this behavior at lower temperatures; k_3 , the deacylation rate constant, shows dependence on one group with $pK \sim 7$ and is pH independent beyond 8.0 at all temperatures studied. At and above 25°, $K_s(k_{-1}/k_1)$ is nearly pH independent up to a pH of 8.5 and rises steeply beyond that point. A protein transition which has been reported in an earlier paper manifests itself at pH 7.5 and 8.0 but not below or above these pH values. ΔH^\ddagger and ΔS^\ddagger for the rate constants and ΔH° and ΔS° for the metastable intermediates compensate each other with a $T_c \approx 290^\circ\text{K}$. These observations and their implications are discussed in detail.

Introduction¹

In a previous paper² we presented a study of the rate parameters for the α -chymotryptic hydrolysis of *N*-acetyl-L-tryptophan ethyl ester (ATEE) as a function of temperature and concentration of first product, ethanol, at a fixed pH of 8.0 where the catalytic process was shown to be nearly pH independent.^{3,4} Analysis of the data on the basis of a simple catenary chain mechanism proved to be adequate. In addition to providing conventional thermodynamic information, the study demonstrated the catalytic importance of the substate transition ($A_bH_2 \leftrightarrow A_fH_2$)² previously reported by Kim⁵ in fluorescence studies of the protein and detected by Martin⁶ and Kaplan and Laidler⁷ in the chymotryptic hydrolysis of several other substrates. Recently, Berezin, *et al.*,⁸ reported data on the temperature dependence of inhibitor binding to α -chymotrypsin which indicate the participation of this substate transition in this process also. Of more general interest was the finding that the major "metastable" intermediates, ES, the enzyme substrate noncovalent complex, EA, the acyl enzyme compound formed from the *N*-acetyl-L-tryptophan moiety of the substrate (the second product P_2 is *N*-acetyl-L-tryptophan) gave enthalpies and entropies of formation relative to separated reactants which are fit, within error, by the linear "compensation" relationship, eq 1, established by Yapel and Lumry for the binding of substrate-analog inhibitors.⁹ The con-

stants γ and T_c in eq 1 thus appear to be characteristic of the enzyme and not of the substrates or substrate-analog inhibitors. The value of the parameter, T_c , which we call the "compensation temperature" is near 285°K, which is that found in a number of linear enthalpy-entropy compensation processes of small molecules in water. As is discussed elsewhere,¹⁰ this pattern of behavior now appears to be a universal characteristic of liquid water so that eq 1 suggests a direct participation of water in the reactions of α -CT. It is thus necessary to expand the initial kinetic study and we present in this paper the values of kinetic and thermodynamic quantities characterizing rate processes and equilibria for the reaction of α -CT with ATEE at a variety of pH values both above and below 8.0.

(1) This is paper number LBC 61. Please request reprint by number. This work was supported by United States Public Health Service through National Institutes of Health Grant No. 2R01-AM-05853 and by National Science Foundation through Grant No. GB 7896.

(2) S. Rajender, M. Han, and R. Lumry, *J. Amer. Chem. Soc.*, **92**, 1378 (1970).

(3) M. L. Bender and F. J. Kezdy, *ibid.*, **86**, 3704 (1964).

(4) M. L. Bender, F. J. Kezdy, and C. R. Gunter, *ibid.*, **86**, 3697, 3714 (1964).

(5) Y. D. Kim and R. Lumry, *ibid.*, **93**, 1003 (1971).

(6) C. Martin, personal communication.

(7) H. Kaplan and K. J. Laidler, *Can. J. Chem.*, **45**, 547 (1967).

(8) I. V. Berezin, A. V. Levashev, and K. Martinek, *Eur. J. Biochem.*, **16**, 472 (1970); *FEBS (Fed. Eur. Biochem. Soc.) Lett.*, **7**, 20 (1970).

(9) R. Lumry and R. Biltonen in "Structure and Stability of Biological Macromolecules," S. Timashev and G. Fasman, Ed., Marcel Dekker, New York, N. Y., 1969, Chapter 2.

(10) R. Lumry and S. Rajender, *Biopolymers*, **9**, 1125 (1970).

$$\Delta H_f^\circ = \gamma + T_c \Delta S_f^\circ \quad (1)$$

Table I: The Phenomenological Rate Constants α_0 , α_p , β_0 , and β_p as Functions of pH at Six Temperatures, in the Hydrolysis of *N*-Acetyl-L-tryptophan Ethyl Ester by α -CT in 0.2 M KCl

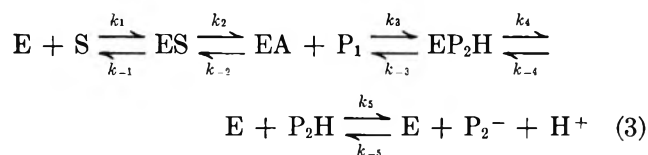
	pH									
	5.5	6.0	6.5	7.0	7.5	8.0	8.5	9.0	9.5	10.0
$T = 5^\circ$										
β_0, sec^{-1}		1.2	3.0	6.2	9.0	12.0	12.0	12.0	12.0	12.5
$\Delta F^\ddagger_{\beta_0}, \text{kcal/mol}$		16.13	15.63	15.23	15.02	14.86	14.86	14.86	14.86	14.84
β_p, sec^{-1}		6.5	16.0	33.0	48.0	60.0	61.0	58.0	45.0	30.0
$\Delta F^\ddagger_{\beta_p}, \text{kcal/mol}$		15.20	14.70	14.30	14.10	13.97	13.96	13.99	14.13	14.36
$\alpha_0 \times 10^{-5}, m^{-1} \text{sec}^{-1}$		0.40	1.60	3.50	4.20	5.03	4.80	3.80	1.50	0.40
$\Delta F^\ddagger_{\alpha_0}, \text{kcal/mol}$		10.38	9.62	9.18	9.08	9.00	9.01	9.14	9.65	10.38
$\alpha_p \times 10^{-5}, m^{-1} \text{sec}^{-1}$		0.40	1.00	2.80	4.40	4.80	4.90	4.70	2.50	0.90
$\Delta F^\ddagger_{\alpha_p}, \text{kcal/mol}$		10.38	9.87	9.31	9.06	9.00	9.00	9.02	9.37	9.87
$T = 15^\circ$										
β_0, sec^{-1}	1.2	3.0	7.0	13.0	18.0	15.0	24.0	24.0	25.0	24.0
$\Delta F^\ddagger_{\beta_0}, \text{kcal/mol}$	16.74	16.21	15.73	15.37	15.19	15.00	15.02	15.02	15.00	15.02
β_p, sec^{-1}	8.5	16.0	35.0	60.0	76.0	102.0	102.0	98.0	80.0	50.0
$\Delta F^\ddagger_{\beta_p}, \text{kcal/mol}$	15.62	15.25	14.81	14.50	14.36	14.19	14.19	14.22	14.33	14.60
$\alpha_0 \times 10^{-5}, m^{-1} \text{sec}^{-1}$	0.31	0.50	2.20	3.60	4.00	4.90	4.60	3.50	1.30	0.30
$\Delta F^\ddagger_{\alpha_0}, \text{kcal/mol}$	10.92	10.65	9.80	9.52	9.46	9.34	9.38	9.53	10.10	10.94
$\alpha_p \times 10^{-5}, m^{-1} \text{sec}^{-1}$	0.30	0.60	1.50	3.10	4.70	4.60	4.70	4.20	2.00	0.70
$\Delta F^\ddagger_{\alpha_p}, \text{kcal/mol}$	10.94	10.54	10.02	9.60	9.37	9.36	9.37	9.43	9.86	10.46
$T = 25^\circ$										
β_0, sec^{-1}	3.0	6.3	15.0	30.0	37.0	47.0	47.0	47.0	47.0	46.0
$\Delta F^\ddagger_{\beta_0}, \text{kcal/mol}$	16.80	16.36	15.85	15.44	15.31	15.17	15.17	15.17	15.17	15.18
β_p, sec^{-1}	17.0	30.0	70.0	110.0	130.0	170.0	172.0	170.0	130.0	50.0
$\Delta F^\ddagger_{\beta_p}, \text{kcal/mol}$	15.77	15.44	14.93	14.67	14.57	14.40	14.40	14.41	14.57	14.78
$\alpha_0 \times 10^{-5}, m^{-1} \text{sec}^{-1}$	0.50	0.68	2.70	3.80	4.20	4.70	4.40	3.00	1.20	0.25
$\Delta F^\ddagger_{\alpha_0}, \text{kcal/mol}$	11.04	10.86	10.04	9.84	9.78	9.73	9.75	9.98	10.52	11.45
$\alpha_p \times 10^{-5}, m^{-1} \text{sec}^{-1}$	0.50	0.85	2.00	3.50	4.50	4.50	4.60	4.00	1.80	0.50
$\Delta F^\ddagger_{\alpha_p}, \text{kcal/mol}$	11.04	10.73	10.22	9.89	9.74	9.74	9.73	9.81	10.35	11.04
$T = 35^\circ$										
β_0, sec^{-1}	7.2	14.0	28.0	60.0	65.0	78.0	79.0	80.0	80.0	80.0
$\Delta F^\ddagger_{\beta_0}, \text{kcal/mol}$	16.84	16.43	16.01	15.54	15.49	15.39	15.37	15.37	15.37	15.37
β_p, sec^{-1}	35.0	55.0	110.0	165.0	210.0	250.0	248.0	240.0	200.0	130.0
$\Delta F^\ddagger_{\beta_p}, \text{kcal/mol}$	15.87	15.59	15.17	14.92	14.77	14.67	14.67	14.69	14.80	15.07
$\alpha_0 \times 10^{-5}, m^{-1} \text{sec}^{-1}$	0.70	0.85	3.10	4.00	4.40	4.71	4.40	2.70	1.10	0.20
$\Delta F^\ddagger_{\alpha_0}, \text{kcal/mol}$	11.22	11.00	10.31	10.15	10.09	9.98	10.09	10.39	10.94	11.98
$\alpha_p \times 10^{-5}, m^{-1} \text{sec}^{-1}$	0.80	1.15	2.50	3.80	4.80	5.00	4.60	3.60	1.40	0.30
$\Delta F^\ddagger_{\alpha_p}, \text{kcal/mol}$	11.14	10.91	10.44	10.18	10.04	9.95	10.07	10.23	10.79	11.74
$T = 42^\circ$										
β_0, sec^{-1}	16.5	25.0	50.0	100.0	100.0	115.0	109.0	115.0	110.0	
$\Delta F^\ddagger_{\beta_0}, \text{kcal/mol}$	16.72	16.45	16.02	15.59	15.59	15.50	15.53	15.50	15.53	
β_p, sec^{-1}	65.0	85.0	160.0	230.0	280.0	330.0	327.0	320.0	280.0	
$\Delta F^\ddagger_{\beta_p}, \text{kcal/mol}$	15.86	15.69	15.29	15.07	14.94	14.84	14.85	14.86	14.94	
$\alpha_0 \times 10^{-5}, m^{-1} \text{sec}^{-1}$	0.90	1.00	3.80	4.30	4.80	5.30	4.10	2.80	0.95	
$\Delta F^\ddagger_{\alpha_0}, \text{kcal/mol}$	11.33	11.26	10.43	10.35	10.28	10.22	10.38	10.62	11.30	
$\alpha_p \times 10^{-5}, m^{-1} \text{sec}^{-1}$	1.10	1.50	3.00	4.10	5.30	5.50	4.10	3.50	1.20	
$\Delta F^\ddagger_{\alpha_p}, \text{kcal/mol}$	11.21	11.01	10.58	10.38	10.22	10.19	10.38	10.48	11.15	
$T = 50^\circ$										
β_0, sec^{-1}	31.0	50.0	85.0	165.0	160.0	178.0	179.0	182.0		
$\Delta F^\ddagger_{\beta_0}, \text{kcal/mol}$	16.76	16.45	16.11	15.68	15.70	15.64	15.63	15.62		
β_p, sec^{-1}	100.0	150.0	250.0	335.0	380.0	480.0	476.0	420.0		
$\Delta F^\ddagger_{\beta_p}, \text{kcal/mol}$	16.00	15.74	15.42	15.23	15.15	15.00	15.00	15.08		
$\alpha_0 \times 10^{-5}, m^{-1} \text{sec}^{-1}$	1.15	1.15	4.30	4.50	5.80	5.90	4.00	2.60		
$\Delta F^\ddagger_{\alpha_0}, \text{kcal/mol}$	11.48	11.48	10.63	10.60	10.44	10.42	10.68	10.96		
$\alpha_p \times 10^{-5}, m^{-1} \text{sec}^{-1}$	1.40	1.80	3.70	4.50	6.40	6.30	3.80	3.30		
$\Delta F^\ddagger_{\alpha_p}, \text{kcal/mol}$	11.35	11.19	10.73	10.60	10.38	10.39	10.71	10.80		

Results

At all temperatures and pH values used in this study, the velocity of the hydrolysis of ATEE by α -CT obeyed the rate law given in eq 2 and the reaction has been

$$-dS/dT = v = \frac{e[S_0]}{\frac{1}{\alpha_0 + \alpha_p[P_1]_0} + \frac{1}{\beta_0 + \beta_p[P_1]_0}} \quad (2)$$

shown² to follow the conventional catenary chain mechanism given in eq 3



The fitting parameters for the rate data are $\alpha_0, \alpha_p, \beta_0,$ and β_p . The standard states chosen were unit activity for water and 1 *M* for ethanol and the substrate ATEE. Numerical values for the phenomenological rate constants $\alpha_0, \alpha_p, \beta_0,$ and β_p are given in Table I as functions of pH at six different temperatures, along with the corresponding free energies of activation. As shown previously,² the phenomenological rate parameters are related to the elementary step rate constants in the following way

$$\alpha_0 = [1/k_1 + k_{-1}/k_1k_2]^{-1} \quad (4)$$

$$\alpha_p = [k_{-1}k_{-2}/k_1k_2k_3 + k_{-1}k_{-2}k_{-3}/k_1k_2k_3k_4]^{-1} \quad (5)$$

$$\beta_0 = [1/k_2 + 1/k_3 + 1/k_4 + k_{-3}/k_3k_4]^{-1} \quad (6)$$

$$\beta_p = [k_{-2}k_{-3}/k_2k_3k_4 + k_{-2}/k_2k_3]^{-1} \quad (7)$$

These complex constants can be converted to single-step constants with no ambiguity and small errors, perhaps no greater than a factor of 2 (and thus negligible in the thermodynamic parameters with respect to random and fitting errors) on the basis of two assumptions which are reasonably well supported by data from the literature. The procedure we have adopted is exemplified by the use of the values of the phenomenological parameters for pH 8 and 7: K_s is obtained from a ratio of β_p/α_p without any assumptions as 5×10^{-4} *M* at pH 8.0. Then the value of α_0 establishes lower bounds on k_1 and k_2 as 5×10^5 *M*⁻¹ sec⁻¹ and 200 sec⁻¹, respectively, at 35°. However, Gutfreund and Sturtevant^{11,12} estimate a lower bound for k_1 for a substrate benzoyl-L-tyrosine ethyl ester (which is similar to ATEE) as 2×10^6 *M*⁻¹ sec⁻¹ which establishes an upper bound for k_2 of 300 sec⁻¹. The formation rate constant for proflavine-CT complex can be evaluated from accurate measurements of the corresponding equilibrium constant¹³⁻¹⁵ and the dissociation rate constant^{14,15} as 5×10^6 *M*⁻¹ sec⁻¹. Bender, *et al.*,¹⁶ have assumed that K_s is a true equilibrium constant and Himoe and Hess,¹⁴ using transient rate data and an analysis which requires that K_s be very nearly a true

equilibrium constant, have obtained excellent agreement with our value for K_s for ATEE at pH 6. These comments suggest that $k_{-1} \gg k_2$ in which case k_1 might be at least one order of magnitude larger than 10^6 *M*⁻¹ sec⁻¹. We have chosen to assume $k_{-1} \gg k_2$ realizing that this will introduce a small variable error in the k_2 values obtained from α_0 and K_s . However, the error introduced even at 50° is unlikely to be as large as a factor of 2 unless the activation energy for k_1 is very small. Hence at the worst, the error introduced into the values of the thermodynamic changes is no greater than our random and fitting errors. Additional justification for our assumption will appear in the Discussion section.

The second approximation, $k_4 > k_{-3}$, appears to be equivalent to the first approximation although we have only binding and competitive inhibition studies of *N*-acetyl-L-tryptophan on which to base it but, of course, ATEE and the free acid form of *N*-acetyl-L-tryptophan might be expected to be very similar in their association rate constant behavior.

These two approximations are sufficient to convert the phenomenological constants to values for $K_{EA}, k_2, k_{-2},$ and k_3 which are as precise as our experimental precision in ΔH and ΔS requires. However, to allow more precise use of the phenomenological parameters when better k_1 data become available, we have listed their values in Table I. The corresponding enthalpies and entropies are given in Table II. (See also Table III.)

Values for $k_{-3}k_{-4}/k_4$ can be determined using α_p and the two assumptions that $\Delta G^\circ \approx \Delta H^\circ \approx 0$ for the overall reaction $S + H_2O \leftrightarrow P_1 + P_2H$ and $k_4 \gg k_{-3}$. Recently, the value of ΔH° has been determined (see Appendix) as 0.8 ± 0.5 kcal/mol;¹⁷ the other assumption based on eq 18-20 is correct to ± 1.0 kcal/mol for ΔG° . As will be shown, the value of k_{-3} and thence $k_{-3}/k_3 = K_{EP_2H}$ and k_{-4}/k_4 can be estimated on a very tentative basis by invoking the idea of symmetry about the acylenzyme intermediate in the reaction scheme which we find in the *G, H,* and *S* profiles of the total

(11) H. Gutfreund and J. M. Sturtevant, *Proc. Nat. Acad. Sci., U. S.*, **42**, 719 (1956).

(12) H. Gutfreund, *Discuss. Faraday Soc.*, **15**, 167 (1955).

(13) S. A. Bernhand, B. F. Lee, and Z. H. Tashjian, *J. Mol. Biol.*, **18**, 405 (1966).

(14) A. Himoe and G. P. Hess, *Biochem. Biophys. Res. Commun.*, **23**, 234 (1966).

(15) S. A. Bernhard and H. Gutfreund, *Proc. Nat. Acad. Sci., U. S.*, **53**, 1238 (1965).

(16) B. Zerner and M. L. Bender, *J. Amer. Chem. Soc.*, **86**, 3669 (1964).

(17) See Appendix for a recent calorimetric value for the enthalpy of hydrolysis of *N*-acetyl-L-tryptophan ethyl ester to the protonated acid.

(18) G. S. Parks and H. S. Huffman, "The Free Energies of Some Organic Compounds," The Chemical Catalog, Reinhold, New York, N. Y., 1932.

(19) F. H. Carpenter, *J. Amer. Chem. Soc.*, **82**, 1111 (1960).

(20) T. C. Bruice and S. J. Benovic, "Bioorganic Mechanisms," W. A. Benjamin, New York, N. Y., 1966.

Table II: Some of the Calculated Single-Step Rate Constants in the Hydrolysis of ATEE in 0.2 M KCl by α -CT, at Various pH Values and Temperatures

	pH									
	5.5	6.0	6.5	7.0	7.5	8.0	8.5	9.0	9.5	10.0
$T = 25^\circ$										
$K_s \times 10^4, M$	3.40	3.53	3.50	3.41	2.89	3.78	3.74	4.25	8.10	18.0
$\Delta F^\circ_{K_s}, \text{kcal/mol}$	4.73	4.71	4.71	4.78	4.83	4.66	4.67	4.60	4.22	3.74
$\Delta F^\circ_{\beta_0/\alpha_0}, \text{kcal/mol}$	5.76	5.50	5.81	5.60	5.53	5.44	5.42	5.19	4.65	3.73
k_{21}, sec^{-1}	17.0	24.0	94.5	119.3	122.4	177.7	174.6	127.5	97.2	45.0
$\Delta F^\ddagger_{k_{21}}, \text{kcal/mol}$	15.76	15.57	14.76	14.62	14.60	14.42	14.43	14.58	14.74	15.19
$k_{-2}, m^{-1} \text{sec}^{-1}$	3.0	5.4	20.3	32.5	34.8	49.1	45.0	35.2	35.1	23.0
$\Delta F^\ddagger_{k_{-2}}, \text{kcal/mol}$	16.79	16.45	15.67	15.39	15.35	15.04	15.19	15.34	15.34	15.59
$T = 35^\circ$										
$K_s \times 10^4, M$	4.40	4.78	4.40	4.34	4.38	5.00	5.40	6.86	14.30	43.3
$\Delta F^\circ_{K_s}, \text{kcal/mol}$	4.73	4.68	4.73	4.74	4.73	4.72	4.60	4.46	4.01	3.33
$\Delta F^\circ_{\beta_0/\alpha_0}, \text{kcal/mol}$	5.62	5.43	5.70	5.39	5.49	5.41	5.28	4.98	4.43	3.39
k_{21}, sec^{-1}	30.8	40.63	136.4	173.6	192.7	235.0	237.6	185.2	157.3	86.6
$\Delta F^\ddagger_{k_{21}}, \text{kcal/mol}$	15.95	15.78	15.04	14.89	14.83	14.71	14.70	14.85	15.09	15.32
$k_{-2}, m^{-1} \text{sec}^{-1}$	7.1	10.3	34.7	63.1	59.6	73.3	75.7	61.7	62.9	53.3
$\Delta F^\ddagger_{k_{-2}}, \text{kcal/mol}$	16.86	16.62	15.86	15.51	15.54	15.41	15.40	15.52	15.51	15.61

Table III: Free Energies, Enthalpies, and Entropies of Activation of the Phenomenological Rate Constants at 25° and Different pH Values for ATEE in 0.2 M KCl (Hydrolysis by CT)

pH	$\Delta F^\ddagger, \text{kcal/mol}$				$\Delta H^\ddagger, \text{kcal/mol}$				$\Delta S^\ddagger, \text{kcal/mol}$			
	α_0	α_p	β_0	β_p	α_0	α_p	β_0	β_p	α_0	α_p	β_0	β_p
5.5	11.22	11.14	16.84	15.87	5.7	6.0	16.5	14.5	17	17	1	4
									(5.52)	(5.14)	(0.34)	(1.30)
6.0	11.00	10.91	16.43	15.59	3.5	5.2	15.1	14.0	24	19	4	5
									(7.50)	(5.81)	(1.3)	(1.59)
6.5	10.31	10.44	16.01	15.17	2.3	3.8	14.5	13.3	26	22	5	6
									(8.01)	(6.64)	(1.51)	(1.67)
7.0	10.15	10.18	15.54	14.92	1.0	2.0	13.3	11.5	30	27	7	11
									(9.15)	(8.18)	(2.24)	(3.42)
7.5	10.09	10.04	15.49	14.71	0	0	12.6	9.6	33	33	10	17
									(10.09)	(10.04)	(3.09)	(5.11)
8.0	9.98	9.95	15.39	14.67	-1.1	-1.3	12.4	8.6	36	37	10	20
									(11.08)	(11.25)	(2.99)	(6.07)
8.5	10.09	10.07	15.37	14.67	-1.5	-1.5	12.6	8.8	38	38	9	19
									(11.59)	(11.57)	(2.77)	(5.87)
9.0	10.38	10.23	15.37	14.69	-1.0	-1.0	12.4	9.0	37	36	10	18
									(11.39)	(11.23)	(2.97)	(5.69)
9.5	10.94	10.79	15.37	14.80	-1.5	-1.6	12.3	9.7	37	37	10	17
									(11.44)	(11.39)	(3.07)	(5.10)
10.0	11.98	11.74	15.37	15.07	-1.2	-1.3	12.3	10.3	39	38	10	16
									(12.18)	(12.04)	(3.07)	(4.77)

Quantities in parentheses are
 $T\Delta S^\ddagger$ values at 308°K (350°)

reaction at all pH values below 8.5. (See Figure 9 or the previous paper for examples.) This assumption is probably somewhat safer than it appears on first exposure. We have therefore calculated the quantities for k_{-3} and EP₂H to demonstrate that symmetry in the reaction mechanism does indeed appear. It should be noted, however, that the latter quantities are highly uncertain relative to those appropriate to the other single-step rate constants and their ratios. We have

presented them to emphasize the probable existence of symmetry which appears to be required by the sequence of chemical events.

pH Dependence of the Single-Step Rate Constants. The single-step rate constants or ratios of such constants thus obtained from the phenomenological rate constants along with their respective free energies of activation at two temperatures are given in Table II. Logarithmic plots of the rate constants *vs.* pH are

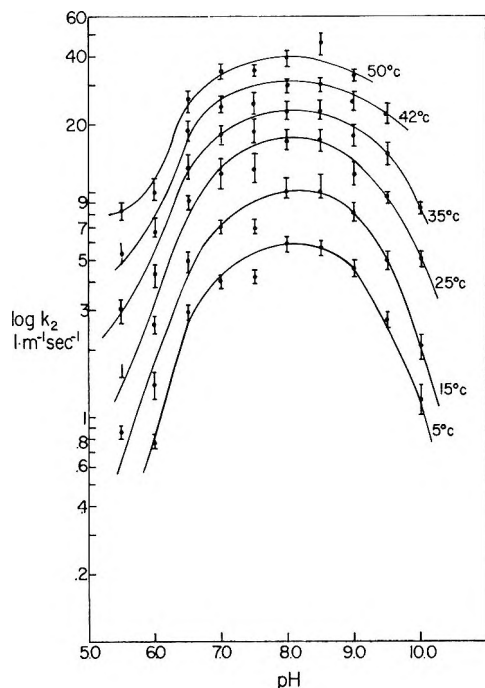


Figure 1. $\log k_2$ vs. pH at different temperatures for the hydrolysis of *N*-Ac-*L*-tryptophan ethyl ester by α -CT, 0.2 *M* KCl.

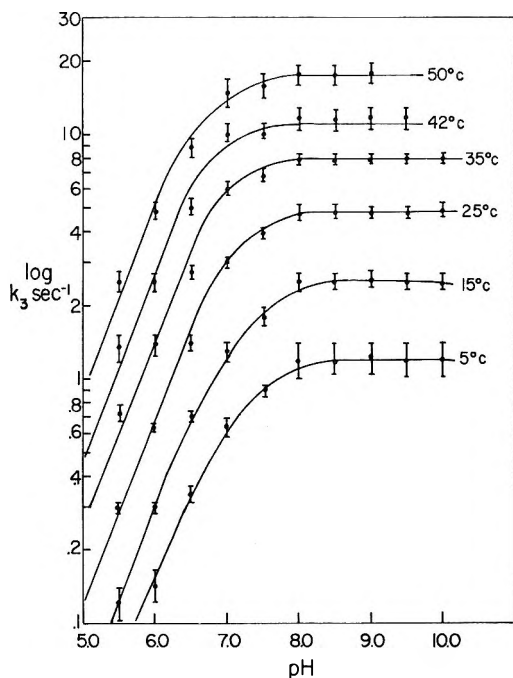


Figure 2. $\log k_3$ vs. pH at six temperatures.

shown in Figures 1-4. k_2 , the first-order rate constant for acylation,³ exhibited a bell-shaped pH-rate profile, implicating two ionizing groups in the lower temperature region. At higher temperatures, however, the k_2 -pH plots showed marked deviation from unit slope and some curvature in the low pH region indicating other ionizing groups or other processes that influence catalysis. In kinetic studies in the

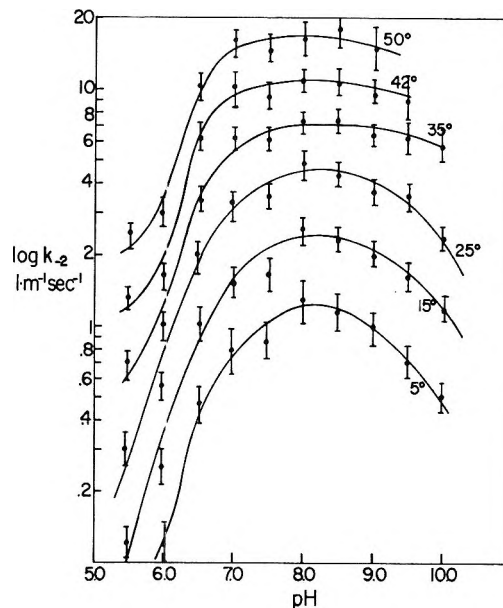


Figure 3. $\log k_{-2}$ vs. pH at six temperatures.

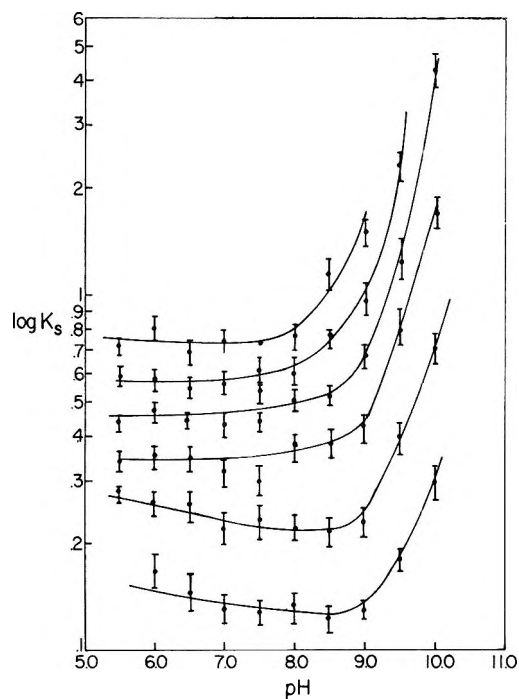


Figure 4. $\log K_s(k_{-1}/k_1)$ vs. pH at six temperatures.

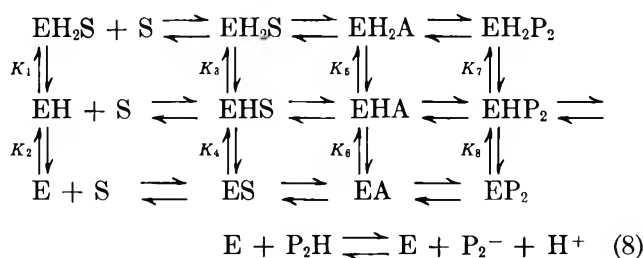
low pH region, Stewart and coworkers^{21,22} reported the appearance of an ionizing group with a $pK \sim 4$ which they believed to be a carboxyl group.

k_{-2} , the off-acylation rate constant, is pH dependent up to a pH of about 8 and in the higher temperature range remains nearly pH independent beyond that point. At lower temperatures, k_{-2} drops slowly with

(21) J. A. Stewart, H. S. Lee, and J. B. Dobson, *J. Amer. Chem. Soc.*, **85**, 1537 (1965).

(22) J. A. Stewart and J. B. Dobson, *Biochemistry*, **4**, 1086 (1965).

pH above 8.5. Like k_2 at higher temperatures, it also shows deviation from unit slope and a curvature in the pH-rate plots. At all temperatures, k_3 , the deacylation rate constant, shows a sigmoid curve, characteristic of one ionizing group. At 25° and above, $K_s = k_{-1}/k_1$ is nearly pH independent up to a pH of about 8.5 and shows a steep rise beyond that point. Since there is no leveling off observed in the equilibrium constant up to a pH of 10.0, it is impossible to estimate the pK of the ionizing group involved in this process with any degree of confidence. At temperatures below 25°, the K_s -pH plot also shows some curvature implicating at least one ionizing group in the lower pH region. This suggests that the nature of the ionizing group(s) at lower temperatures is not the same in the free enzyme and the enzyme-substrate complex and therefore that the effects do not exactly cancel each other to leave K_s independent of pH. Disregarding for the time being, the implications of the enthalpy-entropy compensation behavior, on the basis of the conventional analysis of pH dependence, the minimum elaboration of the scheme given in eq 1 which is required to account for the pH dependence is that of eq 8



The manner in which these prototropic equilibria are depicted does not imply that each step involves only one proton ionization. They are ionization processes and may involve one or more protons. Other analyses are the same as presented before.²

Temperature Dependence of the Phenomenological Rate Constants. Arrhenius plots for the phenomenological parameters α_0 , α_p , β_0 , and β_p at two pH values are shown in Figures 5–8 and a plot of free energy *vs.* reaction coordinate at 35° for four representative pH values is shown in Figure 9. (It should be borne in mind that α_0 , α_p , β_0 , and β_p are complex constants and there is no *a priori* reason to expect Arrhenius plots for these parameters to be linear at all temperatures and pH values.) It is obvious from Figure 9 that the near symmetry of the reaction about the acyl-enzyme intermediate is preserved at all temperatures and pH values studied, indicating the general validity of our reaction scheme. Exact symmetry appears to be an accidental consequence of the relative nucleophilicities of water and ethanol and our choice of standard states.

The deacylation parameters β_0 and β_p show, within error, linear Arrhenius patterns suggesting that these steps have no large heat capacities of activation, no change in the dominant step, nor does the substrate

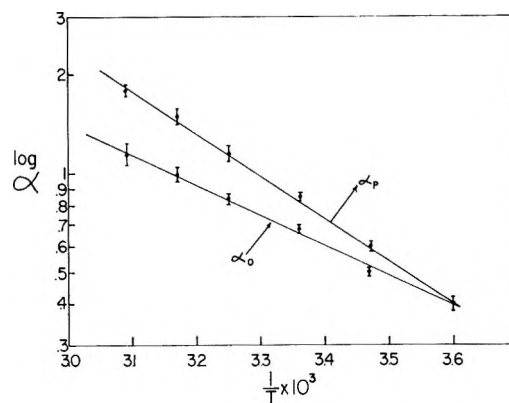


Figure 5. Arrhenius plots for α_0 , α_p , β_0 , and β_p at two representative pH values for the chymotryptic hydrolysis of ATEE (pH 6.0).

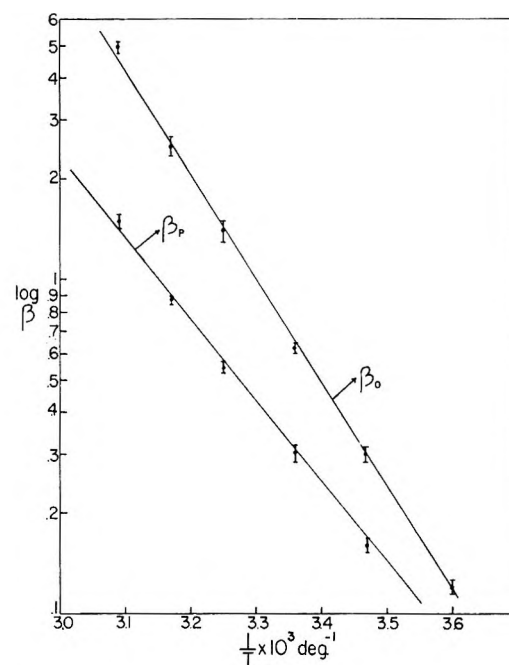


Figure 6. For details see Figure 5 (pH 6.0).

transition $\text{A}_b\text{H}_2 \leftrightarrow \text{A}_f\text{H}_2$ manifest itself in these processes. On the other hand, Arrhenius plots for both α_0 and α_p show small but distinct curvature at pH 8.0, as reported earlier,² and also at pH 7.5. Below pH 7.5, the apparent activation enthalpies are positive. Above pH 8.5, the slopes become positive, so that the apparent enthalpies of activation are negative. We have previously interpreted this change to be a consequence of a transition between two substates A_bH_2 and A_fH_2 of α -CT. The midpoint of the transition is near 25°. A_bH_2 is the lower pH-lower temperature form and A_fH_2 is the higher pH form at higher temperatures. Both substates are catalytically active.

Plots of ΔF^\ddagger , ΔH^\ddagger , and ΔS^\ddagger *vs.* pH for α_0 and α_p are shown in Figures 10 and 11, along with the corresponding quantities for β_0 and β_p , all at 25°. At this temperature, the free energies of activation change very

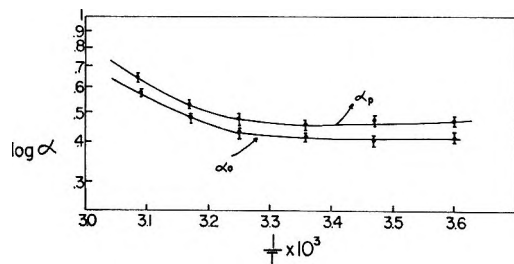


Figure 7. For details see Figure 5. (pH 7.5)

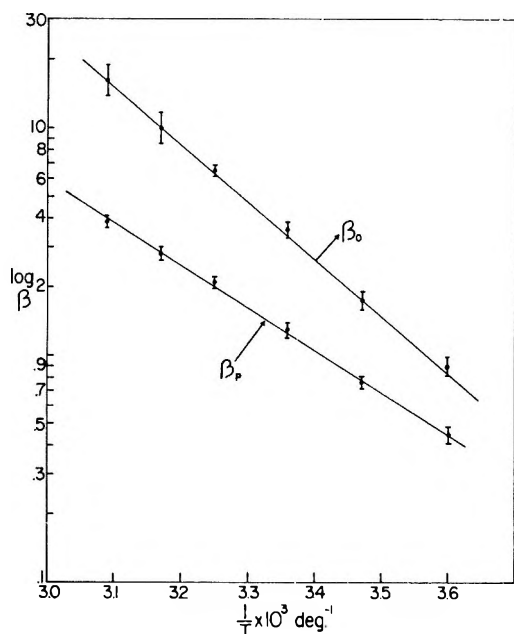


Figure 8. For details see Figure 5 (pH 7.5).

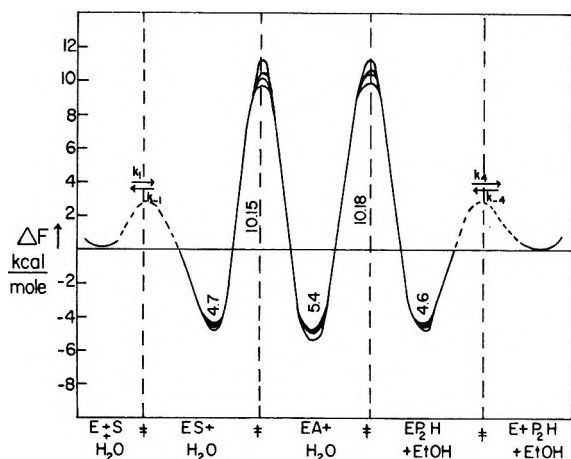
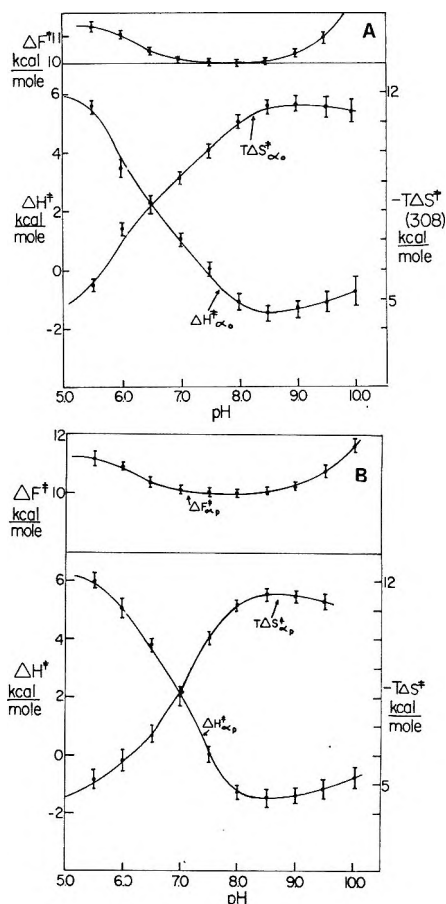


Figure 9. Free energy vs. reaction coordinate for the hydrolysis of ATEE at four pH values, at 35°: 0.2 M KCl (pH 5.5, 7.0, 8.0, 9.0).

little with pH, whereas the enthalpies and entropies of activation change appreciably but compensate each other such that the free energies do not reflect these fairly large changes. The temperature dependence of the elementary-step rate constants and the implications

Figure 10. Free energies, enthalpies, and entropies of activation of α_0 , α_p , β_0 , and β_p in the hydrolysis by CT of ATEE.

of the compensation pattern exhibited will be discussed in a subsequent paper.

Discussion

The $A_bH_2 \leftrightarrow A_fH_2$ Transition. The Arrhenius plots for α_0 and α_p show marked curvature at pH 7.5 and 8.0 but not at the other pH values. There is no reason at the moment to doubt that the curvature is due to the A_bH_2 to A_fH_2 transition detected in other catalytic and inhibitor-binding studies and roughly characterized by Kim and Lumry.⁵ The latter authors found the transition to be temperature dependent but could detect no pH dependence. It is not possible with the precision possible in most enzyme rate studies to obtain reliable estimates of the enthalpy and entropy change in the process from the indirect information provided by Arrhenius plots but the real or apparent sharpness of the slope changes thus far attributable to this transition suggest large enthalpy and entropy changes. The direct fluorescence studies of Kim and Lumry were somewhat more suitable for this purpose but though they gave the rough values, 48 kcal in ΔH and 160 eu in ΔS , the true values could be half or double these values. The maximum in the effect observed by these authors was near pH 8 and the characteristics, *i.e.*,

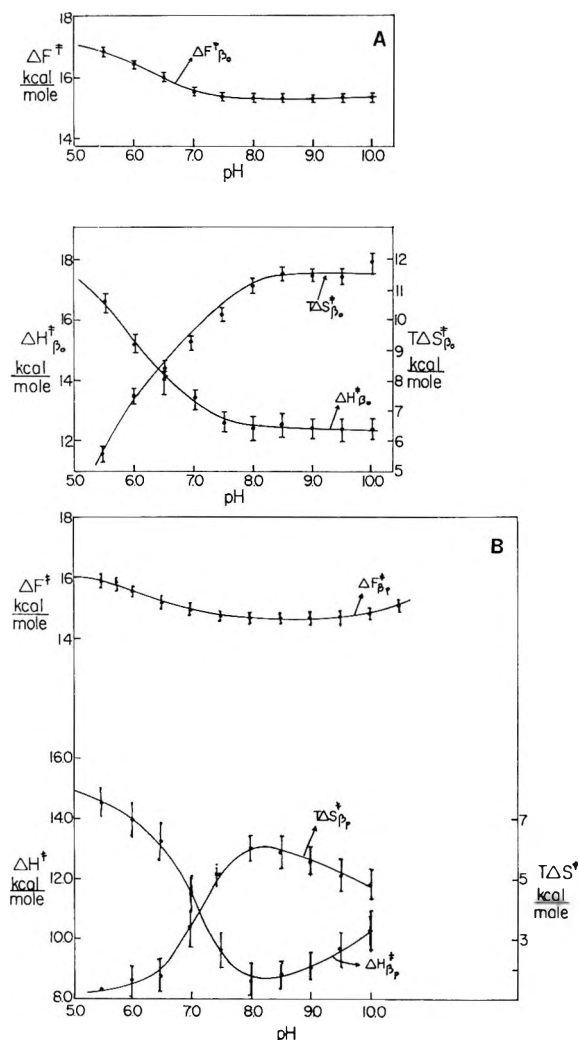


Figure 11. For details see Figure 10.

two-state nature and negligible heat-capacity change, led these authors to suggest that the process is a "subtle conformation change." However, it will be shown in the subsequent paper that the process may involve only protein solvation. It is currently of considerable interest in relation to the enthalpy-entropy compensation pattern found with chymotrypsin and some other proteins.

By fitting the Arrhenius plots of α_0 and α_p with two straight lines the activation energies above and below the transition temperature range can be estimated. Starting from values of 6 kcal/mol at pH 5.5 the activation enthalpies decrease to about 0 kcal/mol at pH 8.0 and 8.5 and become increasingly negative with additional increase in pH. This behavior suggests that α -CT is almost entirely in the A_bH_2 form below pH 7.5 and almost entirely in the A_fH_2 form above pH 8.5. The enzyme is catalytically active in both substrates.

Since curvature is not detected in the Arrhenius plots for the β_0 and β_p parameters, it is possible to delineate the elementary steps which manifest the transition. The dominant term in α_0 is k_{-1}/k_1k_2 ; in α_p it is

$k_{-1}k_{-2}/k_1k_2k_3$; in β_0 it is $1/k_2 + 1/k_3$ and k_{-2}/k_2k_3 in β_p , so that by a process of elimination, we find that only k_{-1}/k_1 is sensitive to the transition; *i.e.*, the quantitative substrate-binding properties of the two species are different. There are, of course, several elementary steps between $E + S$ and ES which are neither detectable nor separable in our study and since, as noted earlier, K_s is pH independent up to 8.5 at temperatures above 25° but below 25° shows a weak pH dependence in the lower pH region, it is possible that there is a change of dominance in K_s as a result of pH change.

Formal Analysis of the pH Dependence. Subject to the assumptions made in our analysis, the acylation steps k_2 and k_{-3} and the deacylation steps k_3 and k_{-2} all show dependence on acid groups with pK values ~ 7 at 25°. The near constancy of the pK_a values within a range of 0.2 pH unit suggests that the same kind of acid group is involved. On the basis of information available from X-ray diffraction experiments, the formal symmetry of the reaction scheme, and the chemical evidence for an acyl enzyme intermediate, it is reasonable to deduce that this is the imidazolium group of His 57, an assignment which has been made several times in the literature.^{3,7,23,24} Yapel^{25,26} has estimated the protolysis, hydrolysis, and direct transfer equilibrium constants for the transfer of protons from the two acid groups of α -CT with pK_a values of about 7 to freely dissolved indicator molecules in solution. Within the errors of the analysis, the two groups are not only quantitatively identical but his rate and equilibrium constants agree within factors of two or three with those for free imidazole. It is thus reasonable to identify the two acid groups of α -CT studied by Yapel as the imidazolium groups of His 40 and His 57. Only the group assignable to His 57 participates in inhibitor-binding reactions of substrate-analog inhibitors and our results are consistent with the involvement of this group and not that of His 40 in the catalytic process. On this assumption, the deprotonated form of His 57 is a necessary partner in the activated complexes for acylation and deacylation since it enters k_2 , k_{-2} , k_3 , and perhaps k_{-3} in the same way. If the enthalpy and entropy of activation were the same for k_2 and k_{-2} , the formation process for EA would be independent of this group under all conditions. However, there are small differences in the thermodynamic changes so that a weak dependence of the EA-formation process on this group can be detected. The simplicity of this behavior suggests that His 57 functions as a simple base

(23) D. E. Koshland, Jr., D. H. Strumeyer, and W. J. Ray, Jr., *Brookhaven Symp. Biol.*, **15**, 101 (1962).

(24) M. L. Bender and F. J. Kezdy, *Annu. Rev. Biochem.*, **34**, 49 (1965).

(25) A. Yapel and R. Lumry, *J. Amer. Chem. Soc.*, submitted for publication.

(26) A. Yapel, Ph.D. Thesis, University of Minnesota, Minneapolis, Minn., 1967.

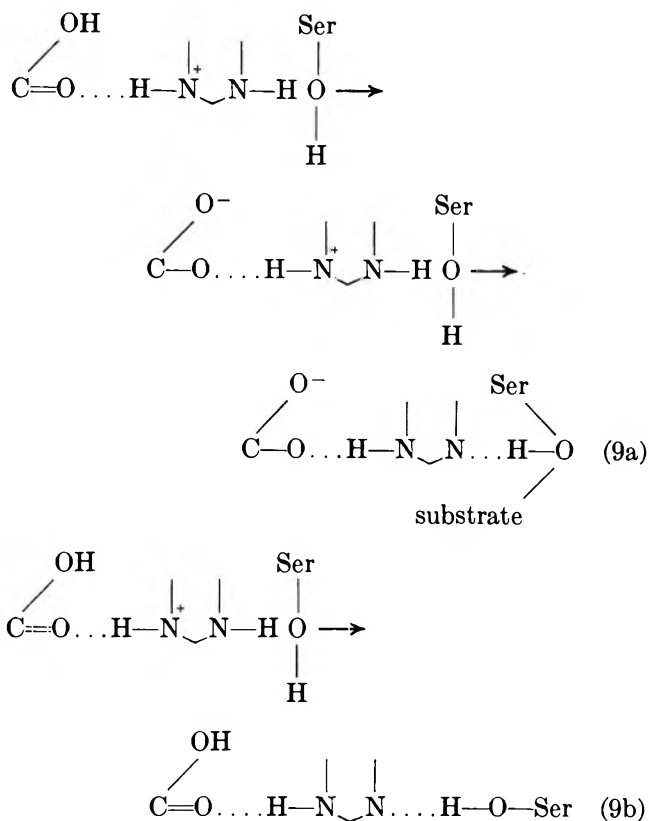
catalyst in the acylation and deacylation processes and has no other apparent function in the catalytic mechanism. We shall see below that the apparent simplicity may be misleading.

The pairs of activation enthalpies $\Delta H^\ddagger_{k_{-2}}$ and $\Delta H^\ddagger_{k_3}$, $\Delta H^\ddagger_{k_2}$ and $\Delta H^\ddagger_{k_{-3}}$ by the present analysis are 12.0 and 12.4 kcal/mol and 10.0 and 11.2 kcal/mol, respectively, at pH 8.0. (Table III.) Although the similarity within these pairs is somewhat accidental, as already mentioned, it is also consistent with the similarity within pairs of the apparent enthalpies and entropies of ionization of this acid group as estimated from the temperature dependence of the apparent pK_a values corresponding to the rate constants k_2 , k_{-3} , k_{-2} , and k_3 . (pK_a values are obtained from the corresponding $\log k$ vs. pH plots by the method of Laidler, fitting the curves to a slope of $n = 1$.) The $\Delta H^\circ_{\text{ion}}$ values are 5.0, 5.4, 4.4, and 4.1 kcal/mol, respectively; the $\Delta S^\circ_{\text{ion}}$ values are given in Table IV.

Table IV: Free Energies, Enthalpies, and Entropies of Ionization of the $pK \sim 7$ Ionizing Group Calculated from the Temperature Dependence of the Single-Step Rate Constants

	ΔF° , kcal mol ⁻¹	ΔH° , kcal mol ⁻¹	ΔS° , Gibbs, mol ⁻¹
k_2 , l. m ⁻² sec ⁻¹	1.34	5.0	12
k_3 , sec ⁻¹	1.57	4.1	8
k_{-2} , l. m ⁻¹ sec ⁻¹	1.68	4.4	9
k_{-3} , sec ⁻¹	1.46	5.4	13

Blow, *et al.*,^{27,28} have suggested that the carboxylate group of Asp 102 facilitates the basic role of the imidazolium group of His 57 by a "charge-relay" mechanism as shown in eq 9a. A passive mechanism of this type would not appear to be effective for the following reasons. Although mechanisms of this kind can convey to any group in the chain the basicity of the most basic member of the chain or the acidity of the most acidic member of the chain, for base catalysis to be effective by this transfer mechanism, the group participating directly in the catalytic process must be less basic than some other member of the chain. Otherwise the chain is irrelevant. The requirements for this type of transfer do not seem to be met by a passive "charge-relay" system. If the environment of the Asp 102 carboxylate group does not shift the pK_a of this group above that of the imidazolium group, eq 9a is adequate, in which case the negative charge on the carboxylate group should increase the pK_a of the imidazolium group (the effect is the net result of the stabilization of the positive charge on the imidazolium group and the weakening of the ion-dipole interaction between carboxylate C-O and imidazolium N-H). As a consequence, the



imidazolium group becomes a slightly stronger base. It does not gain this base strength by proton migration. Alternatively, if the environment pushes the carboxyl pK_a above that of the imidazolium group, it cannot increase the basicity of the imidazole group (eq 9b). The experimental pK_a values are higher by about 0.5 pK unit than those of imidazole itself or the imidazole groups of model histidine compounds. This small shift is consistent with an effective pK_a for the Asp 102 carboxylic acid group well below 7. Hence our data which show that a group with pK_a of 7 enters and leaves the activated complexes as a reasonably normal imidazole group suggest that the charge-relay system does not play an important role in the hydrolysis of small esters and amides. The latter conclusion may be misleading. If changes in the conformation and solvent near the Asp carboxylate group occur as a consequence of some other step in the overall mechanism, the local dielectric constant can be greatly reduced and the carboxylate group will become a strong base, so that the steps envisioned by Blow, *et al.*, will take place. This set of transient changes, "a dynamic charge-relay system" functioning roughly as a paper stapler involves no change in the protonation and thus no dependence on hydrogen-ion activity. As a result, our experiments cannot provide any direct measurement of the increase in basicity of the imidazole group in the activated complexes. The dynamic mechanism

(27) D. M. Blow, J. J. Birktoft, and B. S. Hartley, *Nature*, **221**, 337 (1969).

(28) D. M. Blow, *Biochem. J.*, **112**, 261 (1969).

as opposed to the passive one offers an attractive explanation for the enhanced catalytic effectiveness of the carboxylate-imidazole-hydroxyl grouping. Long-chain substrates bound in close proximity to the Asp 102 carboxylate group might produce the required change in local electrostatic situation but even for small substrates there are attractive possibilities. For example, the aggregate of our data discussed elsewhere^{9,10} are consistent with a mechanism in which the B chain "cap" of the chymotrypsin molecule is compressed down onto the C chain "anvil" in a process triggered by side-chain binding. This "rack" process could force the functional groups into the activated complex conformation and produce the required transient increase in basicity at the same time. Even without the "charge-relay" feature, *i.e.*, without proton transfer, the enforced cooperation of charge with charge and with conformation and solvent provides a wide range of mechanisms for interconversion of mechanical and electronic energy, the adjustment of the acidity or basicity of functional groups, and the transmission of free energy from one point to another. Because charged groups must generally be situated near the surface of proteins where the dielectric constant tends to be the highest, such mechanisms should tend to involve residues near protein surfaces. As a consequence, rearrangements of subunits in multisubunit protein assemblies would be particularly effective as a means for changing the balance positions of the "charge-relay" system. In this sense, conformationally dependent processes of proteins may be more a surface than a bulk phenomenon.

The Acid Group. There is some evidence for the participation of a group with a pK value below 5.5. Stewart, *et al.*,^{21,22} found a pH dependence at lower pH values and attributed it to a carboxylic group. At temperatures above 35°, our k_2 -pH plot (Figure 1) shows a well developed inflection in the vicinity of pH 5.5. This behavior is also found in a k_{-2} -pH profile (Figure 3) and since these two constants have only the on-acylation activated complex in common, the pH dependence must be that of this activated complex. k_3 shows only the acid titration behavior to be expected for a single acid group with pK near 7.

pH Dependence in the Alkaline Region. No clear picture of the behavior of the ATEE + α -CT system in the alkaline pH region emerges from our data. Of the individual rate constants, only k_2 is strongly influenced by an acid group with a pK_a of about 8.8 at 25°. Our data appear to be consistent with a loss of ability of the enzyme to participate in the acylation step (for which k_2 is the rate constant) when the group is deprotonated, but they do not have sufficient accuracy above pH 9.5 to establish firmly the quantitative characteristics of the pH behavior in this region.

The dissociation equilibrium constant for the enzyme-substrate complex, K_s , within the relatively large errors

at alkaline pH values, shows about the same pH dependence as k_2^{-1} . It is independent of pH up to about 8.5 above 25° and then rises rapidly as the pH is increased beyond this point. Since k_2 and K_s have in common only the equilibrium species ES, these observations indicate that the pH dependence is that of ES. At temperatures below 25°, K_s shows a well-defined inflection due to ionizing groups in the neutral pH region. Since this behavior does not appear in k_2 , and k_2 and K_s have a common starting point in ES, this group must be in the free enzyme and it appears in the k_1 step. The ionizing properties of this group must be similar in the free enzyme and the enzyme-substrate complex at temperatures above 25° but below this temperature, the cancellation of the effects in k_1 and k_{-1} are not exact. However, as will be shown in the following paper, the enthalpy and entropy changes in the formation of ES, EA, and EP₂H are all pH dependent in quantitatively similar ways, so that the situation is more complicated than the analyses of this paper indicate.

k_{-2} may have a weak pH dependence on a group with an apparent pK_a greater than 9. k_3 is free of pH dependence in this region and so is k_{-3} insofar as we can determine with our set of assumptions.²⁹ Oppenheimer *et al.*,^{30a} and McConn, *et al.*,^{30b} have presented evidence in support of their claim that the ionizing group on the alkaline pH side is the α -ammonium group of Ileu 16 which according to X-ray diffraction pictures^{27,28} is buried in an ion pair with the carboxylate group of Asp 194. This assignment is consistent with the results of solvent perturbation studies by Kaplan and Laidler⁷ which they interpreted to mean that the acid group is a cation, but it is by no means certain that the effects of alterations in solvent composition can be interpreted in such simple terms.

Marini and Martin,³¹ whose work suggests a much more complicated story, and more recently Bender and coworkers^{32,33} have questioned the assignment of Oppenheimer, *et al.*,^{30a} and at the present time the matter is in dispute. The behavior of α -CT in the alkaline pH region has been studied by several workers³⁴⁻³⁷ and

(29) In calculating k_{-3} and ΔG° , ΔH° , ΔS° for EP₂H, we made use of the reaction symmetry about the acyl-enzyme intermediate and the nearly identical values of ΔG^\ddagger for α_0 and α_p and those for β_0 and β_p . The thermodynamic parameters may be in error by about 1 kcal in ΔG° , 2 kcal in ΔH° , and 6-8 eu in ΔS° , and k_{-3} by a factor of 2 or 3. These values are computed only to demonstrate chemical consistency.

(30) (a) H. L. Oppenheimer, B. Labouesse, and G. P. Hess, *J. Biol. Chem.*, **241**, 2720 (1966); (b) J. McConn, E. Ku, C. Odell, G. Czerninski, and G. P. Hess, *Science*, **161**, 274 (1968).

(31) M. Marini, personal communication.

(32) F. C. Wedler and M. L. Bender, *J. Amer. Chem. Soc.*, **91**, 3894 (1969).

(33) P. Valenzuela and M. L. Bender, *Biochemistry*, **9**, 2440 (1970).

(34) J. R. Garel and B. Labouesse, *J. Mol. Biol.*, **47**, 41 (1970).

(35) C. H. Johnson and C. R. Knowles, *Biochem. J.*, **103**, 428 (1967).

although they all find a pH dependence which can be assigned to the α -ammonium group of Ileu 16, a great deal of interpretation is necessary in order to reconcile the variation in pK_a values observed and the differences in pH behavior between α - and δ -chymotrypsin with the normal pK_a value of an α -ammonium group in model compounds. Part of the variation in apparent pK_a values is probably experimental. Part of it may be due to the use of different substrates and different solvent composition and part may be due to the large temperature dependence of the ionization process. In addition, Kim and Lumry^{5,38} have found evidence for the existence of two acid groups with pK_a values above 8.

Validity of the Interpretation. The analyses given in this paper are restricted to free-energy changes and follow a conventional approach. Only at pH 8 where the hydrolysis is nearly pH independent do the Arrhenius and van't Hoff plots give simple behavior. Within the last few years, it has become reasonably certain that there is a previously hidden but nonetheless ubiquitous property of liquid water which can play a direct role in protein reactions.¹⁰ This process is revealed by the linear relationship between enthalpy and entropy changes given as eq 1. Because the slope parameter, T_0 in this equation, is near 285°K, experiments carried out at temperatures near this value yield free-energy changes in which the enthalpy contributions from the water process are nearly compensated by entropy changes. As a result, in studies carried out at one temperature, the water process is nearly hidden. Studies of temperature dependencies are essential if pH dependencies are to be correctly interpreted. Similarly, variations in solvent composition produced by adding organic cosolvents produce quantitative changes in the water process which must be taken into consideration in solvent-perturbation studies such as those of Kaplan and Laidler.⁷ In the following paper of the series, we begin the much more difficult analysis of the pH dependencies of the various enthalpy and entropy changes in the chymotryptic hydrolysis of ATEE.

Experimental Section

Materials. α -Chymotrypsin, three times crystallized, was a Worthington product and was further purified by the method of Yapel, *et al.*³⁹ Active site concentration was estimated by several methods as described earlier.² Total protein concentration was measured spectrophotometrically using an extinction coefficient of 50,000 at 280 nm, and a molecular weight of 25,000 for α -CT.

N-Acetyl-L-tryptophan ethyl ester was purchased from either Mann or Cyclo Chemical Corp. and was used without further purification since both products gave identical results. Ethanol was a Fisher product, 95% USP grade.

Methods. The pH-stat assembly and the method of measuring initial velocities have been described.² The

system was continuously flushed with CO₂-free water saturated nitrogen in order to eliminate CO₂ interference in more than one way.² Alcohol solutions were made up by volume at 25°. Corrections were not made for small electrode errors in pH measurements in alcohol solutions, as mentioned earlier. Treatment of data was exactly the same as described in an earlier paper.² Initial velocities were calculated by means of a computer program, fitting the time-progress curves to a higher order polynomial in P . Any errors due to progressive denaturation of the enzyme particularly at high pH values and any product inhibition are eliminated by this procedure. Systematic errors in the operation were minimized by randomizing preparation of enzyme and substrate stock solutions, concentration of enzyme and substrate used in each experiment, and the order of determining concentration dependence of initial velocities or time-progress curves. At pH values above 9.5, small corrections had to be made for spontaneous hydrolysis of the ester at temperatures below 35°. At temperatures above 40°, this correction was fairly large so that these values were not used in computing kinetic and thermodynamic parameters at high pH values and high temperatures.

Acknowledgment. We are indebted to Dr. F. Schaub of the LKB Instrument Company for making the flow microcalorimeter available to us. One of us (S. R.) wishes to express her gratitude to Professor Rex Lovrien, Department of Biochemistry, University of Minnesota, for making available the batch calorimeter used in these experiments. Our thanks are also due to Dr. Ingemar Wadsö, Thermochemical Laboratories, Lund, Sweden, for very helpful comments and suggestions.

Appendix

A Calorimetric Determination of the Heat of Hydrolysis of N-Acetyl-L-Tryptophan Ethyl Ester at pH 8.0. In computing some of the thermodynamic parameters from kinetic measurements,² we assumed, on the basis of available data,^{4,41-43} that $\Delta G^\circ \approx \Delta H^\circ = \Delta S^\circ \approx 0$ for the overall reaction, ester \leftrightarrow unionized acid. In order to estimate the errors introduced by these assumptions, we have determined the ΔH° for the hydrolysis by direct calorimetry, using a locally built, constant-

(36) P. Valenzuela and M. L. Bender, *Proc. Nat. Acad. Sci., U. S.*, **63**, 1214 (1969).

(37) M. L. Bender and F. C. Wedler, *J. Amer. Chem. Soc.*, **89**, 3052 (1967).

(38) Y. D. Kim, Ph.D. Thesis, University of Minnesota, Minneapolis, Minn., 1967.

(39) A. Yapel, M. Han, R. Lumry, A. Rosenberg, and D. F. Shiao, *J. Amer. Chem. Soc.*, **88**, 2573 (1966).

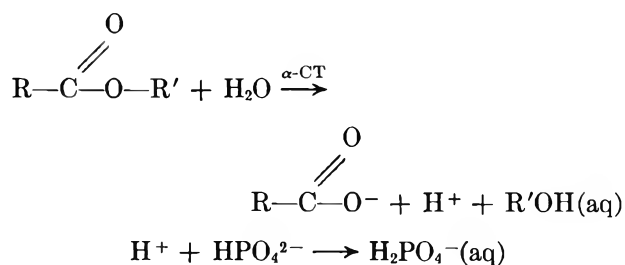
(40) R. Lovrien and W. Anderson, *Arch. Biochem. Biophys.*, **139**, 140 (1969).

(41) J. M. Sturtevant in "Experimental Thermochemistry," H. A. Skinner, Ed., Interscience, New York, N. Y., 1962.

(42) R. Bates and G. Pinching, *J. Res. Nat. Bur. Stand.*, **42**, 419 (1949).

(43) L. Nelander, *Acta. Chem. Scand.*, **18**, 973 (1964).

temperature, Wadsö-type "heat burst" twin microcalorimeter system.⁴⁰ One calorimeter contains the reaction vessel and the other the reference vessel. During the course of a reaction, the two calorimeters are maintained at a constant temperature by electrical heating so that the heat absorbed or evolved in a reaction is directly proportional to the area under the voltage-time displacement curve. Materials were the same as those used in kinetic measurements. The ester solution for calorimetric measurements was buffered in 0.05 *M* total phosphate. The ester was hydrolyzed enzymically with α -chymotrypsin at 25°, pH 7.5 at an ionic strength of 0.1 with KCl. Enzyme concentrations were chosen such that the reaction went to completion in less than 5 min so that thermal equilibrium in the calorimetric cells could be achieved in about 30 min or less, an optimum condition for the operation of the apparatus. In a typical experiment, 4 ml of a 4×10^{-3} *M* solution of the ester and 2 ml of a 4×10^{-5} *M* solution of α -chymotrypsin were fed into the two compartments of the reaction cell while the reference cell held 4 ml of the same ester solution and 2 ml of double-distilled water. This procedure automatically corrects for the heat of dilution of the ester, although in separate experiments the dilution heats proved to be immeasurably small. The measured heat is the total enthalpy of the reaction plus contributions from the ionization of the acid product and buffer components. The heat of ionization of *N*-acetyl-L-tryptophan was measured by calorimetric titration while that for phosphate was obtained from the literature.⁴¹⁻⁴³ The reactions involved are thus



At the pH of the experiment, the product acid is totally ionized. For the reaction given, then, the standard heat of hydrolysis, ΔH_b° is computed from the following expression

$$\Delta H_b^\circ = \Delta H_{\text{obsd}} - \Delta H_1 - \Delta H_2 - \Delta H_3 - \Delta H_4$$

in which ΔH_{obsd} is the experimental heat of the total reaction, ΔH_1 is the heat of dilution of the reactants, ΔH_2 is the heat of ionization of acid products, ΔH_3 is the heat of protonation of the buffer components, and ΔH_4 is the heat of dilution of ethanol, one of the products of the reaction. The standard states used were unit activity for water, 1 *M* for the ester and the corresponding acid, and 1 *M* EtOH (all in unit-activity water). ΔH_{obsd} was -1.4 kcal/mol; ΔH_1 was negligible and was also compensated in the experimental design; ΔH_2 was measured to be -1.0 kcal/mol; ΔH_3 for phosphate buffer was taken from the literature as -1.2 kcal/mol. ΔH_4 was found to be very small relative to experimental errors and was neglected. Under the conditions of the experiment, no autolysis, irreversible denaturation, or aggregation of the enzyme occurred nor were any unaccounted for heat effects observed. Therefore, the heat of hydrolysis of ATEE to the unionized acid form is

$$\begin{aligned} \Delta H_b^\circ &= -1.4 - (-0.1) - (-1.2) = \\ &0.8 \pm 0.5 \text{ kcal/mol of the ester} \end{aligned}$$

Errors reported are average deviations in four experimental runs. Using free energy values reported by Bender, *et al.*,⁴ the thermodynamic changes for the hydrolysis of *N*-acetyl-L-tryptophan ethyl ester to ethanol and free acid at 1 *M* standard state at pH 7.5, 25° and an ionic strength of 0.1 are thus

$$\begin{aligned} \Delta G^\circ &= 1.0 \text{ kcal/mol;} \\ \Delta H^\circ &= 0.8 \text{ kcal/mol;} \quad \Delta S^\circ = -1 \text{ eu} \end{aligned}$$

Errors in entropy change have not been estimated since errors in free energy are not given.

In two separate experiments, using an LKB Model 10700 Wadsö-type microflow calorimeter, we determined the same heat of hydrolysis of ATEE in tris-HCl buffer. Due to uncertainties in the large heat of ionization of the buffer acid under varying solvent conditions, the value obtained, $+1.6 \pm 1.0$, is not highly reliable although it is in reasonable agreement with the batch-calorimeter value.

Studies of the Chymotrypsinogen Family of Proteins. XVI.

Enthalpy-Entropy Compensation Phenomenon of α -Chymotrypsin and the Temperature of Minimum Sensitivity¹

by Rufus Lumry* and Shyamala Rajender

*Laboratory for Biophysical Chemistry, Department of Chemistry, University of Minnesota, Minneapolis, Minnesota 55455 (Received February 23, 1971)**Publication costs assisted by the National Institutes of Health and the National Science Foundation*

The pH and temperature dependencies of the rate constants and rate-constant ratios for the elementary steps in the α -chymotryptic (CT) hydrolysis of *N*-acetyl-L-tryptophan ethyl ester (ATEE) demonstrate a considerably greater complexity of mechanism than has been suggested heretofore by free-energy data and by force-fitting of the phenomenological parameters to conventionally assumed forms. The involvement of an imidazole group is relatively obvious only in the hydrolysis rate process for the acyl-enzyme, EA. Otherwise even below pH 8, several acid groups participate to spread the pH dependence over many pH units. All of the elementary steps are marked by a relationship between enthalpy and entropy changes which is usually linear with linearity coefficients, T_c , roughly in the range from 280 to 300°K. The entropy change tends to compensate the enthalpy change and the quantitative relationship between them suggests a common basis for this phenomenon regardless of the elementary steps or species involved. In addition, since this same enthalpy-entropy compensation pattern is found in examples of many types of small-solute processes in water and has been attributed to the properties of water itself, our results suggest a direct participation of water in the enzymic process. Some other protein reactions have already been found to manifest the same behavior. In the (CT + ATEE) system compensation behavior enters the reaction primarily through the free enzyme and the activated complex for EA formation. Because the free-energy changes in the elementary steps can be operationally divided into contributions from part processes demonstrating compensation behavior and part processes comprising the remaining factors in the reactions, it is possible to extract a "compensation-free" free-energy profile for the total process. With this profile it is found that most of the pH dependence disappears. Furthermore the available data for other ester substrates of CT suggest that the specificity of the enzyme with respect to substrate side chain also is minimized in the sense that the "compensation-free" free-energy profile is quantitatively very similar for all substrates of a common family. This suggestion is consistent with a similar minimization of the ability of the enzyme to discriminate among competitive inhibitors at $T = T_c$. Although this minimization of specificity is probably not a common characteristic of protein reactions in general, the concept of a "temperature of minimum sensitivity" is necessary for systems of CT plus ester substrates or competitive inhibitors and includes sensitivity toward pH variation as well. The temperature of minimum sensitivity is equal to T_c . Substrate specificity is directly related to the compensation phenomenon but the high catalytic efficiency of α -CT is independent of the phenomenon and as a consequence the remarkable pattern of enthalpy and entropy changes along the reaction pathway is associated primarily or entirely with specificity rather than high catalytic efficiency. This situation excludes for chymotrypsin several popular mechanisms proposed for enzymic catalysis. Of equal importance, it suggests a certain futility in attempts to elucidate the mechanisms of protein processes from free-energy data alone. Enthalpy and entropy information appears to be essential for an understanding of the complexities of such reactions.

Introduction

In previous papers^{2a,b} we reported rate data for the chymotryptic hydrolysis of ATEE at different temperatures and pH values. In analyzing the data, we found a linear relationship between the enthalpies and entropies of activation for the activated complexes as well as for the enthalpies and entropies of formation of the metastable intermediates. The slope values, T_c , in the "compensation relation," eq 1, were all near

$$\Delta H_b = \gamma + T_c \Delta S_b \quad (1)$$

285°K. In 1952-1953, Vaslow and Doherty^{3,4} ob-

served that substrate-similar inhibitors such as *N*-Ac-L-tyrosine manifest a linear relationship between the values of the total standard enthalpies of binding

(1) This is paper No. 71 from this laboratory. Please request reprints by number. This work was supported by United States Public Health Service through National Institutes of Health Grant No. 5R01-AM05853 and by National Science Foundation through Grant No. GB 7896.

(2) (a) S. Rajender, M. Han, and R. Lumry, *J. Amer. Chem. Soc.*, **92**, 1378 (1970); (b) S. Rajender, R. Lumry, and M. Han, *J. Phys. Chem.*, **75**, 1375 (1971).

(3) D. G. Doherty and F. Vaslow, *J. Amer. Chem. Soc.*, **74**, 951 (1952).

(4) F. Vaslow and D. G. Doherty, *ibid.*, **75**, 928 (1953).

($\Delta H_a^\circ + \Delta H_b^\circ$) and the total standard entropies of binding ($\Delta S_a^\circ + \Delta S_b^\circ$) produced by varying pH. Yapel and Lumry^{5,6} in extending these studies found that on varying pH this relationship was maintained at a high level of precision over large ranges of enthalpies and entropies of binding for indole, hydrocinnamate ion, and *N*-acetyl-L-tryptophan. For each of these inhibitors as well as *N*-acetyl-D-tryptophan the pH dependence of the total free energy of binding disappears at the T_c value appropriate to a given inhibitor. Furthermore, although these authors also found small differences in the "compensation temperature," T_c , with different substrate-analog inhibitors, to a good approximation, the quantitative differences in the standard free energies of binding among different inhibitors were very small when the experimental temperature was near 280°K. That is, at this temperature the components of the total enthalpy and entropy changes responsible for the linear relationship of eq 1, *i.e.*, ΔH_b° and ΔS_b° , nearly cancel each other in eq 3 to leave the standard free-energy changes in the binding processes essentially invariant with inhibitors structure.

$$\Delta H^\circ = \Delta H_a^\circ + \Delta H_b^\circ = \Delta H_a^\circ + \gamma + T_c \Delta S_b^\circ \quad (2a)$$

$$\Delta S^\circ = \Delta S_a^\circ + \Delta S_b^\circ \quad (2b)$$

$$\Delta G^\circ = \Delta H_a^\circ - T \Delta S_a^\circ + \Delta H_b^\circ - T \Delta S_b^\circ \quad (3)$$

This situation becomes more obvious if eq 1 is inserted into eq 2a and 3 to give eq 2a' and 6. Not only are the

$$\Delta H^\circ = \gamma + \Delta H_a^\circ - T_c \Delta S_a^\circ + T_c \Delta S^\circ \quad (2a')$$

$$\Delta G^\circ = \Delta H_a^\circ - T \Delta S_a^\circ + \frac{T}{T_c} \gamma + \Delta H_b^\circ \left(1 - \frac{T}{T_c}\right) \quad (6)$$

T_c values very nearly the same for the several inhibitors studied but $\Delta G^\circ(T = T_c)$ is identical for these inhibitors. We may thus speak of a *temperature of minimum specificity* or, more generally, *minimum sensitivity*, of about 280°K. For the sake of generality we shall use only the more general term, *temperature of minimum sensitivity*, *e.g.*, for CT, minimum sensitivity to inhibitor and substrate structure and minimum sensitivity of inhibitor binding to changes in pH. Minimum sensitivity behavior of both kinds has been reported for some other proteins (see Discussion) and may have broad implications since the phenomenon of linear enthalpy-entropy compensation with T_c values near 280° appears to be a ubiquitous consequence of the properties of liquid water.⁷ It thus becomes of interest to extend the studies of enthalpy-entropy compensation behavior found in inhibitor-binding processes to a typical catalytic process of α -chymotrypsin. In this paper we present those data which complete the grid of dependencies of the chymotryptic hydrolysis of ATEE on temperature, pH, substrate and alcohol concentrations, and begin to explore the different ways

in which data from the complete study appear to manifest linear enthalpy-entropy relationships.

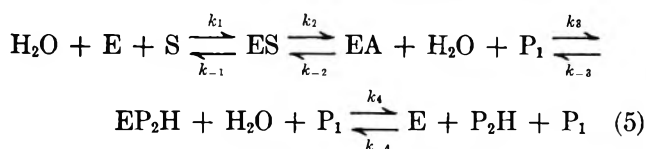
Results

Enthalpy and Entropy Changes for Single-Step Rate or Equilibrium Constants. In previous publications we have presented values for the phenomenological rate parameters α_0 , α_p , β_0 , and β_p and the associated enthalpy and entropy changes obtained from analysis of steady-state rate data for the hydrolysis of ATEE according to eq 4 which has been found to be accurate for all experimental values of pH, temperature, and concentration of first product, ethanol.

$$-\frac{dS}{dt} = V = \frac{E[S]}{\frac{1}{\alpha_0 + \alpha_p [P_1]_0} + \frac{1}{\beta_0 + \beta_p [P_1]_0}} \quad (4)$$

S = ATEE
P₁ = Ethanol

This equation is that for a catenary chain mechanism shown in eq 5 and has been repeatedly found to be



appropriate for the chymotryptic hydrolysis of "good" ester and amide substrates. As discussed in previous papers, since k_{-1} is several-fold greater than k_2 and by analogy k_4 is equally large with respect to k_{-3} , the errors in converting the phenomenological parameters into single-step rate constants are at the most less than a factor of 2 even at the highest experimental temperatures. Even a factor of 2 is within the errors in calculating the enthalpy and entropy changes corresponding to the constants $K_{ES} = k_{-1}/k_1$, $K_{EA} = k_{-1}k_{-2}/k_1k_2$, k_2 , k_{-2} , and k_3 . Since the overall thermodynamic changes for the process $\text{S} + \text{H}_2\text{O} = \text{P}_1 + \text{P}_2\text{H}$ are known or can be estimated within small errors it is also possible to estimate $k_{-3}k_{-4}/k_4$. Examination of the resulting values suggests that the reaction is symmetrical about the acyl-enzyme intermediate EA at all but our highest and lowest pH values. Bender, *et al.*,^{8,9} first demonstrated this symmetrical behavior at pH 8.¹⁰ It is possible to estimate k_{-3} and k_{-4}/k_4 on the assumption of symmetry but we shall not do so in this report since the symmetry begins to look illusory when we compare k_{-2} and k_3 and it is possible that important elementary

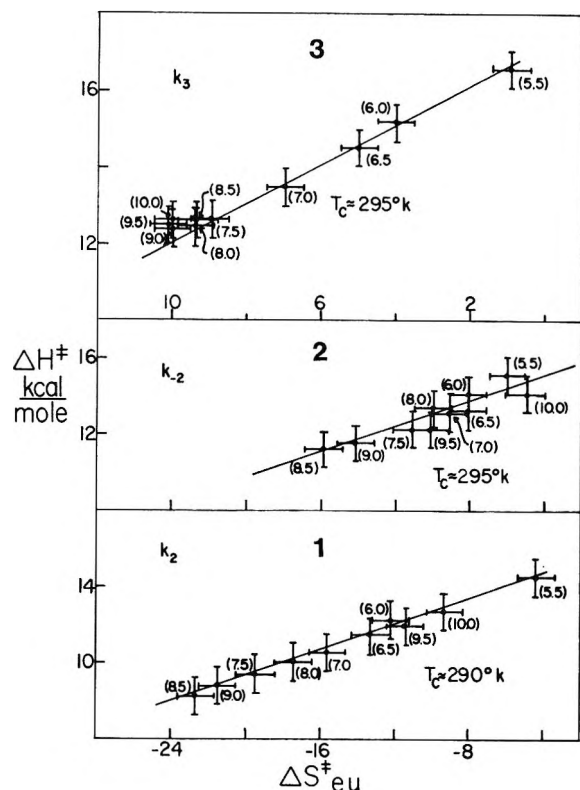
(5) A. Yapel and R. Lumry, *J. Amer. Chem. Soc.*, submitted for publication.

(6) A. Yapel, Ph.D. Thesis, University of Minnesota, Minneapolis, Minn., 1967.

(7) R. Lumry and S. Rajender, *Biopolymers*, **9**, 1125 (1970).

(8) M. L. Bender and F. J. Kezdy, *J. Amer. Chem. Soc.*, **86**, 3704 (1964).

(9) M. L. Bender, F. J. Kezdy, and C. R. Gunter, *ibid.*, **86**, 3714 (1964).



Figures 1-3. Compensation plots for the single-step rate constants k_2 , k_{-2} , and k_3 in the α -chymotryptic hydrolysis of ATEE. Numbers in parentheses indicate the pH. Note that ΔH^\ddagger and ΔS^\ddagger values change above pH 8.5 only for k_2 and k_{-2} but not for k_3 .

steps in the true mechanism are represented inadequately as single steps in the mechanism of eq 5.

Enthalpy and entropy changes for the other parameters are shown in Figures 1-4 which are "compensation plots" of ΔH vs. ΔS . Numerical values of ΔH and ΔS are also condensed in Table I. They form a comprehensive and perhaps unique collection of such information for a single-enzyme-substrate system.

Analysis of Thermodynamic Parameters for Compensation Behavior. Exner has criticized^{11,12} the conventional method of obtaining these thermodynamic quantities, *i.e.*, the enthalpy change from a van't Hoff or Arrhenius plot and the entropy change from a single free-energy change and the enthalpy change. On the other hand, the plotting procedure he proposes over-emphasizes experimental errors though it is certainly a more desirable way of manipulating the data. The best compromise appears to involve determination of ΔH by properly weighted least-squares analysis of a conventional van't Hoff or Arrhenius plot and the entropy change by an equally reliable statistical analysis of plots of $T \ln K$ vs. T or $T \ln k/T$ vs. T for equilibrium or rate parameters.¹³ Transforming weights, often large and frequently neglected, are of course necessary when fitting data to any linear form.¹⁴ This procedure, when applied to our phenomenological rate

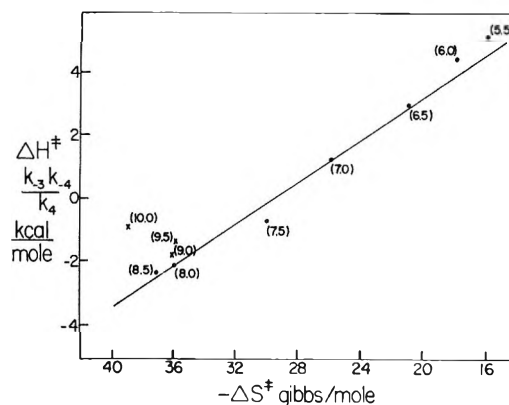


Figure 4. ΔH^\ddagger vs. ΔS^\ddagger plot for the complex rate constant $k_{-2}k_{-4}/k_4$ in the α -chymotryptic hydrolysis of ATEE. Different pH values are indicated in parentheses.

constants assuming negligible heat capacity changes gives, in general, good linear relationships between ΔH and ΔS . Although the propagation of errors in the computation of single-step rate constants increases the values of the estimated standard deviations and standard errors for these constants, the general trend of the corresponding ΔH - ΔS plots and the self-consistency observed in terms of the ordering of the ΔH - ΔS points along the compensation line establishes the existence of the compensation behavior^{15,16} (although not always its linear characteristic) as being a consequence of the properties of the system rather than due to errors of measurement.

As can be seen in Figures 1-4, the variation in the positions along the compensation line of the ΔH - ΔS points with changes in pH, in all cases except k_3 , demonstrates qualitatively the same pattern: a monotonic decrease to some characteristic pH near 8 followed by

(10) Here as in the previous papers the species ES, EA, and EP₂H are defined by the Hartley-Kilby mechanism, eq 5, and although we will follow common practice in assuming that they are first major Michaelis-Menten complex (no covalent bonding), acyl-enzyme species (covalent bond to protein), and major Michaelis-Menten complex for enzyme and second product, P₂H, respectively, much remains to be done to provide correct and detailed descriptions of the metastable intermediates and the rate-limiting steps k_2 and k_3 by which they interconvert. It is possible, for example, that ES is a tetrahedral carbon species and it is also possible that the mechanism and the important intermediates differ greatly from one type of a substrate to another. Hence many of the conclusions drawn with respect to ATEE may not carry over directly to amide, peptide or poor ester substrates, *e.g.*, ethylcinnamate.

(11) O. Exner, *Nature*, **201**, 488 (1964).

(12) O. Exner, *Collect. Czech. Chem. Commun.*, **29**, 1094 (1964).

(13) This procedure was first proposed to us by J. F. Brandts as an improvement over those discussed by Lumry and Rajender⁷ and does make maximum use of the data without introducing correlations in pairs of ΔH and ΔS values due to experimental errors. None of these procedures, however, properly takes into account curvature in van't Hoff and Arrhenius plots due to any significant heat capacity changes. However, by the use of two methods of analysis it is possible to show errors. See footnote to Table I.

(14) G. Johansen and R. Lumry, *C. R. Trav. Lab. Carlsberg*, **32**, (13) 185 (1961).

(15) J. E. Leffler, *Nature*, **205**, 1101 (1965).

(16) J. E. Leffler, *J. Org. Chem.*, **31**, 533 (1966).

Table I: Free Energies, Enthalpies, and Entropies of Activation at Different pH Values for the Single-Step Rate Constants k_2 , k_{-2} , and k_3 , and the Complex Constant $k_{-3}k_{-4}/k_4$ in the α -Chymotryptic Hydrolysis of ATEE.^a Free Energies and Entropies are Calculated for 25°

	pH									
	5.5	6.0	6.5	7.0	7.5	8.0	8.5	9.0	9.5	10.0
$\Delta F_{k_2}^\ddagger$, kcal/mol	15.76	15.36	14.76	14.62	14.60	14.42	14.43	14.58	14.74	15.19
$\Delta H_{k_2}^\ddagger$, kcal/mol	14.0	12.0	11.0	10.0	9.0	9.0	8.0	9.0	10.0	11.0
$\Delta S_{k_2}^\ddagger$, Gibbs/mol	-6	-11	-13	-16	-19	-18	-22	-19	-17	-13
$\Delta F_{k_{-2}}^\ddagger$	16.79	16.32	15.67	15.39	15.35	15.04	15.19	15.34	15.64	15.59
$\Delta H_{k_{-2}}^\ddagger$	16.0	14.0	13.0	12.8	12.5	13.0	10.5	11.0	12.0	14.0
$\Delta S_{k_{-2}}^\ddagger$	-3	-8	-9	-9	-10	-7	-16	-15	-11	-5
pH	5.5	6.0	6.5	7.0	7.5	8.0	8.5	9.0	9.5	10.0
$\Delta F_{k_3}^\ddagger$	16.80	16.38	15.83	15.48	15.40	15.21	15.21	15.19	15.20	15.20
$\Delta H_{k_3}^\ddagger$	16.5	15.0	14.0	13.0	12.5	12.0	12.3	11.8	12.1	12.0
$\Delta S_{k_3}^\ddagger$	-1	-5	-6	-8	-10	-11	-10	-11	-10	-11
$\Delta F_{k_{-3}k_{-4}/k_4}^\ddagger$, kcal/mol	10.14	9.91	9.44	9.18	9.04	8.95	9.07	9.23	9.79	10.74
$\Delta H_{k_{-3}k_{-4}/k_4}^\ddagger$, kcal/mol	5.2	4.4	3.0	1.2	-0.8	-2.1	-2.3	-1.8	-1.4	-1.1
$\Delta S_{k_{-3}k_{-4}/k_4}^\ddagger$, Gibbs/mol	-16	-18	-21	-26	-30	-36	-37	-36	-36	-39

^a All thermodynamic parameters have been obtained by a computerized, weighted least-squares analysis of the rate data, as mentioned in the preceding papers. ΔS values in particular were obtained by two different methods of analysis, one by the conventional way of getting the difference between ΔF and ΔH and the other by fitting the rate data to equations of the form $T \ln K$ vs. T or $T \ln k/T$ vs. T for equilibrium and rate data, respectively. ΔS values obtained by the two methods agreed within 2 entropy units, in the pH region from 5.5 to 9.0 for all the different rate constants. This agreement indicates that the heat capacities of activation and other sources of error (incorrect analysis, systematic errors) for these parameters are too small to be detected at our level of precision. At pH values higher than 9, the difference between the two sets of ΔS values differed by about 3 or 4 eu, which could be due to experimental errors in this region as pointed out in the text. However, for K_{ES} , the pH values for 7.5 and 8.0 the two sets of ΔS values differed by 4 to 5 eu. This is expected since the van't Hoff plots for this parameter at pH 7.5 and 8.0 were nonlinear. We have attributed this to a protein substate transition $A_b \rightarrow A_f$ (see text and the preceding paper). In these cases the $T \ln K_{ES}$ vs. T plots give average values of the entropy changes over the entire temperature range. Hence the ΔH and ΔS values reported for this equilibrium constant in Table I and also in compensation plots are those obtained for the lower temperature form of this enzyme from ΔH and ΔF and have been so designated. The choice does not affect the compensation plots nor the conclusions which have been drawn from the data since the nonlinearity of the van't Hoff plots is that of a sharp break over a small temperature interval.

an abrupt change in direction of motion of the ΔH - ΔS points and a monotonic increase beyond that point. The data at high pH values (above 9) are less precise due to autolysis of the enzyme and may also contain systematic errors associated with changes among substates of the protein, of which there are several in the higher pH region.^{17,18} The constant k_3 (Figure 3) appears to show only the lower pH segment of the compensation pattern. Detail in this pattern can be seen with an alternative compensation plot based on eq 3'. This type of plot emphasizes the sharpness of the "turn-around" behavior near pH 8 much more effectively as can be seen in Figures 5a and b. Although the errors in the compensation plot of k_{-2} are relatively large, there seems to be little doubt that the T_c values for the two linear segments of the plots for k_2 and k_{-2} are different though not greatly so. The pattern is qualitatively identical with that observed by Beetlestone and coworkers¹⁹⁻²³ in ligand-binding reactions of

mammalian ferri hemoglobins using a variety of species and a variety of ligands with the shift from one segment to the other taking place over a narrow pH interval (see Discussion).

The ΔF vs. ΔH plot for k_3 shows no turn around behavior as is also to be seen in Figure 3. Turn around behavior is perhaps suggested for $k_{-3}k_{-4}/k_4$ in Figure 4 but is certainly not established by the data now avail-

(17) R. Lumry and R. Biltonen in "Structure and Stability of Biological Macromolecules," Vol. II of "Biological Macromolecules," S. Timasheff and G. Fasman, Ed., Marcel Dekker, New York, N. Y., 1969, p 65.

(18) Y. D. Kim and R. Lumry, *J. Amer. Chem. Soc.*, in press.

(19) A. C. Anusiem, J. G. Beetlestone, and D. Irvine, *J. Chem. Soc. A*, 357 (1966).

(20) J. G. Beetlestone, D. H. Irvine, *ibid.*, 951 (1968).

(21) A. C. Anusiem, J. G. Beetlestone, and D. H. Irvine, *ibid.*, 960 (1968).

(22) J. G. Beetlestone and D. H. Irvine, *ibid.*, 735 (1969).

(23) J. Beetlestone and D. Irvine, *Proc. Roy. Soc.*, 277, 414 (1964).

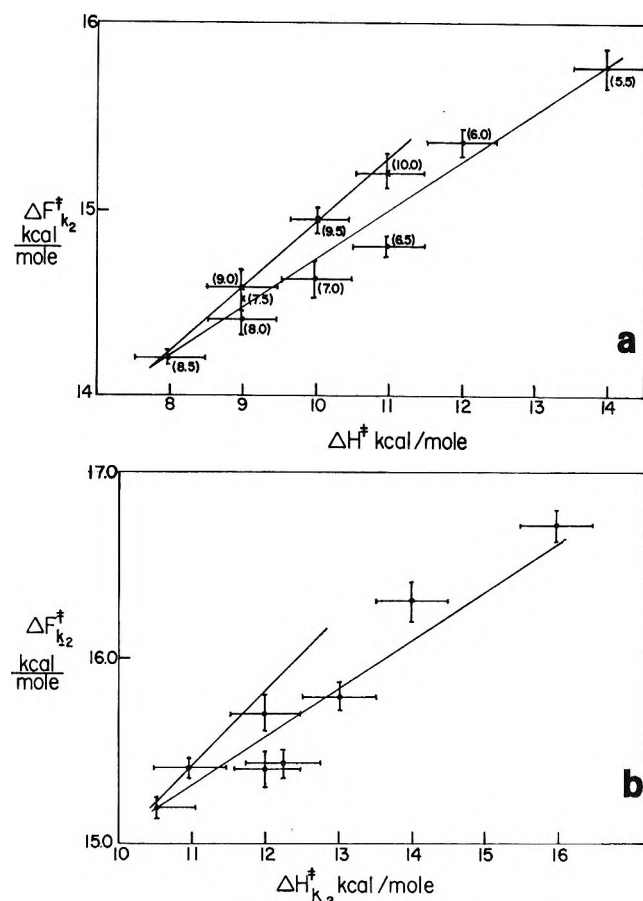


Figure 5. (a) ΔF^\ddagger vs. ΔH^\ddagger plot for k_2 , the on-acylation rate constant. (b) ΔF^\ddagger vs. ΔH^\ddagger plot for k_{-2} , the off-acylation rate constant. This type of plot demonstrates "turn-around" behavior more clearly. Numbers in parentheses indicate pH values. Errors shown are one standard deviation on either side of mean.

able. The value of T_c is also considerably higher and the linearity of the fit somewhat less than convincing though the presence of compensation below pH 8.5 is unmistakable. It must also be remembered that in computing $k_{-3}k_{-4}/k_4$, there is an error of ± 1 kcal introduced in ΔG° and ΔH° for the overall reaction so that the errors in the parameter itself can be as large as a factor of 7.

The compensation plots for the two "metastable intermediates" ES and EA (Figures 6 and 7) are very nearly identical, that for EA being displaced by about 0.5 kcal vertically with respect to a single compensation line for ES. All these lines parallel within error the compensation line found by Yapel and Lumry⁵ for binding of the competitive inhibitor indole and are displaced from it by less than 1 kcal. It will be noticed that the ΔH - ΔS points for pH 7.5 do not follow the pattern of consistent change with pH manifested by the points for the other pH values. The inversion of order of the pH 7.5 and 8.0 points appears to be real and can be tentatively attributed to the substrate transition $A_b \leftrightarrow A_f$ discussed in earlier papers^{2a,b,18} as will be explained below.

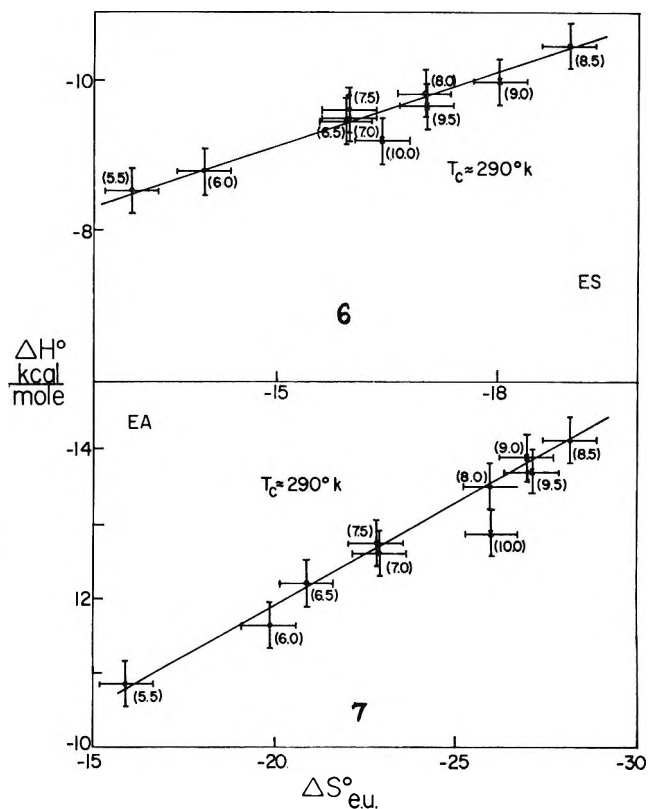


Figure 6. Compensation plot for the metastable intermediate ES. pH values are shown in parentheses.

Figure 7. Compensation plot for the acyl-enzyme intermediate EA at different pH values (shown in parentheses).

"Turn-around" behavior can be seen but is not as obvious as in Figures 5a and b.

The data are uniformly consistent with the existence of enthalpy-entropy compensation behavior in all the single-step rate or equilibrium constants and in general suggest linear behavior possibly with a common basis since the T_c values all fall within a rather narrow temperature interval. It is now necessary to establish insofar as possible with the data available whether the compensation pattern is characteristic of the free enzyme, the metastable intermediates, the activated complexes, or some combination. As pH is varied, the points for ES and EA move in phase along their compensation plots. That is, the ratio of their changes in ΔH° , $(\Delta\Delta H^\circ_{K_{ES}}/\Delta\Delta H^\circ_{K_{EA}})$, and ΔS° , $(\Delta\Delta S^\circ_{K_{ES}}/\Delta\Delta S^\circ_{K_{EA}})$ are constant. The ΔH - ΔS points for EA move twice as much for the same change in pH as do the ES points but the ordering of the points for the two relative to each other remains unchanged. This observation suggests that the pH dependence of the compensation pattern lies primarily in the free enzyme. This possibility is not vitiated by the solubility characteristics of the free substrate or their pH dependence. Rajender and Lumry²⁴ have studied the standard enthalpy and entropy of transfer of ATEE

(24) S. Rajender and R. Lumry, 160th National Meeting of the American Chemical Society, Los Angeles, Calif., March 1971.

from several weakly polar organic solvent mixtures and octanol to water. This transfer process shows small negative enthalpy changes and the entropy changes are large and negative as is consistent with the standard pattern of hydrophobic solvation. Insofar as the transfer process simulates substrate binding (*vide infra*) or binding of ATEE to chymotrypsin we would expect positive enthalpy and entropy contributions from the desolvation of the substrate, that is, from the "hydrophobic binding" of the substrate to the enzyme, if that were the predominant process in ES formation etc. However, an inspection of the thermodynamic quantities for the formation of the two metastable intermediates demonstrates that these "hydrophobic" contributions are heavily overbalanced by the negative contributions from some other part process in the formation of ES, EA, and EP₂H so that the overall enthalpies and entropies of formation of these complexes are negative. Furthermore, the hydrophobic bonding contributions to enthalpy and entropy change should be pH independent in which case they should not demonstrate compensation behavior with pH variation and would be expected to appear in the contribution from the compensation-free part process (*cf.* eq 9).

Substates of α -CT and Related Information of Potential Importance. Studies of CT by optical rotation methods²⁵⁻²⁷ show at lower salt concentrations a continuous production of the catalytically active species A_b and A_f from the inactive species A_a over the pH range from about 3 to 8.5 where an extremum occurs. At higher pH values the catalytically active species are converted reversibly into inactive substate species. It has been shown using fluorescence that there are a number of substates at higher pH values.¹³ The conversion of A_a as measured by ORD is strongly dependent on salt concentrations. At low salt concentrations the conversion occurs over at least 5 pH units and thus is a complicated consequence of multiple ionization processes. The total molar rotation change at 202 nm is about 10⁶ deg and is closely related to substrate and inhibitor binding. However, at the higher salt concentrations used in our work the conversion of A_a as studied by Parker^{25,26} and by Hess and their respective coworkers^{27,28} appears to be a simple first-order process with an apparent pK_a between 2.5 and 3. The latter observations suggest that the fraction of CT in substate A_a in our experiments was always very small. Nevertheless there is a considerable similarity between the ORD pattern obtained as a function of pH at low salt concentrations and the pH dependence of the enthalpies and entropies of formation of the intermediates ES and EA shown in Figure 8a and b and the ΔH^\ddagger and ΔS^\ddagger values for k_2 and k_{-2} though not k_3 (see Figures 9-11). The points in these figures were calculated from the phenomenological parameters with considerable care in error estimation and there is no reason at the present time to simplify the curves. It is thus

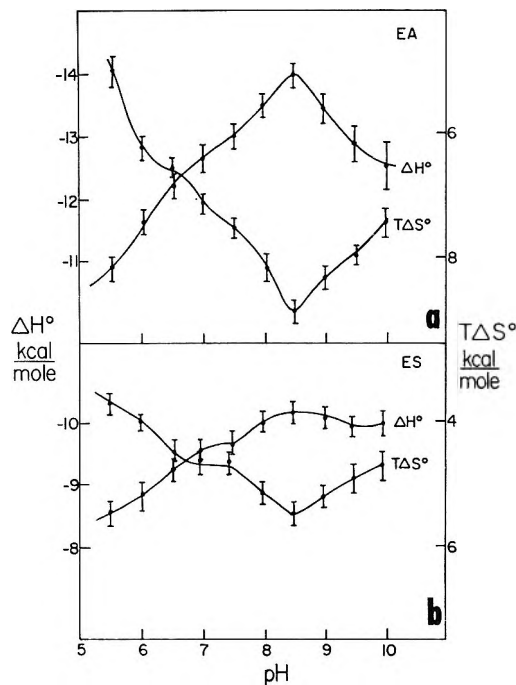


Figure 8. Plots of ΔH° and $T\Delta S^\circ$ as a function of pH for the metastable intermediates ES and EA in the α -chymotryptic hydrolysis of ATEE. EP₂ follows the same pattern.

necessary to accept the possibility that the pH dependence is as complicated as shown in these figures and also to retain an open mind about the proportions of the various substates of CT which were present in our experiments at different pH values. As already mentioned^{2a,b} there are two catalytically active substates, A_b and A_f, in equilibrium between pH 7 and 9 so that some unusual pH dependence is to be expected in this region. Other substates may account for the peculiarities of the curves at higher pH values.

Additional Analysis through pH Dependence. As shown in Figures 6 and 7 the enthalpies and entropies of formation of EA and ES tend to compensate each other when pH is varied and compensation is linear at least at pH 8 and below. The pH dependence of ΔH° and ΔS° for the formation of ES and EA from E + S shows that these intermediates cannot be formed unless some set of acid groups is converted to base form. The pH dependence is that of the free enzyme E since the changes in ΔH° for ES and EA shown in Figure 8a and b are very similar in form even though the changes are considerably larger for EA than for ES.

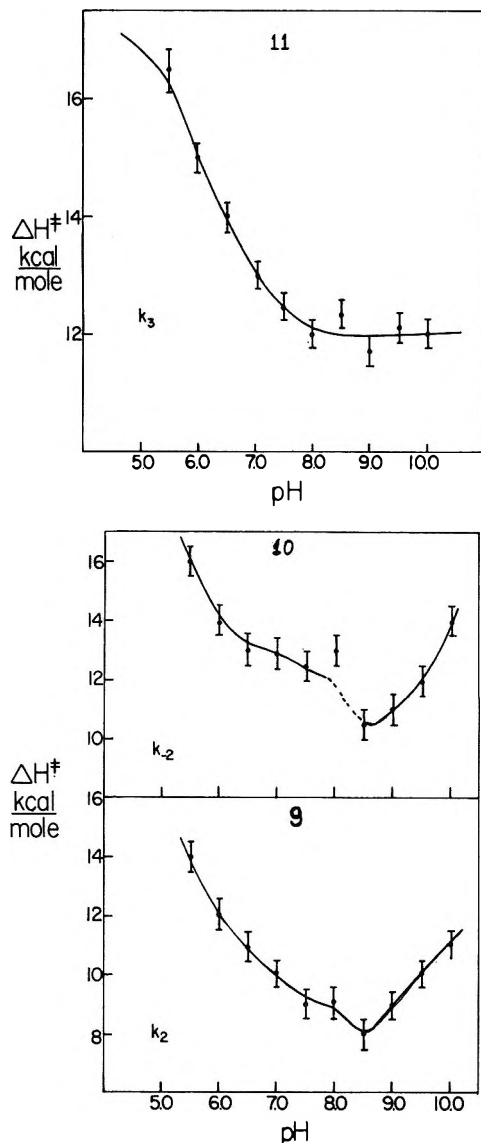
It is noteworthy that the involvement of these acid groups which prevent formation of ES and EA can

(25) H. Parker, Ph.D. Thesis, University of Minnesota, Minneapolis, Minn., 1967.

(26) H. Parker and R. Lumry, *J. Amer. Chem. Soc.*, **85**, 483 (1963).

(27) B. Havsteen and G. P. Hess, *ibid.*, **85**, 791 (1963).

(28) G. P. Hess, *Brookhaven Symp. Quant. Biol.*, **22**, 1 (1968); H. L. Oppenheimer, B. Labouesse, and G. P. Hess, *J. Biol. Chem.*, **241**, 2720 (1966).



Figures 9-11. ΔH^\ddagger vs. pH for the single-step rate constants k_2 , k_{-2} , and k_3 . Errors shown are one standard deviation.

and apparently has escaped detection because the previous experiments were carried out at temperatures at which compensation is nearly exact relative to experimental errors. As a result, the free energies were insensitive to pH variation. The presence of compensation has produced the same type of omission in inhibitor-binding studies as will be discussed below.

The arguments just given indicate that a major part of the compensation behavior demonstrated below pH 8 in the formation of ES and EA is attributable to the pH dependence of the free enzyme E.

The free enzyme is not a participant in the k_2 or k_3 processes so that the compensation behavior shown by k_2 , k_{-2} , and k_3 is controlled either by an intrinsic dependence of these constants on some or all of the same acid groups or different acid groups must be involved. It has been repeatedly reported that V_{\max} for good ester substrates of CT observed under the condition

of zero P_1 concentration has a pH dependence characteristic of an imidazolium group. Since V_{\max} for ATEE under these circumstances is dominated by k_3 , our determination of k_3 should show this behavior and, as shown in Figure 11, this is the case at least over most of the experimental pH range. The failure of the system to approach a low pH plateau at pH 5.5 may be a result of experimental errors, failure of our analysis of the β_0 parameter, or a real effect. We have shown in the previous paper^{2b} that our phenomenological parameters suggest the existence of an additional acid group which begins to appear in some of the parameters around pH 6.

The problem presented by Figures 9 and 10 is more serious. If our assignment of the peculiar pattern of Figures 8a and b primarily to E is correct, the patterns shown in Figures 9 and 10 although quite similar must be attributed to ES^\ddagger and although the ionization of an imidazolium group can be part of the observed complexity, it is certainly only one group considerably overshadowed by other effects of pH. Furthermore, the patterns for k_{-2} and k_3 are quite different, showing that the process is less symmetric than was previously suggested. In the preceding paper we analyzed only the phenomenological parameters as functions of pH and temperature and, following customary procedures, forced the fitting to conventional titration curves and conventional straight-line Arrhenius plots. Of course this procedure produced a relatively simple and conventional description of the reaction. In this paper we have converted the phenomenological parameters to close estimates of the single-step constants and ratios for many constant temperatures and have then analyzed the temperature dependence of each resulting rate or equilibrium constant. The temperature and particularly the pH dependence of the computed constants are notably different than the previous force-fit values. This is to be expected for the more complex phenomenological parameters but the model used for force fitting was clearly inadequate. Even if our mechanism is still incomplete due to the substate complexity of the protein or because we have not provided enough steps in the catenary chain to approximate the true situation, the pH dependence of the enthalpy change associated with none of the computed constants except perhaps k_3 is simple. Those for $\Delta H_{k_2}^\ddagger$ and $\Delta H_{k_{-2}}^\ddagger$ resemble each other closely and are also similar to those for $\Delta H^\circ_{K_{ES}}$ and $\Delta H^\circ_{K_{EA}}$ but the former appear to reflect the behavior of ES^\ddagger and the latter primarily the behavior of E.

Analysis of Compensation Behavior for k_3 . If $\Delta H_{k_3}^\ddagger$ varies as a result of the deprotonation of a single imidazolium group, the existence of linear compensation for k_3 may be trivial insofar as it is an immediate consequence of the shift in equilibrium populations of protonated and deprotonated forms of this group. If the ionization process is labeled d with standard enthalpy

and entropy of ionization ΔH_d° and ΔS_d° , and the formation of the activated complex from the deprotonated species, either ES or EA, is labeled c with ΔH_c^\ddagger and ΔS_c^\ddagger , the observed enthalpy of activation is given by eq 7a and the corresponding entropy by eq 7b. The fraction of protonated ES or EA is f . Eliminating f yields the linear compensation expression, eq 8, and defines T_c as the ratio $\Delta H_d^\circ/\Delta S_d^\circ$. The latter ratio is about 295°K. This value is not a reasonable value for imidazole or small imidazole compounds ($\Delta H_d^\circ \approx 8$ kcal/mol, $\Delta S_d^\circ \approx -2$ eu/mol if $pK_a = 6$) but may be correct for this protein-bound imidazole group. The ratio can be only weakly dependent on temperature if linear compensation is to be observed over a significant temperature range.

$$\Delta H^\ddagger = \Delta H_c^\ddagger + f\Delta H_d^\circ \quad (7a)$$

$$\Delta S^\ddagger = \Delta S_c^\ddagger + f\Delta S_d^\circ \quad (7b)$$

$$\Delta H^\ddagger = \Delta H_c^\ddagger - \left(\frac{\Delta H_d^\circ}{\Delta S_d^\circ}\right)\Delta S_c^\ddagger + \left(\frac{\Delta H_d^\circ}{\Delta S_d^\circ}\right)\Delta S^\ddagger \quad (8)$$

Application of a similar argument to the processes $E + S \leftrightarrow ES$, $E + S \leftrightarrow EA$, $ES \leftrightarrow ES^\ddagger$, and $EA \rightarrow ES^\ddagger$ is complicated by the participation of more than one acid group. When more than two species of E, ES, etc. have to be taken into account, the linear form of eq 8 can be preserved only by rare accident unless the groups ionized cooperatively so that there are effectively only two forms of each of these species. The acid groups responsible for the variation of enthalpy and entropy changes associated with K_{ES} , K_{EA} , k_2 , and k_{-2} remain to be accounted for and assigned. It is probable that this cannot be done reliably without data of considerably higher precision, a formidable experimental undertaking, but experiments of other types calculated to reveal inadequacies in our assumed mechanism and errors in the conversion of the phenomenological parameters into rate constants are also necessary. Such improvements are unlikely to simplify the picture but they will make it possible to describe in more detail the underlying complexity demonstrated by our findings.

The ionizing groups responsible for the upper pH part of the compensation pattern may be related to the ion pair seen in X-ray diffraction models. Considerable evidence²⁹⁻³¹ has been presented particularly for δ -CT³²⁻³⁴ to suggest that the pH dependence of the phenomenological parameter K_m obtained at zero P_1 concentration and which for ATEE + α -CT is equal to $(k_{-1}k_3/k_1k_2)$ is due to the disruption of the ILE 16 α -ammonium and ASP 194 carboxylate with an effective pK_a value near 9.³⁵⁻³⁷ However, according to Martin and Marini³² there are reasons to doubt this interpretation. Kim and Lumry¹⁸ have shown that there are two rather than one acid groups involved in the several substrate transitions of free α -CT in the alkaline region

and little can be gained by attempting to make assignments of the acid groups involved in compensation behavior. Much work remains to be done in these several areas.

Discussion

The presence of compensation phenomena greatly complicates the analysis of equilibrium and kinetics data and their interpretation. Conventional kinetics studies do not afford any means for separating the experimental enthalpy and entropy changes into contributions from the part processes manifesting compensation behavior and those that do not. In short, total enthalpy and entropy changes cannot be used to give reliable chemical information until ways are devised to separate them into part contributions from the various processes that make up the overall reaction. Rate and equilibrium data obtained at temperatures near T_c can often be misleading as a result of a minimization of the free-energy change due to the compensation part process as we have already shown.

Source of Compensation Behavior. Despite the ubiquitous appearance of similar enthalpy-entropy compensation behavior in the α -CT + ATEE system, it is not necessary to conclude that all manifestations of this behavior are due to a single common source. There are several possible sources. Electrostatic theories usually predict a roughly linear relationship between enthalpy change and entropy change with change in charge number and distribution and with some variations in solvent composition. King³⁸ has discussed these matters and calculates a value for the ratio $\Delta H/\Delta S$ in water systems to be about 80°K although he notes that it is usually found in experiment to be near room temperature. Beutlestone and Irvine²³ have considered the behavior of $\Delta H^\circ/\Delta S^\circ$ for the human ferri hemoglobins A, S, and C at constant pH. ΔH° and ΔS° are predicted to be linearly related on strictly electrostatic grounds if the dielectric constant of the medium and its partial derivative with respect to temperature are constant. Their estimated T_c for the charged groups of the proteins on this basis is about

(29) D. M. Blow, J. Birkoft, and B. S. Hartley, *Nature*, **221**, 337 (1969).

(30) T. A. Steitz, R. Henderson, and D. M. Blow, *J. Mol. Biol.*, **46**, 337 (1969).

(31) D. M. Blow, *Biochem. J.*, **112**, 261 (1969).

(32) C. Martin and M. Marini, *Eur. J. Biochem.*, in press.

(33) P. Valenzuela and M. L. Bender, *Biochemistry*, **9**, 2440 (1970).

(34) F. C. Wedler and M. L. Bender, *J. Amer. Chem. Soc.*, **91**, 3894 (1969).

(35) A. Y. Moon, J. M. Sturtevant, and G. P. Hess, *J. Biol. Chem.*, **240**, 4204 (1965).

(36) D. Karibian, C. Laurent, J. Labouesse, and B. Labouesse, *Eur. J. Biochem.*, **5**, 260 (1968).

(37) J. Garel and B. Labouesse, *J. Mol. Biol.*, **47**, 41 (1970).

(38) E. J. King, "Acid-Base Equilibria," "The International Encyclopedia of Physical Chemistry and Chemical Physics," Topic 15, "Equilibrium Properties of Electrolyte Solutions," Vol. 4, Pergamon Press, New York, N. Y., 1965.

335°K. However, these authors, in subsequent studies^{20,21} found that electrostatic arguments are inadequate to account for the behavior of their ferri hemoglobin systems with changes in pH, particularly in the region of the isoelectric point. A more complete electrostatic theory may ultimately provide better consistency and as matters now stand a strictly electrostatic basis for compensation behavior cannot be ruled out for the α -CT-ATEE system.

Turning now to the protein, it is reasonable to expect that changes in the protein conformation, whether they are outright changes in the amount of folding, simpler expansion-contraction processes, or many small atom displacements, can produce enthalpy and entropy changes of the same sign which furthermore might provide a linear relationship between these two quantities if the changes are sufficiently small.

Finally, the accumulation of examples of small-solute as well as protein processes in water solutions which manifest a linear enthalpy-entropy compensation pattern and appear to be attributable to liquid water itself⁷ introduces the strong possibility that liquid water is responsible for some or all of the compensation behavior observed with our system. We shall examine these alternatives in greater detail to see if one or a combination of these can account for the observed behavior.

Among the compensation patterns demonstrated by our system, the simplest appears to be that associated with the formation of the activated complex for deacylation of the protein by the acid moiety of the substrate, k_3 , in the pH region below 8. This pattern is roughly consistent with the ionization of the imidazolium group of HIS 57 and thus appears to be a consequence of electrostatic considerations involving only this group and its environment. However, eq 8 which describes this situation may be more complex than it appears. It has been found in many studies of the ionization of congener or homologous families of weak organic acids³⁹⁻⁴² that the electronic contributions to the total ΔH° and ΔS° are quantitatively in accord with variations in the appropriate Hammett and Taft σ and σ^* parameters. The nonelectronic contributions, attributed primarily to variations in solvation with substitution of the parent member of a series, yield an expression of the form (*cf.* eq 1, *et seq.*)

$$\Delta H_{\text{sol}}^\circ = \gamma + T_c \Delta S_{\text{sol}}^\circ \quad (9)$$

with small values for γ and T_c values near 285°K. It has been proposed elsewhere⁷ that this linear relationship is due to changes in solvation water at some distance from the acid and its ion products. Thus if eq 8 is applicable for the ATEE-CT system, the fact that $(\Delta H_d^\circ / \Delta S_d^\circ)$ in the equation is found near 285°K may be coincidental or it may also be due to participation of the same property of liquid water apparently responsible for compensation behavior in the weak-acid sys-

tems. If it is the latter, some or all of the compensation behavior observed with the ATEE-CT system, although certainly dependent on changes in the state of ionization of a few acid groups which play a central role in the catalytic scheme and on other properties of the system, also must be in some way connected with the properties of liquid water itself. Subsequent sections of the discussion will be found to support this possibility.

The compensation patterns which are observed with k_{-2} , k_2 , and K_{ES} and perhaps with K_{EA} and $(k_{-3}k_{-4}/k_4)$ exhibit turn-around behavior at about pH 8.5. The sharpness of the turn-around point as clearly seen in Figures 5a and b suggests a higher than first-order dependence on hydrogen-ion activity. As will be discussed, the turn-around behavior observed by Beetlestone, *et al.*,¹⁹⁻²³ in ligand binding to ferrihemoglobins is completed over a fraction of a pH unit so that a number of protons must be involved in the compensation behavior studied by these workers. More precise determination of the turn-around pH, called "characteristic pH" by Beetlestone, *et al.*, is made difficult by the occurrence of the $A_b \rightarrow A_f$ transition. Turn-around behavior may be a direct consequence of this transition if substate A_b predominates at pH 8.0 and below and substate A_f is the predominant species at pH 8.5 and above. That is, the lower pH segment of the compensation behavior may be attributable to A_b and the higher-pH segment to A_f . However, the relationship of these substates to each other and to the substates found at still higher pH values by Kim and Lumry^{17,18} and by Yapel⁶ argue against this relatively simple assignment and further discussion is not useful until the transitions among the various substates are better understood and their relationship to the elementary steps of the catalytic process better established.

The Loss of Specificity. Although there are clear indications that a few ionizable groups of CT play specific roles in most and perhaps all of the compensation patterns observed with the ATEE + CT system, there has also accumulated evidence that other factors are involved. Thus far in this report the similarity of the values of T_c for the different compensation patterns and the fact that these values lie close together in the range in which T_c values for linear enthalpy-entropy compensation behavior in small-solute systems in highly aqueous solvents are almost universally found are the major indications that compensation behavior in our system may be closely related to the more general water-based phenomenon already mentioned. We shall not discuss this possibility in any more detail but

(39) D. I. G. Ives and P. D. Marsden, *J. Chem. Soc.*, 649 (1965).

(40) W. G. O'Hara and L. G. Hepler, *J. Phys. Chem.*, 65, 2107 (1961).

(41) R. M. Izatt, D. Eatough, and J. Christensen, *ibid.*, 72, 2720 (1968).

(42) J. Konicek and I. Wadsö, *Acta Chem. Scand.*, in press.

it is necessary to present evidence from CT studies and from studies of other proteins to illustrate the possible significance and the utility of compensation behavior in protein study. For this undertaking it is useful to introduce a new concept which we call the "temperature of minimum sensitivity." By this we mean that there exists for protein systems a small range of experimental temperatures in which the sensitivity, as measured by rate constants, ratios of rate constants, or their corresponding free energy changes, with respect to one or more important variables of the system is minimal. The term sensitivity can often be used very broadly and the temperatures of minimum sensitivity for the protein systems for which the values are available are very similar. Sensitivity may mean the ability of an enzyme to make quantitative selections in binding and bond-rearrangement steps among members of a related family of substrates, or it may mean the ability of a protein to distinguish among inhibitors, *e.g.*, the ability of ferrihemoglobin, chymotrypsin, acetylcholinesterase, etc. to make quantitative distinctions among ligands or substrate-analog inhibitors. Alternatively the term may be applied to the response of the kinetics or equilibrium constants to salt concentration and type or to pH. And finally we shall also apply it to the quantitative differences in a given type of process when a particular protein with the same physiological function is isolated from a number of different organisms.

Other Examples of a Temperature of Minimum Sensitivity. The possible existence of a temperature of minimum sensitivity with respect to inhibitor structure is implicit in the studies of Belleau, *et al.*,⁴³⁻⁴⁵ on acetylcholinesterase and with respect to inhibitor binding as well as enzyme behavior in the discussions of Likhstenshtein^{46,47} on linear compensation. The concept is clearly demonstrated in Yapel's studies of inhibition of CT using indole, *N*-acetyl-L- and D-tryptophan, and hydrocinnamate ion.^{5,6} This set of studies is important for three reasons. The first of these is the demonstration that precisely linear compensation lines for the standard enthalpies and entropies of binding are produced by pH variation and that the changes produced in both quantities by pH variation can be quite large; *e.g.*, over the pH range 7-8 for *N*-acetyl-L-tryptophan ΔH° varies by 17 kcal and ΔS° by 63 eu. Calorimetric studies of the binding of these inhibitors to CT at a constant pH of 7.8 by Shiao and Sturtevant⁴⁸ and by Shiao⁴⁹ produced somewhat smaller values of ΔH° and ΔS° , possibly as a result of complications introduced by the need to correct for aggregation of the protein, but they confirm the existence of linear compensation behavior with a T_c in the 278-300° range. Yapel's compensation lines obtained by pH variation for his inhibitors except indole are nearly superimposable with an average T_c value of 270°K. His indole line is equally precise and has the same intercept at $\Delta S^\circ = 0$ but has a significantly different slope, $T_c = 285^\circ\text{K}$.

Hence the second conclusion from Yapel's work is that apart from these small quantitative differences in T_c which are not yet understood, a single compensation line is roughly adequate for all his inhibitors at all the pH values he examined. As a consequence, if the experimental temperature is near 280°K the variations in the standard free energies of binding for different inhibitors are very small despite the large changes in ΔH° and ΔS° obtained under these experimental conditions. Thus there exists a temperature of minimum sensitivity for CT with respect to the affinity for inhibitors at least those studied by Yapel^{5,6} and by Shiao.^{48,49} Furthermore, this temperature of minimum sensitivity is independent of experimental pH. In other words, the specificity with respect to the pH dependence is also minimized at the same temperature.

The temperature of minimum sensitivity is, of course, equal to the compensation temperature but is a conceptual rather than an experimental quantity, an observation which should be kept in mind during the remainder of this discussion.

Belleau and Lavoie⁴³⁻⁴⁵ have shown that in the binding of about 30 ligands of the tetramethylammonium ion series to acetylcholinesterase, the free energy of binding is constant within 0.5 kcal, whereas the enthalpies and entropies of binding undergo large fluctuations which compensate each other with a $T_c \approx 288^\circ\text{K}$.

The most fully developed experimental demonstrations of the temperature of minimum sensitivity are those of Beetlestone and Irvine and their collaborators.^{19-23,50,51} Their observations in studies of ligand-binding by ferrihemoglobins are represented below.

1. The standard enthalpies and entropies of binding of the ligands F^- , CN^- , N_3^- , SH^- , and methylamine are pH dependent so as to yield linear compensation patterns with turn-around behavior ("characteristic pH behavior") very similar to that demonstrated in the present study. The T_c values are nearly the same for the different ligands and fall in the range found with all the CT systems. At sufficiently high concentrations of salt, the descending and ascending segments of the compensation line have the same T_c value for a given ligand. Thus with respect to pH variation there is a

(43) B. Belleau and J. Lavoie, *Can. J. Chem.*, **46**, 1397 (1968).

(44) B. Belleau, *Ann. N. Y. Acad. Sci.*, **144**, 705 (1967).

(45) B. Belleau and V. DiTullio, *J. Amer. Chem. Soc.*, **92**, 6320 (1970).

(46) G. I. Likhstenshtein, *Biofizika*, **11**, 23 (1966).

(47) G. I. Likhstenshtein, "Water in Biological Systems," I. Kayushin, Ed., Consultants Bureau, New York, N. Y., 1969.

(48) D. D-F. Shiao and J. M. Sturtevant, *Biochemistry*, **8**, 4910 (1969).

(49) D. D-F. Shiao, *ibid.*, **9**, 1083 (1970).

(50) A. C. Anusiem, J. A. Beetlestone, and D. H. Irvine, *J. Chem. Soc. A*, 1337 (1968).

(51) J. E. Bailey, J. A. Beetlestone, D. H. Irvine, and A. Ogunmola, *ibid.*, 749 (1970).

temperature of minimum sensitivity which is very nearly the same, about 290°K, for all the ligands studied.

2. The dependence of the thermodynamic quantities on sodium chloride concentration at fixed pH values has been investigated for the binding of hydroxyl ion to heme iron. Examination of their data shows that the same compensation line is obtained at constant pH with varying salt concentration as is obtained at constant salt concentration with varying pH. The T_c value is about 290°K. There is thus a temperature of minimum sensitivity with respect to variation in sodium chloride concentration.

3. The binding of hydroxyl ion to the ferric iron ion of ferrimethemoglobin ("alkaline methemoglobin formation") has associated with it variations in ΔH° of about 10 kcal/mol of heme for the 30 ferrihemoglobin species investigated, yet the $\Delta H^\circ - \Delta S^\circ$ values fall with good precision on a single compensation line with at T_c value of 300°K. Recently, the binding of F^- , methylamine, N_3^- , CN^- , and SH^- has also been studied as a function of species variation of ferri hemoglobin. All yield linear compensation behavior with very similar T_c values. Thus there exists a temperature of minimum sensitivity with respect to species variation. In this connection their data show that all or nearly all charged groups of these proteins play a quantitative role in compensation behavior. Substitution of even a single group at a considerable distance from the heme iron group, *e.g.*, from glutamic acid in human Hb A, to valine in Hb C and to lysine in Hb S, produces large changes in ΔH° and ΔS° though the changes in ΔG° are negligible if the experimental temperature is near T_c .

In contrast to the situation encountered in inhibitor binding by CT, the compensation lines for CN^- , F^- , N_3^- , and SCN^- obtained by pH variation are not superimposable but rather lie very nearly parallel. The ΔH° intercepts are all different so that there does not exist a temperature of minimum sensitivity with respect to the binding of ligands. This difference in minimum sensitivity behavior is perhaps not surprising. We can explore the situation by following Hepler and Ives and their respective coworkers.³⁹⁻⁴¹ We divide the total binding process into part processes using the simple device introduced at the end of the Results section. ΔH_a° is due to desolvation of CT substrate, ligand, or CT inhibitor plus the electronic features of the total binding process not associated with the source of compensation behavior. ΔH_b° is contributed by the part process responsible for compensation behavior. So also for ΔS_a° and ΔS_b° . Then if $\Delta H_b^\circ = \gamma + T_c \Delta S_b^\circ$, by elimination of ΔH_b° and ΔS_b° from eq 2a and b, eq 10 results.

$$\Delta H^\circ = (\gamma + \Delta H_a^\circ - T_c \Delta S_a^\circ) + T_c \Delta S^\circ \quad (10)$$

The ordinate intercepts of the compensation lines, $(\gamma + \Delta H_a^\circ - T_c \Delta S_a^\circ)$, should vary strongly with

ligand in the ferrihemoglobin studies as indeed they do. On the other hand, the intercept variation need not be very large for the inhibitors studied by Yapel^{5,6} and Shiao.^{48,49} If the water-to-octanol transfer process is an appropriate model for the "hydrophobic-bonding" part of the enzyme-substrate or enzyme-inhibitor combination, partitioning studies²⁴ show that the contribution to ΔH° from this transfer process is small so that variations with inhibitors and substrates are too small to be detected within our errors. The entropy changes are also small since the positive entropy of transfer from water to octanol (a unitary quantity) must be offset almost completely by the negative entropic entropy change and the entropy reduction due to restrictions on rotational and side-chain motion resulting from the union. Furthermore, additional enthalpy-entropy compensation with respect to solubility in water is to be expected among substrates and inhibitors and this will tend to reduce the variations in $\Delta H_a^\circ - T_c \Delta S_a^\circ$. Apparently the remaining aspects of the part-processes we have labeled a, whatever they may be, do not vary much from inhibitor to inhibitor in Yapel's group.

Since we have no models to estimate the contribution from water molecules displaced from the protein binding regions into bulk water, it is not possible to rationalize this situation but the fact is that the variations in the ordinate intercepts are very small for the CT systems which have been studied.

Possible Existence of a Temperature of Minimum Sensitivity in Chymotryptic Catalysis. The small variation in ordinate intercept with variation in inhibitors for CT seems to show up in substrates as well. In Figure 12 are plotted the enthalpy and entropy changes corresponding to K_m for several substrates as well as the activation enthalpies and entropies corresponding to the maximum velocity V_m . The data, collected from the literature, are very spotty. If the mechanism of chymotryptic catalysis is the same for all these substrates in the sense that the significant metastable intermediates and the activated complexes occur at the same positions along the total reaction coordinate, then the compensation lines shown in this figure are reasonable and should also be found to be appropriate for other CT substrates still to be studied provided they belong to this same class. Some of the data were obtained in relatively high alcohol concentrations and since alcohols are not only cosolvents but also act as nucleophiles in the deacylation process, there is considerable uncertainty in adding them to the collection. Nevertheless, both K_m and V_m data are fit reasonably well by single lines in Figure 12 and the lines have T_c values in the range established by the other studies. Hence the figure does suggest that there is a temperature of minimum sensitivity with respect to substrate differentiation within a given substrate family.

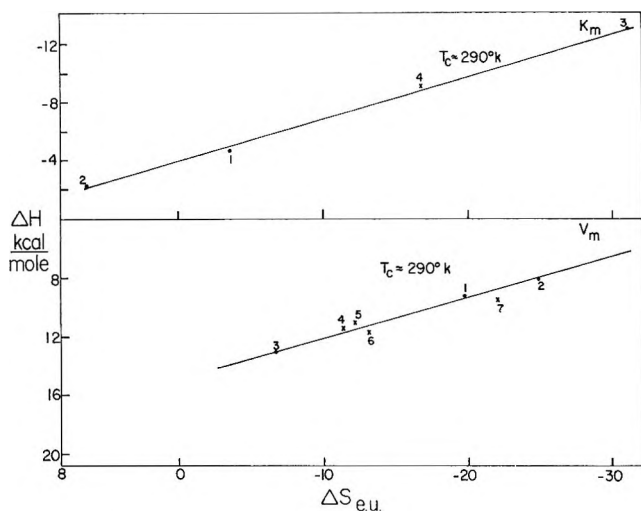


Figure 12. Compensation plot for K_m and V_m for the hydrolysis by α -CT of *N*-acetylphenylalanine methyl ester (1), (2) *D*-1-keto-3-carbomethoxytetrahydroisoquinoline and (3) *D*-methyl-3,4-dihydroisocoumarin-3-carboxylate at pH 7.8, 10% acetonitrile (data from Cohen, *et al.*⁵⁷ K_m and k_{cat} values for ATEE hydrolysis at pH 8.0 from the present study (4) are shown to fall on the same compensation line as also k_{cat} for ATEE (5) (from Bender, *et al.*^{5,9}), *N*-benzoylphenylalanine ethyl ester (6) and *N*-benzoyltyrosine ethyl ester. (7) (from Laidler "Chemical Kinetics of Enzyme Action," Oxford University Press, London, 1956, Chapter 9).

Lumry and Biltonen¹⁷ have shown that the activation enthalpies and entropies obtained by Cane⁵² for the deacylation of the acyl-enzymes (acetyl-, propionyl-, butyryl-, valeryl-, and caproyl-) demonstrate compensation behavior within the errors so that CT appears to have a temperature of minimum specificity with respect to the deacylation rate process for this series of compounds. Rüterjans⁵³ finds a linear compensation pattern with T_c of 290°K in the binding of inhibitors to ribonuclease A and T, and the data of Hammes and coworkers^{54,55} as well as those recently obtained by Biltonen and coworkers⁵⁶ on ribonuclease A support this finding. Hence ribonuclease A and perhaps ribonuclease T appear to have a temperature of minimum specificity with respect to inhibitor binding.

The Compensation-Free Reaction Profile for Chymotrypsin. The results obtained by a variety of workers show that in the binding of inhibitors by α -CT the hydrophobic-bonding contributions to enthalpy and entropy change are dominated by the negative contributions from a second part process of the total. The latter process which demonstrates compensation behavior has already been discussed here and elsewhere.^{6,7,21} The most that can be said about it at this time is that it involves the protein and may involve, in an equally important way, liquid water. Cohen and coworkers⁵⁷ have discussed this matter in terms of solvation of substrate with emphasis on hydrophobic bonding, as have Canady and coworkers.^{58,59} We have shown that these arguments are quite irrelevant insofar

as transfer reactions in which a substrate or inhibitor is transferred from water to a polar organic solvent give enthalpy and entropies of transfer which are small relative to those found in inhibitor binding to CT systems, and, indeed, have the wrong sign. The arguments of Cohen and coworkers may take on new significance if it can be shown that displacement of water from the binding region of CT, as proposed by Bernhard,⁶⁰ involves several water molecules and varies with substrate and inhibitor. The X-ray diffraction evidence shows that a few water molecules must be displaced.²⁹⁻³¹ The enthalpy change in this displacement may be negative due to some improvement in hydrogen bonding but is probably small. The entropy change attributable to these molecules must be roughly equal to that in the melting of ice, *i.e.*, about +5 eu per mole of water, the change being in the wrong direction to be identified with the part process which manifests compensation and dominates the enthalpy and entropy changes in the binding processes.

The specificity of α -chymotrypsin with respect to substrate side chains, inhibitors, and pH has been shown to be directly related to the part processes of the individual elementary steps which introduce compensation behavior. It has been necessary to introduce a phenomenological coordinate in describing the reactions of CT which takes into account these part processes. This coordinate was originally called the "functional conformation coordinate"^{62,64} but with the rapid development of evidence suggesting the participation of liquid water, the term appears increasingly inappropriate although much remains to be done to establish the actual participation of liquid water. Except for new examples and the fact that there is now considerable agreement among water specialists that pure liquid water and many highly aqueous solutions do manifest "two-state" behavior, which is important because the linear enthalpy-entropy compensation pattern with T_c near 285°K is an immediate consequence of this behavior, the subject is adequately covered by Lumry and Rajender⁷ elsewhere. In any event, the "compensation coordinate" is now phenomenologically identifiable with the compensation line and thus with the concept of a temperature of minimum

(52) W. Cane, Ph.D. Thesis, University of Minnesota, Minneapolis, Minn., 1967.

(53) H. Rüterjans, personal communication.

(54) G. Hammes and P. R. Schimmel, *J. Amer. Chem. Soc.*, **87**, 4665 (1965).

(55) T. C. French and G. Hammes, *ibid.*, **87**, 4569 (1965).

(56) R. Biltonen, personal communication.

(57) S. Cohen, V. Vaidya, and R. Schultz, *Proc. Nat. Acad. Sci. U. S.*, **66**, 249 (1970).

(58) G. Cuppett and W. Canady, *J. Biol. Chem.*, **245**, 1069 (1970).

(59) C. Royer and W. Canady, *Arch. Biochem. Biophys.*, **124**, 530 (1968).

(60) S. A. Bernhard and G. L. Rossi, in "Structural Chemistry and Molecular Biology," A. Rich and N. Davidson, Ed., Freeman Co., San Francisco, Calif., 1968, pp 110-113.

sensitivity. The existence of a temperature of minimum sensitivity with respect to the effects of side-chain variation on ES and EA is reasonably certain. The more common situation is likely to be that exemplified by ligand-binding to the ferri hemoglobins, *i.e.*, each ligand has its own compensation line based on pH and salt variation but the lines themselves are displaced along the ordinate due to variations in $(\Delta H_a - T_c - \Delta S_a)$. With enzyme systems, compensation in rate processes such as $ES \rightarrow ES^\ddagger$ and $EA \rightarrow EA^\ddagger$ due to side-chain variation may be found to be a more general phenomenon. With CT, side-chain specificity occurs in both kinds of elementary steps, *i.e.*, those of secondary bonding not thought to include primary-bond rearrangements and the rate processes for processes thought to include bond rearrangement. We have seen that this kind of sensitivity as well as pH dependence can be minimized or eliminated by working at experimental temperatures equal to the T_c values. Operationally it is necessary to use some suitable compromise temperature since the T_c values vary slightly from step to step but we can eliminate sensitivity in a formal fashion from the free-energy profile of the ATEE-CT reaction by plotting the values of the ordinate intercepts for each of the steps of the total process. Where the compensation lines at higher pH values above the turn-around point have significantly different intercept values than those below pH 8, we have used the lower pH intercepts. The result, Figure 13, is essentially a compensation-free description of the ATEE-CT process since all part-processes contributing compensation behavior have been eliminated. As already mentioned, the data shown in Figure 12 suggest that Figure 13 will prove to be quantitatively nearly identical with similar diagrams constructed for other ester substrates of CT. We believe Figure 13 represents a conceptual development of considerable potential importance in the study of some enzyme mechanisms.

Implications of the Compensation-Free Reaction Profile for Chymotryptic Catalysis. The figure has several interesting implications of which undoubtedly the most important is that the high efficiency of CT in ATEE hydrolysis is in no obvious way related to side-chain specificity. The introduction of side-chain specificity effects or pH effects, by carrying out the reaction at temperatures well removed from the T_c values, increases or decreases rate constants and equilibrium constants by factors which may at most achieve no more than a few orders of magnitude even at pH extremes with large temperature deviations. These changes are relatively small and it is clear that the efficiency of CT in the k_2 , k_{-2} , k_3 , and k_{-3} steps, which are believed to be those of bond rearrangement, is due in major part to factors which are not related to pH or side-chain sensitivity. One exception is, of course, stereospecificity but this is, in effect, a special

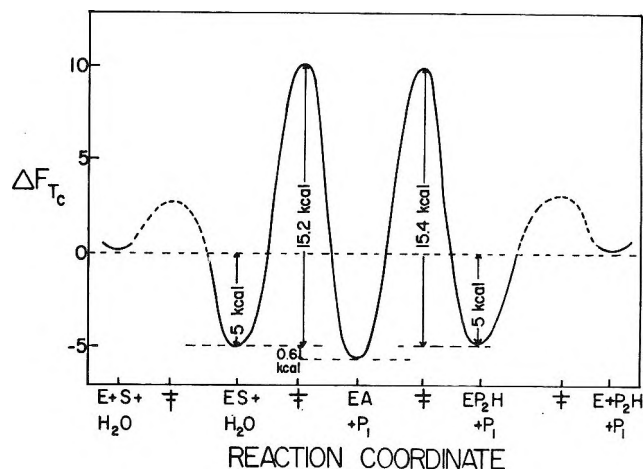


Figure 13. "Specificity-free" free-energy profile for the hydrolysis of ATEE by α -CT. Free-energy values are obtained from ΔH intercept values at $\Delta S = 0$ of the compensation plots for the several steps. Experimental conditions have been described.

situation since the details of the "conformational coordinate" and the mechanism are different for the D-enantiomorph of ATEE. Another special case is provided by substrates and acylating groups such as *p*-nitrophenyl acetate which have side chains that are too small to engage the protein "conformation coordinate." This case has been discussed elsewhere.^{17,61}

Figure 12 suggests that small activation energies and large negative activation enthalpies for the acylation and deacylation activated complexes (see free-energy profile, Figures 4 and 5 in ref 1), which are very abnormal relative to model studies of basic ester catalysis by imidazole groups, may be deceptive as a clue to the mechanism responsible for the high catalytic efficiency of the enzymic processes. The values of these quantities vary with pH indicating that at least part of the negative enthalpy and entropy contributions responsible for the abnormal values are due to the compensation part processes. It is possible that nearly all of the negative enthalpy and entropy contributions from the protein-water part of the system are from the compensation part process rather than the compensation-free part process. Unfortunately, it is not yet possible to separate total enthalpy or entropy changes into contributions from the two kinds of part processes and we are forced to work with free-energy changes only.

Figure 13 is not immediately consistent with the simple rack proposal due to Lumry⁶²⁻⁶⁴ and detailed by Jencks.⁶⁵ In its simplest form according to this pro-

(61) L. Faller and J. M. Sturtevant, *J. Biol. Chem.*, **241**, 4825 (1966).

(62) R. Lumry and H. Eyring, *J. Phys. Chem.*, **58**, 110 (1954).

(63) H. Eyring, R. Lumry, and J. D. Spikes in "Mechanism of Enzyme Action," McElroy and Glass, Ed., Johns Hopkins Press, Baltimore, Md., 1954.

(64) R. Lumry, *Enzymes*, **1**, 157 (1959).

posal, the substrate is bound in a distorted form. Some of the free energy released by the favorable features of the enzyme-substrate union is diverted to increase the free energy of the reactant states ES and/or EA relative to the free energies of the activated complexes ES[‡] and EA[‡]. It can be seen in Figure 13 that both ES and EA have about the same free energy of formation at T_c as has been found for the compounds of CT with the inhibitors indole, hydrocinnamate ion and *N*-acetyl-*L*-tryptophan at T_c (which is about -4 kcal/mol).⁶⁵ These comparisons may prove deceptive but they do not indicate any remarkable increase in free energy of ES and EA due to this type of rack mechanism. The diagram does not, in fact, reveal any obvious way in which free energy released in ES formation can be used to accelerate the acylation and deacylation rates. Relative to the separated reactants and thus relative to a small-molecule model the catalytic efficiency is seen to be due to the stabilization of the metastable intermediates rather than a destabilization. The reduction of the "on-acylation" and "off-acylation" free energy barriers is probably also important but the free energies of formation of the corresponding activated complexes from the metastable intermediates are not much lower than would be expected for base or nucleophile catalyzed hydrolyses in small models. However, conclusions such as these are based on chemical descriptions of ES, EA, and the activated complexes which are still imperfect despite the excellent foundation established by Bender and coworkers in particular. In fact, these same deductions can be made using the free-energy diagram for ATEE published by Bender, *et al.*,^{8,9} despite the fact that the latter was computed for 25° rather than for the appropriate T_c values. However, it is worth reiterating that Figure 13 is conceptually very different. Whatever the special tricks nature has developed to produce the catalytic acceleration of electron (*i.e.*, bond) rearrangement steps in CT systems, our study shows that they can be clearly divorced from those aspects of the protein function responsible for specificity in the selection of substrates. Bond-rearrangement steps do show quantitative variation with substrate side chain in a related family of substrates but only at temperatures different from T_c and the quantitative effect is small relative to the effect of the fundamental catalytic mechanism whatever it may be. Figure 13 is the free-energy description of this fundamental mechanism and its understanding provides one goal in the study of enzymic mechanisms, substrate specificity being the other. Thus we have started this discussion, which summarizes the results of our steady-state studies of the ATEE-CT system, with a reasonably simple explanation based on a few acid groups of the protein. This explanation was superficially satisfying in the framework of most studies of enzymic mechanisms and it was sufficient to show that entropy and enthalpy changes must be measured in systems

which manifest enthalpy-entropy compensation behavior if important details of mechanism are not to be hidden. The near constancy of the T_c values found in the ATEE-CT system compared with those found in other small solute and protein reactions and the ubiquitous occurrence of compensation phenomena suggested that the simple explanation was incorrect although certain key acid groups undoubtedly play a central role in the complex mechanism responsible for compensation. Comparisons of the catalytic data with the inhibitor-binding data demonstrated a close relationship which could not be explained on the basis of simple ionization processes and these comparisons were made more impressive by reference to other protein systems in which compensation behavior has been found to involve charged groups but only as one part of a complex phenomenon. The observation that the ubiquitous compensation line can be generated at constant pH by varying inhibitors in the case of CT and the abundance of examples showing that linear enthalpy-entropy compensation is a normal characteristic of reactions in water solution forced us to examine compensation in the ATEE-CT system as a potential member of this large group. This examination led to a clean separation between fundamental electron-rearrangement processes responsible for the speed of catalysis and the mechanism responsible for specificity characteristics. It seems quite possible that these two aspects of chymotryptic catalysis are independent at least to the first order of approximation and that they developed more or less independently in evolution.

The discussion of the new approach presented here is of necessity brief. The reader is referred to a paper on compensation by Lumry and Rajender⁷ and a discussion of chymotryptic catalysis given by Lumry and Biltonen¹⁷ for the amplification necessary to appreciate the phenomenological simplicity of the entropy-enthalpy compensation behavior. It is to be noted that the phenomenological parameters have provided a rather inaccurate description of the mechanism of chymotryptic catalysis if the single-step rate and equilibrium

(65) W. P. Jencks in "Catalysis in Chemistry and Enzymology," McGraw-Hill, New York, N. Y., 1969, Chapter 9 and earlier references therein.

(66) As is discussed elsewhere [R. Lumry, *Advan. Chem. Phys.*, 21, 567 (1971)], comparisons of inhibitor-enzyme compounds with metastable intermediates in the catalytic process which have the same chemical composition (*e.g.*, *N*-acetyl-*L*-tryptophan combined with CT as an inhibitor and the intermediate EP₂H) is not safe. Although the standard free energies of formation of the latter pair as can best be estimated are not very different, the standard enthalpies and entropies of formation similarly estimated are quite different. In addition, the rates of formation and dissociation of enzyme-inhibitor complexes may be many orders of magnitude slower than for the metastable intermediate of the same composition as is the case for this pair. The differences in behavior are often not seen except when enthalpies and entropies are measured. The idea does not appear to have been recognized previously although there is no *a priori* reason why it should not be of general applicability. It renders dubious the common technique of studying equilibrium binding between substrates or products and enzymes as a source of information about the metastable intermediates in a complete and reacting enzyme-substrate system.

constants evaluated in this report are correct. Single-step constants and their associated enthalpy or entropy changes provide a minimum basis on which to analyze enzymic mechanism although these quantitative parameters must be supplemented by precise X-ray-diffraction information before the undertaking can be completed. Just how much use studies of the mechanisms of small molecule "models" will prove to be remains to be established. Judging from the information available in this series of papers from our laboratory and the remarkably large number of structural differences which exist between chymotrypsinogen and α -CT the mechanism of chymotryptic catalysis is at least one order of magnitude more complex than most current literature on the subject assumes. A certain degree of symmetry in the reaction about the acyl-enzyme species EA is found in this more refined analysis but it is probable that there are distinct differences between the activated complex for EA formation and that for its hydrolysis which will require breaking down of what we have written as a single elementary step $ES \leftrightarrow EA$ into at least two steps. A recent publication by Rossi and Bernhard⁶⁷ shows that the k_3 step as we have written it may include at least two true elementary steps. This modification does not in any way invalidate the analysis we have given.

It should also be borne in mind that α -CT is not the stable form of the enzyme in the pH region of this study.⁶⁸ The stable form is γ -CT, which is above pH 5, but the interconversion of the two conformers is so slow that it is unlikely to have occurred in our experiments as a source of complication in our results.^{17,69}

The importance of entropy in protein processes is emphasized by the results we have obtained. The

conventional application of absolute rate theory usually positions the important activated complexes at saddle-points on the potential energy surface. In protein reactions the role of entropy is often equal in importance to that of enthalpy so that the activated complexes must be correctly established by saddle-points on the free-energy surface at any given temperature. It will be noted that in the reaction we have studied the free energies of activation are dominated by the entropy behavior.

More or less as a result of a process of elimination, Lumry and Rajender⁷ have been forced to the tentative conclusion that the interaction between protein conformation and water responsible for enthalpy-entropy compensation behavior is a manifestation of expansion and contraction of the protein. If this proves to be the correct interpretation, proteins held tightly together in insoluble or soluble particulate systems, *e.g.*, the mitochondrial or hemoglobin, can be linked for free-energy exchange by the same type of expansions and contractions which are responsible for compensation behavior in freely dissolved single-subunit proteins.

Acknowledgments. We are very much indebted to Drs. A. Alfsen, J. Beetlestone, R. Biltonen, and H. Rüterjans for data provided prior to publication and to Drs. J. Beetlestone, B. Belleau, J. F. Brandts, M. H. Han, and A. Yapal for suggestions and criticism.

(67) G. L. Rossi and S. Bernhard, *J. Mol. Biol.*, **55**, 215 (1971).

(68) S. T. Freer, J. Kraut, J. D. Robertus, H. T. Wright, and Ng. H. Xuong, *Biochemistry*, **9**, 1997 (1970).

(69) T. Hopkins and R. Lumry, unpublished observations from this laboratory.

Nuclear Magnetic Resonance Spectral Interpretation by Pattern Recognition

by B. R. Kowalski and C. A. Reilly*

Shell Development Company, Emeryville, California 94608 (Received November 30, 1970)

Publication costs assisted by the Shell Development Company

A pattern recognition method is applied to high-resolution nmr data for the purpose of detecting the presence of various molecular structural features. Pattern vectors, derived from calculated nmr spectral frequencies and intensities, comprise the training set used to calculate weight vectors for classification. The spectra are preprocessed with the autocorrelation function to remove the translational frequency variance produced by chemical shift variations from spectrum to spectrum. Truncation of the autocorrelation function, necessary to keep the pattern dimension relatively small, is possible because of a redundancy in the information. Weight vectors for ethyl, *n*-propyl, and isopropyl groups were trained by a regression procedure and tested on unknown spectra (not in the training set).

Spectral interpretation can be the most tedious and time consuming step in a spectroscopic experiment. Yet, if this arduous task is not properly done, valuable information may be lost. The analysis of a spectrum is usually accomplished *via* determination of intermediate parameters (*i.e.*, chemical shifts and coupling constants in the case of nmr) which are then related to structural and/or elemental information. In order to free the chemist from this labor, a more direct path leading from spectral data to structural and/or elemental information is very desirable.

The transformation of N pieces of spectral information into M pieces of desired structural and/or chemical information can be thought of as mapping the experimental data in N space into the derived features in M space ($N \gg M$). For example, a digitized spectrum is actually a series of experiments resulting in the relative intensities measured at N incremental units along some axis (time, frequency, mass, etc.). The spectrum can be thought of as a vector in N -dimensional space. There is a variety of ways of achieving such a mapping. Some of these ways actually correspond to an analysis of the spectrum on theoretical grounds (*e.g.*, assignment of absorption frequencies in vibrational spectroscopy) while others are strictly empirical methods that use some criterion, such as minimum variance, for the mapping. The objective of most of these methods is the same: to reduce the large amount of information in the N space to a comparable amount in the smaller M space.

Probably the newest and most interesting approach to performing this task is the broad and incohesive discipline called pattern recognition. It is rather difficult to think of pattern recognition as a discipline when in reality it consists of a number of algorithms that have been used to solve problems from many diverse fields. Basically, it involves the analysis of unknown data by mathematical models trained on known data. Although the largest amount of published research is

found in the area of alphanumeric character recognition, a few of the other applications include particle tracking in cloud, bubble, and spark chambers, fingerprint analysis, speech analysis, weather prediction, medical diagnosis, and aerial and microphotographic processing. An excellent review by Nagy evaluates many of the algorithms used for pattern recognition and discusses several interesting applications.¹

Molecular structural information has been obtained directly by applying a computerized learning machine to digitized spectra from mass spectrometry,²⁻⁵ infrared spectrometry,⁶ and a combination of both.⁷ The successful results of these studies and the work of others⁸ indicate that spectral interpretation can be performed on an empirical basis by a computer without imparting the characteristics of the spectroscopic method or rules for determining molecular structure.

One of the most useful tools for determining the molecular structure of molecules is high resolution nuclear magnetic resonance (nmr). This paper will be concerned with proton magnetic resonance only, but the ideas developed should be transferable to the nmr spectra of other nuclei (such as ¹³C) as well.

The block diagram in Figure 1 shows the present method and two proposed methods of determining molecule structural units from nmr. Path 1 is the con-

(1) G. Nagy, *Proc. IEEE*, **56**, 836 (1968).

(2) P. C. Jurs, B. R. Kowalski, and T. L. Isenhour, *Anal. Chem.*, **41**, 21 (1969).

(3) P. C. Jurs, B. R. Kowalski, T. L. Isenhour, and C. N. Reilly, *ibid.*, **41**, 690 (1969).

(4) B. R. Kowalski, P. C. Jurs, T. L. Isenhour, and C. N. Reilly, *ibid.*, **41**, 695 (1969).

(5) P. C. Jurs, B. R. Kowalski, T. L. Isenhour, and C. N. Reilly, *ibid.*, submitted for publication.

(6) B. R. Kowalski, P. C. Jurs, T. L. Isenhour, and C. N. Reilly, *ibid.*, **41**, 1945 (1969).

(7) P. C. Jurs, B. R. Kowalski, T. L. Isenhour, and C. N. Reilly, *ibid.*, **41**, 1949 (1969).

(8) L. R. Crawford and J. D. Morrison, *ibid.*, **41**, 994 (1969).

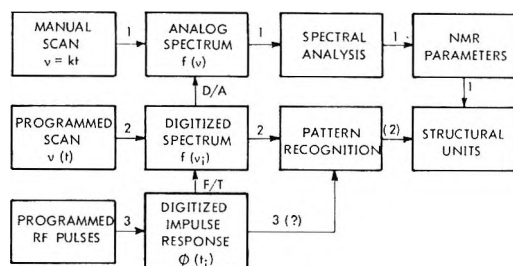


Figure 1. Schematic procedure for nmr data acquisition and processing.

ventional method that has been yielding important information for many years. The manual scan produces an analog spectrum which shows the relative intensities of the various proton groups as a function of frequency (usually measured with respect to some standard such as the TMS line). An experienced spectroscopist can analyze the analog spectrum for nmr parameters (chemical shifts and spin-spin coupling constants) for the various nuclei present. This analysis is relatively easy when the spectrum is close to first order and contains no overlapping multiplets. When either or both of these conditions are not met, the analysis is best done with the aid of a computer⁹ and can be tedious and time consuming to say the least. Specialized experiments (e.g., double resonance) can be performed, provided the necessary equipment is available. The fact is that all of the information is present in the analog spectrum (unless it is first order) and most of these experiments serve only to simplify the spectrum so that it can be analyzed more readily.

Path no. 2 shows the method of nmr data analysis that is proposed and partially tested in this paper. A sample is analyzed by having a computer or other device first collect a spectrum in digitized form. After preprocessing to convert the spectrum to a pattern vector, it is analyzed by pattern recognition techniques. Chemically meaningful information or structural parameters can be produced without ever determining a chemical shift or a coupling constant explicitly.

Path no. 3 is a proposed method that is closely related to that of path no. 2. An elaboration of this proposed method will be made in the last section.

The Pattern Recognition Method. A primary objective of pattern recognition is to develop a mathematical pattern classifier that can be trained on a set of known patterns (training set) and used to classify other new, unknown patterns. For spectrometric applications, this translates into using knowledge obtained from known spectra to analyze unknown spectra. This larger objective can be broken down into smaller objectives each presenting problems of a different nature. These subobjectives are: formation of pattern vectors, selection of a classification algorithm, training, and finally, testing and application. These topics and their accompanying problems will be discussed individually

in this paper with a definite slant towards an application to nmr spectrometry.

Pattern vector formation can be the most formidable problem in any application of pattern recognition. It is sometimes called preprocessing and can be defined as: given an amount of information on a large number of samples, what is the best possible vector representation of this information with respect to the algorithm chosen? In the case of nmr spectral analysis, the information is the digitized, continuous wave (cw) spectrum measured at a constant resolution and referenced to a constant frequency. Each such spectrum is called a spectrum vector. The samples are the actual chemical compounds that were used to obtain the spectrum vectors. The specific problem in the application of pattern recognition to nmr is: given a number of spectrum vectors representing digitized nmr spectra, what must be done to form pattern vectors so that an optimal amount of the information present in the spectra can be used by the pattern classifier to obtain structural information? In many cases, the unprocessed data (e.g., normalized mass spectra in the case of mass spectrometry) are adequate and no further pretreatment is necessary. Unfortunately, this is not the case in nmr as will be discussed in the next section.

Another objective in a pattern recognition application is the selection of a pattern classification algorithm. The algorithm includes a training method and a classification scheme. There are several powerful algorithms to choose from¹ and new methods along with improvements on existing methods are being introduced at a rapid rate. Spectroscopic applications however, because of the large amount of data that can be collected, impose certain constraints on the selection of an algorithm. For example, it may be necessary and practical to digitize hundreds of nmr spectra in order to obtain satisfactory performance for a given analysis. For high-resolution spectra, the digitization procedure could produce as many as 10,000 intensities for each spectrum vector. This, of course, means that millions of numbers must be processed. If the algorithm is mathematically complicated, the application can be quite costly. Due to the large amount of data and the complexity of the pretreatment necessary for the applications in this study, a simple pattern classifier (linear discriminant function^{1,10,11} and a relatively fast training algorithm (regression analysis)¹² were used. It must be emphasized that the linear discriminant function is an extremely powerful pattern classifier and was chosen

(9) J. W. Emsley, J. Feeney, and L. H. Sutcliffe, "Progress in Nuclear Magnetic Resonance Spectroscopy," Vol. 1, Pergamon Press, New York, N. Y., 1966.

(10) N. J. Nilsson, "Learning Machines," McGraw-Hill, New York, N. Y., 1965.

(11) G. S. Sebestyen, "Decision-Making Processes in Pattern Recognition," Macmillan, New York, N. Y., 1962.

(12) A. Ralston and H. Wilf, "Mathematical Methods for Digital Computers," Wiley, New York, N. Y., 1966.

over *possibly* more powerful ones not only for economic reasons but also because it served as a vehicle to help solve the more serious problem of forming useable pattern vectors from the nmr spectrum vectors. The linear pattern classifier uses the dot product of the input pattern vector (\mathbf{y}) and a trained weight vector (\mathbf{w}) to produce a scalar output (s) as

$$s = \mathbf{w} \cdot \mathbf{y} + c \quad (1)$$

where c is a scalar constant and is determined, along with \mathbf{w} , during the training procedure. If s is a positive number for a particular \mathbf{y} , we say that the classifier has generated an affirmative output. If s is negative or zero, the output is negative.

Training consists of selecting a set of known pattern vectors called the training set and using a training algorithm to calculate a corresponding weight vector. The weight vector consists of one parameter (adjustable weighting factor) for each dimension of the training patterns. (It will henceforth be assumed that the constant in eq 1 is part of the pattern classifier and therefore part of the weight vector. In reality, it is calculated along with the weight vector by augmenting the pattern vectors, thereby increasing the pattern space by one dimension.) As an example of training, it may be desired to calculate a weight vector that can be used by the pattern classifier to determine whether or not a compound (represented here by its pattern vector) contains an isopropyl group. The procedure would be first to select a number of representative compounds from the two groups (*i.e.*, those containing and those not containing isopropyl groups). Then, the spectra obtained from these compounds are used to form the training set of pattern vectors. The training algorithm calculates a weight vector that can be used by the pattern classifier to determine whether or not unknown compounds contain the isopropyl group. A properly chosen training set could be used to train many weight vectors, each determining a different functional part of the molecule. Together, these weight vectors would aid immensely in the automatic computer interpretation of spectroscopic data.

There are a number of training algorithms that could be used to obtain a weight vector. Early applications to spectroscopic data analysis used a feedback algorithm^{2,3} and the method of least squares.⁴ In the feedback method a training pattern is presented to the classifier containing an arbitrarily initiated weight vector and the response is checked against the correct answer. If it is the desired response (a correct determination of the presence or absence of the sought for structural unit in the molecule), no action is taken and the next pattern is presented. If an incorrect response is given, the weight vector is adjusted (a fraction of the training pattern is added or subtracted) to produce the correct response. This is continued in a cyclic process with the hope that all of the training set patterns can be

classified correctly. The feedback method is an acceptable training procedure provided that the size of the training set is not too large. At this point it should be mentioned that a particular weight vector is not unique and many factors must be considered in a discussion of the "best" weight vector for a specific determination. This discussion is beyond the scope of this paper.

The feedback algorithm can be expected to produce a weight vector rapidly, provided that the entire training set resides in the core memory of the computer. As the training set gets larger and overflows onto peripheral storage devices (*i.e.*, drum, disk, tape) the advantage of this method disappears. Even when the data are stored on a high-speed drum, and accessed using true random accessing methods (calculation of a hardware address) the calculations can be prohibitively costly. This is mainly due to the multiple accessing required for complete training. Most practical applications of pattern recognition to spectroscopy will probably require training sets of spectral vectors exceeding core storage limits of most computers. The data used in this study, for example, required more than a quarter of a million words of storage and were, therefore, stored permanently on a drum (Univac 1108 Fastrand). For this reason, it is desirable to use an algorithm that requires reading the training set only once, processing it one pattern at a time as it is brought into the core from a peripheral device. One method that satisfies this requirement is multiple regression analysis.¹² The method starts by setting up the normal equations from the system of linear equations (one equation for every pattern in the training set) using eq 1. The desired responses(s) are input as +1 for a positive pattern (representing a compound containing the sought-for-structure) and -1 for a negative pattern. The Gaussian elimination method is used to solve the normal equations.

Stepwise regression, used to calculate the weight vector for this study, makes use of intermediate regression equations and allows a one-at-a-time addition or removal of parameters to the solution. The parameter that is added at any step is the one that will reduce the standard error by the greatest amount. Parameters are removed from the equations if the removal will not increase the standard error by more than a specified amount. This procedure can be stopped at any time or it may be allowed to use all of the available parameters for the solution (the latter case corresponds to the complete multiple regression analysis). This procedure permits a careful examination of the importance and interrelation of the parameters. In the present study the procedure was stopped when the addition of a parameter did not lower the standard deviation by more than a specified amount proportional to the ratio of the error in the parameter to the absolute value of the parameter.

The final step in the development of a pattern recog-

nition method is testing the weight vectors. This simply amounts to obtaining pattern vectors that are not present in the training set, presenting them to the pattern classifier, and checking the responses. The test vectors must represent typical patterns that might be expected to turn up in a practical application. If performance is not adequate, assuming that all of the other problems have been solved, the training set should be enlarged.

Problems in Pattern Formation from Nmr Spectra.

The first experiments in this study attempted direct applications of pattern recognition to normalized spectrum vectors. Three hundred cw proton spectra (60 MHz) from 0 to 500 Hz relative to TMS were digitized manually at 2.5-Hz intervals to give pattern vectors of 200 dimensions each. This is an obvious starting point in a study of this type because it represents the minimum amount of preprocessing. The results of these experiments showed that it was possible to derive a weight vector that performed well on the training set but gave results on test patterns that were only slightly better than random.

The key to understanding the results of these early experiments is found in the nature of the representation of the information in an nmr spectrum. Usually the spectrum is analyzed in terms of chemical shifts and coupling constants. The positions of the multiplets on the frequency axis give information as to the types of protons in the compound. The detailed fine structure within a multiplet provides information about the locations of other nuclei in the molecule. Figure 2 shows two calculated ethyl spectra with the same line width (0.5 Hz) and the same coupling constant (7.0 Hz). Their spectra are similar because of the obvious pattern of two very similar multiplets. It is obvious to the eye that the spectra represent ethyl groups even though there are rather large differences in the corresponding chemical shifts. The eye ignores the translational differences and minor differences in fine structure and easily identifies each pattern as consisting of a triplet and a quartet. The large translational differences make a direct application of pattern recognition to such cw nmr spectra unfeasible. The mathematical model used by the pattern classifier cannot tolerate large translational shifts in the patterns. This is not to say that chemical shifts are unimportant in the analysis of an nmr spectrum. They are, indeed, of paramount importance. However, they must be present in the pattern vector in a different representation. In other words, a transformation of the data (preprocessing) is necessary in order to map the translational information into a translationally invariant form while preserving the important multiplicity information. These translational shifts in a spectrum are ordinarily produced by two different effects. The first effect is a solvent shift. Although it is a relatively small problem, molecules can absorb energy at different frequencies depending on the

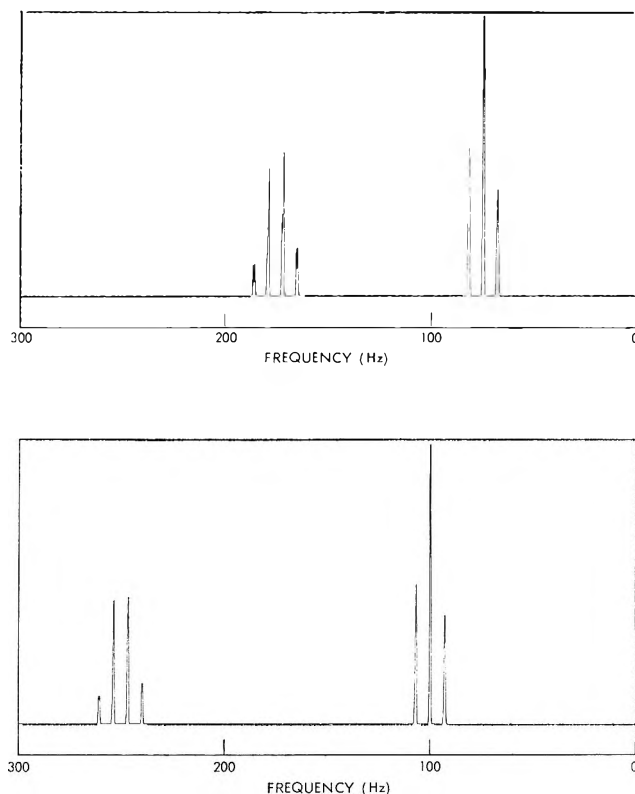


Figure 2. Calculated nmr spectra of ethyl groups with different chemical shifts.

solvent used. Of greater importance are the frequency shifts produced by structural differences. The large shifts in the two spectra in Figure 2 could arise only because of the different environments of the groups. These shifts represent important information and, even though the spectral data must be transformed so as to make pattern recognition possible, the chemical shift information must be preserved.

Another problem that plagues an application to nmr (and actually to any kind of high resolution spectroscopy) is the sheer size of the spectrum vectors (*i.e.*, volume of information contained, much of which is redundant). Consider the digital recording of a cw 60-MHz nmr spectrum over the region 0–500 Hz. If the instrument resolution is 0.5 Hz and a reasonable representation of line shape is necessary, about 10 readings should be recorded per 0.5-Hz increment. This amounts to a spectrum vector containing 10,000 values. In other words, the weight vector will need 10,000 parameters to separate the pattern vectors that, geometrically represented, are in a 10,000-dimensional hyperspace. Aside from the large amount of computer time necessary to calculate a weight vector (assuming such a calculation is possible) there exists an even larger problem. From an elementary knowledge of the theory of linear algebra, it is clear that perfect training results are guaranteed with a training set containing $\leq 10,000$ patterns. There is serious doubt, however, that the resulting weight vector would perform acceptably on

unknown patterns. For this reason, having more patterns than parameters is desirable, but unfortunately not practical with spectrum vectors of so many dimensions.

Derivation of Pattern Vectors by Autocorrelation. There are essentially two kinds of resolution in a digitized nmr spectrum. First there is the "instrumental resolution" usually defined by the full width at half-height of a single resonance line and this is found by direct measurement of the plotted cw spectrum. It is essentially a measure of the ability of the instrument to identify two closely spaced lines. The second resolution or the "digital resolution" (R) is the calibrated size of the stepping increment on the frequency axis during digitization. It is a measure of the faithfulness with which the digital spectrum represents the analog spectrum. Considerable information could be lost if digital data are obtained at intervals of only 1 Hz from an instrument capable of a resolution of 0.2 Hz. Conversely, an R of 0.001 Hz is in excess of the amount necessary to record a spectrum from an instrument with a 0.5-Hz resolution. It should be clear that R is an important quantity in any computer application and should be chosen carefully. This digital resolution is of particular importance to the transformation used by this study to eliminate the translational difficulties discussed in the last section. This transformation consists of autocorrelating the digitized nmr spectrum vector. The autocorrelation function $A(x)$ of a continuous function $F(f)$ is defined¹³ as

$$A(x) = \int_f F(f)F(f+x)df \quad (2)$$

where x in this case can take on any desired value. $F(f)$ is the cw nmr spectrum which is a function of frequency (f) and $F(f+x)$ is the spectrum offset by x . The discrete form of this definition is

$$A(nR) = \sum_f F(f)F(f+nR), \quad n = 0, 1, 2, \dots \quad (3)$$

where R is the digital resolution discussed above. Keeping n positive produces only half of this symmetric function. Autocorrelation has an interesting effect on a digital function $F(f)$ that is most easily demonstrated by a simple example. The top part of Figure 3 is a simplified AB stick spectrum. It is important to remember that although such multiplets can be found almost anywhere on the frequency axis, there is a very definite internal structure which is essentially constant and independent of the distance from a reference. The lower part of Figure 3 shows the positive part of the autocorrelation function for this AB spectrum. The most important point in this figure is the fact that autocorrelating the AB pattern will produce exactly the same pattern no matter where the center of gravity of the AB spectrum is found on the frequency axis. The values of the autocorrelation function can be readily

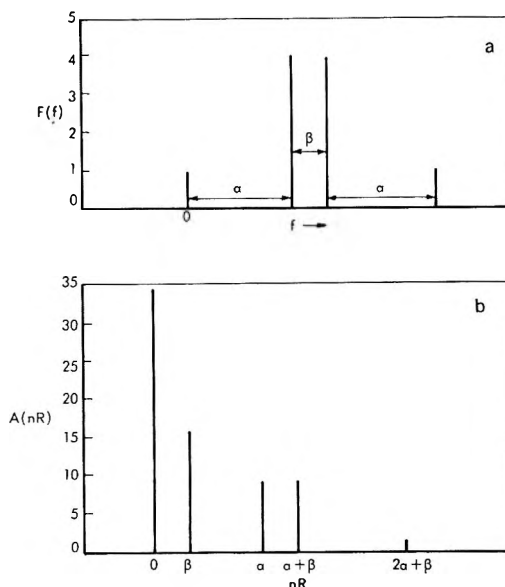


Figure 3. AB stick spectrum (a) and its autocorrelation function (b).

found from definition 3 using the various values for nR ($0, \beta, \alpha, \alpha + \beta$) where nonzero intensities exist. For example, for $nR = 0$, $A(nR)$ is simply the sum of the squares of the peak intensities in the spectrum.

Calculation of the autocorrelation of a digitized spectrum can be quite a costly process. The number of multiplications alone is approximately $1/2N^2$ where N is the size of the spectrum. Fortunately, as will be explained later in this section, only a small part of the autocorrelation spectrum was needed for this study. However, where it is necessary to calculate the entire function, a faster procedure can be used. The procedure consists of taking the Fourier transform of the spectrum in order to obtain the complex waveform $G(t)$ where

$$G(t) = \int F(f)e^{-i2\pi ft}df \quad (4)$$

Next, $G(t)$ is multiplied by its complex conjugate to form the power function $|G(t)|^2$ of the waveform. The power function is then inverse transformed as in (5) below to obtain the autocorrelation function. Thus, the autocorrelation function actually requires

$$A(f) \int \int F(f)e^{-i2\pi ft}df |e^{i2\pi ft}dt \quad (5)$$

fewer mathematical operations and consequently less computer time than a straightforward autocorrelation procedure.

The autocorrelation function provides a better pattern vector than does the original nmr spectrum vector. This is essentially due to the removal of translational variance from the data. A certain amount of information (phase) is indeed lost during the transform and this

(13) R. Bracewell, "The Fourier Transform and Its Applications," McGraw-Hill, New York, N. Y., 1965.

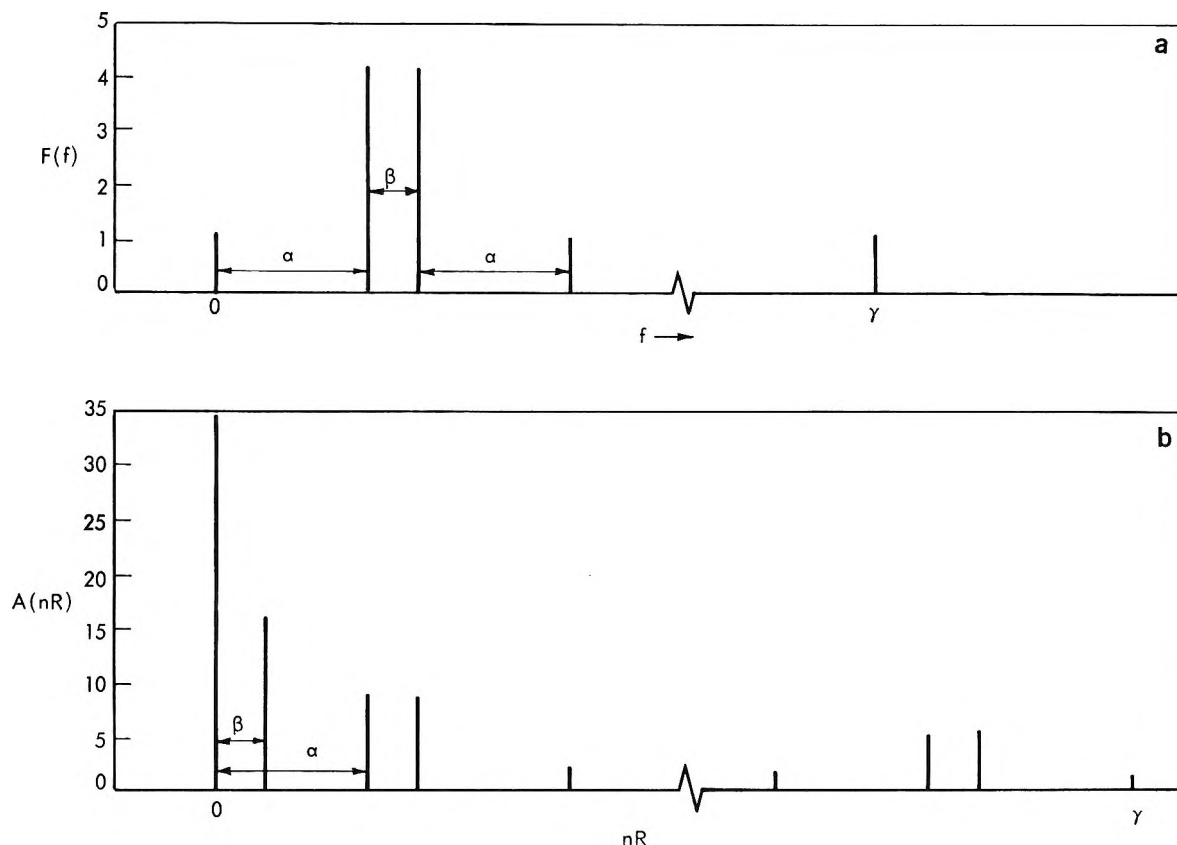


Figure 4. AB stick spectrum plus a single reference line (a) and its autocorrelation function (b).

is consistent with the fact that the autocorrelation function does not have an inverse. A few observations are in order before proceeding. (1) The value of $A(nR)$ at $n = 0$ is used to normalize $A(nR)$ at $n = 1, 2, \dots$. This makes $A(nR)$ of equivalent spectra recorded at different instrument gains the same. (2) The dimension of the pattern vector obtained is only one less than the original spectrum vector. (3) Line shape information is preserved.

The use of the total autocorrelation function does not solve the problem of vectors with a large number of dimensions. Observation no. 2 above states that the dimensionality is not significantly reduced. The interesting point, however, is that there is a certain redundancy of information that can be eliminated from the autocorrelation function. This is not the case for simple examples such as the one in Figure 3. However, it becomes clearer by examining a spectrum with a large difference in chemical shifts between two multiplets. Figure 4 shows the AB spectrum exactly as in Figure 3 with the addition of a single line with unit intensity at a distance γ from the origin. The broken axis is meant to show that this singlet is a large distance from the multiplet ($\gamma \gg 2\alpha + \beta$). The effect of the additional peak on the autocorrelation function is most interesting. The lower part (nR near 0) of the autocorrelation function is identical to that of Figure 3 while the upper part (nR near γ) is an exact reproduction of the original

spectrum. Unfortunately, this upper part suffers from the same translational problems as found in the original spectrum. This suggests using only the lower part of the autocorrelation function as a pattern vector. The problem of too large a pattern vector would thereby be solved. In practice, a 500-Hz spectrum is autocorrelated and only the lowest 25-Hz portion is used for pattern formation. The 25-Hz range was chosen as a compromise between two conflicting factors. The first factor was the necessity for keeping the pattern vector dimension below 250. Since the regression analysis program operates on the correlation matrix stored in core memory, the above limit was set by core storage limits. The second factor was the desire to maintain high resolution by setting the digital resolution, R , equal to 0.1 Hz. A larger or smaller value of R could conceivably produce better results but with an instrument resolution of 0.5 Hz (obtainable on most high resolution instruments) an R of 0.1 Hz was deemed necessary. These two limits allowed a range of 25 Hz of the autocorrelation function. This range actually contains a contribution from every peak in most typical nmr spectra.

This truncated autocorrelation function would seem to contain only coupling constant and multiplicity information but a closer examination shows that this is not necessarily so. Unless the spectrum is first order, some chemical shift information is actually retained in

the form of deviations of peak intensities from those observed in a first-order nmr spectrum. This representation is best described by considering two possible extreme cases in nmr spectra. One extreme is a spectrum that contains only widely spaced singlets. This condition can occur when proton couplings are too small to be detectable. The autocorrelation function is clearly of little value in this case. The other extreme is the pure first-order splitting patterns obtained when the chemical shift differences are much larger than the observable constants. Only multiplicity and coupling constant information appears in the lower part of the autocorrelation function because all of the differences in chemical shifts are greater than 25 Hz. In between these two extremes, chemical shift information appears as extra lines or as deviations in peak intensities which come from distorted multiplet intensities in the original spectrum.

An example of the combined benefits is illustrated by comparing Figure 2 with Figure 5. For the application of pattern recognition, it is clear that an intolerable distortion of the pattern (actually in the form of important information) is seen in Figure 2 going from the top spectrum to the bottom one simply by changing the two chemical shifts. Figure 5 shows the lower portion (2.0–25.0 Hz) of the normalized autocorrelation function for each spectrum of Figure 2. (The lowest 2.0 Hz is not shown and in actual practice is not used because it is redundant except for $A(0)$.) Two important features should be noted. (1) The translational differences between the two spectra are eliminated in the truncated autocorrelation functions. (2) The chemical shift information is not lost but can be seen as differences in the shapes of the autocorrelation functions.

The two subjects discussed in the previous section were (1) translational difficulties and (2) the large size of the spectrum vectors. Using the lower 2.0–25.0 Hz of the autocorrelation function as a pattern vector represents a significant step in solving these problems as the experimental results will show.

Derivation of a Training Set. One important requirement of a training set for deriving weight vectors is that it must contain spectra from a representative distribution of compounds of practical interest. For many applications it would be a rather time consuming and expensive task to obtain such a set. Compounding this difficulty is the fact that, at this time, the authors know of no collection of high quality nmr spectra in a computer-compatible format (card, tape, etc.).

Until such time as a large number of representative nmr spectra in digital form have been collected experimentally, such spectra can readily be simulated by means of any one of a number of well known computer programs.⁹ The stripped down noniterative part of the Ferguson–Marquardt version of program NMRIT⁹ was incorporated into a larger program, MRCALC, used to calcu-

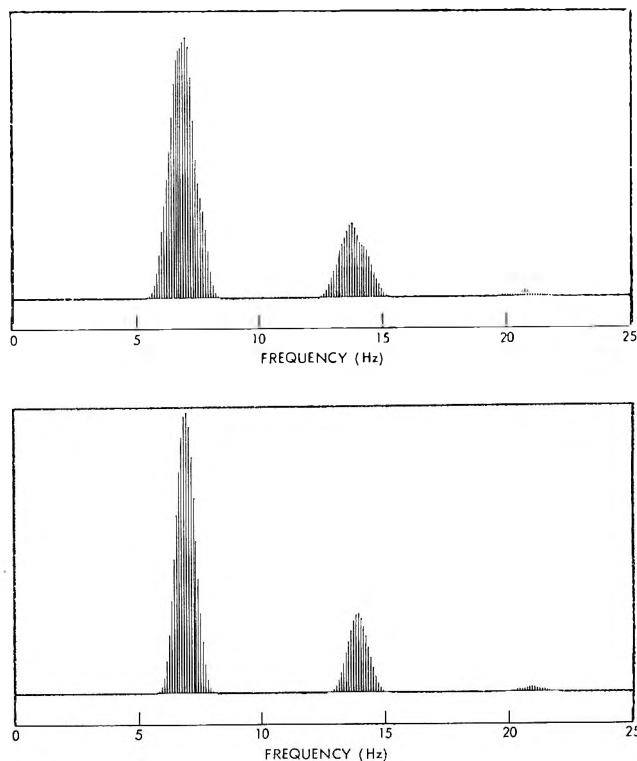


Figure 5. Lower portion (2.0–25.0 Hz) of autocorrelation functions for calculated ethyl group nmr spectra of Figure 2.

late the training set for this study. Program MRCALC needs the same information used by NMRIT but in the form of limits for the constants normally found in instrument run spectra. The program can calculate a number of spectra that will span the range of those normally found in an application. For example, in order to calculate representative spectra of ethyl groups, the program would be given the following information: (1) CH_3 chemical shifts that run between 50 and 150 Hz at intervals of 50 Hz (all frequencies in this paper refer to spectra run on a 60-MHz instrument); (2) CH_2 chemical shifts that start at a few Hertz above the CH_3 shift and range to 275 Hz at intervals of 25 Hz; (3) the coupling constant between the two groups with possible values of 7.0, 7.5, and 8.0 Hz.

Program MRCALC proceeds to calculate a number of stick spectra (63 in the case of the ethyl group) that form a good distribution of the ethyl spectral patterns. The output from MRCALC in this study consisted of punched cards containing the frequencies and intensities of the lines in the calculated spectrum. These cards form the input to program MRDATA which in turn calculates the pattern vectors. The first step in the pattern formation process is autocorrelating the stick spectrum obtained from MRCALC. Since only 25 Hz is used in the pattern, the calculation was discontinued when $nR = 25.0$ ($R = 0.1$ Hz). Applying the autocorrelation function to the spectrum before the line shape is added amounts to a calculational savings of several orders of magnitude and has been justified by

experiment. A Gaussian line shape is next added to each line in the autocorrelation function of the stick spectrum. The half-width required was determined experimentally. The 230 intensities at every 0.1 Hz from 2.1 Hz to 25.0 Hz become part of the pattern. In order to introduce information on absolute chemical shifts into the pattern vectors, five moments, calculated over five 100-Hz frequency intervals (0–100 Hz, 100–200 Hz, etc.) were also added to the pattern vectors. These five intervals were chosen because they were equal and they roughly corresponded to frequency intervals of chemical interest. The moments $M(f_1, f_2)$ were calculated over the intervals f_1 and f_2 by

$$M(f_1, f_2) = \frac{\sum_{nR=f_1}^{f_2} I(nR)f(nR)}{\sum_{nR=f_1}^{f_2} f(nR)} \quad (6)$$

where the $I(nR)$ array contained the spectral intensities relating directly to the frequency array $f(nR)$. The intensities were normalized to a constant while $f(nR)$ ranged from 0.0 to 500.0 Hz. This gave a total pattern dimension of 235 with the augmentation to add the constant making a 236-dimensional pattern space. Table I shows the actual structures and the number of spectra of these structures that were used for training. The nine different structural groups generated 634 patterns with each pattern having a total of 236 dimensions.

Table I: Structures for Data Base

CH ₃ —CH ₂ —	63	—CH ₂ —CH ₂ —	45
CH ₃ —CH<	63	CH ₃ —CH=CH—	84
CH ₃ —CH ₂ —CH ₂ —	63	—CH ₂ —CH=CH—	84
CH ₃ —CH ₂ —CH<	64	>CH—CH=CH—	84
(CH ₃) ₂ —CH—	84		

At first glance it would appear that a pattern would change drastically if any group were connected to another proton containing group instead of to heteroatoms or carbons without protons. This is indeed the case in the original spectrum as addition of a —CH— to the chain would give rise to a new splitting pattern in the spectrum. Fortunately, the lower part of the autocorrelation function which makes up the majority of the pattern still retains the pattern structure. This is seen by comparing the two ethyl patterns in Figure 5 with the pattern calculated from the spectrum of 1-nitropropane shown in Figure 6. They are quite similar even though the ethyl group in the *n*-propyl compound undergoes splitting by the second methylene. Figure 7 shows the pattern obtained by autocorrelating the spectrum of isopropyl cyanide which does not contain an ethyl group. The pattern is considerably different from the others shown in Figures 5 and 6. The most important

point demonstrated by a comparison of these spectra is that the spectrum of the basic molecular group is transformed to a pattern that dominates the autocorrelation function regardless of its environment but that the environmental information is still present to some extent. This makes the detection of the molecular group possible and allows for future determination of its environment.

Results and Discussion

Several weight vectors were calculated and tested during the course of this study. The results were generally excellent indicating the effectiveness of the autocorrelation function for generating pattern vectors to describe spectral features in high-resolution nmr spectra. The weight vector trained to detect the presence of the *n*-propyl group, for example, easily detected the presence of the group in test spectra as long as the chemical shifts and coupling constants were within the limits used for calculating the training set. Table II shows the training results for four weight vectors. The first column indicates the structural group that the vector was trained to detect. The first ethyl vector was determined by placing only the 63 ethyl pattern vectors in the positive category (+1.0) and the remaining 571 pattern vectors in the negative category (−1.0). The strategy behind this decision was that the spectral pattern of an ethyl group is considerably different from an *n*-propyl spectral pattern. The relatively poor results obtained by testing the vector (shown later) prompted further investigation. Close examination of the numerical values found for the pattern vectors indicated that the characteristic ethyl structure was present in both the *n*-propyl and CH₃CH₂CH₁ pattern vectors. The second ethyl vector in the table was trained by defining ethyl, *n*-propyl, and CH₃CH₂CH₁ pattern vectors as members of the positive category. The two remaining vectors are self-explanatory. The second column contains the number of dimensions that were actually calculated by the stepwise regression procedure. For example, the first ethyl weight vector used only 41 dimensions out of the 236 available. Even with these small numbers of dimensions, each weight vector was able to correctly classify every pattern vector in the training set. Being able to train a weight vector to classify 634 patterns using only 41 dimensions is indicative of a correct representation of the information in the pattern vectors. The "positive" and "negative" columns give the numerical accuracy for the classification of the training set into positive and negative categories. The first number is the average of all the responses after training (value of *s* in eq 2) of the members in that category. The number in parentheses is the standard deviation of this average for the category. The isopropyl weight vector is an ideal case in that the averages (0.94 and −1.00) are close to the desired responses of 1.0 and −1.0, respectively, and the

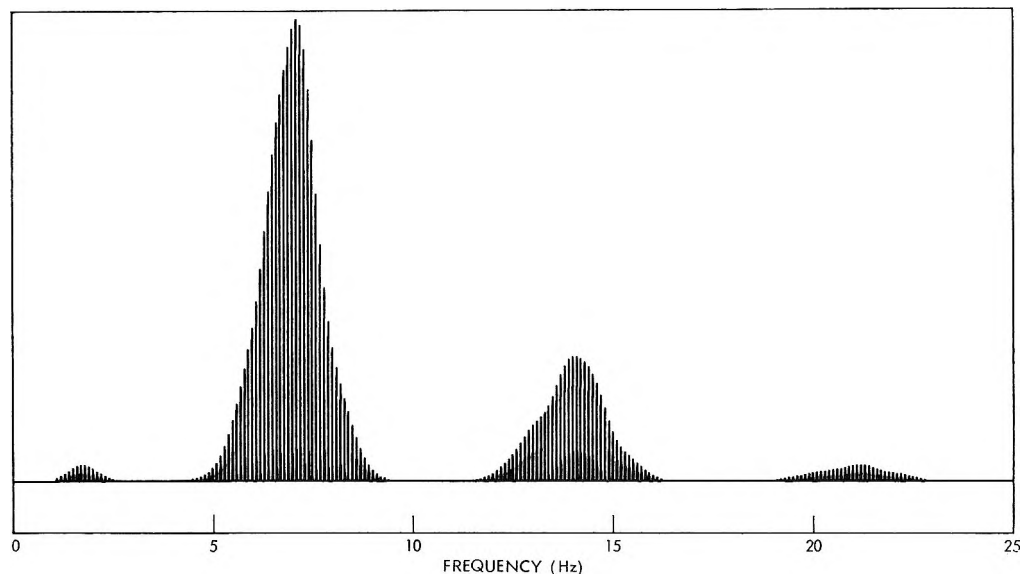


Figure 6. Autocorrelation function obtained from the calculated nmr spectrum of 1-nitropropane at 60 MHz.

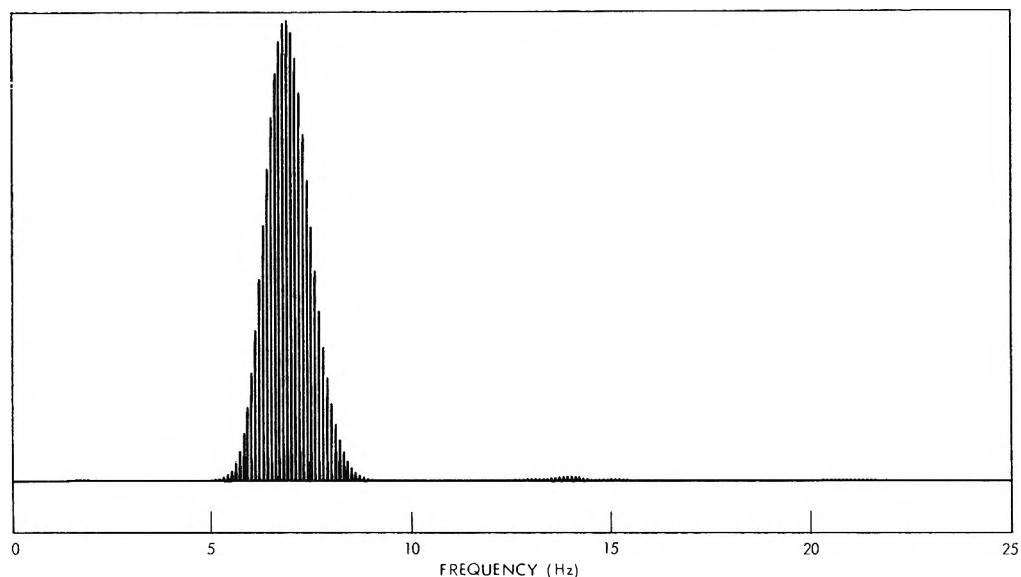


Figure 7. Autocorrelation function (2.1–25.0 Hz) obtained from the calculated nmr spectrum of isopropyl cyanide (60 Hz).

Table II: Training Results for Four Weight Vectors^a

Weight vector	No. of parameters used	Positive	Negative
(No. 1) CH ₃ CH ₂ -	41	0.60 (0.44)	-1.04 (0.26)
(No. 2) CH ₃ CH ₂ -	41	1.30 (0.34)	-0.83 (0.26)
CH ₃ CH ₂ CH ₂ -	44	0.84 (0.20)	-0.98 (0.18)
(CH ₃) ₂ CH-	47	0.94 (0.18)	-1.00 (0.12)

^a 634 patterns in training set, 236 total dimensions available for each pattern vector.

standard deviations are small. Applying a 95% one-sided confidence limit on each of these results would allow positive responses down to 0.58 and negative

responses as large as -0.76. These distributions are far from overlapping (giving rise to incorrect responses) at high confidence levels. Since the cases tested gave correct responses using the midpoint (0.0) between the desired responses (+1.0 and -1.0) as a decision surface, this value was used for all further tests.

Of considerably more interest than tabulating correct responses from several test cases were the attempts to use the trained weight vectors for classifications beyond reasonable limits. These studies provided valuable information on the limits to which the weight vector could be used and still provide useful information. This was done by asking the weight vectors to classify test patterns significantly different from any of those in the training set. It is difficult to imagine anything but random results from these weight vectors when used

to classify molecular types other than the nine contained in the training set. Table III shows the results of applying the four weight vectors of Table II to nine test cases. Incorrect responses (according to the training definition) are in parentheses. The most important point to note is that *none* of the test cases is in the training set. The first four test cases represent groups that are structurally the same as those contained in the training set. Correct responses are mandatory for

Table III: Application of Trained Weight Vectors to Unknown Test Cases

Test pattern	Responses for			
	Ethyl (No. 1)	Ethyl (No. 2)	n-Propyl	Iso- propyl
① CH ₃ CH ₂ Br	Yes	Yes	No	No
② CH ₃ CH ₂ CH ₂ NO ₂	(Yes)	Yes	Yes	No
③ (CH ₃) ₂ CHCN	No	No	No	Yes
④ CH ₃ CH ₂ CH<	(Yes)	Yes	No	No
⑤ ① + ②	Yes	Yes	Yes	No
⑥ ① + ③	Yes	Yes	No	Yes
⑦ ③ + ④	(Yes)	Yes	Yes	(No)
⑧ CH ₃ CH ₂ - (10 Hz)	Yes	(No)	No	No
⑨ CH ₃ CHCH ₂ -	No	No	No	(Yes)

these cases. The next three cases are 50/50 mixtures of two of the first three. Since there were no mixtures in the training set, correct responses cannot be expected. They are, however, desirable from the standpoint of practical routine applications. The next test case, CH₃CH₂ (10 Hz), is an ethyl group pattern calculated from a spectrum with a difference of only 10 Hz between the chemical shifts of the two groups. This is outside the limits used in calculating the training set and therefore cannot be expected to produce the correct answer. This pattern and others like it could be added to the training set, however, to increase the useable range. The last test case is completely unlike any in the training set.

The results of the first ethyl weight vector were unacceptable according to the definition of an ethyl group

used for training. As was mentioned earlier in this section, the autocorrelation pattern is actually contained in the *n*-propyl autocorrelation pattern and therefore the real problem was a human error in definition. Even though the training procedure tried to force negative responses from *n*-propyl groups and other CH₃CH₂ containing groups, the classification of the test vectors from these groups produced positive responses. The second weight vector was trained by defining all CH₃CH₂ containing groups as having an ethyl group. The results are much improved.

Several improvements are being considered that either obtain more information from the autocorrelation function, add data from other analytical sources, or return to the original spectrum in order to perform different types of transformations. The greatest emphasis, however, will be centered on further use of the information contained in the pattern vector derived from the autocorrelation function. The beneficial information representation as related to the pattern recognition application is enough justification for this emphasis but there is an added incentive stemming from the use of proposed path no. 3 in Figure 1. For this approach to nmr analysis, the free induction decay waveform, $G(t)$, of a molecule could be analyzed by pattern recognition to produce molecular structure information. A direct application of pattern recognition to the pulsed nmr waveform suffers from a translational problem of the type discussed earlier. Fourier transform theory, however, supplies the solution. The autocorrelation function $A(f)$ can be obtained by taking the Fourier transform of the square of $G(t)$, which is now a real function of time

$$A(f) = \int G^2(t)e^{i2\pi ft} dt$$

There is no need to derive $F(f)$ unless chemical shift information is required in forming the pattern vector. Thus, it is seen that full utilization of Fourier transform theory would allow a computerized structure analysis in a pattern recognition to be performed on either of the two main forms of nmr spectra (cw or pulsed).

Chemistry of Barium Released at High Altitudes

by *N. W. Rosenberg** and *G. T. Best*

Air Force Cambridge Research Laboratories, L. G. Hanscom Field, Bedford, Massachusetts 01730
(Received January 18, 1971)

Publication costs assisted by the Air Force Cambridge Research Laboratories

Release of barium vapor at high altitude provides a useful geophysical tool by forming a visible tracer for motions of ions and neutrals in the ionosphere. The excitation, ionization, and oxidation of atomic barium released in sunlight between 100 and 200 km altitude is examined in this paper. Observed spectral measurements of resonance Ba and Sr atoms, excited Ba atoms, Ba ions, and BaO molecules provide the basis for estimating relative importance of the several processes. Excitation of ground-state barium to excited metastable levels with a time constant of 1 sec is followed by photoionization with a time constant of 30 sec. Oxidation of the metastables has an altitude-dependent time constant, ranging from a fraction of a second at 100 km to 40 sec at 200 km. Thus oxidation dominates over ionization at low altitudes and limits observations of ion clouds to altitudes above about 150 km.

Introduction

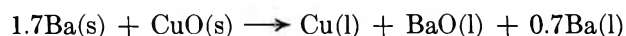
Chemical releases have been made into the earth's upper atmosphere for geophysical measurements for about 15 years. Released metal atom vapor reflects sunlight at its resonance radiation wavelengths, and can be photographed at twilight against the dark sky background. Injections of 1 kg of vapor can create a trail 1 km in diameter and 100 km long, the distortion and motion of which permit atmospheric winds to be derived from observations over a period of 100–1000 sec.

The release of barium vapor is a method of generating a high-density plasma in a sunlit upper atmosphere. Both neutral and ionized components resulting from the release may be separately tracked at twilight by ground-based optics in the light of their visible spectral emissions. The use of these releases to determine electric and magnetic fields and the dynamics of the atmosphere at altitudes from 160 km to several earth radii has been described in the literature.¹ The chemistry of the released barium vapor at high altitudes (where interaction with sunlight is the only factor in the kinetics) has also been discussed elsewhere,² but at altitudes below 200 km oxidation processes are also important. This paper will present recent data and interpretation concerning the competition between ionization and oxidation found in some 40 releases made in the last 5 years at heights from 95 to 200 km. The discussion is based on the time history of observed spectral emissions of four components: barium neutral, barium ion, barium oxide, and strontium neutral. The structure and composition of the upper atmosphere into which the barium vapor is released is defined by Table I.^{3,4} These values are subject to variations due to diurnal, seasonal, and solar effects, but serve to indicate that electron densities of more than 10^6 cm^{-3} would constitute a detectable perturbation of the iono-

sphere, while a corresponding initial barium density would be a minor constituent. In fact electron densities as high as 10^7 to 10^8 cm^{-3} have been achieved by the barium release technique.

Experimental Section

A few kilograms of a mixture of copper oxide and barium metal (1:1.7 mole ratio) is carried in a vaporizer aboard a rocket to the desired release point. Ignition at altitude results in substantially complete reaction within 30 msec to a 2500–3000°K liquid phase mixture of Cu, BaO, and Ba (and a small quantity of Ba vapor and outgassing products) at about 100 atm pressure. A



vented diaphragm is ruptured at 100 msec, and the entire canister contents are ejected (about 90% in 200 msec after vent.)

The vented material consists principally of barium vapor and liquid droplets of a mixture of barium, barium oxide, and copper (ground tests show that very little remains in the vaporizer). Barium vaporizes from the liquid droplets as the cloud of vapor and liquid moves along the rocket trajectory and expands radially, but cooling by radiation and evaporation reduces the vaporization to a negligible rate within 100 msec after release. The total barium vapor yield in our releases, which ranged from 2 to 6 kg of initial chemical mix, was between 7 and 10% of the original excess barium over a wide range of release altitudes and pay-

(1) G. Haerendel and R. Lust, *Sci. Amer.*, 219, 80 (1968).

(2) G. T. Best and N. W. Rosenberg, "Spectroscopic Studies of Barium Release," paper presented at IAGA Symposium, Madrid, Sept 1969.

(3) U. S. Standard Atmosphere Supplements, U. S. Government Printing Office, Washington, D. C., 1966.

(4) COSPAR International Reference Atmosphere, North Holland, Amsterdam, 1965.

Table I: Structure of Upper Atmosphere^a

Altitude, km	Temperature, °K	$N(N_2)$, cm^{-3}	$N(O_2)$, cm^{-3}	$N(O)$, cm^{-3}	$N(e)$, cm^{-3}	Collision frequency, sec^{-1}	Mean free path, cm
100	208	8.2 (12)	2.0 (12)	5.0 (11)	1 (5)	2.4 (3)	1.7 (1)
120	355	4.0 (11)	7.5 (10)	7.6 (10)	1.5 (5)	1.6 (2)	3.3 (2)
160	721	1.9 (10)	2.6 (9)	9.8 (9)	3 (5)	1.4 (1)	7 (3)
200	934	3.3 (9)	3.6 (8)	3.2 (9)	5 (5)	4.7 (0)	2.1 (4)

^a The number in parentheses is the exponent of 10, *i.e.*, 8.2 (12) = 8.2×10^{12} .

load sizes. There is an apparent increase in the yield of releases larger than 12 kg of chemical mix. In the experiments reported here, vaporized barium totaled about 1 mol, which would occupy about 0.1 km³ at ambient number density at 200 km.

A small quantity of vaporized barium oxide and barium ion is also observed in ground-state resonance lines in streak spectra for the first 200 msec. The barium metastable levels may also be thermally populated to a small extent, but are not seen because of the lower oscillator strengths of their "resonance lines".⁵

These transient features disappear as the spherical shell expands and the number density along the line of sight drops below the threshold for detection. After the vapor cloud has come to rest, a ring of particulate matter continues to expand with a radial velocity of 1 km sec⁻¹ perpendicular to the rocket trajectory and moves along the rocket trajectory with the original velocity of the rocket. This ring is identified as particulates because it scatters all wavelengths of the solar spectrum, even to the point of showing the solar Fraunhofer lines. A montage of photographs of a release is shown in Figure 1 and shows early time growth of vapor and particulates as well as late-time configurations of the ionized and neutral clouds.

Reaction Processes Following Release

The processes following the generation of a cloud of neutral barium vapor at high altitude in sunlight may be described qualitatively as excitation to metastable levels followed by the competing processes of ionization and oxidation. We shall now discuss each of these separately.

(a) *Excitation.* A partial term diagram of neutral barium is shown in Figure 2 and indicates the spectral features observed in emission from sunlit barium releases. Intensity data from spectra taken during the first 3 sec using $1/30$ sec resolution TV scanning are shown in Figure 3. Note that the ground-state resonance features of strontium and barium show a peak intensity at 0.1–0.3 sec, then falling rapidly to a more nearly constant level. This is believed to be due to the greater doppler width of the resonance lines before the cloud reaches thermal equilibrium with the ambient. The singlet and triplet metastable features are also seen to peak at about 1 sec after release. Optical

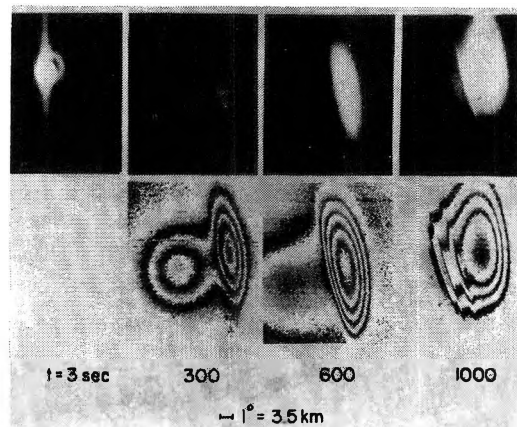
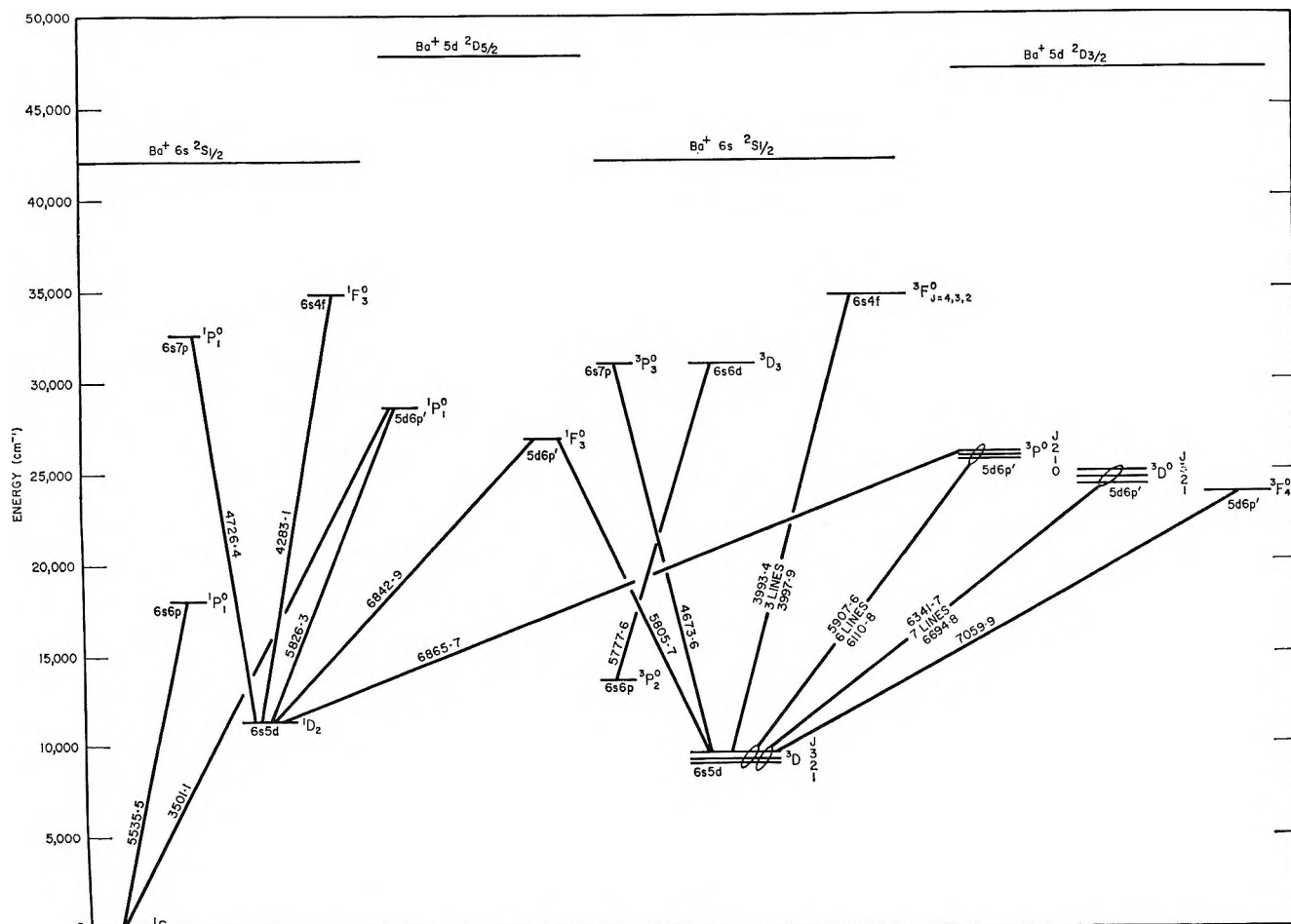


Figure 1. Montage of Ba release photographs. The lower row presents density contours of the unfiltered photographs above, and shows more clearly the weak neutral cloud. The 3-sec frame shows a neutral Ba sphere surrounded by a particulate ring. (The vertical line is caused by smearing of the bright central image in shutterless camera operation.) The 300-sec frame shows the separation of the ion cloud which has diffused preferentially along the earth's magnetic field lines from the spherical neutral cloud which is moving with the ambient wind. By this time, there is no significant Ba atom content remaining in the neutral cloud, which is scattering light only in Sr resonance and BaO band emissions. The 600-sec frame shows further separation, and development of a "bridge" connecting the ion cloud and the very weak neutral cloud. Spectroscopy shows that this bridge consists of ions, and is discussed in the text. The 1000-sec frame shows development of striations in the ion cloud by drift-caused instabilities.

pumping of the metastable ¹D level has been calculated to have a time constant of $\tau = 1.24$ sec, and it may be shown that solar irradiation will rapidly populate the 6s5d ³D metastable levels *via* the 5d6p' ¹F₃^o level ($\tau = 0.42$ sec) and *via* the 5d6p' ³P₂^o level ($\tau = 1.08$ sec). The 6s5d ³D₃ level is first populated but the multiplets between the ³D^o, ³P^o terms and the ³D term ensure rapid pumping of all ³D levels. The decay of 6s6p ³P₁^o (which is produced by the absorption of solar photons at 7911 Å) will also produce some metastable ³D barium atoms, but the time constants involved are 10–20 sec. The intensities of all the metastable lines decay as the barium ion lines grow in with the same time constant, which increases with altitude, asymptotically approach-

(5) B. M. Miles and W. L. Wiese, *Nat. Bur. Stand. (U. S.) Tech. Note*, No. 474 (1969).



Ba I TERM DIAGRAM

Figure 2. Term diagram of Ba I showing emission features observed in sunlit high altitude releases.

ing 30 sec at altitudes above 260 km. This behavior will be explained in terms of removal of the neutral metastable barium by the competing processes of ionization and oxidation.

Strontium is present in the barium as a 1% contaminant, but displays only its resonance line at 4607 Å in these experiments. Because the 5s5p 3P term for strontium is lower than the 5s4d 3D term, the latter is not metastable in strontium, whereas the corresponding 6s5d 3D term for barium is lower than the 6s6p 3P term, and is metastable. If strontium were to ionize to any significant extent the SrII resonance lines at 4078 and 5215 Å would be seen. Likewise if significant SrO were produced the blue bands of the $B^1\pi-X^1\Sigma$ system would be seen.

(b) *Ionization.* As has been documented by Foppl, *et al.*,⁶ the reason for the choice of barium for the production of an ionized plasma was that the resonance lines of both neutral and ionized barium lay in the visible region of the spectrum. The expected time constant for solar photoionization from the ground state was estimated by Foppl, *et al.*, as 2000 sec⁻¹, due to both continuum photoionization and the exci-

tation of autoionizing levels. Using the recent cross section measurements of Hudson, Carter, and Young⁷ this estimate could be doubled, giving a photoionization time constant of about 1000 sec. The observed time constant for photoionization is in fact much closer to 30 sec, and is explained by a two-step process *via* one or more of the $^1,^3D$ metastable levels of barium. Consequently the wavelength required for photoionization is not 2380 Å, but in the region 3000–3260 Å, which provides a photon irradiance some 20–40 times greater in the solar flux, as shown in Table II.

The presence of strongly autoionizing levels in barium was first pointed out by Garton and Codling,⁸ who showed that the large photoionization cross section near the $6^2S_{1/2}$ limit was due to the presence of the 5d8p $^1P_1^o$ level close to the series limit, and which combined strongly with the $6s^2\ ^1S_0$ ground state. Autoionizing levels 5d9p and 5d10p $^3P_1^o$ were also noted in absorp-

(6) H. Foppl, G. Haerandel, J. Loidl, R. Lust, F. Melzner, B. Meyer, H. Neuss, and E. Reiger, *Planet. Space Sci.*, **13**, 95 (1965).

(7) R. D. Hudson, V. L. Carter, and P. A. Young, *Phys. Rev. A*, **2**, 643 (1970).

(8) W. R. S. Garton and K. Codling, *Proc. Phys. Soc.*, **75**, 87 (1960).

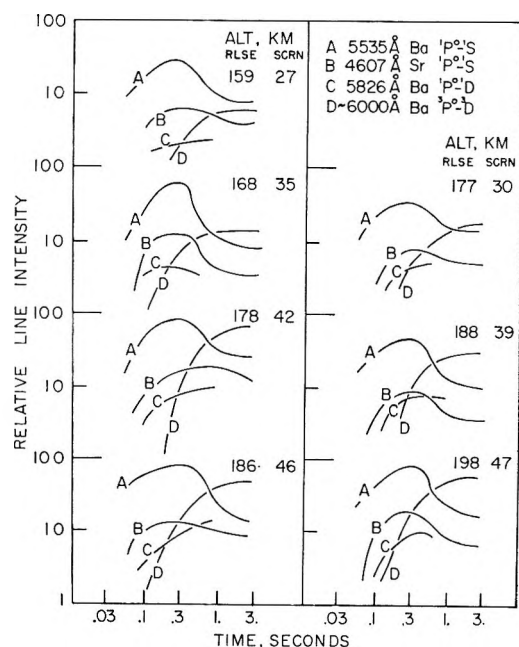


Figure 3. Relative intensities of spectral features of a barium release in the first 3 sec obtained by a slitless TV spectrograph.

contributions to the rate of photoionization. However, the natural lifetime of the 1D level is reported to be 0.5 sec,^{10a} so it is concluded that the major source of ions is the 3D metastable term.

(c) *Oxidation.* At release the Ba inventory is almost entirely ground state. By times of the order of 1 sec (Figure 3) the neutral cloud is found to emit at wavelengths corresponding to ground state and metastable Ba, but only ground-state Sr (present as an impurity). By times of the order of 100 sec, the neutral cloud has lost all of its atomic Ba emissions and is radiating only in BaO bands and the ground-state atomic Sr line. Barium atoms disappear as the result of two competing processes, one of which is seen to be photoionization. Correcting for the fixed photoionization rate we may determine the altitude dependence of the other process from the observed rate of neutral disappearance. We find that over a large altitude (*i.e.*, density) range this rate constant is directly proportional to the number density of O_2 , with a two-body rate coefficient of $0.9 \times 10^{-10} \text{ cm}^3 \text{ molecule}^{-1} \text{ sec}^{-1}$. This rate coefficient is sufficiently large to indicate that the activation energy is small.

The bond strength of BaO is most recently reported by Gaydon^{10b} as 5.7 eV, which makes the $Ba + O_2$ reaction exothermic by 0.6 eV. However, metastable barium oxidation will be exothermic by an additional 1.2 eV and, because of the electronic excitation, may have a significantly lower activation energy. Reaction between barium and atomic oxygen is believed to be insignificant because it would require three-body collisions, which are too infrequent above 120 km.

We believe that oxidation by O_2 involves metastable rather than ground-state barium since the Sr present, which has no metastable levels, persists with no evidence for oxide formation. The slitted spectrograph which was used to give time-resolved atomic line spectra could not detect the barium oxide band spectrum with sufficient time resolution to determine directly the rate of barium oxide formation as a function of altitude. However, it has been determined that low-altitude releases form dense oxide clouds and the quantity of oxide produced decreases with increasing altitude. Additional evidence for the role of O_2 in oxidizing atomic barium comes from the laboratory measurements of Sakurai, Johnson, and Broida,¹¹ who find that there is an optimum ratio of O_2/Ba which produces a maximum yield of BaO, as detected by its fluorescence spectrum. A microwave discharge in the oxygen before mixing reduced the BaO fluorescence. Presumably the pro-

(9) W. R. S. Garton, W. H. Parkinson, and E. M. Reeves, *Proc. Phys. Soc.*, **80**, 860 (1962).

(10) (a) A. Gallagher, private communication, June 1969; (b) A. G. Gaydon, "Dissociation Energies," Chapman and Hall Ltd., London, 1968.

(11) K. Sakurai, S. E. Johnson, and H. P. Broida, *J. Chem. Phys.*, **52**, 1625 (1970).

Table II: Integrated Solar Photon Irradiance $\int_0^\lambda \theta_\lambda d\lambda$ above the Earth's Atmosphere

Wavelength λ , Å	Integrated photon irradiance, photons $\text{cm}^{-2} \text{ sec}^{-1}$
2200	5.0 (13)
2400	1.6 (14)
2600	3.5 (14)
2800	9.0 (14)
3000	2.3 (15)
3200	4.6 (15)
3400	8.1 (15)

tion from the ground state. A subsequent attempt to find transitions from the metastable $5d6s \ ^1,^3D$ levels to these autoionizing levels failed to detect any significant lines.⁹ It thus appears probable that the photoionization is due to continuum absorption by one or more of the $^1,^3D$ metastable levels. An attempt to isolate the particular level responsible, using the selective ultraviolet absorption of atmospheric ozone, has been reported elsewhere.² In the experiments described the earth's ozone layer was used to screen selectively, as a function of release altitude and solar depression angle, various wavelengths of solar radiation. The experiments were designed to find how late in evening twilight a barium release would still generate ion clouds. The rate of production of ions under various release conditions was measured and compared with rates computed according to various assumptions regarding the photoionization process. The conclusion was that both the 1D and 3D levels made significant

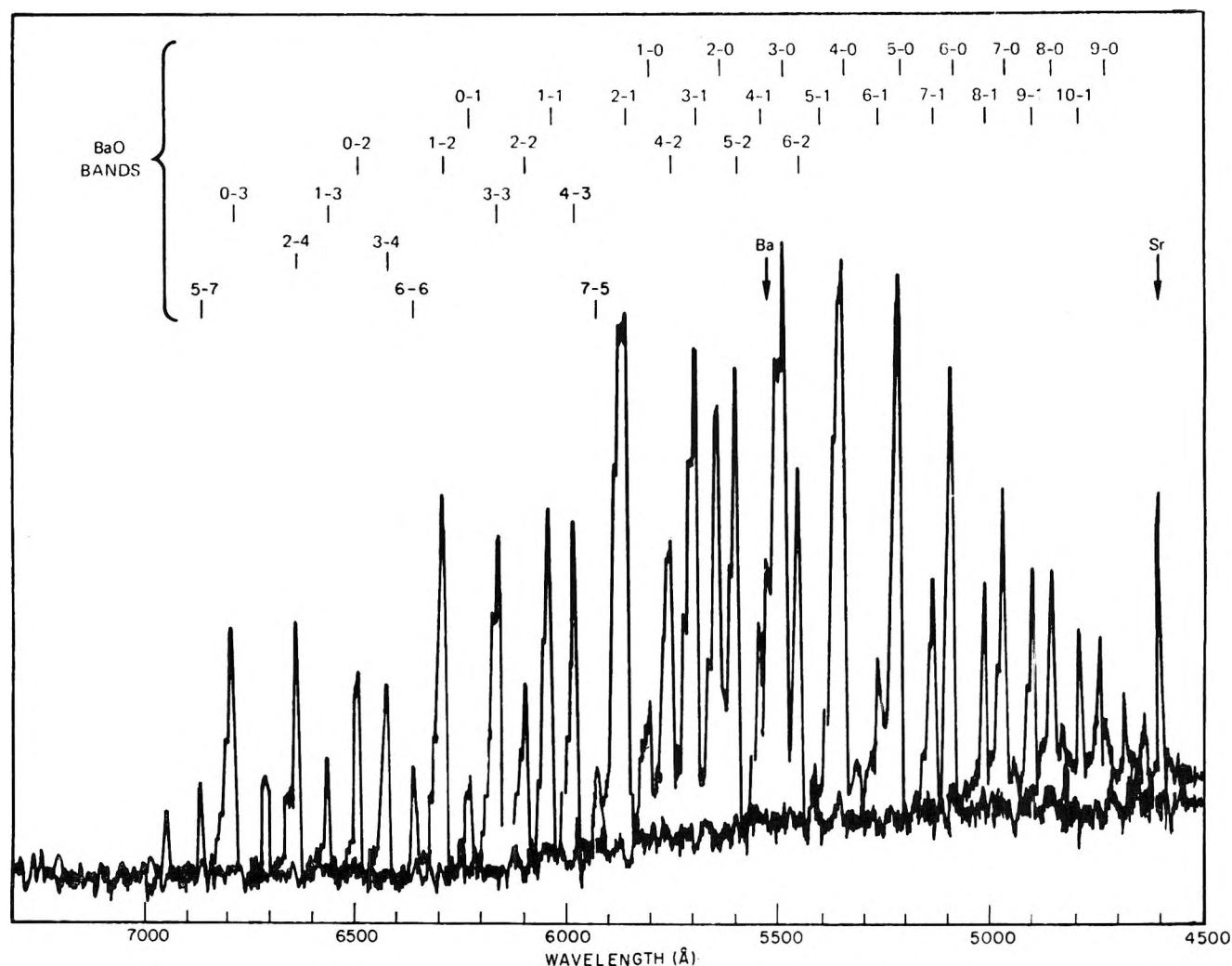


Figure 4. BaO spectrum obtained from release at 106 km.

duction of a small amount of atomic oxygen was accompanied by a corresponding reduction in the O_2 density. They favor the view that an excessive increase in the amount of O_2 present quenches the $A^1\Sigma$ state of BaO. However in upper atmosphere releases at 100 km the BaO fluorescence is strongly extinguished, yet the time between collisions (0.4 msec) is much longer than the measured lifetime of the excited state (12 μ sec). Therefore absence of BaO fluorescence at 100 km is attributed to a lack of BaO. A mass spectrometric study of species present in the barium-oxygen system¹² showed no reaction of BaO with O_2 , and no Ba-O species in which the ratio O/Ba was greater than unity were observed. Possibly the high temperature or the ionizing beam prevent such species from being observed.

One curious feature of the ultraviolet-screened experiments already referred to was the slow observed rate of disappearance of the low neutral barium clouds which could only be explained by assuming a rate of oxidation some ten times slower than for releases in full sunlight. With the data available it cannot be

determined whether the boundary between slow oxidation and normal oxidation depends on altitude or screening height. No major change in atmospheric composition at twilight exists which can be invoked to explain this phenomenon. The experiment is to be repeated with simultaneous rocket-borne measurements of the solar uv irradiation at selected wavelengths.

Other Observed Reactions

The foregoing three reactions are accompanied or followed by other reactions which are only significant under certain conditions. We shall discuss each of these separately below.

(a) *Recombination.* At the electron temperatures found in the upper atmosphere, radiative recombination has been shown to be much more significant than dielectronic recombination.¹³ The rate coefficient for

(12) M. G. Inghram, W. A. Chupka, and R. F. Porter, *J. Chem. Phys.*, **23**, 2159 (1955).

(13) L. Goldberg, "Autoionization," A. Temkin, Ed., Baltimore, Md., 1966, p 14.

radiative recombination of barium ions is probably about $10^{-12} \text{ cm}^3 \text{ sec}^{-1}$ so that a plasma density as large as 10^7 cm^{-3} would have a half-life of 10^5 sec . Thus recombination is negligible at high altitudes and the ultimate disappearance of the ion cloud is due to diffusion. At lower altitudes, other reactions play some role.

(b) *Photodissociation.* Following the release of larger payloads it is noticed that after the ion and neutral clouds have separated there is a much weaker ion "bridge" joining the neutral and ionized clouds. This is believed to be due to photodissociation of BaO to form fresh neutral barium atoms which are again subject to the competing processes of ionization and oxidation. The bridge is due to the ions created from these neutrals. Most of the spectral features of the neutral barium atom have been weakly detected in the "oxide clouds". The photodissociation threshold for BaO is 2637 \AA and this process is considered much more probable than photoionization ($\lambda \leq 2100 \text{ \AA}$). In the ultraviolet-screened experiments an ion bridge did not form. A time constant for photodissociation of a few thousand seconds would permit a detectable ion bridge to be formed without significantly depleting the barium oxide cloud.

(c) *Subsequent Consumption of Barium Oxide.* The barium ion actually constitutes a minor constituent in the ambient neutral atmosphere. For example at 200 km altitude a Ba ion density of $10^7/\text{cm}^3$ is about the highest achieved (and is much higher than ambient ion density of $5.10^6/\text{cm}^3$) yet is only $1/1000$ of the local neutral ambient density. Even the local O_2 number density at this altitude is about 40 times as great as the barium ion density, so appreciable depletion of O_2 should not be observed. On the other hand, at altitudes near 100 km, the expanding barium vapor release actually pushes the ambient atmosphere aside and it is therefore possible to produce a photoionized core before the ambient O_2 molecules reach the center. In recent releases performed in the 100-km region, persistent ionization with a density of $4 \times 10^6 \text{ cm}^{-3}$ was detected by radiofrequency techniques. Optical detection of ions was unsuccessful using conventional techniques due to the bright sky background at the release conditions necessary for photoionization and because of the dense barium oxide cloud which was generated. The barium oxide bands scatter efficiently throughout the visible spectrum (see Figure 4) and ion and neutral clouds do not separate at these altitudes.

Spectroscopic observations of these 100-km region releases showed that BaO itself may be consumed. At altitudes below 100 km the BaO disappeared within 1 sec to a cloud of white smoke. At 107 km the BaO cloud intensity reached a peak within 1 or 2 sec of release and then decayed over 20 sec.

These releases have yielded many spectra of the BaO band system and over 40 bands have been identified, almost filling the Deslandres table out to $v' = 10$ by

$v'' = 4$. Peak intensities appear to follow closely the first three Condon parabolaes.¹⁴ These releases may prove to be useful sources of oxide band spectra where relative intensity data will yield information concerning the variation with internuclear distance of the electronic transition moment. In laboratory spectra such measurements may be rendered inaccurate due to the intense electric fields of the exciting arc or other aspects of the excitation mechanism. Information concerning the absolute oscillator strength of the $A'\Sigma-X'\Sigma$ transition may also be derived from spectroscopic data on releases in the 150–200-km range.

As has already been pointed out, strontium has no metastable levels and neither oxidizes nor ionizes to any significant extent compared with barium at high altitudes. There is, however, some evidence that strontium is slowly consumed at 108 km, and at 98 km the strontium decays as rapidly as the barium.

Concluding Remarks

Many of the processes leading to the generation of an ionized plasma following a release of barium vapor are now well understood. There are many other associated mechanisms which become important under certain conditions, and which are yet to be completely documented. The present state of our knowledge concerning barium releases may be summarized by Figure 5. The major limitation to barium yield in the

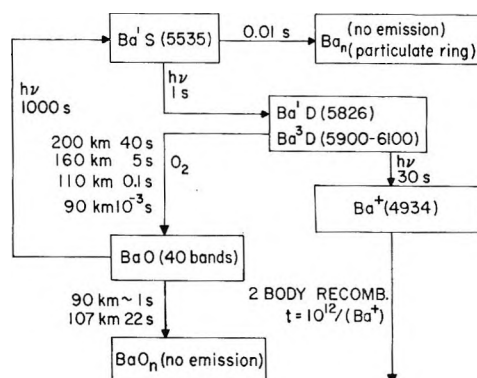


Figure 5. Diagram showing overall state of knowledge of processes involved in upper atmospheric barium releases.

thermite reaction mixture is that 80–90% of the "free" barium is trapped in the solidifying droplets expelled from the canister and significant increases in release temperature are limited by materials used. The use of larger payloads will not give a corresponding increase in ion density since optical thickness effects limit the rate of production of metastable barium.

(14) W. M. Vaidya, D. D. Desai, and R. G. Bidaye, *J. Quant. Spectrosc. Radiat. Transfer*, **4**, 353 (1964).

Acknowledgments. We wish to acknowledge the cooperation of W. K. Vickery of AFCRL responsible for design of the barium payloads; E. F. Allen of Space

Data Corp. responsible for fabrication of the payloads; and I. Kofsky of PhotoMetrics, Inc. responsible for much of the data reduction necessary for the study.

Difference Chromatography of Sea Water¹

by Paul C. Mangelsdorf, Jr.,*

Department of Physics, Swarthmore College, Swarthmore, Pennsylvania 19081

and T. Roger S. Wilson

Woods Hole Oceanographic Institution, Woods Hole, Massachusetts 02543 (Received January 11, 1971)

Publication costs assisted by the Woods Hole Oceanographic Institution

When sea water samples are analyzed by the method of difference chromatography the composition differences are resolved into the coherent waves described by Helfferich and Klein. The predicted sequence of affinity cuts is found. Cation composition variations produced in the initial anion front by changes in total normality are found to be satisfactorily predicted by the theory. Similar variations produced by changes in the SO_4/Cl ratio are found to be consistent with the theory and with previously verified consequences of a sea water model due to Garrels and Thompson. However the activity coefficient of K^+ is more strongly reduced by SO_4^{2-} enrichment than the model predicts.

Introduction

Sea water is a concentrated mixed electrolyte solution containing large proportions of ions of certain lithophilic elements² plus trace amounts of everything else that can be leached from a planetary surface. The specific composition of sea water is of theoretical interest only to geochemists. To the physical chemist sea water represents one instance of a large class of possible mixed electrolyte solutions, therefore of practical interest only because there is so much of it.³

The constancy of the relative proportions of the major ions in sea water has long been recognized,⁴ and has been amply verified by the recent work of Morris and Riley,⁵ Culkin and Cox,⁶ and Riley and Tongudai,⁷ summarized in Table I.

The reported variations in ionic proportions are small and not very systematic. However, all the geochemical factors controlling the composition of sea water must be reflected in such small residual variations from place to place and from time to time.

At Woods Hole we have been attempting to study these variations by the use of "difference chromatography,"⁸ a form of ion-exchange chromatography in which a sample of an unknown mixture is injected into a carrier stream of a standard mixture closely similar to the unknown. The method is a null method: if the mixtures are identical a detector at the column output will give a steady undeflected reading. When compo-

sition differences do exist between the two mixtures these are resolved into a set of "coherent" composition pulses,⁹ eigenvectors in composition space,⁸ each of which travels separately down the column at a characteristic speed. The theory of such coherent pulses and steps has been fully developed in the recent definitive volume by Helfferich and Klein.⁹

It should be strongly emphasized that the response pattern obtained is *not* (as might have been expected) one in which each component has its own separate pulse or step across which the concentrations of all other components are constant. On the contrary the concentrations of *all* sorbed components will, in general, change during each pulse or step.

(1) Contribution No. 2623 from the Woods Hole Oceanographic Institution.

(2) V. M. Goldschmidt, "Geochemistry," A. Muir, Ed., Oxford University Press, 1954, Chapter II, Table VI.

(3) About 1.37×10^{21} l., all told: H. U. Sverdrup, M. W. Johnson, and R. H. Fleming, "The Oceans," Prentice-Hall, Englewood Cliffs, N. J., 1942, Table 4.

(4) J. P. Riley in "Chemical Oceanography," Vol. 1, J. P. Riley and G. Skirrow, Ed., Academic Press, New York, N. Y., 1965, Chapter I, Historical Introduction.

(5) A. W. Morris and J. P. Riley, *Deep-Sea Res.*, **13**, 699 (1966).

(6) F. Culkin and R. A. Cox, *ibid.*, **13**, 789 (1966).

(7) J. P. Riley and M. Tongudai, *Chem. Geol.*, **2**, 263 (1967).

(8) P. C. Mangelsdorf, Jr., *Anal. Chem.*, **38**, 1540 (1966).

(9) F. Helfferich and G. Klein, "Multicomponent Chromatography," Marcel Dekker, New York, N. Y., 1970.

Table I: The Major Ion Composition of Sea Water as Determined by Recent Investigators

Ion	Ratio to chlorinity ^a	No. samples	Ref
Na ⁺	0.5555 ± 0.0007	49	b
	0.5567 ± 0.0007	93	c
Mg ²⁺	0.06692 ± 0.00004	66	b
	0.06667 ± 0.00007	91	c
Ca ²⁺	0.02126 ± 0.00004	66	b
	0.02128 ± 0.00006	81	c
K ⁺	0.0206 ± 0.0002	54	b
	0.0206 ± 0.00015	84	c
Sr ²⁺	0.00040 ± 0.00002	58	b
	0.00042 ± 0.00002	38	c
SO ₄ ²⁻	0.14000 ± 0.00023	345	d
Br ⁻	0.003473 ± 0.000012	219	d

^a Expressed as the weight ratio gram/gram. "Chlorinity" exceeds the true total chloride, being the total number of equivalents of all halide precipitated in a silver titration, multiplied by the equivalent weight of chlorine. See ref 22. ^b Reference 6. ^c Reference 7. ^d Reference 5.

With an appropriate calibration it is possible to interpret each pulse amplitude—as measured on any suitably sensitive detector—in terms of all the composition changes associated with that pulse.¹⁰ For each component the concentration difference between the unknown and the standard can be reconstructed as the sum of all the concentration changes (in that component) occurring in the several pulses.

The fundamental equations for the speed of a coherent front are given by Helfferich and Klein as¹¹

$$u = u_{c_i} = u_{c_j} \text{ for all } i \text{ and } j \quad (1)$$

and

$$u_{c_i} = \frac{u_0}{1 + (\partial \bar{c}_i / \partial c_i)} \text{ for all } i \quad (2)$$

where u_{c_i} is the "concentration velocity" of species i ,¹² u_0 is the flow velocity of the mobile phase, and \bar{c}_i and c_i are concentrations (per unit volume of column) of species i in the stationary and mobile phases, respectively.

These equations are derived solely from considerations of continuity and therefore hold for *any* definable extensive component regardless of binding coefficients, activity coefficients, ionic associations, etc. Effects of the latter sort will be reflected in the velocity eigenvalues and in the composition eigenvectors.

According to these equations any component not bound on the column ($\bar{c}_i \equiv 0$) can only change its solution concentration in a front travelling with the flow speed. After this initial solution front there will be as many different steps (pulses) as there are compositional degrees of freedom in the stationary pulse. For ion exchange this number will be, in general, one less than the number of exchangeable ions. Thus, in our cation-

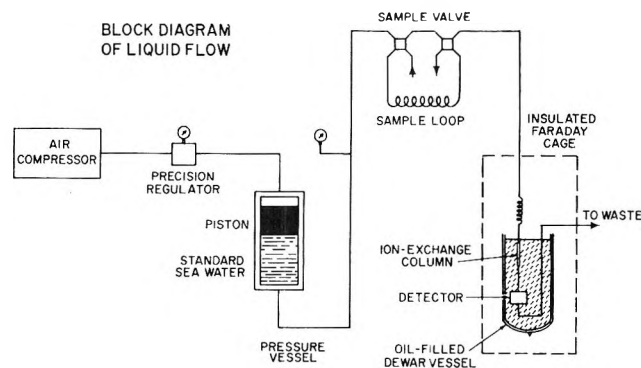


Figure 1. Schematic diagram of difference chromatograph.

exchange analysis we should expect that all the variation in anion composition, including *total anion normality*, will take place in an initial front travelling with the flow speed.¹³ All subsequent cation composition changes should take place at constant anion composition and constant total normality. One might therefore expect that these cation pulses would reflect changes only in the proportions of the cations to one another and would be entirely independent both of the total normality of the original mixture and of its anionic composition. To a good first approximation this is true. However, precise calibrations reveal two necessary refinements.

1. Large initial differences in total normality of sea water give rise to measurable cation pulses even in the absence of initial differences in the cation ratio. To compensate for this effect we have to make an "anion peak correction" in our cation analyses.

2. Changes in the anion ratios, specifically in the $\text{SO}_4^{2-}/\text{Cl}^-$ ratio, give rise to small cation pulses, even at constant total normality.

It is the purpose of this paper to attempt to relate the observed behavior of the difference chromatograph, including these two refinements, to the theoretical framework provided by Helfferich and Klein, and to the fundamental physical chemistry of sea water.

Experimental Section

For the work described here the apparatus was as indicated in Figure 1, except that the air pressure/piston drive has been replaced with a pump in the most recent work. The temperature of the oil-filled dewar flask containing the column and the detector is not

(10) Since the theory is the same for *steps* (produced by a single switch from one mixture to another) as for *pulses* (produced by switching over and back) and since the notion of stepwise composition changes from an initial mixture to a final mixture is easier to visualize, the discussion here is couched in terms relating to the step picture though the experimental work is all done with pulses.

(11) See ref 9, eq 3.37 and 3.13.

(12) The concentration velocity of a species is defined as the rate of advance of a specified concentration of that species: $u_{c_i} \equiv (\partial z / \partial t)_{c_i}$.

(13) This conclusion would be modified by the occurrence of significant *electrolyte sorption* on the column, cf. F. Helfferich, "Ion Exchange," McGraw-Hill, New York, N. Y., 1962, Section 5-3c

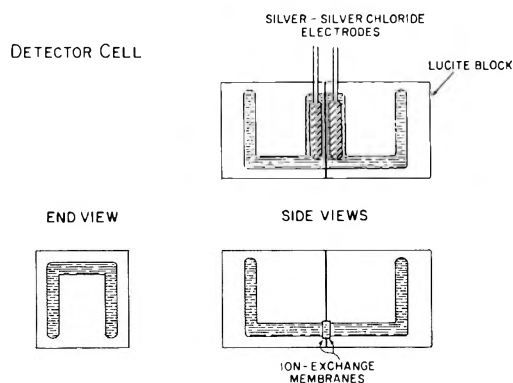
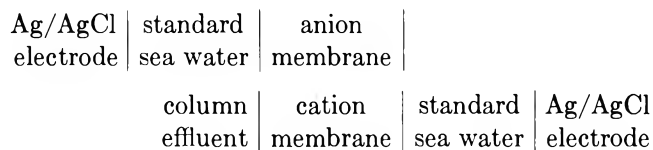


Figure 2. Schematic diagram of membrane cell detector.

regulated since steady drifts are much more acceptable to us than cyclic fluctuations. Instead we keep this part of the apparatus packed in styrofoam insulation inside a wooden case in a temperature-controlled room held at $21 \pm 1^\circ$. Thermal equilibration between the inside and outside is mainly provided by the sea water flowing, at the rate of about a liter per day, through the 3 or 4 l. of oil bath.

The actual column temperature will run slightly higher than the room temperature since 0.8–2.0 kJ/l. of Joule heat is developed in the column by the flowing water.

For all our work the detector consists of an ion-exchange membrane cell¹⁴ of the form



For the membranes we have used AMF ion C-103C cation membrane and A-104B anion membrane manufactured by American Machine and Foundry Co., Springdale, Conn. This cell has been extensively employed for membrane salinometry here and at other laboratories,^{15–20} and its response to various electrolyte mixtures has been determined.¹⁹ The response to ordinary salinity changes is about 95 mV/decade, or 40 mV/neper, at room temperature.

The detector geometry, indicated schematically in Figure 2, is arranged to permit good thermal contact between the metallic electrodes (whose compartments are separated only by a thin Teflon insulating film) while resisting convective exchange from the ion-exchange membranes to the electrode compartments. The sensing volume between the membranes is about 0.1 ml. The body of the cell is assembled from Lucite blocks and spacers suitably machined and clamped together longitudinally.

Output of the detector cell is amplified by a Keithley 150B Microvolt-ammeter and recorded on a chart recorder. Any initial asymmetry potential in the detector is biased out before amplification so that our rou-

tine measurements can be run at a recorder full-scale sensitivity of $6 \mu\text{V}$. We try optimistically to read our peak heights to the nearest $0.01 \mu\text{V}$ but should probably claim $\pm 0.05 \mu\text{V}$ for resolution and detection limits. There is also a typical chromatographic irreproducibility in peak heights, proportionate to the peak heights, amounting to several per cent.

Because the initial anion peak is due only to the total salinity (normality) difference between the unknown and standard which can be determined routinely by a number of methods, and because a large initial anion peak tends to perturb, or even obliterate, subsequent cation peaks, we customarily titrate the sample to our standard salinity, before running, using distilled water as a titrant and a membrane salinometer as the indicator. To obtain a standard more dilute than any pelagic or coastal samples we are likely to encounter we dilute Sargasso Sea surface water²¹ with distilled water from its typical salinity of $36.0/00$ to a standard $27.30/00$.²² Thus, all observations reported here refer to a diluted sea water about $3/4$ as salty as typical pelagic sea water.

Calibration Procedure. To calibrate the difference chromatograph we spike samples of our dilute standard sea water with small increments (1–5%) of the various cations in the chloride form and of the various anions in the sodium form, or with distilled water. Figure 3 shows the kinds of traces produced by such spikes. A least-squares linear regression of peak height against amounts of salts and against anion peak height is obtained for each of the three cation peaks we observe.²³ This regression matrix is then post-multiplied by a matrix which expresses the salt increments in terms of the fractional increments in total normality, $d \ln c_0$, and in the equivalent fractions $d \ln X_{\text{Mg}}$, $d \ln X_{\text{Ca}}$, $d \ln X_{\text{K}}$, $d \ln X_{\text{SO}_4}$. The increments $d \ln X_{\text{Na}}$ and $d \ln X_{\text{Cl}}$ are not independent but can be related to the others

$$d \ln X_{\text{Cl}} = -(X_{\text{SO}_4}/X_{\text{Cl}}) d \ln X_{\text{SO}_4} \quad (3a)$$

$$d \ln X_{\text{Na}} = -\sum (X_j/X_{\text{Na}}) d \ln X_j \quad j = \text{Mg, Ca, K} \quad (3b)$$

(14) Broadly discussed by G. J. Hills in "Reference Electrodes," D. J. G. Ives and G. J. Janz, Ed., Academic Press, New York, N. Y., 1961, Chapter 9.

(15) P. Ballard, report to fellowship committee, Woods Hole Oceanographic Institution, 1962, unpublished manuscript.

(16) P. H. Koske, *Kieler Meeresforsch.*, **20**, 138 (1964).

(17) H. L. Sanders, P. C. Mangelsdorf, Jr., and G. R. Hampson, *Limnol. Oceanogr.*, **10**, R216 (1965).

(18) P. C. Mangelsdorf, Jr., in "Estuaries," G. M. Lauff, Ed., AAAS Publications, Washington, D. C., 1967.

(19) J. M. T. M. Gieskes, *Kieler Meeresforsch.*, **24**, 18 (1968).

(20) T. R. S. Wilson, *Limnol. Oceanogr.*, in press.

(21) Sargasso Sea surface water is low in nutrients and therefore relatively sterile.

(22) Salinity is measured in parts per thousand: $0/00$. It is easier to measure than to define. Roughly: salinity = $1.805 \times$ chlorinity. Cf. R. A. Horne, "Marine Chemistry," Wiley-Interscience, New York, N. Y., 1969, Chapter 4, Section 5.

(23) A fourth peak due to Sr^{2+} differences can be demonstrated but it is naturally small and so slow in moving through the column that it is broadened beyond all detection in our normal operation.

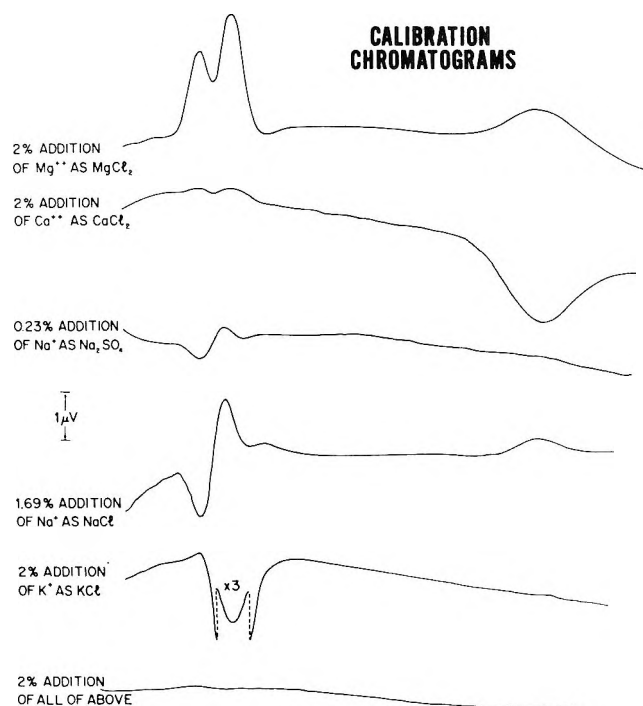


Figure 3. Difference chromatograms produced by various salts. The large initial anion peaks have been omitted from the left-hand ends of these traces, though some residual tailing can be seen. Each trace corresponds to about 20 min of operation.

The resulting product matrix should have all zeros in the column associated with $d \ln c_0$. This must be rigorously true since there should be no peaks whatsoever if the equivalent fractions all remain constant and if the anion peak has been adjusted to zero by titration. Because of this inherent constraint we usually make a least-squares adjustment of the coefficients of the original regression matrix such that each of the expected peak heights would vanish if the salts were all added in sea water proportions and if the anion peak were zero. (See Figure 3.)

Finally, the matrix dependence of peak heights on the cation equivalent fraction increments, $d \ln X_{\text{cation}}$, is inverted, yielding a calibration matrix which expresses the $d \ln X_{\text{cation}}$ as linear combinations of the peak heights and of the one anion composition variable, $d \ln X_{\text{SO}_4}$.²⁴

Results and Discussion

Five different calibration matrices obtained independently for different sample sizes and different operating conditions are given in Table II. For each of the cation peaks the set of calibration coefficients represent the corresponding composition eigenvector in units determined by the detector sensitivity.

In the first two calibrations two sets of coefficients are listed for cation peak no. 1. This peak has a marked shape peculiarity in that the initial pulse (either positive or negative) is always followed by a pronounced reverse pulse which tails back to the base line in a quasiexponential manner.²⁵ To complicate

matters the whole pattern overlaps peak no. 2. Peak no. 1 was therefore measured independently at two positions: one near the initial maximum before the onset of peak no. 2, and one on the tail after the conclusion of peak no. 2. The close proportionality between the two calibrations for the two readings of peak no. 1 was not imposed but emerges from the statistical analysis, confirming both our prior interpretation of the peak no. 1 pattern, and the validity of the statistical procedures.

Because of the overlap peak no. 2 is read as near as possible to the reversal point of peak no. 1 but the readings are probably affected somewhat by peak no. 1. The resulting calibration for peak no. 2 is empirically valid but may differ slightly from the true composition eigenvector.

Affinity Cut Sequence. The most important qualitative result here is the verification of the sequence of affinity cuts predicted theoretically by Helfferich,²⁶ and elaborated by Helfferich and Klein.²⁷ We can order the cations in a sequence of increasing affinities Na^+ , K^+ , Mg^{2+} , Ca^{2+} , such that: 1. each coherent boundary represents a cut in the sequence; 2. each successive cut travels with a slower velocity than the previous one; 3. at each boundary all components on one side of the cut change in one direction while the com-

(24) Algebraically this may be expressed simply as

$$d\vec{P} = \vec{\alpha}A + \beta d\vec{c}$$

But

$$d\vec{c} = \mathbf{M} d \ln X + \vec{D} d \ln c_0, \text{ where } \beta \vec{D} = 0$$

so

$$d\vec{P} = \vec{\alpha}A + \beta \mathbf{M} d \ln X = \vec{\alpha}A + \beta \mathbf{M}_{\text{cat}} d \ln X_{\text{cat}} + \beta \mathbf{M}_{\text{SO}_4} d \ln X_{\text{SO}_4}$$

Whence

$$d \ln X_{\text{cat}} = (\beta \mathbf{M}_{\text{cat}})^{-1} \{d\vec{P} - \vec{\alpha}A - \beta \mathbf{M}_{\text{SO}_4} d \ln X_{\text{SO}_4}\}$$

or

$$d \ln X_{\text{cat}} = f d\vec{P} + \vec{f}_A A + \vec{f}_{\text{SO}_4} d \ln X_{\text{SO}_4}$$

where

$d\vec{P}$ = cation peak heights

A = anion peak height

$d\vec{c}$ = amounts of added salts

$\vec{\alpha}$, β are regression matrices

$d \ln X$ = fractional increments in equivalent fractions

$d \ln c_0$ = fractional increment in total normality

\mathbf{M} and \vec{D} are transformation matrices for the composition variables

f , \vec{f}_A and \vec{f}_{SO_4} are the final calibration matrices

In cases where peak heights are measured at more than one position so that there are more components in $d\vec{P}$ than in $d \ln X_{\text{cations}}$ the matrix \mathbf{M}_{cat} is not square and the final inversion is performed by a least-squares method which minimizes the normalized errors in the redundant set $d\vec{P}$.

(25) For steps rather than pulses the corresponding behavior would be a step in which an initial overshoot decays slowly to the plateau value. A rate process is evidently at work here but whether in the column or in the detector we do not know.

(26) F. Helfferich, *Advan. Chem. Ser.*, **79**, 30 (1968).

(27) F. Helfferich and G. Klein, ref 9: Chapter 3, Section IV B; Chapter 5, Section IV A.2.

Table II: Calibration Matrices Obtained with Different Sample Sizes and Different Resins^a

Ion	Sulfate correction ($\partial \ln X_i / \partial \ln X_{SO_4}$)	Anion peak corrections ($\partial \ln X_i / \partial V_A$) in $10^{-4}/\mu V$	Cation peak coefficients ($\partial \ln X_i / \partial \text{peak}_j$), in $10^{-2}/\mu V$		
			Peak 1	Peak 2	Peak 3
Resin: CG-120, Type 3, 400-600 mesh Column: 15 cm \times 0.4 cm i.d. Flow: \sim 2 ml/min at 80-100 psi; air driven					
2-ml Samples					
Na	-0.11	-0.02	+0.25, -0.93	+0.02	-0.01
K	+0.21	-0.14	-0.66, +2.47	+0.36	-0.53
Mg	+0.40	+0.05	-0.98, +3.60	-0.11	-0.11
Ca	+0.22	+0.18	-0.30, +1.23	-0.03	+1.09
4-ml Samples					
Na	-0.03	-0.04	+0.28, -0.14	-0.01	+0.02
K	-0.02	-0.12	-0.89, +0.53	+0.36	-0.17
Mg	+0.10	+0.13	-1.05, +0.52	0.00	-0.26
Ca	+0.14	+0.22	-0.47, +0.23	-0.02	+0.94
Resin: BioRad 50W \times 12, 400 mesh Column and flow as above					
2-ml Samples					
Na	-0.02	-0.04	+0.15	-0.02	-0.07
K	+0.02	-0.07	-0.08	+0.64	+0.03
Mg	+0.05	+0.18	-0.60	+0.03	-0.12
Ca	+0.06	+0.14	-0.26	+0.05	+2.25
4-ml Samples					
Na	-0.04	-0.03	+0.10	+0.01	-0.03
K	+0.02	0.00	-0.13	+0.42	-0.04
Mg	+0.14	+0.10	-0.42	-0.02	-0.18
Ca	+0.09	+0.26	-0.10	+0.01	+1.70
Resin as above Column: 20 cm \times 0.04 cm i.d. Flow: 2 ml/min at 100-350 psi, pump driven					
4-ml Samples					
Na	-0.04	-0.06	+0.13	0.00	-0.02
K	+0.01	+0.06	-0.05	+0.36	-0.06
Mg	+0.14	+0.21	-0.53	-0.02	-0.08
Ca	+0.18	+0.17	-0.14	-0.01	+0.94
Typical peak appearance time		1.8 min	6.4 min	8.6 min	20 min

^a Units are chosen so that cation peak heights in microvolts and anion peak height in hundreds of microvolts give the $d \ln X_i$ as percentage increments.

ponents on the other side change in the opposite direction.

The affinity sequence which we ascribe to our sea water system, and the corresponding cuts, is indicated in Table II. There are small apparent exceptions to prediction 3 (above), mainly associated with peak no. 2. The fraction of K^+ in sea water is so small that the changes in other constituents required to accommodate changes in K^+ are almost negligible. Ordinary experimental errors in determining these coefficients, plus the possible influence on peak no. 2 of the overlap from peak no. 1, could cause sign errors on small num-

bers. It will be noted that in no case does a sign violation of prediction 3 exceed 0.05 for 2-ml samples nor exceed 0.02 for the more reliable 4-ml samples.

Because peak no. 2 is so specific for K^+ it is difficult to be certain that K^+ comes before Mg^{2+} , rather than after, in the affinity sequence. For the purposes of the affinity cut picture it may be safer to regard our calibrations as showing two definite cuts in the sequence Na^+ , Mg^{2+} , and Ca^{2+} , with the location of K^+ relative to Mg^{2+} still undetermined. Indeed the sequence might even be different for the two different resins.

This behavior of K^+ , in peak no. 2, represents the

Table III: Comparison between Calculated and Measured Anion Peak Corrections (in $10^{-4}/\mu\text{V}$)

	Calculated	Measured (mean of 5)
$d \ln X_{\text{Na}} = d \ln X_{\text{Na}}$	$= -0.054$	$= -0.05$
$d \ln X_{\text{K}} = d \ln X_{\text{Na}} - (d \ln \gamma_{\text{K}} - d \ln \gamma_{\text{Na}})$	$= -0.054 + 0.008$	$= -0.05$
$d \ln X_{\text{Mg}} = 2 d \ln X_{\text{Na}} - (d \ln \gamma_{\text{Mg}} - 2 d \ln \gamma_{\text{Na}}) + d \ln c_0$	$= -0.107 + 0.058 + 0.25 = +0.20$	$+0.13 \pm 0.03$
$d \ln X_{\text{Ca}} = 2 d \ln X_{\text{Na}} - (d \ln \gamma_{\text{Ca}} - 2 d \ln \gamma_{\text{Na}}) + d \ln c_0$	$= -0.107 + 0.062 + 0.25 = +0.20$	$+0.19 \pm 0.02$

"trace species" case, elucidated by Helfferich and Klein, for which the concentration velocity is the same as the species velocity.²⁸ The derivative in eq 2 can be replaced by the ratio \bar{c}_i/c_i so that we may deduce directly from the ratio of appearance times that the amount of K^+ bound on the resin is at least 3.8 times as great as the amount in the surrounding sea water (per unit column volume).²⁹ The two other appearance times and composition eigenvectors have no such simple interpretation. It should be possible in principle to reconstruct the Jacobian matrix which represents the differential form of the exchange isotherm,³⁰ but the information thus gained would be entirely specific to our particular experimental conditions.

Anion Peak Correction. The second column in Table II gives the corrections which must be made for each $100 \mu\text{V}$ of anion peak magnitude. That is, when a $+100\text{-}\mu\text{V}$ anion peak occurs the sums of the composition changes in the subsequent cation peaks are less than the actual input changes by the amounts of the corrections. Since the sums of the composition changes in all the peaks must be equal to the input changes (the step picture makes this obvious), it necessarily follows that these corrections represent actual changes in cation composition which occur in the initial anion front traveling with the flow velocity.

On the other hand, eq 2 tells us that no species can change its stationary phase concentration \bar{c}_i in that initial anion front. Therefore, these cation composition changes associated with the anion front must occur while the solution composition remains in equilibrium with an unchanging column composition. However, if the column composition does not change neither should the activity coefficients of the bound ions (though the overall Donnan potential of the exchange resin might shift). The equilibrium constraint on the solution cations must be

$$d \ln a_{\text{Mg}} = d \ln a_{\text{Ca}} = 2 d \ln a_{\text{Na}} = 2 d \ln a_{\text{K}} \quad (4)$$

where a_i is the activity of species i in solution, and

$$d \ln a_i \equiv d \ln \gamma_i + d \ln m_i \equiv$$

$$d \ln \gamma_i + d \ln X_i + d \ln c_0 \quad (5)$$

in which c_0 is the total normality, m_i is the molality of species i , X_i is its equivalent fraction,³¹ and the γ_i are the conventional activity coefficients.³²

It appears that our anion peak corrections should be

quite independent of column-exchange characteristics and should only depend on the sea water composition and on the detector.

In Table III we have used eq 4 and 5 to estimate the percentage increments, $d \ln X_i$, per $100\text{-}\mu\text{V}$ anion peak. The values of $(d \ln \gamma_{\text{Mg}} - 2 d \ln \gamma_{\text{Na}})$, etc., were estimated from the concentration dependence of the mean activity coefficients of chloride solutions at 25° , tabulated by Robinson and Stokes,³³ by taking such quantities as

$$\Delta(3 \ln \gamma_{\pm, \text{MgCl}_2} - 2 \ln \gamma_{\pm, \text{NaCl}}) / \Delta \ln c_0$$

across the ionic strength interval 0.3–0.6. The quantity $d \ln c_0 = 0.25 \times 10^{-4}/\mu\text{V}$ comes from the detector sensitivity of 40 mV/neper .³⁴ The value for $d \ln X_{\text{Na}}$ was obtained by applying the constraint that

$$\sum dX_i = \sum X_i d \ln X_i = 0$$

From the agreement in Table III between the measured and calculated corrections it appears that the principal factors have been taken account of. Our theoretical characterization of the anion front as a composition variation constrained to preserve equilibrium with a cation column of constant composition is borne out. The effect we see is mainly due to valence differences, an extra term $d \ln c_0$ appearing in the expressions for the divalent ions.

Sulfate Enrichment Correction. Changing the $\text{SO}_4^{2-}/$

(28) F. Helfferich and G. Klein, ref 9, eq 3.18 and surrounding discussion; also p 60; also Chapter 4, Section VB.

(29) All of the pulses are delayed somewhat by an unknown flow volume between the sample valve and the detector, but outside the column proper. Thus the ratio of two appearance times is always closer to unity than it should be.

(30) F. Helfferich and G. Klein, ref 9, eq 5.66.

(31) $\sum X_i = \sum X_j = 1$
cations anions

From Table I and similar data for a few other minor components we estimate the approximate values

$$\begin{array}{ll} X_{\text{Na}} = 0.77271 & X_{\text{Cl}} = 0.90134 \\ X_{\text{Mg}} = 0.17619 & X_{\text{SO}_4} = 0.09332 \\ X_{\text{Ca}} = 0.03395 & X_{\text{Br}} = 0.00139 \\ X_{\text{K}} = 0.01686 & X_{\text{HCO}_3} = 0.00384 \\ X_{\text{Sr}} = 0.00029 & X_{\text{F}} = 0.00011 \end{array}$$

(32) R. A. Robinson and R. H. Stokes, "Electrolyte Solutions," 2nd ed, Butterworths, London, 1959, Chapter 2.

(33) See ref 32, Appendix 8.10.

(34) Strictly speaking we should include a correction to this number because some of the anion peak signal is caused by the composition changes we are studying as well as by the initial normality difference. However these corrections can be shown to be negligible here.

Table IV: Sulfate Effects Deduced from Sulfate Enrichment Corrections^a

Ion	$(\partial \ln X_i / \partial \ln X_{\text{SO}_4})_\eta$			—Fraction of ion in sulfate ion pair—	
	$\eta = V_A$	$\eta = c_0$	$\eta = \Gamma$	These measurements	Garrels-Thompson sea water model
Na	-0.032 ± 0.005	-0.018 ± 0.005	-0.011 ± 0.005	$+0.007 \pm 0.005$	0.012
K	$+0.008 \pm 0.005$	$+0.018 \pm 0.011$	$+0.02 \pm 0.02$	$+0.04 \pm 0.02$	0.01
Mg	$+0.11 \pm 0.02$	$+0.06 \pm 0.02$	$+0.03 \pm 0.03$	$+0.11 \pm 0.03$	0.11
Ca	$+0.12 \pm 0.03$	$+0.05 \pm 0.03$	$+0.02 \pm 0.03$	$+0.10 \pm 0.03$	0.08

^a Sulfate corrections from the first set of calibrations are considered unreliable and are not included in these averages.

Cl⁻ ratio in the sample necessitates the corrections indicated in the first column of Table II. As with the anion peak effects these corrections must correspond to actual cation composition changes which occur in the initial anion front. Again these must be of such a nature as to preserve the exchange equilibrium without altering the composition of the stationary phase.

The nature of our calibration procedure is such that these sulfate enrichment corrections, estimated at zero anion peak V_A , are of the form

$$(\partial \ln X_i / \partial \ln X_{\text{SO}_4})_{V_A=0}$$

subject, of course, to the column equilibrium constraint. To obtain thermodynamic quantities independent of our detector we need to estimate the related expressions

$$(\partial \ln X_i / \partial \ln X_{\text{SO}_4})_\eta = (\partial \ln X_i / \partial \ln X_{\text{SO}_4})_{V_A} + (\partial \ln X_i / \partial V_A)_{X_{\text{SO}_4}} (\partial V_A / \partial \ln X_{\text{SO}_4})_\eta \quad (6)$$

where η could be the normality c_0 or the ionic strength Γ .

The coefficients $(\partial \ln X_i / \partial V_A)_{X_{\text{SO}_4}}$ are just the anion peak corrections previously discussed. The detector sensitivities $(\partial V_A / \partial \ln X_{\text{SO}_4})_\eta$, subject to the equilibrium constraint, have not been measured. However, Gieskes¹⁹ studied the effects of chemical variations on the emf of a membrane cell chemically identical with ours. From his results we estimate the quantities $(\partial V_A / \partial \ln X_i)_{c_0}$, unconstrained, which are combined with the measured quantities $(\partial \ln X_i / \partial \ln X_{\text{SO}_4})_{V_A}$ and with the detector sensitivity to give us $(\partial \ln c_0 / \ln X_{\text{SO}_4})_{V_A}$. Since, as assumed earlier, the quantity $(\partial V_A / \partial \ln c_0)_{X_{\text{SO}_4}}$ is not significantly different from 40 mV even when the equilibrium constraint is applied, we are able to deduce

$$(\partial V_A / \partial \ln X_{\text{SO}_4})_{c_0} = -3.3 \text{ mV}$$

In a similar fashion we estimate $(\partial V_A / \partial \ln X_{\text{SO}_4})_\Gamma = -5.0 \text{ mV}$. Using these values we obtain the estimates shown in Table IV.

At constant normality the term $d \ln c_0$ drops out of eq 5 and the equilibrium constraint becomes

$$d \ln \gamma_{\text{Mg}} - 2 d \ln \gamma_{\text{Na}} = -(d \ln X_{\text{Mg}} - 2 d \ln X_{\text{Na}}) \text{ etc.}$$

Therefore we obtain

$$[\partial (\ln \gamma_{\text{K}} - \ln \gamma_{\text{Na}}) / \partial \ln X_{\text{SO}_4}]_{c_0} = -0.037 \pm 0.011$$

$$[\partial (\ln \gamma_{\text{Mg}} - 2 \ln \gamma_{\text{Na}}) / \partial \ln X_{\text{SO}_4}]_{c_0} = -0.09 \pm 0.02$$

$$[\partial (\ln \gamma_{\text{Ca}} - 2 \ln \gamma_{\text{Na}}) / \partial \ln X_{\text{SO}_4}]_{c_0} = -0.09 \pm 0.03$$

$$[\partial (\ln \gamma_{\text{Ca}} - \ln \gamma_{\text{Mg}}) / \partial \ln X_{\text{SO}_4}]_{c_0} = +0.00 \pm 0.03$$

all at a total normality of 0.48 equiv/kg.

In order to estimate the activity coefficients of various species in sea water Garrels and Thompson devised a simple self-consistent model in which the amount of ion pairing was determined by the activities of free ions while the activity coefficients for the free ions depended on the total ionic strength in the same fashion as in pure solutions without association.³⁵ According to this model, then, at constant ionic strength Γ there should be no changes in the activity coefficients of free ions.³⁶

When these assumptions are applied to our system at constant Γ the equilibrium constraint becomes

$$d \ln [\text{Mg}^{2+}] = d \ln [\text{Ca}^{2+}] = 2 d \ln [\text{Na}^+] = 2 d \ln [\text{K}^+] \quad (4a)$$

Combining this with the mass action equilibria for the ion pairing with sulfate we obtain

$$d \ln X_{\text{Na}} + d \ln c_0 = d \ln [\text{Na}^+] + ([\text{NaSO}_4^-] / \text{Na}_{\text{total}}) d \ln [\text{SO}_4^{2-}]$$

$$d \ln X_{\text{Mg}} + d \ln c_0 = 2 d \ln [\text{Na}^+] + ([\text{MgSO}_4] / \text{Mg}_{\text{total}}) d \ln [\text{SO}_4^{2-}] \text{ etc.} \quad (7a)$$

plus

$$d \ln X_{\text{SO}_4} + d \ln c_0 = d \ln [\text{SO}_4^{2-}] + Q_{\text{SO}_4} d \ln [\text{Na}^+]$$

where

(35) R. M. Garrels and M. E. Thompson, *Amer. J. Sci.*, **260**, 57 (1962).

(36) The well-demonstrated existence of Harned α coefficients, even in nonassociating solutions, underlines the roughness of this approximation, ref 32, Chapter 15.

$$Q_{\text{SO}_4} = ([\text{NaSO}_4^-] + 2[\text{MgSO}_4] + 2[\text{CaSO}_4] + [\text{KSO}_4^-]) / \text{SO}_4^{\text{total}} \quad (7b)$$

Using the percentages of sulfate ion pairing calculated by Garrels and Thompson we estimate that at constant Γ the quantities $d \ln X_{\text{SO}_4}$, $d \ln [\text{SO}_4^{2-}]$, $d \ln [\text{Na}^+]$, and $d \ln c_0$ should be in the proportions $1/1.00/(-0.061)/(-0.043)$. Our sea water is only $3/4$ as concentrated as the sea water for which their model was constructed, but these particular numbers are relatively insensitive to the assumed amounts of ion pairing: with no pairing at all we would have the proportions $1/0.96/(-0.032)/(-0.038)$. Consequently we commit no serious error if we insert the values $d \ln [\text{SO}_4^{2-}] = 1.00$, $d \ln [\text{Na}^+] = -0.06$, and $d \ln c_0 = -0.04$, along with the estimated values of $(\partial \ln X_i / \partial \ln X_{\text{SO}_4})_{\Gamma}$, into eq 7a to obtain estimates of the proportions of the various cations combined as the sulfates. Thus

$$\begin{aligned} [\text{MgSO}_4] / \text{Mg}_{\text{total}} &= (d \ln X_{\text{Mg}} + d \ln c_0 - \\ &\quad 2 d \ln [\text{Na}^+]) / d \ln [\text{SO}_4^{2-}] \\ &\cong (0.03 - 0.04 + 0.12) / 1.00 \\ &\cong +0.11 \end{aligned}$$

These calculated values for the degrees of ion pairing based on our measurements are compared in Table IV with the predictions of the Garrels-Thompson model. There is surprising agreement although we find K^+ to be somewhat more strongly paired with SO_4^{2-} (*i.e.*, showing a more rapid decline in activity coefficients when SO_4^{2-} is added) than the model predicts. This discrepancy does not arise from our approximations since these affect K^+ and Na^+ equally, but can be traced back to the original calibrations in Table II.

A number of workers have tested the Garrels-Thompson model and have found evidence for ion pairing of Mg^{2+} to about the extent predicted by the model.³⁷⁻⁴²

Published estimates range from 3%^{37a} to 40%^{37b} with most values running about 10%. Ultrasonic absorption results demonstrate the existence of MgSO_4 as a distinct species with a finite dissociation rate, amounting to about 9% of total Mg^{2+} .⁴⁰

The percentage of Ca^{2+} ion tied up by ion pairing, presumably mostly as the sulfate, has been estimated by Thompson as 16%, from emf measurements with a calcium-selective electrode.⁴³ Kester and Pytkow-

icz⁴⁴ recalculated the amount of Ca^{2+} in the sulfate ion pair as $10.8 \pm 0.5\%$.

So far as we know experimental comparisons with the model predictions involving K^+ have not been previously published.

Conclusion

We conclude that the characteristic behavior of the difference chromatograph agrees in all particulars with the theory of coherent fronts developed by Helfferich and elaborated by Helfferich and Klein. To the extent that thermodynamic properties of sea water are involved in our work the coherent front theory implies values which are consistent with the previously confirmed predictions of the Garrels-Thompson model of sea water.

Acknowledgments. The continuing program in difference chromatography has been supported by AEC Contract AT(30-1)-3838. One of the sets of calibrations was obtained on an apparatus constructed and operated with the support of National Science Foundation Grant GA18347. Computer time for the calibration regressions and matrix inversions was supplied by the Swarthmore College Computer Center. The careful experimental work of Helen Stanley, Carol Taylor, and Charles Olson is especially appreciated. Our original conception of difference chromatography arose from the apparent resemblance of the composition waves of displacement analysis and frontal analysis to the finite amplitude shock waves, detonation waves, and rarefaction waves of gas dynamics. This resemblance suggested that there should also be well-behaved infinitesimal waves analogous to ordinary sound waves, which proved to be the case. For the necessary familiarity with shocks and detonations and their ways P. C. M. is indebted to a fondly remembered apprenticeship in the Gibbs Laboratory under the incomparable guidance of George B. Kistiakowsky.

(37) (a) R. F. Platford, *J. Fish. Res. Bd. Can.*, **22**, 113 (1965); (b) R. M. Pytkowicz, I. W. Duedall, and D. N. Connors, *Science*, **152**, 640 (1966).

(38) M. E. Thompson, *ibid.*, **153**, 866 (1966).

(39) J. M. T. M. Gieskes, *Z. Physik. Chem.*, **50**, 78 (1966).

(40) F. H. Fisher, *Science*, **157**, 823 (1967).

(41) R. M. Pytkowicz and R. Gates, *ibid.*, **161**, 690 (1968).

(42) D. R. Kester and R. M. Pytkowicz, *Limnol. Oceanogr.*, **13**, 670 (1968).

(43) M. E. Thompson, *Science*, **154**, 1643 (1966).

(44) D. R. Kester and R. M. Pytkowicz, *Limnol. Oceanogr.*, **14**, 686 (1969).

Dynamics of the Reactions of O_2^+ with H_2 and D_2

by M. H. Chiang, E. A. Gislason, B. H. Mahan,* C. W. Tsao, and A. S. Werner

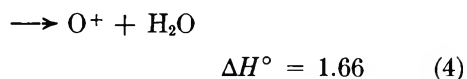
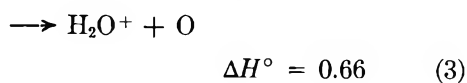
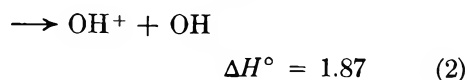
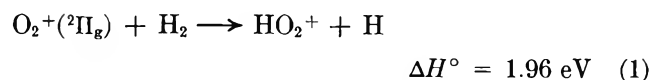
Inorganic Materials Research Division of the Lawrence Radiation Laboratory and Department of Chemistry, University of California, Berkeley, California 94707 (Received December 31, 1970)

Publication costs assisted by the U. S. Atomic Energy Commission

Velocity vector distributions of the ionic products of the reactions $O_2^+(H_2,H)HO_2^+$, $O_2^+(H_2,OH)OH^+$, $O_2^+(H_2,O)H_2O^+$, $O_2^+(D_2,O)O^+$ as well as nonreactively scattered O_2^+ are reported for several initial relative kinetic energies of collision. For relative energies below 5 eV, the distributions of HO_2^+ , OH^+ , and H_2O^+ all show the forward-backward symmetry characteristic of a reaction mechanism which involves a persistent $H_2O_2^+$ collision complex. At higher initial relative energies, a transition to direct or impulsive reaction mechanism is observed. The O^+ product appears to be formed by a direct interaction mechanism at all energies at which it can be detected. The distributions of nonreactively scattered O_2^+ give evidence of both direct and complex scattering mechanisms. The behavior of the system is qualitatively consistent with predictions based on the known major features of the potential energy surface.

As reported in a series of recent publications,¹⁻⁴ this laboratory has investigated the dynamics of exothermic ion-molecule reactions in which a hydrogen or deuterium atom is transferred from the neutral target to the projectile ion such as Ar^+ or N_2^+ . These reactions typically have large total cross sections, and the product ion velocity vector distributions in the center-of-mass system are strongly peaked in the original direction of the projectile ion beam. Rebound scattering of the product through barycentric angles as large as 180° is observed, and at initial relative energies above 4 eV, the contribution of this process is nearly as great as that of the small angle stripping process.

It seemed clear to us that an entirely different dynamical behavior might be found in endothermic ion-molecule reactions, particularly those in which the intermediate collision complex had a substantial potential energy minimum with respect to both reactants and products. The reactions 1-4 all satisfy these criteria,



and can be conveniently explored with our ion beam apparatus. Accordingly, we undertook investigations of reactions 1-4 and certain of their isotopic variations, and report the results here. Preliminary communications on this system have already appeared.^{5,6}

Experimental Section

The instrument used in this work has been described in detail previously.² It consists of a magnetic mass spectrometer for preparation of a collimated beam of primary ions of known energy, a scattering cell to contain the target gas, and an ion detection train made up of an electrostatic energy analyzer, a quadrupole mass spectrometer, and an ion counter. The detector components and the exit slit of the scattering cell are mounted on a rotatable lid, which permits the intensity of scattered ions to be measured at various angles and energies.

The primary ions were extracted from a microwave discharge through oxygen. Because of the low electron temperature (~ 5 eV) that is characteristic of these discharges, relatively few electrons have energies greatly in excess of 10 eV. Consequently, most of the ionization is produced by electrons which have energies which are not much greater than the ionization energy of the gas (12.2 eV), and the number of metastable excited ions such as $O_2^+(^4\Pi_u)$, which requires 16 eV to be produced, is much smaller in a microwave discharge than in a conventional 50 eV electron impact source.

Beam attenuation experiments of the type described by Turner, *et al.*,⁷ showed that the momentum analyzed

(1) W. R. Gentry, E. A. Gislason, Y. T. Lee, B. H. Mahan, and C. W. Tsao, *Discuss. Faraday Soc.*, **44**, 137 (1967).

(2) W. R. Gentry, E. A. Gislason, B. H. Mahan, and C. W. Tsao, *J. Chem. Phys.*, **49**, 3058 (1968).

(3) E. A. Gislason, B. H. Mahan, C. W. Tsao, and A. S. Werner, *ibid.*, **50**, 142 (1969).

(4) M. Chiang, E. A. Gislason, B. H. Mahan, C. W. Tsao, and A. S. Werner, *ibid.*, **52**, 2698 (1970).

(5) E. A. Gislason, B. H. Mahan, C. W. Tsao, and A. S. Werner, *ibid.*, **50**, 5418 (1969).

(6) M. Chiang, E. A. Gislason, B. H. Mahan, C. W. Tsao, and A. S. Werner, *ibid.*, **53**, 3752 (1970).

(7) B. R. Turner, J. A. Rutherford, and D. M. J. Compton, *ibid.*, **48**, 1602 (1968).

O₂⁺ beam contained less than 3% excited metastable ions. The vibrational excitation of the ions in the ²Π_g ground state of O₂⁺ is not known, but Franck-Condon factors⁸ suggest that most molecules are in the excited vibrational levels 1-5, with the average vibrational energy being approximately 0.3 eV. This is probably a realistic upper limit to the vibrational energy of O₂⁺, since we estimate that the ions undergo at least one and perhaps as many as 50 collisions with O₂ in this relatively high pressure (20-50 μ) source before being extracted from the plasma. Measurements of the kinetic energy threshold for the reaction and dissociation of O₂⁺ also suggested that the ions have approximately 0.3 eV internal energy.

Our experimental results are presented in the form of contour maps² of the specific intensity, $\bar{I}(\theta, u)$, or the intensity of ions per unit velocity space volume normalized to unit beam strength, scattering gas density, and collision volume. A polar coordinate system is used, with the radial coordinate u representing the speed of the ion relative to the center of mass of the target-projectile system, and the angular coordinate θ measured with respect to the original direction of the projectile ion beam. The specific intensity is normalized so that

$$\bar{\sigma} = 2\pi \int_0^\pi \sin \theta \, d\theta \int_0^\infty u^2 \bar{I}(\theta, u) \, du$$

is always proportional to the true total cross section σ .

While the original experimental points are not usually shown on the intensity contour maps, each map is generated from 10-20 scans of the laboratory energy and angular distributions, in each of which 10-20 intensity measurements are made. For the more complicated intensity distributions, even more data are collected. All of the contour maps show circles of constant Q , the difference between the final and initial relative translational energies. Assuming ground-state reactants we can write

$$Q = \frac{1}{2}\mu'(g')^2 - \frac{1}{2}\mu g^2 = -\Delta E_0^\circ - U' + U$$

where ΔE_0° is the energy change for reactants and products in their ground states, and U and U' are the internal excitation energies of reactants and products, respectively.

Results and Discussion

In analyzing the experimental results, it is helpful to consult Table I, which lists the enthalpy changes⁹ for forming various products and the intermediate H₂O₂⁺ from ground state O₂⁺ and H₂. It is clear that all possible reactions are endothermic, and that the collision complex H₂O₂⁺ represents a substantial potential energy minimum. It must be borne in mind, however, that while the energies of the separated products and reactants are known, there is very little information available about potential energy barriers which may

Table I: Enthalpies and Appearance Potentials

	ΔH_0° , eV ^a	V_{app} , eV ^b
H ₂ O ₂ ⁺	-2.38	10.92 ± 0.05
H + HO ₂ ⁺	1.96	15.36 ± 0.05
H + H + O ₂ ⁺	4.47	
OH ⁺ + OH	1.87	15.35 ± 0.1
OH ⁺ + O + H	6.26	
H ₂ O ⁺ + O	0.66	14.09 ± 0.1
H ₂ O + O ⁺	1.66	
H ₂ + O + O ⁺	6.78	
H ₂ ⁺ + O ₂	3.37	
H ₂ + O ₂ ⁺	0	15.8 ± 0.5

^a Enthalpy for forming specified products from O₂⁺ and H₂

^b Appearance potential for products from ionization of H₂O₂⁺.

lie between reactants and various products. Such barriers of course could profoundly affect the reaction dynamics. The appearance potentials of the various ions formed from H₂O₂ by electron impact do indicate the magnitudes of potential barriers which lie between H₂O₂⁺ and its various decomposition products. Accordingly, the appearance potentials measured by Foner and Hudson¹⁰ are listed in Table I.

We now shall present the results and discussion successively for each channel proceeding approximately in increasing order of complication.

A. O₂⁺ + D₂ → O⁺ + O + D₂. Figure 1 shows the intensity distribution of O⁺ produced by the collisional dissociation of O₂⁺ by D₂ at an initial relative energy of 11.2 eV. The distribution is asymmetric about the ±90° line in the barycentric system. This clearly shows that the dissociation occurs by a direct or short-lived collisional interaction. In addition, the O⁺ intensity peaks at a velocity which is very nearly equal to the velocity of the original O₂⁺ projectile. This indicates that in the most probable collision process, one of the atoms of the projectile is only slightly disturbed by the dissociation, and proceeds on as O⁺ at nearly the velocity of the original projectile.

In interpreting Figure 1 and other maps of the specific intensity, it must be kept in mind that the contribution of scattering out of the plane of the beam and detector is not included. To take account of the products scattered out-of-plane, one could multiply each specific intensity by sin θ, where θ is the barycentric scattering angle. This would remove the intensity maximum from θ = 0 and place it at some greater angle in the forward scattering hemisphere. In a strict sense, inclusion of the sin θ factor is inappropriate and can be somewhat misleading if the apparatus resolution is

(8) R. W. Nichols, *Proc. Phys. Soc. London (At. Mol. Phys.)*, **1**, 1192 (1968).

(9) J. L. Franklin, *et al.*, "Ionization Potentials, Appearance Potentials, and Heats of Formation of Gaseous Positive Ions," NSRDS-NBS 26, 1969.

(10) S. N. Foner and R. L. Hudson, *J. Chem. Phys.*, **36**, 2676 (1962).

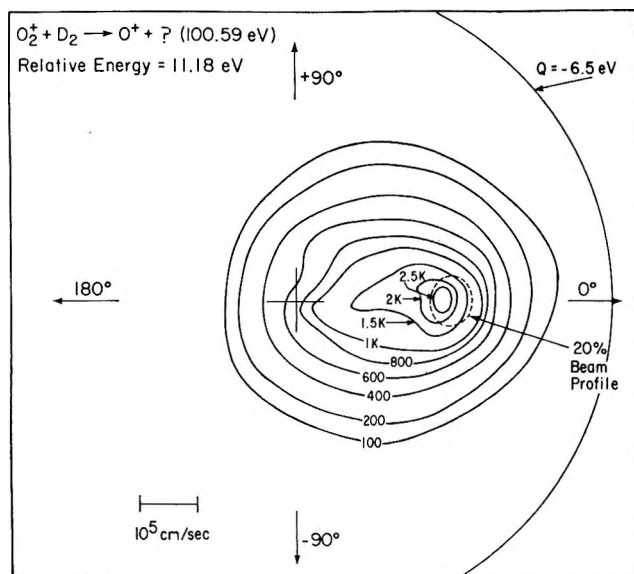


Figure 1. A contour map of the specific intensity of O^+ from $O_2^+ + D_2$ collisions at an initial relative energy of 11.2 eV. The radial coordinate is the speed of O^+ relative to the center of mass, and the angular coordinate is the center-of-mass system scattering angle, measured relative to the direction of the O_2^+ beam. The circle labeled $Q = -6.5$ is located assuming the D_2 and neutral O products retreat from O^+ with no kinetic energy relative to each other.

relatively poor, as is true for the case at hand. Consequently, we omit this factor in the maps presented here. However, a map which includes the $\sin \theta$ factor still leads to the conclusion that the free O^+ ion has, in the dissociation process, been subject to the finite but relatively small forces which produce forward scattering.

Figure 2 shows that when the D_2 target is replaced by He, a very similar distribution of O^+ results. In another paper,¹¹ we have reported extensive measurements of the dissociation of O_2^+ , NO^+ , N_2^+ , and N_2O^+ by collision with helium. Our conclusion from that work was that these dissociations occur principally by a version of the stripping process in which the target atom collides with one of the atoms of the projectile and breaks the projectile bond either adiabatically or through excitation to a weakly bound or slightly repulsive electronic state. The other projectile atom, which is ultimately detected as O^+ , is thus subject only to relatively weak forces and proceeds at nearly its original velocity throughout the dissociation. The great similarity between Figures 1 and 2 suggests that the dissociation of O_2^+ by collision with D_2 proceeds in a similar manner.

In an experiment in which O_2^+ collided with D_2 at 5.55 eV relative energy, no O^+ was observed, despite the fact that only 1.6 eV is required to form D_2O and O^+ . Thus, aside from our observation that the total cross section for dissociation of O_2^+ by D_2 is larger than for dissociation by He at the same relative energy, we have no evidence that either the existence of a long-lived $D_2O_2^+$ complex or the possibility of forming D_2O

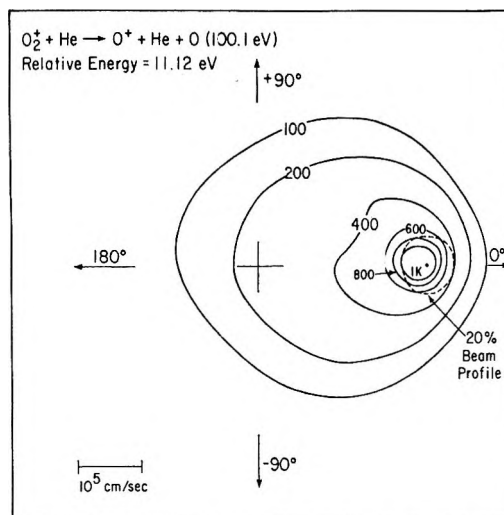


Figure 2. A contour map of the specific intensity of O^+ from $O_2^+ + He$ collisions at 11.1 eV relative energy. The intensities are directly comparable to those in Figure 1.

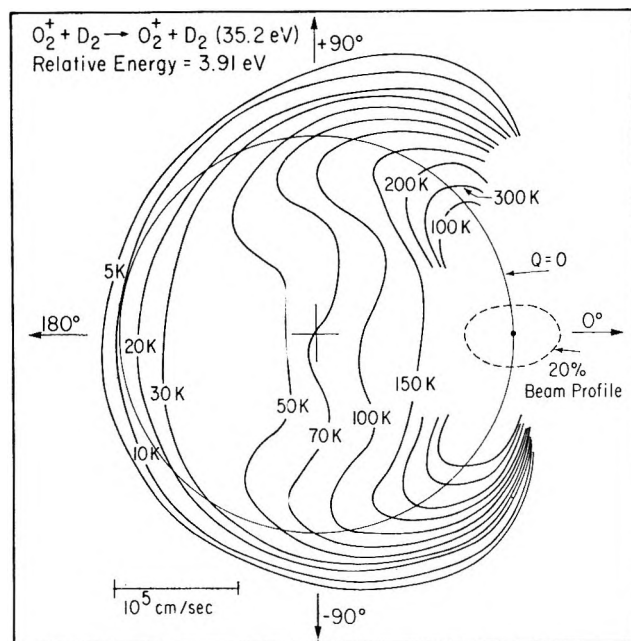


Figure 3. A contour map of the specific intensity of O_2^+ scattered from D_2 at 3.91 eV relative energy. The circle marked $Q = 0$ is the locus of elastic scattering. Points closer to the origin correspond to negative Q values and hence inelastic scattering.

product has any influence on the dynamics of the dissociation process. It seems of considerable interest that the dissociation occurs by a direct interaction with D_2 , for we shall see that the other reaction channels in this system are strongly affected by the potential energy minimum which corresponds to $D_2O_2^+$.

B. $O_2^+ + D_2 \rightarrow O_2^+ + (D_2)$. The nonreactive scattering of O_2^+ by D_2 depends in an interesting man-

(11) M. H. Cheng, M. Chiang, E. A. Gislason, B. H. Mahan, C. W. Tsao, and A. S. Werner, *J. Chem. Phys.*, **52**, 5518 (1970).

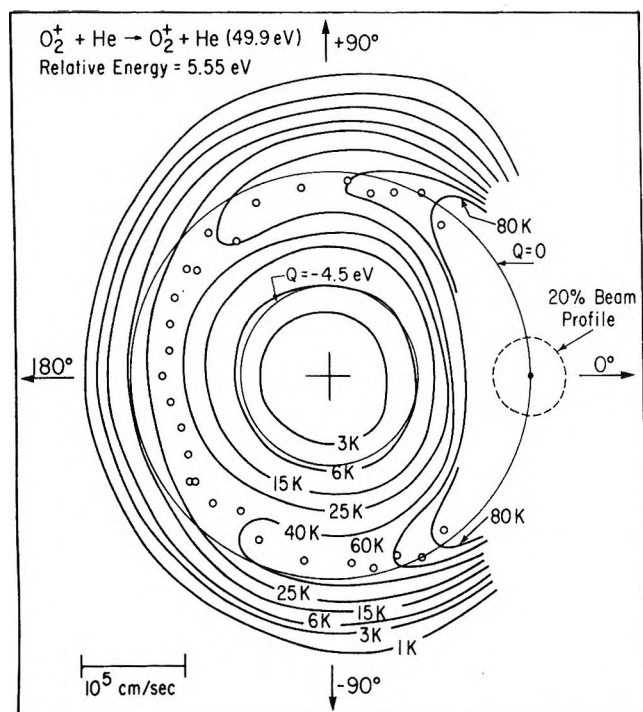


Figure 4. A contour map of the specific intensity of the O_2^+ scattered by He at an initial relative energy of 5.55 eV. The small circles locate the actual intensity maxima found in each energy and angular sweep through the scattering pattern.

ner on the scattering angle and the relative energy of collision. Figure 3 shows that when the initial relative energy is 3.91 eV, there is considerable small-angle scattering which is elastic within experimental uncertainty. As the angle increases past 60° , the scattered intensity greatly decreases and the intensity maxima lie in regions for which Q , the difference between the final and initial relative kinetic energies, is increasingly negative. Thus the scattering which produces this outer ridge becomes progressively more inelastic as the scattering angle increases. The monotonic evolution of this ridge from high intensity elastic scattering at small angles to lower intensity inelastic scattering at large angles suggests that the entire ridge is caused by direct interaction processes which occur in moderate to large impact parameter collisions.

This direct interaction mechanism seems to be considerably attenuated at angles greater than 135° , where the intensity ridge disappears. Apparently, the small impact parameter collisions which would be expected to contribute to scattering in this very large angle region in fact lead to chemical reaction or inelastic scattering with a broad distribution of internal excitations. There is also a substantial scattered intensity of O_2^+ at or near to the center of mass velocity. This indicates that a considerable fraction of the collisions are very inelastic, and leave the O_2^+ and D_2 sharing up to 3.91 eV as internal excitation energy.

In analyzing scattering from a reactive target, it is often very enlightening to compare it to the scattering

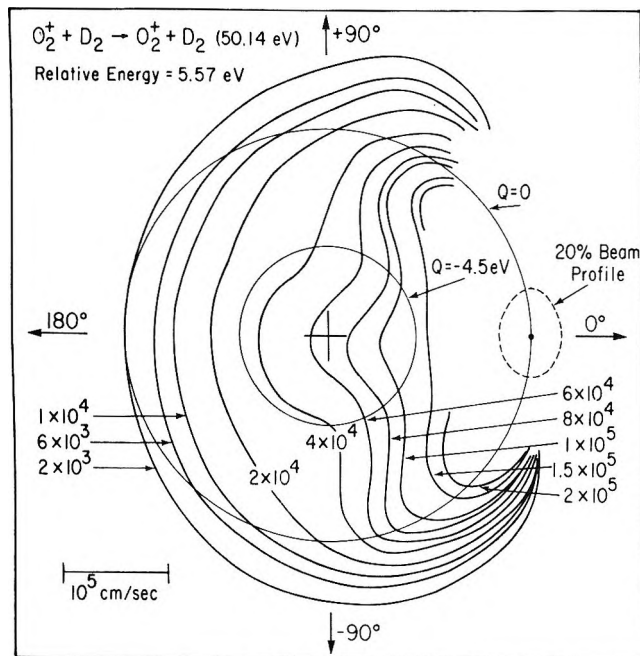


Figure 5. The distribution of the specific intensity of O_2^+ scattered from D_2 at 5.57 eV relative energy. Note the smaller intensity near 180° and $Q = 0$, in comparison with Figure 4.

of the same projectile from an inert target of the same mass. In Figure 4 we show the intensity of O_2^+ scattered from a helium target at 5.55 eV initial relative energy. At angles greater than 90° the scattering becomes increasingly inelastic as the angle increases. At 180° , the most probable value of Q is -1.5 eV. In another paper¹² we have reported more extensive measurements of inelastic scattering in this and other such nonreactive systems, and have successfully interpreted the scattering in terms of classical theories of vibrational excitation. Thus Figure 4 represents the vibrational excitation of O_2^+ that can be expected from collisions in which the interaction is of the direct, non-chemical type.

Figure 4 should be compared with Figure 5, which shows O_2^+ scattered from D_2 at 5.57 eV initial relative energy. In the $O_2^+-D_2$ system, virtually all the O_2^+ at large angles has been scattered very inelastically. In fact, the back-scattering of greatest intensity lies very close to the center-of-mass velocity, and therefore involves collisions in which nearly 5.57 eV is shared as internal excitation of O_2^+ and D_2 , or is used to dissociate D_2 .

The fact that the inelasticities found for the $O_2^+-D_2$ and O_2^+-He systems differ greatly is consistent with the existence of a collision complex $D_2O_2^+$ in which the atoms interact through strong chemical forces. However, the data for nonreactive scattering do not, by themselves, prove that this complex is necessarily long-lived. For example,^{2,4} in the systems $N_2^+-D_2$ and

(12) M. H. Cheng, M. Chiang, E. A. Gislason, B. H. Mahan, C. W. Tsao, and A. S. Werner, *J. Chem. Phys.*, **52**, 6150 (1970).

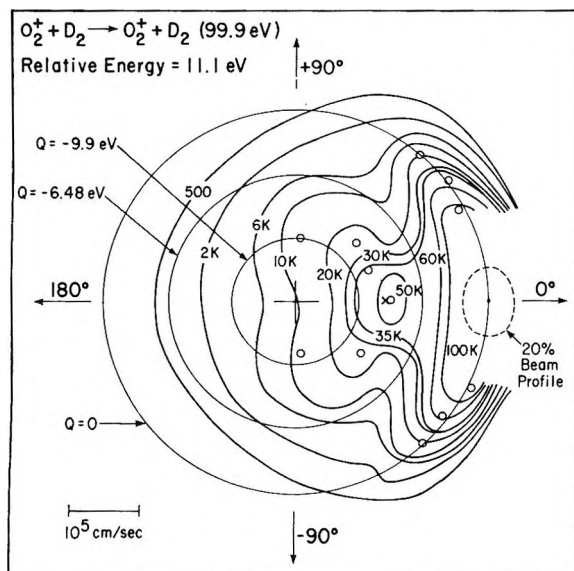


Figure 6. The distribution of the specific intensity of O_2^+ scattered from D_2 at 11.1 eV relative energy. The small circles locate intensity maxima as in Figure 4. The circle marked $Q = -6.48$ is the approximate locus of scattered O_2^+ excited to nearly its dissociation limit (6.8 eV), while the $Q = -9.9$ eV circle locates O_2^+ which has excited D_2 vertically to its dissociative ${}^3\Sigma_u$ state. The cross at the inelastic peak is the velocity which DO_2^+ formed by the spectator stripping process would have.

Ar^+-D_2 which involve reaction by direct, short-lived interaction, the N_2^+ that does not react is scattered very inelastically, while the unreacted Ar^+ shows only very small inelasticity. On the basis of our experience, it appears that the existence of strong chemical interactions does not necessarily lead to nonreactive collisions of great inelasticity. However, inelasticity which is substantially greater than that predicted by classical vibrational energy transfer theory does indicate either electronic excitation or strong coupling of the nuclear motions through valence forces.

When the initial relative energy of O_2^+ and D_2 exceeds 6 eV, the intensity distribution of the scattered O_2^+ shows a secondary maximum in the small angle inelastic region. Figure 6 shows that when the initial relative energy is 11.1 eV, this feature has developed into a fairly well-defined intensity ridge (see the ellipse of intensity 50 K). The asymmetry of this feature about the $\pm 90^\circ$ line makes it seem very unlikely that it is connected with the existence of a long-lived collision complex. It also seems unlikely that the cause of this ridge is vibrational excitation of the collision partners by direct interaction, since we should expect large rather than small-angle scattering, and a broad, rather than well-defined range of inelasticities from such a process. Much the same argument eliminates simple adiabatic one-step or knock-on collisional dissociation of D_2 as a likely origin of this scattering.

The inelastic feature in Figure 6 resembles the one which we found² in the nonreactive scattering of N_2^+

by D_2 . From a determination of the energy threshold for the $N_2^+-D_2$ inelastic process, we concluded that it arose principally from the excitation of D_2 to its lowest ${}^3\Sigma_u$ state by grazing collisions. A similar finding was made³ in the $N_2^+-CD_4$ system, and was rationalized in a similar manner. The same explanation may in fact be valid for the inelastic feature in the $O_2^+-D_2$ system. However, the existence in this system of large amounts of elastic and inelastic scattering which cannot be unequivocally separated from the inelastic ridge makes it impossible for us to determine a partial cross section and energy threshold for this feature, and thereby to test the electronic excitation hypothesis thoroughly.

Another possible explanation for the inelastic peak is that it arises from the dissociation of DO_2^+ molecules which are formed by a stripping-type process² and have internal energies in excess of the 2.6 eV dissociation energy of the $D-O_2^+$ bond. It can be easily demonstrated that the internal energy U' of DO_2^+ formed by the spectator stripping process is given by

$$U' = E_a - \Delta E_0^\circ$$

where E_a is the energy of the projectile O_2^+ relative to the atom abstracted. The excitation energy of any DO_2^+ formed by spectator stripping thus rises linearly with the projectile energy until U' equals 2.6 eV. At this point (a relative energy of 8.6 eV for $O_2^+-D_2$) any DO_2^+ formed by spectator stripping becomes unstable with respect to dissociation to O_2^+ and D . The resulting O_2^+ should have a velocity approximately equal to that calculated for DO_2^+ formed by spectator stripping.

The well-defined inelastic peak or ridge in Figure 6 first makes its appearance at approximately 8 eV initial relative energy, quite close to the value of 8.6 eV predicted from the spectator stripping. These observations strongly suggest that, at least at relative energies above 8 eV, some or all of the small angle inelastic feature may represent collisional dissociation of D_2 by O_2^+ through the spectator stripping mechanism. However, careful examination of Figures 3 and 5 shows that at energies below 8.6 eV, there is important, if not particularly well-defined inelastic scattering in the small angle region. Experiments with H_2 targets also show this feature. Since the dissociative stripping mechanism cannot operate in this low-energy regime, we are inclined to attribute these small-angle inelastic features to electronic excitation of H_2 to the ${}^3\Sigma_u$ state. Thus there is evidence for dissociation of D_2 both by electronic excitation and the dissociative stripping process, and it seems likely that both occur at relative collision energies above 8.6 eV.

C. $O_2^+ + D_2 \rightarrow DO_2^+ + D$. In a preliminary communication,⁵ we have briefly summarized our findings for this reaction. At low relative energies of collision (<5 eV) the DO_2^+ product (or HO_2^+ from $O_2^+-H_2$ collisions) has a very nearly isotropic specific intensity

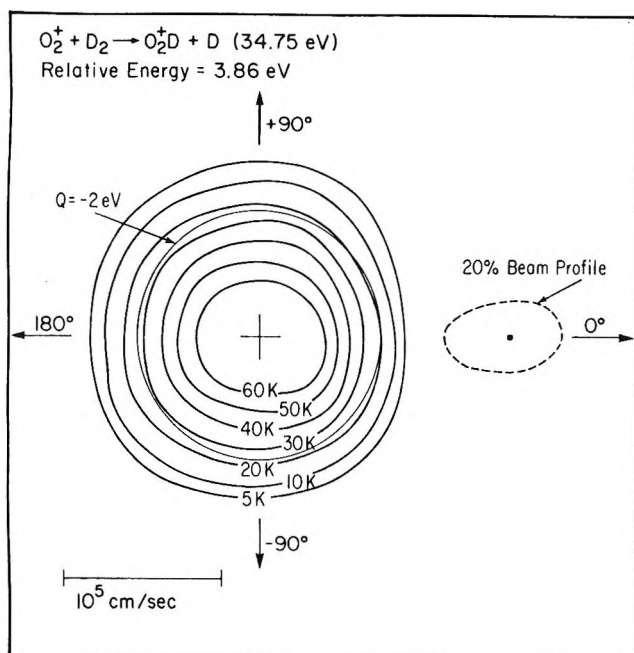


Figure 7. A contour map of the specific intensity of DO_2^+ from $O_2^+-D_2$ collisions at a relative energy of 3.86 eV. The circle marked $Q = -2$ eV is the locus of the maximum product velocity, assuming no motion of the target gas, no beam energy and angular spread, and infinite detector resolution.

distribution in the center-of-mass system. This is illustrated in Figure 7, which is typical of several of the maps which we have determined in this low-energy regime. The isotropy indicates the occurrence of a long-lived collision complex of relatively small total angular momentum and large internal energy per vibrational and rotational mode. The small total cross section ($\sim 2 \text{ \AA}^2$) and large bonding energy (2.4 eV) with respect to D_2 and O_2^+ are consistent with such a deduction.

Another factor that may contribute substantially to the isotropy is the rotational angular momentum of the O_2^+ drawn from the microwave discharge. While the temperature of the discharged gas was not measured, it could easily be 400°K, which would correspond to a most probable J of 9 for O_2^+ . The plane of rotation, and thus the angular momentum vector of O_2^+ , is randomly oriented with respect to the $O_2^+-D_2$ relative velocity vector. Therefore, rotation of O_2^+ is a factor which tends to randomize the relation between the initial relative velocity vector and the total angular momentum vector or orientation of the complex, and thus tends to produce an isotropic product distribution.

In investigations of O_2^+-HD collisions,^{5,6} we have found that at low initial relative energies, both HO_2^+ and DO_2^+ are distributed isotropically in the center of mass system, and that the intensity of DO_2^+ exceeds that of HO_2^+ by as much as a factor of 8. These results constitute further evidence that the $O_2^+(D_2,D)-DO_2^+$ reaction proceeds by a long-lived collision complex at these lower relative kinetic energies. The

prevalence of DO_2^+ over HO_2^+ is the opposite of the isotope effect that we found for reactions which proceed by a direct interaction mechanism. Because DO_2^+ has a lower zero-point energy and higher density of states than does HO_2^+ , the isotope effect expected from the statistical decay of a long-lived HDO_2^+ collision complex should favor formation of DO_2^+ over HO_2^+ , as is observed in the experiments.

In an attempt to determine whether there is an activation energy barrier which exceeds the endothermicity of 1.96 eV, we studied the $O_2^+(H_2,H)HO_2^+$ reaction down to initial relative energies of 1.47 eV. While the relative reaction cross section decreased as the relative energy was lowered past 2.0 eV, considerable product intensity remained even when the nominal initial relative energy was as low as 1.47 eV. In view of the uncertainty of ± 0.20 eV in the initial relative energy due to target gas motion and ion beam energy spread, and the estimated 0.3 eV vibrational excitation of the O_2^+ , it is not surprising that a reaction threshold was not observed at 1.96 eV, nor even in the 1.47-eV experiment. Diminished beam intensities prevented significant experiments at lower energies. However, it seems clear that if there is an activation barrier for the $O_2^+(H_2,H)HO_2^+$ reaction, its height is not significantly in excess of 2.1 eV. These experiments also indicate that the barrier for formation of the $H_2O_2^+$ complex from O_2^+ and H_2 is not significantly greater than 2.1 eV. On the other hand, if all products are formed by decomposition of an $H_2O_2^+$ complex, the fact that significant products are formed at all suggests that the barrier for formation of the complex from reactants is not much lower than the endothermicity for formation of HO_2^+ or OH^+ . If this were not so, most complexes would simply redissociate to reactants over the low barrier between reactants and complex. The picture that emerges then is that the barrier for formation of the $H_2O_2^+$ complex with a hydrogen peroxide structure from O_2^+ and H_2 is comparable in height with the energy plateau which represents HO_2^+ product formation.

Support for this conclusion is found in the work of Foner and Hudson¹⁰ on the mass spectrometry of H_2O_2 . These authors found that the appearance potential of O_2^+ and H_2 from H_2O_2 is 15.8 ± 0.5 eV, whereas the thermodynamic minimum energy required for this change is 13.42 eV. Therefore, $O_2^+ + H_2$ are formed from $H_2O_2^+$ with internal or kinetic energy amounting to 2.4 ± 0.5 eV. This means there is a 2.4 ± 0.5 eV barrier for forming $H_2O_2^+$ from O_2^+ and H_2 , which is consistent with our earlier conclusion.

Figures 8–10 show that as the initial relative kinetic energy is increased above 5 eV, the angular distribution of DO_2^+ loses its isotropy, and acquires an intensity maximum in the forward scattering region. The forward peaking increases in relative importance with increasing energy. These distributions of DO_2^+ found in high-energy experiments are qualitatively similar

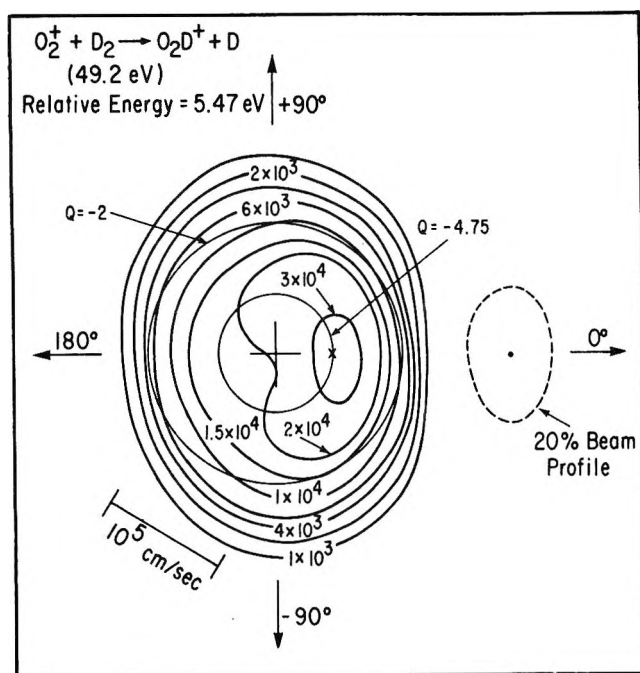


Figure 8. A contour map of the specific intensity of DO_2^+ from the O_2^+-D_2 reaction at 5.47 eV initial relative energy. The circles marked $Q = -2$ and -4.75 eV are, respectively, the velocity limits for products with the minimum and maximum allowable internal excitation. The cross marks the velocity of DO_2^+ formed by the spectator stripping process.

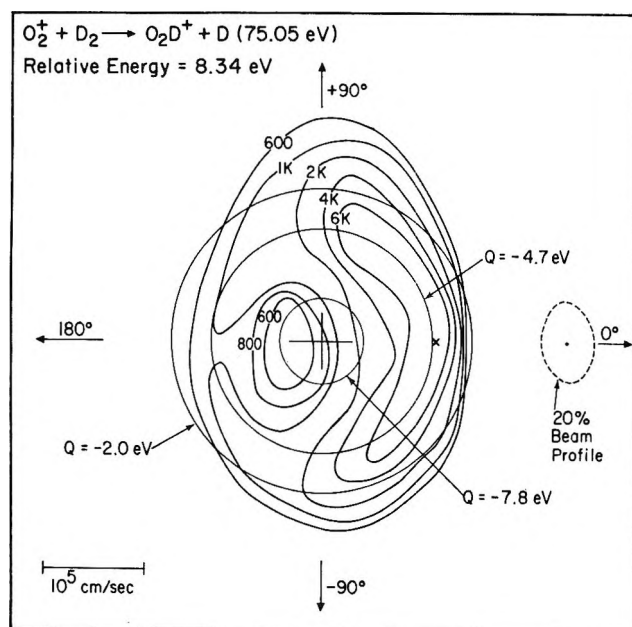


Figure 9. A contour map of the specific intensity of DO_2^+ from the O_2^+-D_2 reaction at 8.34 eV initial relative energy. The cross locates the velocity of DO_2^+ formed by the spectator stripping process.

but clearly broader than the product distributions from the $\text{Ar}^+(\text{D}_2, \text{D})\text{ArD}^+$ and $\text{N}_2^+(\text{D}_2, \text{D})\text{N}_2\text{D}^+$ reactions.^{2,4} Thus the DO_2^+ distributions indicate that as the initial relative energy is increased, the lifetime of the D_2O_2^+

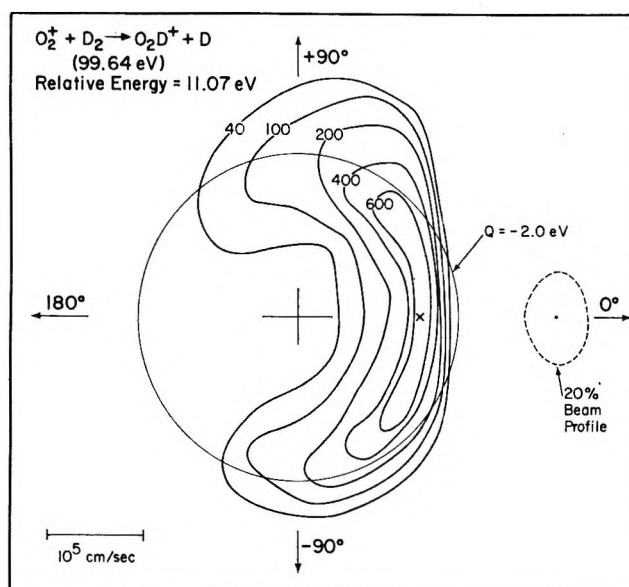


Figure 10. A contour map of the specific intensity of DO_2^+ from the O_2^+-D_2 reaction. Note that the total intensity is small, and rather broadly distributed about the spectator stripping velocity, which is marked by a cross.

collision complex decreases to less than one full rotational period, and the reaction mechanism tends toward the direct or impulsive types of interaction.

The reaction $\text{O}_2^+(\text{D}_2, \text{D})\text{DO}_2^+$ has recently been investigated by Ding and Henglein,¹³ who determined the translational energy spectrum of DO_2^+ in the primary beam direction without angular intensity measurements. The O_2^+ was prepared by impact of 100-eV electrons in a conventional mass spectrometer source, and contained substantial amounts of the metastable $^4\Pi_u$ state of O_2^+ . Ding and Henglein were able to separate the effects of this excited state from the reactions of ground-state O_2^+ , and showed that below 4 eV relative energy the reaction of ground-state O_2^+ produced DO_2^+ moving at the velocity of the center of mass, as would be expected from the decay of a long-lived complex. When the initial relative energy was above 5 eV, the maximum intensity of DO_2^+ fell at velocities greater than that of the center of mass, and with increasing initial energy eventually reached the value expected from the ideal stripping process. A threshold for production of DO_2^+ from ground-state O_2^+ was found at approximately 1.9 eV relative energy. In view of our failure to observe a sharp threshold for this reaction, this finding of Ding and Henglein is somewhat surprising. In other respects, however, the two investigations are nicely consistent in the regions in which they overlap.

The qualitative reason for the change in reaction mechanism with increasing relative kinetic energy is clear from unimolecular reaction rate theory. The

(13) A. Ding and A. Henglein, *Ber. Bunsenges. Phys. Chem.*, **73**, 562 (1969).

lifetime of the collision complex is determined by its total internal energy as compared with the minimum amount needed to decompose, and by the total number of internal modes which share the total energy. The simplest expression for the lifetime τ of the collision complex is that derived from the Rice-Ramsperger-Kassel theory,¹⁴ which treats the energized molecule as a collection of s degenerate oscillators of frequency ν

$$\tau = (1/\nu)[E/(E - E_0)]^{s-1}$$

Here E is the total internal energy and E_0 is the minimum energy needed for decomposition. Because of failures of the assumptions of the model, this expression can give lifetimes which are incorrect by orders of magnitude, and therefore should not be used for quantitative calculations of τ . However, the formula does correctly indicate the important quantitative trends that τ decreases as the internal energy E increases, and the molecular complexity decreases.

In order to calculate the lifetime of the D₂O₂⁺ collision complex quantitatively, we used the RRKM theory¹⁴ of unimolecular decomposition. The vibration frequencies for D₂O₂⁺ were estimated by analogy to those of D₂O₂, with allowance for the increased O-O bond strength in D₂O₂⁺. The vibrational energy level densities were evaluated by the method of Whitten and Rabinovitch.¹⁵ The total internal energy of the complex was set equal to the sum of the initial relative kinetic energy and the binding energy of reactants, plus 0.6 eV to allow for the vibrational energy of O₂⁺. The maximum impact parameter for reaction was evaluated from the approximate cross section for DO₂⁺ formation, and from this, the reduced mass, and the initial relative velocity, the maximum angular momentum was calculated.

In Table II we give a comparison between the lifetime

Table II: Lifetimes for the D₂O₂⁺ Collision Complex

E_{rel} , eV	$\tau_{\text{calcd.}}^a$ sec	$\tau_{\text{rot.}}^b$ sec	$\tau_{\text{rot.}}^c/\text{radis}$
3.86	4.7×10^{-13}	1.4×10^{-13}	≥ 5
5.47	1.1×10^{-13}	1.2×10^{-13}	~ 1
8.3	3.5×10^{-14}	0.9×10^{-13}	≤ 0.3

^a Calculated using RRKM theory with all channels. ^b Calculated assuming that the total orbital angular momentum appears as rotation about a nonunique axis. ^c Estimated using the fall-off function of ref 16.

of the complex with respect to dissociation to DO₂⁺ and D as calculated using RRKM theory, and the "experimental" lifetime. The possibility of the complex decomposing to O₂⁺ + D₂, DO₂⁺ + D, OD⁺ + OD, and D₂O⁺ + O was included in the calculation. The experimental lifetime was estimated from the experimental intensity ratio of forward to back scattered DO₂⁺ using the falloff function for osculating complexes

given by Fisk, McDonald, and Herschbach.¹⁶ In calculating the rotational frequencies used in constructing Table II, we have assumed that D₂O₂⁺ has approximately the same geometry as D₂O₂. It is, therefore, nearly a prolate symmetric top with one small moment of inertia I_A corresponding to the rotation of the deuterium atoms around the O-O axis, and two large and nearly equal moments of inertia I_B and I_C corresponding to the tumbling of the oxygen atoms.

One sees from Table II that in the experiment at 5.5 eV relative energy, the D₂O₂⁺ complex had a maximum experimental lifetime of approximately one rotational period. For the same experiment, RRKM theory predicts a lifetime of 0.8 rotation about the B or C axes, or 5 rotations with the same angular momentum about the unique A axis. Since the reaction occurs in effect by ejection of a D atom from the D₂O₂⁺ complex, it would appear that the significant motion in determining the forward-backward symmetry of the product angular distribution is the high-frequency rotation about the unique axis. That is, the circulation of the deuterium atoms about the O-O axis destroys any memory of the direction from which O₂⁺ came much more rapidly than does the precession or tumbling of the O-O axis about the total angular momentum vector. If this argument were valid, then we would be forced to conclude that RRKM theory overestimates the lifetime of the D₂O₂⁺ complex by approximately a factor of 6.

There is reason to expect that complexes will tend to have only a small fraction of their total angular momentum present as rotation about the unique axis. The assumption of statistical equilibrium corresponding to a rotational temperature T_r leads to a distribution function $P(K)$ for the quantum number K for rotation about the unique axis which is given by¹⁷

$$P(K) = \exp(-1/2 K^2 / K_a^2)$$

where

$$K_a = |kT_r I_r / \hbar^2|^{1/2}$$

and

$$I_r = I_B I_A / (I_B - I_A)$$

Thus high values of K are not favored, and the rotational angular momentum will tend to reside in the low-frequency tumbling motions of the O-O axis.

It can also be argued that complexes which do have large amounts of their angular momentum present as

(14) D. Bunker, "Theory of Elementary Gas Reaction Rates," Pergamon Press, New York, N. Y., 1966.

(15) G. Whitten and B. S. Rabinovitch, *J. Chem. Phys.*, **38**, 2466 (1963).

(16) G. A. Fisk, J. D. McDonald, and D. R. Herschbach, *Discuss. Faraday Soc.*, **44**, 228 (1967).

(17) W. B. Miller, S. A. Safron, and D. R. Herschbach, *ibid.*, **44**, 108 (1967).

rotation about the unique axis will not dissociate to the products DO_2^+ and D. If we treat the separation of the products as a two-body problem with a (negative) potential energy $\phi(r)$, then rotation of the complex creates a maximum in the effective potential V_{eff} for separation of the products

$$V_{\text{eff}} = L^2\hbar^2/(2\mu r^2) + \phi(r)$$

Here $L\hbar$ is the orbital angular momentum of the separating products, μ is their reduced mass, and t is their separation. This two-body approximation is appropriate if the maximum in the effective potential comes at a value of r large enough so that the internal motions of the fragments are essentially decoupled from their motion along the reaction coordinate.

The maximum which occurs in the effective potential energy curve can be viewed as a barrier which complexes must cross in order to become products. Alternatively, and perhaps more satisfactorily, it can be pictured as an ejection potential which supplies final relative kinetic energy to product particles that have crossed it. The height of this barrier (with respect to products) is given by

$$V_B = (L\hbar)^4/(C_4)(4\mu)^2 \quad (5)$$

when ϕ is the ion-induced dipole potential $-C_4/r^4$.

We see from eq 5 that large amounts of angular momentum L coming from rotation of the complex combined with small reduced masses for the products can create a high barrier in the exit channel. In the case at hand, the barrier height may be as much as 1 eV above the asymptotic product potential energy. Products would be expected to have this much relative translational energy, and therefore to lie well away from the center of mass velocity. This is not found experimentally. In fact, the intensities of Figure 8 have maximum values on the $Q = -4.75$ eV circle, which corresponds to the minimum possible final translational energy consistent with product stability. It appears, therefore, that in the dissociation of D_2O_2^+ to DO_2^+ and D, the angular momentum of the complex must be converted to angular momentum of rotation of the DO_2^+ entity, rather than appear as orbital angular momentum (and thus product translational energy) of DO_2^+ and D.

In order to explain the high internal excitation of the DO_2^+ product, we must find a mechanism by which the total angular momentum of the complex ($\sim 150\hbar$) is converted to rotation of DO_2^+ rather than to orbital motion of D and DO_2^+ . This conversion requires that angle dependent forces act between the D and DO_2^+ fragments as they begin to separate to products. Since D_2O_2^+ in the hydrogen peroxide structure would have an equilibrium OOD angle of approximately 105° , separation of D from DO_2^+ in a direction approximately parallel to the O-O axis would produce torques which could result in excitation of rotation of DO_2^+ . This

mode of separation might be particularly favored in D_2O_2^+ complexes in which most angular momentum was contained in the tumbling around the B and C axes. Indeed, this type of rotation would seem to be required if the incipient orbital rotation of D about DO_2^+ were to be converted efficiently to rotation of DO_2^+ .

In contrast, separation of D from DO_2^+ in a direction more nearly perpendicular to the O-O axis would seem to be an inefficient way to convert orbital momentum to product rotation. There are, of course, angle dependent forces which are responsible for the internal rotation barrier in hydrogen peroxide, but these are relatively weak compared with the forces required to bend chemical bonds. Thus, it seems that rotation of the complex about the unique axis cannot be readily converted to rotation of the DO_2^+ fragment.

In view of the foregoing considerations, we feel that there will tend to be relatively few D_2O_2^+ complexes which have substantial amounts ($150\hbar$) of angular momentum present as rotation about the unique axis. Those which do apparently do not dissociate to D and DO_2^+ because of the high effective potential energy barrier and the difficulty of converting this angular momentum into product rotation. Thus the high frequency rotation about the unique axis of the complex is not effective in maintaining the isotropy of the DO_2^+ angular distribution as the collision energy is increased. The predictions of the RRKM theory for the lifetime of the complex should therefore be compared with the period for rotation about the B and C axes of D_2O_2^+ .

The data in Table II show that the RRKM calculation of the lifetime of the D_2O_2^+ complex is consistent with experimental observations of the symmetry of the DO_2^+ angular distribution, provided that rotation of the complex about the B and C axes of the prolate top determines this symmetry. There is, however, considerable uncertainty in the molecular parameters and total angular momentum of the complex, and this fact tends to make the agreement between calculated and experimental lifetimes less significant as a test of RRKM theory.

It is also worth noting that it may not be entirely valid to test a statistical model like the RRKM theory in an energy region where we expect to see the beginning of the failure of the statistical picture of rapid distribution of energy among all internal modes. In the experiment done at 5.5 eV relative energy, the calculated lifetime of the complex is long enough to allow only 3-10 vibrations in the various modes of D_2O_2^+ . Even considering the strong anharmonic coupling, this would seem to be nearly the minimum number of vibrations necessary for complete randomization of the internal energy. Failure to distribute the total energy over the entire molecule would result in a lifetime of the complex shorter than that calculated from RRKM theory.

We should also remark that while RRKM theory gives a satisfactory indication of the lifetime of the

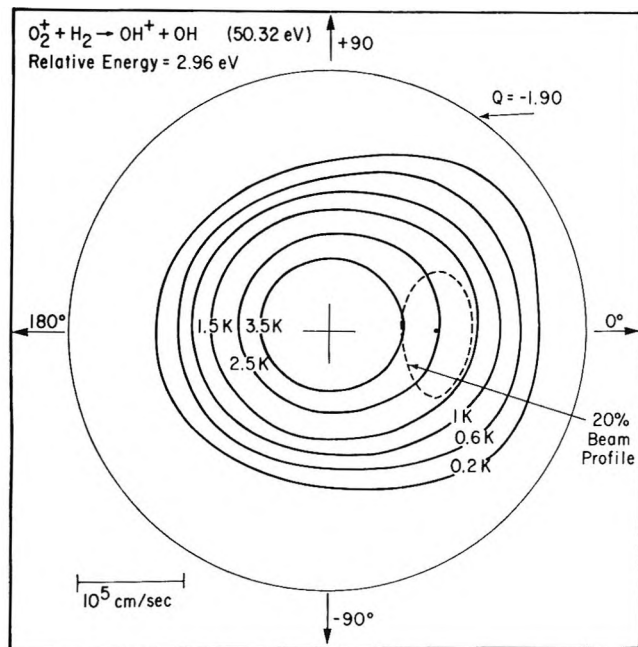


Figure 11. A contour map of the specific intensity of OH^+ from $O_2^+-H_2$ collisions at 2.96 eV initial relative energy. The circle marked $Q = -1.9$ eV is the locus of OH^+ scattered without internal excitation in either product molecule.

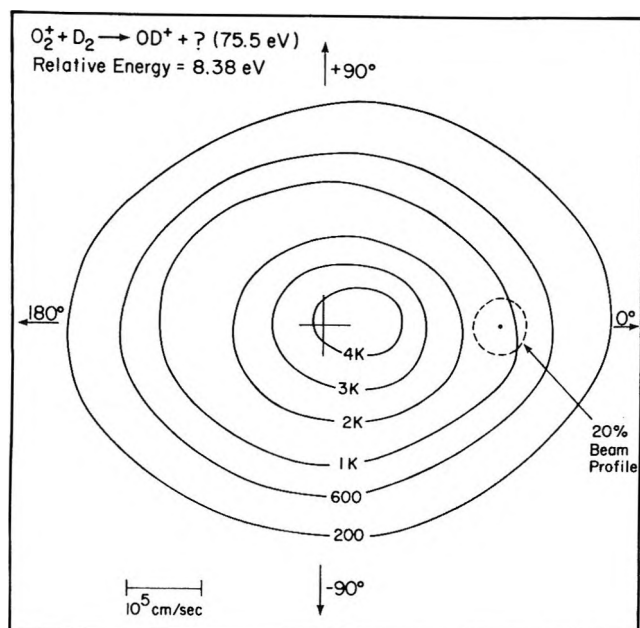
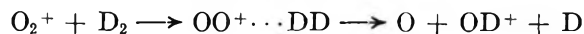


Figure 12. A contour map of the specific intensity of OD^+ from $O_2^+-D_2$ collisions at 8.38 eV relative energy.

complex $D_2O_2^+$, the relative yields of products depart noticeably from what one would calculate using this theory. Relative to the OD^+ formed the amount of DO_2^+ exceeds, and the amount of D_2O^+ is less than, that expected on the basis of the simplest application of RRKM theory. This suggests that some DO_2^+ may be formed by direct interaction at all energies, or that complexes with other than the hydrogen peroxide geometry may be involved. These points will be

explored in a subsequent paper on the isotope effects and product velocity distributions for this system.

D. $O_2^+ + D_2 \rightarrow OD^+ + OD$. Several maps of the intensity of OD^+ or OH^+ from the reaction of O_2^+ with D_2 and H_2 were obtained. Two of these are shown in Figures 11 and 12. It is clear that at both low and high initial relative energies the distribution of OH^+ or OD^+ shows considerable symmetry about the $\pm 90^\circ$ line in the center-of-mass coordinate system. However, this reaction represents a situation in which such symmetry cannot be taken as proof of the existence of a long-lived collision complex. The products OD^+ and OD are very nearly identical, and there is no reason to expect that even direct, impulsive interactions will lead to preferential scattering of OD^+ in either the forward or back direction, as long as the complex has, on the average, a symmetry that maintains the dynamical equivalence of the two oxygen atoms. On the other hand, if the potential energy surface were such as to allow reaction by a process such as



where in the linear collision complex the oxygen atoms are not equivalent, then there would be no reason to expect symmetry in the distribution of OD^+ at high energies.

It appears, therefore, that the observed highly symmetric distribution of OH^+ found in the experiment carried out at 2.93 eV relative energy (Figure 11) implies *primarily* that the $H_2O_2^+$ collision complex has oxygen atoms which are dynamically equivalent. If, as seems highly likely, the OH^+ occurs as an alternate decomposition product of the same collision complex that produces HO_2^+ , then this complex not only has equivalent oxygen atoms, but also it is long-lived when its energy is low.

The high degree of symmetry of the OD^+ distribution found in the experiment performed with 8.3 eV relative energy (Figure 12) also implies the prevalence of a collision mechanism in which the oxygen atoms are equivalent. While this equivalence could be the consequence of a long-lived complex of the hydrogen peroxide structure, it would seem impossible to maintain that a long-lived complex exists when the relative energy is so high. This is particularly true in view of the fact that formation of DO_2^+ occurs by a direct interaction at these high energies. We conclude, therefore, that OD^+ is formed at high energies by a direct, impulsive interaction in which the collision complex has geometries resembling the hydrogen peroxide structure. The small excess intensity of OD^+ in the small-angle scattering region may be a consequence of formation of OD^+ by processes in which the oxygen atoms are not equivalent.

E. $O_2^+ + H_2 \rightarrow H_2O^+ + O$. This reaction is the least endothermic (0.66 eV) of all the reaction channels. It therefore would be expected to be the most important

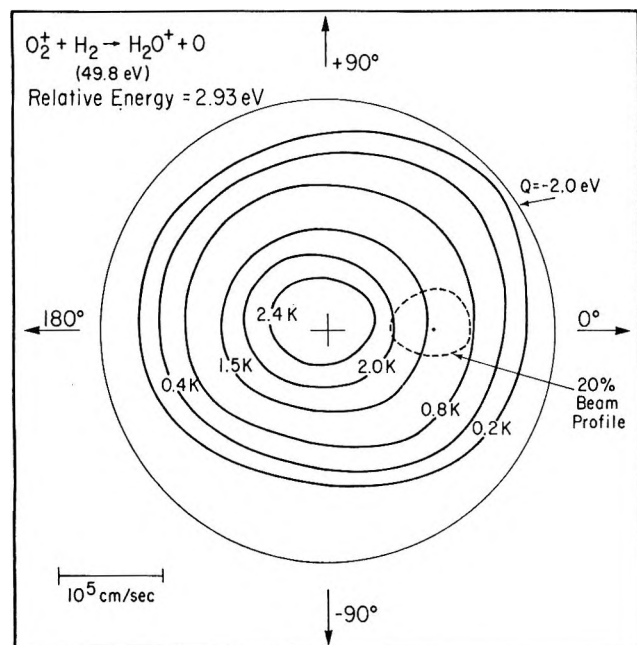


Figure 13. A contour map of the specific intensity of H_2O^+ formed by the $\text{O}_2^+ - \text{H}_2$ reaction at 2.93 eV relative energy.

reactive process if products were formed at a rate proportional to their total phase space. Figure 13 shows that the angular distribution of H_2O^+ is isotropic even though the initial relative energy of collision (2.93 eV) is markedly greater than the endothermicity of reaction. Moreover, the total intensity of H_2O^+ is less than those of OH^+ and HO_2^+ at the same relative collision energies. Both these facts suggest that the reaction path for decay of the H_2O_2^+ complex to H_2O^+ and O, and prevents these products from being of greatest importance. On the other hand, Foner and Hudson¹⁰ find that in the mass spectrum of H_2O_2 , the products H_2O^+ and O appear at the thermodynamic threshold energy, and therefore are formed without significant internal or translational excitation. This finding refutes the postulate of an energy barrier in the H_2O^+ product channel.

It is also possible that the critical configuration of the H_2O_2^+ complex which leads to H_2O^+ is of highly constrained geometry. Such a "tight" complex would be consistent with both the small yield of H_2O^+ , and the low appearance potential found by Foner and Hudson. A configuration in which H_2O_2^+ resembled a nonplanar formaldehyde molecule would have the necessary characteristics of high vibration frequencies in all but the reaction coordinate.

Figure 14 shows that even when the initial relative energy of collision is 5.9 eV, the distribution of H_2O^+ has considerable symmetry about the $\pm 90^\circ$ line in the center-of-mass coordinate system. This persistence of the long-lived complex mechanism at higher energies is consistent with the low product yield, for if the critical

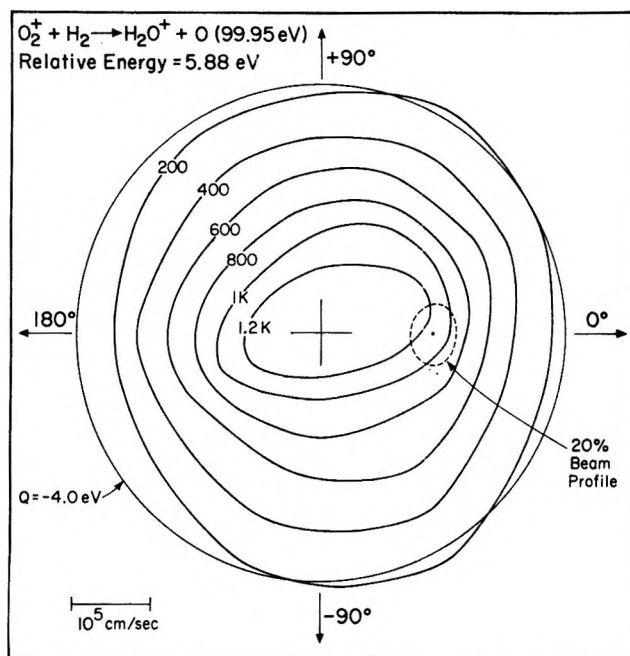


Figure 14. A contour map of the specific intensity of H_2O^+ formed by the $\text{O}_2^+ - \text{H}_2$ reaction at 5.88 eV initial relative energy. Product ions formed with zero velocity relative to the center of mass are unstable with respect to dissociation to $\text{H} + \text{OH}^+$ if the neutral O product is not electronically excited.

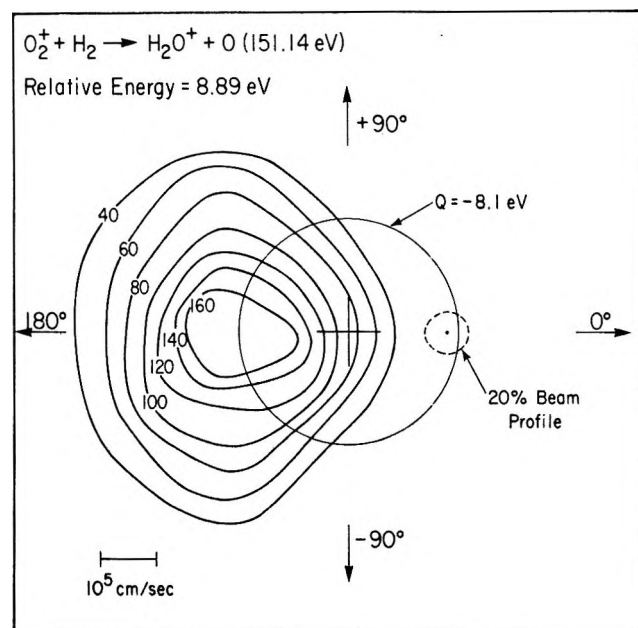


Figure 15. A contour map of the specific intensity of H_2O^+ formed from O_2^+ and H_2 at 8.89 eV initial relative energy. Note the low intensity relative to that in Figure 14. The circle marked $Q = -8.1$ eV passes through the broad intensity maximum. A Q value of -7.9 at $\theta = 180^\circ$ corresponds to spectator stripping of the O^+ from O_2^+ .

configuration for forming H_2O^+ and O is of very low probability, it is likely that these products tend to be formed from complexes which have existed several rotational periods.

Figure 15 gives the velocity vector distribution of H_2O^+ formed from very energetic collisions (8.89 eV) of O_2^+ and H_2 . The distribution is highly anisotropic, which indicates that H_2O^+ is formed by a direct interaction mechanism in this high energy regime. The velocity vector distribution is rather broad, and has a rather poorly defined maximum in the vicinity of the velocity H_2O^+ would have if it were formed by the spectator stripping mechanism. The latter would correspond to abstraction of O^+ from O_2^+ by H_2 with no momentum transfer to the free O atom. However, because of the extreme breadth of the H_2O^+ distribution, the term spectator stripping is a very poor description of the high energy mechanism. Moreover, since H_2O^+ can absorb only 5.7 eV as internal energy before dissociating, and most of the product in Figure 15 lies in regions where Q is more negative than -5.7 eV, the oxygen atom formed with H_2O^+ must be electronically excited.

Summary

In this paper we have demonstrated the existence of three reactions which proceed through a persistent collision complex at low initial relative kinetic energies. For the $\text{O}_2^+(\text{D}_2, \text{D})\text{DO}_2^+$ and $\text{O}_2^+(\text{H}_2, \text{O})\text{H}_2\text{O}^+$ reactions, we have shown that as the relative kinetic energy of collision is increased, the product angular distributions become asymmetric, and direct interaction mechanisms begin to dominate the dynamics. For the $\text{O}_2^+(\text{D}_2, \text{OD})-$

OD^+ reaction, the product distribution remains quite symmetric even in the high energy regime, evidently because of the near identity of the OD and OD^+ products, and dynamical equivalence of the oxygen atoms. These observations of the reaction dynamics can be qualitatively rationalized using thermodynamic and ion appearance potential data. The experimentally estimated lifetime of the collision complex formed in 5.5 eV relative energy collisions is in agreement with the prediction of the RRKM version of unimolecular reaction rate theory.

The nonreactive collisions between O_2^+ and D_2 lead to scattering patterns which are consistent with direct or potential scattering for small angles or large impact parameters, and with strongly interacting collision complexes for small impact parameter, large-angle scattering. Collisions between O_2^+ and D_2 which produce O^+ appear to proceed only by a direct interaction, despite the influence of the persistent collision complex in the other product channels.

Acknowledgment. This work was supported by the U. S. Atomic Energy Commission. E. A. G. acknowledges a postdoctoral fellowship from the National Center for Pollution Control. B. H. M. wishes to express his appreciation of the early scientific guidance and continuing inspiration provided by Professor George B. Kistiakowsky, to whom this paper is dedicated.

The Thermal Unimolecular Decomposition of 1,1,2-Trimethylcyclobutane

by A. T. Cocks and H. M. Frey*

Chemistry Department, Reading University, Reading, England (Received January 18, 1971)

Publication costs borne completely by The Journal of Physical Chemistry

The gas phase thermal decomposition of 1,1,2-trimethylcyclobutane has been studied from 387 to 455°. The primary decomposition proceeds by two pathways, one to yield propylene and 2-methylpropene and the other to yield ethylene and 2-methylbut-2-ene. Rate constants for these processes were independent of initial reactant pressure above 5 Torr and were fitted by the Arrhenius equations: $\log k_{\text{propylene}}/\text{sec}^{-1} = 15.75 \pm 0.07 - 60,170 \pm 230 \text{ cal mol}^{-1}/2.303RT$; and $\log k_{\text{ethylene}}/\text{sec}^{-1} = 15.93 \pm 0.06 - 63,880 \pm 190 \text{ cal mol}^{-1}/2.303RT$. Secondary reactions of the products occur, but these are much slower than the primary processes.

Introduction

In an earlier paper,¹ we developed a semiquantitative procedure for predicting the rates of reaction of substituted cyclobutanes from a mechanistic model which involved a twisting of the cyclobutane ring in forming

the transition state. The present work was undertaken to test the predictions of this model.

Experimental Section

1,1,2-Trimethylcyclobutane was prepared by two methods, one starting from 2,2,3-trimethylcyclobu-

tanone² and the other from 1,2,2-trimethylbicyclo[1.1.0]butane.

A small sample of 2,2,3-trimethylcyclobutanone was converted to the semicarbazone and this was reduced to the hydrocarbon with sodium in diethylene glycol.³ The crude 1,1,2-trimethylcyclobutane was separated by steam distillation.

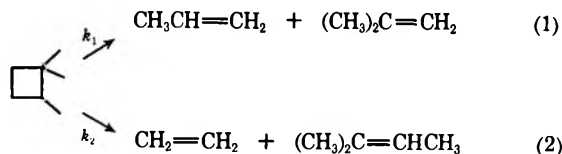
A small sample of 1,2,2-trimethylbicyclo[1.1.0]butane was reduced to 1,1,2-trimethylcyclobutane with lithium in ethylenediamine.⁴ Water was added to the reaction mixture and the cyclobutane distilled out.

The crude 1,1,2-trimethylcyclobutane from both preparations was washed with sulfuric acid, followed by water, dried, and then distilled on a vacuum line. Final purification was by preparative gas chromatography using a 5-m \times 6-mm column packed with 60–80 mesh Chromosorb P containing 20% w/w of squalane and operated at 80°. The cyclobutane was dried over a 4A molecular sieve for 24 hr. The final purity was better than 99.8%. Its identification was confirmed by nmr spectroscopy.

Apparatus. The kinetic apparatus and experimental techniques were virtually the same as described previously.⁵ The gas handling lines and gas pipets were heated and maintained at about 60° to minimize adsorption problems. Gas chromatographic analysis was performed with a Perkin-Elmer 452 instrument fitted with a gas sampling valve, flame ionization detector, and a 5-m \times 2-mm column packed with 20% w/w silicone oil on 60–80 mesh Chromosorb P. For the determination of product ratios the column was operated at ambient temperature and for kinetic analyses at 70°. Signals from the detector were integrated with a Perkin-Elmer D2 instrument. Reaction products were identified by comparison of their retention times with those of authentic samples on four different columns.

Results

In the temperature range 387–455°, 1,1,2-trimethylcyclobutane decomposed by two pathways to yield propylene and 2-methylpropene by one and ethylene and 2-methylbut-2-ene by the other.



Before any kinetic studies were made, the reaction vessel was "aged" by pyrolyzing a large sample of reactant for 24 hr at 455°. After this treatment reproducible kinetic results were obtained for the decomposition of the reactant. Plots of $\log(2P_0 - P_t)$ against time, where P_0 and P_t are the pressures at the start and at time t , respectively, obtained from the recorder trace of the pressure transducer output, were linear to greater than 60% decomposition. No corrections were made

for dead space ($\sim 0.5\%$). Preliminary runs in which the initial reactant pressure was varied from 5 to 25 Torr showed that the rate constant was independent of pressure in this range. Subsequent decompositions always employed initial reactant pressures between 10 and 12 Torr. Two complete runs were carried out at each of eight temperatures within the stated range. Overall rate constants were obtained from the slopes of the plots of $\log(2P_0 - P_t)$ against time (by a least-squares analysis). Values obtained for rate constants from duplicate runs agreed within 2%. In addition, at each temperature, several pyrolysis mixtures taken to low percentage decomposition were analyzed to obtain the ratio of propylene to ethylene and 2-methylpropene to 2-methylbut-2-ene. The latter ratios were more scattered than the former but the mean values were in good agreement. Values of k_1 and k_2 were determined at each temperature using the values of the overall rate constants together with the value of the ratio of ethylene to propylene. These are shown in Table I. Arrhenius plots of the data given in Table I gave good straight lines from which the following equations were obtained by a least-squares analysis

$$\log k_1/\text{sec}^{-1} = 15.75 \pm 0.07 - 60,170 \pm 230 \text{ cal mol}^{-1}/2.303RT$$

$$\log k_2/\text{sec}^{-1} = 15.93 \pm 0.06 - 63,880 \pm 190 \text{ cal mol}^{-1}/2.303RT$$

The error limits are standard deviations. It is surprising that the error limits are smaller for the smaller rate constant, but this arises by a fortuitous cancellation of errors due to pressure and analytical measurements.

Table I: Rate Constants for the Decomposition of 1,1,2-Trimethylcyclobutane

Temp, °C	387.4	395.1	405.5	417.0
$k_1 \times 10^4, \text{sec}^{-1}$	0.686	1.19	2.36	4.99 (5)
$k_2 \times 10^4, \text{sec}^{-1}$	0.0622	0.111	0.229	0.502 (5)
Temp, °C	425.6	436.0	446.1	455.8
$k_1 \times 10^4, \text{sec}^{-1}$	8.34	16.0	29.4	51.5
$k_2 \times 10^4, \text{sec}^{-1}$	0.867	1.75	3.32	6.03

Runs were carried out at 415.7° in a reaction vessel packed with glass tubes to give it a surface to volume ratio 25 times that of the unpacked reaction vessel. The rate constants obtained in this series were within 2% of that calculated from the Arrhenius equation.

(1) A. T. Cocks and H. M. Frey, *J. Chem. Soc. A*, 2566 (1970).

(2) H. Bestian and D. Gunther, *Angew. Chem., Int. Ed. Engl.*, **2**, 608 (1963).

(3) H. L. Herzog and E. R. Buchman, *J. Org. Chem.*, **16**, 99 (1951).

(4) W. R. Moore, S. S. Hall, and C. Largman, *Tetrahedron Lett.*, 4353 (1969).

(5) A. T. Cocks and H. M. Frey, *J. Chem. Soc. A*, 1671 (1969).

Table II

Reactant	Products	$\log A/\text{sec}^{-1}$	$E_a/\text{kcal mol}^{-1}$	$\Delta G_{723}^\ddagger/\text{kcal mol}^{-1}$
<i>trans</i> -1,2-Dimethylcyclobutane	Propylene	15.45	61.6	54.08
	Ethylene + but-2-enes	15.46	63.4	55.84
<i>cis</i> -1,2-Dimethylcyclobutane	Propylene	15.48	60.4	52.79
	Ethylene + but-2-enes	15.57	63.4	55.49
1,1,2-Trimethylcyclobutane	Propylene + 2-methylpropene	15.75	60.2	51.66
	Ethylene + 2-methylbut-2-ene	15.93	63.9	54.80

The reaction cannot therefore have any appreciable surface component.

A series of runs at 415.5° was followed by gas chromatographic analysis. Due to the limited supply of reactant only six runs were performed. A first-order plot of the first five points (up to 60% decomposition) gave a good straight line, but the sixth point (~75% decomposition) lay off this line. At this relatively high percentage decomposition, further products were observed on the chromatogram. Pyrolysis of mixtures of the product olefins for similar times to those required for about 75% decomposition of the cyclobutane gave products with the same retention times to the further products observed in the trimethylcyclobutane pyrolyses. It would appear that a small amount of secondary decomposition of the olefins occurs but that this will not have an appreciable effect on rate constants determined from data up to 60% decomposition. The rate constant obtained from the first-order plot of the chromatographic data agreed within 2% of that calculated from the Arrhenius equation based on pressure measurements.

Discussion

Studies of product stereochemistry^{6,7} suggest that the decomposition of cyclobutanes occurs predominantly by a pathway involving a biradical intermediate. Evidence has been presented for the existence of a transition state with a twisted ring configuration, in which 1-3 transannular interactions are increased in going from reactant to biradical.⁵ Interaction energies, required to account for the observed rates of decomposition of the monoalkylcyclobutanes, have been shown to have reasonable magnitudes.

The model on which these calculations were based assumes that the overall rate constant is the sum of a set of independent rate constants, corresponding to decomposition processes initiated by the rupture of each of the C-C bonds in the cyclobutane ring. This bond breaking is assumed to take place by a simultaneous twisting of one end of the bond into a given face of the ring and of the other end out of this face and into the opposite face. Thus, each bond can be rup-

tured in two modes and there are eight separate pathways to decomposition. (Because of symmetry considerations some of these may have identical rates, and in the case of cyclobutane itself all eight modes will have the same rates).

The Arrhenius parameters and ΔG_{723}^\ddagger values (*i.e.*, at 723°K) for cyclobutane substituted in the 1 and 2 positions which have been studied to date⁸ are shown in Table II.

Inspection of Table II shows that 1,1,2-trimethylcyclobutane decomposes faster by both pathways than the 1,2-dimethyl compounds. We consider first the major decomposition pathways. For the formation of propylene from *trans*-1,2-dimethylcyclobutane we take the methyl stabilization of the diradical to be twice that for monomethyl substitution, and using the free energies of interaction calculated previously, a value for ΔG_{723}^\ddagger of 54.22 kcal mol⁻¹ is obtained, which is in good agreement with the experimental value.

The decomposition of *cis*-1,2-dimethylcyclobutane to yield propylene is faster than the *trans* compound, presumably due to destabilization of the reactant by the 1-2 interaction of the methyl groups. If it is assumed that no relief of this interaction occurs as a result of cleavage of the C₃-C₄ bond, then it is possible to calculate the magnitude of this effect from the difference in free energies of activation of the *cis* and *trans* compounds. This yields a value of 1.64 kcal mol⁻¹.

For the reaction of 1,1,2-trimethylcyclobutane to yield propylene and 2-methylpropene, twisting the methyl group on C₂ into the ring relieves 1-2 interaction, whereas twisting this group away from the ring leaves a residual interaction with the *trans* methyl group on C₁. The limits for ΔG_{723}^\ddagger can be obtained assuming either that the residual interaction is zero, or by assuming it is unchanged and equal to the ground-state interaction. Such calculations lead to 51.31 kcal

(6) A. T. Cocks, H. M. Frey, and I. D. R. Stevens, *Chem. Commun.*, 458 (1969).

(7) J. E. Baldwin and P. W. Ford, *J. Amer. Chem. Soc.*, **91**, 7192 (1969).

(8) H. R. Gerberich and W. D. Walters, *ibid.*, **83**, 3935 (1961); **83**, 4884 (1961).

$\text{mol}^{-1} < \Delta G_{723}^{\ddagger} < 51.91 \text{ kcal mol}^{-1}$. The observed value of $51.66 \text{ kcal mol}^{-1}$ lies between these limits.

Calculations for the free energies of activation for the minor pathways in the *cis*-dimethyl- and the trimethylcyclobutanes are complicated by a number of changes in interactions for which no values are available from other systems. However, such complications are not obvious for the decomposition of *trans*-1,2-dimethylcyclobutane. Nevertheless the calculated value for $\Delta G_{723}^{\ddagger}$ yields a rate constant which is twice that observed. Indeed on any reasonable model it is difficult

to reconcile the relatively slow rate of this pathway with the rate of decomposition of methylcyclobutane.

It would appear that our model can provide a rationalization of the observed rates of decomposition of most cyclobutanes investigated to date, but the agreement is still only semiquantitative.

Acknowledgment. We thank Dr. H. Bestian for a sample of 2,2,3-trimethylcyclobutanone and Dr. L. Skattebøl for a sample of 1,2,2-trimethylbicyclo-[1.1.0]butane. A. T. C. thanks the Science Research Council for the award of a research studentship.

Circular Dichroism of Chlorophyll and Related Molecules Calculated

Using a Point Monopole Model for the Electronic Transitions

by Kenneth D. Philipson, S. Cheng Tsai, and Kenneth Sauer*

Department of Chemistry and Laboratory of Chemical Biodynamics, Lawrence Radiation Laboratory, University of California, Berkeley, California 94720 (Received December 24, 1970)

Publication costs assisted by the U. S. Atomic Energy Commission

Agreement between calculated and observed rotational strengths for solution monomers of chlorophyll, bacteriochlorophyll, and related molecules has been improved by an order of magnitude through the use of a model which distributes the $\pi-\pi^*$ transitions over the porphyrin ring. Using the Kirkwood-Tinoco coupled oscillator approach, the electronic transitions are described using point monopoles located at the porphyrin macrocycle nuclei. Asymmetrically-placed substituents are replaced by anisotropic polarizabilities and the sum of monopole-polarizability potentials is used to calculate the rotational strengths. An improved geometry for the chlorin ring system is based on recent X-ray diffraction data. The discussion considers the possibilities for theoretical treatment of more complicated systems of molecules.

The application of circular dichroism measurements to materials of photosynthetic origin promises to provide important information about the internal organization and structure of the photoactive pigmented membranes.¹ In order to provide a sound basis for interpreting the CD spectra of these complex biological materials, it is important to develop a better understanding of the corresponding properties of the individual (isolated) molecules.

The present paper is an extension of a previous study of the origins of molecular optical activity in chlorophyll and related molecules.² These molecules consist of an extended, planar porphyrin chromophore, whose symmetry can be considered to be perturbed by substituents placed asymmetrically around the periphery. The absolute configuration at the asymmetric centers in many of these molecules is known,^{3,4} which enables them to provide a rigorous test for the theoretical

treatment. The agreement between experiment and calculations utilizing a model involving a point monopole approximation for the electric transition moment is a considerable improvement over that resulting from the use of point dipole transition moments, but there is still some discrepancy in the quantitative nature of the calculations.

Theory

In the Kirkwood coupled oscillator model, the origin of optical activity is the interaction potential between electric transition dipoles located asymmetrically with

(1) K. Sauer in "Photosynthesis and Nitrogen Fixation," A. San Pietro, Ed., "Methods in Enzymology," Vol. 24, Academic Press, New York, N. Y., in press, 1971.

(2) C. Houssier and K. Sauer, *J. Amer. Chem. Soc.*, **92**, 779 (1970).

(3) I. Fleming, *Nature*, **216**, 151 (1967).

(4) H. Brockmann, Jr., *Angew. Chem., Int. Ed. Engl.*, **7**, 221 (1968).

respect to one another.⁵ Tinoco has derived a general formalism for the rotational strength (R_A) for the case of an electrically allowed, magnetically forbidden transition, $a \leftarrow 0$, located on group i , starting from perturbation theory.⁶ The pertinent equation contains two sets of terms

$$R_A = - \left[\frac{2\pi}{c} \sum_{j \neq i} \sum_{b \neq a} \frac{V_{i0a;j0b} \nu_a \nu_b (\mathbf{R}_j - \mathbf{R}_i) \cdot (\mathbf{u}_{j0b} \times \mathbf{u}_{i0a})}{h(\nu_b^2 - \nu_a^2)} \right. \quad (1a)$$

$$\left. + 2 \sum_{j \neq i} \sum_{b \neq a} \frac{\text{Im } V_{i0a;j0b} \nu_a \mathbf{u}_{i0a} \cdot \mathbf{m}_{j0b}}{h(\nu_b^2 - \nu_a^2)} \right] \quad (1b)$$

where \mathbf{R}_j and \mathbf{R}_i are position vectors of the j th and i th group, respectively, and \mathbf{u} 's are electric dipole transition moments in groups i and j for transitions $a \leftarrow 0$ and $b \leftarrow 0$ where the subscript 0 represents the ground state. $V_{i0a;j0b}$ is the coulomb potential energy due to the interaction of transition charge densities in group i with those in group j . ν_a and ν_b are the frequencies of the transitions $a \leftarrow 0$ and $b \leftarrow 0$, h is Planck's constant, and c is the velocity of light. Im means "the imaginary part of" and \mathbf{m}_{j0b} is the magnetic dipole transition moment for the transition $b \leftarrow 0$ on group j . The second term in this formula is extremely difficult to calculate and is usually ignored. It is expected on theoretical grounds⁷ to be much smaller than the first term and one explicit calculation⁸ has it accounting for about $1/10$ of the observed rotational strength in cyclopentanone derivatives. Hence, only the more familiar first term, equivalent to the Kirkwood contribution, will be considered in this paper.

For each of the pigments the long wavelength Q_y and Q_x transitions are examined.^{9,10} These electrically allowed transitions are $\pi-\pi^*$ in nature and are delocalized over the porphyrin chromophore. For each of the molecules considered here the Q_y band is lower in energy and has a greater absorption intensity (Table I). The x and y axes are defined in Figure 1. Typical absorption and circular dichroism spectra are shown in Figure 2. The band assignments are from experimental studies of fluorescence polarization and linear dichroism,^{11,12} and from the theoretical studies of Gouterman.^{9,10} Each of the bands is slightly complicated by higher vibrational components. These components, however, are not strongly polarized,¹⁰ due to mixing with higher electronic states. Because of this, the higher vibrational components tend not to contribute to the circular dichroism and are ignored in the calculations. The shorter wavelength Soret bands (occurring in the range 350–450 nm) overlap one another strongly, and no calculations were attempted on them.

From the fundamental equation of rotational strength¹³

$$R_A = \text{Im } \mathbf{u}_{0a} \cdot \mathbf{m}_{a0} \quad (2)$$

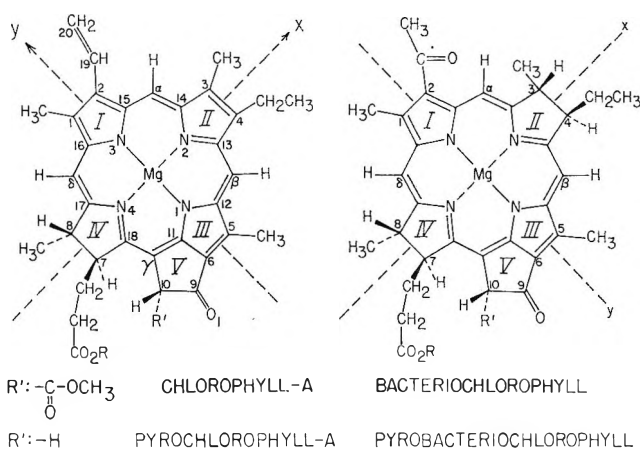


Figure 1. Molecular structures of chlorophyll a, pyrochlorophyll a, bacteriochlorophyll, and pyrobacteriochlorophyll, showing the absolute configuration of the asymmetrically placed ring substituents, R = phtyl.

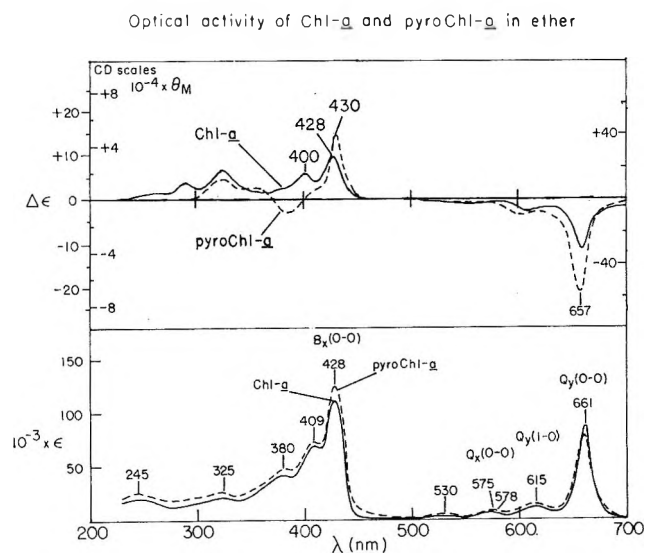


Figure 2. Circular dichroism and absorption spectra of chlorophyll a and pyrochlorophyll a in ether (from ref 2).

a molecule must possess nonperpendicular electric and magnetic transition dipole moments in order to be optically active. Electrically allowed transitions of planar aromatic chromophores, such as the Q transitions of the simple porphyrins, cannot possess the required magnetic dipole from symmetry

- (5) J. G. Kirkwood, *J. Chem. Phys.*, **5**, 479 (1937).
- (6) I. Tinoco, Jr., *Advan. Chem. Phys.*, **4**, 113 (1962).
- (7) W. Moffitt, *J. Chem. Phys.*, **25**, 467 (1956).
- (8) L. L. Jones, Ph.D. Thesis, University of Utah, Salt Lake City, Utah, 1961.
- (9) M. Gouterman, *J. Mol. Spectrosc.*, **6**, 138 (1961).
- (10) M. Gouterman, *J. Chem. Phys.*, **30**, 1139 (1959).
- (11) J. C. Goedheer in "The Chlorophylls," L. P. Vernon and G. R. Seely, Ed., Academic Press, New York, N. Y., 1966, p 147.
- (12) M. Gouterman and L. Stryer, *J. Chem. Phys.*, **37**, 2260 (1962).
- (13) L. Rosenfeld, *Z. Phys.*, **52**, 161 (1928).

Table I: Experimental Values of Absorption and Rotational Strengths (in Ether)

		Chl a	pyroChl a	BChl	pyroBChl
λ_{\max} , nm	Q_y	661	661	770	770
	Q_z	575	578	570	583
ω_{\max} , cm^{-1}	Q_y	15,130	15,130	12,987	12,987
	Q_z	17,390	17,300	17,540	17,150
Band width, $\Delta\omega$, cm^{-1}	Q_y	390	420	550	490
	Q_z	760	780	910	920
$10^{-3}\epsilon_{\max}$, $(\text{mol/l.})^{-1} \text{cm}^{-1}$	Q_y	86.3	80	96	96
	Q_z	6.8	8	22	22
Oscillator strength, $f = 4.33 \times 10^{-9} \int \epsilon(\omega) d\omega$	Q_y	0.155	0.155	0.309	0.30
	Q_z	0.024	0.029	0.110	0.110
Rotational strength, $10^{40}R_A$, cgs	Q_y	-8.7	-14.3	5.0	
	Q_z	~ 0	~ 0	-4.4	

considerations. The necessary magnetic dipole, in the case of chlorophyll and related biological pigments, is supplied as a perturbation resulting from interaction with asymmetrically-placed substituents.

With this in mind, we can make the form of eq 1a seem plausible. The interaction potential, $V_{i0a;j0b}$, and the dependence on frequency originate in the perturbation method. The vector relationships come from equations such as

$$\mathbf{m}_{j0b} = \frac{i\pi}{c} \nu_b (\mathbf{R}_j \times \mathbf{u}_{j0b}) \quad (3)$$

where $i = \sqrt{-1}$. The two summations of eq 1a indicate that the transition of interest, \mathbf{u}_{i0a} , is interacting with all the transitions, $b \leftarrow 0$, of each of the asymmetrically-placed substituents, j .

The specific molecules for which calculations were done are chlorophyll a (Chl a), pyrochlorophyll a (pyroChl a), bacteriochlorophyll a (BChl), and pyrobacteriochlorophyll a (pyroBChl). Calculated rotational strength is compared with experimental circular dichroism (CD) results for the first three of these for both the Q_y and Q_z bands. The relevant experimental absorption and CD data for these molecules are shown in Table I. The molecular structures of these molecules differ in two important respects: (1) the number of asymmetric substituents and (2) the number of rings which have reduced outer bonds. As shown in Figure 1, BChl has five porphyrin ring carbon atoms substituted asymmetrically at positions C-3, C-4, C-7, C-8, and C-10. In pyroBChl, the carboxymethyl group is replaced with a hydrogen atom and so the C-10 position is no longer asymmetrically substituted. Likewise Chl a and pyroChl a are asymmetrically substituted at positions C-7, C-8, C-10, and at C-7, C-8, respectively. The absorption spectra of these molecules, in contrast to the CD, are relatively insensitive to the nature of the asymmetric substituents and are more a function of the extent of unsaturation of the pyrrole rings. Therefore, it is expected, and found experimentally, that the absorption spectrum of Chl a closely

resembles that of pyroChl a. The same relationship holds between BChl and pyroBChl.

In a previous model used to calculate the interaction potential, $V_{i0a;j0b}$ was evaluated by treating the porphyrin transitions as point dipoles, substituting a dipole-dipole interaction expression in eq 1a and then using the Kirkwood polarizability approximation.² The actual $\pi-\pi^*$ transitions involved, however, are delocalized over the entire porphyrin ring, which has a radius of the order of 5 Å, while the distance between the asymmetric centers and the nearest carbon of the aromatic part of the porphyrin ring can be as small as 2 Å. Thus, a more realistic attempt must take into account the effect of this delocalization of the transition on the interaction potential. For the results presented here, this was done by considering the transition dipole to be the sum of transition electric monopole moments located at each of the conjugated atoms of the ring. The potential can then be determined by treating separately the interaction of each of the monopoles of the porphyrin ring with the effective transition dipoles of the asymmetric centers according to the equation

$$V_{i0a;j0b} = - \sum_t \frac{q_{i0a} \mathbf{R}_{i0a;j} \cdot \mathbf{u}_{j0b}}{|\mathbf{R}_{i0a;j}|^3} \quad (4)$$

where q_{i0a} is the electric transition monopole located at the t th atom for transition $a \leftarrow 0$ (the Q_y or Q_z transition) for group i (the porphyrin ring) and $\mathbf{R}_{i0a;j}$ is a position vector from the j th asymmetrically-placed substituent to monopole t .

The transition monopoles were obtained from the self-consistent field molecular orbital calculations of Weiss,¹⁴ who used the configuration interaction method of Pariser, Parr, and Pople (SCMO-PPP-CI).¹⁵ Good qualitative agreement with the visible and near-uv absorption spectra was obtained. The monopole charge at the t th atom of a π system is proportional to $C_{t0}C_{ia}$ for a transition from the ground state to a singly

(14) C. Weiss, Jr., work in progress.

(15) R. G. Parr, "Quantum Theory of Molecular Electronic Structure," W. A. Benjamin, New York, N. Y., 1963.

Table II: Atomic Coordinates and Transition Monopoles

Atom ^a	Coordinates, Å, for methyl pheophorbide a ^b	Transition monopoles ^c			
		BChl		Chl a	
		Q _y	Q _z	Q _y	Q _z
N ₁	(0.20, -2.01, 0.02)	-0.035	0.007	-0.049	0.001
N ₂	(2.10, 0.00, -0.04)	0.001	-0.115	0.005	-0.055
N ₃	(-0.13, 2.07, -0.04)	0.035	-0.007	0.047	0.004
N ₄	(-2.16, -0.06, 0.06)	-0.001	0.115	0.004	0.109
C _α	(2.33, 2.46, -0.03)	0.035	-0.129	0.107	-0.112
C _β	(2.63, -2.40, 0.03)	-0.033	-0.124	-0.086	-0.136
C _γ	(-2.30, -2.45, -0.02)	-0.035	0.129	-0.054	0.108
C _δ	(-2.57, 2.35, 0.03)	0.033	0.123	0.044	0.109
C ₁	(-0.85, 4.25, 0.02)	-0.051	0.037	-0.039	0.029
C ₂	(0.52, 4.26, -0.01)	-0.046	-0.035	-0.028	-0.041
C ₃	(4.26, 0.83, 0.07)	0.000	0.000	0.040	0.027
C ₄	(4.36, -0.54, 0.07)	0.000	0.000	-0.046	0.017
C ₅	(0.80, -4.20, -0.02)	0.051	-0.037	0.045	-0.037
C ₆	(-0.61, -4.11, -0.03)	0.046	0.035	0.036	0.031
C ₇	(-4.83, -0.92, 0.30)	0.000	0.000	0.000	0.000
C ₈	(-4.46, 0.61, 0.01)	0.000	0.000	0.000	0.000
C ₉	(-1.83, -4.88, -0.09)	0.000	0.001	-0.001	0.002
C ₁₀	(-3.02, -3.81, -0.13)	0.000	0.000	0.000	0.000
C ₁₁	(-0.93, -2.73, -0.02)	0.081	-0.078	0.067	-0.079
C ₁₂	(1.30, -2.89, 0.02)	0.091	0.070	0.075	0.059
C ₁₃	(2.99, -1.06, 0.01)	0.112	0.055	0.069	0.062
C ₁₄	(2.85, 1.13, 0.01)	-0.103	0.063	-0.084	0.050
C ₁₅	(1.00, 2.87, -0.02)	-0.081	0.078	-0.085	0.050
C ₁₆	(-1.26, 2.84, 0.00)	-0.091	-0.070	-0.075	-0.085
C ₁₇	(-3.01, 1.00, 0.04)	-0.112	-0.055	-0.111	-0.058
C ₁₈	(-2.92, -1.19, 0.08)	0.103	-0.063	0.106	-0.056
C ₁₉	(1.43, 5.43, 0.00)	0.000	-0.001	0.000	0.000
C ₂₀ ^d	(1.12, 6.61, -0.22)	-0.015	-0.008	0.000	0.000
O ₁	(-2.01, -6.09, -0.11)	0.015	0.008	0.019	0.010

^a See Figure 1 for numbering system. ^b See ref 23. ^c See ref 14. ^d C₂₀ is replaced with an oxygen in BChl.

excited state, a , where C_{t0} and C_{ta} are, respectively, the molecular orbital coefficients at the t th center for the ground- and excited-state molecular orbitals. The monopoles (Table II) for BChl and pyroBChl were derived from a calculation for 2,6-dicarbonyl OPP-tetrahydroporphin and those for Chl a and pyroChl a from 2-vinyl-6-carboxylchlorin. The calculated monopoles were scaled so that the summation

$$\sum_t \mathbf{R}_{i0a} q_{i0a}$$

equaled the experimental value for \mathbf{u}_{i0a} . In order to improve the approximation to the transition charge densities of π -type orbitals, each monopole strength was separated into two parts. New monopoles, with magnitudes equal to $1/2$ those of the calculated monopoles, were placed 1 Å above and below the conjugated atom.¹⁶ The number of monopoles used, therefore, was actually twice the number of conjugated atoms. Molecular orbital calculations on protochlorophyll were not very successful. For this more symmetric molecule polarized transitions for the long wavelength absorption bands, in contrast to experiment,² were not predicted and therefore a rotational strength calculation was not attempted.

If we now substitute eq 4 into eq 1a

$$R_A = -\frac{2\pi}{c} \sum_{j \neq i} \sum_{b \neq a} \sum_t \frac{\nu_a \nu_b}{h(\nu_b^2 - \nu_a^2)} \frac{q_{i0a}}{|\mathbf{R}_{i0a;j}|^3} \times [\mathbf{R}_{i0a;j} \cdot \mathbf{u}_{j0b}] [\mathbf{u}_{j0b} \cdot (\mathbf{R}_{i0a;j} \times \mathbf{u}_{i0a})] \quad (5)$$

we find that any calculation would be extremely difficult, because knowledge of the transition dipoles of each of the asymmetric groups, j , for all transitions, $b \leftarrow 0$, is needed. A majority of these transitions occur in the far-ultraviolet region and have never been classified. To overcome this, we use Kirkwood's polarizability approximation

$$(2/h\nu_0) \sum_b \mathbf{u}_{j0b} \mathbf{u}_{j0b} = (\alpha_{33} - \alpha_{11})_j \mathbf{e}_j \mathbf{e}_j \quad (6)$$

where ν_0 is an average frequency of the transitions, α_{33} and α_{11} are the polarizabilities parallel and perpendicular to the axis of symmetry for each group (assuming cylindrical symmetry), and \mathbf{e}_j is a unit vector pointing along the axis of cylindrical symmetry. Each covalent bond in an asymmetric center is considered in the calculations to be a group, j . A polarizability anisotropy

(16) R. W. Woody, *J. Chem. Phys.*, **49**, 4797 (1968).

$(\alpha_{33} - \alpha_{11})_j$ is associated with each bond, and its magnitude is based on values found in the literature. By considering each bond separately, and therefore distributing each asymmetric substituent in space, better results can be expected than if each group is approximated by a single polarizability value. Bond polarizabilities are difficult to determine and considerable variation in values is found in the literature. The values used for the C—H,¹⁷⁻¹⁹ C—C,^{20,21} C=O,^{21,22} and C—O^{21,22} bonds are shown in Table III and are judged to be the best available. By putting eq 6 into eq 5 and by using the good approximation

$$\frac{\nu_0^2}{\nu_0^2 - \nu_a^2} \approx 1$$

we obtain our final equation

$$R_A = -\frac{\pi}{c} \sum_{j \neq i} \sum_t \frac{\nu_a Q_{it0a}}{|\mathbf{R}_{it0a;j}|^3} (\alpha_{33} - \alpha_{11})_j \times (\mathbf{R}_{it0a;j} \cdot \mathbf{e}_j) [\mathbf{e}_j \cdot (\mathbf{R}_j - \mathbf{R}_{i0a}) \times \mathbf{u}_{i0a}] \quad (7)$$

Table III: Bond-Bond Polarizabilities

Bond	Polarizability anisotropy $10^{24} (\alpha_{33} - \alpha_{11})$, cm^2
C—C	0.71
C=O	1.24
C—O	0.96
C—H	-0.312

Coordinates for the molecules (Table II) are taken from a recent crystal structure determination of methylpheophorbide a²³ (Chl a with the central Mg atom removed and with a methyl group replacing the phytol chain). Thus, the geometry of the side groups in solution is taken to be the same as that in the crystal. Although this may seem to be a crude approximation, molecular models show that each side group has significant steric hindrances. Thus, the assumption used is that, even in solution, the side groups are unable to rotate freely. Because eq 7 predicts a dependence of rotational strength on the inverse square of the distance of separation, the part of the side group which makes the greatest contribution to the optical activity is expected to be that which is closest to the conjugated ring, and it is precisely this part of the group which will feel the bulk of the steric forces. Calculations in which all side groups were allowed to rotate freely (Table IV) were also attempted. In all cases the agreement with experiment was not so good as that in which the "crystal conformation in solution" was assumed. In certain cases the results did not even agree with the sign of the experimental rotational strength.

The phytol chain is ignored in the calculations. This probably introduces no serious error since this substit-

uent is a larger distance from the porphyrin ring than any other group, thereby decreasing its interaction potential. Evidence from nmr measurements^{24,25} indicates that the phytol does not strongly interact with the other substituents. Measurements in this laboratory show that the CD of methylchlorophyllide a is identical with that of Chl a, implying that the phytol may safely be ignored in a theoretical treatment. This result would seem to resolve a conflict between the results of Houssier and Sauer² on pheophytin a and those of Briat, *et al.*,²⁶ on methylpheophorbide a (pheophytin a with a methyl replacing the phytol). The difference in the magnitude of the CD reported for these molecules can most likely be attributed to a calibration problem of one of the spectrometers or to a partial epimerization of the substituents at C-10, as has already been suggested.²

Results

Results of the calculations are given in Table IV. All experimental measurements^{2,27} were made on solutions in ether and, to account for the dielectric effect of the solvent,²⁸ all calculated rotational strengths were multiplied by $(n^2 + 2)/3$, where n is the refractive index of the solvent. In all cases there is qualitative agreement between the theoretically derived rotational strengths and the experimental values. In the previous study,² in which the Q transitions were approximated by a point dipole, the experimental measurements gave larger rotational strengths than the calculations by factors from 8 to 40. In one case (Chl a; Q_y transition) the wrong sign was predicted. In the point monopole calculations (Table IV) the range of discrepancies is reduced to 1.5-6 and the signs are all correctly predicted. Most of the improvement reported here can be attributed to the use of monopoles and the use of a fixed geometry for the substituents. It is clear that in calculations such as these, a highly delocalized transition cannot be accurately represented as a point dipole.

(17) B. C. Vickery and K. G. Denbigh, *Trans. Faraday Soc.*, **45**, 61 (1949).

(18) T. Yoshino and H. J. Bernstein, *J. Mol. Spectrosc.*, **2**, 241 (1958).

(19) A. T. Amos and G. G. Hall, *Theor. Chim. Acta*, **6**, 159 (1966).

(20) C. W. Bunn and R. P. Daubeny, *Trans. Faraday Soc.*, **50**, 1173 (1954).

(21) C. G. LeFevre and R. J. W. LeFevre, *Rev. Pure Appl. Chem.*, **5**, 261 (1955).

(22) K. G. Denbigh, *Trans. Faraday Soc.*, **36**, 936 (1940).

(23) M. Fischer, Ph.D. Thesis, University of California, Berkeley, 1969 (UCRL-19524).

(24) K. Sauer, J. R. Lindsay Smith, and A. J. Schultz, *J. Amer. Chem. Soc.*, **88**, 2681 (1966).

(25) G. L. Closs, J. J. Katz, F. C. Pennington, M. R. Thomas, and H. H. Strain, *ibid.*, **85**, 3809 (1963).

(26) B. Briat, D. A. Schooley, R. Records, E. Bunnenberg, and C. Djerassi, *ibid.*, **89**, 6170 (1967).

(27) L. Coyne, unpublished data.

(28) A. Moscowitz, *Advan. Chem. Phys.*, **4**, 67 (1962).

Table IV: Comparison of Calculated and Experimental Rotational Strengths

Molecule	Transition	Point dipole model, ^a $RA \times 10^{40}$ cgs	Point monopole model					Calculated sum, $RA \times 10^{40}$ cgs	Experimental, $RA \times 10^{40}$ cgs
			Calculated $RA \times 10^{40}$ cgs contribution for each asymmetry center						
			C-3	C-4	C-7	C-8	C-10		
BChl	Q_y	-1.3	1.9	1.9	-3.3	-2.3	5.2	3.4	5.0
	Q_z	-0.1	-0.005	-0.31	0.14	0.20	-3.1	-3.1	-4.4
pyroBChl	Q_y	0	1.9	1.9	-3.3	-2.3		-1.8	
	Q_z	0	-0.005	-0.31	0.14	0.20		0.03	
Chl a	Q_y	0.5			-2.9	-2.1	3.6	-1.4	-8.7
	Q_z	0.02			0.07	0.1	-1.6	-1.4	~0
pyroChl a	Q_y	0.4			-2.9	-2.1		-5.0	-14.3
	Q_z	0.3			0.07	0.1		0.2	~0
Bchl (monopoles in plane)	Q_y		3.2	3.9	-5.0	-4.1	5.2	2.8	5.0
Chl a (with BChl monopoles)	Q_y				-1.6	-1.0	2.4	-0.2	-8.7
BChl (with freely rotating side groups)	Q_y		0.1	0.8	-0.4	-0.8	0.4	0.1	5.0

^a Calculated from data in ref 2.

Results are also presented for a calculation in which all monopoles were placed in the plane of the chromophore (for all other calculations, monopoles were divided by two and placed 1 Å above and below the plane; see above). It is seen that this can change the contribution of an individual asymmetric center by as much as a factor of 2. The implication from this is that if the true wave function (with the transition charge densities distributed continuously through space) were used to calculate the interaction potential, the result would be an improvement over that obtained by using monopoles (even if the monopoles were an extremely accurate set). That is, there is still an inherently large approximation in the use of point monopoles.

A calculation is presented for Chl a in which BChl monopoles were used. This changes the result by a large amount and appreciably reduces the agreement with experiment. Since Chl a and BChl are closely related molecules with monopole patterns which are rather similar, this test shows that relatively small changes in monopoles can cause large changes in the calculated rotational strengths. Fairly accurate monopoles are, therefore, essential for this type of calculation.

Attempts were made to prepare and to obtain a CD spectrum for pyroBChl. For this molecule the contribution to the rotational strength induced by the groups at C-3 and C-4 is expected approximately to cancel the contributions of the asymmetric centers at C-7 and C-8 (these groups are related by an approximate center of inversion) and a small CD signal is expected. However, the rotational strength of the Q_y transition of pyroBChl was observed to be generally greater than that for BChl and with a large variability from sample

to sample. Although the infrared spectrum confirmed the absence of the C-10 carboxymethyl group following pyrolysis and the visible and near-infrared absorption was virtually indistinguishable from that of BChl, the CD results lead us to doubt whether we had the correct molecule. As a consequence, the experimental rotational strengths for pyroBChl are not included in Table IV.

Conclusions

The nature of the optical activity of the chlorophyll molecules studied can now be considered to be understood qualitatively. The general features of the CD spectra can be accounted for in terms of the interactions described by the Kirkwood-Tinoco approach. It is possible that this type of calculation may prove useful in assigning absolute configurations to molecules where this information is not known.

The origin of the circular dichroism of chlorophylls in photosynthetic membranes differs from that described here. Exciton interactions between chlorophylls cause rotational strengths of a much larger magnitude than those exhibited by monomers. Nevertheless, the theory for such interactions has much in common with that presented here. The results presented above thus make calculations on more complicated systems feasible.

Acknowledgments. The authors wish to thank Dr. Charles Weiss, Jr., and Dr. Mark Fischer for many helpful discussions. This research was supported in part by the U. S. Atomic Energy Commission, and in part by a grant from the National Science Foundation (GB-6738).

Liquid Crystal–Isotropic Phase Equilibria in the System

Poly- γ -benzyl- α ,L-glutamate–Dimethylformamide¹

by Elizabeth L. Wee and Wilmer G. Miller*

Department of Chemistry, University of Minnesota, Minneapolis, Minnesota 55455 (Received December 31, 1970)

Publication costs assisted by the U. S. Public Health Service

The temperature–composition phase diagram has been determined for the system polybenzylglutamate–dimethylformamide in the temperature range -20 to $+140^\circ$ and the composition range 0–40 wt % polymer. The detailed phase diagram was determined with a polymer of molecular weight 310,000 (M_w). The molecular weight dependence of the phase equilibria was estimated using polymers of molecular weights 120,000, 310,000, and 900,000. Nuclear magnetic resonance, hydrodynamic, and polarizing microscope measurements were employed to locate the phase boundaries between the isotropic and liquid crystal phases. At low temperatures ($<35^\circ$) the phase diagram is strikingly similar to that predicted by Flory for impenetrable rods. At higher temperatures considerable difference occurs. An upper critical solution temperature is observed for the liquid crystal phase. No evidence was found for a critical temperature in the isotropic–liquid crystal equilibrium.

Introduction

Liquid crystal phases containing high molecular weight components have been known for many years. The earliest involved polyelectrolytes such as tobacco mosaic virus.² Approximately 20 years ago liquid crystals were observed with the nonionic helical polymer poly- γ -benzyl- α ,L-glutamate (PBLG) as one constituent.^{3,4} Shortly thereafter Flory proposed a phase diagram for the two component system solvent–stiff chain polymer based on a lattice treatment.^{5,6} The more important results of this treatment were that an entropically driven phase transition could occur, that a biphasic (isotropic, liquid crystal) region may exist with a rather small difference between the concentrations in the two phases, and that endothermic polymer–solvent mixing results in a large concentration difference between the two phases in equilibrium. Although other methods have been used to treat the isotropic–liquid crystal phase equilibrium,^{7–10} no complete temperature–composition phase diagram has been presented.

Robinson showed by polarizing microscope observations that the liquid crystal phase was cholesteric.⁴ At room temperature the biphasic region was found to be in substantial agreement with Flory's predictions with respect to concentrations and molecular weight dependence,¹¹ assuming the heat of polymer–solvent mixing was zero or negative. Vapor sorption studies by Flory and Leonard¹² later cast doubt on the applicability of the original Flory model at high polymer concentrations. Parallel, impenetrable rods mixing with solvent should show ideal entropy of mixing, which was not observed. Solvent–side chain mixing was invoked to account for the discrepancy.

A temperature–composition phase diagram has not been determined previously. A three component system, polymer–solvent–nonsolvent, has been investigated¹³ where the variation of nonsolvent content corresponds thermodynamically to a variation in temperature. Unfortunately, it is difficult to connect the nonsolvent content to theoretical parameters.

Variable temperature studies on dilute, isotropic PBLG–dimethylformamide (DMF) solutions have been reported recently.¹⁴ These studies indicated that at some temperatures polymer–solvent mixing should be endothermic, thus altering the phase equilibria if the lattice theory is applicable.

In this communication the temperature–composition phase diagram for the PBLG–DMF system is reported for the temperature range -20 to $+140^\circ$ and the com-

(1) This work was supported in part by research grants from the U. S. Public Health Service (GM16922) and by funds from the University of Minnesota Graduate School.

(2) J. D. Bernal and I. Fankuchen, *J. Gen. Physiol.*, **25**, 111 (1941).

(3) A. E. Elliott and E. J. Ambrose, *Discuss. Faraday Soc.*, **9**, 246 (1950).

(4) C. Robinson, *Trans. Faraday Soc.*, **52**, 571 (1956).

(5) P. J. Flory, *Proc. Roy. Soc. Ser. A*, **234**, 60 (1956).

(6) P. J. Flory, *ibid.*, **234**, 73 (1956).

(7) L. Onsager, *Ann. N. Y. Acad. Sci.*, **51**, 627 (1949).

(8) A. Isihara, *J. Chem. Phys.*, **19**, 1142 (1951).

(9) E. A. DiMarzio, *ibid.*, **35**, 658 (1961).

(10) M. A. Cotter and D. E. Martire, *Mol. Cryst. Liquid Cryst.*, **7**, 295 (1969).

(11) P. J. Flory, *J. Polym. Sci.*, **49**, 105 (1961).

(12) P. J. Flory and W. J. Leonard, Jr., *J. Amer. Chem. Soc.*, **87**, 2102 (1965).

(13) A. Nakajima, T. Hayashi, and M. Ohmori, *Biopolymers*, **6**, 973 (1968).

(14) K. G. Goebel and W. G. Miller, *Macromolecules*, **3**, 64 (1970).

position range 0–40 wt % polymer. The phase equilibria were investigated by solvent proton magnetic resonance, polarizing microscopic, and hydrodynamic measurements. The phase equilibria are compared with existing theory.

Experimental Section

Three samples of PBLG were employed. Sample PBLG3 ($M_w \approx 310,000$) was purchased from New England Nuclear Corp. Sample PBLG1 ($M_w \approx 120,000$) was obtained by polymerizing benzylglutamate *N*-carboxyanhydride in DMF with a primary amine initiator. Sample PBLG9 ($M_w \approx 900,000$) was prepared from anhydride polymerization in benzene-dioxane (4:1, v:v) with a secondary amine initiator. All samples were vacuum dried for 24 hr at 60° before use. Except in the molecular weight studies, sample PBLG3 ($M_w \approx 310,000$) was used throughout the whole work.

Dimethylformamide (Eastman Kodak, reagent grade) was vacuum distilled over CaSO_4 .

For the nmr and polarizing microscope studies solutions less than 0.1 volume fraction polymer were prepared directly in nmr sample tubes (5 mm o.d.). Samples with concentrations 0.1 or greater were prepared outside the sample tubes and transferred by syringe. All tubes were sealed. In calculating volume concentrations the density of PBLG was taken¹³ as 1.283 g ml^{-1} . The polymer and solvent specific volumes were assumed to be concentration independent. Volume fractions are reported at 25°. No temperature corrections were made.

The nmr spectra were taken using a Varian A-60D spectrometer equipped with a Varian variable temperature controller. The spectra were obtained without sample tube spinning, unless otherwise specified. The spectrum was recorded at proper time intervals until a more or less time independent spectrum was observed. Frequently this took many hours. The slowness appears to be a characteristic phenomenon in macromolecular liquid crystals. It may be a consequence of the coupling mechanism for the orientation of the bundles in a magnetic field.

A Leitz microscope having a temperature controlled stage was employed for all polarizing microscope studies.

A Haake Rotovisco Couette type rotational viscometer with NV rotator was employed for hydrodynamic studies. The rate of shear was calculated at the rotor surface.

Results

System with Three Components. Initially we attempted to determine the temperature dependence of the phase equilibrium by the approach of Nakajima, Hayashi, and Ohmori.¹³ To a PBLG-DMF solution at constant temperature the nonsolvent methanol was added until turbidity occurred. A slight increase in

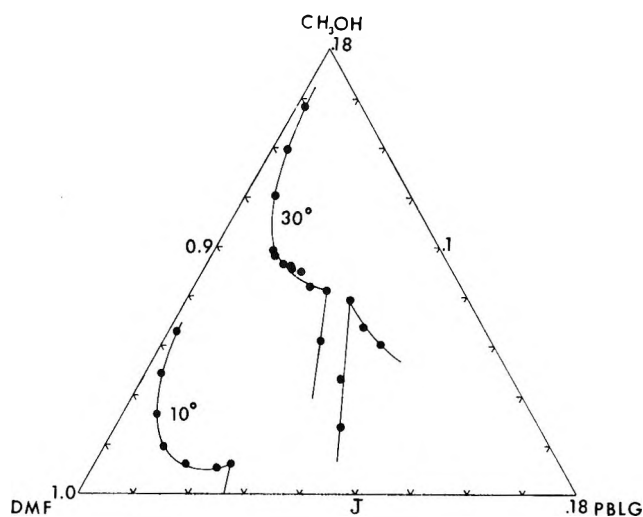


Figure 1. Turbidity points for the system. PBLG-DMF- CH_3OH at 10 and at 30°. The solid line is calculated from the Flory model.⁶

temperature resulted in a clear solution. Turbidity again appeared upon returning to the original temperature. Results of such studies at 10 and 30° are shown in Figure 1, where the turbidity temperature was taken to be the temperature of phase equilibrium. Viewing the turbid phase through crossed polars gave inconclusive evidence as to its being the liquid crystal phase. The striking similarity between the general features of these diagrams with the Flory diagram encourages one to force a fit between the two by finding the value of the Flory χ parameter necessary for superposition. The solid lines in Figure 1 were calculated using Flory's equations.⁶ The χ values are shown in Figure 2 as a function of the volume fraction nonsolvent (v_{NS}). Linear extrapolation to 0% nonsolvent yields a positive and temperature dependent χ . A positive and temperature dependent χ is consistent with the results of Goebel and Miller,¹⁴ who found the dilute solution osmotic second virial coefficient to be temperature dependent, and to change sign in this temperature region.¹⁵ A linear relation between χ and the nonsolvent content assumes the "single liquid approximation" of Scott.¹⁶ In this approximation the solvent composition in the coexisting phases must be the same so that the solvent-nonsolvent mixture behaves as a single liquid. Thus the entropy of mixing remains the same as in binary component systems, whereas the heat of mixing depends on solvent composition. A further consequence of the "single liquid approximation" is that the χ value extrapolated to $v_{\text{NS}} = 0$ should be independent

(15) The solvent can presumably interact with the polymer side chain and not the helical backbone. A model side chain, benzyl *n*-butyrate, when mixed with DMF gave a calorimetric heat of mixing of +130 cal per mole of butyrate, thus providing another indication of a positive heat of mixing. We wish to thank Dr. Warren Puhl for this determination.

(16) R. L. Scott, *J. Chem. Phys.*, 17, 268 (1949).

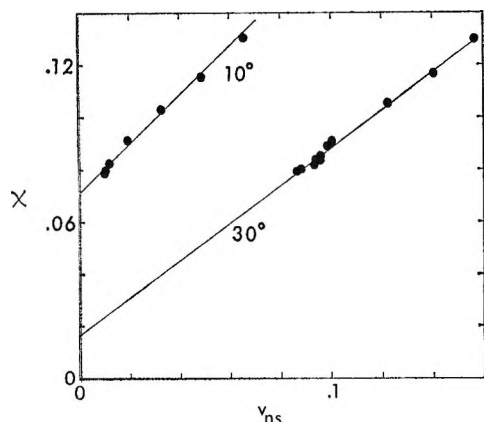


Figure 2. The Flory χ values needed to fit the experimental data in Figure 1.

of the nonsolvent employed. The data of Nakajima, *et al.*,¹³ for the nonsolvents methanol and water do not extrapolate to the same χ . Consequently we abandoned this approach.

Solvent Proton Magnetic Resonance Studies. Normally in proton magnetic resonance of solutions the nuclear spin-magnetic field interactions and the indirect spin-spin interactions are the only terms in the Hamiltonian which are important. The direct dipole-dipole intramolecular and intermolecular interactions are averaged to zero. In helical PBLG the protons are held in relatively fixed orientations thus providing an anisotropic environment. The intramolecular dipolar coupling is not averaged to zero, thus removing the degeneracy among the many protons otherwise equivalent. As the Zeeman resonance must be distributed over all these splittings the intensity of each peak is reduced to such an extent that the high molecular weight PBLG spectrum consists of a broad envelope of unresolved lines which becomes part of the background signal. This is true for the isotropic as well as the liquid crystal phase.

In a strong magnetic field the rodlike PBLG molecules in the liquid crystal phase are aligned in the direction of the field, thereby converting the cholesteric into a nematic phase.¹⁷⁻²⁰ The spectrum of the DMF protons is a time average over their environment. When in the vicinity of the polymer the environment of the DMF molecule is anisotropic, consequently the direct intramolecular dipolar terms are not averaged to zero. However, the protons in DMF are split by a much smaller number of direct dipole-dipole interactions. With the total intensity distributed over a smaller number of splittings, the DMF signal is much more intense than that of the polymer.

A typical magnetic field oriented DMF spectrum taken on the Varian A-60D is shown in Figure 3A. Although the spectrum shown here is not fully resolved, it has been shown using a 220-MHz spectrometer to consist of nine lines for the methyl protons, and a quar-

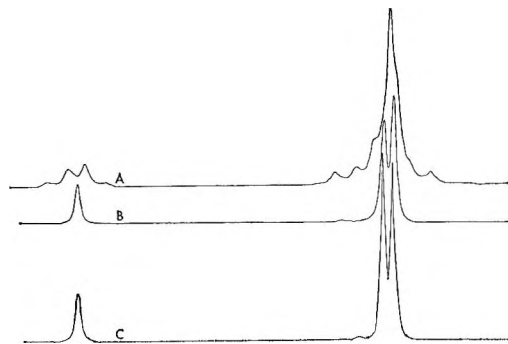


Figure 3. Proton magnetic resonance spectrum of DMF in the magnetic field oriented liquid crystal phase (A), in the biphasic region (B), and in the isotropic phase (C). Polymer concentration (volume fraction) and temperature was (A) 0.165 at 44°; (B) 0.110 at 4°; (C) 0.070 at 44°.

tet for the formyl proton.²⁰ On occasion the nine line resolution could be obtained on the 60-MHz instrument. A typical spectrum for DMF in the isotropic phase is shown in Figure 3C, and in the biphasic region in Figure 3B. The DMF spectra in the isotropic and biphasic regions differ only in the relative heights of the methyl proton peaks. From a number of measurements of this type we concluded that the phase boundary between the liquid crystal and the biphasic region could be investigated reliably by nmr, but not the isotropic-biphasic boundary.

Our experimental approach was to place a sample in the spectrometer and wait several hours to see if dipolar splitting appeared. If it did, the system was considered to be a single, liquid crystal phase. The temperature was then adjusted and the sample held at the new temperature until a sensibly time independent spectrum was obtained. So long as there was no collapse of the multiplets we assigned each temperature-composition point to the liquid crystal phase. When a temperature was reached in which the multiplets collapsed, the system was assigned to the biphasic region. In order to determine if our measurements were the equilibrium ones, the sample was temperature cycled through the suspected phase boundary. Figure 4 is an example of such a cycle, confirming the equilibrium nature of the measurements.

All temperature-composition points investigated by magnetic resonance measurements are shown in Figure 5 for the PBLG3 polymer. The equilibrium line bounding the liquid crystal phase, determined by nmr measurements, is shown in Figure 6.

As the polymer composition is increased the intensities are decreased and the spectrum is broadened. A

(17) S. Sobajima, *J. Phys. Soc. Jap.*, **23**, 1070 (1967).

(18) E. T. Samulski and A. V. Tobolsky, *Mol. Cryst. Liquid Cryst.*, **7**, 433 (1969).

(19) B. M. Fung, M. J. Gerace, and L. S. Gerace, *J. Phys. Chem.*, **74**, 83 (1970).

(20) M. Panar and W. D. Phillips, *J. Amer. Chem. Soc.*, **90**, 3880 (1968).

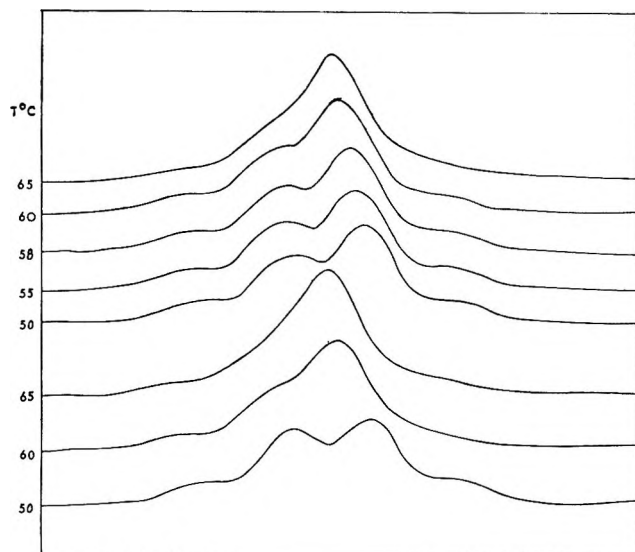


Figure 4. Formyl DMF proton spectrum as the temperature is cycled through a suspected phase boundary. Starting point is the bottom spectrum. Volume fraction polymer was 0.122.

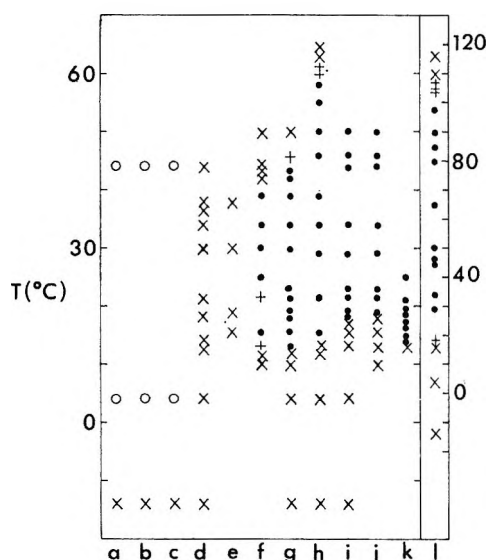


Figure 5. Classification of the DMF spectrum as a function of temperature for various compositions. The volume fraction of PBLG3 was 0.0098 (a), 0.050 (b), 0.070 (c), 0.089 (d), 0.097 (e), 0.101 (f), 0.110 (g), 0.122 (h), 0.165 (i), 0.203 (j), 0.30 (k), or 0.150 (l). Spectrum is classified as to whether it resembles that in Figure 3A (●), 3B (×) or 3C (○). Occasionally, formyl proton split slightly giving a single peak with shoulders while methyl protons exhibited no dipolar splitting (+).

50 vol % solution gave a very broad, unresolved spectrum.

Polarizing Microscope Studies. Robinson in his initial study of polypeptide liquid crystals employed the polarizing microscope for phase determination.⁴ Placed between crossed polars the liquid crystalline phase transmits light, the isotropic phase does not. Upon heating a sample in a sealed tube between crossed polars the temperature at which light ceased to be

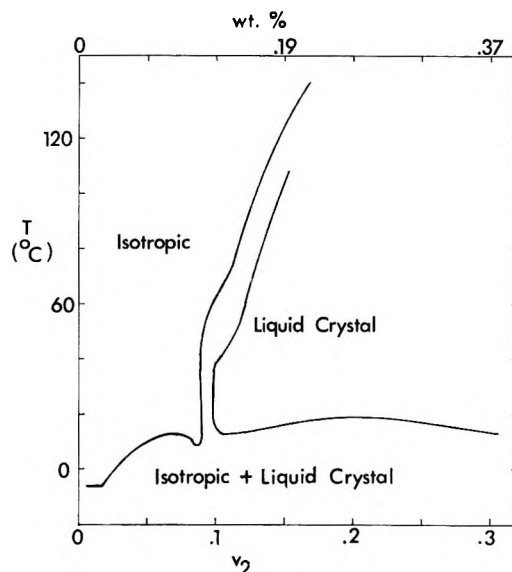


Figure 6. Phase diagram for PBLG3. Equilibrium line bounding the liquid crystal phase was determined by nmr, while the line bounding the isotropic phase was determined from polarizing microscope studies.

transmitted was taken as the biphasic to isotropic equilibrium temperature. Cycling the temperature through this point indicated the system was reversible. The equilibrium line bounding the isotropic phase, determined by polarizing microscope measurements, is shown in Figure 6 for PBLG3.

At temperatures where a solution is biphasic some areas of the sample transmit light when placed between crossed polars, others do not. We found it difficult to determine the point when no dark areas remained, *i.e.*, the point where only the liquid crystal phase was present. No polarizing microscope determinations are reported for the biphasic to liquid crystal transition.

Hydrodynamic Studies. In Figure 7 the viscosity is shown as a function of temperature for several polymer concentrations. The shear rate at the rotor surface in all cases was 19.4 sec^{-1} , and the polymer was PBLG3. The phase transition temperatures determined by nmr and by the polarizing microscope are indicated for reference. Viscosities greater than 10,000 cP were not measurable with the viscometer employed. Most of the liquid crystal solutions are highly non-Newtonian. As our interest here is in phase boundaries no shear rate studies are reported.

Molecular Weight Studies. A few nmr and microscope studies were made with PBLG1 and PBLG9. These are shown in Figure 8. Using these points and assuming that the phase boundaries have shapes similar to that for PBLG3, approximate phase boundaries have been sketched in.

Discussion

Comparison of Methods and Reliability of the Phase Diagram for PBLG3. Some of the more interesting

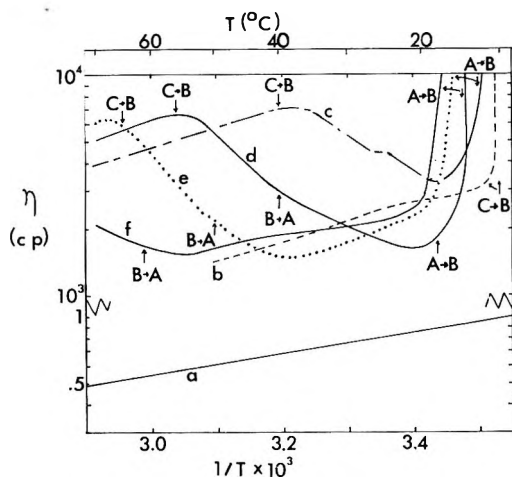


Figure 7. Temperature dependence of the viscosity. The volume fraction polymer was 0 (a), 0.05 (b), 0.09 (c), 0.10 (d), 0.11 (e), and 0.12 (f). Vertical arrows indicate the temperatures at which the transitions occur obtained from Figure 6. The symbols A, B, and C represent liquid crystal, biphasic, or isotropic region, respectively.

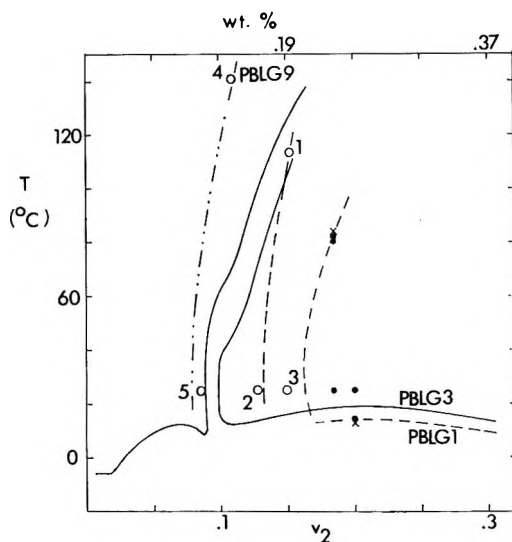


Figure 8. Effect of molecular weight on phase boundaries. Classification of nmr spectra (●, ×) as in Figure 5. Microscopic results (○) indicate a phase boundary (1, 4), an isotropic region (2), or a biphasic region (3,5). Points 1-3 and nmr data are for PBLG1, points 4 and 5 are for PBLG9.

portions of the phase diagram were determined only through the use of nuclear magnetic resonance measurements. Figure 4 illustrated the reversibility of the spectrum when the temperature was cycled through a suspected phase transition. This was typical of all above room temperature transition points. The reversibility across the 10–20° transition ($v_2 > 0.1$) differed slightly. When the temperature was lowered across the transition the dipolar split nmr spectrum collapsed. If the temperature was increased to a degree above the transition, it was exceedingly difficult to get the spectrum to split again. However, increasing the tempera-

ture 2–5° above the transition resulted in splitting, which persisted as before down to the phase equilibrium temperature. Inasmuch as most of these solutions at temperatures near the transition temperatures have very high viscosities (see Figure 7) which rapidly decrease as one goes across the phase boundary, a kinetic effect appears to be a reasonable interpretation of this hysteresis phenomenon.

Occasionally a spectrum near a phase transition was observed to be intermediate between Figures 3A and 3B (+ in Figure 5). We interpret this to mean that magnetic field orientation of the liquid crystal can take place if a small amount of isotropic phase is present. Although this puts some ambiguity into the phase boundary, most of the nmr studies locate the boundary to within $\pm 1^\circ$.

An additional systematic error may result in that the presence of the magnetic field may alter the transition temperature. In the concentration region $v_2 > 0.1$ there is a lower as well as an upper temperature bound on the stability of the liquid crystal phase. The low temperature boundary between 10 and 20° is controlled primarily by favorable polymer-polymer interaction, which decreases as the temperature increases. Any magnetic field effects would raise the transition temperature of the lower boundary, while lowering the upper boundary. Although the interaction with the magnetic field is weak and hopefully unimportant, it is difficult to estimate. However, there is one observation which indicates that the effect is negligible. At room temperature the polymer concentration necessary to produce a biphasic system is the same whether determined by nmr or by the polarizing microscope.

In the liquid crystal phase the cholesteric screw axis, perpendicular to the polymer helix axis, is not oriented in the same direction in all parts of the system. Consequently when placed between polars no setting of the polars will extinguish light transmission from all parts of the system, in contrast to the isotropic phase. This is the basis for determining the equilibrium line bounding the isotropic phase. The optical rotation in the liquid crystal phase is wavelength dependent. White light was used to illuminate the microscope. The pitch of the screw axis is a function of both polymer composition and temperature, becoming greater as the polymer concentration is lowered or the temperature increased. It is possible that under some conditions the optical rotation may become too small to be observed in the light microscope with the wavelengths employed, thus rendering the microscope technique unsuitable for cholesteric phase determination.

If certain compositions of the cholesteric phase are unobservable, the line bounding the isotropic phase in Figure 6 may be in error. Above 10° the liquid crystal phase in equilibrium with the isotropic phase is 11–18 vol % polymer. It is easy to prepare liquid crystals of this composition and to determine their optical

properties. As we know they can be observed in the polarizing microscope, this portion of the isotropic boundary should not be in error. In the biphasic region when the overall polymer composition is less than 9 vol % the isotropic phase is in equilibrium with a liquid crystal phase of unknown composition and structure, though presumably very rich in polymer. As we do not know the composition of the liquid crystals which may be unobservable, this low concentration portion of the phase boundary may be somewhat in error.

The viscosity data have been presented here as a technique for phase boundary determination. The use of viscosity for determining the concentration of the isotropic to biphasic boundary has been reported.^{13,21} In the isotropic region, irrespective of concentration, the normal exponential decrease in viscosity with inverse temperature is observed over most of the temperature range. When the polymer concentration is less than 0.09 the solutions gel at a temperature above the phase boundary temperature determined by the microscope technique. This gel has been observed previously by more qualitative measures.¹⁴ It appears in Figure 7 as a very rapid rise in viscosity. Its structure is unknown.

If the polymer concentration is greater than 0.09 the temperature coefficient of the viscosity is very complex. In the high-temperature region the isotropic-biphasic transition temperatures in Figure 6 correlate well with change of sign in the viscosity temperature coefficient in Figure 7. At low temperatures a gel is formed. Whether it occurs above or below the nmr determined phase boundary depends on the concentration. As the temperature is raised above the gel point the viscosity initially decreases and eventually reverses itself and rapidly increases. At the temperature of the upper liquid crystal phase boundary there is a perceptible increase in the viscosity temperature coefficient, thus correlating the two methods. The remaining features of the viscosity-temperature-composition curves are of little importance to the phase diagram.

In summary we believe the phase diagram to be reliable except for the region $v_2 < 0.09$.

Comparison of Experimental Results with Theory. Phase diagrams calculated from Flory's equations⁶ are shown in Figure 9 for three axial ratios (x). Axial ratios of 50, 150, and 450 correspond approximately to the three molecular weights studied. The shapes of the equilibrium lines differ somewhat from those originally calculated. This is probably a result of more precise numerical methods available today. A zero or negative χ leads to a narrow biphasic region. A positive χ corresponds to a positive excess free energy of mixing. As a consequence of the large number of polymer segment-segment contacts upon alignment, a slightly positive heat of mixing widens the biphasic

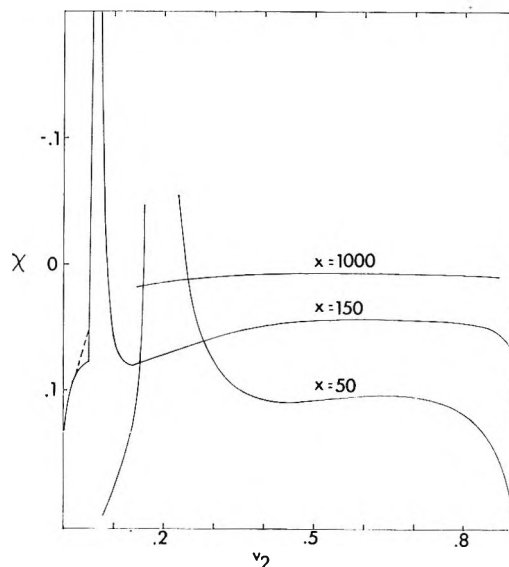


Figure 9. Flory phase diagram as a function of axial ratio x . Only high concentration end of $x = 1000$ diagram shown. In the $x = 150$ diagram dashed portion results from assuming equilibrium degree of disorientation as unity.

region to such an extent that the ordered phase is very rich in polymer while the isotropic phase is very rich in solvent. Inasmuch as χ may contain entropic as well as enthalpic contributions a positive χ cannot be formally identified with a positive heat of mixing. To the right of the narrow biphasic region the phase boundary goes through a maximum, and hence the liquid crystal phase has a critical solution temperature. In the case of infinite molecular weight the critical solution temperature corresponds to $x = 0$.

Comparison of Figure 6 with the $x = 150$ phase diagram in Figure 9 shows a large number of similarities, and some discrepancies. From previous studies¹⁴ we know that the osmotic second virial coefficient has a positive temperature dependence, and becomes negative below *ca.* 22°. Thus χ varies inversely with temperature. To the right of the narrow biphasic region the phase boundary goes through a maximum, but at a lower polymer concentration than the theoretical one. We find a liquid crystal upper critical solution temperature of *ca.* 18°. Slightly below this temperature the system should split into two liquid crystal phases. We made no attempt to observe this directly. In order for the isotropic-liquid crystal biphasic region to exhibit a critical point the amount of disorder in the liquid crystal phase must approach the disorder in the isotropic phase.²² We find no experimental evidence for such a critical point. In the temperature region 15-35° the experimental phase diagram is similar to the Flory diagram in the $\chi \approx 0$ region. The experimental miscibility gap is slightly narrower and occurs

(21) J. Hermans, Jr., *J. Colloid Sci.*, **17**, 638 (1962).

(22) L. Landau and E. Lifshitz, "Statistical Physics," Addison-Wesley, 1958.

at a slightly higher polymer composition. The major deviations from the Flory diagram occur at the higher temperatures. From 40 to 140° the miscibility gap becomes slightly greater and the equilibrium concentrations increase approximately 50%. The Flory theory of impenetrable, rigid rods is incapable of predicting this effect.

Comparison of Figures 8 and 9 indicates that the general features of the molecular weight dependence of the Flory theory are observed. Lowering the molecular weight widens the liquid crystal-isotropic miscibility gap and shifts it to higher polymer concentrations. The liquid crystal critical solution temperature is lowered. As only a few points were taken, detailed features of the phase diagram are unknown.

The Flory-Huggins lattice theory for random coil polymers predicts the correct molecular weight dependence of the critical temperature if the χ parameter is taken to be a linear function of inverse temperature. The critical concentrations and the shape of the phase boundary correspond only semiquantitatively to the experimental results.

If by analogy we assume a linear relation of χ with $1/T$, and that the lattice treatment gives the correct molecular weight dependence of the liquid crystal critical temperature, a χ - T scale can be estimated from the approximately 5° lowering of the critical solution temperature in going from PBLG3 to PBLG1. The scale so determined, $\chi = -3.51 + 1035/T$, yields a χ value of 0 at 22°, 0.28 at 0°, and -1.0 at +140°. Osmotic pressure studies on the dilute isotropic phase indicated somewhat larger values of χ around room temperature.¹⁴ The existence of an upper critical

solution temperature requires a positive heat of mixing. Appropriate differentiation of the approximate χ - T relationship indicates a positive entropy contribution as well. This indicates that the Flory treatment of the ordered phase for impenetrable rods underestimates the entropy of mixing. This underestimation has been suggested previously from solvent activity measurements at high polymer concentrations in other solvent systems.¹²

The existence of a truly athermal phase transition is of considerable theoretical interest. All theories which predict an athermal transition are approximate. If we take χ to be of the form $a + b/T$, with a and b as given above, the enthalpy of mixing is positive and temperature invariant. As we do not know the true relationship between χ and T , we cannot establish from this work whether or not the athermal transition exists.

The other theoretical model applicable to concentrated solutions, thermal as well as athermal, is that of Cotter and Martire,¹⁰ based on a quasichemical treatment of a face-centered cubic lattice system. Inasmuch as their primary interest was in a one component small molecule liquid crystal, they did not consider biphasic equilibria nor large values of the axial ratio. In order to calculate the phase diagram four binary interaction terms must be specified, in contrast to the one parameter (χ) theory of Flory. Because of the large number of parameters which must be arbitrarily specified, we have not attempted to calculate a phase diagram. It is possible that the portion of the experimental phase diagram not in agreement with the Flory treatment may be fitted by their equations.

Thermodynamics of cis-trans Isomerizations. II. The

1-Chloro-2-fluoroethylenes, 1,2-Difluorocyclopropanes, and Related Molecules¹

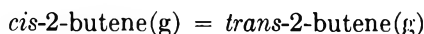
by Norman C. Craig,* Lawrence G. Piper, and Vicki L. Wheeler

Department of Chemistry, Oberlin College, Oberlin, Ohio 44074 (Received January 4, 1971)

Publication costs assisted by the Petroleum Research Fund

For the cis-to-trans reaction of 1-chloro-2-fluoroethylene the equilibrium constant over the temperature range 475–760°K is given by $\log K = -171.0^\circ\text{K}/T + 0.0462$. As a consequence $\Delta H^\circ_{615} = 780 \pm 20$ cal/mol and $\Delta S^\circ_{615} = 0.21 \pm 0.04$ cal/deg-mol. For the cis-to-trans reaction of 1,2-dichloroethylene $K = 0.645 \pm 0.013$ at 562°K. This gas chromatographically derived value confirms previous dielectric constant measurements. Critically evaluated electronic energy differences for a series of cis-trans isomerizations in the gas phase are: N_2F_2 , 3050 ± 400 ; $\text{C}_2\text{F}_2\text{H}_2$, 1080 ± 120 ; C_2ClFH_2 , 870 ± 110 ; $\text{C}_2\text{Cl}_2\text{H}_2$, 720 ± 160 ; $\text{C}_2\text{Br}_2\text{H}_2$, 250 ± 330 ; and $\text{C}_2\text{F}_2\text{ClH}$, 80 ± 230 cal/mol. In each case the cis isomer has the lower energy. This cis effect is rationalized in terms of "nonbonded" forces. The synthesis of the cis and trans isomers of 1,2-difluorocyclopropane is described. A preliminary value for the equilibrium constant for the cis-to-trans isomerization of these isomers is 11.7 ± 0.5 at 585°K, from which it appears that the trans isomer has the lower energy. This result is remarkable in view of $H^\circ_{\text{gauche}} - H^\circ_{\text{trans}} = 0$ for 1,2-difluoroethane as well as the low energy of cis- $\text{C}_2\text{F}_2\text{H}_2$.

In the 1930's Kistiakowsky and his coworkers at Harvard made a series of precise measurements of enthalpies of hydrogenation from which accurate resonance energies and energies of isomerization were derived. In particular, for the reaction



they found that the energy change at 355°K was -950 ± 120 cal/mol.² Subsequent application of this method to more elaborately substituted ethylenes has given values for isomerization energies which include -940 cal/mol for $\text{MeHC}=\text{CH}(i\text{-Pr})$,^{3a} -4220 for $\text{EtOCHC}=\text{CHCOEt}$,^{3b} -5700 for $\text{PhHC}=\text{CHPh}$,^{3b} and -9370 for $(\text{tert-Bu})\text{HC}=\text{CH}(\text{tert-Bu})$.^{3a} The presently available spectroscopic and thermodynamic data are, however, insufficient to permit separation of the electronic energy contribution in ΔE° from the contributions due to other degrees of freedom of the molecules. Nonetheless, it seems likely that the nonelectronic contributions nearly cancel out (*vide infra*), and thus the trans configuration has the lower electronic energy. These electronic energy differences for isomeric ethylenes are a part of the experimental basis for the concept of steric crowding, which is apparently important even in the case of 2-butenes.⁴

In contrast to the foregoing examples, a growing body of experimental data on haloethylenes (and a diazene) strongly suggests that cis isomers can have the lower electronic energy. Reasonably well established gas-phase examples of this effect include the 1,2-dichloroethylenes,⁵ the 1,2-difluoroethylenes,^{1,6} and the 1,2-difluorodiazenes.⁷ Fragmentary data exist for many others.^{6,8} In mixed dihaloethylenes the preference (free energy) for the cis configuration is sustained

throughout the series C_2FCIH_2 to C_2FIH_2 .^{6,8a,b} Enthalpy differences ranging from 700 to 3000 cal/mol are found in fluorine- and chlorine-substituted species. Haloethylenes are sufficiently simple that complete spectroscopic data may be confidently sought and employed to isolate the electronic energy change. In addition to giving experimental results from the isomerization equilibrium of the 1-chloro-2-fluoroethylenes and, secondarily, confirmatory data for the 1,2-dichloroethylenes, the main purpose of the present paper is to provide a thorough analysis for the whole series of halogenated ethylenes (and a diazene) for which reasonably complete data are now available.

(1) Part I: N. C. Craig and E. A. Entemann, *J. Amer. Chem. Soc.*, **83**, 3047 (1961).

(2) G. B. Kistiakowsky, J. R. Ruhoff, H. A. Smith, and W. E. Vaughan, *ibid.*, **57**, 876 (1935). See also E. J. Prosen, F. W. Maron, and F. D. Rossini, *J. Res. Natl. Bur. Stand.*, **46**, 106 (1951), who obtained -750 ± 580 cal/mol from enthalpies of combustion.

(3) (a) R. B. Turner, D. E. Nettleton, and M. Perelman, *J. Amer. Chem. Soc.*, **80**, 1430 (1958); (b) R. B. Williams, *ibid.*, **64**, 1395 (1942); (c) for values for other ethylenes see E. L. Eliel, "Stereochemistry of Carbon Compounds," McGraw-Hill, New York, N. Y., 1962.

(4) W. G. Dauben and K. S. Pitzer in "Steric Effects in Organic Chemistry," M. Newman, Ed., Wiley, New York, N. Y., 1956.

(5) (a) L. Ebert and R. Bull, *Z. Phys. Chem. Abt. A*, **152**, 451 (1931); (b) A. R. Olson and W. Maroney, *J. Amer. Chem. Soc.*, **56**, 1320 (1934); (c) R. E. Wood and D. P. Stevenson, *ibid.*, **63**, 1650 (1941).

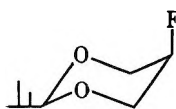
(6) H. G. Viehe, *Chem. Ber.*, **93**, 1697 (1960).

(7) (a) C. B. Colburn, F. A. Johnson, A. Kennedy, K. McCallum, L. C. Metzger, and C. O. Parker, *J. Amer. Chem. Soc.*, **81**, 6397 (1959); (b) G. T. Armstrong and S. Marantz, *J. Chem. Phys.*, **38**, 169 (1963).

(8) (a) H. Van der Walle, *Bull. Soc. Chim. Belges*, **47**, 217 (1938); (b) H. G. Viehe and E. Franchimont, *Chem. Ber.*, **96**, 3153 (1963); (c) H. G. Viehe, J. Dale, and E. Franchimont, *ibid.*, **97**, 244 (1964); (d) A. Demiel, *J. Org. Chem.*, **30**, 2121 (1965); (e) N. C. Craig and D. A. Evans, *J. Amer. Chem. Soc.*, **87**, 4223 (1965).

Preference (free energy) for the cis configuration is apparently not limited to halogenated ethylenes. It is also found in 1-halopropylenes⁶ with 1-chloropropylene⁹ and 1-bromopropylene¹⁰ being the best documented examples in the recent literature. For crotonitrile ($\text{CH}_3\text{HC}=\text{CHCN}$), Butler and McAlpine have obtained a positive enthalpy change for the cis-to-trans reaction from the temperature coefficient of the equilibrium constant.¹¹ These propylene examples have been rationalized in terms of polar attraction between CH and CX bonds with and without hyperconjugation. Such an explanation has also been given for the remarkably low barriers for CH_3 -group rotation in *cis*-1-fluoropropylene¹² and in *cis*-1-chloropropylene.¹³ A dipole attraction argument will not serve, however, to explain the effect in the symmetrically substituted haloethylenes.

There is evidence that the double bond is not required for an apparent net attraction to occur between two identical (or neighboring) halogen atoms.¹⁴ From vibrational spectroscopic studies Klaboe and Nielsen deduced a 0 ± 200 cal/mol energy difference between *gauche* and *trans* conformers of 1,2-difluoroethane near room temperature.¹⁵ Abraham and Parry have alluded to unpublished nmr observations¹⁶ that support the conclusions of Klaboe and Nielsen. El Bermani and Jonathan found only -200 ± 80 cal/mol for the *gauche*-to-*trans* conversion in 1-chloro-2-fluoroethane.¹⁷ These particular ethane cases are made all the more noteworthy by the failure of Abraham and Parry's empirical potential function to account for the rotameric energy differences. In contrast, their function which includes an ethane-like threefold barrier term, a pair of Buckingham-like van der Waals terms, and a dipole term, was moderately successful in accounting for conformational energy differences in many other halogenated ethanes.¹⁶ Yet, Dellepiane and Zerbi have recently shown that similar empirical potential functions for internal rotation give a poor account of the shape of the barrier for a number of experimentally well-developed cases.¹⁸ Nmr studies, supported by a partial vibrational assignment, also suggest that 1,2-dimethoxyethane is another example in which the *gauche* configuration is of lower energy than the *trans*.^{19,20} Further evidence for a *cis* preference in the absence of a double bond comes from the studies by Eliel and Kaloustian of the equilibrium for the *cis*-*trans* isomerization of 5-substituted 2-isopropyl-1,3-dioxanes such as



for which $\Delta G^\circ_{298} = 830$ cal/mol for the *cis*-to-*trans* conversion in benzene.²¹

It has seemed to us that a thorough investigation of the 1,2-difluorocyclopropanes, which are spectroscopi-

cally manageable and configurationally well defined, would clarify the importance of the double bond in the *cis* effect. Models show that the FF distance in the *cis* and *trans* isomers of these cyclopropanes should be within 0.1 Å of the corresponding distances in the 1,2-difluoroethylenes and 1,2-difluoroethanes. Preliminary results of the cyclopropane study are reported in this paper.

Experimental Section

1-Chloro-2-fluoroethylenes. The preparation and characterization of the *cis* and *trans* isomers of C_2FCIH_2 have been described before.²² As in the earlier study of the $\text{C}_2\text{F}_2\text{H}_2$ isomerization equilibrium,¹ gas chromatography was employed to analyze the equilibrium mixtures of the iodine-catalyzed, gas-phase isomerization. Samples were handled on a vacuum system as described before, but the oven was improved. A Bayley Instrument Co. (Model 117) controller was installed with its resistance element in the aluminum cylinder which enclosed the reaction cell, and three chromel-alumel thermocouples were positioned in and around the cell to check for temperature uniformity. At most the temperature varied about 1° over the cell volume. At each temperature equilibrium was approached from both the *cis*-rich and *trans*-rich sides. Gas chromatographic analyses were performed at 65° on a 4-m column packed with dibutyl phthalate on firebrick. Peaks representing the two isomers were well separated and had near-Gaussian shapes. Areas of the peaks were calculated by the triangle approximation after initial planimeter measurements gave the same results for ratios of areas within experimental error. Measurements on prepared mixtures showed that no correction was needed to observe *trans*/*cis* ratios within 0.5%. In most cases samples were equilibrated for several days and showed little evidence of volatile side products and only slow pressure decreases due to polymerization.

(9) J. W. Crump, *J. Org. Chem.*, **28**, 953 (1963).

(10) (a) K. E. Harwell and L. F. Hatch, *J. Amer. Chem. Soc.*, **77**, 1682 (1955); (b) P. S. Skell and R. G. Allen, *ibid.*, **80**, 5997 (1958).

(11) J. N. Butler and R. D. McAlpine, *Can. J. Chem.*, **41**, 2487 (1963).

(12) R. A. Beaudet and E. B. Wilson, Jr., *J. Chem. Phys.*, **37**, 1133 (1962).

(13) (a) R. A. Beaudet, *ibid.*, **40**, 2705 (1964); (b) V. W. Weiss, P. Beak, and W. H. Flygare, *ibid.*, **46**, 981 (1967).

(14) R. G. Ford and R. D. Beaudet, *ibid.*, **48**, 1352 (1968); **48**, 4671 (1968).

(15) P. Klaboe and J. R. Nielsen, *J. Chem. Phys.*, **33**, 1764 (1960).

(16) R. J. Abraham and K. Parry, *J. Chem. Soc. B*, 539 (1970).

(17) M. F. El Bermani and N. Jonathan, *J. Chem. Phys.*, **49**, 340 (1968).

(18) G. Dellepiane and G. Zerbi, *J. Mol. Spectrosc.*, **24**, 62 (1967).

(19) T. M. Connor and K. A. McLauchlan, *J. Phys. Chem.*, **69**, 1888 (1965).

(20) R. G. Snyder and G. Zerbi, *Spectrochim. Acta*, **23A**, 391 (1967).

(21) E. L. Eliel and M. K. Kaloustian, *Chem. Commun.*, 290 (1970).

(22) N. C. Craig, Y.-S. Lo, L. G. Piper, and J. C. Wheeler, *J. Phys. Chem.*, **74**, 1712 (1970).

Pressures in the reaction vessel ranged from 100 to 300 Torr.

1,2-Dichloroethylenes. Samples of Aldrich Chemical Co. *cis*-C₂Cl₂H₂ and *trans*-C₂Cl₂H₂ were used without further purification other than degassing and vacuum distillation. The equilibrium study at 288° followed the same procedure as for the 1-chloro-2-fluoroethylenes. For the gas chromatographic analyses a 4-m column packed with silicone oil on firebrick was used at 90°. Sketching was employed to untangle the small region of overlap between the two peaks, and areas were measured with a planimeter. Side reactions were not extensive.

1,2-Difluorocyclopropanes. *cis*- and *trans*-1,2-difluorocyclopropane were prepared by a photolytic reaction between diazomethane²³ and 1,2-difluoroethylene (source, Peninsular Chem Research Co.). Photolysis of approximately 1:1 mixtures of diazomethane and olefin in the liquid phase at -80° gave a yield of cyclopropanes of about 20%.²⁴ The vented reaction tube was immersed in an ethanol-Dry Ice mixture in an un-silvered Pyrex dewar flask and irradiated from the outside with light from a medium pressure mercury arc. Pure samples of *cis* and *trans* isomers were obtained by gas chromatographic fractionation on a 4-m column packed with tricresyl phosphate on firebrick. After the *trans* isomer (bp ~11°) was eluted at room temperature, the column temperature was raised to 75° to hasten the elution of the *cis* isomer (bp ~46°). Identities of the isomers were established by means of vapor densities, proton nmr, and infrared spectra.²⁵ The exploratory isomerization studies were carried out in a tube furnace with temperature control of ±5°. Both *cis*-rich and *trans*-rich samples were equilibrated. At temperatures below 300° the reaction was too slow even with iodine catalysis. Above 340° side reactions were overwhelming. Relatively large amounts of iodine were used. Gas chromatographic analyses were done at a constant temperature of 57° on the tricresyl phosphate column.

Statistical Thermodynamic Calculations. Calculations based on the rigid-rotor, harmonic oscillator model²⁶ were performed with program STATHEM on an IBM 360/44 computer. Input consisted of Cartesian coordinates and masses for atoms, vibrational fundamentals, and rotational symmetry numbers. Output included principal moments of inertia as well as tables of thermodynamic functions from 100 to 2000°K in 100° intervals. Tables of output data are on file.

Results

For the reaction

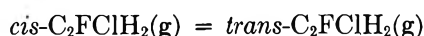


Table I summarizes the equilibrium constant measurements and Figure 1 shows the temperature dependence of log *K* over the 280° range. A least-squares fit gives

$$\log K = (-171.0 \pm 4.9^\circ\text{K})/T + (0.0462 \pm 0.0083)$$

from which $\Delta E^\circ_{620} = 780 \pm 20$ cal/mol and $\Delta S^\circ_{620} = 0.21 \pm 0.04$ cal/deg-mol. Figure 1 also includes two "ungefährer" values of the equilibrium constant reported by Viehe.⁶ They were not used in the least-squares analysis. A rigid-rotor, harmonic-oscillator treatment of the spectroscopic data gives $\Delta S^\circ_{620} = 0.24 \pm 0.2$ cal/deg-mol, $\Delta E^\circ_{620} = 185 \pm 20$ cal/mol, and $\Delta E_{zp} = -270 \pm 70$ cal/mol.^{22,27} As a consequence $\Delta E_e = \Delta E^\circ_{620} - \Delta E^\circ_{620} - \Delta E_{zp} = 860 \pm 110$ cal/mol. The excellent agreement between the entropy change derived from the equilibrium constant measurements and the entropy change calculated from the spectroscopic data is reassuring. The ±0.2 uncertainty in the calculated ΔS° is due primarily to the estimated uncertainties in the assignments of the vibrational fundamentals.

Table I: Observed Equilibrium Constants for the Reaction $cis\text{-C}_2\text{FCIH}_2(\text{g}) = trans\text{-C}_2\text{FCIH}_2(\text{g})$

Temp. °K	—Number of analyses ^a —		Equilibrium constant ^b
	<i>cis</i> - rich	<i>trans</i> - rich	
474	1		0.485
		3	0.485 ± 0
540	4		0.536 ± 0.003
		4	0.549 ± 0.002
		5	0.527 ± 0.003
554		3	0.533 ± 0.005
	4		0.544 ± 0.011
615		5	0.558 ± 0.007
	5		0.587 ± 0.007
681		6	0.576 ± 0.007
	5		0.621 ± 0.007
756		3	0.630 ± 0.003
	5		0.661 ± 0.004
		2	0.669 ± 0.002

^a After mixture had apparently reached equilibrium. ^b With average difference from the average. All 55 values of the equilibrium constant were used in the least-squares analysis.

(23) W. von E. Doering and W. R. Roth, *Tetrahedron*, **19**, 715 (1963). *N*-Methyl nitrosourea was obtained from Columbia Organic Chemical Co.

(24) This methylene reaction was not stereospecific. No reaction was observed in repeated attempts to photolyze ketene-difluoroethylene mixtures in the liquid phase at -80°. Gas-phase photolysis of the ketene-ethylene mixtures gave complex product mixtures and low yields of the difluorocyclopropanes.

(25) Paper II4, 23rd Symposium on Molecular Structure and Spectroscopy, Columbus, Ohio, September 1968. Principal gas-phase ir bands, *cis*-c-C₃F₂H₄: 3103B, 3063C, 1449B, 1346A, 1225B, 1150A, 1136C, 1060A, 1047C, 860B, 785B, 739A, 621A, 468C, 318A, ~210 cm⁻¹; *trans*-c-C₃F₂H₄: 3110C, 3070A, 1457 distorted B?, 1304A, 1159A, 1072A, 1003C, 961B, 842B, 782A, 452A, 414B, ~300 twc bands overlapped.

(26) G. N. Lewis and M. Randall, revised by K. S. Pitzer and L. Brewer, "Thermodynamics," 2nd ed, McGraw-Hill, New York, N. Y., 1961, Chapter 27.

(27) θ = thermal energy; zp = zero point vibrational energy; and e = electronic energy.

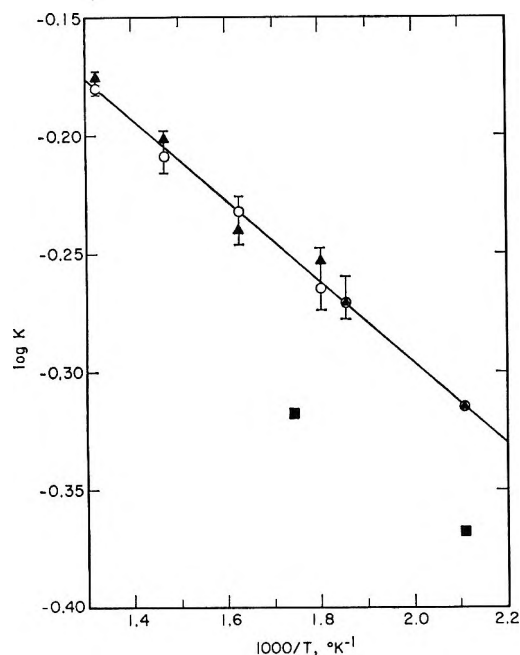
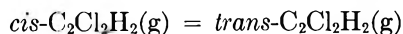


Figure 1. Temperature dependence of the equilibrium constant for the cis-trans isomerization of C_2ClFH_2 . Viehe (ref 6) ■, this research: cis-rich, ○; trans-rich, ▲. Line is from least-squares analysis.

Figure 2 is a composite of all of the published values for the equilibrium constant for the reaction



Our single equilibrium constant measurement, $K = 0.645 \pm 0.013$ at $562 \pm 1^\circ K$, is also included. The agreement of this gas chromatographically derived value with the ones based on dielectric constant measurements decreases the possibility that the latter method was confounded by side reactions (*vide infra*). All of the published values save the one of Ebert and Büll^{5a} were obtained from dielectric constant measurements. The line in Figure 2 was drawn by eye. In drawing this line the single value of Ebert and Büll, based on boiling point measurements, was disregarded as were the two high temperature measurements of Maroney.²⁸ Side reactions were probably significant at these high temperatures. Nonetheless, the line fits the two high temperature values reasonably well. The equation for this line is

$$\log K = (-141^\circ K)/T + 0.066$$

from which $\Delta E^\circ_{540} = 650 \pm 70$ cal/mol and $\Delta S^\circ_{540} = 0.30 \pm 0.20$ cal/deg-mol. The upper limits on these values are based on the line which fits the data of Wood and Stevenson alone.^{5c}

From the published spectroscopic data we calculate $\Delta S^\circ_{540} = 80.40 - 80.05 = 0.35 \pm 0.2$ cal/deg-mol, $\Delta E^\circ_{6540} = 8010 - 7800 = 210 \pm 20$ cal/mol, $\Delta E_{zp} = 20500 - 20775 = -275 \pm 80$ cal/mol. Consequently, ΔE_e is 720 ± 160 cal/mol. The small differences be-

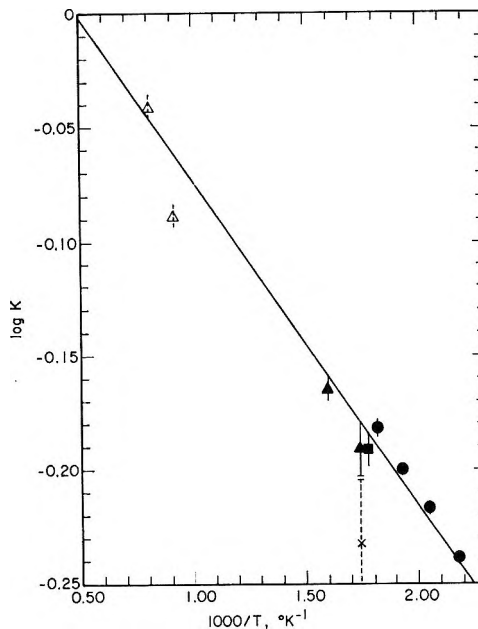


Figure 2. Temperature dependence of the equilibrium constant for the cis-trans isomerization of $C_2Cl_2H_2$: ●, Wood and Stevenson (ref 5c); ▲, Olson and Maroney (ref 5b); △, Maroney (ref 28); ×, Ebert and Büll (ref 5a); ■, this research.

tween these statistical thermodynamic quantities and those given by Pitzer and Hollenberg²⁹ are due to the use of the updated vibrational assignment of Hopper³⁰ and the geometric parameters preferred by Bernstein and Ramsay.³¹

The present value of 650 cal/mol for ΔE°_{540} is consistent with the value of $\Delta E^\circ_{300} = 200 \pm 500$ cal/mol obtained from the enthalpy of combustion of $C_2Cl_2H_2$ isomers in the liquid phase^{32a} and the enthalpies of vaporization.^{32b} Compared with the present value of $\Delta E^\circ_0 = 440$ cal/mol, values of 530 and 500 were calculated from Wood and Stevenson equilibrium constant data alone^{5c,31} and a value of 445 was calculated from the combined lower temperature data.²⁹

Statistical thermodynamic calculations were also carried out for cis- and trans- N_2F_2 . The vibrational fundamentals were from King and Overend's assignment^{33a} augmented with gas-phase Raman bands for the

(28) W. Maroney, *J. Amer. Chem. Soc.*, **57**, 2397 (1935).

(29) K. S. Pitzer and J. L. Hollenberg, *ibid.*, **76**, 1493 (1954).

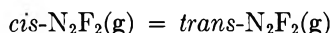
(30) M. Hopper, Ph.D. Thesis, University of Minnesota, 1967. For *cis*- $C_2Cl_2H_2$: (*a*₁) 3077¹, 1587¹, 1183¹, 714¹, 173¹; (*a*₂) 876¹, 406¹; (*b*₁) 3087¹, 1303¹, 857¹, 571¹; (*b*₂) 697¹. For *trans*- $C_2Cl_2H_2$: (*a*_g) 3071¹, 1576¹, 1270¹, 844¹, 349¹; (*a*_v) 895, 226; (*b*_g) 758¹; (*b*_v) 3090, 1200, 817, 245 cm^{-1} . 1 = liquid-phase values; others for gas phase.

(31) H. J. Bernstein and D. A. Ramsay, *J. Chem. Phys.*, **17**, 556 (1949).

(32) (a) L. Smith, L. Bjellerup, S. Krook, and H. Westermark, *Acta Chem. Scand.*, **7**, 65 (1953); (b) J. A. A. Ketelaar, P. F. Van Velden, and P. Zahm, *Recl. Trav. Chim. Pays-Bas*, **66**, 731 (1947).

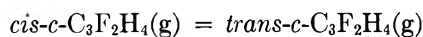
(33) (a) S.-T. King and J. Overend, *Spectrochim. Acta*, **23A**, 61 (1967); (b) J. Shamir and H. H. Hyman, *ibid.*, **23A**, 1191 (1967); *cis*- N_2F_2 : (*a*₁) 1525, 896, 341; (*a*₂) ~550; (*b*₁) 952, 737; *trans*- N_2F_2 : (*a*_g) 1523, 1018, 603; (*a*_v) 364; (*b*_v) 990, 423 cm^{-1} . All except the ~550 cm^{-1} band of the *cis* isomer are for the gas phase.

trans isomer observed by Shamir and Hyman.^{33b} Separate geometric parameters used for the two isomers were those reported by Bohn and Bauer from an electron diffraction study.³⁴ Microwave measurements concur on the cis geometry,³⁵ and high resolution infrared measurements concur on the trans.³⁶ For use with $\Delta E^\circ_{298} = 3000 \pm 300$ cal/mol obtained by Armstrong and Marantz from enthalpies of reduction with ammonia,^{7b} $\Delta E^\circ_{\theta 298} = 2915 - 2850 = 65 \pm 40$ cal/mol, and $\Delta E_{zp} = 7030 - 7145 = -115 \pm 75$ cal/mol. Also $\Delta S^\circ_{298} = 62.60 - 61.85 = -0.25 \pm 0.2$ cal/deg-mol. The difference in electronic energy between the two isomers is 3050 ± 400 cal/mol. All of these thermodynamic quantities are for the reaction



Colburn and coworkers have reported several measurements of the cis-trans equilibrium at 558°K .^{7a} From the average equilibrium constant, $K = 0.152$, and calculated values of $\Delta S^\circ_{560} = -0.15$ cal/deg-mol and $\Delta H^\circ_{560} - \Delta H^\circ_{298} = 40$ cal/mol, one calculates $\Delta E^\circ_{298} = 1990$ cal/mol. Given the difficulty of making equilibrium measurements on this highly reactive system, this value appears to be in reasonable agreement with the thermochemical one.

For the iodine-catalyzed reaction



at $586 \pm 5^\circ\text{K}$, the equilibrium constant is 11.7 ± 0.5 , from which $\Delta G^\circ_{585} = -2900 \pm 200$ cal/mol. Although considerable infrared and Raman data are in hand, we do not yet have a complete assignment of the fundamentals for the two isomers. Therefore, for the present we assume $\Delta S^\circ_{585} \approx 0$ and $\Delta E_e \approx \Delta E^\circ_{585} \approx \Delta G^\circ_{585}$. In this cyclopropane case, the trans isomer has lower electronic energy. In view of the difficulties in observing equilibrium in this system we consider this result to be preliminary.

Discussion

Table II is a compilation of thermodynamic quantities for the cis-to-trans isomerization of haloethylenes (and difluorodiazene) for which rather complete spectroscopic and thermodynamic data are available. The quantity of particular interest, the difference in electronic energy of the two isomers, is given in the last column. In addition to the data for difluorodiazene, chlorofluoroethylene, and dichloroethylene which were presented in the Results section, Table II includes data for 1,2-difluoroethylene, 1,2-dibromoethylene, 1,2-diiodoethylene, and one trihaloethylene.

Pertinent thermodynamic quantities for the iodine-catalyzed isomerization of $\text{C}_2\text{F}_2\text{H}_2$ have been reported previously.^{1,37} A shock tube study of the rate of isomerization from both the cis and trans directions gives $\Delta E^\circ_{1200} = 2700 \pm 2400$ cal/mol³⁸ in general agree-

ment with the value derived from the temperature dependence of the equilibrium constant.

Two sets of measurements of the gas-phase, iodine-catalyzed isomerization of $\text{C}_2\text{Br}_2\text{H}_2$ have been reported.^{39,40} The 80° temperature range is too small to reveal a believable temperature dependence of the equilibrium constant. In choosing $K = 0.960 \pm 0.06$, for the cis-to-trans reaction we have placed somewhat greater weight on the more recent measurements, which are based on gas chromatographic analysis. Statistical thermodynamic values of $\Delta S^\circ_{475} = 0.58 \pm 0.3$ cal/deg-mol and $\Delta E^\circ_{\theta 475} = 220 \pm 40$ cal/mol⁴¹ have been used to extract ΔE°_{475} and ΔE_e from ΔG°_{475} . Dowling and coworkers gave $\Delta E_0^\circ = -100 \pm 160$ cal/mol (present value 90 ± 240) based on the dubious ΔE° calculated by Noyes and Dickinson.³⁹ In the liquid phase the polar, cis isomer is favored ($K = 0.59-0.67$ at $25-150^\circ$)^{5b} over the gas phase as expected.¹⁵

The published spectroscopic data for the diiodoethylenes do not permit meaningful statistical thermodynamic calculations. Although the assignment for the trans isomer⁴² appears to be sound, the assignment for the cis isomer is in doubt. The cis assignment is based on spectra measured on the eutectic mixture (20% trans, 80% cis).⁴³ A number of bands of the two isomers are overlapped. The standing assignment gives $\Sigma_i \nu_i(\text{cis}) < \Sigma_i \nu_i(\text{trans})$ in contrast to all of the other dihalo cases considered in this paper. Also two of the frequencies for *cis*- $\text{C}_2\text{I}_2\text{H}_2$ ($\nu_6 \approx 664$ and $\nu_7 = 176$ cm^{-1}) fall below values that would fit the group frequency pattern established by the other dihaloethylenes. In contrast, a similar group frequency comparison for the trans isomer is satisfactory.⁴²

Furuyama, Golden, and Benson have recently reported the equilibrium constant ($K = 1.69 \pm 0.13$) for the gas phase isomerization (inherently iodine catalyzed) and have found no significant temperature dependence over a 140° range.⁴⁴ They give $\Delta E^\circ_{590} =$

(34) R. K. Bohn and S. H. Bauer, *Inorg. Chem.*, **6**, 369 (1967). Calculated moments of inertia were: *cis*- N_2F_2 : $I_a = 26.58$, $I_b = 64.04$, $I_c = 90.62$; *trans*- N_2F_2 : $I_a = 6.633$, $I_b = 109.80$, $I_c = 116.42$.

(35) R. L. Kuczkowski and E. B. Wilson, Jr., *J. Chem. Phys.*, **39**, 1030 (1963).

(36) S.-T. King and J. Overend, *Spectrochim. Acta*, **23A**, 2875 (1967).

(37) N. C. Craig and J. Overend, *J. Chem. Phys.*, **51**, 1127 (1969).

(38) P. M. Jeffers and W. Shaub, *J. Amer. Chem. Soc.*, **91**, 7706 (1969).

(39) R. M. Noyes and R. G. Dickinson, *ibid.*, **65**, 1427 (1943).

(40) Viehe and Franchimont (ref 8b) have shown an equilibrium is established between $\text{HBrC}=\text{CBrH}$, $\text{HBrC}=\text{CIH}$, and $\text{HIC}=\text{CIH}$, all of which were present in significant amounts in their system. We have not observed any such halogen exchange in the fluorochloroethylene systems.

(41) J. M. Dowling, R. G. Puranik, A. G. Meister, and S. I. Miller, *J. Chem. Phys.*, **26**, 233 (1957). Most of the frequencies used in the statistical thermodynamic calculations were liquid phase values.

(42) R. H. Krupp, E. A. Piotrowski, F. F. Cleveland, and S. I. Miller, *Develop. Appl. Spectrosc.*, **2**, 52 (1962).

(43) S. I. Miller, A. Weber, and F. F. Cleveland, *J. Chem. Phys.*, **23**, 44 (1955).

Table II: Thermodynamic Functions for *cis*-*trans* Isomerization of Haloethylenes
cis-HXC=CXH(g) = *trans*-HXC=CXH(g)

	Tem- perature, °K	$\Delta S^\circ_{\text{obsd.}}$ cal/deg-mol	$\Delta S^\circ_{\text{calcd}}$	$\Delta E^\circ_{\text{obsd.}}$ cal/mol	ΔE_0°	ΔE_{elect}
FN=NF	300		-0.25 ± 0.2	3000 ± 300	2930 ± 330	3050 ± 400
HFC=CFH (480-760)	620	0.14 ± 0.03	-0.01 ± 0.2	930 ± 20	780 ± 40	1080 ± 120
HFC=CClH (475-760)	615	0.21 ± 0.04	0.24 ± 0.2	780 ± 20	600 ± 40	870 ± 110
HClC=CClH (460-620)	540	0.30 ± 0.20	0.32 ± 0.2	650 ± 70	440 ± 90	720 ± 160
HBrC=CBrH (420-500)	475		0.58 ± 0.3	$(320 \pm 200)^a$	90 ± 240	250 ± 330
HIC=CIH (470-610)	540	1.1 ± 0.1		0 ± 200		
HFC=CFCl	590		-0.12 ± 0.3	$(10 \pm 180)^a$	30 ± 20	80 ± 230

^a Calculated from a single equilibrium and $\Delta S^\circ_{\text{calcd}}$. Literature citations are given in the text.

0 ± 200 cal/mol and $\Delta S^\circ_{590} = 1.1 \pm 0.1$ cal/deg-mol. It is disturbing, however, that equilibrations at 400–430°K in the liquid phase in decalin gave $\Delta E^\circ = -1550$ cal/mol.⁴³ However, this liquid phase value is a recalculated one. In the original report the eutectic mixture was mistaken for pure *cis*.⁴⁵ Further doubt is introduced by the fact that a 30° temperature range is insufficient to accurately determine a small ΔE° .

The thermodynamic values in Table II for the one trihaloethylene, 1,2-difluoro-1-chloroethylene, are from a previous paper.⁴⁶ Error estimates have been revised somewhat as a consequence of the present comparative analysis.

Although much of the evidence for the *cis* effect depends on small differences between large numbers, the data in Table II, considered as a whole, provide rather strong support for the existence of this effect. The pattern of the entropy and energy values is reasonable, and, where checks on the entropy change from second-law and third-law treatments are possible, the agreement is good. Of course, contributions from second-order effects including anharmonicity, rotation-vibration interaction, Fermi resonance, and gas nonideality have been neglected in the statistical thermodynamic calculations. It is reasonable, however, to assume that these contributions tend to cancel out for molecules as similar as pairs of *cis*-*trans* isomers.

At first thought gas nonideality, particularly in the form of strong hydrogen bonding between pairs of *cis* isomers, is of greater concern. Qualitatively, dimerization of *cis* isomers (an exothermic process) could produce an apparent positive temperature coefficient for the overall *cis*-to-*trans* isomerization that could dominate a true negative temperature coefficient (exothermic) for the simple isomerization involving monomers. Evaluation of expressions for the competing equilibria with representative values for the overall temperature coefficient and *trans*/*cis* ratio showed that

the necessary degree of dimerization of the *cis* isomer would be unreasonably large. At room temperature the dimerization would be essentially complete. Yet, separate gas density measurements for the *cis* (and *trans*) isomers of $C_2F_2H_2$ gave molar weights within a few per cent of ideal gas values.¹ Also, enthalpies and entropies of vaporization are normal for both *cis*- and *trans*- $C_2Cl_2H_2$ ^{32b} and *cis*- and *trans*- $C_2F_2H_2$.⁴⁷

In every instance in Table II the observed, composite ΔE° reflects the difference in electronic energy rather well, as has been often assumed. Since $\Delta S^\circ \approx 0$, particularly for the fluoro systems, the approximation $\Delta E^\circ \approx \Delta G^\circ$ is useful.

At least one kind of nonthermodynamic evidence exists in support of the *cis* effect. It is the difference in torsional force constants for *cis*- and *trans*- $C_2F_2H_2$ ³⁷ and *cis*- and *trans*- $C_2Cl_2H_2$.²² In both cases the *cis* isomer has the larger force constant for incipient torsion around the double bond. The difference is well outside the uncertainty in these force constants as calculated by a normal coordinate analysis of complete hydrogen-deuterium isotopic sets. In contrast, the force constants for CH out-of-plane wagging are very nearly the same in each case. The larger torsional force constant for *cis* isomer presumably reflects some additional force holding this isomer in the planar configuration.

Though more supporting evidence would be desirable, the *cis* effect in haloethylenes now seems to be rather

(44) S. Furuyama, D. M. Golden, and S. W. Benson, *J. Phys. Chem.*, **72**, 3204 (1968). The *cis*-*trans* isomerization competes with the dehalogenation reaction, $HIC=CIH \rightarrow I_2 + CH \equiv CH$. In the bromoiodo system (ref 40) the equilibrium constant for the *cis*-*trans* isomerization of $C_2I_2H_2$ was found to be 2.13 (175°) and 2.07 (225°).

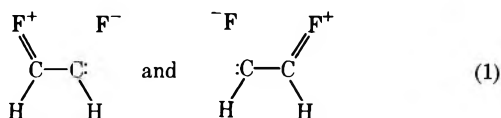
(45) R. M. Noyes, R. G. Dickinson, and V. Schomaker, *J. Amer. Chem. Soc.*, **67**, 1319 (1945).

(46) N. C. Craig, D. A. Evans, L. G. Piper, and V. L. Wheeler, *J. Phys. Chem.*, **74**, 4520 (1970).

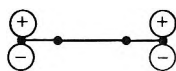
(47) From unpublished vapor pressure equations, for *cis*- $C_2F_2H_2$: $\Delta H^\circ = 5450$ and $\Delta S^\circ = 22.0$; for *trans*- $C_2F_2H_2$: $\Delta H^\circ = 4970$ cal/mol and $\Delta S^\circ = 22.6$ gibbs/mol.

well established in experiment. Rationalizations for it are, however, a much more uncertain matter. At first glance the 3000 cal difference in energy between the isomers of N_2F_2 (Table II) appears anomalously large compared with the 1100 cal difference for the isomers of $C_2F_2H_2$. However, in $C_2F_2H_2$ the repulsion energy between the CF bond dipoles is approximately 1400 cal greater in the cis isomer.⁴⁸ The corresponding difference in dipole-dipole repulsion in N_2F_2 must be considerably smaller since the cis isomer has a dipole moment of only 0.16 D.³⁵ Thus, for comparative purposes each for the electronic energy difference for a dihaloethylene pair in Table II should be increased from about 1400 to 400 cal, the latter being for $C_2I_2H_2$.¹⁶

At the present time no quantum mechanical calculations appear to be available that are sufficiently precise to corroborate the experimental evidence for the cis effect and to explain it. However, Pitzer and Hollenberg²⁹ and others have ascribed this effect to contributions from resonance structures of the type



More recently Hoffmann and Olofson⁴⁹ have argued for a preferred cis structure of electronically excited or anionic butadiene due to overlap of the p orbitals in the π HOMO



This molecular orbital argument applies to *cis*- $C_2F_2H_2$, which may be considered to have a six-electron π system if a nonbonded pair from each fluorine atom is involved. Both the valence bond and the MO arguments require double bond character in the CX bonds at the expense of the unshared pairs on each of the halogen atoms. The nuclear quadrupole coupling constants for chloroethylenes have been interpreted as indicating about 5% double bond character for CCl bonds.⁵⁰ The corresponding double bond character for *cis*- $C_2Cl_2H_2$ is not exceptional, however, and no data are available for *trans*- $C_2Cl_2H_2$. An apparent weakness in this electron delocalization explanation is the trend in the ΔE_e values in Table II. These ΔE_e values do not seem to decrease in proportion to the presumed weakening of the p-p overlap between carbon and larger halogen atoms. Steric repulsion of nonbonding electrons might also be expected to add to this rate of decrease in ΔE_e .¹⁶ However, these effects are offset to some extent by the previously cited decrease in the CX dipole-dipole repulsion. If the polar valence bond structures (1) were important, the cis effect would be marked in the mixed chlorofluoroethylenes. Yet, the electronic energy differences for the two chlorofluoro examples in Table II seem to fit a smooth trend between CFH=CFH and

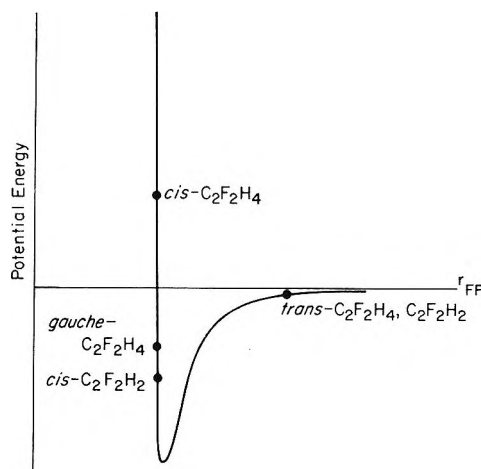


Figure 3. An approximation to the van der Waals intramolecular potential function for FF interaction. Estimated FF distances are shown for molecular structures of interest.

CClH=CClH. (The fragmentary data for CFH=CBrH and CFH=CIH suggest otherwise, however.^{6,8} Although the case for the electron delocalization interpretation of the cis effect is far from complete, it seems the most reasonable proposal for haloethylenes (and diazenes).⁵¹

The electron delocalization argument will not serve to explain the apparent cis effect in saturated compounds. Although $H^\circ_{\text{gauche}} - H^\circ_{\text{trans}} = 0$ for 1,2-difluoroethane, allowance for about 1000 kcal/mol greater CF dipole-dipole repulsion in the gauche conformer makes $\Delta H^\circ = 0$ more significant. It must be emphasized, however, that $\Delta H^\circ = 0$ for the $C_2F_2H_4$ conformers is tentative, and further, ΔE_e might yet prove to favor the trans form. However, on the basis of presently available data (see the Introduction for other examples) a nonbonded, van der Waals attraction between the halogen atoms may be important. van der Waals attractions based on potential energy parameters obtained from noble gases are too small to support this hypothesis,¹⁶ although it is possible that noble gas parameters are inadequate for bound halogen atoms. Thus, for 1,2-dihaloethanes containing fluorine Abraham and Parry's calculations were 0.5–1.0 kcal too low for the gauche-to-trans conversion. Figure 3 is a schematic representation of the location of various fluorocyclopropanes on a deepened $-F \cdots F-$ potential curve. Based on rotation barriers in various fluoroethanes¹⁶ it appears that the cis (eclipsed) form of $C_2F_2H_4$ falls in the repul-

(48) Estimated from a point charge model based on the geometry and dipole moment from the microwave study (ref 35). Neglect of moment for the CH bond favors the cis isomer.

(49) R. Hoffmann and R. A. Olofson, *J. Amer. Chem. Soc.*, **88**, 943 (1966).

(50) (a) J. H. Goldstein, *J. Chem. Phys.*, **24**, 106 (1956); (b) R. G. Stone and W. H. Flygare, *J. Mol. Spectrosc.*, **32**, 233 (1969).

(51) For 1-halopropylenes simple dipole-dipole attraction seems to be an adequate explanation as shown by Abraham and Parry's calculation for rotamers of 1-halopropanes (ref 16).

sive region. Of course, the steepness of the potential curve on the repulsive side implies that small differences in geometry would cause sizeable changes in the van der Waals interaction energy. Unfortunately, the fact that the rotation barrier in *cis*-1-fluoropropylene is little different from that for 1,1-difluoropropylene,^{13a} in which the apparent equilibrium HF distance is 0.05 Å longer, seems to contradict this explanation—if the $-H \dots F-$ van der Waals potential is anything like that for $-F \dots F-$. For *cis* haloethylenes both double bond induced and direct van der Waals attractions may be involved, since the FF distance in *cis*-1,2- $C_2F_2H_2$ ⁵² is close to that in *gauche*-1,2- $C_2F_2H_4$.

cis-1,2-Difluorocyclopropane with a predicted FF distance⁵³ close to that of *gauche*- $C_2F_2H_4$ might be expected to exhibit the single bond *cis* effect alone. However, our preliminary equilibrium constant value implies a remarkably low energy for the *trans* configuration. Of course, it is possible that the true FF distance in the *cis*-cyclopropane is sufficiently small to place it well up the repulsive side of the van der Waals potential. Such a shortened FF distance could possibly be related to diminished opportunity for steric relief in the cyclopropane, which should be reflected in a large HCF bending force constant. It is also possible that the difluorocyclopropane result is the only one permitting direct interpretation, in which case the true *cis* effect is

only to be found along with double bonds. In the near future we expect to have more critical vibrational and thermodynamic data on the difluorocyclopropanes. It is also hoped that the *trans* cyclopropane isomer has a sufficient dipole moment to make possible a detailed microwave investigation of it as well as the *cis* isomer.⁵⁴

Acknowledgments. This research was supported by the Petroleum Research Fund (Grant No. 2422B) and a grant from the A.S.T.M. Charles D. Jonah wrote program STATHERM. N. C. C. is grateful for the hospitality extended to him at the University of California, Berkeley, during tenure of an N.S.F. Science Faculty Fellowship (1970–1971).

(52) FF distance in *cis*- $C_2F_2H_2$ is 2.74 Å [V. W. Laurie and D. T. Pence, *J. Chem. Phys.*, **38**, 2693 (1963)]; in the corresponding *trans* isomer it is 3.56 Å. Based on the geometric parameters (ref 15): $r_{CF} = 1.37$, $r_{CC} = 1.54$ Å, $\angle CCF = 109.5^\circ$, and dihedral angle in *gauche* of 60° ; the FF distance in *cis*- $C_2F_2H_4$ is 2.45 Å, in *gauche*- $C_2F_2H_4$ is 2.77 Å, and in *trans*- $C_2F_2H_4$ is 3.56 Å.

(53) With $r_{CF} = 1.33$, $r_{CC} = 1.52$ Å, $\angle CCC = 60^\circ$, $\angle HCF = 118^\circ$, and $\angle CCF = 116.5^\circ$, the FF distance in *cis*- $C_2F_2H_4$ is 2.71 Å. See Hs. H. Günthard, R. C. Lord, and T. K. McCubbin, Jr., *J. Chem. Phys.*, **25**, 768 (1956), for cyclopropane geometric parameters.

(54) NOTE ADDED IN PROOF. D. Sianesi and R. Fontanelli, *Ann. Chim. (Rome)*, **55**, 850 (1965), have measured the bromine-catalyzed isomerization of 1*H*-pentafluoropropylene over the temperature range 300–550°. For the *cis*-to-*trans* reaction $\Delta H^\circ = 3.9$ kcal/mol (sign changed to conform to the data) and $\Delta S^\circ = 1.45$ cal/deg-mol.

Photoionization Mass Spectrometric Study of XeF₂, XeF₄, and XeF₆^{1a}

by J. Berkowitz,* W. A. Chupka, P. M. Guyon, J. H. Holloway,^{1b} and R. Spohr

Argonne National Laboratory, Argonne, Illinois 60439 (Received December 20, 1970)

Publication costs assisted by the U. S. Atomic Energy Commission

The process $\text{XeF}_2 + h\nu \rightarrow \text{Xe}^+ + \text{F}^- + \text{F}$ has been observed, and from its threshold the value $\Delta H_f^\circ(\text{XeF}_2) = -28.0 \pm 0.5$ kcal/mol has been derived. Subsequent studies of the thresholds for XeF_2^+ from XeF_4 and XeF_4^+ from XeF_6 then yield $\Delta H_f^\circ(\text{XeF}_4) = -57.6 \pm 2$ kcal/mol and $\Delta H_f^\circ(\text{XeF}_6) = -(90_{-3}^{+8})$ kcal/mol, respectively. The first ionization potentials of the compounds studied are: 12.35 ± 0.01 eV for XeF_2 , 12.65 ± 0.1 eV for XeF_4 , and 12.19 ± 0.02 eV for XeF_6 —all higher than that of atomic xenon and in good agreement with photoelectron spectroscopic values. The evidence presented indicates that the ground states of XeF_4^+ and XeF_6^+ have some asymmetric character. The ions XeF^+ , XeF_3^+ , and XeF_5^+ are found to be distinctly more stable to loss of a fluorine atom than are those containing an even number of fluorine atoms. The implications of these observations as regards the bonding in xenon-fluorine compounds are discussed. These studies give no evidence regarding the existence of low-lying excited states of XeF_6 ; more extensive experiments involving long equilibration times will be required to decide this question.

I. Introduction

The very existence of noble gas fluorides has presented an exciting challenge to theoretical chemists. A number of molecular calculations^{2a,b} have indeed been performed to explain the structure of these interesting chemical entities, but in order to test some of these calculations it is necessary to have more accurate data. For example, several independent experimental approaches³⁻⁵ aimed at determining the heats of formation of XeF_2 , XeF_4 , and XeF_6 have yielded significantly different results. The electron-impact mass spectrometric measurements⁶ are rather crude and cannot hope to achieve quantitatively conclusive numbers. A photoionization mass spectrometric study⁷ of XeF_2 was able to deduce a fairly accurate first ionization potential of XeF_2 , but little else. Recently, some photoelectron-spectroscopic investigations⁸ of XeF_2 , together with vacuum-ultraviolet absorption work,^{8,9} have provided additional information regarding the ionization potentials of XeF_2 which has helped to elucidate the present photoionization mass spectrometric study.

II. Apparatus

The basic design of the vacuum-ultraviolet monochromator and high-transmission mass spectrometer have been described in an earlier publication,¹⁰ as have subsequent improvements in the detection system.¹¹ The inlet system of the mass spectrometer was replaced by one made with stainless steel and Kel-F tubing and Monel valves. Before use, it was seasoned thoroughly, first with fluorine gas and then with the substance under investigation. The xenon fluorides were subsequently deposited, stored, and dispensed from Kel-F tubes fitted with Kel-F valves.

III. Sample Preparation

A. *Xenon Difluoride, XeF₂*. Xenon difluoride was prepared by reaction of a tenfold excess of xenon with fluoride in a nickel reactor, as described elsewhere.^{12,13} Traces of impurity were removed by discarding the vapor-pressure heads from the sample until the infrared spectrum attested to the purity of the residual difluoride.¹³ About 3% of the original sample was lost in the purification process.

B. *Xenon Tetrafluoride, XeF₄*. Xenon tetrafluoride was prepared by the reaction of xenon and fluoride in an atomic ratio of 1:5 at 400°. Xenon hexafluoride and xenon difluoride present in the product were dis-

(1) (a) Work performed under the auspices of the U. S. Atomic Energy Commission; (b) on leave from The Department of Chemistry, University of Aberdeen, Old Aberdeen, AB9 2UE, Scotland.

(2) (a) See, for example, "Noble-Gas Compounds," H. H. Hyman, Ed., University of Chicago Press, Chicago, Ill., 1963; (b) J. H. Holloway, "Noble-Gas Chemistry," Methuen & Co., Ltd., London, 1968, Chapter 8.

(3) L. Stein and P. L. Plurien, ref 2a, p 144.

(4) B. Weinstock, E. E. Weaver, and C. P. Knop, *Inorg. Chem.*, **5**, 2189 (1966).

(5) V. I. Pepekin, Yu. A. Lebedev, and A. Ya. Apin, *Zh. Fiz. Khim.*, **43**, 1564 (1969).

(6) H. J. Svec and G. D. Flesch, *Science*, **142**, 954 (1963).

(7) J. D. Morrison, A. J. C. Nicholson, and T. A. O'Donnell, *J. Chem. Phys.*, **49**, 959 (1968).

(8) (a) C. R. Brundle, M. B. Robin, and G. R. Jones, *ibid.*, **52**, 3383 (1970); (b) B. Brehm, M. Menzinger, and C. Zorn, *Can. J. Chem.*, **48**, 3193 (1970).

(9) J. Jortner, E. G. Wilson, and S. A. Rice, ref 2a, p 358.

(10) J. Berkowitz and W. A. Chupka, *J. Chem. Phys.*, **45**, 1287 (1966).

(11) W. A. Chupka and J. Berkowitz, *ibid.*, **47**, 2921 (1967).

(12) W. E. Falconer and W. A. Sunder, *J. Inorg. Nucl. Chem.*, **29**, 1380 (1967).

(13) F. Schreiner, G. M. McDonald, and C. L. Chernick, *J. Phys. Chem.*, **72**, 1162 (1968).

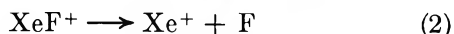
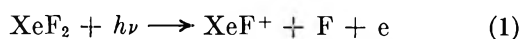
carded by the stepwise removal of the vapor above the reaction products. In this way the hexafluoride impurity was rapidly disposed of, but about 25% of the original sample had to be removed before infrared spectra indicated pure XeF_4 .

C. Xenon Hexafluoride, XeF_6 . Xenon and fluorine were mixed in a ratio of 1:20 and heated at a temperature of 300° and a total pressure of about 40 atm. The hexafluoride was purified from the other binary fluorides of xenon by taking advantage of the reversible reaction of xenon hexafluoride with sodium fluoride. The detailed purification procedures are described elsewhere.¹⁴⁻¹⁶ Final purification was effected by the stepwise removal of vapor above the reaction products until the infrared spectrum indicated a pure specimen.

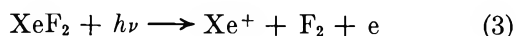
IV. Experimental Results

A. XeF_2 . A photoionization mass spectrum¹⁷ of this sample, taken at 800 \AA , is shown in Figure 1. This figure illustrates two advantages enjoyed in this experiment, when compared with the previous⁷ photoionization work. The earlier work was limited to the hydrogen lamp as a light source, and hence insufficient photon energy was available to explore the fragmentation reaction that yields Xe^+ as product. Secondly, it was found in the earlier work that all Xe^+ observed was attributable to chemical decomposition of the XeF_2 sample en route to the ionization chamber of the mass spectrometer; its characteristic autoionization spectrum clearly distinguished parent Xe^+ from fragment Xe^+ .

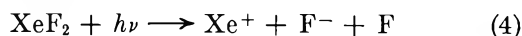
By contrast, the chemical decomposition occurring in our experiment was reduced to virtually undetectable proportions with the precautions described in section II. Hence, the Xe^+ intensity in Figure 1 is representative of fragment Xe^+ from XeF_2 . When the mass spectrometer was focused on the Xe^+ peak and the photon wavelength was scanned, a relatively intense threshold appeared at $\sim 800\text{--}810 \text{ \AA}$ ($\sim 15.3 \text{ eV}$), as seen in Figure 2. From the heretofore available bond energies of XeF_2 , this onset could be attributed to the stepwise fragmentation



rather than



A search for contributions from process 3 was not fruitful, but there was a weak residual Xe^+ intensity that persisted to longer wavelength. From its threshold and the subsequent analysis of a concomitant F^- peak, we were able to conclude that this weak Xe^+ intensity was attributable to the process



The wavelength dependence of this F^- intensity, ob-

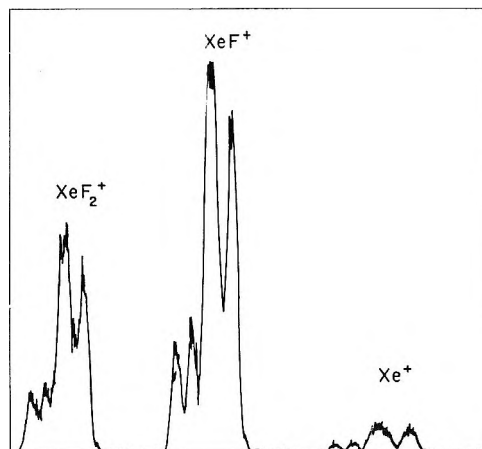


Figure 1. Photoionization mass spectrum of XeF_2 , taken at 800 \AA .

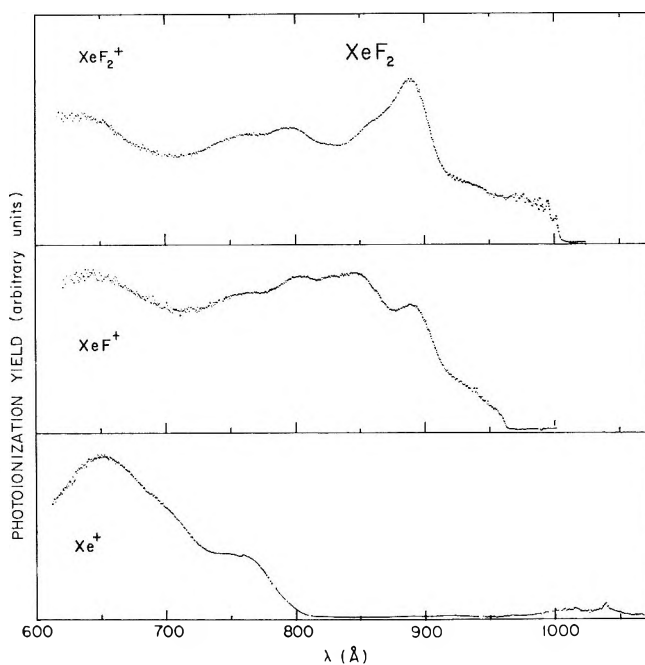


Figure 2. Photoionization efficiency curves of (a) XeF_2^+ , (b) XeF^+ , and (c) Xe^+ from XeF_2 , obtained at a resolution width of 0.4 \AA (FWHM).

tained with the hydrogen many-line pseudo-continuum as a light source, is shown in Figure 3.

The peaked structure of this F^- curve is immediately suggestive of a predissociation, rather than a direct

(14) I. Sheft, T. M. Spittler, and F. H. Martin, *Science*, **145**, 701 (1964).

(15) R. D. Peacock, H. Selig, and I. Sheft, *Proc. Chem. Soc. London*, 285 (1964).

(16) J. G. Malm, F. Schreiner, and D. W. Osborne, *Inorg. Nucl. Chem. Lett.*, **1**, 97 (1965).

(17) In this instance the Hopfield continuum of helium served as the light source and the photon resolution width (FWHM) was 0.8 \AA . The mass resolution could be significantly improved when necessary by narrowing the slits of the mass spectrometer, but for the present purposes it was more productive not to use high mass resolution, but rather to increase the signal strength in order to minimize the data-acquisition time.

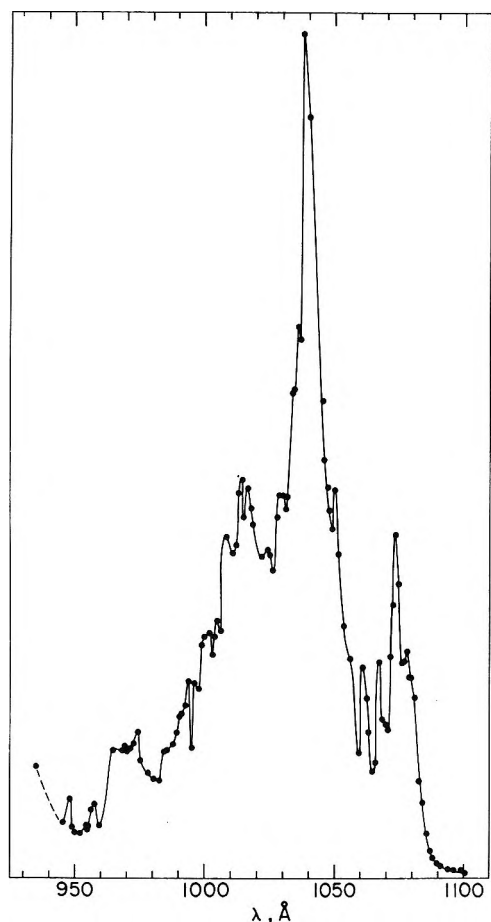


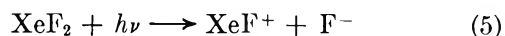
Figure 3. Wavelength dependence of the F⁻ intensity from the process XeF₂ + hν → Xe⁺ + F⁻ + F.

dissociative ionization process. Rather similar behavior was recently observed by us¹⁸ in the pair-formation processes involving F₂ and HF, respectively. In these diatomic molecules it was possible to show convincingly that the pair formation proceeds through a two-stage process: (a) the molecule in its electronic ground state (and vibrational ground state) absorbs a photon and goes into Rydberg series which converge upon the ionic ground state and (b) these Rydberg terms are "crossed" by potential curves that correlate with the ions in their ground states. Landau-Zener-type crossings can then occur at energies rather close to the limit for dissociation into ground-state ions.

A similar process is quite likely occurring here. The spacings between the first three sharp peaks is about 520 cm⁻¹, which is just the spacing Brundle, *et al.*,⁸ found in the photoelectron spectrum of the ionic ground state and attributed to excitation of a stretching vibration in the triatomic ion. The Rydberg states should experience a similar excitation. The corrected Rydberg formulas given by Brundle, *et al.*,^{8,19} have been used to calculate possible Rydberg members that might contribute to the peaks observed in the pair formation. Of the s-type orbitals, the *n* = 8 (1031 Å) converging to ²P_{1/2} and the *n* = 8, 9, and 10 (1073, 1045, and 1030

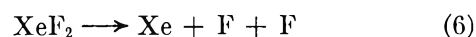
Å) converging to P_{3/2} appear to be likely candidates. Of the d-type orbitals, the *n* = 6 and *n* = 7 (1048 and 1013 Å) converging to ²P_{1/2} also appear as attractive possibilities. The s-type orbitals are usually narrower,²⁰ and it is noteworthy that the sharp peaks near threshold are calculated to be of s type.

If the predominant contribution to the ion-pair process is predissociation, then selecting a precise threshold for this process is somewhat uncertain since one must hope that a Rydberg state and a curve crossing occur somewhere near threshold. One can set rather rigorous upper limits on the endothermicity of the dissociation, but one must look into the detailed structure of the ionization of each specific molecular system to deduce whether or not the value obtained is close to the true thermodynamic value. In the present instance, there seems to be evidence that states occur near threshold. In fact, this process has a precursor



which extends to still longer wavelength (lower energy). The sudden drop in structure and in ionization yield at the apparent threshold, the quasi-linear behavior of the ionization yield at the apparent threshold, and the tail (probably having contributions from internal thermal energy and monochromator slit width) all suggest a process that occurs at or very near the true threshold.

An objective technique²¹ for treating the threshold region is as follows. The linear region is extrapolated to the background level, and to the energy corresponding to the intercept is added the average internal energy. For the linear XeF₂ molecules, the average rotational energy at 298°K is 0.025 eV. From the observed²² vibrational frequencies, the average vibrational energy at this temperature can readily be computed to be 0.040 eV. The linearly extrapolated threshold for reaction (4) is 1086 Å = 11.416 eV, and hence the value corrected to 0°K is 11.481 eV. From the accurately known ionization potential²³ of Xe and the electron affinity²⁴ of F⁻, one can deduce that the dissociation energy for the reaction



is 2.800 eV, and hence the average XeF bond energy in XeF₂ is 32.3 kcal/mol at 0°K. From our recently re-

(18) Photoionization mass spectrometric study of F₂, HF, and DF, J. Berkowitz, W. A. Chupka, J. H. Holloway, P. M. Guyon, and R. Spohr, *J. Chem. Phys.*, in press.

(19) The convergence limits of the Rydberg series given in ref 8a are evidently the vertical, rather than the adiabatic ionization potentials.

(20) R. E. Hoffman, Y. Tanaka, and J. C. Larrabee, *J. Chem. Phys.*, **39**, 902 (1963).

(21) P. M. Guyon and J. Berkowitz, *ibid.*, **54**, 1814 (1971).

(22) H. H. Claassen, P. Tsao, and C. C. Cobb, in published work; P. A. Agron, G. M. Begun, H. A. Levy, A. A. Mason, C. G. Jones, and D. F. Smith, *Science*, **139**, 842 (1963).

(23) C. Moore, *Nat. Bur. Stand. (U. S.) Circ.*, **3**, No. 467 (1949).

(24) R. S. Berry, *Chem. Rev.*, **69**, 533 (1969).

determined dissociation energy¹⁸ of F₂ (1.586 ± 0.006 eV) we can then compute $\Delta H_f^\circ(\text{XeF}_2) = -28.0$ kcal/mol. A reasonable estimate of the error in threshold determination is *ca.* 2 Å, which in this wavelength region corresponds to 0.5 kcal/mol. By way of comparison, Weinstock, *et al.*,⁴ obtained the value -25.32 kcal/mol on the basis of their determination of gas-phase equilibrium constants, while the value from the calorimetric measurement of Pepekin, *et al.*,⁵ is $\Delta H_f^\circ(\text{XeF}_2) = -28.6 \pm 0.8$ kcal/mol. This observation, together with subsequent results on XeF₄ and XeF₆, suggests some systematic error in ref 4.

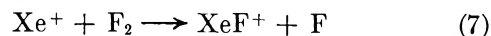
The formation of parent ion XeF₂⁺, which is a much more intense process than that forming Xe⁺ at energies below ~15.5 eV, is seen in Figure 2. There is distinct evidence for autoionization in the region between threshold and the onset of the next electronic state⁸ at *ca.* 960 Å. This could be due to vibrational autoionization from Rydberg states converging to the ionic ground state but having vibrational excitation (as in F₂ and HF, ref 18), or it may be due to Rydberg states converging upon the excited ²Π_{1/2} state (akin to the behavior in xenon, ref 20), or perhaps it is due to both. The spectrum of the light source in this wavelength region contains some peaks which prevent accurate measurement of structure in the ionization curve. There is a hint of structure in the older photoionization work⁷ as well, but evidently the authors did not feel secure in this interpretation. In addition, their technique for deducing ionization potentials assumes a specific kind of direct ionization (step function) whose derivative would yield the desired quantity. When pronounced structure is evident in the photoionization curve, as in the present case, other techniques are required.

The first peak in the XeF₂⁺ curve occurs at ~1003 Å, and the true first ionization potential is almost certainly at a longer wavelength. If the tailing at threshold were due entirely to the monochromator slit width, it should extend for *ca.* 0.8 Å (as discussed in ref 21). The observed tailing extends for *ca.* 4 Å and therefore probably has contributions from internal thermal energy at ~300°K. Of this, the rotational energy should make negligible contribution to the parent ionization, but vibrational contributions can be significant. This behavior seems most similar to that described in ref 21 in the section on thresholds for diatomic oscillators. In the latter work, it was shown that in the case of idealized step-function behavior, convolution of a Boltzmann distribution would yield an exponential tail originating at a point of discontinuity. The tangent at the point of discontinuity (our peak at 1003 Å) intercepts the energy axis at a distance *kT* from threshold (for diatomics). For an idealized linear cross section, convolution of a thermal distribution yields a linear portion plus an exponential, such that the extrapolated linear portion intercepts the energy axis at a

distance *kT* (for diatomics) from the true threshold. This behavior for diatomics was predicted on the condition that $h\nu < kT$.

Here we are dealing with a linear triatomic, which has two stretching frequencies with $h\nu \approx 0.065$ eV (*i.e.*, with energies much larger than *kT* and hence contributing little to the threshold) and one doubly degenerate bending mode with $h\nu \approx 0.026$ eV (*i.e.*, with an energy about equal to *kT*). Hence, the shift from the linearly extrapolated intercept should (most probably) be less than *2kT*. A shift of *kT* would place the adiabatic 0°K ionization potential at 12.35 eV, while the 1003-Å peak (the upper limit) is equivalent to 12.36 eV. Thus, it seems rather conclusively established that the first ionization potential of XeF₂ is 12.35 ± 0.01 eV, a value significantly different from the earlier photoionization result⁷ (12.28 eV), but in good agreement with the photoelectron spectroscopic results of Brundle, *et al.*,⁸ (12.35 ± 0.01 eV) and Brehm, *et al.*,⁸ (12.33 ± 0.02 eV).

A rather striking phenomenon now appears. The second adiabatic ionization potential (the ²Π_{1/2} companion of the ionic ground state) is given by Brundle, *et al.*, as 12.89 ± 0.01 eV (top of first vibrational peak) and by Brehm, *et al.*, as 12.83 ± 0.02 eV (estimated onset of ionization). This first excited ionic state is narrow, and it has a hint of vibrational structure. Hence, it is not a repulsive state. In the XeF₂⁺ curve, no significant change occurs in this energy range, but the XeF⁺ fragment appears precisely in this region (linearly extrapolated threshold = 965.5 Å = 12.84 eV, 0°K corrected onset = 12.90 eV). It appears, therefore, as if this first excited state is crossed by a repulsive curve, and predissociation takes place to form XeF⁺ + F. Predissociation evidently does not take place from the ionic ground state because the Franck-Condon region does not encompass sufficiently high vibrational levels of the ground state. From the photoelectron spectrum, it appears that there is no significant population of vibronic states in XeF₂⁺ in the energy range 12.6–12.8 eV. Hence the value (12.90 eV) for the threshold of reaction 1 should be regarded as an upper limit for thermochemical purposes, and from this it follows that $D_0(\text{XeF}^+) \geq 2.03$ eV. The latter result is important in that it demonstrates that $D_0(\text{XeF}^+)$ is significantly larger than the average Xe-F bond energy (1.40 eV) previously found for XeF₂ and also implies that the reaction



should be exothermic. Recent kinetic studies²⁵ of reaction 7 at this laboratory indicate that the cross section rises with increasing kinetic energy, a behavior normally associated with endothermic reactions. The

(25) J. Berkowitz and W. A. Chupka, *Chem. Phys. Lett.*, **7**, 447 (1970).

interpretation of this behavior must somehow involve the mechanism of this reaction rather than its thermochemistry.

The value for $D_0(\text{XeF}^+)$ is not unreasonable when compared with those for the isoelectronic interhalogens. The direct isoelectronic analog is IF, whose dissociation energy has been somewhat uncertain. Of the two possible values (1.99 eV and 2.88 eV) that stem from observed predissociations, the higher value seems currently^{26,27} to be distinctly favored. The value²⁸ of D_0 for ICl is 2.152 eV, and of the two permissible values²⁸ (2.19 eV and 2.60 eV) for $D_0(\text{FBr})$, the higher one is favored.²⁷ Hence, in this case of XeF^+ , as well as two others (the KrF^+ ion²⁹ and the ArF^+ ion²⁵), the diatomic ions of the rare gas fluoride behave as pseudohalogens. However, as is discussed in ref 25, this is not the case for HeF^+ and NeF^+ .

As one now examines the ionization at shorter wavelengths in Figure 2, one finds that both the XeF_2^+ and XeF^+ curves show several weak peaks, commencing at ca. 935 Å and terminating at the onset of a large increase in ionization at ca. 918 Å. These are presumably Rydberg levels formed by excitation of an electron from the inner a_{1g} molecular orbital (notation of ref 9) or $10\sigma_g$ (notation of ref 8). The convergence limit cannot be determined accurately, but the onset of the steep rise at 918 Å = 13.5 eV corresponds very closely to the adiabatic ionization potential obtained in photoelectron spectroscopy (Brundle, *et al.*,⁸ ~13.5 eV; Brehm, *et al.*, 13.58 ± 0.05 eV). Both the XeF_2^+ and XeF^+ acquire significant additional contributions to their intensities as the wavelength is scanned across this band. However, at the adiabatic onset (14.00 ± 0.05 eV, ref 8a; 14.06 ± 0.05 eV, ref 8b) reported for the next band (presumably ejection of an electron from an e_{1g} molecular orbital [ref 9] or $3\pi_g$ [ref 8]), the XeF_2^+ intensity has begun to decline, while the XeF^+ begins to rise again at about the onset of this state and continues to rise through most of the wavelength region corresponding to the energy band of this state. For both the $10\sigma_g$ state and the $3\pi_g$ state we are well above the dissociation limit but a major contribution to parent ionization continues to be made by $10\sigma_g$, although not by $3\pi_g$. It is evident that a simple statistical theory cannot explain this behavior and perhaps should not be expected to for a triatomic molecule.

As one proceeds to shorter wavelength, the next major contribution to ionization appears to be the onset of significant Xe^+ intensity, at ca. 810 Å ≡ 15.3 eV. This corresponds quite closely to the next observed adiabatic ionization potential (Brundle, *et al.*, 15.25 ± 0.05 eV; Brehm, *et al.*, 15.40 ± 0.05 eV) and is attributed to the ejection of an electron from the e_{1u}^- ($4\pi_u$) orbital. Slight changes in the XeF^+ and XeF_2^+ intensities also occur in this region. This onset of Xe^+ clearly corresponds to a process involving concomitant formation of two F atoms (rather than F_2) since the

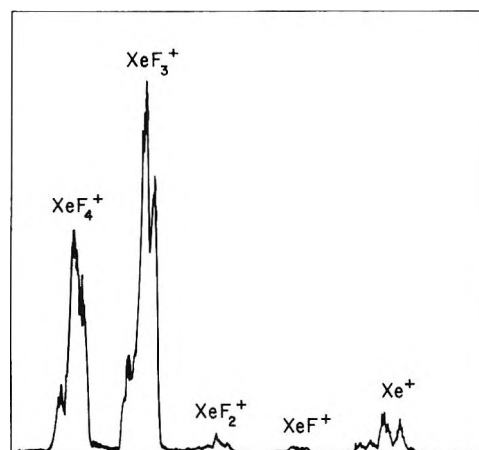


Figure 4. Photoionization mass spectrum of XeF_4 , obtained with the undispersed central-image light of the hydrogen lamp.

latter process would be expected to occur around 905 Å. No evidence for any significant contribution from the F_2 formation process exists in the Xe^+ curve.

On the basis of the previously determined threshold (11.481 eV) for reaction 4 and the electron affinity of F, one would anticipate this new Xe^+ threshold (effectively the sum of reactions 1 and 2) to occur at 14.93 eV. A glance at the photoelectron spectrum of Brundle, *et al.*, indicates that this corresponds to a deep valley in the ionization process. Very few, if any, ionic states are being made in this energy range; thus it is not surprising that the apparent threshold occurs at higher energy (~15.3 eV) and hence this process is not a useful one for thermochemical purposes.

Finally, at still shorter wavelengths, another significant process for production of Xe^+ becomes evident, with an onset at ca. 735 Å (16.87 eV) which also agrees well with the photoelectron spectroscopic studies (Brundle, *et al.*, 16.80 ± 0.05 eV; Brehm, *et al.*, 17.10 ± 0.1 eV). The output of the helium continuum is too weak in the 600–620-Å region to enable us to reach any significant conclusion regarding the next ionic state, which has tentatively been placed at ca. 20–22 eV in the photoelectron-spectroscopic work.⁸

B. XeF_4 . The mass spectrum of photoionized XeF_4 , obtained at central image with the hydrogen many-line continuum, is depicted in Figure 4. There is no measurable XeF_n^+ intensity with mass higher than XeF_4 (*i.e.*, no XeF_6 impurity) and the XeF_2^+ intensity is so weak that it may be attributable to fragmentation of XeF_4 ; the appearance potential of XeF_2 (to be discussed later in this subsection) bears this out.

(26) R. A. Durie, *Can. J. Phys.*, **44**, 337 (1966).

(27) E. H. Wiebenga, E. E. Havinga, and K. H. Boswijk, *Advan. Inorg. Radiochem.*, **3**, 133 (1961).

(28) G. Herzberg, "Molecular Spectra and Molecular Structure. II. Spectra of Diatomic Molecules," Van Nostrand, Princeton, N. J., 1950.

(29) J. Berkowitz, J. H. Holloway, and W. A. Chupka, "Photoionization Mass Spectrometric Study of KrF_2 ," unpublished work.

The Xe^+ has some contribution from a very small xenon impurity. No ion-pair formation was detected for this system.

In Figure 5, the parent XeF_4^+ ion intensity is shown as a function of incident wavelength. This intensity rises rather slowly from a threshold at *ca.* 980 Å (12.65 eV) to a maximum intensity at *ca.* 950–952 Å (13.02 eV). This range of energy is much larger than can be accounted for by monochromator slit width (*ca.* 0.8 Å) or Boltzmann distribution (average vibrational energy²² at 300°K \approx 0.09 eV). Brundle, *et al.*,³⁰ report similar values (12.72 and 13.06 eV) from their photoelectron spectrum. Therefore, it appears as if the

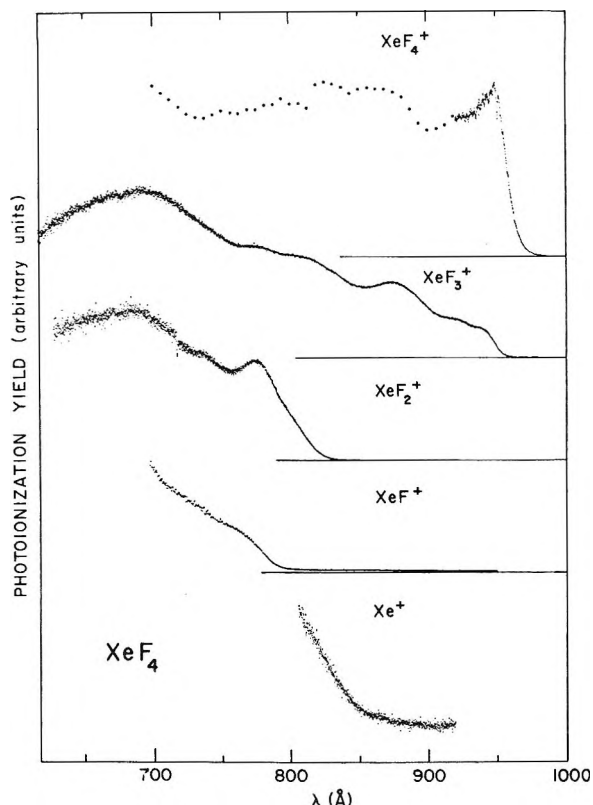


Figure 5. Photoionization efficiency curves of (a) XeF_4^+ , (b) XeF_3^+ , (c) XeF_2^+ , (d) XeF^+ , and (e) Xe^+ from XeF_4 .

Franck–Condon factors are not favorable at the adiabatic ionization potential. The XeF_3^+ fragment intensity, also shown in Figure 5, has an apparent threshold at *ca.* 906 Å (12.91 eV). The photoelectron spectrum of Brundle, *et al.*,³⁰ does not show the onset of another state until *ca.* 13.3 eV. Hence the dissociative ionization must somehow involve the ionic ground state of XeF_4^+ . The *ab initio* calculations of Basch, *et al.*,³¹ on XeF_4 show the uppermost occupied orbital to be $10a_{1g}$ (the calculated Koopman's theorem ionization potential \approx 12.6 eV) and the next deeper orbital to be $5a_{2u}$ (\approx 15.1 eV). Since both of these orbitals are non-degenerate, ionization from these orbitals should not give rise to Jahn–Teller splitting. Yet one must ac-

count for the apparent distortion in the XeF_4^+ , which can so readily yield $\text{XeF}_3^+ + \text{F}$, and also for the weak Franck–Condon probability at the adiabatic ionization limit. Within the framework of simple molecular orbital theory, ionization from an a_{1g} orbital (totally symmetric) should only yield concomitant vibrational excitation which is also totally symmetric. This cannot account for the above phenomena. It appears as if there must be an interaction that distorts the symmetry of XeF_4^+ in its ground state. Configuration mixing of a_{1g} with the $5a_{2u}$ can presumably give this kind of distortion. Basch, *et al.*,³¹ have presumably not solved the configuration–interaction problem. An alternative approach that can rationalize the low-energy fragmentation of XeF_4^+ proceeds as follows. The doubly degenerate asymmetric stretching mode ν_6 of XeF_4 has been reported by Claassen, *et al.*,²² to have a vibrational frequency of 586 cm^{-1} . At room temperature, the first excited state of this normal mode represents 12% of the molecular concentration. The act of ionization would approximately preserve this concentration and also permit the total wave function (electronic and vibrational) to be asymmetric. The fragmentation could then proceed without violating symmetry restrictions.

The higher vibrational levels of an antisymmetric vibration are symmetric for even values of the vibrational quantum number. Therefore, it is possible in principle to excite antisymmetric modes by $\Delta\nu_K = 0, \pm 2, \pm 4, \dots$. However, the transition with $\Delta\nu_K = 0$ is by far the most intense.³² Therefore, while this represents a mechanism for breaking the symmetry, it does not seem likely that it can account for the relatively strong XeF_3^+ intensity just beyond threshold.

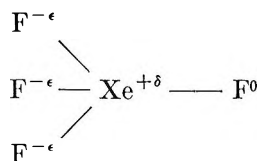
It may be useful to describe this ionic ground state in a hybrid of valence-bond and molecular-orbital terminology. Coulson³³ has given a qualitative picture of bonding in the xenon fluorides, in which about one unit of electronic charge is donated by the central Xe and apportioned among the appropriate number of fluorine ligands. The bonding between each fluorine and xenon is then primarily Coulombic. If an electron primarily localized on one of the fluorines is removed, the bonding of that particular fluorine to the rest of the structure would be drastically weakened. We note that from the description of their uppermost orbital ($10a_{1g}$) by Basch, *et al.*,³¹ it has *ca.* 90% fluorine contribution and 10% Xe. Hence, removal of an electron from this orbital is effectively removing a fluorine electron, and an appropriate description may be

(30) C. R. Brundle, G. R. Jones, and H. Basch, submitted for publication in *J. Chem. Phys.*

(31) H. Basch, J. Moskowitz, C. Hollister, and D. Hankins, unpublished work.

(32) G. Herzberg, "Molecular Spectra and Molecular Structure. III. Electronic Spectra and Electronic Structure of Polyatomic Molecules," Van Nostrand, Princeton, N. J., 1966, pp 150–153.

(33) C. A. Coulson, *J. Chem. Soc.*, 1442 (1964).



The four equivalent resonance structures of this type could be combined to give a wave function of a_{1g} symmetry.

It should be noted that this behavior (forming a fragment ion very near to threshold) is not a rare anomaly. It will be encountered again (section IV C) when we discuss XeF₆ and probably occurs for most hexafluorides, for alkali halides,³⁴ and for CF₄.³⁵ The explanation given above (removal of an electron localized on the halogen, which then destroys the Coulombic bond of that halogen to the remaining positive entity) may not be appropriate for CF₄, but it offers a plausible interpretation for the other ionic systems.

Returning now to the XeF₄⁺ spectrum, we only briefly point out that there appears to be evidence for autoionization, particularly at $\sim 951 \text{ \AA}$, where a dip occurs in the ionization yield. This dip is presumably a form of the Fano profile³⁶ that characterizes the interaction of a quasidecrete state with the underlying continuum.

The peak Brundle, Jones, and Basch observed at 13.38 eV has no obvious correlation with a noticeable increase in ionization, either in XeF₄⁺ or XeF₃⁺. On the other hand, the XeF₃⁺ intensity does begin rising at ca. 910 \AA ($\sim 13.6 \text{ eV}$) and reaches a local maximum at ca. 879 \AA (14.1 eV), which corresponds to a valley in the spectrum of Brundle, *et al.*³⁰ The next feature, a very broad maximum in the XeF₃⁺ intensity, has an onset at ca. 844 \AA (14.6 eV) and reaches a maximum at ca. 693 \AA (17.99 eV), and again does not bear close resemblance to the spectrum of Brundle, *et al.*

Meanwhile, in the 820–828- \AA region, XeF₂⁺ has begun to appear (Figure 5). The increase in ionization at this energy may roughly correlate with the very broad band (maximum at 15.18 eV) in the spectrum of Brundle, *et al.* An accurate determination of this threshold is quite useful, since it enables us to set a good lower limit and to obtain an approximate value for $\Delta H_f^\circ(\text{XeF}_4)$. We extrapolate the long linear region of the XeF₂⁺ curve near threshold to the background level and subtract the average internal energy.²¹ The extrapolated threshold is 821.5 \AA (15.092 eV), the average rotational energy is 0.039 eV, and the average vibrational energy²² is 0.090 eV. Therefore, a fairly rigorous upper limit to this threshold is 15.22 eV. By combining this with the previously determined $\Delta H_f^\circ(\text{XeF}_2)$ and ionization potential of XeF₂ and with $D_0(\text{F}_2)$, we deduce $\Delta H_f^\circ(\text{XeF}_4) \geq -57.6 \text{ kcal/mol}$ (*i.e.*, more positive). From the photoelectron spectrum of Brundle, *et al.*, in this energy region, we see that ionic states are being populated, and a significant activation

barrier is not likely for this dissociation. Hence, we feel that the true 300°K threshold is not likely to be more than 0.1 eV lower than 15.09 eV, and therefore $\Delta H_f^\circ(\text{XeF}_4) = -57.6 \pm 2 \text{ kcal/mol}$.

The linearly extrapolated onset for XeF⁺ occurs at 790.5 \AA (15.68 eV). The value corrected to 0°K is 15.81 eV. From this result, we can deduce another (somewhat less accurate) value for $\Delta H_f^\circ(\text{XeF}_4)$ by making use of the previously measured $\Delta H_f^\circ(\text{XeF}^+)$, reported in section III A, and $D_0(\text{F}_2)$. The errors in the limiting values for the onset of XeF⁺ from XeF₂ and of XeF⁺ from XeF₄ tend to cancel. The result, $\Delta H_f^\circ(\text{XeF}_4) = -58.6 \text{ kcal/mol}$, is in excellent agreement with that based on the XeF₂⁺ threshold. The error in the latter determination is estimated to be 3 kcal/mol.

Because of a slight xenon impurity from decomposition of XeF₄, no meaningful threshold could be deduced for Xe⁺.

Our best value $\Delta H_f^\circ(\text{XeF}_4) = -57.6 \pm 2 \text{ kcal/mol}$ is in good agreement with the calorimetric value of Stein and Plurien³ [$\sim 60 \text{ kcal/mol}$ when corrected for the newer $\Delta H_f^\circ(\text{HF})$] but distinctly diverges from the value of ref 4 (-50.2 kcal/mol). Errors are not clearly assessed in ref 3 and 4, but the impression given is that they are $\leq 1 \text{ kcal/mol}$.

We can now estimate a lower limit to $\Delta H_f^\circ(\text{XeF}_3^+)$. The linearly extrapolated threshold is 955.5 \AA ; corrected to 0°K, this yields 13.10 eV for the appearance potential of XeF₃⁺ from XeF₄, and hence $\Delta H_f^\circ(\text{XeF}_3^+) \geq 226.3 \text{ kcal/mol}$. For the dissociation energy for XeF₄⁺ \rightarrow XeF₃⁺ + F, we estimate 13.10 eV $- 12.65 \text{ eV} = 0.45 \text{ eV}$.

C. XeF₆. The photoionization mass spectrum of XeF₆ obtained at central image with the helium Hopfield continuum is shown in Figure 6. Two points are noteworthy: the XeF₆⁺ parent ion is barely detectable, and the xenon impurity is small. The XeF₅⁺ is clearly the major ion, but it is necessary to make ap-

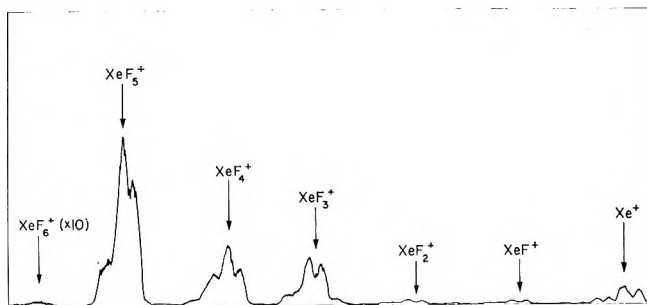


Figure 6. Photoionization mass spectrum of XeF₆, obtained with the undispersed central-image light of the helium lamp.

(34) J. Berkowitz, *J. Chem. Phys.*, **50**, 3503 (1969).

(35) T. A. Walter, C. Lifshitz, W. A. Chupka, and J. Berkowitz, *ibid.*, **51**, 3531 (1969).

(36) U. Fano, *Phys. Rev.*, **124**, 1866 (1961).

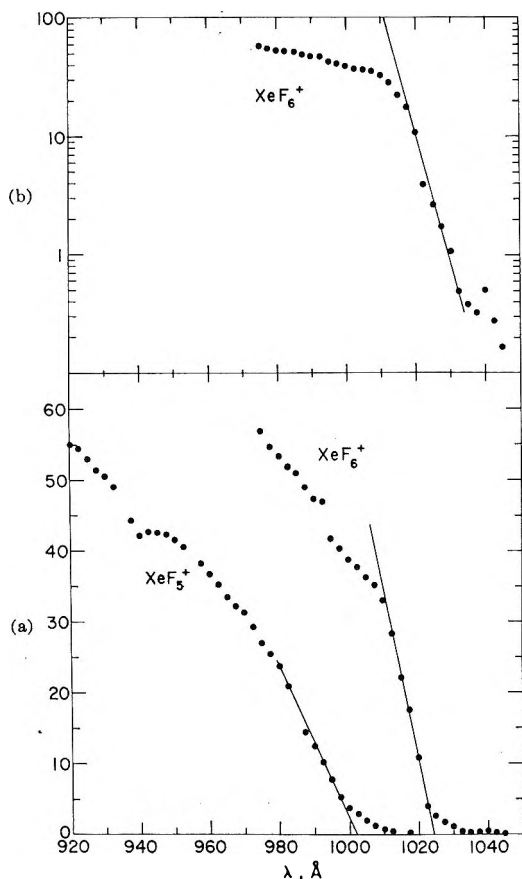


Figure 7. Photoionization efficiency curve of XeF_6^+ , plotted on (a) linear and (b) semilogarithmic coordinates. The photoionization efficiency curve of XeF_5^+ is also shown in (a).

pearance-potential measurements on the other fragments to demonstrate that they do not arise from XeF_4 and XeF_2 present as impurities. No ion-pair process could be detected.

In order to perform meaningful measurements on the parent ion XeF_6^+ , it was necessary to use 1-mm entrance and exit slits on the monochromator, together with a hydrogen-lamp light source. In Figure 7 the results in the threshold region are shown on both linear and semilogarithmic coordinates. The latter display is now more useful, since the exponential Boltzmann tail should be linear on such a plot, whereas it is somewhat more difficult to perform the subtraction of hot bands for complex molecules on the linear plot. A more accurate approach would be to determine the density of vibronic states populated at the temperature of the experiment, as was shown²¹ for S_8^+ and S_6^+ . However, there is insufficient information regarding the possibility of low-lying electronic states in neutral XeF_6 , and the vibrational spectrum is also not adequately established. Hence, the departure from linearity on a semilogarithmic plot (at 1019 \AA) is a useful lower limit to the first ionization potential; the curvature between 1016 and 1019 \AA may reflect the density-of-states factor,²¹ and hence an upper energy limit is

probably 1016 \AA . We therefore set the first ionization potential of XeF_6 at 12.19 ± 0.02 eV.

The threshold region of XeF_5^+ was examined under the same conditions as for XeF_6^+ (described above); the results are also displayed in Figure 7. We note a linear rise in the threshold region on linear coordinates, which is treated by extrapolating this linear region to the background level and subtracting the internal thermal energy.²¹ The slit width of the monochromator, although contributing 8.3 \AA FWHM in this experiment, should not affect the extrapolated threshold of a linearly rising function.²¹ From the linearly extrapolated threshold (1003 \AA = 12.36 eV) and the internal thermal energy³⁷ (~ 0.20 eV), we deduce 12.56 eV as the 0°K appearance potential of XeF_5^+ , and hence the bond energy for the dissociation $\text{XeF}_6^+ \rightarrow \text{XeF}_5^+ + \text{F}$ is 0.37 ± 0.05 eV. This value is very similar to the values 0.45 and ~ 0.55 eV found for removing the corresponding first fluorine from XeF_4^+ and XeF_2^+ , respectively. The trend in these bond energies is also implied in Coulson's analysis,³² since the partial negative charge on the fluorine (and hence the strength of the ionic bond) diminishes in the order $\text{XeF}_2 > \text{XeF}_4 > \text{XeF}_6$.

It is appropriate at this point to compare the photoelectron spectrum of Brundle *et al.*,³⁰ and the *ab initio* calculations of Basch, *et al.*,³¹ for XeF_6 because the next fragment (XeF_4^+) occurs at significantly higher energy, where successively higher ionic states are involved. Brundle, *et al.*, find one relatively narrow peak (~ 0.45 eV FWHM) corresponding to the removal of the most loosely bound electron in XeF_6 . The threshold for removal of this electron (the adiabatic first ionization potential) appears to be in fair agreement with our value (12.19 eV), although a small xenon atomic impurity in their measurement may interfere with a more accurate determination of this threshold. The vertical ionization potential, according to Brundle, *et al.*, is 12.51 eV. Although XeF_6 has 15 vibrational degrees of freedom whereas XeF_4 has only 9, this peak in XeF_6 is not appreciably wider than the corresponding one in XeF_4 . The next (very broad) peak in the photoelectron spectrum of XeF_6 has an onset at *ca.* 14 eV and a maximum at *ca.* 15.2 eV. Hence, the parent XeF_6^+ and first fragment XeF_5^+ , and only these ionic

(37) Since the vibrational spectrum of XeF_6 is not well established, we have estimated the internal (vibrational + rotational) energy of this molecule at 300°K in two somewhat independent ways. The vibrational spectrum of MoF_6 is rather well established [D. W. Osborne, F. Schreiner, J. G. Malm, H. Selig, and L. Rochester, *J. Chem. Phys.*, **44**, 2802 (1966)]. Its mass is not very different from that of XeF_6 , and its stretching frequencies are comparable with (though slightly higher than) the stretching frequencies of XeF_6 heretofore observed. Taking the value of $H_{300}^\circ - H_0^\circ$ from Osborne, *et al.*, and subtracting $3/2kT$ (for translation) and kT (for the $C_p - C_v$ correction), we obtain 4.3 kcal/mol. Alternatively, H. Kim, H. H. Classen, and E. Pearson [*Inorg. Chem.*, **7**, 616 (1968)] have crudely estimated 200 cm^{-1} for all three triply degenerate bending modes and 600 cm^{-1} for the stretching fundamental of an octahedral XeF_6 . From these we compute 4.7 kcal/mol (~ 0.20 eV) for the sum of vibrational and rotational energy.

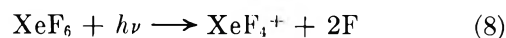
species, correlate with the removal of an electron from the uppermost populated molecular orbital.

According to Basch, *et al.*,³¹ this uppermost occupied orbital is the totally symmetric and nondegenerate 8a_{1g}. This orbital has properties similar to those of the 10a_{1g} encountered in XeF₄; it has a 78% fluorine contribution. The arguments advanced for XeF₄ would then also be applicable here, *i.e.*, removal of an electron localized on a fluorine would disrupt the ionic bond between that fluorine atom and the residual structure, and the ground state of XeF₆⁺ may be distorted by mixing with either of the degenerate orbitals e_g, t_{1g}, or t_{2u}.

Goodman³⁸ believes that low-lying excited states of XeF₆ can exist by population of the next higher (8t_{1u}) orbital. The calculation of Basch, *et al.*, indicates that this t_{1u} lies ~10.6 eV above their uppermost populated orbital (8a_{1g}). It is, of course, recognized that promotion of an electron from 8a_{1g} to t_{1u} would result in new interactions, *i.e.* electron repulsion and spin-orbit interactions. Nevertheless, the calculated energy of this t_{1u} state lies so much higher than 8a_{1g} that even taking into account the configuration interaction of singly excited configurations, the energy of this excited state is still likely to be quite large compared with *kT*, and hence one would not expect any appreciable population of excited states on the basis of this calculation. It has already been noted that in the photoelectron spectrum of XeF₆ the ionic ground state appears no broader than the corresponding XeF₄ states. If there were several low-lying ionic states near the ground state, one might expect a significant broadening. Hence, one is forced to conclude that neither the photoelectron spectrum nor the photoionization spectrum provides evidence for low-lying excited states in XeF₆. These experiments also do not shed any light on the much discussed, but still uncertain, symmetry of XeF₆ in its neutral ground state. Although the evidence points to distortion in the ionic ground state, it is not likely to be of Jahn-Teller-type, since the highest degenerate orbital (5e_g) lies some 7 eV deeper than the uppermost 8a_{1g}, according to Basch, *et al.*³¹

The next increase in ionization in going to higher energy (Figure 8) occurs for XeF₆⁺ at ca. 875 Å (~14.17 eV). This correlates well with the onset of a new ionic state in the photoelectron spectrum (~14 eV). The XeF₄⁺ intensity rises from this new threshold, more or less linearly, for the remainder of the energy range covered (to ca. 20 eV). The photoelectron spectrum also shows a very broad ionization region that extends to ca. 20 eV and contains unresolved peaks at ca. 15.2, 16.0, and 17.65 eV. This implies that at the threshold for XeF₄⁺ from XeF₆, there should be many states available, and hence this latter threshold should be reliable.

From Figure 8, we obtain the value 801.5 Å (15.47 eV) as an extrapolated linear threshold for the process



When corrected²¹ for the estimated internal energy (0.20 eV), this becomes 15.67 ± 0.05 eV. One can now complete a cycle employing the previously determined Δ*H*_{f°}(XeF₄) = -57.6 ± 2 kcal/mol, the ionization potential of XeF₄ = 12.65 eV, and the dissociation energy of F₂ = 1.586 eV. The result of this cycle is Δ*H*_{f°}(XeF₆) = -90.6 kcal/mol. Probably the major source of uncertainty in this calculation is the ionization potential of XeF₄ (section IV B) because the adiabatic and vertical ionization potentials are so widely separated that it is difficult to deduce the precise adiabatic value. It is almost certainly ≤ 12.9 eV, however, so this uncertainty is ≤ 0.25 eV. The next largest source of error is in the true threshold for process 8. An upper limit to the threshold wavelength would appear from Figure 8 to be 810 Å = 15.3 eV. Both of these possible errors would act in the same direction and would reduce Δ*H*_{f°}(XeF₆) to ~-81.1 kcal/mol. The thermal energy correction may have been estimated too low, however, if XeF₆ turns out to have many low-frequency modes of vibration.³⁷ This could make

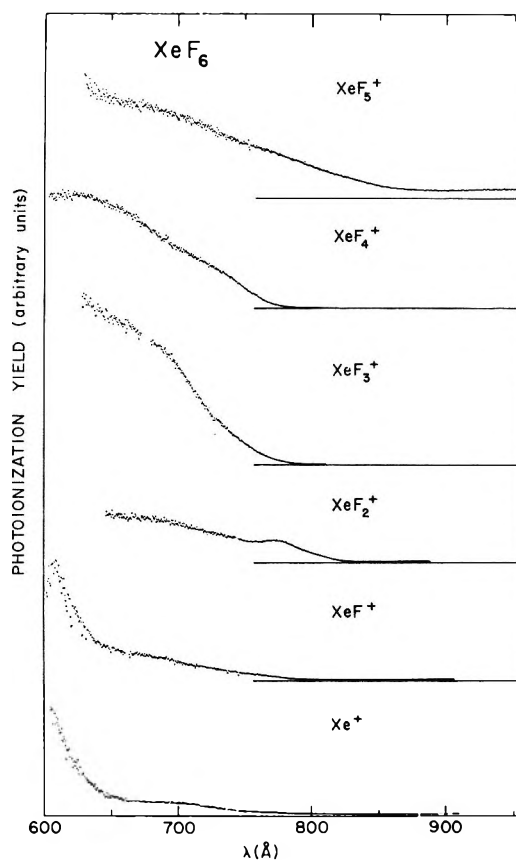


Figure 8. Photoionization efficiency curves of (a) XeF₅⁺, (b) XeF₄⁺, (c) XeF₃⁺, (d) XeF₂⁺, (e) XeF⁺, and (f) Xe⁺ from XeF₆.

(38) G. L. Goodman, private communication. See also Symposium on Noble Gas Compounds, Fluorine Division, American Chemical Society, Chicago, Ill., Sept 1970.

$\Delta H_f^\circ(\text{XeF}_6)$ more negative by about 2 kcal/mol. Hence, the analysis based on reaction 8 leads to -91 kcal/mol $\leq \Delta H_f^\circ(\text{XeF}_6) \leq -81$ kcal/mol, with the more negative value favored.

We can also study the reaction



The threshold for this process appears to be between 770 and 780 Å (between 16.1 and 15.9 eV), although not readily apparent from the scale in Figure 8. When combined with $\Delta H_f^\circ(\text{XeF}_3^+)$ previously deduced and $D_0(\text{F}_2)$, this leads to $-90.2 \leq \Delta H_f^\circ(\text{XeF}_6) \leq -94.8$ kcal/mol. Since the threshold for XeF_3^+ is at higher energy, it must compete with the lower energy processes, and this effect (according to the quasiequilibrium theory of mass spectra) will tend to shift its apparent threshold to higher energy. The effect is noticeable in the rather slow increase of XeF_3^+ with increasing energy. Hence, a value $\Delta H_f^\circ(\text{XeF}_6) = -90$ kcal/mol, or perhaps slightly less negative, is again indicated.

The thresholds for the fragments XeF_2^+ , XeF^+ , and Xe^+ occur at still higher energy, and thus become less significant because of the aforementioned competitive processes. In addition, there may be several possible neutral products accompanying these fragments, and these would confuse the interpretation of their threshold still further. By contrast, the occurrence of the processes forming XeF_4^+ and XeF_3^+ from XeF_6 were confirmed in this work by observing the pertinent metastable ions corresponding to the transitions $\text{XeF}_5^+ \rightarrow \text{XeF}_4^+ + \text{F}$ and $\text{XeF}_4^+ \rightarrow \text{XeF}_3^+ + \text{F}$.

A best value $\Delta H_f^\circ(\text{XeF}_6) = -(90_{-3}^{+8})$ kcal/mol is indicated by our photoionization threshold data. This is in good agreement with the result of Stein and Plurien³ [-86 kcal/mol, when corrected for the new $\Delta H_f^\circ(\text{HF})$] but very far from the value of Weinstock, *et al.*⁴ (-68.1 kcal/mol). One can never discount the possibility that the true threshold for reaction 8 has not been achieved. However, it seems clear that states are being formed in the molecular ion, and an activation barrier of some 20 kcal/mol against decomposition according to reaction 8 is unlikely, since the molecule is large and has many vibrational degrees of freedom. The XeF_4^+ ion is formed by a second-stage decomposition, and this would tend to increase the threshold somewhat, but probably by only a small fraction of an electron volt.

V. Discussion

In Table I we list the adiabatic ionization potentials for XeF_2 , XeF_4 , and XeF_6 deduced from this work and comparative values obtained by photoelectron spectroscopy^{8,30} and electron-impact mass spectrometry.⁶ The agreement between photoionization mass spectrometry and photoelectron spectroscopy is very good; the electron-impact values are higher by about 0.25 eV. Both the direction and magnitude of the deviation of

Table I: Adiabatic Ionization Potentials (eV) of the Xenon Fluorides

	XeF_2	XeF_4	XeF_6
Electron impact ^a	12.6 ± 0.1	12.9 ± 0.1	...
Photoelectron spectroscopy ^b	12.35 ± 0.01	12.72	12.2 ± 0.2 ^c
Photoionization mass spectrometry ^d	12.35 ± 0.01	12.65 ± 0.1	12.19 ± 0.02

^a Reference 6. ^b References 8 and 29. ^c Estimated from data of ref 29. ^d This work.

the electron-impact data are about what one would expect from past experience.³⁹

Coulson³³ has stated that the π_u orbital in XeF_2 "must lie a little higher (perhaps 1 eV) than the xenon 5p orbital." He therefore expects an ionization potential of ~ 11 eV for XeF_2 . The *ab initio* calculations of Basch, *et al.*,³¹ for this π_u orbital yield 13.6 eV which, when corrected by the empirical factor used by Brundle, *et al.*,⁸ corresponds to 12.5 eV. The experimental value (12.35 ± 0.01 eV) is clearly *higher* than that of the xenon 5p orbital. For XeF_4 and XeF_6 , Basch, *et al.*, obtain 12.6 and 11.7 eV for the removal of an electron from $10a_{1g}$ and $8a_{1g}$, respectively. The experiments do indicate a higher value for XeF_4 (12.65 eV) than for XeF_6 (12.19 eV). In fact, the variation appears not to be monotonic; XeF_4 has the highest ionization potential, but each of these xenon fluorides seems to have a higher ionization potential than atomic xenon.

While the gross features of the ionization processes seem to be in accord with the calculations of Basch, *et al.*, the more precise features would appear to require extensive configuration-interaction calculations. Thus, the order of the two uppermost filled orbitals in XeF_2 appears to be reversed, as already noted by Brundle, *et al.*,⁸ and the asymmetrically distorted nature of the ionic ground states in XeF_4^+ and XeF_6^+ cannot be inferred at the current level of sophistication of these calculations.

The heats of formation of the xenon fluorides deduced from this work, and earlier values obtained by other techniques, are summarized in Table II. The discrepancy between our values and those of Weinstock, *et al.*,⁴ increases with the complexity of the molecule. This is also the direction of increase of our experimental error. The nature of our bootstrap experiment bases the measurement of ΔH_f of a higher fluoride upon a measured value of the next lower fluoride, so that errors may accumulate. The types of errors that can be anticipated ("lagging thresholds") are such as to

(39) K. Watanabe, *J. Chem. Phys.*, **26**, 542 (1957).

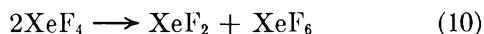
Table II: Heats of Formation (kcal/mol at 0°K) of the Xenon Fluorides

	XeF ₂	XeF ₄	XeF ₆
Stein and Plurien ^a		-60	-87
Weinstock, Weaver, and Knop ^b	-25.3	-50.2	-68.1
Pepekin, Lebedev, and Apin ^c	-28.6 ± 0.8		
Present work	-28.0 ± 0.5	-57.6 ± 2	-(90 ₋₃ ⁺⁸)

^a Reference 3. ^b Reference 4. ^c Reference 5.

cause departure from the values of Weinstock, *et al.*, in just the direction that we observe. Nevertheless, the magnitude of the discrepancy appears very large by the usual standards applied to thresholds for mass spectrometric fragment ions. It is of interest to note that the Xe-F bond energy that can be deduced from the results of ref 4 is 31.0, 30.9, and 29.7 kcal/mol for XeF₂, XeF₄, and XeF₆, respectively. The corresponding numbers from our data are 32.35, 32.85, and 33.35 kcal/mol. The experimental bond distances are 2.00 ± 0.01 Å for XeF₂,⁴⁰ 1.95 ± 0.01 Å for XeF₄,⁴¹ and 1.89 ± 0.005 Å for XeF₆.⁴² One might normally expect a shorter bond distance to imply a stronger bond, in agreement with our results, but the variation is small and hence we do not consider this correlation as strong support for our values.

Also implicit in our results is the conclusion that the disproportionation reaction



is almost thermoneutral, perhaps slightly exothermic. This might be an interesting reaction to test the overall conclusions of the photoionization experiments.

An amusing exercise that can be performed with the photoionization-threshold data is to calculate the successive bond energies in the decomposition XeF₆⁺ → XeF₅⁺ → XeF₄⁺ → ... This can be done by combining the heats of formation of the ions from all of the xenon fluorides and assuming that the structure of XeF₄⁺ from XeF₆ is the same as that of XeF₄⁺ from XeF₄, etc. (This assumption is implicit in the fragmentation-threshold method of deducing bond energies, in any event.) The results are graphically illustrated

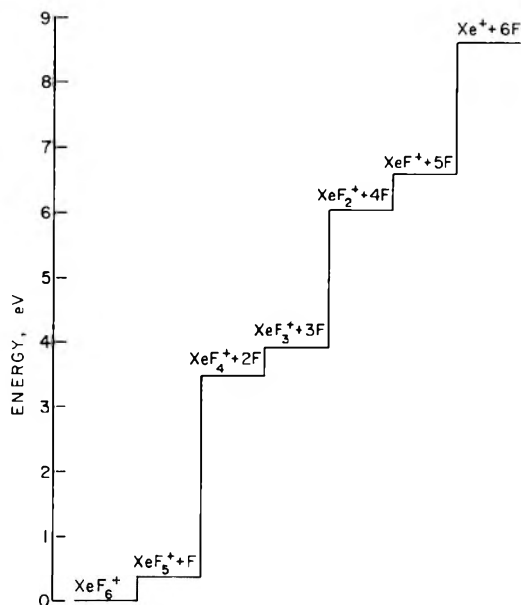


Figure 9. The relative stabilities of the various XeF_n⁺ ions toward loss of a fluorine atom, plotted on an energy level diagram.

in Figure 9. It is obvious that the ions having an odd number of fluorine atoms are more stable toward ejection of a fluorine; these are also the ions having an even number of electrons. The XeF₄⁺ and XeF₆⁺ apparently have an unpaired electron in an orbital, and this seems to favor an asymmetric distortion of these molecular ions in their ground states. The XeF₅⁺ → XeF₄⁺ transition appears to require significantly more energy than the others, and this once again raises the possibility that a "lagging threshold" or excess energy may perhaps be necessary for rupture of this bond.

The controversy regarding possible low-lying electronically excited states of neutral XeF₆ has certainly not been settled by this investigation, but no evidence for their existence has been found in this or the photoelectron study. More laborious investigations which permit long-term equilibration in the gas phase are obviously required.

(40) H. A. Levy and P. A. Agron, ref 2a, p 221.

(41) J. H. Burns, P. A. Agron, and H. A. Levy, ref 2a, p 211.

(42) R. M. Gavin and L. S. Bartell, *J. Chem. Phys.*, **48**, 2460 (1968); L. S. Bartell and R. M. Gavin, *ibid.*, **48**, 2466 (1968); R. D. Burbank and N. Bartlett, *Chem. Commun.*, 645 (1968).

Predissociation and Dissociation Energy of HBr^+

by Michael J. Haugh and Kyle D. Bayes*

Department of Chemistry, University of California, Los Angeles, California 90024 (Received January 13, 1971)

Publication costs assisted by the U. S. Air Force Office of Scientific Research

A predissociation in the $A^2\Sigma^+$ state of HBr^+ and DBr^+ is described. The electronic state responsible for the predissociation is a stable $^4\pi$ state. The dissociation limit of $2180 \pm 20 \text{ cm}^{-1}$ above the $A^2\Sigma^+$ ($v = 0$) level of HBr^+ corresponds to dissociation into $\text{H}(^2S)$ and $\text{Br}^+(^3P_{3/2})$ atoms. This results in a dissociation energy of $\text{HBr}^+(X^2\pi_{3/2})$, $D^{\circ}_0(\text{HBr}^+) = 3.893 \pm 0.003 \text{ eV}$, which is compatible with current thermodynamic data.

Introduction

The electronic spectrum of HBr^+ was first described by Norling,¹ and additional work has been reported by Barrow and Caunt.² Emission has been observed from the lowest two vibrational levels of the upper $A^2\Sigma^+$ state. Although no emission has been observed from higher vibrational levels of the $A^2\Sigma^+$ state, the possibility of predissociation has not been mentioned. Recently emission from the lowest vibrational level of $\text{DBr}^+(A^2\Sigma^+)$ has been reported.³

While recording the emission spectrum from the charge exchange reaction



we observed a breakoff in the rotational structure of the 1,0 band of the $A^2\Sigma^+ \rightarrow X^2\pi_1$ system. The high rotational excitation created in this reaction aided in the recognition of this predissociation. This paper will attempt to use this predissociation to establish an accurate dissociation limit for the HBr^+ molecule.

Experimental Section and Results

The excited HBr^+ was formed by colliding a beam of 2500-eV Ar^+ with HBr at room temperature and a pressure of a few milliTorr. The apparatus has been described previously.⁴ Spectra were recorded on a 1-m Ebert spectrometer with a cooled EMI 6256S photomultiplier. Lines were identified by using previously measured wavelengths along with occasional atomic argon or bromine lines that also appeared in the spectrum.

A photoelectric trace of the 1,0 band is shown in Figure 1. Several branches are indicated above the spectrum, with the first missing lines indicated by dashed lines. The predissociation appears to be essentially complete in all of the observed branches, with the first missing lines being at most 5% as intense as the preceding line. The breakoff occurs in both the $^2\Sigma^+ \rightarrow ^2\pi_{3/2}$ and $^2\Sigma^+ \rightarrow ^2\pi_{1/2}$ bands.

In order to use a predissociation limit to establish a bond energy, it is necessary to find breakoffs in more than one vibrational band. A search in the 0,0 bands

of HBr^+ indicated a predissociation, but not with the sharp cutoff observed in the 1,0 bands. The effect can be seen in a Boltzmann plot, as shown in Figure 2.

For most diatomic emission spectra, a plot of eq 2

$$\ln(I/S) = -B'N'(N' + 1)/kT \quad (2)$$

gives a simple straight line, indicating a Boltzmann distribution among the rotational levels of the emitting state. Here I is the emission intensity of an individual rotational line, S is a line strength factor⁵ that depends on the particular branch and the rotational quantum number N' , B' is the rotational constant for the emitting state, k is the Boltzmann constant, and T is a "rotational temperature," which need not be the same as the average temperature of the emitting gas.

When the intensities of lines within the 0,0 band are placed on a Boltzmann plot (Figure 2) the lines of low rotational quantum number give a straight line corresponding to a rotational temperature of about 3000°K. At high values of N' , the intensities fall below the expected line, and the effect becomes larger for higher N' . The first significant drop in intensity occurs for $N' = 21$, for which the $^3Q_{21}$ line was 25% less intense than expected. Unfortunately, the corresponding R_1 line was overlapped. By $N' = 23$, the R_1 line was less than 20% of the expected intensity. Other branches could not be identified due to overlapping and background emission. The abrupt change in slope observed in Figure 2 will be taken as the onset of predissociation. This change occurs for $N' = 21$, with a possible uncertainty of ± 1 .

Due to the unusual method of ionizing and exciting the HBr^+ , it is possible that these breakoffs are due to a collision-induced predissociation, caused by the departing neutral Ar. Additional spectra of the 1,0 bands

(1) F. Norling, *Z. Phys.*, **95**, 179 (1935).

(2) R. F. Barrow and A. D. Caunt, *Proc. Phys. Soc., Ser. A*, **66**, 617 (1953).

(3) L. Marsigny, J. Lebreton, and Y. Petit, *C. R. Acad. Sci. Paris, Ser. C*, **270**, 1632 (1970).

(4) M. J. Haugh and K. D. Bayes, *Phys. Rev. A*, **2**, 1778 (1970).

(5) L. T. Earls, *Phys. Rev.*, **48**, 423 (1935).

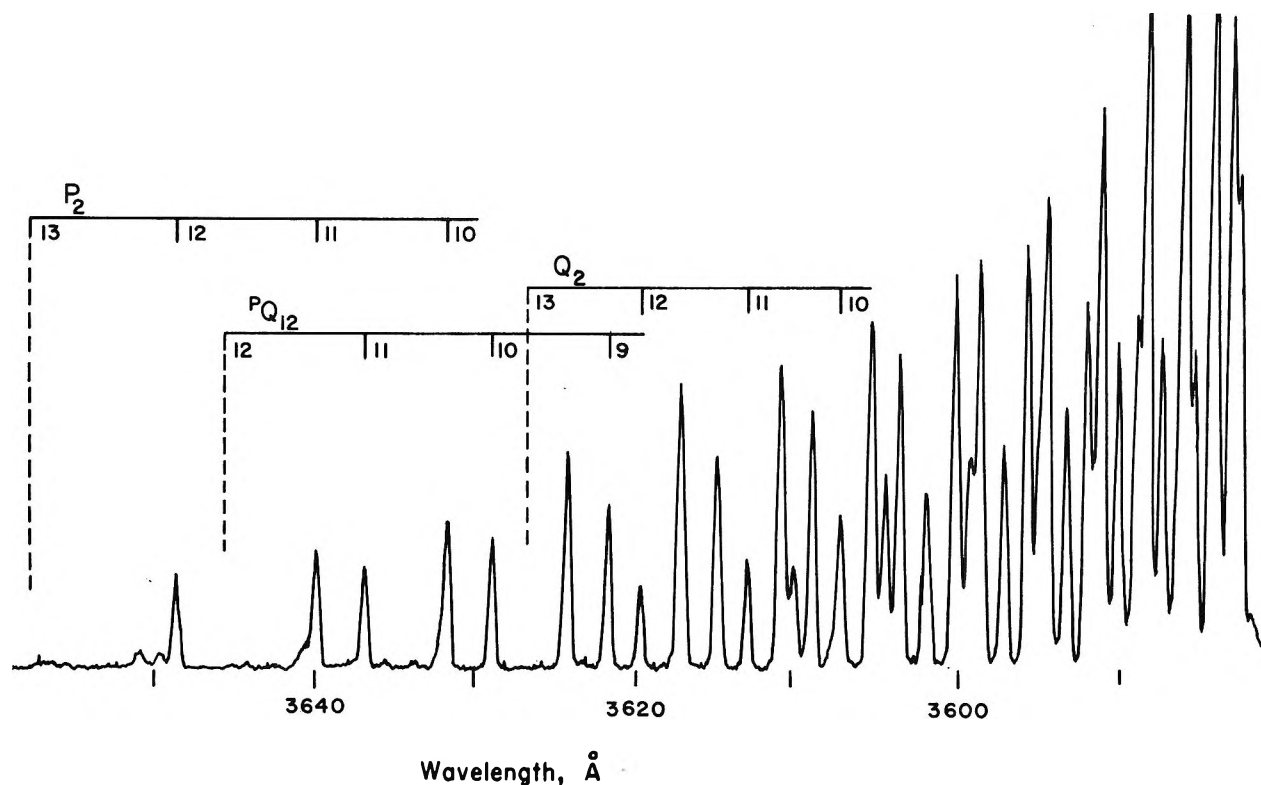


Figure 1. Spectrum of the $\text{HBr}^+(\text{A}^2\Sigma^+(v' = 1) \rightarrow \text{X}^2\pi_{1/2}(v'' = 0))$ band in emission. The breakoffs in three of the branches are indicated. The numbers shown are N' , rather than the usual J'' .

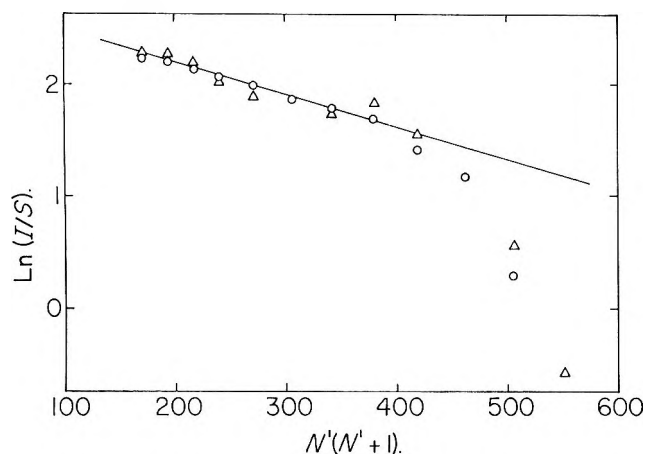


Figure 2. Boltzmann plot for the $\text{HBr}^+(\text{A}^2\Sigma^+(v' = 0) \rightarrow \text{X}^2\pi_{3/2}(v'' = 0))$ band. The $\text{R}_{\text{Q}_{21}}$ lines are indicated by circles, the R_1 lines by triangles.

were taken using a microwave discharge (2450 MHz) in pure HBr at a total pressure of 7 mTorr. The same breaking-off points were observed, showing that the predissociation is not collisionally induced.

The emission spectrum of DBr^+ was also observed in the charge-exchange reaction of Ar^+ with DBr . In addition to the expected emission from the 0 and 1 vibrational levels of the $\text{A}^2\Sigma^+$ state, strong bands from $v' = 2$ were present. This additional vibrational level is the result of the lowering of vibrational levels within the potential energy curve due to the isotope effect.⁶

Break-offs in the rotational structure of the 2,0 bands of DBr^+ were very evident, as can be seen in Figure 3. There is some uncertainty in assigning rotational quantum numbers to the 2,0 band since a complete rotational analysis has not been carried out. The numbers shown in Figure 3 are derived by using the spectroscopic constants for HBr^+ and applying the appropriate isotopic factors to calculate the constants for DBr^+ .⁷ Due to the uncertainties in some of these factors, the rotational assignments shown in Figure 3 should be considered tentative.

The break-off in the 2,0 band of DBr^+ is not as complete as that observed for the 1,0 band of HBr^+ . For example within the P_1 branch, emission from $N' = 13$ is about 30% as intense as the $N' = 12$ line, while the $N' = 14$ line is very weak. (A comparable decrease in intensity can be observed in the Q_{21} , Q_1 , and $\text{R}_{\text{Q}_{21}}$ branches.)

The observed predissociations are summarized in Table I. When the break-offs in the various branches are compared, it can be seen that the break comes between the doublet splitting of the $N' = 12$ level of $\text{HBr}^+(\text{A}^2\Sigma^+, v = 1)$, defining the predissociation to within that 25- cm^{-1} interval. Similarly, the break in

(6) G. Herzberg, "Molecular Spectra and Molecular Structure. I. Spectra of Diatomic Molecules," Van Nostrand, Princeton, N. J., 1950, p 162.

(7) M. J. Haugh, Ph.D. Thesis, University of California, Los Angeles, Calif., 1968.

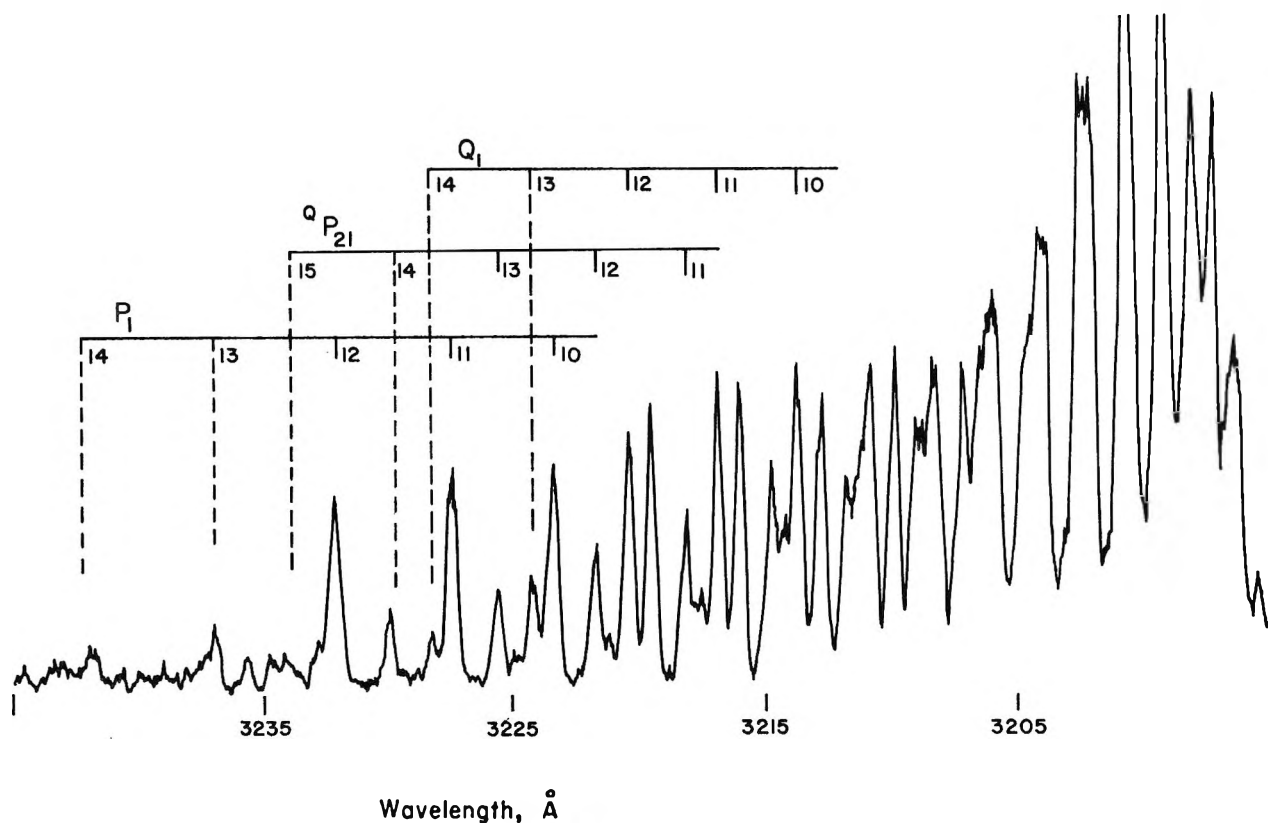


Figure 3. Spectrum of the $\text{DBr}^+(\text{A}^2\Sigma^+(v' = 2) \rightarrow \text{X}^2\pi_{3/2}(v'' = 0))$ band in emission. The weak lines are indicated by dashed lines. The numbers shown are N' .

Table I: The Predissociations Observed in the $\text{A}^2\Sigma^+ \rightarrow \text{X}^2\pi_i$ System of HBr^+ and DBr^+ . All Energies Are Relative to the $\text{HBr}^+(\text{A}^2\Sigma^+, v = 0, N = 0)$ Level

Band	Branch	Last normal level				Energy (cm^{-1})	First level of reduced intensity	
		J''	J'	N'	Level		Level	Energy (cm^{-1})
$\text{HBr}^+(1,0)$	P_2	25/2	23/2	12	$\text{F}_2(12)$	2213.1	$\text{F}_2(13)$	2357.6
	P_1	25/2	23/2	11	$\text{F}_1(11)$	2103.1	$\text{F}_1(12)$	2238.5
	Q_2	23/2	23/2	12	$\text{F}_2(12)$	2213.1	$\text{F}_2(13)$	2357.6
	Q_1	23/2	23/2	11	$\text{F}_1(11)$	2103.1	$\text{F}_1(12)$	2238.5
	PQ_{12}	23/2	23/2	11	$\text{F}_1(11)$	2103.1	$\text{F}_1(12)$	2238.5
$\text{HBr}^+(0,0)$	RQ_{21}	23/2	23/2	12	$\text{F}_2(12)$	2213.1	$\text{F}_2(13)$	2357.6
	RQ_{21}	39/2	39/2	20	$\text{F}_2(20)$	2433.4	$\text{F}_2(21)$	2677.8
$\text{DBr}^+(2,0)$	R_1	39/2	41/2	20	$\text{F}_1(20)$	2476.5	$\text{F}_1(22)$	2935.1
	P_1	27/2	25/2	12	$\text{F}_1(12)$	2128.7	$\text{F}_1(13)$	2202.0
	Q_1	25/2	25/2	12	$\text{F}_1(12)$	2128.7	$\text{F}_1(13)$	2202.0
	QP_{21}	27/2	25/2	13	$\text{F}_2(13)$	2188.5	$\text{F}_2(14)$	2266.5
	RQ_{21}	25/2	25/2	13	$\text{F}_2(13)$	2188.5	$\text{F}_2(14)$	2266.5

the $\text{DBr}^+(\text{A}^2\Sigma^+, v = 2)$ structure occurs between the two $N' = 13$ levels, which are only 13.5 cm^{-1} apart.⁸

Discussion

A predissociation may be used to establish a dissociation limit, but only if the type of predissociation can be established. This usually requires the observation of predissociation in three or more different vibrational levels.

One type of predissociation, called type III by Herzberg,⁹ occurs when the effective potential energy curve (electronic plus vibrational plus rotational) becomes entirely repulsive. For low vibrational levels, this occurs only for high rotational quantum numbers. With more vibrational energy, less rotation is required, but always the total energy must be above the dissociation limit for that particular *electronic* state. This type of "predissociation by pure rotation" can be eliminated for

HBr⁺, since the dissociation limit for the A²Σ⁺ state should be well above the observed predissociations. (Compare the corresponding A²Σ⁺ state of HCl⁺.¹⁰)

Then the predissociation must be caused by another electronic state crossing the A²Σ⁺ state. Herzberg distinguishes three different cases,⁹ depending on whether the crossing point is above the dissociation limit (case Ic), below it (case Ib), or just at the dissociation limit (case Ia). Case Ic can be most easily distinguished by comparing the break-off in two different vibrational states. Consider the general formula for the effective potential energy $U_N(r)$ of the predissociating state

$$U_N(r) = U_0(r) + \frac{\hbar^2}{8\pi^2\mu r^2} N(N+1) \quad (3)$$

where the first term, $U_0(r)$, gives the purely electronic potential, and the second term is the rotational energy at a particular internuclear distance r . The reduced mass is μ , and N represents the nuclear rotation quantum number. If the crossing point for the rotationless curves is above the dissociation limit at an internuclear distance r_c , then the maximum in $U_N(r)$ for values of $N > 0$ will also occur at approximately r_c . Now by considering the energy difference between two observed break-offs, ΔU , and the two rotational quantum numbers corresponding to the break-offs, N_1 and N_2 , the value of r_c can be calculated.

$$\Delta U = \frac{\hbar^2}{8\pi^2\mu r_c^2} \{N_2(N_2+1) - N_1(N_1+1)\} \quad (4)$$

When this is done with the HBr⁺ ($v' = 1$ and $v' = 0$) predissociations, the calculated crossing point is about 3.3 Å. Since this internuclear distance is considerably larger than the distances involved in the lower part of the A²Σ⁺ state, for which $r_e = 1.68$ Å, this type of curve crossing is not compatible with the observations in HBr⁺. For the same reason it is unlikely that the predissociating state crosses the A²Σ⁺ state close to the dissociation limit. Therefore, the predissociating state is stable, crossing the A²Σ⁺ curve at a point below the dissociation limit. As will be seen later, this state is almost certainly the ⁴π state arising from the ground-state atoms H(²S) and Br⁺(³P₂).

Even though the predissociation in HBr⁺ has been established as case Ib, it is still possible that the rotationless predissociating state has a potential maximum at large internuclear distances. If that were true, any extrapolation of the break-off energies to the rotationless state would not yield a true dissociation limit, but rather the dissociation limit plus the unknown barrier height. Only if there is no potential maximum will an extrapolation to the rotationless state give a true dissociation limit. These two possibilities, case Ib with or without a potential maximum, can be distinguished by making a plot of total energy at the observed break-

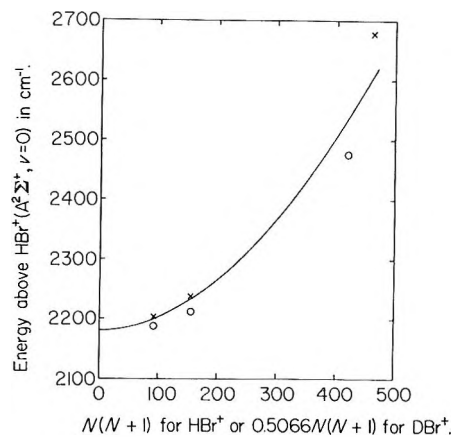


Figure 4. The limiting curve of dissociation for HBr⁺ and DBr⁺. The pair of points to the left are for DBr⁺, the others for HBr⁺. The energy intercept is 2180 ± 20 cm⁻¹.

offs as a function of $N'(N'+1)$. If there is a significant potential maximum, the plot will be a straight line, since the critical internuclear distance, r_m , at which $U_N(r)$ has its maximum, will remain approximately constant as N' increases. If there is no potential maximum, the r_m values increase rapidly as $N' \rightarrow 0$, and the plot of break-off energy vs. $N'(N'+1)$ is curved, with a slope that approaches zero as $N' \rightarrow 0$. Only in this latter case does the energy limit for $N' \rightarrow 0$ correspond to a true dissociation limit.

The break-off energy plot of HBr⁺ is shown in Figure 4. For each break-off the first rotational level which has a significantly decreased emission is given as a cross, while the last normal level is indicated with a circle. The limiting curve of dissociation has been sketched in so as to pass between each pair.

Since there are only two break-offs for HBr⁺, these cannot distinguish between a straight line and a curve. However, when the break-off for DBr⁺ ($v' = 2$) is added to the plot, a straight line cannot be drawn through the three intervals, but a curved line with zero slope at $N' = 0$ can be drawn. It is concluded that

(8) By chance, the energy of the DBr⁺(A²Σ⁺, $v = 2$) level, relative to the HBr⁺(A²Σ⁺, $v = 0$) level, can be calculated quite accurately, even though the vibrational constants of the A²Σ⁺ state are not known accurately. Letting a superscript *i* denote the heavier molecule, then the vibrational energy difference

$$G^i(v=2) - G^i(v=0) = \rho\omega_e(2.5) - \rho^2\omega_e x_e(2.5)^2 - \omega_e(0.5) + \omega_e x_e(0.5)^2$$

where ω_e and $\omega_e x_e$ refer to the HBr⁺ molecule, and ρ^2 equals the ratio of reduced masses, μ/μ^i . Inserting values for ρ and ρ^2 and simplifying gives

$$G^i(v=2) - G^i(v=0) = 1.27941[\omega_e - 2\omega_e x_e] - 0.3575\omega_e x_e$$

Now although neither ω_e nor $\omega_e x_e$ is known accurately, the difference ($\omega_e - 2\omega_e x_e$) is, since this is just the $\Delta G^{1/2}$ measured by Barrow and Caunt² as 1328.7 cm⁻¹. Thus using their estimated value of $\omega_e x_e \cong 40$ cm⁻¹ gives a value for $G^i(v=2) - G^i(v=0)$ of 1685.7 cm⁻¹, while an error of $\pm 20\%$ in the value of $\omega_e x_e$ will cause an error of only ± 3 cm⁻¹ in the energy separation.

(9) See pages 420–432 of ref 6.

(10) F. Norling, *Z. Phys.*, **104**, 638 (1935).

there is no maximum in the $U_0(r)$ curve and that the extrapolated energy limit, $2180 \pm 20 \text{ cm}^{-1}$, represents a true dissociation limit.^{11,12} The error limits on this value represent only the uncertainty in the curve, and not the possible uncertainties in the analysis of the DBr^+ spectrum. When a proper rotational analysis has been done, Figure 4 should be redone using the measured parameters for DBr^+ .

The states of the atoms formed by the predissociation cannot be determined from the predissociation alone. However, by using the relationship between ionization potentials, I , and dissociation energies, D

$$I(\text{HBr}) + D^{\circ}_0(\text{HBr}^+) = D^{\circ}_0(\text{HBr}) + I(\text{H or Br}) \quad (5)$$

combined with other measurements it is possible to determine the products. The dissociation energy, $D^{\circ}_0(\text{HBr}^+, \text{X}^2\pi_{3/2})$, will be just the sum of the ν_{00} for the transition $\text{A}^2\Sigma^+ \rightarrow \text{X}^2\pi_{3/2}$, which Norling¹ measured as $29,227 \text{ cm}^{-1}$, and the predissociation limit shown in Figure 4; thus $D^{\circ}_0(\text{HBr}^+)$ is $31,407 \pm 20 \text{ cm}^{-1}$, or $3.894 \pm 0.003 \text{ eV}$, where the products of the dissociation are not yet specified. The ionization potential of HBr has been measured several times recently,¹³⁻¹⁶ and the range $11.67 \pm 0.05 \text{ eV}$ encompasses the measured values. The dissociation energy for neutral HBr can be calculated from thermodynamic tables¹⁷ as 86.64 kcal/mol , or $30,303 \text{ cm}^{-1}$. When the possible atomic ionization energies are added to this dissociation energy, the possible energy limits are shown in Table II. Since the sum of $D^{\circ}_0(\text{HBr}^+)$ and $I(\text{HBr})$ is $125,500 \pm 400 \text{ cm}^{-1}$, this energy limit is compatible only with the atomic states $\text{H}(^2\text{S})$ and $\text{Br}^+(^3\text{P}_2)$.

Table II: The Lowest Energy States for the System $(\text{H} + \text{Br})^+$

Atomic states	Total energy above HBr
$\text{H}(^2\text{S}) + \text{Br}^+(^3\text{P}_2)$	$125,588 \text{ cm}^{-1}$
$\text{H}(^2\text{S}) + \text{Br}^+(^3\text{P}_1)$	$128,724 \text{ cm}^{-1}$
$\text{H}(^2\text{S}) + \text{Br}^+(^3\text{P}_0)$	$129,425 \text{ cm}^{-1}$
$\text{H}^+(^1\text{S}) + \text{Br}(^2\text{P}_{3/2})$	$139,982 \text{ cm}^{-1}$

Since the ionization potential of the bromine atom has been measured accurately as $95,285 \text{ cm}^{-1}$,¹⁸ the spectroscopic measurements now may be combined to provide an accurate relationship between $I(\text{HBr})$ and $D^{\circ}_0(\text{HBr})$.

$$I(\text{HBr}) = D^{\circ}_0(\text{HBr}) + 63,878 \pm 30 \text{ cm}^{-1} \quad (6)$$

If the above value for $D^{\circ}_0(\text{HBr})$ is used, the calculated value for $I(\text{HBr})$ becomes $11.677 \pm 0.004 \text{ eV}$. Since this value agrees well with recent measurements,^{15,16} the energetics of the HBr system appear to be well established.

The combination of a ^2S hydrogen atom and a ^3P Br^+ can result in a total of four molecular states: $^2\Sigma^-$, $^2\pi$, $^4\Sigma^-$, $^4\pi$. The resulting $^2\pi$ state can be identified with the ground state of HBr^+ , $\text{X}^2\pi_i$. Since both of the Σ states are Σ^- states, they cannot be predissociating the $\text{A}^2\Sigma^+$ state, due to the rigorous selection rule, $+ \leftarrow | \rightarrow -$, for perturbations.¹⁹ Therefore the predissociating state must be $^4\pi$, as was previously concluded by Lemka, *et al.*¹⁵ Since the predissociation is spin forbidden, the break-off may not be complete, which could explain the fact that Norling was able to observe lines photographically beyond the break-off.¹ The conclusion that the $^4\pi$ state must have a potential minimum is in contrast to the potential energy curves drawn by Lemka, *et al.*

Acknowledgments. This paper is offered as an encomium to Dr. G. B. Kistiakowsky for his gracious help and inspiration during the past 15 years. For financial support we thank the Air Force Office of Scientific Research (AF-AFOSR 687-64) and the National Aeronautics and Space Administration for a Predoctoral Traineeship (to M. J. H.).

(11) This reasoning would not be valid if there were a significant maximum in the $U_0(r)$ curve and tunnelling were occurring. Since HBr^+ and DBr^+ have different reduced masses, their tunnelling probabilities are different and the points for HBr^+ would lie on a curve below those for DBr^+ (*cf.* AlH and AlD^2). However, as was shown earlier, if there is a maximum in $U_0(r)$ then its position occurs at about 3.3 \AA . It has not been possible to construct a curve $U_0(r)$ with a maximum at 3.3 \AA that can give the observed break-offs as sharply as observed, and *at essentially the same energy* for $\text{HBr}^+(v' = 1)$ and $\text{DBr}^+(v' = 2)$. Although tunnelling may be responsible for the incomplete break-off observed in $\text{HBr}^+(v' = 0)$, there is at present no evidence for a potential maximum in $U_0(r)$.

(12) C. Herzberg and L. C. Mundie, *J. Chem. Phys.*, **8**, 263 (1940).

(13) K. Watanabe, T. Nakayama, and J. T. Mottl, *J. Quant. Spectrosc. Radiat. Transfer*, **2**, 369 (1962).

(14) D. C. Frost, C. A. McDowell, and D. A. Vroom, *J. Chem. Phys.*, **46**, 4255 (1968).

(15) J. H. Lemka, T. R. Passmore, and W. C. Price, *Proc. Roy. Soc. Ser. A*, **304**, 53 (1968).

(16) D. W. Turner, C. Baker, A. D. Baker, and C. R. Brundle, "Molecular Photoelectron Spectroscopy," Wiley-Interscience, London, 1970.

(17) D. D. Wagman, W. H. Evans, V. B. Parker, I. Halow, S. M. Bailey, and R. H. Schumm, "Selected Values of Chemical Thermodynamic Properties," National Bureau of Standards (U. S.) Technical Note 270-4, U. S. Government Printing Office, Washington, D. C., 1969.

(18) R. E. Huffman, J. C. Larrabee, and Y. Tanaka, *J. Chem. Phys.*, **47**, 856 (1967).

(19) See p 416 of ref 6.

Selective Solvation of Ions by Water in Propylene Carbonate

by David R. Cogley, James N. Butler,*¹ and Ernest Grunwald

Tyco Laboratories, Inc., and Brandeis University, Waltham, Massachusetts 02154 (Received December 17, 1970)

Publication costs assisted by Harvard University

Proton magnetic resonance (chemical shift) measurements of water at low concentrations in propylene carbonate (PC) containing various salts have been made at 60 MHz and 36.4°. From these data the equilibrium constants for association of water with individual ions have been obtained under a relatively mild set of extra-thermodynamic assumptions. The molal association constants K_1 are 6.5 for Li^+ , 1.4 for Na^+ , 0.4 for K^+ , and 6.2 for Cl^- . Additional order-of-magnitude estimates are 0.3 (Et_4N^+), 0.3 (BF_4^-), 0.3 (ClO_4^-), 0.1 (BPh_4^-), and 0.4 (LiCl ion pair). Stepwise constants for addition of 2 and 3 water molecules to Li^+ are $K_2 = 2.7$ and $K_3 = 1.9$. The chemical shift of protons on a water molecule associated with an ion, compared with a water molecule in PC alone, varies from approximately 150 Hz for BPh_4^- to +95 Hz for Li^+ . The affinity of water at low concentrations in PC for alkali metal cations correlates well with the free energy of transfer of these ions from PC to bulk water; but the free energy of transfer for a chloride ion (-11.3 kcal) is more than 10 times the free energy of formation of a chloride-water bond in PC. This reflects the stabilization of chloride ion in water by cooperative interactions which are at least as important as the direct coordination of the ion by H_2O molecules.

Introduction

The wide variation in reactivity of ions in different solvents is well known, and is usually discussed in terms of solvation energies and medium effects, or thermodynamic functions of transfer from one pure solvent to another.²⁻⁵ In mixtures of solvents, where the first solvation shell of different ions may have substantially different compositions, the additional concept of selective solvation becomes an important part of understanding chemical interactions.^{3,6-9}

From the study of ionic reactions such as nucleophilic substitution,^{4,10,11} acid dissociation,^{5,12,13} solubility,¹⁴ and electrochemical potentials,¹⁵ it has become clear that a fruitful distinction can be made between dipolar aprotic solvents (dielectric constant greater than 30) and hydroxylic or hydrogen-bonding solvents. In particular, the reactivity of small anions is dramatically greater in dipolar aprotic solvents compared to hydroxylic solvents, whereas the reactivity of cations is much less sensitive to the nature of the solvent.^{3,4,13,14} For instance, the nucleophilic displacement of iodide from CH_3I by chloride ion proceeds 10^6 to 10^7 times as fast in dipolar aprotic solvents (dimethylformamide, dimethylacetamide, acetone) as in hydroxylic solvents (water, methanol).⁴ Another example is the marked reduction in basicity when small amounts of water are added to benzyltrimethylammonium hydroxide in dimethyl sulfoxide.¹²

However, a more general question may be raised. Is the high affinity of small anions for water a result of specific coordination effects (which should be apparent at low water concentrations in a dipolar aprotic solvent) or is it a cooperative phenomenon which becomes apparent only when one approaches the structure of pure water? In the case of hydroxide ion in dimethyl sulf-

oxide-water mixtures, one may infer that the water is specifically coordinated to the hydroxide ion and deactivates it,¹² but this need not be the only possible explanation in other cases. One approach to the elucidation of this problem is to measure the first association constant of water with a series of ions in dipolar aprotic solvents, and we report here a relatively direct method of obtaining this information.

For these studies we chose as solvent propylene carbonate [4-methyl-1,3-dioxolan-2-one, PC], a dipolar

(1) Visiting lecturer on applied chemistry, Harvard University, 1970-1971. Division of Engineering and Applied Physics, Harvard University, Pierce Hall, Cambridge, Mass. 02138.

(2) B. Gutbezahl and E. Grunwald, *J. Amer. Chem. Soc.*, **75**, 565 (1953).

(3) E. Grunwald, G. Baughman, and G. Kohnstam, *ibid.*, **82**, 5801 (1960).

(4) A. J. Parker, *Chem. Rev.*, **69**, 1 (1969).

(5) R. G. Bates in "The Chemistry of Nonaqueous Solvents," Vol. 1, J. J. Lagowski, Ed., Academic Press, New York, N. Y., 1966; and in "Solute-Solvent Interactions," J. F. Coetzee and C. D. Ritchie, Ed., Marcel Dekker, New York, N. Y., 1969.

(6) P. Debye, *Z. Phys. Chem.*, **130**, 56 (1927).

(7) G. Scatchard, *J. Chem. Phys.*, **9**, 34 (1941).

(8) H. Schneider in "Solute-Solvent Interactions," J. F. Coetzee and C. D. Ritchie, Ed., Marcel Dekker, New York, N. Y., 1969.

(9) L. S. Frankel, C. H. Langford, and T. R. Stengle, *J. Phys. Chem.*, **74**, 1376 (1970).

(10) R. F. Rodewald, K. Mahendran, J. L. Bear, and R. Fuchs, *J. Amer. Chem. Soc.*, **90**, 6698 (1968).

(11) R. Alexander, E. C. F. Ko, A. J. Parker, and T. J. Broxton, *ibid.*, **90**, 5049 (1968).

(12) C. D. Ritchie in "Solute-Solvent Interactions," J. F. Coetzee and C. D. Ritchie, Ed., Marcel Dekker, New York, N. Y., 1969.

(13) B. W. Clare, D. Cook, E. C. F. Ko, Y. C. Mac, and A. J. Parker, *J. Amer. Chem. Soc.*, **88**, 1911 (1966).

(14) R. Alexander, E. C. F. Ko, Y. C. Mac, and A. J. Parker, *ibid.*, **89**, 3703 (1967).

(15) J. N. Butler, *Advan. Electrochem. Electrochem. Eng.*, **7**, 77 (1970).

aprotic solvent with high dielectric constant (65.0 at 25°)¹⁶ and dipole moment (4.94 D).¹⁷ Unlike water, PC does not exhibit any strong self-association or well defined intermolecular structure, as evidenced by a Kirkwood g factor near unity (1.02 at 213°K).¹⁶ The main intermolecular forces are strong but nonspecific, and the high dielectric constant makes it possible to dissolve salts up to concentrations of several molal. Most salts are completely dissociated in dilute solutions.¹⁸ In this respect, it has been suggested that PC is a close approximation to an "ideal structureless dielectric" solvent for studies of electrolytes.¹⁹

Because PC is only weakly acidic and weakly basic, one does not expect to find highly specific coordination phenomena such as are found in solvents like dimethylformamide or dimethyl sulfoxide. It has a wide liquid range (−49.2 to 247.1° at 1 atm)²⁰ which allows one to study temperature effects easily. It is relatively resistant to chemical attack (except for acid- or base-catalyzed hydrolysis at high water concentrations), a property which has given it an important place in the development of high-energy batteries using lithium anodes. In this application, selective solvation of ions by water or organic impurities may play a crucial role in battery system performance.^{18, 21}

To probe the composition and structure of the first solvation shell, nuclear magnetic resonance provides a valuable method because of the straightforward correspondence between chemical shifts and relaxation times of resonance signals and the details of short-range structures.^{8, 9, 22, 23} We have studied chemical shifts of the proton magnetic resonance of small amounts of water in PC containing dissolved salts. On the basis of relatively mild extrathermodynamic assumptions, we have been able to obtain equilibrium constants for association of water with individual ionic species. We find that the association constant for Cl[−] with water in PC is very close to that for Li⁺ and only slightly greater than that for Na⁺. This result implies that, at least in the case of Cl[−], its much lower reactivity in water compared with dipolar aprotic solvents is due to cooperative effects at least as much as to specific coordination.

Experimental Section

Solvent. Propylene carbonate (Jefferson Chemical Co.)²⁰ was purified by distillation at approximately 2 Torr in a Podbielniak adiabatic vacuum still of approximately 50 theoretical plates. Typical concentrations of impurities (gas chromatographic analysis) were 10 ppm of propylene oxide, 20 ppm of propylene glycol, 2 ppm of allyl alcohol, and less than 2 ppm of water. Details of purification and analysis are given elsewhere.^{24, 25} Doubly distilled, CO₂-free water was used in preparation of solutions containing H₂O.

Salts. Ultrapure lithium perchlorate was obtained from Anderson Physics Laboratories. This sample was prepared from G. F. Smith 99.9% LiClO₄, recrystal-

lized three times from water, heated under vacuum for several days, and finally fused under vacuum and sealed in glass under argon. It contained less than 0.0015% H₂O and less than 0.0005% Cl.²⁶

Lithium tetrafluoroborate (Foote Mineral Company) in the form of a fine, free-flowing white powder was used as received. Flame photometric analysis (Instrumentation Laboratories Model 143A, 1 mM KCl internal standard, 0.02% wetting agent) indicated 0 ± 1 mol % Na and 103 ± 1 mol % of the expected Li content. The Li calibration was made with ultrapure LiCl (see below). The most likely impurity was LiF (*i.e.*, 96 mol % LiBF₄, 4 mol % LiF). Because hydrolysis and solvate formation occur so easily with BF₄[−] and PF₆[−] salts, we did not attempt further purification by recrystallization. The salt as received had already been recrystallized several times from a proprietary solvent which showed the least decomposition effects of more than 60 solvents tested.²⁷

Lithium tetraphenylboride was custom synthesized by Veron, Inc. Flame photometric analysis showed that the salt contained 0 ± 1 mol % Na, but only 58 ± 5 % of the expected Li content. (Since K⁺ is the internal standard for the flame photometer, accuracy was limited in these analyses by corrections for the limited solubility of KBPh₄.) After 3 days under vacuum at 25°, the salt was analyzed for BPh₄[−] by titration with KCl in aqueous solution using a potassium-selective liquid ion-exchange electrode (Orion Research Inc.), and found to contain 58.0 ± 0.6% LiBPh₄, in agreement with the flame photometry. Integration of nmr water peak areas of LiBPh₄ solutions in PC indicated that the salt contained 0.54 mol of water per mol of LiBPh₄, which accounts for only 1.7% additional weight of the impure salt. Since one could detect the odor of acetone (the solvent from which the salt had been recrystallized) after dissolution in water, it seems likely

(16) L. Simeral and R. L. Amey, *J. Phys. Chem.*, **74**, 1443 (1970).

(17) R. Kempa and W. H. Lee, *J. Chem. Soc.*, 1936 (1958).

(18) R. J. Jasinski, *Advan. Electrochem. Electrochem. Eng.*, in press.

(19) H. L. Friedman, *J. Phys. Chem.*, **71**, 1723 (1967).

(20) "Propylene Carbonate, Technical Bulletin," Jefferson Chemical Company, Houston, Texas, ca. 1962. The practical liquid range of PC is even greater because it may be supercooled to as low as −80° for several months.

(21) J. N. Butler, D. R. Cogley, and E. Grunwald, *Ingenieurs EPCI*, in press.

(22) J. F. Hinton and E. S. Amis, *Chem. Rev.*, **67**, 367 (1967).

(23) J. Burgess and M. C. R. Symons, *Quart. Rev., Chem. Soc.*, **22**, 276 (1968).

(24) R. J. Jasinski and S. Kirkland, *Anal. Chem.*, **39**, 1663 (1967).

(25) J. N. Butler, R. J. Jasinski, D. R. Cogley, H. L. Jones, J. C. Synnott, and S. Carroll, "Purification and Analysis of Organic Non-aqueous Solvents," Final Report, Contract F19628-68-C-0052, 1970. AFCRL-70-0605.

(26) J. N. Butler, D. R. Cogley, J. C. Synnott, and G. Holleck, "Study of the Composition of Nonaqueous Solutions of Potential Use in High Energy Density Batteries," Final Report, Contract No. AF 19(628)6131, 1969. AFCRL-69-0470, AD-699589.

(27) R. Carter (Foote Mineral Co.), private communication, 1969.

that the salt received from the manufacturer was actually $\text{LiBPh}_4 \cdot 4(\text{CH}_3\text{COCH}_3)$. (The unaccounted weight fraction corresponds to 3.9 mol of acetone per Li.) LiBPh_4 is quite sensitive to thermal decomposition, so it cannot be recrystallized from a high-boiling solvent such as PC. Since acetone is chemically similar to PC, the salt was used as received. Attempts to recrystallize it from another volatile solvent seemed likely only to introduce additional impurities. Concentrations of solutions used in the actual measurements were calculated from the salt composition determined experimentally.

Lithium chloride was prepared by Anderson Physics Laboratories, by fusion in a molybdenum apparatus under vacuum, flushing with anhydrous HCl and purging with argon while molten, and sealing in quartz under argon. This salt contained less than 0.01% water, hydroxide, or oxide.

Sodium perchlorate (G. F. Smith Co.), sodium chloride, potassium chloride, sodium tetraphenylborate (Fisher Certified), tetraethylammonium perchlorate, and tetraethylammonium chloride (Eastman) were used as received after storage in a dry argon atmosphere to remove any superficial water.

Sample Handling. All materials were stored and all samples were prepared in a Vacuum Atmospheres drybox with an argon atmosphere containing less than 1 ppm of water or oxygen. The atmosphere was recirculated and purified continuously. Purity of the atmosphere was checked with a 60-W incandescent bulb whose glass envelope had been removed. Such a bulb continued to glow in the drybox atmosphere for 6 to 12 hr before burning out. Shiny lithium or lithium-sodium alloys left exposed to the drybox atmosphere as getters did not discolor over a span of 1 year. A vacuum antechamber was used to transfer samples in and out of the box. Neoprene gloves (60 mil) were used to keep moisture and oxygen transport through the gloves to a minimum.

Salt solutions and PC-water mixtures were prepared by weight inside the drybox. Aliquots of stock solutions were diluted by weight to obtain low concentrations. Nmr tubes (Wilma Type 517 PP) were stoppered with plastic pressure caps and care was taken to avoid contact of solution with the plastic. If excess gas space was left above a very small sample of solution, the evaporation of water into this gas space could be observed over a period of several days as a decrease in nmr peak intensity, but this was not a major source of error if the liquid filled most of the tube. Measurements of chemical shift were generally performed immediately after sample preparation. LiPF_6 samples were found to hydrolyze rapidly, and eventually consumed all water present in the solvent, so that results with this salt were irreproducible. LiBF_4 samples hydrolyzed only slightly, and the change in chemical shift was less than 1 Hz over a period of 2 weeks.

Solubilities. The solubility of alkali chloride salts in PC and PC-water mixtures was obtained by magnetically stirring 5–10 g of the finely powdered salt in 30 g of solvent at $20 \pm 1^\circ$ in the drybox for 1 day and then allowing the salt to settle for a day or more before withdrawing an aliquot for analysis. Solutions were analyzed for alkali metal by flame photometry and for chloride by potentiometric titration with aqueous AgNO_3 .^{26,28} A Gran²⁹ plot was used to obtain the end point. For unsaturated LiCl, the chloride content obtained in this manner was within 1% of that prepared by weight; but for NaCl and KCl, which become saturated at concentrations less than millimolar, the error in analysis was about 4%. No trend in solubility with time was found for samples taken after 1 day, indicating that equilibrium had been reached and that no solid salt had been withdrawn with the solution.

Nuclear Magnetic Resonance. Nmr measurements were made at 60 MHz and a constant temperature of 36.4° fixed by the Varian T-60 permanent magnet spectrometer. The frequency lock (Permalock) module overcame the problem of field drift and allowed chemical shifts to be determined to ± 0.1 Hz in most cases. Stability was within 0.3 Hz over a period of 1 day. Frequency calibration was carried out by applying a side band from a square-wave generator (Wavetek Model 112) and measuring the frequency of a synchronized square-wave output on the spectrometer digital indicator in the 10-sec gate mode, taking the average over about 1 min.²⁸ The field was optimized as directed by the manufacturer at the beginning of each series of measurements. Resolution for an acetaldehyde sample at a sweep rate of 0.1 Hz/sec was normally 0.3 Hz.

The lower limit of detection of the water proton resonance was between 2 and 5 mm. Normally, samples contained at least 20 mm water. In this concentration range the water resonance can become obscured by spinning side bands and carbon-13 satellite peaks of the solvent, or base line noise. In most cases, spinning side bands with up to 50 times the amplitude of the water resonance could be moved out of the way by varying the spinning rate.¹⁶ Multiple upfield and downfield scans were used to counteract the effects of filtering.

For each sample, chemical shifts were referenced to the center of the PC methyl doublet, with the spectrometer normally being locked on the strongest resonance (approximately 200 Hz downfield) of the methylene-methine multiplets.²⁶ Comparison of the PC solutions containing water and salt with pure PC and with tetramethylsilane was made using coaxial (Wilma Type 517) nmr tubes. The methyl doublet resonance frequency was found to be independent of

(28) D. R. Cogley, "Water Association and Ion Hydration in Propylene Carbonate," Ph.D. Thesis, Brandeis University, 1970. University Microfilms No. 70-24623.

(29) G. Gran, *Analyst (London)*, **77**, 661 (1952).

Table I: Chemical Shifts for Water in Propylene Carbonate Salt Solutions^a

Salt	Cs, m	Cw, m	$\nu_{\text{expt.}}$ Hz	$\nu_{\text{cor.}}^c$ Hz	Salt	Cs, m	Cw, m	$\nu_{\text{expt.}}$ Hz	$\nu_{\text{cor.}}^c$ Hz			
LiClO ₄	0.754	0.0289	134.6	134.7	NaClO ₄	0.884	0.111	90.8	90.5			
		0.0577	134.1									
		0.1211	133.9									
		0.2754	133.0									
		0.557	131.6									
	0.1544	0.0246	104.1	104.5	NaBPh ₄	0.202	0.111	70.6	70.3			
		0.0487	103.6									
		0.0844	102.8									
		0.218	100.7									
		0.496	98.1									
	0.0298	0.0199	69.9	70.0	Et ₄ NClO ₄	0.197	0.111	56.9	54.9			
		0.0288	69.9									
		0.0820	69.7									
		0.1541	70.6									
		0.386	71.0									
LiBPh ₄ ^b	0.2261	0.213	113.0		Et ₄ NCl	0.0276	0.0263	68.0	68			
		0.1071	93.6									
		0.0890	89.1									
		0.0798	86.6							89.3		
		0.0597	80.6							82.8		
	0.0435	0.114	75.0	76.5		0.0276	0.187	66.4				
		0.0200	65.0	65.1								
		0.0084	63.0 ?									
		0.0645	80.5	82								
		0.0645	0.0828	80.1								
	LiBF ₄ ^d	1.223	0.0304	130.5 ?			0.0645	0.172	77.4			
											1.050	130.1 ?
											0.949	129.7 ?
											0.790	128.6 ?
											0.520	124.2 ?
0.228		0.0304	110.3	110.7	None ^f	0.0	0.0	(53.7)	53.7			
										0.215	109.1	109.6
										0.102	92.4	92.9
										0.0473	77.0	77.4
										0.0286	69.5	69.7
	0.0304	109.1	109.6		0.0303	0.0686	55.0					
									0.102	92.4	92.9	
									0.0473	77.0	77.4	
									0.0286	69.5	69.7	
									0.0276	0.237	137.6 ? ^e	~140
0.5276	1.160	118.2										

^a Spectrometer frequency 60 MHz, 36.4°. Reference frequency is the center of the methyl doublet of neat propylene carbonate. All values corrected for magnetic susceptibility effects. Precision of ν is ~ 0.1 Hz. ^b Salt was LiBPh₄·4(CH₃COCH₃). No attempt has been made to correct for the presence of small amounts of acetone, but these effects are presumed negligible. ^c Corrected or extrapolated to zero water concentration. ^d Concentrations corrected to reflect the small amount of LiF present in the original salt which precipitated out of solution. First 5 points uncertain because of this. ^e Substantial broadening (3–8 Hz) of H₂O peak but not carbon-13 satellite of solvent or ethyl group. ^f Additional data for H₂O-PC mixtures are given in ref 26, 28, and 30.

water concentration but shifted to lower field with increasing salt concentration. The magnitude of these shifts were 1.6 Hz for LiClO₄, 1.0 Hz for LiBPh₄, and 0.8 Hz for LiBF₄ at 1 *m* salt, corrected for differences in magnetic susceptibility.²⁸ All chemical shift data reported in this paper for salt solutions have been corrected for this effect, and thus are referred to the center of the methyl doublet in pure propylene carbonate.

Results

The chemical shift data obtained from small amounts of water in the presence of LiClO₄, LiBPh₄, LiBF₄, NaBPh₄, Et₄NClO₄, and Et₄NCl are given in Table I. The concentration ranges where accurate data could be

obtained were limited by interference from the ethyl resonances in the case of the tetraethylammonium salts. Water concentrations in Table I include the water introduced with the salt, if any. The acetone introduced with the LiBPh₄ reagent was assumed to resemble propylene carbonate sufficiently closely that a few mole per cent of acetone in the solvent would not substantially affect the ion hydration equilibria. This assumption seems to be borne out since the LiBPh₄ data fell on the same curve as the LiClO₄ data. The highest concentration data for LiBF₄ were sufficiently uncertain (because of LiF precipitation) that only the data obtained at 0.228 *m* and below were used in quantitative analysis.

The chemical shift of water in the absence of salt (ν_w) is dependent on water concentration, since self-association of water in PC occurs to some extent²⁸ ($K_{\text{dimer}} \sim 0.1$ kg/mol) and this is discussed in detail in another paper.³⁰ At low water concentrations, the expression

$$\nu_w = 53.7 + 19.4C_w \quad (1)$$

is obtained, where C_w is the concentration of water in mol/kg.

Chemical shifts were extrapolated to zero water concentration where possible or corrected using eq 1 and approximate association constants to obtain the concentrations and chemical shifts of the various water-containing species. In Figure 1, these corrected values are plotted and compared with calculated curves obtained as described below.

The most significant observation to be made is that the chemical shift for LiClO_4 , LiBPh_4 , and, less certainly, LiBF_4 all fall on a single curve. Similarly, the values for both sodium salts fall on a single lower curve in Figure 1. There is virtually no change in chemical shift on adding Et_4NClO_4 , but the change on adding Et_4NCl is as large as that for lithium salts. From these results we may conclude qualitatively that water is strongly bound to Li^+ and Cl^- , less strongly bound to Na^+ , and shows very little preference for the other ions as compared to the solvent.

A quantitative analysis of these results may be made rigorously for data extrapolated to zero water concentration, since in this limit only 1:1 water-ion complexes are appreciable and association of water with itself is negligible. This is further simplified if the rate of proton exchange is either very slow or very fast.

The nmr results for all solutions studied demonstrate that the rate of exchange of protons between the first solvation shell and the bulk of the solution is quite rapid. If very slow exchange took place, one would expect to resolve separate resonances for the different protons.^{8,9,22,23} No more than one resonance which could be attributed to water was ever observed. For intermediate rates of exchange, one might see broadening of a single water peak to a non-Lorentzian shape when the proton exchange rate was approximately $2\pi(\nu_1 - \nu_0)$, where ν_1 is the chemical shift of a proton in the solvation shell and ν_0 is for unbound water in the solvent.^{30,31} Again no broadening of the peaks was observed at any concentration of water or salt studied. A possible exception was the highest concentration range of Et_4NCl and lowest concentrations of H_2O , where broadening of 3–8 Hz was observed for H_2O but not for the ethyl or PC resonances. However, no quantitative analysis of exchange kinetics was made. For all other cases, the exchange rate is considerably faster than $2\pi(\nu_1 - \nu_0)$, and the fast-exchange approximation is valid.

For a system where fast exchange occurs between a

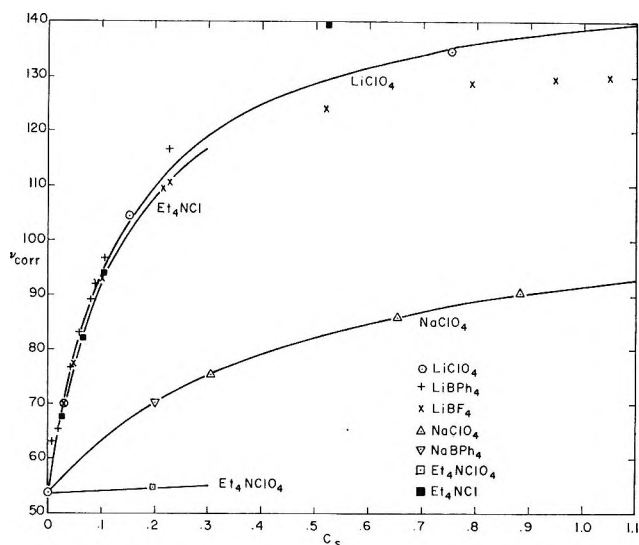


Figure 1. Chemical shift of water at infinite dilution in PC as a function of salt concentration. Data points are from Table I, corrected to zero water concentration, and curves are calculated from eq 5.

set of protons, a single resonance line is obtained, whose frequency shifts with the composition of the solution, according to a relation of the type³¹

$$\nu - \nu_0 = \sum(\nu_i - \nu_0)f_i \quad (2)$$

where f_i are mole fractions of the various solute species, ν_i are the hypothetical chemical shifts for the protons in those species, and ν_0 is a reference frequency which we have chosen to be the water resonance at zero concentration. (If a species contains two or more equivalent protons, ν_i is the weighted average of the chemical shifts for all protons in that species for which fast exchange occurs.) The various concentrations of individual species are related by the usual mass balance and equilibrium conditions.³² Thus, for each unknown equilibrium introduced into the chemical model of the system, two adjustable parameters are obtained: an equilibrium constant and a hypothetical chemical shift. It is therefore desirable to have as many cross-checks as possible, if reliable equilibrium constants are to be obtained.

For a 1:1 salt, MA, at low water concentrations, we may expect monoaquo complexes of each ion to form. If their formation constants are represented by K_1^M and K_1^A , and the hypothetical chemical shift of water protons in these complexes are represented by ν_1^M and ν_1^A , ν_0 is the resonance frequency of water in the absence of salt, C_s is the total salt concentration, C_w is the total

(30) D. R. Cogley, M. Falk, J. N. Butler, and E. Grunwald, unpublished works.

(31) L. M. Jackman and S. Sternhell, "Applications of Nuclear Magnetic Resonance Spectroscopy in Organic Chemistry," Pergamon Press, London, 1969.

(32) J. N. Butler, "Ionic Equilibrium," Addison-Wesley, Reading, Mass., 1964.

water concentration, and $[H_2O]$ is the free water concentration (not bound to any ions), we obtain the relations

$$C_w = [H_2O] \left(1 + \frac{K_1^M C_s}{1 + K_1^M [H_2O]} + \frac{K_1^A C_s}{1 + K_1^A [H_2O]} \right) \quad (3)$$

$$\nu - \nu_0 = \frac{[H_2O]}{C_w} \left(\frac{K_1^M C_s (\nu_1^M - \nu_0)}{1 + K_1^M [H_2O]} + \frac{K_1^A C_s (\nu_1^A - \nu_0)}{1 + K_1^A [H_2O]} \right) \quad (4)$$

which may be simplified in the case of weak association ($K_1[H_2O] \ll 1$) to give

$$\nu - \nu_0 = C_s \left(\frac{K_1^M (\nu_1^M - \nu_0) + K_1^A (\nu_1^A - \nu_0)}{1 + C_s (K_1^M + K_1^A)} \right) \quad (5)$$

This can be used as the basis of a linear plot: a graph of $(\nu - \nu_0)/C_s$ vs. $\nu_0 - \nu$ has slope $K_1^M + K_1^A$ and intercept $K_1^M(\nu_1^M - \nu_0) + K_1^A(\nu_1^A - \nu_0)$. Thus the combined equilibrium constants and the combined hypothetical chemical shifts for cation and anion can be determined. All these relations are exact in the limit of zero water concentration, since any medium effect of water goes to zero; and the medium effect of salt becomes exactly additive, as indicated by eq 5. The curves of Figure 1 were plotted using eq 5, and the fit is excellent. The parameters, together with the standard deviation of ν , are given in Table II. Division of these into single-ion contributions will be discussed in the next section.

Solubilities of the alkali chlorides in anhydrous PC and in PC containing 0.1068 *m* water were measured and are listed in Table III. The values for LiCl are

Table II: Parameters for Salt Effect at Zero Water Concentration

Salt	Slope ^a	Intercept ^b	Std dev ^c
LiClO ₄	6.8 ± 0.3	663 ± 16	0.8
LiBPh ₄	6.8 ± 0.3 ^d	660 ± 20	1.0
LiBF ₄	6.8 ± 0.3 ^d	630 ± 20	1.6
NaClO ₄	1.7 ± 0.2	98 ± 2	0.5
NaBPh ₄	1.7 ± 0.2 ^d	97 ± 5	~0.5 ^d
Et ₄ NClO ₄	<0.5 ^d	6 ± 1	~0.2
Et ₄ NCl	6.5 ± 0.3	624 ± 9	~1.0 ^e

^a $K_1^M + K_1^A$, kg/mol. Error is standard deviation, but absolute values are sensitive to ν_0 (3 Hz error in ν_0 changes K_1 by as much as 20%). ^b $K_1^M(\nu_1^M - \nu_0) + K_1^A(\nu_1^A - \nu_0)$, (kg Hz)/mol. Error is standard deviation. ^c Standard deviation of ν_{cor} (Table I) from ν_{calcd} (eq 5) Hz. ^d Estimated. Observed slopes for LiBPh₄ and LiBF₄ were considered unreliable due to impurities, and were assumed to be equal to the LiClO₄ slope. The point for NaBPh₄ is <0.5 Hz from the NaClO₄ line. The slope for Et₄NClO₄ was inferred by arguments presented in the Discussion. ^e Higher concentration points were given less weight to reflect uncertainties due to line broadening.

Table III: Solubility of Alkali Chlorides^a

Salt	Solubility in dry PC, mm	Solubility in wet PC, mm	Literature values for "dry" PC, mm
LiCl	37.4 ± 0.4	53.0 ± 0.5	38 ^b 40 ^c 0.7 ^d
NaCl	0.122 ± 0.006	0.175 ± 0.009	0.003 ^d
KCl	0.352 ± 0.020	0.476 ± 0.020	0.27 ^d

^a Dry PC: $C_w = 0.0001$ *m*. Wet PC: $C_w = 0.1068$ *m*. ^b R. Keller, J. N. Foster, D. C. Hanson, J. F. Hon, and J. S. Muirhead, "Properties of Nonaqueous Electrolytes," NASA CR-1425, Aug 1969, N69-36413. ^c See ref 33. ^d See ref 34.

consistent with those measured previously by other workers and confirmed in our laboratory.³³ The solubility data for alkali chlorides obtained by Harris,³⁴ although widely quoted (*e.g.*, ref 4), appear to be in error.

The increase in solubility of the alkali chlorides as the water concentration is increased reflects the selective association of water with the ions of the salts, and will be discussed quantitatively in the next section.

Discussion

Chemical Shift Data. The fact that the chemical shift data for all lithium salts fall on one curve and those for all sodium salts fall on another curve (Figure 1), together with the very small effect of Et₄NClO₄, permits us to make a number of rather mild extrathermodynamic assumptions which separate the equilibrium constants and chemical shifts of Table II into individual ionic contributions. For example, we would not expect the contributions of ClO₄⁻ and BPh₄⁻ to be the same unless they were both very small, since ClO₄⁻ is chemically similar to the oxygen in PC, whereas BPh₄⁻ presents four benzene rings, with their magnetically different ring currents, to any coordinating species.

From studies of water in organic solvents it has been shown that the chemical shift of water monomer protons (*vs.* liquid benzene at 36.5°) is 403 Hz in benzene,³⁵ 286 Hz in 1,2-dichloroethane,³⁵ and 256 Hz in PC.^{28,30} From these results we estimate that the chemical shift of a water proton bound to BPh₄⁻ is 150 ± 50 Hz up-field of a water proton bound to ClO₄⁻. (Our estimate is based on the chemical shifts of water protons in benzene and PC.)

$$\nu_1^{ClO} - \nu_1^{BPh} = 150 \pm 50 \text{ Hz} \quad (6)$$

Combining this assumption with the Li⁺ and Na⁺ data in Table II, which imply (7) and (8)

- (33) J. C. Synnott and J. N. Butler, *Anal. Chem.*, **41**, 1890 (1969).
 (34) W. S. Harris, "Electrochemical Studies in Cyclic Esters," Ph.D. Thesis, University of California, Berkeley, 1958. U. S. Atomic Energy Commission Report UCRL-8381.
 (35) L. Ödberg and E. Högfeldt, *Acta Chem. Scand.*, **23**, 1330 (1969).

$$K_1^{\text{ClO}}(\nu_1^{\text{ClO}} - \nu_0) - K_1^{\text{BPh}}(\nu_1^{\text{BPh}} - \nu_0) = 0 \pm 30 \quad (7)$$

$$K_1^{\text{ClO}} - K_1^{\text{BPh}} = 0 \pm 0.3 \quad (8)$$

we obtain (9)

$$K_1^{\text{BPh}} = 0 \pm 0.2 \pm 0.002(\nu_1^{\text{ClO}} - \nu_0) \quad (9)$$

A second mild assumption required is that $\nu_1^{\text{ClO}} - \nu_0 \ll 100$. Since this chemical shift ($\nu_1 - \nu_0$) is less than 100 Hz for Li^+ or Cl^- , where bonding is quite strong, we would expect that for ClO_4^- , which is similar to the solvent, it should be much smaller. (Later, we estimate $\nu_1^{\text{ClO}} - \nu_0$ to be of the order of 15 Hz.) This argument thus leads us to the conclusion that $K_1^{\text{BPh}} < 0.2$, and since physically $K_1 > 0$, we have given the value in Table IV as 0.1 ± 0.1 . From eq 8 and 9, we then obtain in a similar way $K_1^{\text{ClO}} = 0.3 \pm 0.1$.

Table IV: Molal Equilibrium Constants and Chemical Shifts for Association of Water with Ions in PC

Ion	K_1^a kg/mol	$\nu_1 - \nu_0$ Hz
Li^+	6.5 ± 0.3	102 ± 5
Na^+	1.4 ± 0.1	67 ± 7
K^+	0.4 ± 0.2^b	
Et_4N^+	0.3 ± 0.2	0 ± 30
Cl^-	6.2 ± 0.3	100 ± 3
Cl^-	7.0 ± 0.6^b	
ClO_4^-	0.3 ± 0.1	15 ± 30
BF_4^-	0.3 ± 0.2	15 ± 30
BPh_4^-	0.1 ± 0.1	-150 ± 50
LiCl^c	0.4 ± 0.2^b	

^a Nmr, 36.4°, except where noted. ^b Solubility, 20°. ^c Ion pair.

Having established K_1 for ClO_4^- , we can obtain much more accurate values for Li^+ and Na^+ from the slopes in Table III for LiClO_4 and NaClO_4 , and these are listed in Table IV. Since the curve for LiBF_4 is the same as for LiClO_4 , we have taken the same constants for BF_4^- as for ClO_4^- .

From the Et_4NClO_4 data in Table III, we can obtain K_1 for Et_4N^+ and the two chemical shifts, again making rather mild assumptions. Since the difference in chemical shift of water in 1,2-dichloroethane³⁵ is only 30 Hz upfield from that in PC, we may assume

$$\nu_1^{\text{Et}} - \nu_0 = 0 \pm 30 \quad (10)$$

which gives from the intercept of eq 5

$$\nu_1^{\text{ClO}} - \nu_0 = 20 \pm 3 \pm 100K_1^{\text{Et}} \quad (11)$$

For cations, where there are no specific hydrogen-bonding or paramagnetic effects, we might expect that $\nu_1 - \nu_0$ would be correlated with the free energy of association with water (*i.e.*, with $\log K_1$). Extrapolating such a correlation ($\log K_1 = -0.64 + 0.015(\nu_1 - \nu_0)$ for Li^+ and Na^+), we obtain $K_1^{\text{Et}} = 0.35 \pm$

0.25 and from eq 11, $\nu_1^{\text{ClO}} - \nu_0 = 20 \pm 60$. However, the same correlation gives, from $K_1^{\text{ClO}} = 0.3 \pm 0.1$, a corresponding chemical shift of +9 to -4, or $\nu_1^{\text{ClO}} - \nu_0 = 0 \pm 10$ Hz. This in turn implies, *via* eq 11, $K_1^{\text{Et}} \sim 0$. Correlation of $\log K_1$ and chemical shift with the reciprocal of ionic radius³ gives similar results: $K_1^{\text{Et}} \sim 0.1$; $K_1^{\text{ClO}} \sim 0.2$; $\nu_1^{\text{ClO}} - \nu_0 = 15 \pm 30$.

Solubility Data. It is also possible to calculate the sum of ionic hydration constants from the variation of solubility with added water concentration, provided no complex species are formed. The saturation concentrations of NaCl and KCl are sufficiently low that no appreciable ion pairs are formed. This is confirmed by conductance measurements.³⁴ Since the product of the free ionic activities is a constant (K_{so}) independent of whether water is present or not, we may attribute the solubility increase to the formation of hydrated ionic species, and obtain the relation

$$(1 + K_1^{\text{M}}[\text{H}_2\text{O}])(1 + K_1^{\text{A}}[\text{H}_2\text{O}]) = R^2 \quad (12)$$

where R is the ratio of the solubility of MA in the presence of water (total concentration C_w) compared with that in anhydrous PC. A mass balance on water

$$C_w = [\text{H}_2\text{O}](1 + K_1^{\text{M}}[\text{M}^+] + K_1^{\text{A}}[\text{A}^-]) \quad (13)$$

allows correction for the amount of water bound to the ions.

From our solubility data (Table III) for NaCl, together with the ionic hydration constant (1.4) given in Table IV for Na^+ , we obtain from eq 12 and 13 the value $K_1^{\text{Cl}} = 7.0 \pm 0.6$ at 20°. This value is not too sensitive to the hydration constant of Na^+ , and the fact that our Na^+ value was obtained at 36.4° does not introduce as large an error as the uncertainty in the solubility data. This constant for Cl^- is gratifyingly close to that obtained from the nmr measurements on Et_4NCl . Not only do the values agree within the estimated error, but the nmr (36.5°) value is lower than the solubility (20°) value, as might be expected for an exothermic ion hydration reaction.

The solubility of KCl (Table III) gives an estimate of the ionic hydration equilibrium constant for K^+ which is the same order of magnitude as that for the large anions: 0.4 ± 0.2 .

Treatment of the LiCl solubility data by eq 12 and 13 predicts that $R = 1.48$ on the basis of ionic hydration constants obtained by the other methods. This is in reasonable agreement with the experimental value ($R = 1.42$) when the uncertainties of the constants (particularly the temperature effect on K_1^{Li}) are taken into consideration. Since LiCl is known to be strongly ion paired in propylene carbonate, by potentiometric titration,²⁶ activity coefficient,³⁶ and conductance methods,³⁷ this implies that the hydration of the ion

(36) M. Salomon, *J. Phys. Chem.*, **73**, 3299 (1969).

(37) L. M. Mukherjee and D. P. Boden, *ibid.*, **73**, 3965 (1969).

pair is quite weak compared with that of the individual ions. Using an ion-pairing constant³⁷ of $10^{2.75}$ and introducing additional terms into eq 12 and 13 to allow for ion-pair formation and hydration of this ion pair, we estimated that the hydration constant for the ion pair was approximately 0.4 ± 0.2 , similar to that for K^+ or the large ions.

Statistical Estimates of K_1 . A plausible estimate may be made, purely on statistical grounds, for K_1 in the absence of specific interactions. The exact value, of course, depends on the maximum number of solvent molecules admitted to the solvation shell, and this can change as the composition of the solvent changes. However, if one considers an ion with N equivalent solvent molecules surrounding it, and the bulk mole fraction of the minor solvent component (*i.e.*, water) is X_w , then the probability of having one of these solvent molecules in the solvation shell is

$$\frac{[M \cdot H_2O]}{[M]} = \frac{1 - (1 - X_w)^N}{X_w(10^3/M_s + [H_2O])} [H_2O] = K_1[H_2O] \quad (14)$$

where concentrations are in mol/kg of solvent, and M_s is the molecular weight of the solvent (102 g/mol for PC). Evaluating the expression for K_1 implied by eq 14, for $[H_2O] < 0.1$, we obtain approximately

$$K_1 = 0.10 N \quad (15)$$

Thus, for example, if the first solvation shell contains 4 molecules, this model predicts $K_1 = 0.4$ even if there are no specific forces of association between the ion and the solvent. Thus it seems not without significance that most of the K_1 values in Table IV are in the range 0.1–0.4, particularly when the possibility of repulsive as well as attractive interactions is considered.

Multiple Hydration of Li^+ . At high concentrations of water, substantial deviations are observed from the simple plot which assumes only one water molecule bound to an ion. With Na^+ salts and Et_4NCl , these deviations are too small to be quantitatively evaluated, but for Li^+ salts, we have made a quantitative estimate of the second and third hydration equilibrium constants

$$\begin{aligned} [Li^+ \cdot 2H_2O] &= K_2[Li^+ \cdot H_2O][H_2O] \\ [Li^+ \cdot 3H_2O] &= K_3[Li^+ \cdot 2H_2O][H_2O] \end{aligned} \quad (16)$$

An iterative procedure based on evaluation of the slope of the ν vs. C_{H_2O} plot and minimization of the calculated vs. observed frequency values was employed, making use of a time-shared computer system for the calculations. Details are given elsewhere.²⁸ The association constants and the hypothetical chemical shifts obtained are given in Table V; a comparison of calculated and observed resonance frequency values over a range of salt and water concentrations is given in Figure 2 for $LiClO_4$. The agreement is good to concentrations of

Table V: Stepwise Equilibrium Constants and Chemical Shifts for Li^+ Hydration in Dilute Propylene Carbonate^a

Hydration step	K_i , kg/mol	$(\nu_i - \nu_0)$, Hz
1 ^b	6.8 ± 0.3	98 ± 3
2	2.7 ± 0.4	91 ± 5
3	1.9 ± 0.6	78 ± 10

^a Deviations are standard deviations. ^b Includes contribution from ClO_4^- . See Table IV.

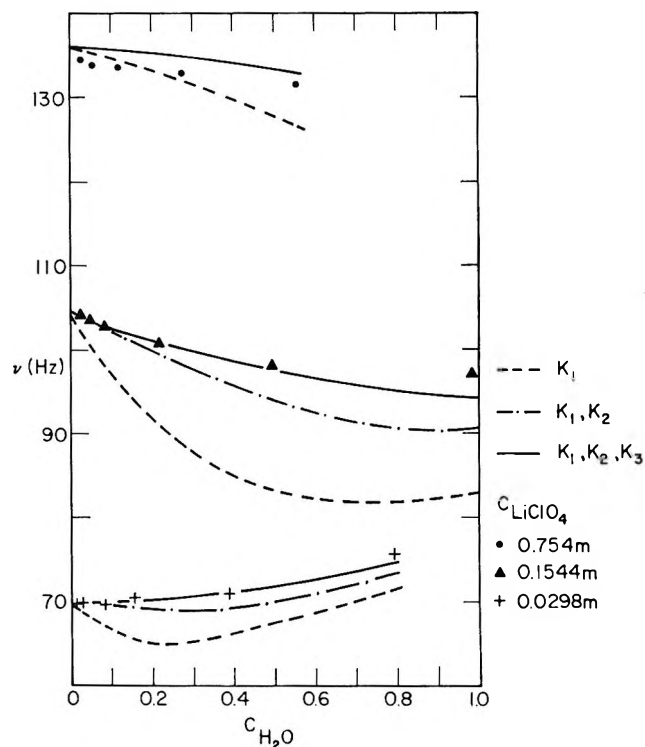


Figure 2. Comparison of calculated and observed data for the chemical shift of water in the presence of $LiClO_4$ in PC. Constants are given in Table V.

approximately 1 *m* in both salt and water. Broken lines show the shape of curves obtained if K_2 or K_3 is set equal to zero. The agreement for $LiBPh_4$ is equally good.

The stepwise constants for association of water with lithium ion decrease as the number of water molecules increases, indicating that there is no cooperative hydration phenomenon in PC, and implying that the much stronger association of water with Li^+ is perhaps not so much a specific chemical bonding as it is simply a geometric factor: the smaller water molecules can fit easily about the lithium ion without seriously disrupting the bulky propylene carbonate molecules which are already there. For larger cations this is less probable, and their selective association with water is correspondingly weaker.

Relation to Free Energies and Enthalpies of Transfer. In this work, we have obtained association constants

between water and various ions in PC, a relatively structureless dielectric medium, and it is of interest to consider the extent to which the interactions we have measured are representative of the hypothetical "first bond" formed when an ion is solvated by water itself. One of the principal pieces of experimental evidence for difference in solvation is the free energy of transfer of an ion between solvents, sometimes expressed by means of a "solvent activity coefficient."²⁻⁴ If the principal contribution to this free energy of transfer is the formation of a strong, specific, coordination bond between ion and solvent, then we would expect to see a good correlation between standard free energies of the first hydration (obtained in our studies) and standard free energies of transfer from bulk water to propylene carbonate. (For a full discussion, and to appreciate the approximations involved, see ref 3.)

In Table VI we have compared the free energy of

Table VI: Correlation of Hydration Equilibria in PC with Free Energies and Enthalpies of Transfer^b

Ion	$\frac{RT}{\ln K_1}$ ^a	ΔG_{tr} ^c	ΔG_{tr} ^d	ΔH_{tr} ^e	ΔG_{tr} ^f	ΔH_{tr} ^f
Li ⁺	+1.14	+3.7	+0.9 ^g	+0.7	+2.8	+1.4
Na ⁺	+0.21	+1.1	-2.4	-2.4	+0.5	-0.3
K ⁺	-0.56	-0.3	-0.3	-5.2	-1.7	-4.2
Et ₄ N ⁺	-0.7			+0.2		
Cl ⁻	+1.20	+11.3	+14.0	+6.3	+12.1	+4.6
ClO ₄ ⁻	-1.0			-3.9		-3.6
BF ₄ ⁻	-0.7					
BPh ₄ ⁻	-1.4	-8.3	-8.4	-3.5		-1.6

^a See Table IV for error limits. ^b $\Delta G_{tr} = G_{PC}^\circ - G_{H_2O}^\circ$. All values in kcal/mol. ^c This work. ^d See ref 4. ^e See ref 38. ^f See ref 39. ^g Using $\Delta G_{tr} = +14.96$ for LiCl (ref 36).

formation of an ion-water bond in PC ($-RT \ln K_1$) with free energies and enthalpies of transfer obtained by other workers.^{4,38,39} Parker and Alexander's values⁴ for the free energies of transfer of K⁺ and Cl⁻ are not consistent with the solubility data obtained in this work, and we have therefore estimated revised values for Cl⁻ (and hence Na⁺ and Li⁺) by a similar method, assuming the free energies of transfer of large ions such as BPh₄⁻ and AsPh₄⁺ to be equal, except for a Born charging term.³ (This method was also used by Krishnan and Friedman to evaluate single-ion enthalpies.³⁸) From measurements of the cell Li|Li⁺Cl⁻|TiCl|Ti(Hg), Salomon³⁶ determined an accurate value (+14.96 kcal/mol) for the standard free energy of transfer of LiCl from water to PC. This avoids the uncertainties in the solubility method due to ion-pairing and activity coefficient corrections. Combining our new value for Cl⁻ with this thermodynamic value for LiCl gives +3.7 kcal/mol for Li⁺. Values obtained by an extrapolation method³⁹ are about 1 kcal lower.

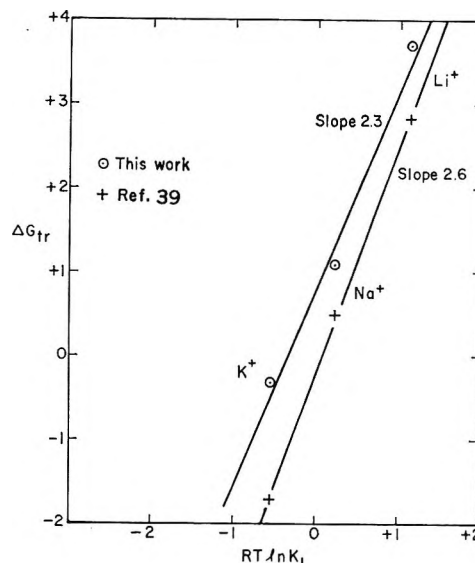


Figure 3. Correlation of free energy for the formation of a water-cation bond at infinite dilution in PC ($-RT \ln K_1$) with the free energy of transfer from bulk PC to bulk water ($-\Delta G_{tr}$).

Based on the model of strong coordinate bond formation between water and ions, one expects to see a correlation between $RT \ln K_1$ and ΔG_{tr} with slope of the order of magnitude of the solvation number in water. For the alkali metal cations (Figure 3) this correlation is quite good, and shows a slope corresponding to the formation of about two or three water-cation bonds. Correlation with ΔH_{tr} is also good, giving a steeper slope. However, the unknown entropy factors in the hydration equilibria make interpretation of this correlation less obvious. When the other ions are included in the correlation of ΔH_{tr} with $RT \ln K_1$ the general trend is preserved, but the slope may be anywhere between 1 and 6.

Two ions deviate dramatically from the correlation of $RT \ln K_1$ with ΔG_{tr} : the free energy of transfer of BPh₄⁻ (large and hydrophobic) is very much lower (-8.3 kcal/mol) than expected, and the free energy of transfer of Cl⁻ is very much higher (+11.3 kcal/mol). The excess free energy of transfer for Cl⁻ over Li⁺ (which has the same K_1) is therefore associated with the formation of a much different water structure compared with bulk water. What is surprising is that this excess free energy due to structural effects should be *ten times* as large as the formation of the initial water-chloride bond, and have a magnitude corresponding to the formation of five to ten new hydrogen bonds in water.

In this connection, it seems to be important to investigate the association of water with other small anions (F⁻ and OH⁻, for example) to see if this effect is widely obtained.⁴⁰

(38) C. V. Krishnan and H. L. Friedman, *J. Phys. Chem.*, **73**, 3934 (1969).

(39) M. Salomon, *ibid.*, **74**, 2519 (1970).

Acknowledgments. The assistance of Mr. James Turner and Mr. John C. Synnott with some of the experimental work, and helpful discussions with Dr. Mark Salomon, are gratefully acknowledged. This work was supported in part by the Petroleum Research Fund of the American Chemical Society and the Air Force Cambridge Research Laboratories, Office of Aerospace Research, but does not necessarily constitute the opinion of these agencies.

(40) NOTE ADDED IN PROOF. Hydration constants of ions and undissociated salts in acetonitrile have been determined by I. M. Kolthoff and coworkers [*J. Amer. Chem. Soc.*, **89**, 1582, 2521 (1967)]. Values of K_1 for the association of water with ions in acetonitrile [4 ± 1 (Li^+), 2.6 (Na^+), 1.3 (K^+), 11 (Cl^-), and 1.0 (ClO_4^-)] closely parallel our values for PC given in Table IV above. Recent reevaluation of the free energy of transfer for anions between PC and water by A. J. Parker and coworkers ["Solvation of Ions XVI," in press] gives $\Delta G_{tr} = +8.6$ kcal for Cl^- and -10.0 kcal for BPh_4^- . This implies $+6.4$ kcal for Li^+ , considerably diminishing the difference between Li^+ and Cl^- , and producing a better correlation with K_1 for these two ions but giving a value for Li^+ in disagreement with both the correlations of Figure 3 and the extrapolation method of ref 39.

Equilibrium Distributions of Some Octane and Nonane Isomers

by *Richard K. Lyon*

Corporate Research Laboratories, Esso Research and Engineering Company, Linden, New Jersey 07036
(Received September 23, 1970)

Publication costs assisted by the Esso Research and Engineering Company

All 18 of the isomeric octanes and four of the nonanes were treated with an isomerization catalyst, AlBr_3 . Relative reaction rates were measured. For three sets of isomers equilibrium distributions were obtained and compared with the API Project 44 data.

Introduction

Equilibrium distributions among isomeric compounds are in general calculated from heat of combustion and heat capacity measurements, a procedure involving small differences in large numbers. In some favorable cases, however, catalysts can bring about isomeric interconversion. If perturbations due to side reactions are negligible, the observed distribution is the equilibrium distribution within the accuracy of chemical analysis.

Aluminum halide catalyzed isomerizations have been used to obtain the equilibrium distribution of the butane, pentane, hexane, and heptane isomer sets.^{1,2} Extension of these measurements to the higher hydrocarbons would be of interest since these equilibrium distributions would show the effect of interaction between remote groups.

In the present study all 18 octane isomers and four nonane isomers were treated with AlBr_3 . Complete equilibrium among all isomer forms of either the octanes or nonanes could not be achieved, since some of the isomerizations necessary for complete equilibrium are slow compared with the concurrent degradation reaction. Three subsets of isomers, the singly branched octanes (SBO), the doubly branched nonquaternary octanes (DBNO), and the triply branched nonanes (TBN),

were found to achieve steady-state distributions. Relative rate measurements for all observable reactions were made and the steady-state distributions are proven to be the equilibrium distributions.

Experimental Section

The hydrocarbons used in these experiments were Chem. Samp. Co. of 99% purity and were used without further purification. The catalyst was AlBr_3 from Matheson Coleman and Bell. As initially received it had a catalytic activity suitable for these measurements and was used as received.

Using a drybox, 0.1 g of AlBr_3 was weighed into a glass vial which was then sealed with a rubber septum. The vial was then placed in a constant temperature bath and 5 cc of the reactant mixture was then injected. The reactant mixture was always 50 vol % isomeric octane or nonane and 50% methylcyclopentane (MCP). At various times after reactant injection, samples were withdrawn *via* syringe, injected into water to deactivate the catalyst, and analyzed by a P&E F-11 gas chromatograph with a 300-ft squalane

(1) F. E. Condon, *Catalysis*, **6**, 43 (1958).

(2) H. Pines and N. E. Hoffman, "Friedel-Crafts and Related Reactions," Vol. II, G. A. Olah, Ed., Interscience, New York, N. Y., 1964.

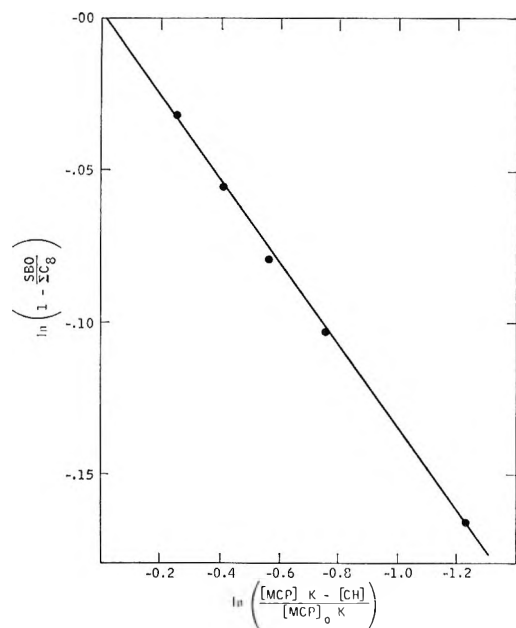


Figure 1. Typical relative rate plot.

capillary column. Peak areas were measured by an Infotronics CRS-100 integrator. Analysis of isomer mixtures of known weight composition showed that within experimental error all the octane isomers had the same sensitivity. The isomeric analysis was complete with two exceptions—3-methylheptane (3-MC₇) and ethylhexane (EtHex) could not be separated. 2-Methyl-3-ethylpentane (2-M-3-EtP) could be detected in the presence of 2,3-dimethylhexane (2,3-DMH) only if the former were more than 15% of the latter.

Numerous rate measurements, all relative to the rate of the methylcyclopentane–cyclohexane (CH) equilibration, were made. Figure 1 is typical of the better results. The vertical ordinate (conversion of doubly branched nonquaternary octane isomers to singly branched octane isomers) is the expression appropriate to a first-order irreversible reaction. This assumption of irreversibility is a valid approximation only at low conversion. Due to the kinetic complexity of the isomer interconversion this approximation was necessary, hence only low conversion measurements were used to calculate the relative rate constants reported here. The horizontal ordinate (conversion of methylcyclopentane to the equilibrium methylcyclopentane–cyclohexane mixture) is the expression appropriate to a first-order reversible reaction, where K is the methylcyclopentane–cyclohexane equilibrium constant.

Results

Normal octane was observed to isomerize slowly to the methylheptanes, the relative rate constant at 59.1° being $0.13k_{\text{MCP}=\text{CH}}$. Dimethylhexanes were also observed, but the ratio of their yield to the methylheptane yield extrapolated to zero at zero conversion of the *n*-octane.

The observed steady-state distributions of the singly branched octane isomers are given in Table I. A sample was judged to have reached steady state *not* from the data to be averaged but from the approach of the methylcyclopentane–cyclohexane ratio to its equilibrium value. The methylcyclopentane–cyclohexane ratio is a good index, since the singly branched octane isomers interconvert faster than do methylcyclopentane–cyclohexane. When this happened the catalyst was still active as proven by the continued slow interconversion of the singly branched octane and doubly branched nonquaternary octane isomers.

During the isomerization of the doubly branched nonquaternary octane isomers at 13°, the distribution of the singly branched octane isomers formed was observed to be 4-MC₇/2-MC₇ = 0.266 ± 0.002 and (3-MC₇ + EtHex)/2-MC₇ = 0.771 ± 0.001 . During the isomerization of the singly branched octane isomers at 13° the distribution of the doubly branched nonquaternary octane isomers was observed to be (2,3-DMH + 2-M-3-EtP)/2,5-DMH = 0.230, 2,4-DMH/2,5-DMH = 0.807, and 3,4-DMH/2,5-DMH = 0.0564.

In Table II, the relative rates at which each singly branched octane isomer converts to the others and at which the equilibrating mixture of singly branched octane isomers form other products are given. The rate of formation of the other products was observed to be independent of the starting singly branched octane isomer. Since the rates of mutual interconversion are high compared with the rates forming other products, this is to be expected.

Table II gives rate constants for the isomerization of singly branched octane to both doubly branched nonquaternary octane and 2,2-dimethylhexane. The latter reaction is a true direct reaction rather than a secondary isomerization of doubly branched nonquaternary octane, since the ratio of 2,2-dimethylhexane to doubly branched nonquaternary octane is 0.05 independent of reaction time. Further using the value of $k_{\text{DBNO} \rightarrow 2,2\text{-DMH}}$ given in Table IV, one calculates that the amount of 2,2-dimethylhexane observed early in the reaction is 25 times as great as that which could be formed by secondary reaction.

Table II does not give rate constants for the direct interconversion of 2-methylheptane with either 4-methylheptane or ethylhexane, only the interconversion of these three with 3-methylheptane. Based on product ratios extrapolated to zero conversion, these direct interconversions do not occur to an observable extent, 5% of the total isomerization.

The steady-state distributions of the doubly branched nonquaternary octane isomers are given in Table III. The amount of 2-methyl-3-ethylpentane present in these distributions could not be determined, since it was always less than 15% of the 2,3-dimethylhexane.

In Table IV the relative rate constants are given for the total rate at which each doubly branched non-

Table I: Equilibrium Distribution of the Singly Branched Octanes

Observed ratio	Start with				Average
	2-MC ₇	3-MC ₇	4-MC ₇	EtHex	
	13.0°				
4-MC ₇	0.273 ± 0.002		0.271		0.272 ± 0.001
2-MC ₇	Av of 2				
3-MC ₇ + EtHex	0.768 ± 0.002		0.764		0.766 ± 0.002
2-MC ₇	Av of 2				
	40.0°				
4-MC ₇	0.276	0.262	0.270	0.268	0.269 ± 0.004
2-MC ₇					
3-MC ₇ + EtHex	0.843	0.823	0.832	0.824	0.830 ± 0.007
2-MC ₇					
	59.1°				
4-MC ₇	0.253 ± 0.006		0.246 ± 0.006		0.250 ± 0.004
2-MC ₇	Av of 2		Av of 2		
3-MC ₇ + EtHex	0.856 ± 0.012		0.855 ± 0.001		0.856 ± 0.001
2-MC ₇					

Table II: Relative Rate Constants for the Singly Branched Octane (SBO) Isomerizations

Reaction	$k/k_{MCP \rightleftharpoons CH}$		
	13.0°	40.0°	59.1°
2-MC ₇ → 3-MC ₇	3.7	3.1	2.1
3-MC ₇ → 2-MC ₇		3.4	
3-MC ₇ → 4-MC ₇		2.9	
4-MC ₇ → 3-MC ₇ + EtHex		8.9	8.3
EtHex → 4-MC ₇		14	
SBO → DBNO	0.10	0.09	0.15
SBO → 2,2-DMH	0.005		
SBO → <i>n</i> -C ₈		0.0064	
SBO → <i>i</i> -C ₈ H ₁₀		0.009	

quaternary octane isomer isomerizes to all of the others. The kinetics of these coupled equilibrations are complex as is illustrated by Figure 2, an isomer distribution *vs.* time plot for the isomerization of 3,4-dimethylhexane. The figure is drawn to show all three products being formed at nonzero rates at time $t = 0$. A separate set of experiments confirmed this. The product ratios, 2,4-DMH/2,3-DMH and 2,5-DMH/2,3-DMH, were measured as a function of conversion at low conversion of the 3,4-dimethylhexane. The zero conversion intercepts of these ratios were 0.23 and 0.03, respectively.

The data obtained in most of our runs were not suitable for determining the ratio in which products are being formed at the start of the reaction, because the thermodynamically less stable product isomers are converted to the more stable isomers by rapid secondary reactions. In Figure 3 the ratio of the thermodynamically more stable isomers, 2,5-dimethylhexane/2,4-dimethylhexane, is plotted as a function of methylcyclopentane conversion for the isomerization of 3,4-dimethylhexane, 2,3-dimethylhexane, and 2-

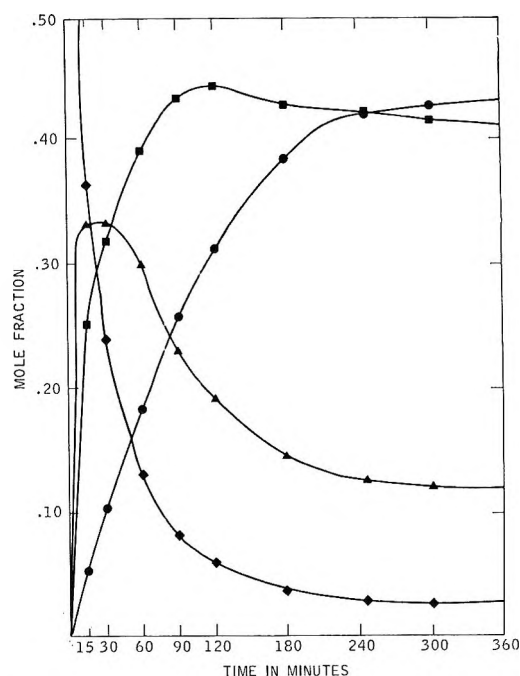


Figure 2. Isomerization of 3,4-dimethylhexane: \blacklozenge , 3,4-dimethylhexane; \blacktriangle , 2,3-dimethylhexane; \blacksquare , 2,4-dimethylhexane; \bullet , 2,5-dimethylhexane.

methyl-3-ethylpentane. The zero conversion intercepts do not appear to differ significantly.

The subset of doubly branched quaternary octane isomers, 2,2-dimethylhexane, 3,3-dimethylhexane, and 3-methyl-3-ethylpentane, were observed to isomerize with the rate constants of 0.03, 0.06, and 0.07 times $k_{MCP \rightleftharpoons CH}$, respectively, at 59.1°. The predominant products were the doubly branched nonquaternary octane isomers. No direct interconversion among the members of this subset was observed.

Table III: Equilibrium Distribution of the Doubly Branched Nonquaternary Octanes

Observed ratio			Start with		
	2,3-DMH	2,4-DMH	2,5-DMH	3,4-DMH	Average
13.0°					
$\frac{2,3\text{-DMH} + 2\text{-M-3-EtP}}{2,5\text{-DMH}}$	0.228 ± 0.001 Av of 2	0.218 ± 0.001 Av of 2	0.237	0.234 ± 0.005 Av of 3	0.229 ± 0.006
$\frac{2,4\text{-DMH}}{2,5\text{-DMH}}$	0.797 ± 0.001 Av of 2	0.793 ± 0.004 Av of 3	0.798	0.795 ± 0.005 Av of 3	0.795 ± 0.001
$\frac{3,4\text{-DMH}}{2,5\text{-DMH}}$	0.0602 ± 0.0016 Av of 2	0.0532 ± 0.0003 Av of 3	0.0554	0.0566 ± 0.0021 Av of 2	0.0561 ± 0.0023
40.0°					
$\frac{2,3\text{-DMH} + 2\text{-M-3-EtP}}{2,5\text{-DMH}}$	0.261 ± 0.008 Av of 5	0.253 ± 0.003 Av of 5	0.254 ± 0.003 Av of 3	0.252	0.255 ± 0.003
$\frac{2,4\text{-DMH}}{2,5\text{-DMH}}$	0.963 ± 0.037 Av of 5	0.943 ± 0.013 Av of 5	0.934 ± 0.007 Av of 3	0.969	0.942 ± 0.033
59.1°					
$\frac{2,3\text{-DMH} + 2\text{-M-3-EtP}}{2,5\text{-DMH}}$	0.337	0.343	0.316	0.327	0.331 ± 0.009
$\frac{2,4\text{-DMH}}{2,5\text{-DMH}}$	0.938	0.940	0.917	0.941	0.934 ± 0.008
$\frac{3,4\text{-DMH}}{2,5\text{-DMH}}$	0.0955	0.0982	0.0952	0.0953	0.0960 ± 0.0011

Table IV: Relative Rate Constants for the Doubly Branched Nonquaternary Octane (DBNO) Isomerizations

Reaction	$k/k_{\text{MCP} \rightleftharpoons \text{CH}}$		
	13.0°	40.0°	59.1°
2,3-DMH → DBNO	3.8	6.8	7
2,4-DMH → DBNO	1.1	2.1	2.7
2,5-DMH → DBNO	0.59	3.4	16.5
3,4-DMH → DBNO	>7	11.4	10
2-M-3-EtP → DBNO	>30	≥30	Not measured
DBNO → 2,2-DMH	0.0073	0.012	0.012
DBNO → 3,3-DMH	Not measured	0.004	Not measured
DBNO → SBO	0.072	0.12	0.134 ± 0.006
DBNO → <i>i</i> -C ₄ H ₁₀	0.008	0.01	0.025

The subset of triply branched octanes undergoes mutual interconversions, but cracks to *i*-C₄H₁₀ at a comparable rate. Hence, the equilibrium distribution of this subset could not be measured. For 2,2,3-trimethylpentane at 40.0°, the relative rate constants for isomerization to other trimethylpentanes, for isomerization to doubly branched nonquaternary octane, and for cracking to *i*-C₄H₁₀ were 0.62, 0.03, and 0.2, respectively.

It is generally believed that the inertness of neopentane to Lewis acid catalysts is due to the difficulty of forming a primary carbonium ion. One would, therefore, expect tetramethylbutane to be inert, and under our experimental conditions, it is.

One subset of C₉H₂₀ isomers, the triply branched nonanes (TBN), was investigated. The isomers 2,2,4-

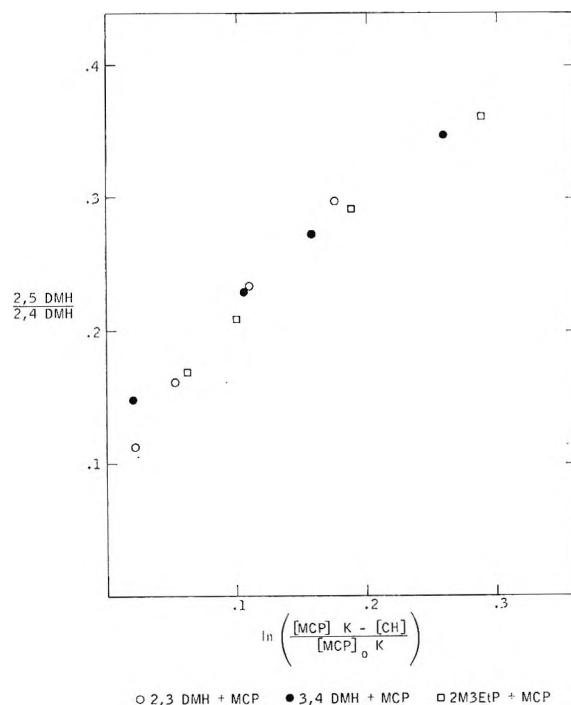


Figure 3. Ratio of 2,5-dimethylhexane (2,5-DMH) to 2,4-dimethylhexane (2,4-DMH) as a function of conversion at 13°.

trimethylhexane, 2,2,5-trimethylhexane, 2,3,4-trimethylhexane, and 2,4-dimethyl-3-ethylpentane were mixed with methylcyclopentane and treated with AlBr₃ at 13°. During the isomerization of each of these nonanes the only isomers formed in observable amounts

Table V: Comparison of Thermodynamic Quantities from This Study with API Project 44 Data

	K 13 ^{°a}	K 13 ^{°b}	K 59.1 ^{°a}	K 59.1 ^{°b}	ΔH_f^a kcal	ΔH 25 ^{°b} kcal	ΔS_f^a eu	ΔS 25 ^{°b} eu
2,5-DMH \rightleftharpoons 2,4-DMH	0.80	0.57	0.93	0.69	0.6	0.77	1.8	1.6
2,5-DMH \rightleftharpoons 3,4-DMH	0.040	0.053	0.071	0.093	2.4	3.07	1.9	2.2
2-MC ₇ \rightleftharpoons 4-MC ₇	0.27	0.19	0.25	0.24	-0.3	0.81	-3.8	-0.46
2-MC ₇ \rightleftharpoons 3-MC ₇ + EtHex	0.74	0.85	0.82	1.03	0.4	0.79	0.9	2.43
2,5-DMH \rightleftharpoons 2,3-DMH + 2-M-3-EtP	0.174	0.065	0.27	0.112	1.8	2.27	2.6	2.5
2,5-DMH \rightleftharpoons 2-M-3-EtP	<0.026	0.018	<0.040	0.035				

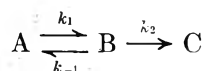
^a This study. ^b API.

(>1%) were 2,2,5-trimethylhexane, 2,4,4-trimethylhexane, 2,2,4-trimethylhexane, and 2,2,3-trimethylhexane. During the isomerization of 2,3,4-trimethylhexane and 2,4-dimethyl-3-ethylpentane, both 2,2,5-trimethylhexane and 2,4,4-trimethylhexane were formed at nonzero rates from the start of reaction. 2,2,5-Trimethylhexane rose steadily to its steady-state value while 2,4,4-trimethylhexane rose to a maximum then decayed to its steady-state value. 2,2,4-Trimethylhexane showed a slight maximum while 2,2,3-trimethylhexane was marginally detectable late in the reaction. At steady state the isomer distribution was observed to be 89 \pm 1% 2,2,5-trimethylhexane, 7.5 \pm 0.3% 2,4,4-trimethylhexane, 2 \pm 1% 2,2,4-trimethylhexane, and 0.8 \pm 0.8% 2,2,3-trimethylhexane.

Due to its high steady-state concentration, a relative rate constant for 2,2,5-trimethylhexane could not be measured. For 2,2,4-trimethylhexane, 2,3,4-trimethylhexane, and 2,4-dimethyl-3-ethylpentane, the relative rate constants for isomerization were 5.4, 84, and 19, respectively, at 18°. The nonane isomers cracked to *i*-C₅H₁₂ with an average relative rate constant of 0.03 at 13°.

Discussion

For the simple system



it can readily be shown that

$$\frac{(B/A)_{eq} - (B/A)_{ss}}{(B/A)_{eq}} = \frac{k_2}{k_1}$$

where (B/A)_{ss} is the ratio of B to A at steady state and (B/A)_{eq} is this ratio at equilibrium. Judged on this basis it is clear from the data in Table II that the only reaction fast enough to cause a significant difference between the steady-state and equilibrium distributions of the singly branched octane isomers is their isomerization to doubly branched nonquaternary octane isomers. However, a steady-state distribution of singly branched octane isomers was also observed during the isomerization of the doubly branched nonquaternary octane iso-

mers. If the reaction SBO \rightarrow DBNO causes the singly branched octane steady-state distribution to depart from equilibrium in one direction the reaction DBNO \rightarrow SBO must cause departure in the opposite direction. Since the two steady-state distributions are within experimental error the same, they are the same as the equilibrium distribution. A similar argument may be made to equate the steady-state and equilibrium distributions of the doubly branched nonquaternary octane isomers.

The observed steady-state distribution of the triply branched nonane isomers is the equilibrium distribution of all triply branched nonane isomers which interconvert rapidly. The data prove this set includes 2,2,4-trimethylhexane, 2,2,5-trimethylhexane, 2,3,4-trimethylhexane, 2,4,4-trimethylhexane, and 2,4-dimethyl-3-ethylpentane. The interconversion of 2,2,3-trimethylhexane, 2,3,5-trimethylhexane, 2,3,3-trimethylhexane, 3,3,4-trimethylhexane, 2,2-dimethyl-3-ethylpentane, and 2,3-dimethyl-3-ethylpentane with the other triply branched nonane isomers should involve carbonium ion rearrangements completely analogous to rearrangements observed to be facile. Hence it is likely that all triply branched nonane isomers interconvert freely and that the observed distribution is the equilibrium distribution of the complete triply branched nonane subset.

Using Raoult's law and vapor pressure data from API Project 44,³ the observed isomer ratios at equilibrium in the liquid phase (Tables I and III) may be converted to the gas phase equilibrium constants shown in Table V.

Using API data for log K_f and ΔH_f at 25° the API values of K given in Table V were calculated. The agreement between the present measurements and API is reasonable for 2,5-DMH \rightleftharpoons 2,4-DMH, 2,5-DMH \rightleftharpoons 3,4-DMH, and 2-MC₇ \rightleftharpoons 3-MC₇ + EtHex. The K values for 2,5-DMH \rightleftharpoons 2,3-DMH + 2-M-3-EtP disagree at both 13 and 59.1°. The upper limit for $K_{2,5\text{-DMH} \rightleftharpoons 2\text{-M-3-EtP}}$ from the present study is not in-

(3) "Selected Values of Properties of Hydrocarbons and Related Compounds," API Project 44, College Station, Texas, 1963.

consistent with the API value, so the API value for $K_{2,5\text{-DMH} \rightleftharpoons 2,3\text{-DMH}}$ is in large error.

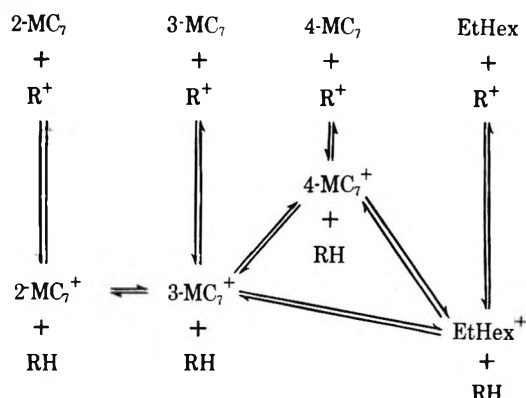
API data are available only for ΔH_f for the triply branched nonane isomers. These data show 2,2,5-trimethylhexane to be more stable than the other triply branched nonane isomers by enthalpy differences ranging from 2.23 to 4.77 kcal/mol. It may be surprising that one of 11 isomers should be 90% of the equilibrium distribution; however, 2,2,5-trimethylhexane is the isomer which minimizes the steric repulsion among the methyl groups.

The observed relative reaction rates may be rationalized in terms of a carbonium ion reaction mechanism. These concepts have been reviewed by Condon¹ and Pines,² and applied in detail to the hexane isomerization by McCaulay⁴ and by Brouwer and Oelderik.⁵ Kramer and Schriesheim⁶ have discussed the heptane isomerization mechanism. In large measure the octane and triply branched nonane isomerizations behave as would be expected from these studies but a few novel features require comment.

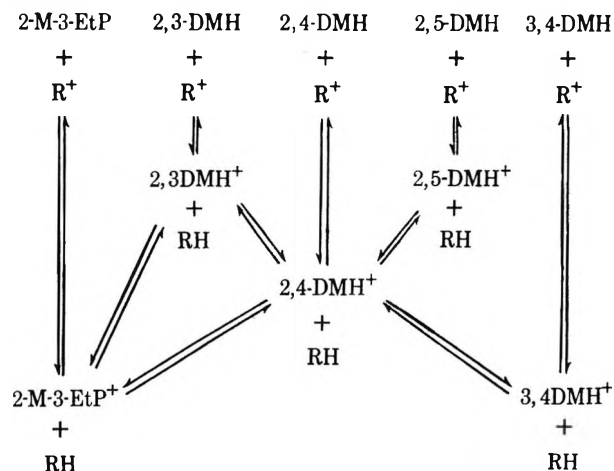
The kinetics of the singly branched octane and doubly branched nonquaternary octane interconversions are in puzzling contrast; the singly branched octane isomerization is a sequential reaction while all products are formed from the start of reaction during the doubly branched nonquaternary octane isomerization. If it is assumed that carbonium ions rearrange *via* shifts of alkyl groups between adjacent carbons, then the kinetics of the singly branched octane and doubly branched nonquaternary octane interconversions will be shown in Schemes I and II. The observed kinetics may be explained by the *ad hoc* assumptions that during the singly branched octane interconversions the hydride transfer steps are all faster than the approach to equilibrium among the isomeric carbonium ions and that during the doubly branched nonquaternary octane interconversions the hydride transfer steps are all slower. The former assumption predicts that there will be no direct interconversion between 2-methylheptane and either 4-methylheptane or ethylhexane, as is observed. The latter assumption implies that all isomers should be formed from the start of the reaction at a rate proportional to the equilibrium concentration of the corresponding carbonium ion times the hydride transfer rate constant. Hence the ratio of any two products at the start of the reaction should be the same irrespective of which isomer is used as the starting material. The data in Figure 3 are in accord with this prediction.

There has been some question in the literature as to whether during carbonium ion rearrangement larger alkyl groups can migrate with the same ease as the methyl group. The isomerization of the EtHex carbonium ion to the 4-MC₇ carbonium ion requires a propyl group shift. Since the overall rate of EtHex \rightarrow 4-MC₇ is comparable with the rates of the other singly branched octane interconversions, and the singly

Scheme I



Scheme II



branched octane interconversions are rate limited by the ion isomerizations, the rates of methyl and propyl shifts are comparable.

The observation that the singly branched octane isomers can isomerize directly to 2,2-dimethylhexane implies that a significant fraction of 2,2-dimethylhexyl ions formed are converted to 2,2-dimethylhexane by hydride transfer before they can isomerize to doubly branched nonquaternary octane ions. Hence, during the isomerization of the doubly branched nonquaternary octane isomers to 2,2-dimethylhexane the hydride transfer step must be facile and the slowness of the overall reaction must be attributed to a slow ion isomerization step.

The isomerization of a carbonium ion containing two tertiary carbons to an ion containing a quaternary carbon ($\text{DBNO}^+ \rightarrow 2,2\text{-DMH}^+$) is a slow process. The isomerization of a carbonium ion containing three tertiary carbons to an ion containing one tertiary and one quaternary carbon is a fast process, since the triply

(4) D. A. McCaulay, Symposium on Isomerization and Related Processes, presented before the Division of Petroleum Chemistry, American Chemical Society, Boston, Mass., April 5-10, 1959.

(5) D. M. Brouwer and J. M. Oelderik, Preprints, Division of Petroleum Chemistry, No. 13, American Chemical Society, Washington, D. C., 1968, p 184.

(6) K. M. Kramer and A. Schriesheim, *J. Phys. Chem.*, **65**, 1283 (1961).

branched nonane isomers interconvert freely between forms which do and do not contain quaternary carbons. The manner in which the third tertiary carbon facilitates the ionic isomerization is obscure.

That the triply branched octanes crack at a rate comparable to their interconversion is consistent with the observations of Condon.⁷ However, it is surprising that the triply branched nonane isomers interconvert with negligible cracking. This anomaly may be tentatively explained if one assumes that the equilibrium distribution among the isomeric ions is similar to the equilibrium distribution of the corresponding paraffins. From the API data 2,2,4-trimethylpentane is most abundant in the triply branched octane equilibrium

distribution. Hence for the triply branched octane system the most abundant carbonium ion would be the 2,2,4-trimethylpentyl ion. In this ion the charged tertiary carbon is β to the quaternary carbon and rapid cracking is to be expected. For the triply branched nonane system the dominant ion would be the stable 2,2,5-trimethylhexyl ion.

Acknowledgment. The author wishes to thank David Benn for his skilled assistance in performing the experimental work described above and George Kramer for helpful discussions.

(7) F. E. Condon, *J. Amer. Chem. Soc.*, **73**, 3938 (1951).

Single-Pulse Shock Tube Studies of Hydrocarbon Pyrolysis. II.

The Pyrolysis of Ethane

by *J. N. Bradley** and *M. A. Frend*

Department of Chemistry, University of Essex, Colchester, Essex, England (Received January 4, 1971)

Publication costs borne completely by The Journal of Physical Chemistry

The pyrolysis of ethane in an argon diluent has been studied over the temperature range 1220–1660°K using a single-pulse shock tube technique. In agreement with previous work, the reaction shows a complex temperature dependence, the activation energy falling almost to zero at the highest temperatures. The transition in kinetic behavior is accompanied by a change in product distribution. Numerical integration of the kinetic equations shows that the behavior cannot be explained in terms either of the falloff characteristics of the unimolecular reactions involved or of inhibition by the products of reaction. The only explanation which has been found to reproduce both the observed kinetics of reaction and the product distribution is the participation of an alternative decomposition step for the ethyl radical, $C_2H_5 \rightarrow C_2H_3 + H_2$, followed by reactions of the vinyl radical, including $C_2H_3 \rightarrow C_2H_2 + H$.

Introduction

The kinetics of the thermal decomposition of ethane have been studied extensively and, although there has been some controversy over the orders of reaction of the separate steps and over the involvement of surface processes, there appears to be qualitative agreement on the basic reaction mechanism, at least below 1000°K. During a program of investigations^{1,2} on the pyrolysis of higher molecular weight hydrocarbons, it was found that some pyrolyses displayed normal linear Arrhenius behavior over a wide range of temperatures while others showed very marked departures from an Arrhenius temperature dependence, accompanied by correspondingly pronounced transitions in product distribution. As previous shock tube studies^{3–5} had

suggested similar behavior for ethane, it was decided to reexamine this reaction at temperatures above 1000°K, in the hope that the system would prove sufficiently simple to permit reliable computer simulation of all the kinetic processes involved.

Experimental Section

The apparatus and experimental method have been described in detail in the first paper of the series.¹

- (1) J. N. Bradley and M. A. Frend, *Trans. Faraday Soc.*, **67**, 72 (1971).
- (2) M. A. Frend, Ph.D. thesis, University of Essex, 1969. J. N. Bradley and M. A. Frend, to be submitted for publication.
- (3) G. I. Kozlov and V. G. Knorre, *Combust. Flame*, **6**, 253 (1962).
- (4) I. F. Miller and S. W. Churchill, *A.I.Ch.E. J.*, **8**, 2, 201 (1962).
- (5) G. B. Skinner and W. E. Ball, *J. Phys. Chem.*, **64**, 1025 (1960).

Briefly, the design of the shock tube follows that constructed originally by Glick, Squire, and Hertzberg.⁶ The timing of the rupture of the diaphragms is achieved electrically,⁷ rather than by the use of an auxiliary shock tube, to give more precise control. The reactants are confined to a small section of the tube separated from the experimental section by two sliding-vane valves which are opened immediately prior to firing the shock. The products are flushed into a small vessel at the end of the tube by introducing a high pressure of nitrogen into the driving section.

The reflected shock conditions are calculated from incident velocity measurements in the usual way. The major source of error in determining the temperature and pressure history of the reacting gas lies in estimating the time of arrival of the rarefaction wave, since the change is not a step transition as in the case of the shock and is more easily obscured by noise. This means that reaction times cannot be measured to better than $\pm 50 \mu\text{sec}$, corresponding to a possible error of ca. 5–10%. This prevents the use of a range of reaction times and makes the results at the ends of the temperature scale rather less accurate.

Ethane was supplied by Cambrian Chemicals Ltd. at better than 99% purity and was further purified by bulb-to-bulb distillation. Argon (99.995%) was supplied by British Oxygen Co. Ltd. Analysis was carried out by vapor phase chromatography using Porapak Q and Porapak T columns. The identity of the peaks was checked by mass spectrometry. The computer simulation was carried out using a program devised originally by Gear⁸ and subsequently modified by Dr. J. Oliver of the Computing Centre, University of Essex. The improved stability characteristics permitted the numerical integration of a series of simultaneous linear differential equations roughly two orders of magnitude faster than corresponding Runge-Kutta-Merson procedures. The considerable improvement in speed offered by this program for integrating systems of stiff differential equations should prove extremely valuable for solving kinetic equations and some further details have been provided in an Appendix to the paper.

Results

The pyrolysis of ethane in an argon diluent has been studied for total pressures of 400–800 Torr over the temperature range 1250–1660°K. Some experiments were conducted with 0.5% mixtures but the majority employed 1% mixtures. The sole detectable products were ethylene, methane, and acetylene and the amount of hydrogen formed was estimated on this basis. Experiments with other hydrocarbon systems^{1,2} showed that the analytical technique would certainly have revealed products present in greater than 0.1% yield. The experimental technique as presently in use would only permit small variations in pressure and/or reaction

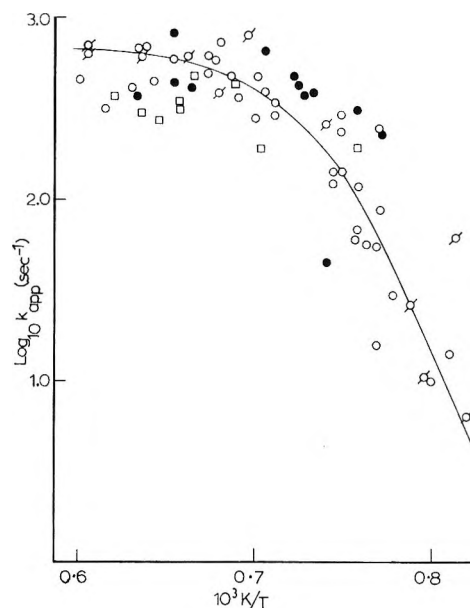


Figure 1. Arrhenius plot of apparent first-order rate constants for ethane decomposition: \circ , 1% C_2H_6 in Ar; \bullet , 0.5% C_2H_6 in Ar; \square , results which do not meet the 100° criterion (see text); \square , 0.4% C_2H_6 , 0.6% C_2H_4 in Ar. The smooth curve is intended to be representative of the results for the 1% C_2H_6 in Ar mixtures.

time so that the principal experimental variable is the reaction temperature.

Reaction times were normally restricted to the range 0.9–1.5 msec and the degree of conversion varied between 1 and 52%. A significant range was achieved at lower temperatures (from 2 to 31% at 1300°K) but only a much smaller range at higher temperatures (37 to 52% at 1500°K).

The data were interpreted in the form of apparent first-order rate constants and an Arrhenius plot of the results is shown in Figure 1. There is already considerable evidence to show that the decomposition of ethane does not display a constant kinetic order over a wide temperature range and the adoption of a first-order representation is merely a convenience. A smooth curve would therefore be expected *only* if the pressure were either constant or varied monotonically with temperature. The latter would be true for ideal shock tube behavior since the driver pressure is held virtually constant and the experimental pressure reduced in order to increase the temperature. Due to nonreproducible losses in the diaphragm rupture this condition cannot always be maintained: experiments in which the temperature deviated by more than 100° from the mean value for the same starting conditions were discarded in the subsequent analysis. It should be em-

(6) H. S. Glick, W. Squire, and A. Hertzberg, *Symp. (Int.) Combust. [Proc.]*, 5th, 393 (1955).

(7) J. N. Bradley, R. N. Butlin, and J. G. Quinn, *J. Sci. Instrum.*, 42, 901 (1965).

(8) C. W. Gear, *Proc. I.F.I.P. Congr.*, A81 (1968).

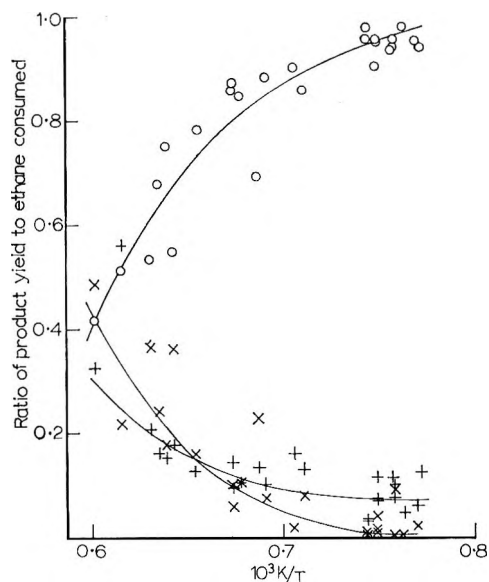


Figure 2. Product yields, expressed as a ratio of the ethane consumed, vs. reciprocal temperature: \circ , C_2H_4 ; \times , C_2H_2 ; $+$, CH_4 .

phasized that there is no suggestion that the data from such experiments were unreliable but simply that inclusion of this small number of results would have made the subsequent analysis intractable. For the same reason results obtained with 0.5% mixtures were not employed in the analysis nor were those experiments in which the products failed to give a satisfactory mass balance. With these restrictions the scatter was well within the experimental error predicted from the reaction times. In order to permit computer simulation, a smooth curve was selected as representative of these data. The curve illustrated has no theoretical significance and was deliberately drawn in such a way as to underestimate the sharpness of the transition and the turnover at high temperatures. This was intended to avoid the danger of very specific features of the behavior being given an undue role in the subsequent analysis.

A number of experiments were conducted with mixtures of 0.6% ethylene, 0.4% ethane, and 99.0% argon, and the results are also shown in Figure 1. The uncertainty in the analysis is much greater in these experiments.

The variation with temperature of the product distribution in the experiments using 1% mixture is illustrated in Figure 2.

Discussion

The most significant feature of the present investigation is the sharp transition in the Arrhenius behavior, the apparent activation energy changing from about 90 kcal/mol at 1250°K almost to zero at 1600°K. Although the total pressure of *ca.* 700 Torr is insufficient to maintain unimolecular rate constants at their high-pressure limiting values at these elevated temperatures

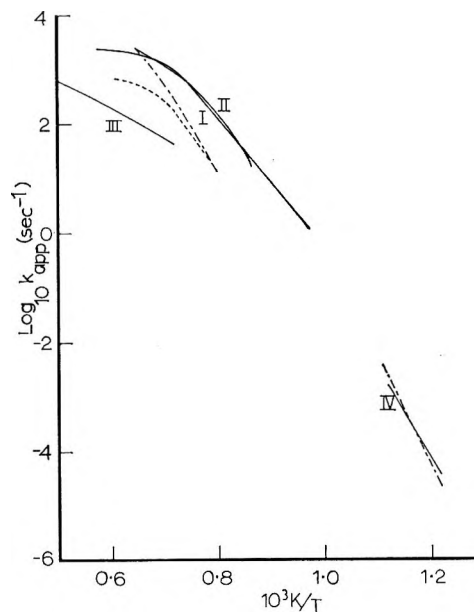


Figure 3. Comparison of present results with those of previous workers: I, Skinner and Ball (ref 5); II, Kozlov and Knorre (ref 3); III, Miller and Churchill (ref 4); IV, Kuchler and Thiele (ref 9); Lin and Back, footnote *c* (Table I); Laidler and Wojciechowski (ref 10). - - - - - denotes present results, - · - · - denotes results of calculations using "basic" mechanism.

such a pronounced effect is quite unpredicted. In addition, the variation of product distribution with temperature demonstrates that a change in mechanism parallels the change in Arrhenius behavior. The change in the nature of the products cannot be explained solely on the basis of the subsequent decomposition of ethylene to acetylene, denoted by



because the total formation of acetylene and ethylene falls relative to the amount of methane produced as the temperature increases.

The results of other investigations on ethane decomposition are shown for comparison in Figure 3.^{9,10} Coincidence of the plots is not to be expected as the investigations cover a wide range of pressure; however, all four high-temperature investigations show the same anomalous kinetic behavior, with the transition occurring at very similar temperatures. Shock tube studies on cyclopropane¹ and butane² pyrolysis have shown a similar effect. However, other systems, studied under the same experimental conditions, display no such deviation and demonstrate that the effect cannot be attributed to an artifact of the experimental technique.

A complete analysis of the ethane pyrolysis reaction would require the inclusion of experimental results at various pressures and compositions as, for example,

(9) L. Kuchler and H. Thiele, *Z. Phys. Chem., Abt. B*, **42**, 359 (1939).

(10) K. J. Laidler and B. W. Wojciechowski, *Proc. Roy. Soc. A*, **260**, 91 (1961).

Table I: High-Pressure Limiting Rate Constants for k_1 and k_4

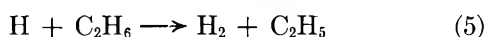
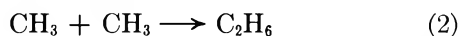
$\log A_1$, sec ⁻¹	E_1 , kcal/mol	$\log k_1$ at 1300°K	Ref	$\log A_4$, sec ⁻¹	E_4 , kcal/mol	$\log k_4$, at 1300°K	Ref
16.3	86.0	1.85	<i>a</i>	10.9	31.0	5.7	<i>f</i>
17.45	91.7	2.05	<i>b</i>	12.6	40.4	5.8	<i>g</i>
16.0	86.0	1.55	<i>c</i>	13.6	38.0	7.2	<i>c</i>
16.3	88.0	1.52	<i>d</i>	14.4	40.9	7.5	<i>h</i>
16.1	87.0	1.49	<i>e</i>				

^a See ref 13. ^b C. P. Quinn, *Proc. Roy. Soc. A*, **275**, 190 (1963). ^c M. C. Lin and M. H. Back, *Can. J. Chem.*, **44**, 2357 (1966). ^d A. B. Trenwith, *Trans. Faraday Soc.*, **62**, 1538 (1966). ^e G. L. Pratt, *Proc. Roy. Soc. A*, **293**, 235 (1966). ^f J. A. Kerr and A. F. Trotman-Dickenson, *J. Chem. Soc.*, 1602, 1611 (1960). ^g J. H. Purnell and C. P. Quinn, *Proc. Roy. Soc. A*, **270**, 267 (1962). ^h L. F. Loucks and K. J. Laidler, *Can. J. Chem.*, **45**, 2795 (1967).

those obtained by previous workers. However the significant feature of all the investigations is the anomalous high-temperature behavior and variation of the apparent first-order rate constant with pressure and composition is readily explained by the occurrence of at least two reactions of intermediate order in the mechanism ((1) and (4) below). It was therefore necessary, and indeed desirable, to attempt in the first instance an explanation of the data obtained with one apparatus at one composition.

The most serious shortcoming of the technique, which applies to *all* the investigations, is that it does not allow a wide variation in the extent of conversion for a given set of starting conditions. In those cases where such variation was obtained the rate appeared to increase with conversion and no evidence was provided for inhibition by reaction products. This observation is far from conclusive and was disregarded in the subsequent analysis.

A very simple mechanism which can be proposed to explain the kinetics of the thermal decomposition of ethane is the following



and it is worthwhile to examine the extent to which this mechanism can explain the experimental observations. The mechanism differs from that known to operate at lower temperatures only by the inclusion of reaction 2. Under high-temperature conditions with a larger value of k_1 , the methyl radical concentration will be appreciable and it becomes necessary to allow competition between reactions 2 and 3.

The first three reactions are together responsible for chain initiation. The various determinations of k_3 are in good agreement¹¹ and a "best" value¹² of $7.95 \times 10^8 \exp(-38.0 \text{ kcal}/RT) \text{ l. mol}^{-1} \text{ sec}^{-1}$ has been

selected. The rate constants k_1 and k_2 are related by the equilibrium constant which has been taken to have the value $1.74 \times 10^8 \exp(-86.1 \text{ kcal}/RT) \text{ atm.}^{13}$ The rate constant k_2 is then completely specified by the selection of the appropriate value for the rate constant k_1 . Experimental determinations of the high-pressure limiting value of k_1 are listed in Table I together with the values at 1300°K. The agreement here is rather less satisfactory, although the variation lies more in the preexponential factor than in the activation energy. A value of $1.26 \times 10^{16} \exp(-87.0 \text{ kcal}/RT) \text{ sec}^{-1}$ has been selected in the knowledge that it is somewhat lower than the average value.

At the high temperatures used here, the high-pressure limiting values are not applicable and it is therefore necessary to make the following correction. As mentioned above, because the formation of the shock wave is not instantaneous, a given set of starting conditions does not always lead to the same experimental conditions and, for this reason, a shock velocity measurement is always necessary to specify the latter. From a series of experiments at or close to a particular shock temperature, a corresponding average reflected shock pressure has been obtained. This shock pressure has then been converted to an apparent ethane pressure by assuming that argon has an energy transfer efficiency of 0.07 relative to ethane. This apparent ethane pressure has then been converted to an "effective" pressure at 978°K using the relation

$$p_2/p_1 = (T_2/T_1)^s$$

which appears in all theories of unimolecular reactions. The value of s has been chosen as 13. The falloff curves at 978°K given by Lin and Laidler¹⁴ have then been used to give the correction factors listed in Table II.

(11) A. F. Trotman-Dickenson and G. S. Milne, "Tables of Bimolecular Gas Reactions," National Bureau of Standards NSRDS-NBS9, 1967.

(12) J. R. McNesby and A. S. Gordon, *J. Amer. Chem. Soc.*, **77**, 4719 (1955).

(13) H. G. Davies and K. D. Williamson, *World Petrol. Congr., Proc.*, **5th**, 4 (1959).

(14) M. C. Lin and K. J. Laidler, *Trans. Faraday Soc.*, **64**, 79 (1968).

Table II: Correction Factors for Falloff Behavior of k_1 and k_4

Temp, °K	k_1/k_1^∞	k_4/k_4^∞
1250	0.166	0.0302
1300	0.132	0.0261
1350	0.104	0.0226
1400	0.083	0.0183
1450	0.062	0.0164
1500	0.050	0.0138
1550	0.035	0.0113
1600	0.022	0.0091
1650	0.011	0.0073

The falloff behavior of k_1 has a lower effect on the overall rate than the table suggests because, at high temperatures, the stationary methyl radical concentration tends to be controlled by competition between reactions 1 and 2, rather than 1 and 3. As microscopic reversibility requires that k_1 and k_2 are related by the equilibrium constant, the falloff of k_1 is paralleled by a corresponding fall in k_2 leaving the stationary methyl radical concentration unaffected. This argument does not apply to the falloff behavior of k_4 , which has been estimated assuming $s = 6$.

Literature values of k_4 are also listed in Table I. The situation here is more serious as two of the rate constant expressions differ from the other two by a factor of about 30. As no reason could be found for preferring one pair of rate constants compared with the other, a rate constant expression of $8.0 \times 10^{16} \exp(-38.0 \text{ kcal}/RT) \text{ sec}^{-1}$ has been selected which is the arithmetic mean of the logarithms of the rate constants at 1250 and 1550°K. Over the temperature range in question, this rate constant expression has a temperature coefficient close to all four literature values. However, the uncertainty in the preexponential term is much greater than that of any of the other rate constants involved in the mechanism. This means that the arbitrariness involved in the selection of the other rate constants, for example k_1 above, is unimportant and the preexponential term in k_4 may be regarded, within limits, as the sole adjustable parameter available for fitting to the experimental data.

In contrast to k_4 , rate constant expressions for k_5 and k_6 are reasonably well known. Schofield¹⁵ has carried out a least-squares analysis on the available values of k_5 and his "best" value of $1.3 \times 10^{11} \exp(-10.45 \text{ kcal}/RT) \text{ l. mol}^{-1} \text{ sec}^{-1}$ has been chosen. Typical radical recombination rate constants are known to lie in the range 10^{10} – $10^{11} \text{ l.}^2 \text{ mol}^{-2} \text{ sec}^{-1}$ and a value of $2.5 \times 10^{10} \text{ l.}^2 \text{ mol}^{-2} \text{ sec}^{-1}$ has been adopted for k_6 . A slightly low value has been chosen because recombination rate constants frequently show small negative temperature coefficients and at sufficiently low pressures falloff behavior would be expected. However, once again, the uncertainty is less than that of k_4 .

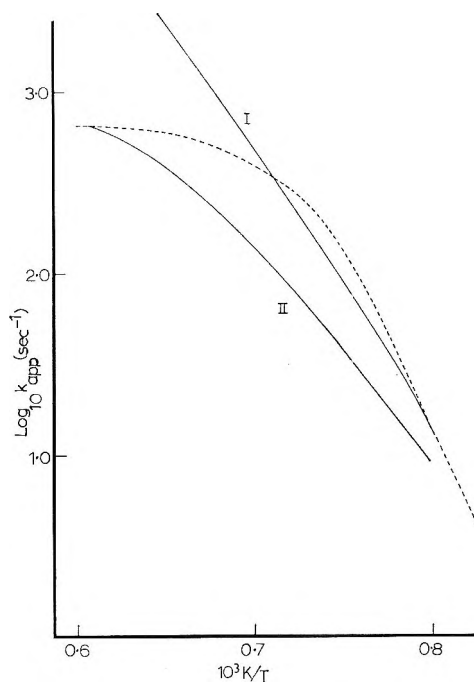
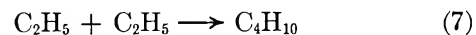


Figure 4. Comparison of experimental curve with the computer simulation: I, basic mechanism; II, basic mechanism plus $\text{CH}_3 + \text{C}_2\text{H}_5 \rightarrow \text{CH}_4 + \text{C}_2\text{H}_4$ (eq 9).

Reaction 6 has been chosen as the sole termination reaction in the mechanism. The alternative which



occurs at lower temperature has been neglected because no butane has been detected in the products, presumably because it breaks down rapidly at these temperatures.

The pyrolysis has been simulated on the computer without invoking any steady-state approximations, using the values of the rate constants discussed above. At the end of the reaction time, all radical concentrations are small compared with those of the stable products, apart from $[\text{CH}_3]$. The final product composition has therefore been calculated by assuming that the methyl radicals recombine to form ethane during the expansion. This assumption is very reasonable in view of the rapid fall in temperature and has been verified by simulating the expansion on the computer for a number of typical cases.

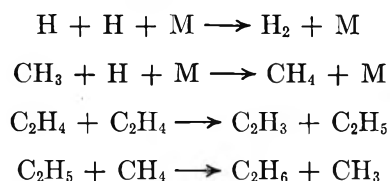
From the computations a plot of the apparent first-order rate constants k_{app} has been constructed for comparison with the experimental data (Figure 4, curve I). The agreement is reasonable at about 1250–1350°K although this agreement is to some extent artificial in view of the uncertainty in the preexponential term of k_4 . It also gives very satisfactory agreement with the low-temperature results shown in Figure 3. For these calculations, the rate constants were assumed to have their limiting values and the concentration chosen

(15) K. Schofield, *Planet. Space Sci.*, 15, 643 (1967).

Table III: Effect of Variation of the Selected Rate Constants on the Rate of Decomposition

Variation	-1300°K			-1550°K		
	Rate constant, sec ⁻¹	Factor	Factor, log units	Rate constant, sec ⁻¹	Factor	Factor, log units
No change	32.75			2368		
$k_1 \times 5$	79.9	$\times 2.44$	+0.387	2840	$\times 1.20$	+0.079
$k_3 \times 5$	83.0	$\times 2.54$	+0.405	3855	$\times 1.63$	+0.212
$k_4 \times 5$	150.4	$\times 4.6$	+0.663	3240	$\times 1.37$	+0.136
$k_5 \times 5$	48.7	$\times 1.49$	+0.173	3135	$\times 1.32$	+0.122
$k_6 \times 5$	25.5	$\times 0.806$	-0.109	1183	$\times 0.5$	-0.301

was that employed in the low-temperature determinations. Each rate constant has been varied in turn by a factor of 5 for temperatures of 1300 and 1550°K and the effect on the overall rate is shown in Table III. The most significant conclusion which can be drawn is that at low temperatures the overall rate is most sensitive to k_4 , which is the rate constant whose value is known with least accuracy. Similar calculations have shown that the reactions



play no significant role in the decomposition.

Although the mechanism gives a satisfactory explanation of the low-temperature behavior it does not explain the falloff observed in this and in other high-temperature investigations of ethane decomposition. It will be noted that some curvature in the calculated k_{app} is observed, arising from the falloff behavior of k_4 , but this is quite inadequate to explain the experimental findings.

A further insight into this behavior is obtained by examining the chain length of the decomposition. For each ethyl radical produced in the initiation sequence (1)–(3) one methane molecule is produced and $3/2$ ethane molecules are consumed. Thus an "effective" chain length ϕ_{eff} may be defined as

$$\phi_{\text{eff}} = \frac{[\text{C}_2\text{H}_6]_{\text{init}} - [\text{C}_2\text{H}_6]_{\text{final}} - \frac{3}{2}[\text{CH}_4]}{[\text{CH}_4]}$$

It should be noted that this is not the true chain length since it neglects the reappearance of some of the ethane in the termination step. The true chain length is therefore greater than the effective chain length. The latter has been chosen to obviate difficulties which would arise if an alternative termination step not involving the formation of ethane becomes important at high temperatures.

In Figure 5, the experimental values of $\log \phi_{\text{eff}}$ have been compared with the computed values as a function of reciprocal temperature. Despite considerable scat-

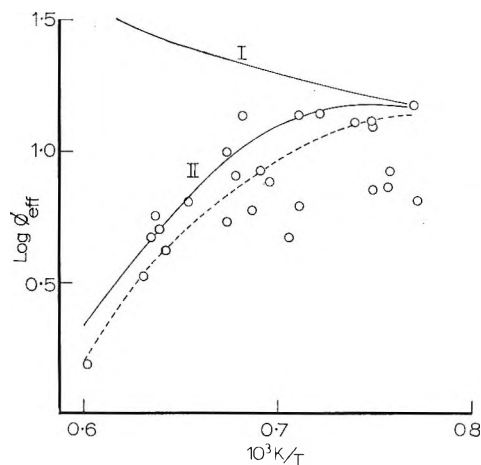


Figure 5. Logarithm of "effective" chain length ϕ_{eff} vs. reciprocal temperature: I, predicted by basic mechanism; II, predicted after inclusion of reactions 13 and 17.

ter it is apparent that the experimental falloff is associated with a reduction in chain length. With the mechanism above such a reduction could occur only if the falloff behavior of k_4 were so acute as to cause its rate actually to fall with increasing temperature. Thus although the falloff characteristics of k_4 calculated above may be imprecise, it would be difficult to reproduce the experimental observations in this way.

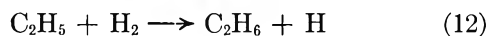
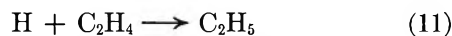
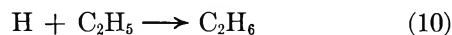
One pair of reactions which might have been expected to occur is



The first of these can be eliminated as propane was not detected in the products even in low-temperature investigations and, because the ratio k_9/k_8 is known to be *ca.* 0.04 at low temperature,¹¹ the same evidence indicates that reaction 9 is also unimportant. It might be expected that the value of k_9 would be intermediate between those of k_2 and k_6 , although the same disproportionation-recombination ratio would indicate a lower value. The possible effect of reaction 9 has therefore been deliberately exaggerated by carrying out the calculation with k_9 set equal to k_6 : the effect on the overall rate is illustrated in Figure 4, curve II.

It is interesting to note that both the overall rate and the effective chain length are significantly reduced. However, although the average temperature coefficient is lowered, the curvature of the Arrhenius plot is not reproduced.

It is therefore necessary to search for additional reactions which could inhibit the chain as the temperature increases. Three such reactions have been suggested previously



Of these, reaction 10 could clearly lead to a genuine reduction in chain length since the stationary radical concentrations will be greater at higher temperatures. On the other hand reactions 11 and 12 provide an explanation of the inhibition of the decomposition by the products which has been observed in some low-temperature investigations.¹⁶ In principle, it should be possible to test the effects of (10) and (12) experimentally either by varying the degree of conversion or by adding ethylene and hydrogen to the reactants.

The experiments with added ethylene proved inconclusive: it appears that, in the range 1500–1600°K, k_{app} may be reduced by a factor of about 2 for an increase in average ethylene concentration of about 10. The relative importance of these reactions is illustrated better by computer simulation.

In the first simulation of the effects of these three reactions, the "best" available values of the rate constants have been used (Table IV) and the result is shown in Figure 6,¹⁷ curve I. It is apparent that incorporation of these reactions into the mechanism leads to a change in the correct direction but the magnitude of the curvature is far from that required. Since the change is of the form expected it is necessary to consider whether the "best" values could be seriously in error. It is perhaps of some significance that Skinner and Ringrose¹⁷ deliberately selected rate constants for these reactions in excess of the literature values in order to explain induction periods in the hydrogen–oxygen reaction. Simulation using these values (Table IV) yielded curves II and III in Figure 6. (The value of k_4 was arbitrarily raised by a factor of 20.7 to obtain the upper curve.) The introduction of these additional reactions clearly reduces the temperature dependence of the decomposition but fails to reproduce the observed variation of the temperature coefficient. The alteration in behavior is almost wholly due to reaction 11 as expected from the relative magnitudes of the rate constants. Reactions 11 and 12 are merely the reverse of reactions involved in chain propagation and reaction 12 is an additional chain termination reaction. The only feasible alternative which might lead to a reduction in chain length with temperature would be a reaction in

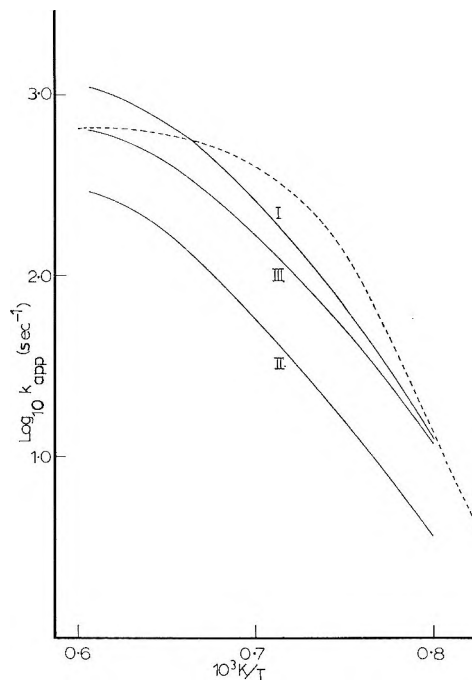
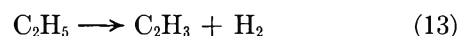
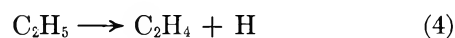


Figure 6. Comparison of experimental curve with the computer simulation including the reactions 10, 11, and 12: I, using "best" rate constants, ref 15 and footnote b in Table IV; II, using rate constants from ref 17; III, using rate constants from ref 17 + $20.7 \times k_4$.

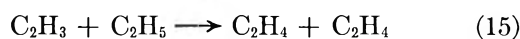
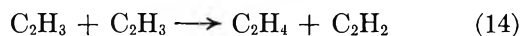
parallel with the propagation step but with a higher temperature coefficient. One possibility is that the reaction



competes with



As both reactions have virtually identical heats of reaction,¹⁸ $\Delta H^\circ_{298} = 38.4$ kcal/mol for (4) *cf.* 38.8 for (13), it is not inconceivable that (13) would have the higher activation energy and hence become predominant at high temperatures. Introducing this reaction necessitates additional reactions removing C_2H_3 radicals and the termination steps



have been added to the mechanism and assigned identical rate constants to that of the major chain termination reaction 6. A value of k_{13} of $7.95 \times 10^{17} \exp(-93.5 \text{ kcal}/RT) \text{ sec}^{-1}$ gave a k_{app} shown by curve I in Figure 7.

(16) M. C. Lin and M. H. Back, *Can. J. Chem.*, **44**, 2369 (1966).

(17) G. B. Skinner and G. H. Ringrose, *J. Chem. Phys.*, **43**, 4129 (1965).

(18) W. M. D. Bryant, *J. Polym. Sci.*, **6**, 359 (1951); A. G. Harrison and F. P. Lossing, *J. Amer. Chem. Soc.*, **82**, 519 (1960); J. B. Farmer and F. P. Lossing, *Can. J. Chem.*, **33**, 861 (1955).

Table IV: Rate Constants for Reactions 10, 11, and 12

Reaction	Rate constants, l. mol ⁻¹ sec ⁻¹		
	Best available value	Ref	Ref 17 value
H + C ₂ H ₅ → C ₂ H ₆ (10)	3.98 × 10 ¹⁰		4.40 × 10 ¹²
H + C ₂ H ₄ → C ₂ H ₃ (11)	2.7 × 10 ¹⁰ exp(-3.04 kcal/RT)	a	4.00 × 10 ¹⁰ exp(-1.58 kcal/RT)
C ₂ H ₃ + H ₂ → C ₂ H ₆ + H (12)	3.24 × 10 ¹⁰ exp(-11.3 kcal/RT)	b	1.56 × 10 ⁹ exp(-4.05 kcal/RT)

^a See ref 15. ^b P. J. Boddy and E. W. R. Steacie, *Can. J. Chem.*, **39**, 13 (1961).

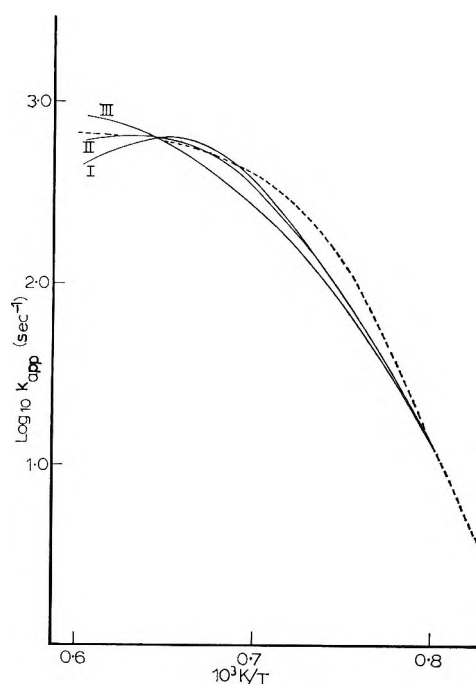
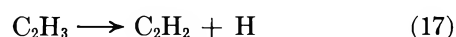


Figure 7. Comparison of experimental curve with the computer simulation: I basic mechanism with (13); II with (13) and (17); and III with (19).

This curve explains the observed kinetic behavior quite well but the acetylene yields of the revised mechanism are still below the experimental values. Manipulation of the termination rate constants within "reasonable" limits, *e.g.*, by a factor of 10 above the selected value or by reducing to a very low value, failed to give any significant improvement.

It is apparent that other reactions must produce acetylene at these high temperatures and an obvious step to follow (13) is the unimolecular decomposition of the vinyl radical



This will clearly lead to the acetylene necessary but at the same time it reduces the effect of (13) as a chain retarding reaction because it yields hydrogen atoms which can continue the chain. The computer simulation was therefore used to determine whether rate constants could be allotted to (13) and (17) which would simulate both the overall rate behavior and the product yields. The results of calculations based on $k_{13} = 3.0 \times 10^{16}$

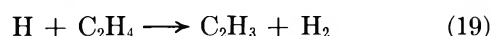
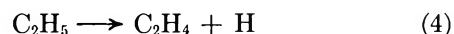
exp(-80.0 kcal/RT) sec⁻¹ and $k_{17} = 2.0 \times 10^4$ sec⁻¹ are shown in Figure 7, curve II and Figure 5, curve II and it can be seen that satisfactory simulation is possible.

It should be emphasized that the numerical values allocated to k_{13} and k_{17} have only limited significance and, in particular, the Arrhenius temperature coefficients should not be equated with activation energies. To begin with both are unimolecular reactions and would not be expected to obey simple Arrhenius relations. Furthermore the simulation did not include reactions 9 and 11 above nor did it include the reaction

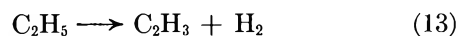


which is a parallel to reaction 17 in that it repropagates the chain. The important feature is that it has only proved possible to simulate the experimental behavior by incorporating reactions 13 and 17 into the mechanism but in order to determine the absolute values of these rate constants it would be necessary to know values for the remaining rate constants with greater certainty.

One further possibility must be investigated. The sequence



would be equivalent in principle to the one-step reaction



A mean value of k_{19} of 1.746×10^{10} exp(-6900 kcal/RT) l. mol⁻¹ sec⁻¹ has been compiled from several sources¹⁵ and has been used in the mechanism as an alternative to (13). Reactions 14-17 were not included to provide the maximum opportunity for reaction 19 to have the desired effect. Figure 7, curve III shows that this reaction is inadequate to explain the behavior: its effect would have been even lower if the other reactions had also been included.

The parallel reaction



is readily discounted because the rate constant is known¹⁹ and incorporation of this step into the mecha-

(19) A. F. Trotman-Dickenson and E. W. R. Steacie, *J. Chem. Phys.*, **19**, 169 (1951).

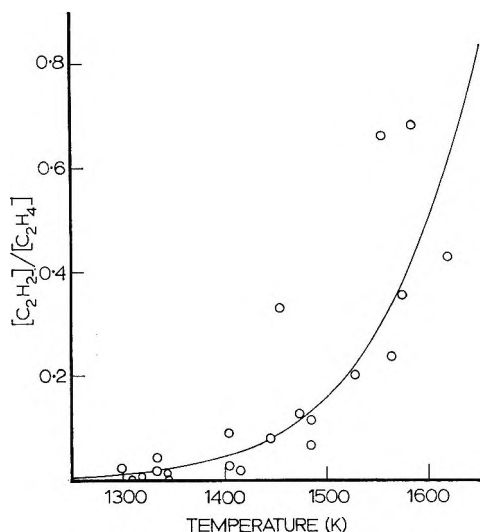


Figure 8. Variation of $[C_2H_2]/[C_2H_4]$ with temperature. The line corresponds to the results predicted by the mechanism which includes reactions 13 and 17.

nism, both with the literature value of the rate constant and with a value ten times greater, had no significant effect on the overall rate.

It is perhaps worth noting that the apparent turnover at the highest temperatures can also be explained by the inclusion of reactions 13 and 17. The minor discrepancy at intermediate temperatures has been removed in subsequent computer simulations by manipulation of k_4 within the limits imposed by the experimental measurements: the results have not been recorded as the exercise appears to be of little quantitative value.

No mention has been made of the subsequent decomposition of ethylene to acetylene (Figure 8). The experiments with ethane-ethylene mixtures demonstrate that the reaction becomes significant at high temperatures. It will not affect the kinetic behavior under discussion, except *via* reactions already mentioned, but it will affect the yield of acetylene. This further emphasizes the difficulty of ascribing reliable values to the rate constants k_{13} and k_{17} . The suggested high-temperature decomposition of the ethyl radical would predict a similar transition in the pyrolysis of any hydrocarbon in which ethyl radicals play a similar role. It should be noted in conclusion that the pyrolysis of butane shows an almost identical transition but the pyrolyses of propane and isobutane are quite normal.

Acknowledgments. The authors wish to express their gratitude to the Institute of Petroleum (Hydrocarbon Research Panel) for the award of a research studentship in support of this work.

Appendix

Unstable propagation of absolute errors occurs in step-by-step methods for the numerical solution of an initial-value differential system

$$y'(x) = f(x, y), y(0) \text{ specified}$$

when the step-length h is such that $h\lambda_i$ lies outside the method's region of stability for any eigenvalue λ_i of $\partial f/\partial y$ having $\text{Re}(h\lambda_i) < 0$. The boundary of this region in the left-half complex plane usually lies within a fairly small distance from the origin (intersecting the real axis near -2.7 for the Runge-Kutta-Merson method, for example), in which case stability requires that $|h|$ be very small for stiff differential systems. Gear (1968) has, however, devised a class of multistep methods whose stability regions include much of the left-half λh plane, and in particular the whole of the negative real axis, so that error propagation is stable for all $|h|$, except possibly when $\text{Re}(h\lambda_i) > 0$ or $|\text{Re}(\lambda_i)| \ll |\text{Im}(\lambda_i)|$ for some λ_i .

Gear's step-by-step method of order k ($1 \leq k \leq 6$) is conveniently written in a Nordsieck form, in which the approximate solution vector

$$a_n = \{y_n, hy_n', h^2y_n''/2!, \dots, h^ky_n^{(k)}/k!\}^T$$

is calculated at each pivotal point $x_n (=x_{n-1} + h)$ in turn using the Newton iterative process

$$a_n^{(0)} = Aa_{n-1}$$

$$a_n^{(m+1)} = a_n^{(m)} - l\{I - hl_0\partial f/\partial y\}^{-1} \times \{hy_n'^{(m)} - hf(x_n, y_n^{(m)})\} \quad (m = 0, 1, \dots, M-1)$$

where A is the Pascal triangle matrix

$$A_{i,j} = \binom{j}{i} \quad (i \leq j) \\ 0 \quad (i > j)$$

and the elements of $l \{l_0, l_1, \dots, l_k\}^T$ are given in Table V.

Table V: Coefficients for Gear's Method

k	1	2	3	4	5	6
l_0	1	2/3	6/11	24/50	120/274	720/1764
l_1	1	3/3	11/11	50/50	274/274	1764/1764
l_2	0	1/3	6/11	35/50	225/274	1624/1764
l_3	0	0	1/11	10/50	85/274	735/1764
l_4	0	0	0	1/50	15/274	175/1764
l_5	0	0	0	0	1/274	21/1764
l_6	0	0	0	0	0	1/1764

The iteration is terminated when

$$\|y_n^{(m+1)} - y_n^{(m)}\| / \|y_n^{(m+1)}\|$$

is comparable with the relative accuracy of the number representation, $\|\cdot\|$ being interpreted as the element of largest magnitude for computational convenience, though another norm could be substituted. The Jacobian $\partial f/\partial y$ is evaluated only when the iteration has not effectively converged after a small number (3, on

empirical grounds) of iterations. It may either be calculated exactly if appropriate code has been generated by the user or by an automatic differentiation package, or alternatively each column $\partial f/\partial y_j$ may be approximated numerically by

$$\{f(x_n, y_n + \delta e_j) - f(x_n, y_n)\}/\delta$$

for some suitable δ , where the j th element of e_j is unity and the remainder zero. A continuing failure to converge is countered by reducing $|h|$.

The step-length may also be reduced by the error control procedure, which ensures that

$$\|y_n^{(M)} - y_n^{(0)}\|/\|y_n^{(M)}\| \leq |h|\eta$$

where η is the maximum relative error which the user will tolerate over a unit interval in x . Failure of this test results in repetition of the step with $|h|$ decreased, while otherwise the probable effect of increasing $|h|$ is assessed on the assumption that the local error behaves like h^{k+1} . Note that changing h by a factor c

is effected by simply multiplying the i th vector element ($i = 1, \dots, k$) of a_n by c^i .

The integration commences with $k = 1$, and k is successively increased to 5 by unit steps, the stability region for $k = 6$ being unsatisfactory. The additional vector element in a_n required at each increase is calculated by approximating

$$\frac{h^{k+1}}{(k+1)!} y_n^{(k+1)}$$

by

$$\frac{1}{(k+1)} \left\{ \frac{h^k}{k!} y_n^{(k)} - \frac{h^k}{k!} y_{n-1}^{(k)} \right\}$$

Whenever h or k are changed, no increase in either is permitted for at least k steps to allow the resulting perturbation to decay.

Further theoretical details are contained in ref 8 and an ALGOL program is available from Dr. J. Oliver, Computing Centre, University of Essex.

Ignition of Aromatic Hydrocarbon-Oxygen Mixtures by Shock Waves

by **Hajime Miyama**

Basic Research Laboratories, Toray Laboratories, Inc., Tebiro, Kamakura, Japan (Received December 21, 1970)

Publication costs borne completely by The Journal of Physical Chemistry

Induction periods τ for the oxidation of various hydrocarbons were measured by using shock-tube technique. The following linear relationships were obtained between $\log \tau[\text{O}_2]$ and $1/T$, where T is temperature behind the reflected shock wave: $\log \tau[\text{O}_2] = (9300 \pm 280)/T - (7.00 \pm 0.77)$ for benzene, $\log \tau[\text{O}_2] = (10,360 \pm 310)/T - (7.22 \pm 0.21)$ for toluene, $\log \tau[\text{O}_2] = (8880 \pm 260)/T - (6.29 \pm 0.20)$ for *o*-xylene, $\log \tau[\text{O}_2] = (8920 \pm 310)/T - (6.24 \pm 0.24)$ for *m*-xylene, $\log \tau[\text{O}_2] = (8420 \pm 310)/T - (5.98 \pm 0.23)$ for *p*-xylene, $\log \tau[\text{O}_2] = (6840 \pm 240)/T - (5.33 \pm 0.17)$ for ethylbenzene, $\log \tau[\text{O}_2] = (9660 \pm 390)/T - (7.52 \pm 0.17)$ for propylbenzene, and $\log \tau[\text{O}_2] = (12,200 \pm 530)/T - (8.72 \pm 0.23)$ for 1,3,5-trimethylbenzene. Here τ is expressed in seconds, $[\text{O}_2]$ in moles per liter, and T is degrees Kelvin.

Induction periods for the oxidation of aromatic hydrocarbons at high temperatures were measured by Mullins¹ in the range 750–1100° by injecting the fuel into a hot air stream. Also, at higher temperatures, Kogarko and Borisov² measured induction periods for 3% benzene–97% air mixtures in shock wave and obtained the relationship

$$\tau = 10^{-13.6} \exp(-26,000/T) \quad (1)$$

where τ is induction period in seconds and T is shock temperature in degrees Kelvin. However, no data are available for other aromatics at higher temperatures. It is expected that aromatics having different substitu-

ents such as methyl, ethyl, and propyl may give different expressions for τ values depending on the kind, number, and position of the substituents in a benzene ring. Therefore, in the present study, we measured induction periods for benzene-, toluene-, *o*-xylene-, *m*-xylene-, *p*-xylene-, ethylbenzene-, propylbenzene-, and 1,3,5-trimethylbenzene-oxygen-argon mixtures.

Experimental Section

A shock tube consisting of a 2.4-m long driver section

(1) B. P. Mullins, *Fuel*, **32**, 363 (1953).

(2) S. M. Kogarko and A. A. Borisov, *Bull. Acad. Sci. USSR*, No. 8, 1255 (1960).

and a 3.5-m experimental section each made of 7.6-cm i.d. diameter stainless steel tubing was used. The velocity of an incident shock wave was measured with two thin platinum film thermometers which were placed at a distance of 130.000 mm from each other, and with an electronic counter. One of the thermometers was stationed 5.5 mm from the end plate where two calcium fluoride windows which were used for infrared emission measurement, a quartz window for ultraviolet emission measurement, and a pressure transducer were inserted flush with walls of the tube. Infrared emission was measured with an InSb infrared detector coupled to a monochromator.³ In the present study, the induction period of pressure increase, that of OH absorption (3067 Å), and that of aromatic hydrocarbon emission (3.29 μ for benzene, toluene, and xylene, 3.30 μ for ethylbenzene and propylbenzene, and 3.33 μ for 1,3,5-trimethylbenzene) were measured simultaneously in reflected shock wave. Since the three induction periods coincided exactly, values of the induction period measured by following the infrared emission were employed. All runs were performed in a fuel-lean region where no soot appeared during the reaction.

The gas mixtures were prepared manometrically in an all-glass apparatus and stirred magnetically in a 10-l. reservoir for 1 hr before use. Commercially available aromatic hydrocarbons of a special grade were used after washing with concentrated sulfuric acid, aqueous sodium hydroxide, and distilled water, successively, dehydration with calcium chloride, and distillation over metallic sodium. Dry oxygen (99.5%) and argon (99.999%) were used without further purification. Other experimental details were the same as in the previous paper.⁴

Results and Discussion

Experimental conditions are summarized in Table I. For all mixtures, the best expression for the dependence of τ on the temperature and on the composition of the mixture was found to be a linear relationship between $\log \tau[\text{O}_2]$ and $1/T$, where T is temperature behind the reflected shock wave. The case of benzene is shown in Figure 1.

The equation (1) of Kogarko and Borisov² was obtained for 3% benzene-97% air mixtures at 1 atm. This can be converted into two plots in Figure 1 by assuming two possible cases: (a) nitrogen is relaxed translationally, rotationally, and vibrationally; and (b) nitrogen is relaxed translationally and rotationally. Our plot for benzene-oxygen-argon is close to their plot corresponding to case a. This agreement was also confirmed by measuring τ for benzene-oxygen-nitrogen mixtures and was discussed in a previous paper.⁵

The least-squares expressions for eight aromatics are

$$\log \tau[\text{O}_2] = (9300 \pm 280)/T - (7.00 \pm 0.07) \quad (\text{for benzene-oxygen-argon}) \quad (2)$$

$$\log \tau[\text{O}_2] = (10,360 \pm 310)/T - (7.22 \pm 0.21) \quad (\text{for toluene-oxygen-argon}) \quad (3)$$

$$\log \tau[\text{O}_2] = (8880 \pm 260)/T - (6.29 \pm 0.20) \quad (\text{for } o\text{-xylene-oxygen-argon}) \quad (4)$$

$$\log \tau[\text{O}_2] = (8920 \pm 310)/T - (6.24 \pm 0.24) \quad (\text{for } m\text{-xylene-oxygen-argon}) \quad (5)$$

$$\log \tau[\text{O}_2] = (8420 \pm 310)/T - (5.98 \pm 0.23) \quad (\text{for } p\text{-xylene-oxygen-argon}) \quad (6)$$

$$\log \tau[\text{O}_2] = (6840 \pm 240)/T - (5.33 \pm 0.17) \quad (\text{for ethylbenzene-oxygen-argon}) \quad (7)$$

$$\log \tau[\text{O}_2] = (9660 \pm 390)/T - (7.52 \pm 0.17) \quad (\text{for propylbenzene-oxygen-argon}) \quad (8)$$

$$\log \tau[\text{O}_2] = (12,200 \pm 530)/T - (8.72 \pm 0.23) \quad (\text{for 1,3,5-trimethylbenzene-oxygen-argon}) \quad (9)$$

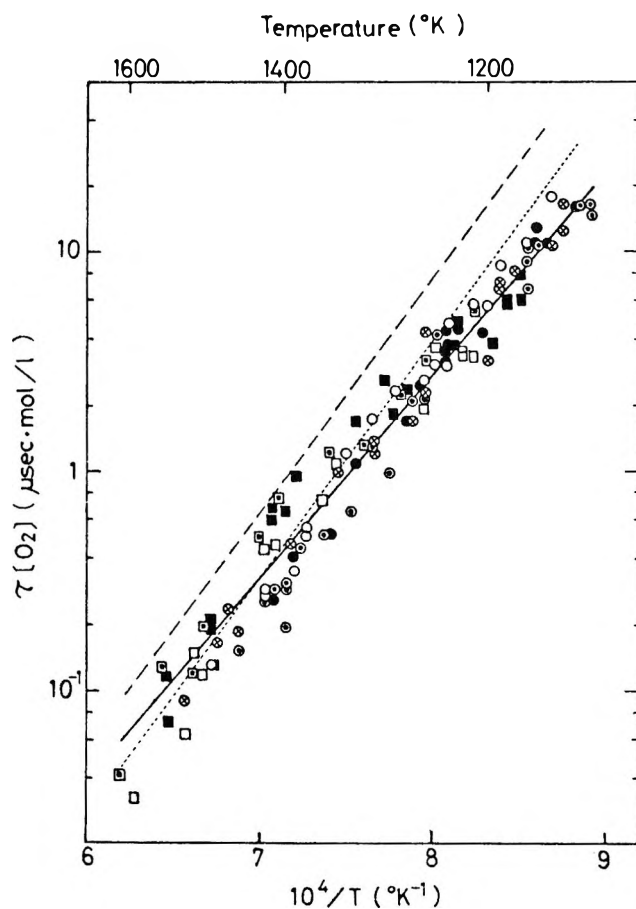


Figure 1. Relation between $\log \tau[\text{O}_2]$ and $1/T$ for benzene-oxygen-argon: O, mixture BI; ●, BII; ○, BIII; ⊗, BIV; □, BV; ■, BVI; ◻, BVII. Dotted line: case a (data of Kogarko and Borisov for benzene-air); dashed line: case b (data of Kogarko and Borisov for benzene-air).

(3) C. R. Orr, *Symp. Combust., 9th, Cornell Univ., Ithaca, N. Y., 1962*, 1034 (1963); K. G. P. Sulzmann, *J. Quant. Spectrosc. Radiat. Transfer*, **4**, 375 (1964).

(4) H. Miyama and T. Takeyama, *Bull. Chem. Soc. Jap.*, **38**, 37 (1965); T. Takeyama and H. Miyama, *Symp. Combust., 11th, Univ. Calif., Berkeley, 1966*, 845 (1967).

(5) H. Miyama, *J. Chem. Phys.*, **52**, 3850 (1970).

Table I: Experimental Conditions

Mixture		Fuel, %	O ₂ , %	Ar, %	Temp, °K	Pressure, atm	Induction period, μsec
Benzene-oxygen-argon	BI	0.5	19.5	80	1150-1490	5.50-7.40	15-1280
	BII	1.0	19.0	80	1130-1410	5.94-7.00	27-1200
	BIII	2.0	18.0	80	1090-1450	5.46-7.00	18-1220
	BIV	4.0	16.0	80	1140-1520	5.40-7.37	13-1375
	BV	1.0	9.0	90	1210-1590	5.90-6.65	8-640
	BVI	2.0	8.0	90	1175-1545	5.58-7.08	20-1125
	BVII	2.75	7.25	90	1210-1615	5.41-6.74	14-1180
Toluene-oxygen-argon	TI	0.25	9.75	90	1255-1795	5.44-6.47	8-825
	TII	0.5	9.5	90	1230-1760	4.85-6.39	9-1300
	TIII	1.0	9.0	90	1265-1745	4.99-6.60	10-1130
	TIV	2.0	8.0	90	1340-1725	5.37-6.46	13-1080
	TV	2.25	7.75	90	1235-1800	4.82-6.45	11-1300
	TVI	2.5	7.5	90	1305-1805	5.21-6.34	18-1420
	TVII	2.75	7.25	90	1330-1770	5.00-6.70	18-1020
<i>o</i> -Xylene-oxygen-argon	OI	0.25	9.75	90	1250-1900	4.60-7.03	7-1250
	OII	0.5	9.5	90	1265-1835	5.15-6.87	5-1000
	OIII	1.0	9.0	90	1285-1870	4.00-5.76	11-960
	OIV	2.0	8.0	90	1360-1940	3.50-6.02	12-520
	OV	2.25	7.75	90	1385-1940	2.77-5.56	20-165
	OVI	2.5	7.5	90	1500-2160	3.38-5.36	10-120
	OVII	2.75	7.25	90	1470-2035	3.98-5.34	10-175
<i>m</i> -Xylene-oxygen-argon	MI	0.25	9.75	90	1270-1685	5.50-6.93	13-1125
	MII	0.5	9.5	90	1245-1765	4.94-6.81	4-1300
	MIII	1.0	9.0	90	1235-1770	4.91-6.79	14-1225
	MIV	2.0	8.0	90	1265-1880	4.71-7.70	18-1160
	MV	2.25	7.75	90	1360-1920	4.91-6.91	17-440
	MVI	2.5	7.5	90	1380-1985	3.35-6.70	14-400
	MVII	2.75	7.25	90	1585-2120	3.98-5.87	4-35
<i>p</i> -Xylene-oxygen-argon	PI	0.25	9.75	90	1235-1625	5.13-6.92	22-1500
	PII	0.5	9.5	90	1265-1715	5.36-6.69	16-860
	PIII	1.0	9.0	90	1280-1720	5.30-6.96	12-800
	PIV	2.0	8.0	90	1240-1790	4.47-7.03	16-1250
	PV	2.25	7.75	90	1285-1875	3.93-6.70	21-890
	PVI	2.5	7.5	90	1330-1875	4.10-6.71	11-460
	PVII	2.75	7.25	90	1330-1985	4.63-6.75	12-470
Ethylbenzene-oxygen-argon	EI	0.25	9.75	90	1140-1625	4.62-5.77	12-450
	EII	0.5	9.5	90	1170-1715	4.77-6.00	7-800
	EIII	1.0	9.0	90	1120-1700	4.66-6.03	12-900
	EIV	2.0	8.0	90	1210-1760	4.23-6.19	22-300
	EV	2.25	7.75	90	1260-1900	4.08-6.10	10-240
Propylbenzene-oxygen-argon	PBI	0.25	9.75	90	1190-1870	4.48-5.90	2-900
	PBII	0.5	9.5	90	1235-1735	4.46-5.72	4-296
	PBIII	1.0	9.0	90	1565-1735	4.66-5.23	2-12
1,3,5-Trimethylbenzene-oxygen-argon	TBI	0.25	9.75	90	1235-1800	4.43-5.69	1-1280
	TBII	0.5	9.5	90	1425-1925	3.96-5.59	2-200
	TBIII	1.0	9.0	90	1810	4.53-5.10	1-4

Here τ is expressed in seconds, $[O_2]$ in moles per liter, and T is degrees Kelvin. Activation energies obtained from these equations are 42.5 kcal/mol for benzene, 47.4 kcal/mol for toluene, 40.6 kcal/mol for *o*-xylene, 40.8 kcal/mol for *m*-xylene, 38.5 kcal/mol for *p*-xylene, 31.3 kcal/mol for ethylbenzene, 44.2 kcal/mol for propylbenzene, and 55.8 kcal/mol for 1,3,5-trimethylbenzene. On the other hand, Mullins' values for aromatic hydrocarbon-air mixtures are 47.2 kcal/mol for benzene, 41.0 kcal/mol for toluene, 34.3 kcal/mol for xylene, and 45.7 kcal/mol for ethylbenzene. There is no close agreement between his and our values.

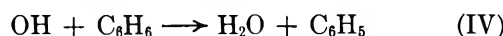
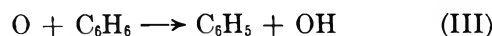
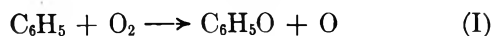
Also, relative values of activation energies among various fuel-oxygen mixtures are different between his and our experiments. These differences cannot be explained even if the difference of experimental methods is taken into account.

Many years ago, the mechanism of benzene oxidation at 500-700° was proposed by Burgoyne⁶ and Norrish and Taylor.⁷ The former assumed the existence of

(6) J. H. Burgoyne, *Proc. Roy. Soc., Ser. A*, **175**, 539 (1940).

(7) R. G. W. Norrish and G. W. Taylor, *ibid.*, **234**, 160 (1955).

$C_6H_6O_2$ and the latter $C_6H_5O_2$ as an intermediate species. However, at higher temperatures as in the present experiment, these intermediates are considered to be very unstable. Thus, the following mechanism assuming C_6H_5 as a chain carrier is considered as one possibility.



If the stationary-state method is applied to this scheme on an assumption that reaction I is rate determining, a linear relationship between $\log \tau[O_2]$ and $1/T$ may be derived as in the case of H_2-O_2 reaction.⁸ If a similar mechanism is applied to other aromatics, these aromatics having different substituents may give different radicals such as $(C_6H_5)CH_2$, $(CH_3C_6H_5)CH_2$,

$(C_6H_5)_2CH_2$, $(C_6H_5)_3CH_2$, and $(CH_3)_2(C_6H_5)CH_2$, which show different reactivity in each reaction corresponding to (I). However, we could not find any reasonable correlation between the above described experimental activation energies and reactivities of different aromatic radicals. In order to explain the difference of activation energies of oxidation among various aromatic hydrocarbons, a more detailed mechanism is desired. The present results are not sufficient for this purpose and further accumulation of experimental evidence is required.

Acknowledgment. The author wishes to express his thanks to Messrs. K. Sugiyama and Y. Oyama for their help in the experiment and to Professor G. B. Kistiakowsky, who initiated the author into the field of combustion kinetics.

(8) H. Miyama and T. Takeyama, *J. Chem. Phys.*, **41**, 2287 (1964).

Initiation Rate for Shock-Heated Hydrogen-Oxygen-Carbon Monoxide-Argon

Mixtures as Determined by OH Induction Time Measurements

by *W. C. Gardiner, Jr.*,* *M. McFarland*, *K. Morinaga*, *T. Takeyama*, and *B. F. Walker*

Department of Chemistry, The University of Texas, Austin, Texas 78712 (Received January 8, 1971)

Publication costs assisted by the Robert A. Welch Foundation

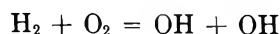
Induction times for OH were determined in incident shock wave experiments with $H_2:O_2:CO:Ar = 1:5:3:91$ mixtures over the temperature range 1400–2500°K. The data are compared to similar experiments with $H_2:O_2:Ar = 1:5:94$ and used to derive a rate constant for the chain initiation reaction $CO + O_2 = CO_2 + O$. The resulting Arrhenius expression $k = 3.1 \times 10^8 \exp(-38,000 \text{ kcal}/RT) \text{ l. mol}^{-1} \text{ sec}^{-1}$ is compared to previous measurements.

I. Introduction

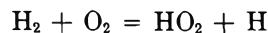
Finding the identity and rate of the homogeneous chain initiation step in the hydrogen-oxygen reaction has proved to be a difficult experimental problem.¹ In mixtures of hydrogen and oxygen containing carbon monoxide, however, some direct experiments on the chain initiation rate can be done.²⁻⁶ It is assumed that the atom transfer reaction



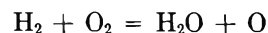
provides an alternative to the pathways usually assumed for chain initiation in absence of CO



or



or



or

(1) C. B. Wakefield, Dissertation, University of Texas, 1969.

(2) B. F. Walker, Dissertation, University of Texas, 1970.

(3) B. F. Myers, E. R. Bartle, and K. G. P. Sulzmann, *J. Chem. Phys.*, **42**, 3969 (1965); **43**, 1220 (1965).

(4) R. S. Brokaw, *Symp. Combust.*, *11th, Berkeley, Calif., 1966*, 1063 (1967).

(5) A. M. Dean and G. B. Kistiakowsky, *J. Chem. Phys.*, **53**, 830 (1970).

(6) T. A. Brabbs, F. E. Belles, and R. S. Brokaw, *Symp. Combust.*, *13th, Salt Lake City, 1970*, to be published.

impurities = atoms or radicals

Shock tube experiments on other systems also yield information on the rate of reaction 10 or its reverse (-10) .⁷⁻¹⁰

Several measurements of the rate constant of reaction 10 have been reported. They are not at all in agreement with one another in the temperature range in which the oxidation of CO in the presence of hydrogen can be studied by shock tube methods, about 1200–2500°K. For a temperature of 1600°K, the Arrhenius expressions recommended give, in $\text{l. mol}^{-1} \text{sec}^{-1}$ units: $k_{10} = 410$ (ref 3); 740 (ref 4); 540 (ref 5); 43,000 (ref 6); 12,000 (ref 7, from $k_1 = 30 \times$ value of ref 3); 300,000 (ref 8); 280 (ref 9); 820 (ref 10); and 990 or 1400 (ref 11). It is clear that the available data do not permit any definite conclusions about the chain initiation rate to be drawn and that additional experiments are needed.

II. Experimental Section

We investigated induction times for appearance of OH radical in mixtures with nominal compositions $\text{H}_2:\text{O}_2:\text{Ar} = 1:5:94$ and $\text{H}_2:\text{O}_2:\text{CO}:\text{Ar} = 1:5:3:91$ heated in incident shock waves to temperatures in the range $1400 < T < 2500^\circ\text{K}$ and pressures in the range $0.15 < p < 0.3$ atm. The apparatus and procedures have been described previously.¹² As in previous experiments with $\text{H}_2\text{-O}_2\text{-Ar}$ mixtures, the induction time was defined by attainment of $[\text{OH}] = 2.5 \times 10^{-7}$ mol/l.¹³ To compensate for random run-to-run variations in the Bi lamp source, the extinction coefficient ϵ in $I = I_0 \exp(-\epsilon[\text{OH}])$ was calculated from the formula $\epsilon_{i,N} = \epsilon_{0.25}(\epsilon_i/\bar{\epsilon})$. Here $\epsilon_{0.25}$ is the average extinction coefficient of the lamp for $[\text{OH}] < 10^{-6} M$ found by Ripley,¹³ ϵ_i is the extinction coefficient found from applying Beer's law to the measured transmission and computed post-combustion value of $[\text{OH}]$ in a given experiment, $\bar{\epsilon}$ is the average extinction coefficient for the range of $[\text{OH}]$ in which the post-combustion value of $[\text{OH}]$ falls, and $\epsilon_{i,N}$ is the normalized extinction coefficient used to determine the transmission at $[\text{OH}] = 2.5 \times 10^{-7} M$. The time between arrival of the shock wave, as detected by a laser-schlieren station, and ignition was multiplied by the shock density ratio σ to convert from laboratory to gas time¹⁴ and by the initial post-shock oxygen concentration $[\text{O}_2]_0$ to scale the ignition rate according to reactant concentration.¹⁵ The results are shown in Figure 1.

The induction time data were subjected to a conventional regression analysis in the $\log(\sigma[\text{O}_2]_0 t_i)$, $10^4/T$ plane¹⁶ using a locally modified version of a standard least-squares routine.¹⁷ An "F" test showed that there was not a significant difference between the variances of the two data sets. Both the $\text{H}_2:\text{O}_2:\text{Ar} = 1:5:94$ and the $\text{H}_2:\text{O}_2:\text{CO}:\text{Ar} = 1:5:3:91$ data sets proved to have virtually identical variances when fit with quadratic $[\log(\sigma[\text{O}_2]_0 t_i) = a + b(10^4/T) + c$

$(10^8/T^2)]$ rather than linear $[\log(\sigma[\text{O}_2]_0 t_i) = a + b(10^4/T)]$ regression lines. Linear regressions were therefore adopted for comparing the two sets of data with one another. The two straight lines generated by the regressions are shown in Figure 1. Their equations are

$$\log(\sigma[\text{O}_2]_0 t_i) = -8.150 \pm 0.0078 + (0.3401 \pm 0.0075)(10^4/T - 5.213)$$

for 33 data points with $\text{H}_2:\text{O}_2:\text{Ar} = 1:5:94$ and

$$\log(\sigma[\text{O}_2]_0 t_i) = -8.122 \pm 0.0064 + (0.3392 \pm 0.0065)(10^4/T - 5.518)$$

for 46 data points with $\text{H}_2:\text{O}_2:\text{CO}:\text{Ar} = 1:5:3:91$. The indicated errors are standard deviations.

A "t" test was first performed to test for a significant difference in slope in the two sets of data. The value $t = 0.0069$, with 75 degrees of freedom, is insignificant. Accordingly, a common slope was computed, giving $b = 0.3395$. A second "t" test was performed to see if the lines might be identical within the scatter of the data. The computed value $t = 7.5$, with 76 degrees of freedom, is significant at the 99.9% confidence level ($t = 3.2$). The lines are therefore not identical: the least-squares regression through the $\text{H}_2:\text{O}_2:\text{CO}:\text{Ar} = 1:5:3:91$ data is statistically different from the least-squares regression through the $\text{H}_2:\text{O}_2:\text{Ar} = 1:5:94$

(7) S. H. Garnett, G. B. Kistiakowsky, and B. V. O'Grady, *J. Chem. Phys.*, **51**, 84 (1969).

(8) T. C. Clark, S. H. Garnett, and G. B. Kistiakowsky, *ibid.*, **51**, 2885 (1969).

(9) E. R. Bartle and B. F. Myers, presented at the 157th National Meeting of the American Chemical Society, Minneapolis, Minn., April 1969; Division of Physical Chemistry Abstract 152.

(10) S. S. Penner, K. G. P. Sulzmann, A. Boni, and L. Leibowitz, *Astronaut. Acta*, **15**, 473 (1970); K. G. P. Sulzmann, L. Leibowitz, and S. S. Penner, *Symp. Combust.*, **13th**, Salt Lake City, 1970, to be published.

(11) Unpublished work of E. R. Bartle and B. F. Myers (B. F. Myers, private communication). The lower value is obtained from the $\text{O}_3\text{-CO}_2\text{-Ar}$ results of these authors when the value of $k(\text{CO}_2 + \text{M} = \text{CO} + \text{O} + \text{M})$ of Fishburne, *et al.* (E. S. Fishburne, K. R. Bilwakesh, and R. Edse, *J. Chem. Phys.*, **45**, 160 (1966)), is used in the data analysis, while the higher value is obtained with $k(\text{CO}_2 + \text{M} = \text{CO} + \text{O} + \text{M})$ from K. W. Michel, H. A. Olschewski, H. Richterling, and H. G. Wagner, *Z. Phys. Chem. (Frankfurt am Main)*, **39**, 9 (1964); **44**, 160 (1965).

(12) W. C. Gardiner, Jr., K. Morinaga, D. L. Ripley, and T. Takeyama, *J. Chem. Phys.*, **48**, 1665 (1968).

(13) D. L. Ripley, Dissertation, University of Texas, 1967.

(14) Boundary layer growth restricts the validity of this procedure. Cf. R. L. Belford and R. A. Strehlow, *Ann. Rev. Phys. Chem.*, **20**, 247 (1969).

(15) G. L. Schott and J. L. Kinsey, *J. Chem. Phys.*, **29**, 1177 (1958). The actual test gas compositions varied slightly from the nominal 1:5:94 and 1:5:3:91 compositions. The actual compositions were used for computing σ , $[\text{O}_2]_0$, and the postcombustion steady value of $[\text{OH}]$. All other computed results were done assuming the nominal compositions.

(16) K. A. Brownlee, "Statistical Theory and Methodology in Science and Engineering," 2nd ed, Wiley, New York, N. Y., 1965, Section 11.6.

(17) Los Alamos "LEAST" least-squares package. Los Alamos Scientific Laboratory Publication LA2367.

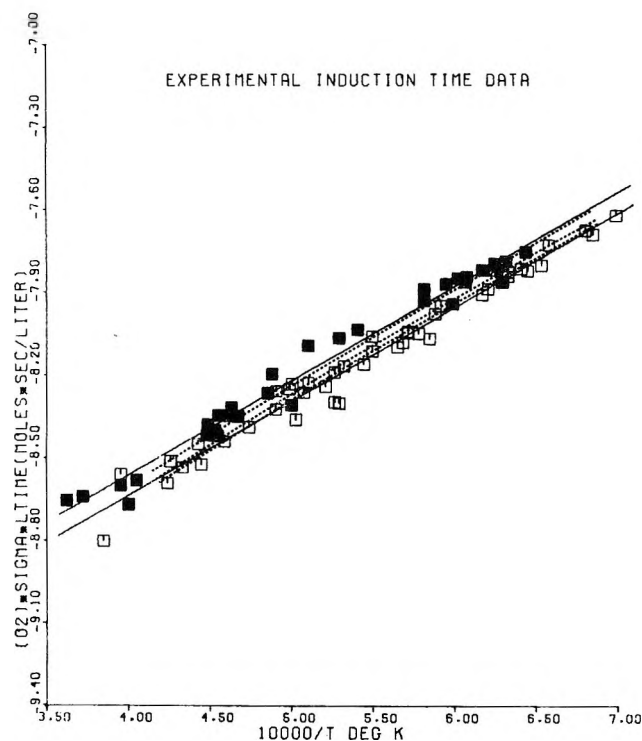
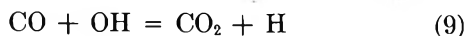


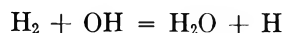
Figure 1. Induction times. The solid symbols are data taken with various mixtures of the nominal composition $\text{H}_2:\text{O}_2:\text{Ar} = 1:5:94$. The open symbols are data taken with various mixtures of the nominal composition $\text{H}_2:\text{O}_2:\text{CO}:\text{Ar} = 1:5:3:91$. The solid lines are the computer-generated least-squares lines through the two sets of data. The three dotted lines were computed using the rate constant set of Table I, except that for the middle dotted line k_{10} had the value given by Brokaw (ref 4). For the upper dotted line the gas composition was $\text{H}_2:\text{O}_2:\text{Ar} = 1:5:94$, while the other two dotted lines were computed for $\text{H}_2:\text{O}_2:\text{CO}:\text{Ar} = 1:5:3:91$.

data. At 1800° K, the difference between the regression lines corresponds to a difference in induction time of 19% or 8 μsec laboratory time.

There is a significant decrease in induction time when CO is added to the experimental gas. The difference is too large to be attributable to an error in the temperature assigned to the gas caused by ignoring the vibrational relaxation of CO, which proceeds on a time scale comparable to the time scale of ignition. It must therefore be due to changes in the chemistry of the induction zone when reactions involving CO are added to the induction zone reactions of the $\text{H}_2\text{-O}_2$ system. Two kinds of reactions are possible. In the induction zone itself, the reaction of CO with OH



can accelerate the conversion of OH into H by supplementing the reaction responsible for this in the $\text{H}_2\text{-O}_2$ system



In the initiation zone, reaction 10 can supplement the $\text{H}_2\text{-O}_2$ initiation reactions. In order to see which of

these reactions of CO is responsible for the observed decrease in induction time, a number of computer simulations of the shock-initiated combustion of these mixtures were made. The simulations were accomplished by numerical integration of the kinetic equations for the mechanism shown in Table I under the constraint of steady shock flow. The rate constant expressions used for reactions 01 to 8 in Table I were chosen as a set which gives optimum reproduction of induction times in $\text{H}_2\text{-O}_2\text{-Ar}$ shocks over wide ranges of temperature and composition. The fit to the induction times of $\text{H}_2:\text{O}_2:\text{Ar} = 1:5:94$ obtained with this set, assuming ideal shock flow, is very good. We experimented with the rate constant parameters for reactions 9 and 10 to determine whether the induction time decreases were occurring in the initiation zone or in the exponential growth region of the induction zone and to deduce a value of the appropriate rate constant.

A complication of the numerical integrations arises due to the effects of the wall boundary layer on incident shock propagation.^{6,14} Extensive computer investigations of these effects were carried out in the course of this study;² they will be reported elsewhere. For the purpose at hand it turns out that as long as a consistent treatment of the shock propagation is made, the results will not be dependent upon whether the shock propagation is assumed to be ideal, or whether the boundary layer flow is laminar or turbulent. This is so because the reaction primarily responsible for the induction time decrease is indeed reaction 10, which participates to a significant extent only in the chemistry immediately behind the shock wave. The calculations reported here are based on the assumption of ideal steady shock flow. The calculations done for the case of steady boundary layer flow, both laminar and turbulent, confirm that the rate constants deduced for the $\text{H}_2\text{-O}_2$ system would change with the flow models, while the rate constant for reaction 10 would not.

The calculated times between shock heating and attainment of $[\text{OH}] = 2.5 \times 10^{-7} M$ were scaled as the experimental data and plotted *vs.* inverse temperature for comparison between calculation and experiment. A number of such calculated induction times are shown in Figure 2, and three of these are compared with the data in Figure 1.

III. Results

The goal of the computer simulations was to explain the difference in induction times between the $\text{H}_2\text{-O}_2$ experiments and the $\text{H}_2\text{-O}_2\text{-CO}$ experiments, the magnitude of which is the separation of the solid lines in Figure 1. Such a difference could be computed in various ways, and it was necessary to decide which of the several possibilities is the proper one.

First it was required to discover whether the thermal effects of changing the gas composition affect the induction time appreciably. To this end the mechanism of

Table I: Mechanism and Rate Constant Expressions for t_i Calculations

Reaction	k	Ref
(01) $H_2 + M = 2H + M$	$2.23 \times 10^9 T^{1/2} \exp(-92,600/RT)$	a
(02) $O_2 + M = 2O + M$	$3.60 \times 10^{16} T^{-1} \exp(-118,000/RT)$	b
(03) $H_2 + M = H_2^* + M$	(Calculated)	c
(04) $H_2^* + O_2 = 2OH$	$6.5 \times 10^7 T^{1/2}$	c
(1) $H + O_2 = OH + O$	$2.34 \times 10^{10} \exp(-10,000/RT)$	c
(2) $O + H_2 = OH + H$	$6.28 \times 10^{10} \exp(-10,900/RT)$	c
(3) $OH + H_2 = H_2O + H$	$2.30 \times 10^{10} \exp(-5150/RT)$	d
(4) $H + O_2 + M = HO_2 + M$	$2 \times 10^9 \exp(+870/RT)$	e
(5) $H + O_2 + H_2O = HO_2 + H_2O$	$6 \times 10^{10} \exp(+870/RT)$	f
(6) $H + OH + M = H_2O + M$	$2 \times 10^{10} \exp(+870/RT)$	g
(7) $OH + OH = H_2O + O$	$7.59 \times 10^9 \exp(-1000/RT)$	h
(8) $H_2 + HO_2 = H_2O + OH$	$2 \times 10^8 \exp(-24,000/RT)$	i
(9) $CO + OH = CO_2 + H$	$3.1 \times 10^8 \exp(-600/RT)$	d
(10) $CO + O_2 = CO_2 + O$	$3.14 \times 10^8 \exp(-37,600/RT)$	j
(11) $CO + O + M = CO_2 + M$	$3.16 \times 10^6 \exp(+23,400/RT)$	k

^a A. L. Myerson and W. S. Watt, *J. Chem. Phys.*, **49**, 425 (1968). ^b M. Camac and A. Vaughan, *ibid.*, **34**, 460 (1961). ^c C. B. Wakefield, Dissertation, The University of Texas, 1969. The rate of reaction 03 was adapted for the composition of these mixtures from J. H. Kiefer and R. W. Lutz, *J. Chem. Phys.*, **44**, 668 (1966). The rates of reactions 04, 1, and 2 were adjusted for optimal fit of H_2 - O_2 -Ar induction times. It should be noted that the initiation mechanism of the H_2 - O_2 explosion is not of importance for the purposes of the present paper. All that is necessary is a correct accounting for the length of the induction period in the one H_2 - O_2 mixture with which we are comparing the H_2 - O_2 -CO mixture. Any other combination of elementary reactions and rate constants which would give the correct induction times would also be satisfactory. ^d G. Dixon-Lewis, W. E. Wilson, and A. A. Westenberg, *J. Chem. Phys.*, **44**, 2877 (1966). ^e D. Gutman, E. A. Hardwidge, F. A. Dougherty, and R. W. Lutz, *ibid.*, **47**, 4400 (1967). ^f The efficiency of H_2O was taken to be 30 times that of Ar; cf. ref. g. ^g The ratio k_6/k_4 was suggested by G. L. Schott and P. F. Bird, *J. Chem. Phys.*, **41**, 2869 (1964); R. W. Getzinger and G. L. Schott, *ibid.*, **43**, 3237 (1965); and R. W. Getzinger, *Symp. Combust., 11th, Berkeley, 1966*, 117 (1967). ^h F. Kaufman and F. P. Del Greco, *Symp. Combust., 9th, Ithaca, 1962*, 659 (1963); $E_A = 1000$ cal was assumed. Recent high-temperature measurements of the reverse rate (E. A. Albers, K. Hoyermann, H. Gg. Wagner, and J. Wolfrum, paper presented at the 13th Symposium (International) on Combustion, Salt Lake City, Aug 1970) confirm that this expression is a suitable extrapolation to shock tube temperatures. ⁱ V. V. Voevodsky, *Symp. Combust., 7th, London, 1958*, 34 (1959). ^j B. F. Walker, Dissertation, The University of Texas, 1970. ^k M. C. Lin and S. H. Bauer, *J. Chem. Phys.*, **50**, 3377 (1969).

Table I was used to calculate the induction times of a $H_2:O_2:CO:Ar = 1:5:3:91$ mixture in which all chemical effects of CO were suppressed by setting the rates of reactions 9 and 10 equal to zero. (The termolecular reaction 11 was found to be too slow to affect any part of the profiles at the low pressures used in these experiments.) The induction times were almost the same as in a mixture in which $[CO] = 0$ (Figure 2).

Next we tested the effect of reaction 9 alone on the chemistry of the induction period. Including reaction 9 with a rate constant expression that was proposed as a consensus of several measurements at high temperatures,¹⁸ while still holding $k_{10} = 0$, gave about half of the necessary correction at 1600°K but had no effect at 2000°K. In order to calculate an acceleration of the right magnitude from reaction 9 alone, it was necessary to increase its rate to about 4 times the consensus value, well beyond the range of the scatter of the measured values of this rate constant¹⁹ (Figure 2).

With the rate constant for reaction 9 set at the consensus value, the rate constant for reaction 10 was varied until good agreement with the experimental values was obtained. It can be seen in Figure 2 that this rate had to be taken somewhat faster than the slower rates assigned by previous authors (e.g., ref 5

and 10), but far slower than the fast rate assigned by other previous authors (ref 6).

Finally, a check was made to see if the assumed nature of the shocked gas flow had an effect upon the results. The absolute value of the effect itself is large (Figure 2 again), but if the rate constants for the H_2 - O_2 system alone were adjusted to give proper agreement once more with H_2 - O_2 induction times, either for laminar or for turbulent boundary layers, the relative change in induction time when CO is added to the mixture is almost the same as in the case when ideal shock propagation is assumed.

IV. Discussion

The rate constant expression for reaction 10 obtained in the final comparison with the data is compared with earlier results on the Arrhenius plot of Figure 3. It is clear from this representation that our results are in good agreement with the lower values obtained by previous authors, but in disagreement by over an order

(18) W. E. Wilson, Report on the Establishment of Chemical Kinetics Tables, Chemical Propulsion Information Agency, 1967.

(19) D. L. Baulch, D. D. Drysdale, and A. C. Lloyd, "High Temperature Reaction Rate Data," No. 1, Leeds University, 1968.

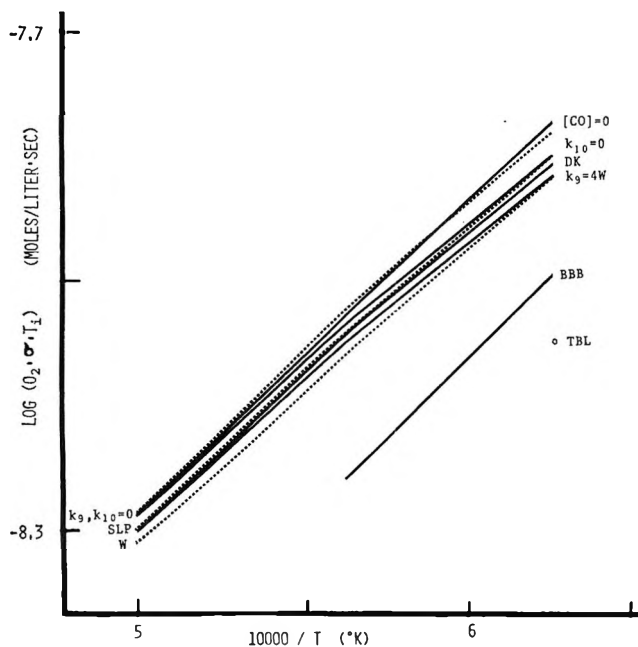


Figure 2. Computed induction times. Except as noted, all computations were done assuming ideal shock propagation, the composition $\text{H}_2:\text{O}_2:\text{CO}:\text{Ar} = 1:5:3:91$, and the rate constant set of Table I. The symbols denote the exceptions: $k_{10} = 0$; SLP, rate constant for k_{10} as given by Sulzmann, Leibowitz, and Penner (ref 10); W, no exceptions; $[\text{CO}] = 0$; $k_9, k_{10} = 0$; DK, rate constant for k_{10} as given by Dean and Kistiakowsky (ref 5); BBB, rate constant for k_{10} as given by Brabbs, Belles, and Brokaw (ref 6); TBL, rate constant for k_{10} of Brabbs, Brokaw, and Belles (ref 6) and turbulent boundary layer growth; $k_{10} = 0, k_9 = 4W$, rate constant for $k_{10} = 0$ and rate constant for $k_9 = 1.24 \times 10^9 \exp(-600/RT)$, 4 times the consensus value recommended by Wilson (ref 18 and 19). The symbols are to the right of the corresponding solid lines and to the left of the corresponding dotted lines.

of magnitude with the higher values obtained previously.

The discrepancy with the rate constant of Brabbs, Belles, and Brokaw⁶ is well outside of the error range of our measurements, as can be seen by comparing Figures 1 and 2. Mechanistic complications seem unlikely, as the compositions, temperatures, and pressures used by these authors were similar to ours. If dissociation of impurities is an important initiation mechanism for experiments under these conditions, then a possible explanation of the difference would be that the purity of our experimental mixtures was greater than that of theirs. In view of the fact that many different mixtures, made with gases from different sources, gave induction times that agreed within experimental error, we believe that impurities do not play a controlling role at least in our experiments.

An interesting possible reconciliation of the discrepancy between the present results and those of ref 6 lies in the fact that the experimental mixtures used by them contained about 5% CO_2 as a catalyst for assuring vibrational relaxation of CO through the rapid V-V

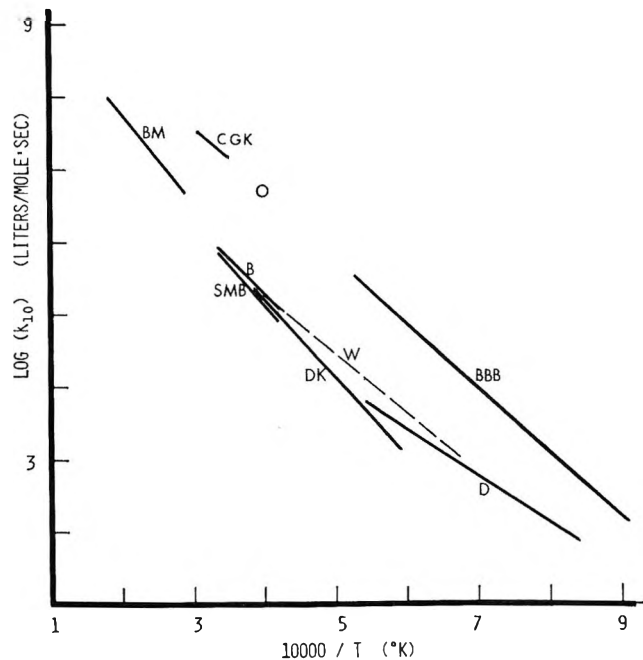


Figure 3. Rate constants for reaction 10. B = Brokaw, ref 4; BBB = Brabbs, Belles, and Brokaw, ref 6; BM = Bartle and Myers, ref 9; CGK, Clark, Garnett, and Kistiakowsky, ref 8; D = L. J. Drummond, *Aust. J. Chem.*, **21**, 2631 (1968); DK = Dean and Kistiakowsky, ref 5; O = Garnett, Kistiakowsky, and O'Grady, ref 7; SMB = Sulzmann, Myers, and Bartle, ref 3; W = this study.

transfer between the ν_3 mode of CO_2 and the $v = 1$ state of CO.²⁰ It may be that the rate constant measured in our experiments (and the other low values as well) pertains to vibrationally cold CO, while the higher value of ref 6 pertains to vibrationally relaxed CO. This would be subject to direct experimental test by repeating the experiments reported here with a CO_2 -containing mixture. The finding of Myers, *et al.*,³ that addition of He to $\text{CO}-\text{O}_2-\text{Ar}$ mixtures did not alter the ignition data speaks against the idea, however.

It is also possible that the use of the CO flame spectrum emission, as in ref 6, provides a mechanistically different diagnostic of reaction progress than in our case and that the present results are to be preferred since they were done directly with observations of a ground state reaction intermediate. This appears unlikely to us, since exponential growth constants have been measured quite successfully in reflected shock waves by monitoring the growth of the CO flame spectrum emission intensity in a manner that is spectroscopically very much like the method employed in ref 6.²¹

It seems most likely to us that the discrepancy between our value for k_{10} and the value derived in ref 6

(20) W. A. Rosser, Jr., R. D. Sharma, and E. T. Gerry, *J. Chem. Phys.*, **54**, 1196 (1971).

(21) D. Gutman and G. L. Schott, *ibid.*, **46**, 4576 (1967); D. Gutman, E. A. Hardwidge, F. A. Dougherty, and R. W. Lutz, *ibid.*, **47**, 4400 (1967).

is attributable to their measurements being affected by scattered light. Downstream scattering of just a small amount of the intense CO flame spectrum radiation from the end of the reaction zone would be sufficient to exaggerate the apparent linear increase of chain center concentrations between the shock front and the exponential growth occurring in the later part of the initiation zone. If this occurs, it would certainly lead to spuriously high values of k_{10} . The k_{10} values inferred by Dean and Kistiakowsky⁵ from ir emission growth measurements in the same temperature range, which would be expected to show less disturbance from scattered radiation, are in good agreement with our results.

Extrapolation of our Arrhenius expression to higher temperatures gives rate constants smaller than the

direct measurements^{9,11} and much smaller than the indirect ones.^{7,8} The inaccuracy of the long extrapolation makes the first comparison of doubtful value, but it would seem to be impossible to increase the activation energy obtained in our experiments to such a high value that agreement with the indirect measurements could be obtained. It has been suggested that the indirect measurements were affected by small concentrations of hydrocarbon impurities.²²

Acknowledgment. This research was supported by the U. S. Army Research Office, Durham, and the Robert A. Welch Foundation.

(22) T. C. Clark, A. M. Dean, and G. B. Kistiakowsky, *J. Phys. Chem.*, **54**, 1726 (1971).

Calculations of the Optical Properties of 1-Methyluracil Crystal by an All-Order Classical Oscillator Theory

by Howard DeVoe

Department of Chemistry, University of Maryland, College Park, Maryland 20742 (Received January 6, 1971)

Publication costs assisted by Department of Chemistry, University of Maryland

An all-order classical oscillator model which takes molecular absorption band shapes into account was used to calculate the polarized refractive indices, reflection spectra, and absorption spectra of 1-methyluracil crystal in the near-ultraviolet region. Lattice sums were evaluated from theoretical transition monopoles for the three lowest $\pi \rightarrow \pi^*$ molecular transitions and point dipoles for the in-plane components of the background polarizability. At the first crystal band the spectral shapes and intensities agree well with experiment for two directions of the light propagation but are uniformly shifted to higher frequencies. At the second crystal band the calculated frequencies, but not the intensities, are satisfactory. The crucial importance of the background polarizability to the crystal optical properties is demonstrated. It is pointed out that molecular transition moment directions cannot be reliably determined from crystal polarization ratios.

Introduction

The optical properties of molecular crystals are usually calculated by tight-binding (Frenkel) exciton theory as originally developed by Davydov.^{1,2} The frequency shifts and intensity changes of absorption lines are derived by first-order quantum mechanical perturbation theory. The present paper is an application of a classical oscillator model³ which differs from exciton theory in treating intermolecular interactions to all orders and in taking the empirical molecular absorption band shapes into account.

In common with exciton theory, the classical oscillator model assumes that intermolecular electron ex-

change and charge transfer are negligible in the ground and excited states so that the crystal differs optically from an oriented gas only because of intermolecular coulomb interactions. The exciton crystal frequency shifts are the same as in the classical theory to first order. Rhodes and Chase⁴ have shown that the classical oscillator model is equivalent to an all-order quan-

(1) A. S. Davydov, "Theory of Molecular Excitons," McGraw-Hill, New York, N. Y., 1962.

(2) D. P. Craig and S. H. Walmsley, "Excitons in Molecular Crystals," W. A. Benjamin, New York, N. Y., 1968.

(3) H. DeVoe, *J. Chem. Phys.*, **43**, 3199 (1965).

(4) W. Rhodes and M. Chase, *Rev. Mod. Phys.*, **39**, 348 (1967).

tum mechanical derivation in which one assumes that the electrons in different chromophores are partially decorrelated and that transitions between excited molecular states are absent.

The model is similar in its use of coupled oscillators to classical dipole treatments applied to hydrocarbon crystals by Mahan⁵ and by Philpott.^{6,7} Their treatments, however, are restricted to absorption lines or Lorentz band shapes.

The classical oscillator model is applied here to calculations of the refractive index, reflection, and absorption of crystals of the pyrimidine base 1-methyluracil. The primary purpose is to see how well the model, with carefully chosen values of the initial parameters, succeeds in reproducing recent measurements of these properties,^{8,9} and to observe the effect of changing some of the parameter values. 1-Methyluracil is a favorable crystal for these calculations because the observed band splitting⁸ of less than 100 cm⁻¹ compared with a band width of about 5000 cm⁻¹ corresponds to weak coupling for which it is appropriate to make use of empirical molecular band shapes in the classical model;¹⁰ furthermore, the crystal symmetry allows one to neglect out-of-plane molecular transitions for the directions and polarizations of the light that are of interest.

Theory

The model employed here is a general one for the interaction of light with an aggregate of interacting chromophores (*e.g.*, a molecular crystal, molecular aggregate, or polymer).^{3,10} Each allowed electronic transition of the chromophore is described by a one-dimensional electronic oscillator fixed in the chromophore along the direction of the transition moment. The complex frequency-dependent polarizability of an oscillator has real (in-phase) and imaginary (out-of-phase) components which one may evaluate empirically from the spectrum of the corresponding molecular absorption band. The aggregate in the electric field of plane polarized light at a fixed frequency is treated as a system of oscillators coupled through coulomb interactions and undergoing forced oscillations which may be evaluated by the simultaneous solution of the coupling equations.

In the case of a crystal with incident light propagating along unit vector \mathbf{k} and incident electric vector polarized along unit vector \mathbf{l} , the resulting complex refractive index n is given by

$$n^2 - 1 = (4\pi/V) \sum_{i,j} A_{ij}(\mathbf{e}_i \cdot \mathbf{l})(\mathbf{e}_j \cdot \mathbf{l}) \quad (1)$$

where V is the unit cell volume, \mathbf{e}_i and \mathbf{e}_j are unit vectors along the directions of oscillators i and j , and the summations are over the oscillators contained in the molecules of one unit cell. The complex quantities A_{ij} are elements of a symmetric matrix \mathbf{A} obtained by inverting a matrix \mathbf{B}

$$\mathbf{A} = \mathbf{B}^{-1} \quad (2)$$

$$B_{ij} = \delta_{ij}/\alpha_i + G_{ij} - (4\pi/3V)[\mathbf{e}_i \cdot \mathbf{e}_j - 3(\mathbf{e}_i \cdot \mathbf{k})(\mathbf{e}_j \cdot \mathbf{k})] \quad (3)$$

Here δ_{ij} is the Kronecker delta; α_i is the complex polarizability of oscillator i at the frequency of the light; and G_{ij} is a spherical lattice sum defined as the coulomb interaction of oscillator i with a sublattice of oscillators translationally equivalent to oscillator j (including oscillator j itself if it belongs to a different molecule) contained within a large spherical region about i when the oscillators all have unit dipole moments. The spherical lattice sums depend on the crystal structure but not on the direction or polarization of the light. The term proportional to V^{-1} in eq 3, on the other hand, depends on the propagation direction \mathbf{k} but not on the detailed crystal structure.

The equations given above for calculating n were derived for a macroscopic crystal from Maxwell's equations.³ They are also valid for a slab-shaped crystal of any thickness relative to the wavelength, oriented perpendicular to the light propagation, provided it is thick enough for the lattice sums to converge and there are no dominating surface effects. It is assumed here that the equations are applicable to the thinnest crystals (0.05 μ or $1/5$ of the wavelength) of 1-methyluracil whose absorbance was measured by Eaton and Lewis.⁸

The polarized molar extinction coefficient ϵ of the crystal (per mole of molecules, in units of liter mole⁻¹ centimeter⁻¹) is evaluated from the imaginary part of n by the relation

$$\epsilon = 3.29\nu(V/N) \text{Im } n \quad (4)$$

where ν is the frequency of the light in kilokaisers (1 kilokaiser = 10³ cm⁻¹), N is the number of molecules per unit cell, and V is the unit cell volume in cubic ångströms. The reflectivity R at normal incidence is evaluated by

$$R = |(n - 1)/(n + 1)|^2 \quad (5)$$

Calculations

Molecular Transitions and Polarizabilities. In the vapor phase absorption spectrum of 1-methyluracil (Figure 1),^{11,12} maxima are seen at frequencies of 39.1 and 49.8 kK with a rise toward a third maximum located somewhere above 52 kK. Figure 1 shows an

(5) G. D. Mahan, *J. Chem. Phys.*, **41**, 2930 (1964).

(6) M. R. Philpott, *ibid.*, **50**, 5117 (1969).

(7) M. R. Philpott, *ibid.*, **52**, 1984 (1970).

(8) W. A. Eaton and T. P. Lewis, *ibid.*, **53**, 2164 (1970).

(9) L. B. Clark, unpublished data.

(10) H. DeVoe, *J. Chem. Phys.*, **41**, 393 (1964).

(11) N. Q. Chako, *ibid.*, **2**, 644 (1934).

(12) N. E. Dorsey, "Properties of Ordinary Water Substance," Reinhold, New York, N. Y., 1940.

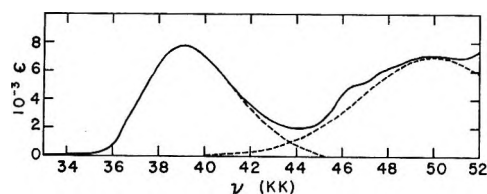


Figure 1. Experimental absorption spectrum of 1-methyluracil vapor (solid curve) with the assumed division into two bands (dashed curves). The solid curve was derived from experimental absorbances of the vapor in contact with crystals of 1-methyluracil in a 120-mm path length cell heated to approximately 107°, measured in a Cary Model 14 spectrophotometer by W. A. Eaton, unpublished work. The absorbances were converted to molar extinction coefficients ϵ (in units of liters mole⁻¹ cm⁻¹) by multiplying by the factor which yielded a value of 7790 at the first band maximum (39.1 kK). This value of $\epsilon(\text{vap})$ is obtained from the measured band height of 1-methyluracil in water⁹ $\epsilon(\text{soln}) = 9500$ by applying a theoretical Lorentz internal field correction^{3,11} $\epsilon(\text{vap}) = [9n/(n^2 + 2)^2]\epsilon(\text{soln})$ where $n = 1.3704$ is the refractive index of water at the frequency (37.5 kK) of the solution maximum.¹²

arbitrary division of the spectrum into an asymmetric band with maximum at 39.1 kK and a symmetric Gaussian band centered at 50 kK with peak height 7000 and half-width 4.5 kK. The third band maximum may be assumed to be located at 53.5 kK, where a maximum is seen in the vapor spectrum of both uracil and 1,3-dimethyluracil.¹³

To obtain theoretical molecular transition moments and transition monopoles for the in-plane $\pi \rightarrow \pi^*$ transitions, a self-consistent field molecular orbital calculation of the π electrons of 1-methyluracil was made followed by configuration interaction of all the excited configurations. Necessary integral values were obtained by using the semiempirical parameterization selected by Berthod, *et al.*,¹⁴ to best fit the transition frequencies and other properties of the π electrons of several organic compounds containing nitrogen and oxygen. The methyl group was treated as two π atomic orbitals having the integral values suggested by Denis and Pullman,¹⁵ with the omission of an inductive effect on the N-Me bond.

The resulting theoretical frequencies, oscillator strengths, and transition moment directions of the four lowest frequency transitions are tabulated in Table I, together with assignments to the observed bands. The first, third, and fourth theoretical transitions are assigned to the three lowest frequency bands; the agreement of frequencies and oscillator strengths is reasonably good. The second theoretical transition, despite its high oscillator strength (0.28), is assumed to be weak or hidden in the observed spectrum (possibly appearing as the shoulder at about 46.5 kK in the spectrum of Figure 1) and was omitted from the optical calculations. These assignments are the same as reported by Berthod, *et al.*,^{14,16} for the corresponding transitions in uracil. The remaining 20 calculated

Table I: Theoretical and Experimental Transitions in the 1-Methyluracil Molecule (the Italicized Values Were Used in the Classical Oscillator Calculations)

Oscillator no.	Theoretical			Experimental	
	ν , kK	f^a	θ , deg ^b	ν , kK	f^a
1	39.6 ^c	0.24 ^c	-2.3 ^c	39.1	0.16
	42.8 ^c	0.28 ^c	-11.5 ^c		
2	45.6 ^c	0.24 ^c	64.5 ^c	50.0	0.24
3	48.5 ^c	0.52, ^c 0.58 ^d	-26.9 ^c	53.5	
4		3.01 ^e	62.6 ^e	84 ^f	
5		2.15 ^e	-27.4 ^e	84 ^f	

^a Oscillator strength. ^b Angle between the N₁-C₄ line and the transition moment direction, measured counterclockwise when viewed as in Figure 1; the N₁-C₄ line makes an angle of 3.2° with the *a* crystal axis. ^c From molecular orbital calculation. ^d Calculated from theoretical transition moment length and experimental frequency. ^e From bond polarizabilities. ^f From vapor spectra of uracil and 1,3-dimethyluracil.

transitions have oscillator strengths below 0.2 and were not included explicitly in the crystal calculations.

The three assigned transitions were represented in the crystal calculations by oscillators 1-3 in each molecule (numbered in order of increasing frequency). The oscillator directions were taken from the molecular orbital calculations (Table I). The position of each oscillator within the molecule (for evaluating lattice sums) was taken as the "center of gravity" of the theoretical transition monopoles defined by a position vector \mathbf{p} from an arbitrary origin

$$\mathbf{p} = \frac{\sum_i \mathbf{p}_i |q_i|}{\sum_i |q_i|} \quad (6)$$

where \mathbf{p}_i is the position vector of atom i and $|q_i|$ is the absolute value of the transition monopole at atom i . The directions and positions are indicated in Figure 2.

The calculated first transition (oscillator 1) is polarized almost parallel to the *a* axis in the crystal, at an angle of 5.5°; this is in close agreement with Eaton and Lewis' determination⁸ of 3.5° from the crystal polarization ratio. It is interesting to note that oscillator 1 is located near the midpoint of the double bond between atoms C₅ and C₆, and that oscillator 3 lies between the two oxygen atoms; these atoms bear the predominant transition charges for the respective transitions.

The complex polarizabilities $\alpha(\nu)$ of oscillators 1 and 2 at any frequency ν were calculated from the extinction coefficients ϵ of the first and second molecular bands, respectively, as indicated in Figure 1, using the relations³

(13) L. B. Clark, G. G. Peschel, and I. Tinoco, Jr., *J. Phys. Chem.*, **69**, 3615 (1965).

(14) H. Berthod, C. Giessner-Prettre, and A. Pullman, *Theor. Chim. Acta*, **5**, 53 (1966).

(15) A. Denis and A. Pullman, *ibid.*, **7**, 110 (1967).

(16) H. Berthod, C. Giessner-Prettre, and A. Pullman, *Int. J. Quantum Chem.*, **1**, 123 (1967).

$$\text{Re } \alpha(\nu) = 0.0925 \int \epsilon(\nu') d\nu' / [(\nu')^2 - \nu^2] \quad (7)$$

$$\text{Im } \alpha(\nu) = -0.1453\epsilon(\nu)/\nu \quad (8)$$

Here, $\alpha(\nu)$ is in units of cubic ångströms, ν and ν' are in kilokaisers, and ϵ is in liters mole⁻¹ cm⁻¹. The integral indicated by eq 7 was evaluated numerically with a frequency interval of 0.2 kK in ν' (omitting the points where $\nu' = \nu$) between limits of 32.8 and 45.2 kK for the first band and 40–60 kK for the second.

Oscillator 3 below its absorption frequency $\nu' = 53.5$ kK was assumed to have a real polarizability with simple Drude dispersion given by

$$\alpha(\nu) = 2.14 \times 10^4 f / [(\nu')^2 - \nu^2] \quad (9)$$

In addition to oscillators 1–3, two additional oscillators (numbered 4 and 5) were included in some of the calculations to take account of the in-plane background polarizability caused by transitions above 53.5 kK. Equation 9 was used for the dispersion of this polarizability, choosing $\nu' = 84$ kK as the apparent source frequency as estimated from the experimental refraction dispersion of benzene and pyridine.

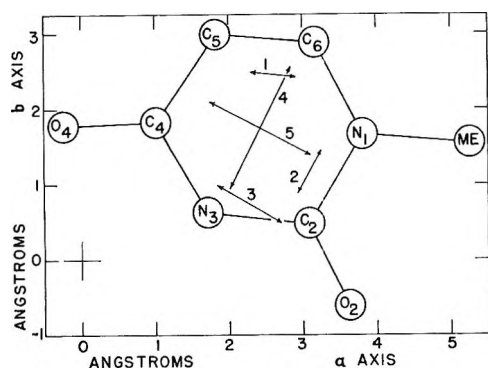


Figure 2. Structure of one of the eight molecules in the unit cell of 1-methyluracil viewed down the c axis. The origin is in the molecular plane at a center of symmetry of the crystal. The coordinates were kindly supplied by Dr. F. S. Mathews. The directions of the oscillators used in the calculations are indicated by double-headed arrows labeled with the oscillator numbers. The midpoints of the arrows are located at the positions assumed in the calculations and the end-to-end distances are equal to the transition moment lengths.

Estimates of the directions and oscillator strengths of oscillators 4 and 5 were made. The in-plane components of the polarizability tensor of the 1-methyluracil molecule at 16.98 kK (the Na D line frequency) were evaluated from the longitudinal and transverse bond polarizability components at this frequency as determined in model compounds by Le Fèvre.¹⁷ This was a necessarily approximate calculation because it neglected any effects of altering the bond environments and hybridizations from the model compounds and assumed the bond tensor components to be additive. The contributions of oscillators 1–3 to the tensor com-

ponents were subtracted from the total values to give the in-plane background polarizability tensor. The resulting principal directions and oscillator strengths at 84 kK are given in Table I. Oscillators 4 and 5 were arbitrarily placed at the center of the ring, midway between atoms N_1 and C_4 .

Crystal Structure. 1-Methyluracil crystallizes in the orthorhombic space group $Ibam$ with eight molecules per unit cell, unit cell dimensions $a = 13.22$ Å, $b = 13.25$ Å, $c = 6.27$ Å, and unit cell volume 1098.3 Å³.¹⁸ The molecular planes lie in layers 3.135 Å apart parallel to the crystal ab plane.

Figure 2 shows the structure of one of the molecules of the unit cell, designated molecule 1 here, looking down the c axis. Positions in molecules 2, 3, and 4 equivalent to crystal coordinates $x, y, 0$ in the plane of molecule 1 are given by

$$-x, -y, 0$$

$$-x, y, c/2$$

$$x, -y, c/2$$

respectively. Since the crystal is body centered, molecules 5–8 are related to these four by a translation $a/2, b/2, c/2$.

Lattice Sums. Interactions among pairs of the oscillators 1–3 located in molecules up to 30 Å apart were calculated as the coulomb interaction between the transition monopoles, using the theoretical transition monopoles. The spherical lattice sums G_{ij} for these interactions were evaluated in this monopole–monopole approximation for a spherical radius out to 30 Å, and in the point dipole approximation from 30 to 50 Å.

Interactions involving oscillators 4 and 5 (which represent the in-plane transitions contributing to the background polarizability) were calculated by treating these oscillators as point dipoles located at the centers of the rings. Thus the term in a lattice sum for the coulomb interaction between oscillator 1, 2, or 3 in one molecule and oscillator 4 or 5 in a second molecule was calculated in a monopole–dipole approximation as

$$(1/\mu_1\mu_2) \sum_i q_i V_i$$

In this expression μ_1 and μ_2 are the transition dipole moments for the first and second molecules, q_i is the theoretical transition monopole at atom i in the first molecule, and V_i is the potential at this point due to the transition charge distribution at the second molecule. This potential in the point dipole approximation is given by

$$V_i = \mathbf{\mu}_2 \cdot \mathbf{R} / R^3 \quad (10)$$

where \mathbf{R} is the vector from the dipole $\mathbf{\mu}_2$ to atom i .

(17) R. J. W. Le Fèvre, *Advan. Phys. Org. Chem.*, **3**, 1 (1965).

(18) D. W. Green, F. S. Mathews, and A. Rich, *J. Biol. Chem.*, **237**, PC 3573 (1962).

It is interesting to note that eq 10 also describes the potential at a point outside a uniformly polarized sphere having a total dipole μ_2 , where \mathbf{R} is measured from the center of the sphere; thus the same lattice sums will be obtained if a uniformly polarized sphere of molecular dimensions is used to replace a point dipole as a (perhaps conceptually superior) model for the transition charge distribution of the background polarizability.

The lattice sums for interactions among oscillators 4 and 5 were obtained by the point dipole approximation. Both the monopole-dipole and dipole-dipole sums were evaluated out to a radius of 50 Å.

Out-of-plane oscillators were omitted for the calculations. This is valid because for the present crystal symmetry and light polarization parallel to the *ab* crystal plane the out-of-plane oscillators are inactive.

A considerable reduction in the computer time needed to invert matrix \mathbf{B} (eq 2) was possible for this particular crystal by performing the calculations on an optical unit cell having 0.25 the volume of the crystallographic unit cell and the oscillators of two molecules instead of eight. This was possible for two reasons: (1) molecules 5-8 (preceding section) are related by translation to molecules 1-4 and so are optically equivalent; and (2) molecules 1 and 2 which are related by a center of symmetry have the same lattice sums and opposite oscillator directions; the same is true of molecules 3 and 4. The oscillators in molecules 1 and 3 constituted the optical unit cell. The calculations require two lattice sums for each combination *i, j* of oscillator types, designated $G_{ij}(\text{eq})$ and $G_{ij}(\text{in})$ depending on whether the oscillators are in equivalent or inequivalent molecules within the optical unit cell. These sums were obtained by the following relations from the calculated lattice sums for the crystallographic unit cell $G_{ik,jl}$ for the interaction of oscillator *i* in molecule *k* with oscillator *j* in molecule *l*

$$\begin{aligned} G_{ij}(\text{eq}) &= G_{i1,j1} - G_{i1,j2} + G_{i1,j5} - G_{i1,j6} \\ G_{ij}(\text{in}) &= G_{i1,j3} - G_{i1,j4} + G_{i1,j7} - G_{i1,j8} \end{aligned} \quad (11)$$

The values of the lattice sums used in the optical calculations are given in Table II.

Results and Discussion

The real part of the refractive index, the reflectivity, and the molar extinction coefficient were calculated at 0.2-kK intervals for frequencies up to 52 kK by eq 1-5.

The values of the refractive indices at 16.98 kK for light incident along the *c* axis and polarized along the *a* or *b* axis, when calculated with the background polarizability included, are fairly close to the experimental values but the magnitudes of n_a and n_b have the wrong relative order (Table III).

The values of n_a and n_b calculated with the background polarizability omitted are low (Table III).

Table II: Calculated Spherical Lattice Sums^a

Oscillators <i>i, j</i>	$G_{ij}(\text{eq}),$ Å ⁻³	$G_{ij}(\text{in}),$ Å ⁻³
Monopole-Monopole Interactions		
1,1	0.02143	0.00488
1,2	0.00228	0.00868
1,3	0.00830	-0.01246
2,2	0.00115	0.01318
2,3	-0.00407	-0.01192
3,3	0.00768	-0.00715
Monopole-Dipole Interactions		
1,4	-0.00823	-0.00262
1,5	0.02355	0.00138
2,4	-0.00481	0.00335
2,5	0.00218	0.01265
3,4	-0.01151	-0.00006
3,5	0.01071	-0.01677
Dipole-Dipole Interactions		
4,4	-0.01119	-0.00840
4,5	-0.00639	0.00077
5,5	0.02505	-0.00732

^a For the calculations each oscillator or transition dipole moment in molecule 1 was taken as having a positive *a* axis component, and in molecule 3 a negative *a* axis component.

Table III: Refractive Indices at 16.98 kK for Light Incident along the *c* Axis and Polarized along the *a* and *b* Axes

	n_a	n_b
Calculated with background polarizability	1.670	1.712
Calculated without background polarizability	1.297	1.134
Experimental ^a	1.830 ± 0.005	1.688 ± 0.002

^a W. A. Eaton and T. P. Lewis, *J. Chem. Phys.*, **53**, 2164 (1970).

One would expect this since even in an oriented gas model the background polarizability (oscillators 4 and 5) contribute more polarization at 16.98 kK than do the low-lying transitions (oscillators 1-3). Philpott,⁷ in classical dipole calculations of the refractive indices of anthracene, came to the same conclusion that the background polarizability makes an important contribution.

The calculated polarized reflection spectra for light normal to the (001) crystal face (Figure 3) are qualitatively similar in appearance to experimental reflection spectra obtained by Rosa¹⁹ and more recently by Clark.⁹ The main differences are that the frequencies of the calculated maxima and minima in both R_a and R_b are about 2 kK too high and the calculated maximum in R_b has about twice the measured intensity. At 30 kK

(19) E. J. Rosa, Ph.D. Dissertation, University of Washington, 1964.

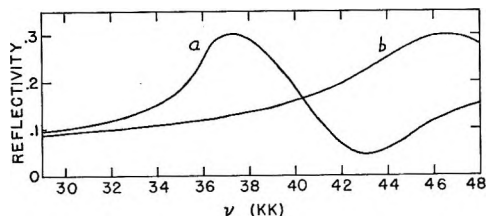


Figure 3. Calculated normal reflectivity for light incident along the c axis and polarized along the a or b axis. The background polarizability was included.

in the transparent region close to the first absorption band edge, where the reflectivities depend only on the real refractive indices, the calculated values are $R_a = 0.10$ and $R_b = 0.09$ which are reasonably close to the measured values⁹ $R_a = 0.13$ and $R_b = 0.08$.

The calculated absorption spectra for light incident along the c axis (Figure 4) agree closely in shape and intensity in the region of the first molecular band with the absorption spectra measured by Eaton and Lewis,⁸ but appear to be shifted by about 2 kK to higher frequencies. The calculated a polarized crystal band (maximum at 37.8 kK) is correctly predicted to be red-shifted from the molecular band (but not as much as observed), and to be skewed in shape with a steep low-frequency edge and a broad tail on the high-frequency side. One may closely superimpose the calculated band spectrum curve on the experimental spectrum if one imagines the vibrational structure appearing in the latter to be smoothed out.

Clark⁹ has recently derived crystal absorption spectra extending to higher frequencies from experimental reflection spectra. The calculated a and b polarized crystal bands in the region of the second molecular band for light incident along the c axis (Figure 4) appear with approximately the same frequencies and splitting as determined by Clark, but with about twice the intensity in the b polarized band.

Omitting the background polarizability from the calculations (Figure 5) greatly alters the crystal band intensities, changes the band positions, and in general decreases the agreement with the experimental spectra.

Compared with the a polarized spectrum for light incident along the c axis, the first crystal band calculated with inclusion of background polarizability for light incident normal to the (110) crystal face and polarized perpendicular to the c axis (Figure 6) appears at a higher frequency (maximum at 39.7 kK) and is much more symmetric in shape. Both differences agree qualitatively with the absorption spectrum obtained by Clark⁹ from the reflection normal to the (110) face. Clark found the band maximum at 38 kK. The calculated band height is about 30% greater than measured by Clark. The calculated second crystal band (Figure 6) is at approximately the measured frequency but has almost twice the measured intensity.

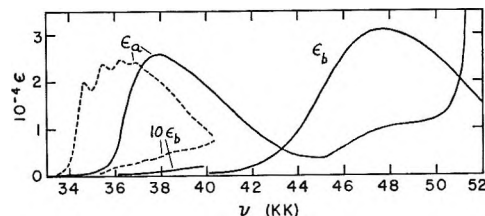


Figure 4. Comparison of calculated and observed polarized absorption spectra for light incident along the c axis and polarized along the a or b axis. Solid curves: calculated with background polarizability included. Dashed curves: measured by direct absorption of thin crystals by Eaton and Lewis.⁸ The molar extinction coefficient ϵ is plotted in units of liters mole⁻¹ cm⁻¹.

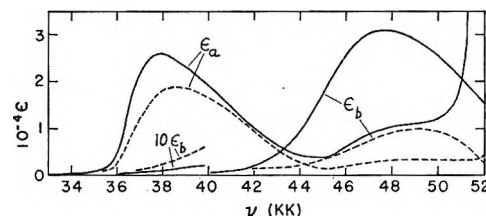


Figure 5. Effect of background polarizability on calculated absorption spectra for light incident along c axis and polarized along the a or b axis: solid curves, with background polarizability (same as solid curves in Figure 4); dashed curves, without background polarizability.

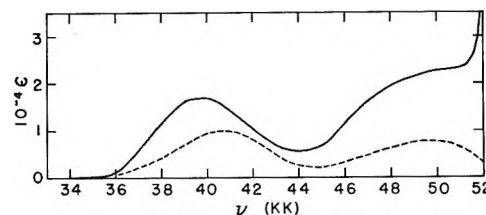


Figure 6. Calculated absorption spectra for light incident normal to (110) face and polarized perpendicular to c axis: solid curve, with background polarizability; dashed curve, without background polarizability.

Omitting the background polarizability (Figure 6) greatly changes the calculated band positions and intensities.

A common pattern emerges in comparing the calculated reflection and absorption spectra with the experimental spectra. In the region of the first crystal band the calculated spectral shapes and intensities are close to the experimental values, but the positions are about 2 kK too high. In the region of the second crystal band the calculated positions are satisfactory but not the intensities.

The errors in the calculated band positions could be resolved if one assumed that the position of the first molecular absorption band appropriate to the time-average (static) crystal environment is 2 kK lower than in the vapor spectrum used for the present calculations. The finding that a 2-kK discrepancy between the calculated and experimental crystal band positions is ob-

tained for two different directions of the light propagation, although the calculated frequency shifts from the molecular band are in opposite directions, suggests that this explanation is correct. The first two absorption bands of 1-methyluracil are observed to shift by 1.6 kK to lower frequencies on going from the vapor phase to aqueous solution;⁸ thus a 2-kK shift seems reasonable in the highly polarizable environment of the crystal. A similar correction of pyrimidine and purine molecular spectra was found to be necessary for calculating the absorption spectrum of helical DNA by the classical oscillator model.²⁰

The errors in the calculated intensities of the second crystal band are probably due to the approximate nature of the derivation of the directions and polarizabilities of the oscillators for the background polarizability. The absorption in the second crystal band region is especially sensitive to the presence or lack of background polarizability, as is clear from Figures 5 and 6. On the other hand, the absorption was not observed to be very sensitive to the polarizability of oscillator 3 (for the molecular band at 53.5 kK); essentially no change in the polarized spectra for light incident along the *c* axis was obtained when the oscillator strength of this oscillator was halved.

Another possible source of significant error is inaccurate values of the spherical lattice sums, which could be due to poor transition monopoles from inaccurate molecular orbitals, inappropriate locations

for the oscillators in point dipole interactions, or an inadequate representation by point dipoles of the coulomb interactions involving the background polarizability.

Finally, it should be pointed out that the calculated polarized crystal absorption spectra in one frequency region have a polarization ratio which is sensitive to the oscillator strengths assumed for oscillators absorbing in other regions. This is seen for instance in Figure 5 where the removal of the background polarizability changes the polarization ratio ϵ_a/ϵ_b in the first crystal band although the absorbing oscillators have not changed directions. Therefore, an oriented gas model of crystal band intensities, in which intensity exchanges among bands are ignored, may lead to a quite inaccurate estimation of a molecular transition moment direction from experimental polarization ratios.

Acknowledgments. I wish to acknowledge the generous help of Dr. William A. Eaton, National Institute of Arthritis and Metabolic Diseases, in providing a vapor phase spectrum of 1-methyluracil; and of Professor Leigh B. Clark, University of California, San Diego, Calif., in allowing me to see unpublished spectra from his laboratory. The computer time for this work was supported in full through the facilities of the Computer Science Center of the University of Maryland.

(20) H. DeVoe, *Ann. N. Y. Acad. Sci.*, **158**, Art. 1, 298 (1969).

Circular Dichroism Studies of Lysine-Rich Histone f-1-Deoxyribonucleic

Acid Complexes. Effect of Salts and Dioxane upon Conformation¹

by Alice J. Adler and Gerald D. Fasman*

Graduate Department of Biochemistry, Brandeis University, Waltham, Massachusetts 02154 (Received January 4, 1971)

Publication costs assisted by the National Institutes of Health, The National Science Foundation, and the American Cancer Society

Nucleoprotein complexes reconstituted from calf thymus DNA and lysine-rich histone (f-1 fraction) in a variety of neutral salts and in dioxane were examined by circular dichroism. The alteration of the DNA ellipticity bands is interpreted as a reflection of conformational change of the DNA in the complexes. Gradient dialysis of DNA and f-1 in various ratios into 0.14 or 0.3 *M* uni-univalent salt solutions results in circular dichroic spectra which can be approximately ordered according to the lyotropic series. This sequence was found to be, in order of the effect on the DNA circular dichroic spectrum (that is, beginning the sequence with salts that alter the circular dichroism spectra the most): guanidine·HCl > NH₄Cl, NH₄OAc ≫ CsCl > KCl, KF > NaOAc, NaBr, NaF, NaCl > LiCl ≫ NaClO₄, KCNS, NaI. Most of the effect is exerted through cations. Alkali metal ions enhance the ellipticity changes of complexes to various extents. Ammonium and guanidinium ions cause the largest changes in the circular dichroism; these specific ion effects are remarkable because of the relatively low salt concentration at which they operate. Most anions (OAc⁻, F⁻, Cl⁻, Br⁻) have little effect, except for ClO₄⁻, CNS⁻, and I⁻, which dissociate the complexes. Very low MgCl₂ concentration (≤0.006 *M*) augments conformational changes; at higher concentration MgCl₂ causes dissociation. Addition of dioxane (up to 40% by volume) enhances distortion of the DNA ellipticity. Different types of complexes result (1) from direct mixing of f-1 histone and DNA in 0.14 *M* NaF, (2) from dialysis into 0.01 *M* NaF, and (3) from dialysis into 0.14 *M* NaF. Filtration experiments indicate that histone binds to DNA in a partially cooperative manner. f-1-DNA interaction is modified by salt concentration, specific salt effects, dioxane, and manner of complex formation. This complicated behavior indicates that charge attraction between histone and DNA, even when supplemented by hydrophobic bonding, is insufficient to account for the observed circular dichroic changes. Specific association of complexes may be involved, mediated by the presence of various salts.

Introduction

In the cell nuclei of higher organisms DNA is found complexed to basic proteins, the histones, as well as to other constituents. These proteins may have two functions—to stabilize the condensed structure of DNA and to regulate transcription (RNA synthesis) from the DNA; the evidence has been reviewed elsewhere.² This laboratory has been studying the interaction of calf thymus DNA with the very lysine-rich histone fraction f-1 from the same source^{3,4} (as well as other histone fractions⁵ and chromatin⁶). The f-1 histone fraction is a protein of molecular weight 21,000, and contains 29% lysine residues, little arginine, and much alanine and proline.⁷ Circular dichroism (CD)⁸ studies of reassociated f-1-DNA complexes has shown that f-1 causes large changes in the conformation of DNA. The distortions of the DNA CD spectrum increase with the ratio of histone in the complex,³ and decrease if the histone is phosphorylated at the ser-37 position.⁴ The solvent used for most previous experiments was 0.14 *M* NaF, a physiological concentration of a salt transparent in the ultraviolet region. The present paper reports an extension of these studies to complexes formed in various concentrations of several uni-univalent salts, MgCl₂, and aqueous dioxane mixtures.

Circular dichroism and the closely related method of optical rotatory dispersion have recently been utilized in studies of native and partially dissociated chromatin (nucleoprotein taken from interphase cells),^{6,9-14}

(1) Publication No. 772 from the Graduate Department of Biochemistry, Brandeis University. This work was supported by research grants from the National Science Foundation (GB-8642), the National Institutes of Health of the U. S. Public Health Service (GM 17533-09), the American Heart Association (69-739), and the American Cancer Society (P-577).

(2) S. C. R. Elgin, S. C. Froehner, J. E. Smart, and J. Bonner, *Advan. Cell Mol. Biol.*, in press.

(3) G. D. Fasman, B. Schaffhausen, L. Goldsmith, and A. Adler, *Biochemistry*, **9**, 2814 (1970).

(4) A. J. Adler, B. Schaffhausen, T. A. Langan, and G. D. Fasman, *ibid.*, **10**, 909 (1971).

(5) T. Y. Shih and G. D. Fasman, *ibid.*, **10**, 1675 (1971).

(6) T. Y. Shih and G. D. Fasman, *J. Mol. Biol.*, **52**, 125 (1970).

(7) M. Bustin and R. C. Cole, *J. Biol. Chem.*, **244**, 5291 (1969).

(8) Abbreviations used: CD, circular dichroism; GuCl, guanidine monohydrochloride.

(9) P. J. Oriel, *Arch. Biochem. Biophys.*, **115**, 577 (1966).

(10) D. Y. H. Tuan and J. Bonner, *J. Mol. Biol.*, **45**, 59 (1969).

(11) V. I. Permogorov, V. G. Debabov, I. A. Sladkova, and B. A. Rebentish, *Biochim. Biophys. Acta*, **199**, 556 (1970).

(12) R. T. Simpson and H. A. Sober, *Biochemistry*, **9**, 3103 (1970).

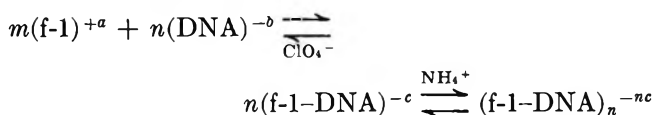
(13) F. X. Wilhelm, M. H. Champagne, and M. P. Daune, *Eur. J. Biochem.*, **15**, 321 (1970).

(14) J. Šponar, M. Boublik, I. Frič, and Z. Šormová, *Biochim. Biophys. Acta*, **209**, 532 (1970).

nucleohistone complexes reconstituted from purified DNA, and isolated histone fractions,^{3-5,10,14-16} and complexes formed from DNA and synthetic, basic polypeptides (such as poly-L-lysine).¹⁷⁻²¹ Other physical techniques applied to these systems include^{22,23} X-ray,²⁴ ultraviolet,²⁵ and infrared spectroscopy,²⁶ fluorescence,²⁷ equilibrium dialysis,²⁸ sedimentation,²⁹ and electron microscopy.²¹ In spite of all this effort the molecular structure of nucleohistone is still largely a matter for conjecture. For example, it is not known definitely whether the B-form of DNA is retained in nucleoprotein.^{21-24,26,30}

Different inorganic salts vary in their ability to destabilize the native conformations of macromolecules. This order of effectiveness, the lyotropic or Hofmeister series,³¹ is roughly the same for lowering the melting temperature of DNA,³² reducing the α -helical content of proteins,³¹ and dissociating actin³³ and other polymerized proteins into subunits.³¹ These specific salt effects usually occur only at very high salt concentration. For example, below 1 M all univalent salts alter the melting temperature of DNA to the same extent,³⁴ exhibiting only an ionic strength dependence. On the other hand, the present work shows that f-1-DNA complexes are sensitive to large, specific salt effects in 0.14 M salt solutions. Organic solvents are known to destabilize the helical structure of DNA;^{35,36} in the present case the circular dichroic spectral changes characteristic of f-1-DNA complexes are progressively enhanced by addition of increasing amounts of dioxane.

Two steps appear to be necessary for production of f-1-DNA complexes whose circular dichroism differs from that of DNA. The first step involves the binding of negatively charged DNA to positively charged histone to form a partially neutralized complex (with a remaining negative charge of -0.7 to -0.85 per nucleotide in typical experiments), and can be reversed by ClO_4^- , for example. The second step is specific association of these complexes, and this process is aided most by NH_4^+ and by dioxane. Schematically



Experimental Section

Materials. The f-1 histone fraction from calf thymus was prepared and characterized as described previously;³ concentrations of stock solutions in water, following centrifugation at 4000g for 10 min, were about 10^{-2} M peptide residues, as determined by a modified⁴ biuret method.³⁷ The same calf thymus DNA preparation was utilized as for previous studies;⁴ its median molecular weight was 12.7×10^6 . Inorganic salts were reagent grade; GuCl was Baker grade. Stock solutions (usually 1 M) of salts were adjusted to pH 7.0, introducing no extraneous ions. Water was redi-

stilled from glass; *p*-dioxane was a Matheson spectro-quality solvent.

Histone-DNA complexes. Unless otherwise specified, complexes of f-1 and DNA were prepared by first mixing these components, at the desired concentration and ratio, in 2 M NaCl. (At such high salt concentration the histone and DNA remain dissociated.) Then stepwise gradient dialysis³⁸ was carried out at 4° (in Union Carbide no. 8 tubing which had been boiled in 0.01 M NaHCO_3 , 0.001 M ethylenediaminetetraacetic acid) in order to reconstitute the complexes. Dialysis was performed first overnight into 0.4 M of the salt under consideration, then for 6 hr into 0.3 M, then overnight usually into 0.14 M salt. In experiments involving various amounts of MgCl_2 or dioxane in the salt solutions, these additives were mixed into the solvents for all stages of dialysis. No buffers were used. The final pH of all solutions examined by CD was 7.0 ± 0.2 (except for solutions to which dioxane was added, in which the apparent pH rose to 8.0 at 40% dioxane). No attempt was made to adjust the pH, since variation of pH between 6.5 and 8.3 did not affect the CD spectra. A few complexes were prepared by further dialysis

- (15) D. E. Olins, *J. Mol. Biol.*, **43**, 439 (1969).
- (16) T. E. Wagner, *Nature*, **227**, 65 (1970).
- (17) P. Cohen and C. Kidson, *J. Mol. Biol.*, **35**, 241 (1968).
- (18) J. T. Shapiro, M. Leng, and G. Felsenfeld, *Biochemistry*, **8**, 3219 (1969).
- (19) B. Davidson and G. D. Fasman, *ibid.*, **8**, 4116 (1969).
- (20) S. Inoue and T. Ando, *ibid.*, **9**, 395 (1970).
- (21) M. Haynes, R. A. Garrett, and W. B. Gratzer, *ibid.*, **9**, 4410 (1970).
- (22) E. M. Bradbury and C. Crane-Robinson in "Histones and Nucleohistones," B. M. P. Phillips, Ed., Plenum Press, London, 1970, Chapter 3.
- (23) J. Pardon and B. Richards in "Biological Macromolecules," Vol. 6, G. D. Fasman and S. N. Timasheff, Ed., Marcel Dekker, New York, N. Y., in press.
- (24) M. H. F. Wilkins, *Cold Spring Harbor Symp. Quant. Biol.*, **21**, 75 (1956).
- (25) T. Y. Shih and J. Bonner, *J. Mol. Biol.*, **48**, 469 (1970).
- (26) K. Matsuo, Y. Mitsui, Y. Iitaka, and M. Tsuboi, *ibid.*, **38**, 129 (1968).
- (27) J. Evett and I. Isenberg, *Ann. N. Y. Acad. Sci.*, **158**, 210 (1969).
- (28) E. O. Akinrimisi, J. Bonner, and P. O. P. Ts'o, *J. Mol. Biol.*, **11**, 128 (1965).
- (29) S. Inoue and T. Ando, *Biochemistry*, **9**, 388 (1970).
- (30) S. Bram and H. Ris, *J. Mol. Biol.*, **55**, 325 (1971).
- (31) P. H. von Hippel and T. Schleich in "Structure and Stability of Biological Macromolecules," S. N. Timasheff and G. D. Fasman, Ed., Marcel Dekker, New York, N. Y., 1969, p 417.
- (32) K. Hamaguchi and E. P. Geiduschek, *J. Amer. Chem. Soc.*, **84**, 1329 (1962).
- (33) B. Nagy and W. P. Jencks, *ibid.*, **87**, 2480 (1965).
- (34) C. Schildkraut and S. Lifson, *Biopolymers*, **3**, 195 (1965).
- (35) T. T. Herskovits, *Arch. Biochem. Biophys.*, **97**, 474 (1962).
- (36) L. Levine, J. A. Gordon, and W. P. Jencks, *Biochemistry*, **2**, 168 (1963).
- (37) S. Zamenhof, *Methods Enzymol.*, **3**, 696 (1957).
- (38) R. C. C. Huang, J. Bonner, and K. Murray, *J. Mol. Biol.*, **8**, 54 (1964).

into 0.01 *M* NaF. Several others were prepared by direct mixing of f-1 and DNA in 0.14 *M* NaF.

Concentrations of DNA in f-1-DNA complexes were obtained by boiling 30 min in 0.5 *M* perchloric acid⁴ and then measuring OD₂₆₀ of the hydrolysate, for which ϵ_{260} (mole nucleotides) = 9.9×10^3 in this solvent. This method could not be used in the presence of dioxane; for these complexes DNA concentrations were calculated from the ultraviolet spectra of the complexes, corrected for scattering, using ϵ_{258} (mole residues DNA) = 6.8×10^3 . (This method agrees with perchloric acid hydrolysis within $\pm 2\%$ for complexes where both methods were compared.) Concentrations of complexes were usually $0.7\text{--}0.9 \times 10^{-4}$ *M* nucleotides. Histone/DNA ratios (*r*) are reported as moles of histone peptide residues per mole of DNA nucleotide residues, and were determined from the input concentrations.

Turbidity was apparent for most complexes in this study. The maximum value of OD₄₀₀/OD₂₅₈, a measure of light scattering, was 0.1 (at OD₂₅₈ \approx 0.7). Attempts to decrease turbidity by shearing complexes in a tissue grinder or blender failed.

Optical Methods. CD measurements were performed at 23° on a Cary 60 spectropolarimeter with 6001 CD attachment, as previously described.⁴ The time constant was 3 or 10 sec; the band pass 1.5 nm. The path length for most f-1-DNA complexes was 1 cm. Mean residue ellipticity $[\theta]$ is reported in degrees centimeter² per decimole of nucleotide residues in the complexes. Typical reproducibility of data in duplicate experiments is indicated by error bars in Figure 2. Ultraviolet spectroscopy was carried out on a Cary 14 instrument.

Membrane Filtration. Several f-1-DNA complexes (1.5-ml aliquots) were passed, by suction filtration, through cellulose membranes. DNA concentrations in the filtrates and in aliquots of unfiltered complexes were then determined by uv spectroscopy, employing light-scattering corrections when needed. Membranes of two types, both 25-mm diameter, 0.45- μ pore size, yielded identical results. The types were mixed cellulose esters (Millipore filters, Type HAWP) and nitrocellulose (Bac-T-Flex filters, Type B-6). Prewashing the filters with boiling water did not affect the results.

Results and Discussion

Various Types of f-1-DNA Complexes Formed in NaF; Stoichiometry. The near-ultraviolet circular dichroism spectrum of native calf thymus DNA is characterized by a double positive ellipticity band ($[\theta]_{277} = 8400$) and a negative band ($[\theta]_{245} = -8900$) of nearly equal intensity. Homologous lysine-rich histone f-1 shows no CD signal at $\lambda > 240$ nm, and has a negative band at lower wavelength ($[\theta]_{201} = -20,000$), characteristic of randomly coiled proteins.³ The calculated sum of the CD spectra for these isolated com-

ponents (as well as the CD of DNA alone) are given in Figure 1; this calculation was made for a histone-to-DNA ratio, *r* (moles of peptide residues/moles of nucleotide residues), of 0.5. As was shown previously,³ when f-1 is complexed with DNA by gradient dialysis annealing into 0.14 *M* NaF, progressive distortion of the DNA circular dichroism spectrum occurs as increasing amounts of histone are included into the f-1-DNA complex. That study indicated a progressive conformational change, which was interpreted in terms of a difference in the asymmetric environment of the DNA nucleotide bases responsible for the near-uv CD bands (although other explanations are certainly feasible^{3,18,21}). The complexes reconstituted by dialysis into 0.14 *M* NaF have reproducible CD spectra at each value of *r*, suggesting specific binding of histone onto DNA. CD spectra for f-1-DNA ratios *r* = 0.5 and *r* = 1.0 are shown in Figures 1 and 3, respectively. At *r* = 1.0 the negative charge on the DNA is 30% neutralized by the histone.

The stoichiometry of binding for these complexes was examined by filtration through cellulose membranes. These filters retain protein-DNA complexes and allow unbound DNA to pass through.³⁹ The results are shown in Table I. As expected, DNA mixed with histone in 2 *M* NaCl passed through the filter, as did plain DNA (with 8-10% loss). However, dialyzed f-1-DNA complexes in 0.14 *M* NaF are partially retained on the membrane (33% at *r* = 0.5, 55% at *r* = 1.0). The filtrates have the CD spectrum of uncomplexed native DNA. Similar results were obtained by centrifugation of complexes (at 10,000*g* for 15 min). For example, at 10^{-4} *M* complex, *r* = 1.0, 56% of the DNA was found in the pellet; the CD of the supernatant was indistinguishable from that of DNA. If the binding of f-1 onto DNA was completely cooperative (in the sense that binding onto any given DNA molecule would be maximal, once it was initiated), the per cent of DNA molecules complexed to f-1 and retained on the filters should equal the per cent of DNA complexed. From the data of Shih and Bonner²⁵ these per cents are 23% at *r* = 0.5 and 38% at *r* = 1.0. On the other hand, if binding was noncooperative, all DNA molecules should be bound to considerable amounts of histone. The results of Table I show that binding is partially cooperative, or nearly cooperative if the results are corrected for the 8-10% of uncomplexed DNA apparently caught by the filters.

Another type of f-1-DNA complex is formed when the components are simply mixed, with rapid stirring, in 0.14 *M* NaF without gradient dialysis. Such complexes do not yield reproducible CD spectra. For example, at 10^{-4} *M*, *r* = 1.0, peak values ranged from those for DNA alone to $[\theta]_{286} = 2400$ and $[\theta]_{248} = -14,500$ (indicating considerable conformational

(39) O. W. Jones and P. Berg, *J. Mol. Biol.*, **22**, 199 (1966).

Table I: Filtration of Complexes^c through Cellulose^a Membranes

Histone/DNA ^b	Solvent	Fraction of DNA held on filter ^d
0 (DNA alone)	0.14 M NaF	0.08
0.5	2 M NaCl ^c	0.11
1.0	2 M NaCl ^c	0.09
1.0	0.14 M NaF ^c	0.60
1.0	0.01 M NaF	0.70
1.0	0.14 M NaF	0.55
1.0	0.14 M NH ₄ OAc	0.53
1.0	0.14 M NaClO ₄	0.46
1.0	{0.05 M MgCl ₂ plus 0.14 M NaCl	0.51
0.5	0.14 M NaF	0.33
0.5	0.14 M NaClO ₄	0.22
0.5	{0.05 M MgCl ₂ plus 0.14 M NaCl	0.25
0.5	0.14 M NaOAc	0.35
0.5	0.14 M NaBr	0.30
0.5	0.14 M KCl	0.33
0.5	0.14 M CsCl	0.37
0.5	0.14 M NH ₄ Cl	0.30
0.5	0.14 M GuCl	0.30

^a Usually mixed cellulose ester filter 0.45- μ pore size. ^b Ratio of amino acid residues/nucleotide residue. ^c Components mixed directly; no gradient dialysis. ^d Average errors from duplicate experiments are about 0.02. All concentrations are about 10⁻⁴ M (nucleotides). ^e Formed by gradient analysis, unless otherwise stated.

change). The CD spectrum for each particular mixture was attained within 15 min of mixing, and remained unchanged for at least 5 days. This variable CD behavior, plus the decrease in binding cooperativity indicated in Table I, suggests that simple mixing of f-1 and DNA produces nonspecific complexes. Histone is certainly bound to DNA; however, without the benefit of annealing through gradient dialysis, it binds irreversibly without reaching the most stable position on the DNA. (Differences between mixed and dialyzed complexes have been observed also with DNA and oligopeptides.²⁹)

Still another type of f-1-DNA complex is obtained upon dialysis down to 0.01 M NaF. The CD spectrum is reproducible, independent of r , and very similar to that of DNA^{3,15} ($[\theta]_{277} = 7800$, $[\theta]_{245} = -9200$). Complex formation occurs under these conditions (as well as after dialysis to 0.14 M salt), as shown by equilibrium dialysis,²⁸ melting curve,²⁵ and precipitation⁴⁰ data. Table I shows that the binding cooperativity of this type of complex (in 0.01 M NaF) is lower than that of complexes formed by dialysis into 0.14 M NaF. Furthermore, there is little aggregation of these complexes, as is seen by their lack of turbidity and light scattering. Once formed, these complexes cannot be reverted to the type formed by dialysis into 0.14 M NaF. Neither simple addition of salt nor dialysis *vs.*

0.14 M NaF accomplished this conversion, even after 6 days. A similar set of two types of complex, one formed at low salt, one at moderate salt concentration, was found for DNA plus arginine-rich histone (IV).⁵ These findings may have implications for chromatin-chromosome conversions within eukaryotic cells.

Circular Dichroism of DNA in Various Solvents. The main purpose of the present investigation was to examine f-1-DNA complexes in a variety of media at moderate ionic strength, since it was known that changes in concentration of NaF and addition of small amounts of organic solvents alter the CD of complexes.³ Before such a study could be initiated, it was necessary to know the concentration limits of various uni-univalent salts, MgCl₂, and dioxane which could be added to calf thymus DNA without causing a large CD change. Table II summarizes the results on DNA. Only the positive band peak values are tabulated, since the remainder of the CD spectrum (including the 245-nm negative band) was remarkably insensitive to solvent conditions.

Table II: Ellipticity of DNA in Various Solvents

Solvent	$[\theta]_{\sim 257}^a$
0.01 M NaCl	8400
0.14 M NaF or NaCl	8400
0.4 M NaF	8200
2.0 M NaCl	5600
0.14 M NaClO ₄	8500
0.4 M NaClO ₄	8400
0.14 M NH ₄ OAc	6800
0.4 M NH ₄ OAc	5700
0.0001 M MgCl ₂	6600
0.0001 M MgCl ₂ plus 0.01 M NaCl	7800
0.0001 M MgCl ₂ plus 0.14 M NaCl	8500
0.001 M MgCl ₂ plus 0.14 M NaCl	8200
0.01 M MgCl ₂ plus 0.14 M NaCl	7800
0.03 M MgCl ₂ plus 0.14 M NaCl	7400
0.2 M MgCl ₂ plus 0.14 M NaCl	6100
10% Dioxane plus 0.14 M NaF	8000
20% Dioxane plus 0.14 M NaF	8000
30% Dioxane plus 0.14 M NaF	8000
40% Dioxane plus 0.14 M NaF	7300 ^b

^a Peak positive ellipticities are listed. There was very little change in the negative band; $[\theta]_{245}$ remained at -9000 ± 300 . DNA concentration 10⁻⁴ M (nucleotides). ^b Solution opalescent. DNA precipitated in 50% dioxane.

The DNA CD spectrum was unaffected by univalent salts at moderate concentration, except for ammonium acetate. The CD spectrum in 0.4 M NH₄OAc was similar to that in very high concentrations of other salts (*e.g.*, 2 M NaCl). (The CD¹¹ and optical rotatory dispersion⁴¹ of DNA at high concentrations of salts has been previously examined.)

(40) M. Sluysers and N. H. Snellen-Jurgens, *Biochim. Biophys. Acta*, **199**, 490 (1970).

(41) M.-J. B. Tunis and J. E. Hearst, *Biopolymers*, **6**, 1218 (1968).

Addition of tiny amounts of MgCl_2 ($10^{-4} M$) greatly affected the CD of DNA in the absence of other electrolytes and, to a smaller extent, in the presence of 0.01 M NaCl . When 0.14 M NaCl was present, in addition to MgCl_2 , much higher concentrations of MgCl_2 resulted in smaller changes in the DNA ellipticity than in the absence of supporting electrolyte.

Similarly, *p*-dioxane added to DNA in the presence of 0.14 M NaF did not affect the CD greatly until 50% (by volume), at which point the DNA precipitated. DNA was not denatured, even by 40% dioxane at 23°; single-stranded DNA ($[\theta]_{273} = 9300$, $[\theta]_{247} = -6000$)³ was never observed.

The CD of f-1 histone alone ($10^{-3} M$ peptide, 1-mm cell) remained unchanged (within experimental error) upon addition of MgCl_2 (as above), various 0.4 M salts including NaClO_4 , and 40% dioxane.

Therefore, univalent salts (with the possible exception of NH_4OAc) up to 0.4 M (the highest concentration used during dialysis), MgCl_2 up to 0.1 M (in the presence of 0.14 M NaCl), and dioxane up to 40% (volume/volume) could safely be used without greatly changing the native conformation of DNA or f-1.

Effect of Various Uni-univalent Salts upon Circular Dichroism of f-1-DNA Complexes. In Figure 1 are seen the CD spectra of f-1-DNA complexes (f-1 histone/DNA ratio, $r = 0.5$, approximately the physiological ratio; complex concentrations $\sim 10^{-4} M$ nucleotides) reconstituted by gradient dialysis into 0.14 M salts. Various degrees of distortion of the DNA CD spectrum are evident, dependent upon the salt. The types of CD changes which occur as increasingly effective salts are used are identical to the progression observed as r is increased for complexes in 0.14 M NaF .³ For example, the CD spectrum for $r = 0.5$ in 0.14 M NaClO_4 is similar to that for $r \sim 0.15$ in 0.14 M NaF ; the CD spectrum for $r = 0.5$ in 0.14 M guanidine hydrochloride looks similar to that for $r = 1.5$ in 0.14 M NaF . (It is difficult to express these changes in spectrum by means of any single quantitative parameter. Analysis with a Du Pont curve resolver show that several CD bands are simultaneously involved in the CD distortions.)

Thus, large specific salt effects on the interaction of f-1 with DNA are apparent, even at the relatively low salt concentration of 0.14 M . This salt sensitivity is unique. Other macromolecular interactions and conformation changes,³¹ including the melting of DNA,^{32,34} are influenced only by nonspecific ionic strength shielding of ions at salt concentrations lower than 1 M . It might have been expected that all uni-univalent salts at 0.14 M would shield the negatively charged phosphates on DNA from the positive lysyl residues on f-1 to the same extent, and thus have the same influence upon DNA-f-1 interactions. This is not the case.

The effect upon the CD of f-1-DNA complexes, $r = 0.5$, of stopping dialysis at 0.3 M uni-univalent salts is

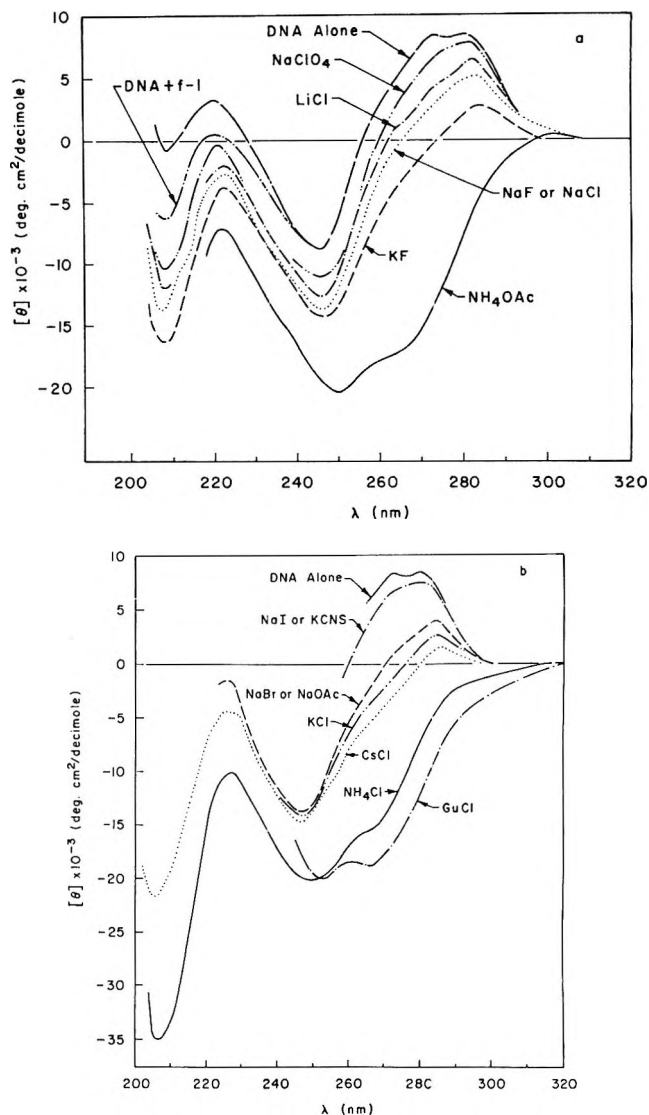


Figure 1. Circular dichroism of f-1-DNA complexes, r (peptide residues/nucleotide) = 0.5, in various 0.14 M salt solutions as labeled. Complex concentration = $7-8 \times 10^{-5} M$ nucleotide residues, path length 1 cm, temperature 23°. Figures 1a and 1b show different salts. The CD of DNA alone ($r = 0$) in 0.14 M NaF or NaCl is given for comparison; the curve "DNA + f-1" is the calculated sum of isolated DNA and f-1 CD contributions (at $r = 0.5$) in the same solvent.

demonstrated in Figure 2. The same order of salt effectiveness in causing CD distortions is apparent as in 0.14 M salts. The magnitude of CD changes is enhanced in 0.3 M salts, except for NaClO_4 and KCNS (where the CD spectra are identical with the sum of uncomplexed DNA and histone). Thus, the specific salt effects are augmented at higher salt concentrations, as expected. (NaCl has the same effect at 0.3 as at 0.14 M ; NaClO_4 and KCNS are causing dissociation, as will be shown later.)

CD curves for f-1-DNA complexes at $r = 1.0$ in several solvents are given in Figure 3. In each case there is greater CD distortion than for the $r = 0.5$ complex in the same solvent. The trends are identical

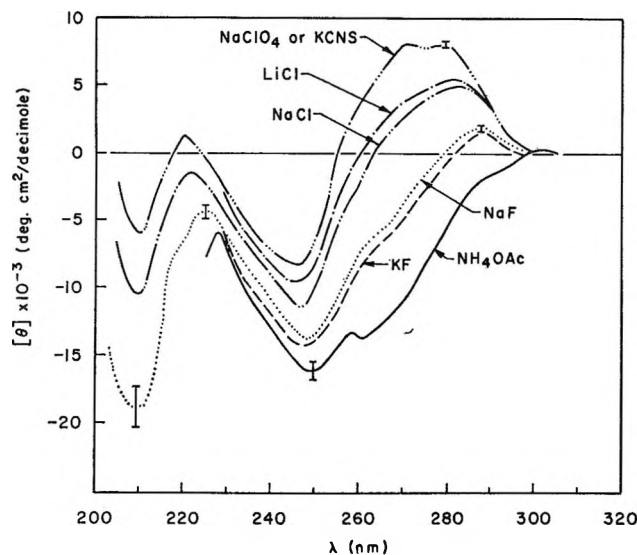


Figure 2. Circular dichroism of f-1-DNA complexes, $r = 0.5$, in various $0.3 M$ salt solutions. The conditions are the same as for Figure 1. Error bars indicate typical average errors between duplicate experiments. Note that the curve for complexes in $0.3 M$ NaClO_4 or KCNS is identical with that for the sum of isolated DNA and f-1 (see Figure 1a). The data for KCNS extend only to 258 nm .

to those at $r = 0.5$: the order of effectiveness in causing CD change at $0.14 M$ is ammonium acetate $>$ NaF $>$ NaClO_4 , and $0.3 M$ NaF is more effective than $0.14 M$ NaF .

It was found that increased opalescence, indicative of aggregation, always accompanied increased CD distortion. For example, values of $\text{OD}_{400}/\text{OD}_{258}$ (a measure of light scattering due to large particles) were, for $r = 1.0$ complexes in $0.14 M$ salt, 0.02 in NaClO_4 , 0.06 in NaF , and 0.10 in NH_4OAc .

The extent to which different salts might cause dissociation of protein from DNA (that is, might not allow the f-1-DNA complexes to form) was examined by filtration through cellulose membranes. It has already been shown that complexes in $0.14 M$ NaF are retained on filters to an extent consistent with nearly cooperative binding of f-1 to DNA. Table I shows that in $0.14 M$ concentration of most salts (including ammonium and guanidinium salts as well as other alkali halides) f-1-DNA complexes at $r = 0.5$ and $r = 1.0$ displayed the same filtration behavior as in NaF . This result indicates, in these uni-univalent salts, that all the histone is bound, that it is bound to DNA in the same manner as in NaF , and that no more DNA is involved in complexation in NH_4OAc than in NaF or NaOAc . The only exception among the salts tested is sodium perchlorate. In this solvent less DNA is caught on the filters, indicating that complex formation is not complete. This result is consistent with the finding⁴² that NaClO_4 causes gradual dissociation of f-1 from native nucleohistone in the range below $0.25 M$ (whereas NaCl does not remove f-1 until 0.4 to $0.6 M$).

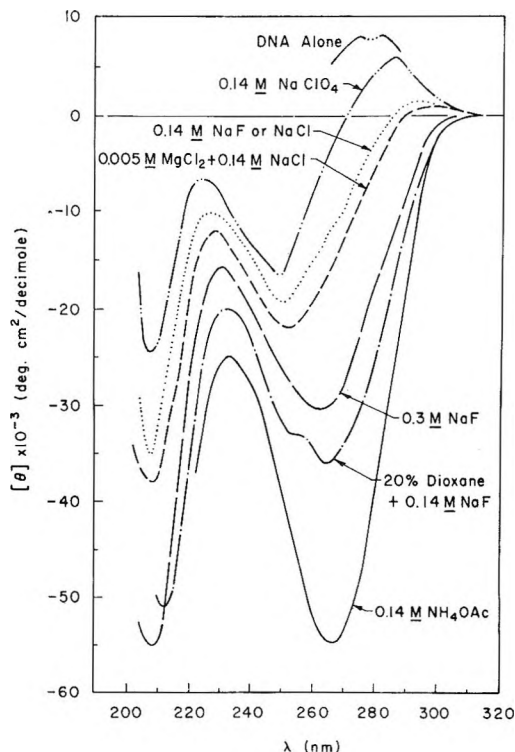


Figure 3. Circular dichroism of f-1-DNA complexes, $r = 1.0$, in selected solvents as indicated. Conditions as in Figure 1.

This dissociation of f-1 from DNA in NaClO_4 could account, in part, for the CD results of Figures 1-3. Thus, NaClO_4 , KCNS , and NaI are inhibiting formation of f-1-DNA complexes. These three salts at $0.3 M$ are more potent than at $0.14 M$ in preventing complex formation. Therefore, the CD spectra in $0.3 M$ of these salts appear more like DNA than in $0.14 M$.

However, the filtration experiments show that simple dissociation of histone from DNA cannot adequately be used to interpret the CD spectra in the remainder of the uni-univalent salts. Furthermore, increasing the concentration of the other salts from 0.14 to $0.3 M$ results in enhancement (not destruction) of the CD distortions. (In contrast, polarization of fluorescence experiments on DNA-polylysine complexes²⁷ could be explained purely by specific salt effects upon complex dissociation; in that study NH_4Cl was found to be more effective at dissociation than was NaOAc .)

An order of effectiveness of uni-univalent salts in bringing about changes in f-1-DNA complex circular dichroism can be obtained from the data of Figures 1 and 2. The sequence is: $\text{GuCl} > \text{NH}_4\text{Cl}, \text{NH}_4\text{OAc} \gg \text{CsCl} > \text{KCl}, \text{KF} > \text{NaOAc}, \text{NaBr} > \text{NaF} > \text{NaCl} > \text{LiCl} \gg \text{NaClO}_4, \text{KCNS}, \text{NaI}$. (Salts are grouped together if they result in identical CD curves, within experimental error. Finer resolution of the series could probably have been obtained by collecting data at

(42) H. H. Ohlenbusch, B. M. Olivera, D. Tuan, and N. Davidson, *J. Mol. Biol.*, **25**, 299 (1967).

higher salt concentrations, as is the case for NaF and NaCl at 0.3 *M*.) From comparison of salts sharing common ions, independent series can be written for cations and for anions. Cations: $\text{Gu}^+ > \text{NH}_4^+ \gg \text{Cs}^+ > \text{K}^+ > \text{Na}^+ > \text{Li}^+$; anions: $\text{OAc}^-, \text{Br}^- > \text{F}^- > \text{Cl}^- \gg \text{ClO}_4^-, \text{CNS}^-, \text{I}^-$.

Differences in anions have relatively little effect upon the CD spectra, except for ClO_4^- , CNS^- , and I^- , which prevent formation of f-1-DNA complexes, even at 0.14 *M*. For example, NH_4Cl and NH_4OAc yield similar data. Cations cause a larger range in spectra, indicating that salts may exert their primary influence upon the complexes through cation binding to negatively charged DNA, and not to histone. (Although the CD of f-1 was not altered by salts, it has been found⁴³ that both KCNS and NaClO_4 bind to and increase the α -helical content of poly-L-lysine at neutral pH. The possibility exists, therefore, that binding of ClO_4^- , CNS^- , or I^- onto f-1 may alter the conformational stability of the protein, thereby influencing its ability to interact with DNA.)

The order of effectiveness in causing CD changes of complexes, given above, is similar to the Hofmeister or lyotropic series; von Hippel and Schleich³¹ have summarized the effectiveness of salts in retaining or altering the native structure of macromolecules. For example, DNA is resistant to heat denaturation³² and F-actin remains associated³³ in $(\text{CH}_3)_4\text{NCl}$ solutions. Perchlorate, thiocyanate, and iodide salts favor denaturation, dissociation, and salting-in. The specific effects of anions upon interaction of f-1 and DNA in reconstituted complexes coincide with the lyotropic series quite well, and can be partially paralleled by the effects of salts on water structure,³¹ and consequent hydration of macromolecules. However, the specific cation effects show some discrepancies. Cs^+ is a large ion and disorders water structure, yet it stabilizes structure in f-1-DNA complexes.

The most difficult specific ion effects to understand are those exerted by ammonium and guanidinium. These ions, at only 0.14 *M*, bring about huge conformational changes in the complexes, as monitored by CD; the magnitude of this stabilization is more than might be expected from the position of NH_4^+ in the lyotropic series. It is likely that these ions bind tightly to DNA itself. The CD spectrum of DNA was seen to be affected by 0.14 *M* NH_4OAc to an extent not observed until very high (~ 2 *M*) concentrations of other univalent salts. In some ways 0.14 *M* (or 0.3 *M*) NH_4OAc has an influence upon DNA and f-1-DNA complexes similar to that of very low concentrations of Mg^{2+} (see later), an ion which binds to DNA more strongly than do monovalent cations.⁴⁴ It may be significant that films of DNA cast from NH_4OAc yield CD spectra⁴⁵ characterized by a large negative band at 265 nm, which are very different from spectra of films cast from NaCl or LiCl. Shapiro, *et al.*,⁴⁶ have demon-

strated a binding preference of tetraalkylammonium ions at 0.15 *M* (but not of alkali metal ions) for adenine-thymine-rich DNAs; calf thymus DNA contains 57% A-T. In the case of oligolysine binding to synthetic polynucleotides,^{47,48} inhibition of this binding by salts was interpreted in terms of competition between inorganic cations and lysine residues for the polynucleotide phosphate groups. On the other hand, for lysine-rich histone interaction with DNA the binding of cations, especially NH_4^+ or Gu^+ , onto DNA appears to assist in whatever aspect of f-1-DNA association leads to CD changes. Strong binding of cations may alter the structural stability of DNA, and thus influence its ability to combine with histone in a manner which results in conformational change or in formation of asymmetric superstructures. Or perhaps these nitrogen-containing cations are sufficiently similar to charged lysine that they are incorporated into f-1-DNA aggregates in the same manner as additional histone would be. This would have the same effect upon the CD spectrum as would an increase in f-1-DNA ratio, as is observed (Figures 1-3).

Effect of MgCl_2 upon Circular Dichroism of f-1-DNA Complexes. The study of the effect of inorganic ions on f-1-DNA complexes was expanded to investigate the effect of Mg^{2+} . Small amounts of MgCl_2 were added to the media used for gradient dialysis. The CD curves for complexes at histone/DNA ratio $r = 0.5$ in the presence of varying amounts of MgCl_2 plus 0.14 *M* NaCl are shown in Figure 4a. The concentration of DNA in the complexes was 8×10^{-5} *M* nucleotides. All solutions contained 0.14 *M* NaCl as supporting electrolyte in addition to the MgCl_2 , in order to prevent large disturbances of the DNA CD by MgCl_2 alone (see Table II). In Figure 4b the peak ellipticity values of the positive band ($[\theta]_{\sim 263}$) for the complexes are plotted as a function of MgCl_2 concentration. The CD curve for $r = 1$ at 0.005 *M* MgCl_2 (plus 0.14 *M* NaCl) is shown in Figure 3.

At very low concentrations of MgCl_2 , 0.00004 to 0.006 *M*, this salt enhances distortion of the DNA CD spectrum. The Mg^{2+} case is another example of a specific cation effect upon the f-1-DNA interaction. The spectral changes cannot be attributed to chloride ion (see above) or to a nonspecific electrostatic influence: at 0.003 *M* MgCl_2 the ionic strength is 0.149 instead of 0.14 (at 0 MgCl_2), and there is a large differ-

(43) (a) A. Ciferri, D. Puett, L. Rajagh, and J. Hermans, Jr., *Biopolymers*, **6**, 1019 (1968); (b) J. Y. Cassim and J. T. Yang, *ibid.*, **9**, 1475 (1970).

(44) G. Felsenfeld and H. T. Miles, *Annu. Rev. Biochem.*, **36**, 407 (1967).

(45) M.-J. B. Tunis-Schneider and M. F. Maestre, *J. Mol. Biol.*, **52**, 521 (1970).

(46) J. T. Shapiro, B. S. Stannard, and G. Felsenfeld, *Biochemistry*, **8**, 3233 (1969).

(47) S. A. Latt and H. A. Sober, *ibid.*, **6**, 3293 (1967).

(48) S. A. Latt and H. A. Sober, *ibid.*, **6**, 3307 (1967).

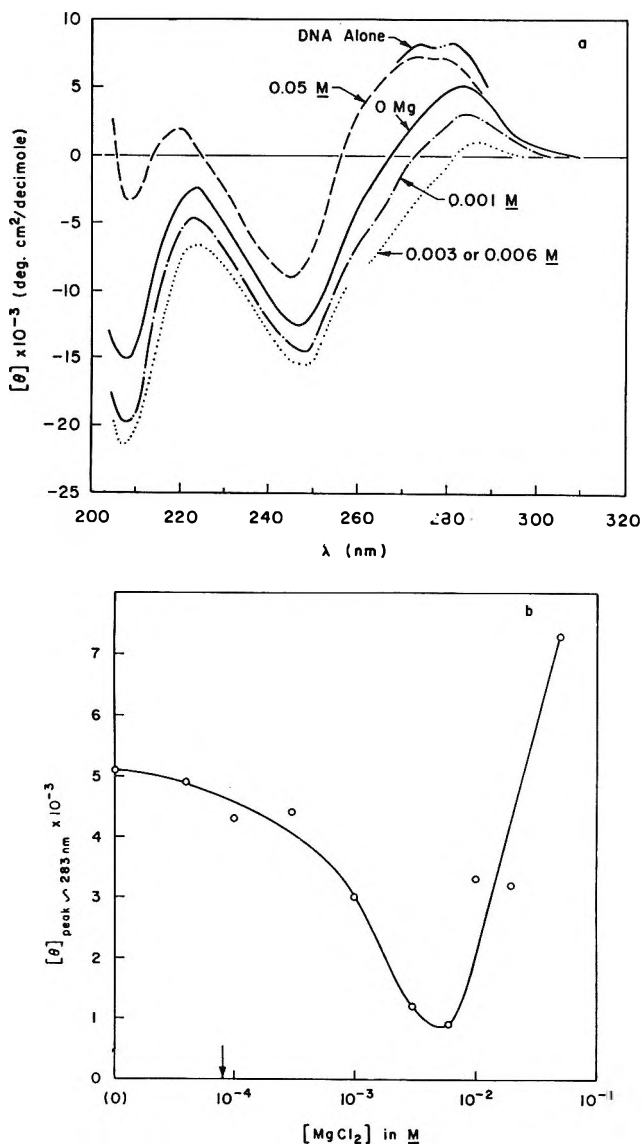


Figure 4. Effect of MgCl_2 upon the circular dichroism of f-1-DNA complexes, $r = 0.5$. All solutions contain 0.14 M NaCl in addition to specified MgCl_2 concentrations: a, circular dichroism spectra at various MgCl_2 concentrations; b, variation of $[\theta]_{\text{positive band}}$ as a function of $[\text{MgCl}_2]$. The arrow indicates concentration of DNA in the complexes.

ence in ellipticity. Figures 1 and 2 show that an increase in ionic strength from 0.14 to 0.30 for NaCl alone induces only a slight change in CD. Figure 4b shows that the Mg^{2+} effect is not stoichiometric (even though Mg^{2+} is tightly bound to DNA phosphate⁴⁴); the curve varies continuously at MgCl_2 concentrations both above and below the concentration of phosphate groups. The type of specific ion effect exhibited by Mg^{2+} at very low concentrations is similar to that shown by NH_4^+ at 0.14 M: both cations shift the f-1-DNA specific association toward a form of complex having a CD spectrum very different from that of DNA. Both cations appear to exert their influence largely through binding to DNA. Perhaps this ion binding alters the stability of the DNA, thus allowing

greater conformational changes upon binding f-1. A previous study⁴⁹ showed that, at 0.01 M, MgCl_2 is more effective than NaCl in causing precipitation of f-1-DNA complexes.

MgCl_2 concentrations above 0.006 M begin to dissociate f-1 from DNA. The ellipticity values are given in Figure 4b. (At 0.01 and 0.02 M MgCl_2 the CD changes are still greater than at zero Mg^{2+} ; both enhancement of change and dissociation are operative in this Mg^{2+} concentration range.) In Figure 4a is seen a CD curve at 0.05 M MgCl_2 , which is very similar to that for a mixture of the isolated components. Further evidence of partial dissociation at 0.05 M MgCl_2 is the filtration data listed in Table I. The disruption of f-1-DNA complexes at $[\text{MgCl}_2] \geq 0.08$ M has been noticed previously,^{28,49} and is not surprising in view of the position of Mg^{2+} in the lyotropic series.³¹

Effect of Dioxane upon Circular Dichroism of f-1-DNA Complexes. 1,4-Dioxane was chosen as a typical organic solvent (dielectric constant 2) for investigation of complexes in partially nonaqueous media. Organic solvents,³⁵ among them dioxane,³⁶ destabilize native DNA structure (observed as a lowering of the melting temperature) largely through disruption of hydrophobic bonding. The present results were obtained under conditions (23°, 10–40% dioxane, by volume, presence of 0.14 M NaF) at which DNA remains double-stranded (see Table II), although its stability may be weakened. At 50% dioxane both DNA and complexes precipitated.

CD curves for f-1-DNA complexes at $r = 0.5$, 10^{-4} M, for several dioxane concentrations are shown in Figure 5. NaF (0.14 M) was present in all solutions. Addition of dioxane progressively enhances the conformational difference between complexes and DNA. A similar effect is demonstrated in Figure 3 for $r = 1.0$ in 20% aqueous dioxane. A set of experiments at $r = 0.5$ and $r = 1.0$ for 10^{-3} M complexes confirmed the nature of the dioxane effect. Thus, the presence of dioxane allows the bound f-1 to exert a greater influence upon the DNA in f-1-DNA complexes, even though organic solvents usually tend to destroy native macromolecular conformations. The DNA may be destabilized as expected, thus allowing larger conformational changes by f-1. (In the case of some proteins, for example β -lactoglobulin,⁵⁰ high concentrations of organic solvents like dioxane cause formation of additional segments of α -helix, but not until after the protein has been partially unfolded.) No unfolding (or dissociation) is observed in the present case.

When dioxane was removed from the complexes by dialysis against 0.14 M NaF, the CD spectra were only partially reverted to values typical of aqueous solutions. For example, for $r = 1.0$, 10^{-4} M complexes (see

(49) E. W. Johns and S. Forrester, *Biochem. J.*, **111**, 371 (1969).

(50) C. Tanford and P. K. De, *J. Biol. Chem.*, **236**, 1711 (1961).

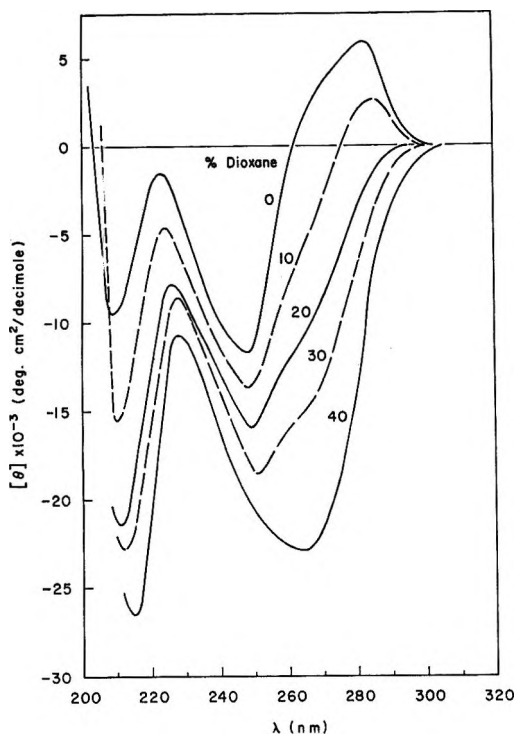


Figure 5. Effect of dioxane upon the circular dichroism of f-1-DNA complexes, $r = 0.5$. In addition to dioxane each solution contained $0.14 M$ NaF. Conditions as given in Figure 1. (See Figure 3 for CD spectrum of a $r = 1.0$ complex in 20% dioxane.)

Figure 3) aqueous dialysis of a sample in 20% dioxane resulted in a change in the relative sizes of the negative peaks ($[\theta]_{247} = -36,000$, $[\theta]_{263} = -32,000$); similar dialysis of a complex in 10% dioxane caused no change in CD spectrum. These results show that formation of complexes in dioxane is a largely irreversible process (*cf.* formation of complexes in $0.01 M$ NaF).

The sensitivity toward salt concentration during complex formation³ is retained in the presence of dioxane. f-1-DNA complexes, $r = 1$, reconstituted in $0.01 M$ NaF plus 10–30% dioxane are characterized by CD spectra very similar to that of DNA alone, as reported for the f-1-DNA complex at $0.01 M$ NaF.³ These spectra cannot be altered significantly by further dialysis against $0.14 M$ NaF plus dioxane.

Conclusions

This study has shown that there are highly selective solvent effects operating upon the interaction of DNA with lysine-rich histone, f-1. The f-1-DNA complexes formed in the presence of dioxane (5–40%) or of quite low concentrations of certain cations are characterized by circular dichroism spectra very different from that of DNA. The counterions which increase this distortion are alkali metals (especially Cs^+) at 0.14 or $0.3 M$, Mg^{2+} up to $0.006 M$ (in the presence of supporting electrolyte), and particularly NH_4^+ and guanidinium⁺ at $0.14 M$. Furthermore, those ions which cause dissociation of histone from DNA (ClO_4^- , CNS^- , and I^-

at $0.14 M$; Mg^{2+} at $> 0.006 M$) do so at unusually low concentrations. An attempt will now be made to correlate the factors that are common to all these effects of neutral salts and organic solvents.

As has been noted, reconstitution of f-1-DNA complexes showing CD alteration (relative to DNA) is always accompanied by a proportional amount of aggregate formation (as shown by turbidity). Under conditions where f-1 is bound to DNA but where there is little CD change (for example, at $0.01 M$ NaF), there is very little light scattering. When a large change in CD occurs (for example, in NH_4OAc) there is no increase in the amount of DNA involved in complex formation (as is shown by filtration experiments), but there is an increase in aggregation. These results imply that the requirements for CD distortion include not only binding of f-1 onto DNA in a cooperative and specific manner, but also specific association of the f-1-DNA complexes formed. (It should be remembered that the DNA in these complexes is only 15–30% neutralized by the f-1, and retains considerable negative charge.)

Other evidence for the ability of lysine-rich histone to bind to DNA and cause a selective sort of aggregation is that f-1 (but not other histone fractions) is apparently important in maintaining the cross-linked structure of nucleoprotein in interphase chromatin⁵¹ and in metaphase chromosomes.⁵² Furthermore, poly-L-lysine-DNA complexes (a similar model system) form aggregated particles of definite, large radius;¹⁸ these complexes have CD spectra characterized by a large, negative band at 269 nm .^{18,21} On the other hand, recent X-ray diffraction⁵³ and hydrodynamic⁵⁴ studies of partially dissociated nucleohistones suggest that the supercoiled structure of nucleoprotein is maintained after removal of the f-1 histone fraction. The CD spectrum characteristic of native nucleohistone is also maintained after removal of f-1.^{12,13,55}

It is not clear by what mechanism complex formation or association of complexes can alter the circular dichroism of DNA. Since there is negligible change in absorption spectrum for DNA when it is incorporated into f-1-DNA complexes at the ratios considered here, an alteration in CD is most likely effected through a change in the asymmetric environment of the nucleotide base chromophores. X-Ray diffraction data on chromatin^{23,24} and on poly-L-lysine-DNA complexes^{21,26} are not yet conclusive, but suggest that the DNA probably retains the geometry of its B conformation in these

(51) V. C. Littau, C. J. Burdick, V. G. Allfrey, and A. E. Mirsky, *Proc. Nat. Acad. Sci. U. S.*, **54**, 1204 (1965).

(52) A. E. Mirsky, C. J. Burdick, E. H. Davidson, and V. C. Littau, *ibid.*, **61**, 592 (1968).

(53) K. Murray, E. M. Bradbury, C. Crane-Robinson, R. M. Stephens, A. J. Haydon, and A. R. Peacocke, *Biochem. J.*, **120**, 859 (1970).

(54) P. Henson and I. O. Walker, *Eur. J. Biochem.*, **14**, 345 (1970).

(55) P. Henson and I. O. Walker, *ibid.*, **16**, 524 (1970).

systems. However, a distortion of base-base distance or of tilt has not been completely ruled out. It has been suggested that polylysine-DNA complexes may form a liquid crystalline system.²¹ However, classical liquid crystal systems derive their circular dichroism from reflection (not absorption); the wavelength of the CD signal in liquid crystals varies with molecular spacing (and concentration) but is not a function of absorption spectrum.⁵⁶ In nucleoprotein systems the wavelength of circular dichroism is close to that of DNA absorption. Thus, the CD distortion for f-1-DNA complexes is not a simple liquid crystal phenomenon, although long-range order of oriented complexes in a supercoil may well be responsible for the CD changes observed here.¹⁸ Perhaps interactions of (or constraints upon) the DNA within the aggregated complexes give rise to CD changes, as appears to be the case with optical rotation of DNA packed within viruses.⁵⁷ Additional alternative interpretations offered for the CD changes upon complex formation are alterations in DNA hydration^{3,18} and interaction between base and peptide chromophores.^{18,21}

Two factors appear to be important in producing f-1-DNA complexes with altered CD: (1) Specific complex formation involves the interaction of DNA (having negatively charged phosphates) and f-1 (containing 29% positively charged lysyl amino groups plus some arginine) to form a partially neutralized complex. The charge remaining on a complex at $r = 1.0$ is still -0.70 per nucleotide. Only complexes reconstituted by dialysis into moderate salt solutions are then capable of the second step. (2) Specific association of complexes involves aggregation of negatively charged molecules, and depends upon the solvent. This association can be prevented by dialysis against $0.01 M$ NaF, enhanced by dioxane, but only partially reversed by removal of dioxane. The effect of different solvents upon the CD of f-1-DNA complexes can be partially understood by a consideration of how various salts and dioxane may influence each step [(1) complexation and (2) association].

Although step 1 (binding) can occur at very low salt concentration,^{25,28,40} greater than $0.01 M$ salt appears necessary for step 2. That is, some shielding of repulsive charges is needed for the association of complexes which results in CD change. However, at salt concentrations high enough to allow aggregation to occur, the influence of salts is not a simple ionic strength dependence, as might be expected in a reaction involving the association of molecules with the same charge. Instead, even at $0.14 M$, each salt has a different specific influence upon the CD change.

DNA is known to interact strongly with cations. Alkali metal counterions are bound to a moderate extent, and Mg^{2+} is bound stoichiometrically, to the phosphates.⁴⁴ It is not yet resolved how much binding can be attributed to the ion atmosphere, and how much is

caused by specific site binding to the phosphates.⁴⁴ Mg^{2+} at very low concentrations would thus neutralize the excess negative charge on f-1-DNA complexes, enhance aggregation (step 2) by allowing the complexes to come together, and lead to increased CD distortion. Since NH_4^+ (at $0.14 M$) has the same effect upon the CD of native calf thymus DNA as does Mg^{2+} (at stoichiometric amounts), it is likely that NH_4^+ is binding to DNA strongly, and in the same manner as Mg^{2+} (although with a smaller binding constant). Then NH_4^+ (and Gu^+) would aid in association of complexes through charge neutralization. Possibly NH_4^+ and Gu^+ act in a more specific manner: they might be incorporated into f-1-DNA complexes as though they were $-NH_3^+$ groups on the histone, thus increasing the apparent f-1/DNA ratio.

Those salts which dissociate f-1 from DNA at $0.14 M$ ($NaClO_4$, $KCNS$, NaI) are also exerting specific ion effects at fairly low concentration. They are not acting merely by reversing step 1 (complex formation) through shielding; $0.5 M$ $NaCl$ is required for destruction of complexes. These anions may denature DNA (and destroy f-1-DNA complexes) by forming complexes with the nucleotide bases,⁵⁸ or by specific binding to the histone, as has been shown to be the case for poly-L-lysine.⁴³

The enhancement of CD change brought about by dioxane cannot be explained simply by a decrease in solvent dielectric constant. If only charge attraction and repulsion were important, dioxane would be expected to aid step 1 and to hinder step 2. Furthermore, if dioxane acted by breaking hydrophobic interactions between nonpolar groups on the DNA and the histone, it would probably interfere with both step 1 (proper, specific binding) and step 2 (complex association). Perhaps step 2 is facilitated by partial removal of water from the histone-DNA complexes, as well as by the binding of certain cations. In addition, dioxane would be expected to enhance ion-pair formation between charged phosphates and lysines; the resultant charge neutralization could aid in aggregation of complexes. Both dioxane and strongly bound cations affect the structural stability of DNA. Although the DNA remains double stranded under the present conditions, it might be more susceptible to conformational change and specific aggregation upon complexing with f-1.

Thus the effects which neutral uni-univalent salts have upon f-1-DNA complexes fall within the Hofmeister series. These specific ion effects have been attributed to their influence upon water structure, hydration of the biopolymer, ion-dipole type interactions, etc., but these concepts as yet do not "account satis-

(56) C. Robinson, *Tetrahedron*, **13**, 219 (1961).

(57) M. F. Maestre and I. Tinoco, Jr., *J. Mol. Biol.*, **23**, 323 (1967).

(58) D. R. Robinson and M. E. Grant, *J. Biol. Chem.*, **241**, 4030 (1966).

factorily for all the observed effects."³¹ However, this study has shown that the interaction between histone f-1 and DNA is extraordinarily sensitive to salt and solvent effects. This interaction results in changes in the CD spectrum of the DNA, implying a conformational change of state. Thus, small alterations in sol-

vent medium may be a selective means of affecting the state of aggregation of these complexes. Both the conformational control and aggregative phenomena have relevance to the purported role that histones may play in association with DNA in the chromatin of eukaryotes.

Reformulation of the Quasiequilibrium Theory of Ionic Fragmentation¹

by **Cornelius E. Klots**

Health Physics Division, Oak Ridge National Laboratory, Oak Ridge, Tennessee 37830 (Received December 2, 1970)

Publication costs assisted by Oak Ridge National Laboratory

An alternative to the transition-state formalism of unimolecular decomposition theory is further developed. When the conservation of angular momentum is heeded, the content of this formulation is seen to be that of phase-space theory. Application to the fragmentation processes of methane ions proves generally successful, although some difficulties are delineated. Tunneling is implicated as a source of the metastable decompositions occurring in methane.

Introduction

The work of Butler and Kistiakowsky² has strongly suggested that the kinetics of unimolecular fragmentation are determined by the energy content of an activated species but not otherwise by its mode of preparation. Since then chemical activation techniques have constituted an important branch of chemical kinetics, and have been instrumental in the ascension of those theories which explicitly predict such behavior and likewise the demise of at least one theory which explicitly does not. Thus, the quasiequilibrium theory of unimolecular decompositions specifically describes an activated species in terms of microcanonical ensemble theory; hence its average lifetime can be a function of only a small number of "constants of motion" and not at all of its past history—precisely as the Butler and Kistiakowsky paper implied.

The essential content of quasiequilibrium theory has found its most common expression within the formalism of the transition state.³⁻⁵ The first-order rate constant for fragmentation of a species with total energy ($E + E_0^\pm$) is given in this formalism by

$$k_i = \sum_{x=0}^{x=E} g_j^\pm(x, \alpha_i) / \rho(E + E_0^\pm, \alpha_i) h \quad (1)$$

where $g_j^\pm(x)$ is the internal statistical degeneracy factor for the transition state of energy (x); the summation extends by energy conservation over the range $0 \leq x \leq E$. E_0^\pm is the activation energy. These degener-

acy factors must further be chosen to be compatible with any additional constraints α_i . Similarly $\rho(E + E_0^\pm, \alpha_i)$ is the density of states of the activated species, again evaluated with the indicated constraints. This expression has found wide use in calculating the rates of unimolecular reaction in the absence of collisions. When coupled with the strong collision hypothesis, the Rice-Ramsperger-Kassel-Marcus description, applicable at all pressures, is obtained.⁶

There is a second formalism available for calculating a fragmentation rate constant

$$k_i = \sum_{x=0}^E g_f(x, \alpha_i) \cdot \frac{\sigma(f, i)}{\pi \lambda^2} / h \rho(E + E_0, \alpha_i) \quad (2)$$

where $g_f(x, \alpha_f)$ is the degeneracy factor for the separated fragments, $\sigma(f, i)$ is the cross section for their association to form the pertinent activated species, and λ is the deBroglie wavelength associated with their relative kinetic energy ($E - x$). Equation 2 follows from the quasiequilibrium hypothesis and microscopic re-

(1) Research sponsored by the U. S. Atomic Energy Commission under contract with Union Carbide Corporation.

(2) J. N. Butler and G. B. Kistiakowsky, *J. Amer. Chem. Soc.*, **82**, 759 (1960).

(3) H. M. Rosenstock, *Advan. Mass Spectrom.*, **4**, 523 (1968).

(4) B. S. Rabinovitch and D. W. Setser, *Advan. Photochem.*, **3**, 1 (1964).

(5) M. L. Vestal in "Fundamental Processes in Radiation Chemistry," P. Ausloos, Ed., Wiley, New York, N. Y., 1968, pp 59-118.

(6) E. V. Waage and B. S. Rabinovitch, *Chem. Rev.*, **70**, 377 (1970).

versibility. It has been used in the contexts of both unimolecular fragmentations⁷ and autoionization.^{8,9}

We shall make extensive use of this latter formalism in the present paper. At this point however we should clarify the relation between eq 1 and 2 and enumerate whatever advantages accrue to the latter. This is most simply done by noting that Marcus¹⁰ and, more recently, Karplus and coworkers¹¹ have shown that the relationship

$$\sum g_f(x, \alpha_i) \frac{\sigma(f, i)}{\pi \lambda^2} = \sum g_j^\pm(x, \alpha_i) \quad (3)$$

defines the thermodynamic properties of the transition state if the latter is to provide numerically consistent answers. Whether or not these properties will correspond to those calculated from the potential energy surface remains an open question. This hinges upon such ancillary matters as whether the concept of a separable reaction coordinate is meaningful and whether transmission coefficients are unity. Recent work has tended to cast some doubt on each of these.^{11,12} Hence we see that eq 2 rests upon the quasiequilibrium hypothesis; eq 1 presupposes both this and the usual further assumptions associated with the theory of the transition state. Any work which purports to test the quasiequilibrium hypothesis itself is evidently more safely rooted in eq 2.

Further advantages of eq 2 may also be noted. Its evaluation requires the thermodynamic properties of the separated fragments. These are amenable to experimental observation, while properties of the transition state are not. The latter can be constructed only after the potential energy surface in the neighborhood of the saddle point has been mapped. Despite impressive recent advances in this direction,¹³ some impatience on the part of the experimentalist is understandable.

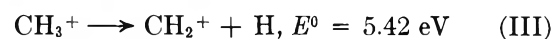
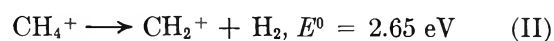
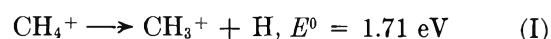
These advantages are not obtained, however, without some cost. One does need good cross-section data for the evaluation of eq 2. But again these are amenable to experimental observation or, again for the impatient, estimation from the interaction potential. This latter procedure is exemplified by the Langevin treatment whereby collision cross sections are obtained from the long-range forces.¹⁴ We shall use this method below.

Before doing so, however, some further general remarks are appropriate. It is well known^{15,16} that bimolecular association rate constants obtained with Langevin cross sections are equal to those obtained from the "loose transition state" models of Gorin¹⁷ and Eyring, Hirschfelder, and Taylor.¹⁸ This is merely a reflection of the fact that eq 3 is fulfilled for such "loose transition states." We conclude then that the Gorin-EHT method for constructing transition states is the correct one for reactions governed by Langevin cross sections. Now, scrutiny of eq 2 shows that it is equivalent to the phase-space methodology¹⁹ for estimating

how a collision couple will fragment. Mies²⁰ has observed that phase-space theory is equivalent to transition state theory for "loose transition states." This also follows from the above remarks. Actually a stronger statement is possible. Phase-space theory is equivalent to quasiequilibrium theory; they are each equivalent to transition state theory whenever the latter is correct.

Illustrative Calculations

We shall illustrate the use of eq 2 in the context of the fragmentation processes of the CH₄⁺ ion. The simplicity of this system lends itself to a scrutiny of the quasiequilibrium hypothesis relatively unobscured by ancillary assumptions. Thus only three reactions need to be considered. These are, together with their activation energies^{21a}



The following observations must be accounted for by any unimolecular decomposition scheme. (1) The appearance potentials for these processes correspond well to the above-indicated activation energies, as determined by independent means.^{21a} Thus there is little, if any, kinetic shift²² for these reactions. (2) Metastable ions have been observed to undergo reaction I for all isotopic variants,^{23,24} and with comparable in-

(7) C. E. Klots, *J. Chem. Phys.*, **41**, 117 (1964).

(8) C. E. Klots, *ibid.*, **46**, 1197 (1967).

(9) Provided one assigns the photon a polarization degeneracy factor of 2, eq 2 also gives the usual Einstein relation between emission lifetimes and photoabsorption cross sections. This is of more than purely formal interest. The energy randomization frequently thought of as underlying unimolecular decompositions is also one of the factors which complicates the use of the Einstein relation; see, for example, A. E. Douglas, *ibid.*, **45**, 1007 (1966).

(10) R. A. Marcus, *ibid.*, **45**, 2138, 2630 (1966).

(11) K. Morokuma, B. C. Eu, and M. Karplus, *ibid.*, **51**, 5193 (1969).

(12) R. A. Marcus, *ibid.*, **41**, 2614 (1964).

(13) I. Shavitt, R. M. Stevens, F. L. Minn, and M. Karplus, *ibid.*, **48**, 2700 (1968).

(14) P. Langevin, *Ann. Chim. Phys.*, **5**, 245 (1905).

(15) B. Mahan, *J. Chem. Phys.*, **32**, 362 (1960).

(16) K. Yang and T. Ree, *ibid.*, **35**, 588 (1961).

(17) E. Gorin, *Acta Physicochim. URSS*, **9**, 691 (1938).

(18) H. Eyring, J. O. Hirschfelder, and H. S. Taylor, *J. Chem. Phys.*, **4**, 479 (1936).

(19) P. Pechukas and J. C. Light, *ibid.*, **42**, 3281 (1965); J. C. Light, *Discuss. Faraday Soc.*, **44**, 14 (1967).

(20) F. H. Mies, *J. Chem. Phys.*, **51**, 798 (1969).

(21) (a) "Ionization Potentials, Appearance Potentials, and Heats of Formation of Gaseous Positive Ions," NSRDS Publication, National Bureau of Standards Report NBS-26, 1969; (b) the structure of CH₄⁺ has been estimated by F. A. Grimm and J. Godoy, *Chem. Phys. Lett.*, **6**, 336 (1970).

(22) W. A. Chupka, *J. Chem. Phys.*, **30**, 191 (1959).

(23) Ch. Ottinger, *Z. Naturforsch. A*, **20**, 1232 (1965).

(24) J. H. Futrell, private communication.

tensity. This is not easily reconciled with the predictions of the usual transition state theory.²⁵ (3) Rotational energy can assist in overcoming the activation energy of reaction I. (4) The breakdown curves, a function of internal energy of the parent ion, are known from the work of vonKoch.²⁶ We shall see that the present formalism is able to account for each of these observations.

The thermodynamic properties of H₂ are well known. Those of the hydrocarbon ions are not^{21b} and so were estimated in the following way. The structures of CH₄⁺, CH₃⁺, and CH₂⁺ were taken as tetrahedral, planar symmetric, and linear symmetric, respectively. For computations of moments of inertia, all their bond lengths were arbitrarily assigned the value 1 Å. The vibrational frequencies of CH₄⁺ were taken as those of CH₄,²⁷ from which were derived in the simplest fashion possible those of the fragment ions. These are summarized in Table I in units $h\nu_i = \epsilon_i(\text{eV})$, together with their degeneracy factors. Also included in the table are the rotational constants which define rotational energy via $E_r(\text{eV}) = BJ(J + 1)$, where J is the rotational quantum number. For CH₄⁺, CH₂⁺, and H₂ these follow from the assumed structures. Since CH₃⁺ will be treated below as a spherical top, its rotational constant was taken as the geometrical mean of those obtained from the three principal moments of inertia.

Table I: Vibrational Energies (with Degeneracy Factors) and Rotational Parameters in Units of eV

CH ₄ ⁺	CH ₃ ⁺	CH ₂ ⁺	H ₂
0.361 (1)	0.361 (1)	0.361 (1)	
0.189 (2)	0.189 (1)		
0.374 (3)	0.374 (2)	0.374 (1)	
0.162 (3)	0.162 (2)	0.162 (2)	
0.771 ^a	1.09 ^a	1.03 ^a	0.545 (2)
			3.75 ^a

^a $B \times 10^3$.

One further preliminary datum, the statistical reaction-path factor for each decomposition, must be discussed. For reactions I, II, and III there are, respectively, four, six, and three equivalent reaction paths. But for the reverse reaction, the total cross section appearing in eq 2 is apportioned among two, two, and one routes, respectively. The net statistical reaction-path factors for these reactions, then, are two, three, and three, respectively. Note that, by a theorem due to Laidler,²⁸ these are also the ratios of the respective symmetry factors for the several reactants.

The manner by which one includes conservation of angular momentum in fragmentation kinetics has been amply illustrated by Nikitin²⁹ and Light,¹⁹ and so need not be belabored here. Reaction I will be treated as a sphere dissociating to a sphere plus an atom. The

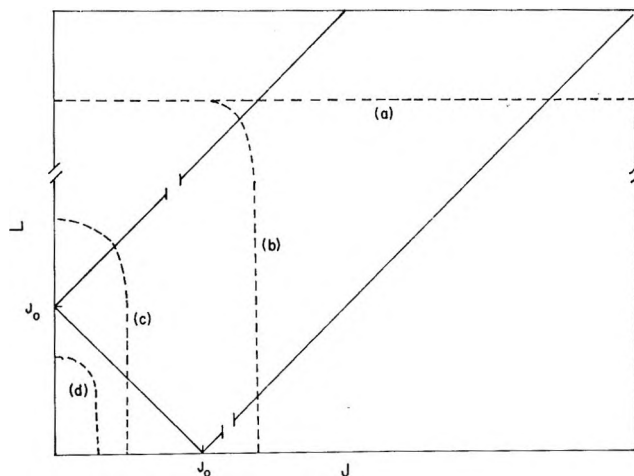


Figure 1. Allowed L, J, J_0 combinations and limitations imposed by Langevin cross sections.

initial angular momentum, indexed as J_0 , must appear as orbital angular momentum L or as product angular momentum J . The cross section ($\sigma/\pi\lambda^2$) for an $(L + J \rightarrow J_0)$ association is $(2L + 1)$ times the fraction of such collisions which result in J_0 , specifically $(2J_0 + 1) \div (2L + 1)(2J + 1)$. At this point it is useful to consider Figure 1; the L, J combinations compatible with a given J_0 are contained within the rectangular area defining $L = J_0 + J \dots |J_0 - J|$. Energy conservation, and the use of the Langevin model for the total cross section, poses the further restriction

$$(L_{\max} + 1)^2 = \gamma[(E - x) - BJ(J + 1)]^{1/2} \quad (4)$$

where $(E - x)$ is the energy not appearing in the vibrations of the products, B is the rotational constant of the product sphere, given by

$$B = \hbar^2/2I$$

where I is the moment of inertia. The parameter γ is given by the Langevin model for ion-molecule collisions

$$\gamma = (2\mu/m)(\alpha/Ra_0^3)^{1/2}$$

where μ is the reduced mass of the separating pair, m that of an electron, α the polarizability of the neutral fragment, a_0 the Bohr radius, and R the Rydberg energy.

With reference again to Figure 1, curve (a) is typical of the restriction obtained with $B = 0$. This is exactly the approximation used in some earlier work of the present author.⁷ But, as Nikitin²⁹ has pointed out, it is extremely limited in its applicability. In fact, a

(25) M. L. Vestal, *J. Chem. Phys.*, **41**, 3997 (1964).

(26) H. vonKoch, *Ark. Fys.*, **28**, 529 (1964).

(27) G. Herzberg, "Infrared and Raman Spectra," Van Nostrand, New York, N. Y., 1945.

(28) D. M. Bishop and K. J. Laidler, *J. Chem. Phys.*, **42**, 1688 (1965).

(29) E. E. Nikitin, *Theor. Exp. Chem.*, **1**, 144 (1965).

quite different limiting approximation, illustrated by curves (b) and (c), is more appropriate. On expansion of eq 4, with $L \sim J$ as will always be the case for not too large J_0 , and assuming

$$(E - x) \ll \gamma^2 B^2 (\simeq R) \quad (5)$$

one finds that the curve defined by eq 4 cuts the allowed rectangle nearly vertically. Since the criterion of (5) is easily justified—the excess energy of fragmentation tends to appear as vibrational excitation⁷—a considerable simplification in the calculation of rate constants is obtained.

Noting that the rotational degeneracy of the product sphere is $(2J + 1)^2$, we have

$$\frac{\sigma}{\pi \lambda^2}(J, L, J_0) = (2J_0 + 1)(2J + 1) \quad (6)$$

This is to be summed, for each J , over the allowed L and then over the allowed J up to $J_{\max} \approx [(E - x)/B]^{1/2}$. We obtain finally

$$k(E + E_0, J_0) = [h(2J_0 + 1)^2 \rho_v(E_v + E_0)]^{-1} \times \left[(2J_0 + 1) \int_0^{BJ_0^2} \rho_v(x) \frac{4}{3} \left(\frac{E - x}{B} \right)^{3/2} d(E - x) + (2J_0 + 1)^2 \int_{BJ_0^2}^E \rho_v(x) \left[\frac{E - x}{B} - \frac{J_0^2}{3} \right] d(E - x) \right] \quad (7)$$

where $\rho_v(x)$ is the density of vibrational states of the products and $\rho_v(E_0 + E_v)$ is the density of vibrational states of the activated species. Except in the immediate vicinity of threshold, this may be written as

$$k(E + E_0, J_0) \simeq \int_0^E \rho_v(x) \left(\frac{E - x}{B} \right) d(E - x) / h \rho_v(E_v + E_0) \quad (8)$$

Through a similar analysis, we obtain for two product linear fragments, as in reaction II

$$k(E + E_0, J_0) = \frac{2}{3} \left[\frac{B_1^{1/2} + B_2^{1/2} - (B_1 + B_2)^{1/2}}{B_1 B_2} \right] \times \int_0^E \sigma_v(x) (E - x)^{3/2} d(E - x) \div h \rho_v(E_v + E_0) \quad (9)$$

where B_1, B_2 are the rotational constants of the two linear fragments. Likewise, when the products include a linear fragment and an atom, as in reaction III

$$k(E + E_0, J_0) = \int_0^E \rho_v(x) \left[\frac{E - x}{B} \right]^{1/2} d(E - x) \div h \rho_v(E_v + E_0) \quad (10)$$

again provided J_0 is not too large. To all of these expressions must then be added the appropriate reaction-path statistical factor, as discussed earlier.

Before passing on to an evaluation of these expressions, it will be appropriate to comment on the use of Langevin cross sections here. Such cross sections have

frequently been compared with the experimental cross sections of ion-molecule reactions and often found wanting, especially at large kinetic energies. But the fragments from the decompositions of reasonably complex species rarely carry much kinetic energy;^{7,30} the weight of this objection is accordingly diminished. Again the cross section for an ion-molecule reaction is the product of two factors, the collision cross section and the probability that the intermediate complex fragments into the observed products. Equation I requires only this first factor and hence is more plausibly evaluated with the Langevin model.

It should be noted that the polarizability appears in eq 4 but not in the final eq 7–10. This insensitivity to the precise magnitude of the collision dynamics is again welcome. It stems from the approximation contained in relation 5.

Evaluation

A large number of recipes for vibrational densities-of-states can be found in the literature. Those of Hoare and Ruijgrok are conceptually appealing and have been used here.³¹ It is to be noted, however, that the integrand in eq 8, for example, contains such a density-of-states together with the factor $(E - x)/B$. This integral can be evaluated by noting that it is just the density-of-states, at energy E , for a fictitious molecule containing the several vibrational degrees of freedom and a four-dimensional rotor. The partition function of the fictitious rotor would be just

$$Q_r = (kT)^2 / B$$

Hoare gives expressions for the density-of-states of such compound systems. Likewise, the integrals appearing in eq 9 and 10 may be evaluated. We have found, incidentally, that these recipes of Hoare give extraordinarily precise results down to the immediate neighborhood of threshold where they are easily supplemented by precise hand calculations.

Figure 2 illustrates the rate constants obtained for reaction I in the vicinity of threshold, presented as functions of the initial vibrational energy content of the ion. Curve (a) is for a nonrotating ion; curve (b) for an ion with rotational energy 0.03 eV. Each curve rises abruptly but smoothly from zero at threshold, as required by eq 7. Thus we do not obtain the step-function behavior in rate constants as implied by the transition-state formalism.^{25,32} The observation of metastable decompositions for all isotopic variants of methane is hence accounted for in principle. (Whether this is indeed the source of the metastables is examined

(30) M. A. Haney and J. L. Franklin, *J. Chem. Phys.*, **48**, 4093 (1968); E. L. Spitz, W. A. Seitz, and J. L. Franklin, *ibid.*, **51**, 5142 (1969).

(31) M. R. Hoare and Th. W. Ruijgrok, *ibid.*, **52**, 113 (1970); M. R. Hoare, *ibid.*, **52**, 5695 (1970); misprints in eq 2.12 and 3.1f of this reference are to be noted.

(32) M. Wolfsberg, *ibid.*, **36**, 1072 (1962).

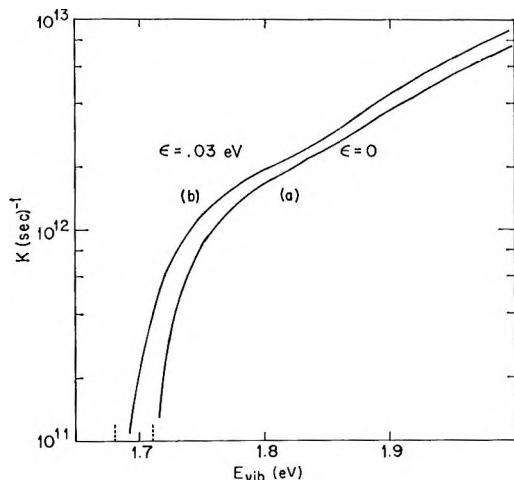


Figure 2. Decomposition rate constants for CH_4^+ near threshold, (a) nonrotating and (b) with 0.03-eV rotational energy.

further, below.) The nevertheless rapid rise with energy, duplicated also in calculations for reactions II and III, explains the absence of significant chemical shifts. Again, the nearly complete availability of rotational energy, indicated by curve (b), mirrors the observation of Chupka³³ to this point.

Before proceeding to calculations of a breakdown curve for methane, we must obtain an expression for the fraction of ions from reaction I which can further dissociate in reaction III. Noting the facility with which rotational energy can promote a dissociation, we identify the fraction of CH_3^+ products which do not further dissociate with the fraction with total vibrational and rotational energy insufficient to do so. This is given by

$$F_{st}(Q, \epsilon) = \int_0^\epsilon \rho_\epsilon(\epsilon - z)(z/B) dz \div \int_0^Q \rho_\epsilon(Q - z)(z/B) dz$$

Here Q is the energy of a CH_4^+ in excess of that needed to undergo reaction I, and ϵ is the activation energy, less than Q , required for the secondary reaction. The vibrational density-of-states function refers to the CH_3^+ . Thus for any CH_4^+ ion with $Q \geq 5.42$, it is a simple matter to obtain that fraction of its CH_3^+ fragments which further dissociate.

The breakdown curve for methane ions thus obtained is displayed in Figure 3. It has been put on an absolute energy basis by using 12.55 eV as the ionization potential of methane.²¹ In the 15.2–19.7-eV region, the relative abundance of CH_3^+ and CH_2^+ follows from the predicted rate constants for reactions I and II. At higher energies the secondary decomposition of CH_3^+ is manifested. The experimental points are from von-Koch.²⁶ The agreement is satisfactory and could be

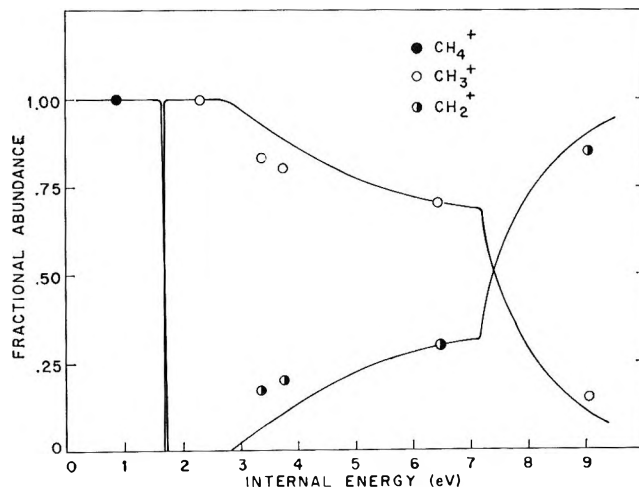


Figure 3. Breakdown pattern for CH_4^+ as a function of internal energy.

further improved by tampering with the assumed parameters of Table I.

We have made no attempt to calculate mass spectra from electron impact or photoionization data, since this would require further assumptions about the internal energy distributions in each such experiment. Indeed, some autoionization apparently occurs in methane³³ and so would further complicate such an analysis. The comparison with the charge-transfer data of vonKoch is much more definitive.

Discussion

It would appear, from the above, that a quasiequilibrium hypothesis is capable of embracing the most pertinent experimental data relating to the fragmentation of the methane ion. Further, since the EHT method for constructing a transition state is equivalent to our use of Langevin cross sections, the transition-state formalism should also lead to numerically identical and hence equally acceptable results. Unfortunately, things are not quite so roseate. Several misgivings about a quasiequilibrium treatment of methane fragmentation must be noted. Figure 2, for example, shows that the absolute magnitudes of the rate constants obtained are quite high—so much so that it is difficult to visualize how a quasiequilibrium hypothesis can be applicable. There have been attempts to estimate the minimum time scale on which such a hypothesis might be meaningful.^{34,35} While only approximate, these estimates suggest that rate constants $\sim 10^{14}$ (sec)⁻¹ are too high.

This difficulty might be ameliorated in the following fashion. As Rice³⁶ has discussed, a fast association reaction implies an abnormally high frequency factor

(33) W. A. Chupka, *J. Chem. Phys.*, **48**, 2337 (1968).

(34) R. L. LeRoy, *ibid.*, **53**, 846 (1970); A. Henglein, *ibid.*, **53**, 458 (1970).

(35) D. L. Bunker, *ibid.*, **40**, 1946 (1964).

(36) O. K. Rice, *J. Phys. Chem.*, **65**, 1588 (1961).

for the reverse dissociation reaction, and this in turn implies drastic "anharmonicity" in the activated species. The density-of-states for this species, appearing in the denominator of eq 1 and 2, must then be accordingly increased. This will have the desired effect of reducing the implied rate constants, perhaps to more plausible magnitudes. At the same time this need not affect the apparent achievements obtained above. Thus, the results of Figure 3 hinge only upon relative rate constants and so will remain unaltered.

Several authors have introduced anharmonicities into density-of-states expressions, usually as minor perturbations.³⁷⁻³⁹ These treatments seem unsatisfactory. The role of the long-range potential, as implied by the use of the Langevin cross sections, would appear to require a more drastic model. It is not presently clear how this is best done. Note that Ottinger⁴⁰ has achieved a similar effect by allowing the flow of energy between vibrations and rotations. The treatment, due originally to Whitten and Rabinovitch,⁴¹ does not conserve angular momentum and hence is not satisfactory.

Figure 2 contains an intimation of still a second difficulty. A role for metastable decompositions in methane is indeed predicted by the monotonic behavior of rate constants near threshold. We would emphasize here that this monotonic behavior is not an artifact introduced by the use of continuous approximations to densities-of-states. It results rather from the monotonic behavior of $\sigma/\pi\lambda^2$ in the Langevin model. Nevertheless, it is also clear that the energy width leading to rate constants characteristic of metastable behavior, and hence $\sim 10^6$ (sec)⁻¹, is vanishingly small. The predicted abundance of such metastables is then much too small to account for Ottinger's observations.²³ Indeed, as a referee has noted, there is a fundamental inconsistency between the absence of significant, kinetic shifts and the presence of metastables in detectable amounts.

Again, a possible explanation can be proffered. The lower limit for the integrations in eq 7, for example, is strictly not zero but rather $\epsilon_r(\epsilon_r/\gamma^2 B_0^2)$ where ϵ_r is the rotational energy of the activated complex and B_0 its rotational constant. This can be understood by reference to region (d) of Figure 1. Conservation of angular momentum and the use of the Langevin model suffice to prohibit decomposition unless $L_{\max}^2 \geq J_0^2$. Except in the neighborhood of threshold, this is of little consequence. But when the excess energy E lies in the range $0 \leq E \leq \epsilon_r(\epsilon_r/\gamma^2 B_0^2)$, the reaction cannot proceed classically. Now Rosenstock³ has suggested tunneling as a source of Ottinger's metastables. Indeed, when E lies in this range, it is the only available mechanism. The great preference for *H* vs. *D* fragmentation and the vanishingly small kinetic energies associated with such metastables⁴⁰ each suggest such an interpretation.

Ionization with light particles is not expected to en-

hance rotational temperatures significantly. Hence, it is not immediately evident that a tunneling mechanism can account for the observed metastable intensities. This can be established, however, by observing that for an ion to have rotational energy ϵ_r and a total energy between E_0 and $E_0 + \epsilon_r(\epsilon_r/\gamma^2 B_0^2)$, the width of possible vibrational energies is also $\epsilon_r(\epsilon_r/\gamma^2 B_0^2)$. When averaged over a rotational equilibrium distribution, the average such width is seen to be

$$\overline{\Delta X} = \frac{(kT)^2 \Gamma(7/2)}{\gamma^2 B_0^2 \Gamma(3/2)} \quad (11)$$

Now only parent ions with vibrational energy less than 1.71 eV are eligible for the tunneling mechanism. If these are roughly equally distributed over this range, then the probability that such an ion will fall into the average tunneling width is $\sim \overline{\Delta X}/1.71$; with $kT \simeq 0.03$ eV and $\gamma^2 B_0^2 = 2.5$ eV, this gives 6×10^{-4} as a predicted metastable to parent ion intensity ratio. The agreement with Ottinger is quite satisfactory.

Two other predictions follow from the above model. In the sequence CH_4^+ , CH_3D^+ , CH_2D_2^+ , CHD_3^+ , the average moment of inertia increases, as then does $\overline{\Delta X}$ of eq 11. The metastable intensity should increase accordingly, as indeed Ottinger observes.⁴¹ Note too that such intensities should go as the square of temperature. This could be easily checked.

The above discussion makes no reference to the rate of tunneling and indeed it is crucial that this rate fall within the metastable range. We shall not attempt any elaboration here other than to observe that tunneling through such centrifugal barriers is of some current interest in bimolecular scattering.⁴² Its probable role in the present context would seem to merit further investigation. Thus, the small but finite intensity of CD_4^+ metastables interestingly reflects its relative tunneling width and with no indication of the usual mass dependence of tunneling.⁴³

Having noted earlier a consistency between the quasiequilibrium calculations and the breakdown curves of vonKoch, we should also point out that Brehm⁴⁴

(37) M. L. Vestal and H. M. Rosenstock, *J. Chem. Phys.*, **35**, 2008 (1961).

(38) K. A. Wilde, *ibid.*, **41**, 448 (1964).

(39) E. W. Schlag, R. A. Sandmark, and W. G. Valence, *ibid.*, **40**, 1461 (1964); W. Forst and Z. Prášil, *ibid.*, **53**, 3065 (1970).

(40) Ch. Ottinger, *Z. Naturforsch. A*, **22**, 20 (1967).

(41) G. Z. Whitten and B. S. Rabinovitch, *J. Chem. Phys.*, **41**, 1883 (1964).

(42) R. E. Roberts, R. B. Bernstein, and C. F. Curtiss, *ibid.*, **50**, 5163 (1969).

(43) L. P. Hills, M. L. Vestal, and J. H. Futrell (to be submitted for publication) have confirmed the observations of Ottinger and have interpreted the metastables in terms of finite reflection coefficients above the potential barrier. This seems unnecessary, but also unlikely for ion-molecule systems. See E. Vogt and G. H. Wannier, *Phys. Rev.*, **95**, 1190 (1954). On the other hand the insensitivity of tunneling through centrifugal barriers to mass is now understood: C. E. Klots, *Chem. Phys. Lett.*, in press.

(44) B. Brehm and E. von Puttkamer, *Z. Naturforsch. A*, **22**, 8 (1967).

has obtained breakdown data which do not agree with those of vonKoch. Brehm's data can only be interpreted as implicating CH_4^+ ions with energy greatly in excess of that required for reaction I and yet not fragmenting. Such a result would require "isolated states" and hence is incompatible with the fundamental premise of the quasiequilibrium model. Again this would warrant the most careful scrutiny.

Experiments such as those of Brehm and of Ottinger are taking much of the guess work out of unimolecular fragmentation studies. The formulation of quasiequilibrium theory that has been presented here is hoped to have a similar result by obviating any need

to estimate transition-state parameters. Our illustration of its use has, by contrast, involved only the most transparent of approximations. And, of course, there is the not inconsiderable advantage that this formalism satisfies microscopic reversibility. Accordingly, while discrepancies between theory and experiment persist, one can be reasonably certain that these are not artifacts of the theory but rather worthy of a more measured study.

Acknowledgment. Discussions with Professors Ch. Ottinger and J. H. Futrell and with Dr. H. C. Schweinler are gratefully acknowledged.

Mass Spectrum of Isocyanic Acid¹

by Denis J. Bogan

Carnegie-Mellon University and the University of Alabama, University, Alabama 35486

and Clifford W. Hand*

Department of Chemistry, University of Alabama, University, Alabama 35486 (Received January 4, 1971)

Publication costs assisted by The University of Alabama

Energies of several possible structures for the HNCO^+ ion have been calculated by INDO methods. Compared with the linear HNCO^+ , a cyclic structure was found to be more stable by 80 kcal. A fragmentation pattern and appearance potentials for the major fragment ions are reported, and a mechanism involving the cyclic structure is presented. The mechanism explains the observed features, including a metastable transition, of the mass spectrum of HNCO^+ . The successful use of INDO calculations in this problem suggests that semiempirical methods may be generally useful in the interpretation of mass spectra.

Introduction

The major product of the thermal decomposition of cyanuric acid has the empirical formula CHON , corresponding to the two possible structures HOCN (cyanic acid) and HNCO (isocyanic acid). Compelling evidence of the true structure comes from an infrared study² in which all the spectral features were accounted for by the structure HNCO , with a linear NCO group and an HNC angle of *ca.* 130° . The structural constants were later very accurately determined by millimeter wave techniques.³ Thus, although some chemical evidence⁴ suggests the existence, in solution, of a tautomeric equilibrium with $\leq 3\%$ HOCN present, and photolytically generated HOCN has been observed in low temperature matrices,⁵ the conclusion is inescapable that gaseous samples at room temperature consist almost exclusively of HNCO .

The mass spectrum of $\text{HNCO}^{6,7}$ shows a large peak at m/e 29, corresponding to an ion of formula HCO^+ ;

this species is the second most abundant fragment ion in the spectrum. This is a curious feature inasmuch as the HCO^+ fragment cannot be formed without extensive rearrangement of the parent structure. Mass peaks corresponding to CH^+ , OH^+ , and NO^+ also appear, and on this basis Smith and Jonassen⁷ suggested that HNCO^+ might have a "triangular structure."

(1) Presented in part at the Southeast-Southwest Regional Meeting of the American Chemical Society, New Orleans, La., Dec 2, 1970.

(2) G. Herzberg and C. Reid, *Discuss. Faraday Soc.*, **9**, 92 (1950); C. Reid, *J. Chem. Phys.*, **18**, 1544 (1950).

(3) R. Kewley, K. L. V. N. Sastry, and M. Winnewisser, *J. Mol. Spectrosc.*, **10**, 418 (1963).

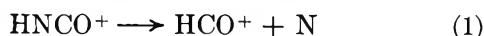
(4) (a) A. Amell, *J. Amer. Chem. Soc.*, **78**, 6234 (1956); (b) N. Groving and A. Holm, *Acta Chem. Scand.*, **19**, 1768 (1965).

(5) M. E. Jacox and D. E. Milligan, *J. Chem. Phys.*, **40**, 2457 (1964).

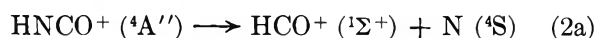
(6) J. M. Ruth and R. J. Philippe, *Anal. Chem.*, **38**, 720 (1966).

(7) S. R. Smith and H. B. Jonassen, *J. Inorg. Nucl. Chem.*, **29**, 860 (1967).

Appearance potentials for HNCO^+ , NCO^+ , HCO^+ , and NH^+ from HNCO have been reported by Rowland, *et al.*,⁸ who also observed a metastable peak at m/e 19.6, corresponding to the process



The metastable peak has a flat-top width corresponding to a kinetic energy release of 0.53 eV. The existence of a metastable peak for such a small molecule was explained⁸ in terms of a slow spin-forbidden predissociation to a repulsive surface, with consequent kinetic energy release in the fragmentation processes. That is, the reaction path (2), (2a) was considered more likely than the simpler reaction 3.



The present work was undertaken in the hope of establishing the structure of the HNCO^+ ion. We report the results of INDO calculations and of redetermination of the molecular ion and principal fragment ion appearance potentials in the mass spectrum of isocyanic acid. A mechanism which satisfactorily explains all of the experimental data is proposed.

Experimental Section

Isocyanic acid was prepared by the thermal decomposition of cyanuric acid under vacuum.⁹ The mass spectrum of the crude product showed 10–20% carbon dioxide and a lesser amount of water. Although hydrogen cyanide has been reported to be a product of this reaction,⁹ the mass spectrum showed that it could not have been present in more than trace quantities.

Water was removed by passing the product gas through phosphorus pentoxide four times, followed by passage through a -20° trap. Carbon dioxide was removed by successive freeze, pump, thaw cycles at -84° . The process was repeated, usually 8–12 cycles, until the mass spectra showed no further change in the ratio m/e 44:43. The final value of this ratio was 0.018, in good agreement with the ratio 0.015 expected from known isotopic abundances. The infrared spectrum of the purified product was identical with that reported by Herzberg and Reid.²

Argon was Matheson ultrahigh purity and was passed through a -196° trap before introduction into the vacuum system.

Most of the experimental work was done with a Bendix Model 12-107 time-of-flight mass spectrometer (TOF) equipped with a 14-107 ion source, in which the pressure was monitored with a cold cathode gauge. For comparison of results, two measurements of the appearance potential of the molecular ion were made with a magnetic deflection mass spectrometer, the CEC 21-104.

Mixtures of *ca.* 2:3 Ar:HNCO were admitted to the TOF from a 2.3-l. reservoir *via* a gold leak. Reservoir pressure was measured by a capacitance manometer (MKS Baratron Type 144). The effusion rate through the pinhole was measured for an air sample, and the pressure drop was found to be about 15%/hr. Therefore, the pressure drop was taken to be linear with time over the shorter duration of appearance potential and fragmentation pattern measurements, and the data were corrected accordingly. Since Smith and Jonassen⁷ found that isocyanic acid trimerizes to cyanuric acid by a first-order mechanism with a half-life of 18 hr at 30° , the pressure drop due to polymerization is also linear over a time span of 1 hr or less.¹⁰

Background pressure in the ion source of the TOF was less than 10^{-7} Torr, and a pressure of 15 Torr in the reservoir resulted in a source pressure of 3×10^{-6} Torr. The background mass spectrum was sufficiently low that the fragmentation pattern required correction only at m/e 17.

INDO calculations were performed using the program CNINDO¹¹ obtained from the Quantum Chemistry Program Exchange, Indiana University, Bloomington, Ind., and the Univac 1108 time sharing system of the University of Alabama Research Institute at Huntsville, Ala.

Results

The fragmentation pattern and appearance potentials of the major fragments from HNCO are shown in Tables I and II, together with previously reported values. The appearance potential for the parent ion is the result of five determinations, all of which agreed to within 0.05 eV, made with both TOF and magnetic instruments. Appearance potentials were measured relative to that of argon, used as an internal standard, and the data were treated by the extrapolated potential difference method.¹² This method is discussed by Field and Franklin¹³ and is considered to be the best method of obtaining appearance potentials from electron impact data, exclusive of those methods utilizing monoenergetic electron beams. Ionization efficiency curves for HNCO^+ and Ar^+ were of the same shape at low ion currents, and therefore the simpler linear ex-

(8) C. G. Rowland, J. H. D. Eland, and C. J. Danby, *Chem. Commun.*, 1535 (1968).

(9) M. Linhard, *Z. Anorg. Allg. Chem.*, **236**, 200 (1938).

(10) In the present work, a sample of isocyanic acid kept in the reservoir for 3 days showed no mass spectral evidence of trimer formation.

(11) (a) J. A. Pople and D. L. Beveridge, "Approximate Molecular Orbital Theory," McGraw-Hill, New York, N. Y., 1970, Appendix A; (b) J. A. Pople and G. A. Segal, *J. Chem. Phys.*, **44**, 3289 (1966); (c) J. A. Pople, D. L. Beveridge, and P. A. Dobosh, *ibid.*, **47**, 2026 (1967).

(12) (a) J. W. Warren, *Nature*, **165**, 810 (1950); (b) J. W. Warren and C. A. McDowell, *Discuss. Faraday Soc.*, **10**, 53 (1951).

(13) F. H. Field and J. L. Franklin, "Electron Impact Phenomena and the Properties of Gaseous Ions," Pure and Applied Physics Series, Vol. 1, Academic Press, New York, N. Y., 1957, Section II-D.

trapolation method yields the same value for $V(\text{HNCO}^+)$ as the extrapolated potential difference method. Four measurements were taken using the linear extrapolation method in order to check on the reproducibility of results.

Table I: Fragmentation Pattern of HNCO at 70 eV Ionizing Energy

m/e	Intensity relative to m/e 43 according to		
	This work	Ref a	Ref b
45	0.1	0.5	0.10
44	1.8	10	1.56
43	100.0	100.0	100.0
42	21.7	26	22.77
30	1.5	3	2.04
29	13.8	27	17.77
28	6.5	12	4.08
27	2.0	5	3.53
26	2.4	7	3.51
22	0.0		0.02
21.5	1.0	1	1.83
21	0.06		0.21
17	0.08	1	0.09
16	0.4	2	0.94
15	6.9	14	13.49
14	1.2	3	3.35
13.5	0.0		0.03
13	0.08	0.4	0.35
12	1.2	5	4.39

^a See ref 6. ^b See ref 7. Ionizing energy not stated.

Table II: Mass Spectrometric Appearance Potentials of Ions Arising from HNCO

Ion	Appearance potentials in eV according to	
	This work	Ref a
HNCO	12.15 ± 0.05	11.60 ^b
NCO	16.66	<16.1
NO	15.76	
HCO	15.76	15.1–15.3
NH	17.26	<17.7

^a See ref 8. ^b Determined by photoelectron spectrometry.

The ionization efficiency curve for the HCN fragment has an unusually long tail (even for a fragment ion), and four determinations of $V(\text{HCN}^+)$ gave results ranging from 13.5 to 14.3 eV with an average of 13.9 eV. The inconsistency of the results and the close agreement of the average with the known electron impact ionization potential of HCN¹⁴ led us to suspect the presence of HCN, formed by pyrolytic decomposition of HNCO on the ion source filament. The existence of a similar pyrolytic decomposition of NO₂ has been established.¹⁵

In order to test this hypothesis, a tungsten filament was placed in the glass line between the pinhole leak and the ion source, and ionization efficiency (I.E.) curves of the m/e 27 species were taken with the fila-

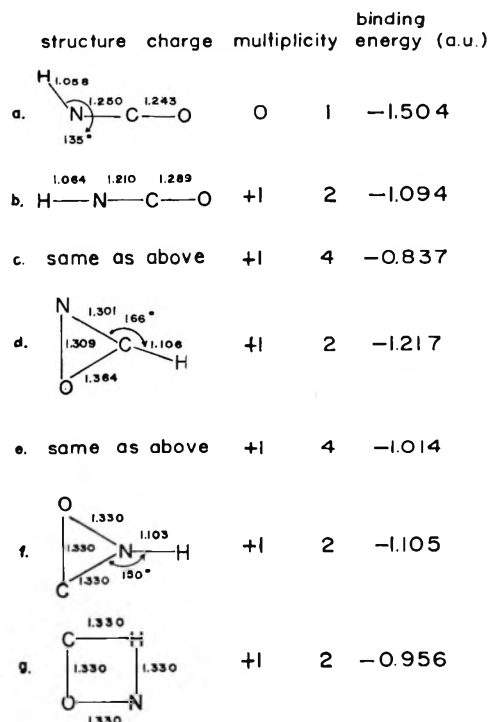


Figure 1. Structures and energies calculated by INDO. All structures are planar, and all bond lengths are in ångströms. Structures a, b, and d are the result of an optimization procedure to find the geometry of minimum binding energy. Energies of structures c, e, f, and g are the result of a single calculation of the designated geometry.

ment power on and off. The results show a significant difference between the two situations. In addition, an I.E. curve of HCN⁺ from pure HCN was taken. Comparison of this curve with the curves of HCN⁺ from HNCO clearly showed that neutral HCN was being formed prior to ionization and that the amount formed was a function of the power applied to the filament upstream of the ion source.

Several attempts to estimate $V(\text{HCN}^+ \text{ from HNCO})$ indicate a value of approximately 17.5 ± 1 eV; however, this result is not given in Table II because of the magnitude of the error limits. Similar difficulties were encountered for the CO⁺ fragment; furthermore, there is reason to believe that the pyrolytic decomposition of HNCO produces an appreciable amount of N₂ and, therefore, no attempt was made to estimate $V(\text{CO}^+ \text{ from HNCO})$. The I.E. curves for NCO⁺, NO⁺, HCO⁺, and NH⁺ show no irregularities and their appearance potentials are reproducible to ±0.15 eV; therefore, it is assumed that each of these ions has a single origin.

The kinetic energy released in fragmentation processes was determined for all species whose appearance

(14) J. D. Morrison and A. J. C. Nicholson, *J. Chem. Phys.*, **20**, 1021 (1952).

(15) (a) J. D. Morrison, *ibid.*, **22**, 1219 (1954); (b) E. C. G. Stueckelberg and H. D. Smyth, *Phys. Rev.*, **36**, 478 (1939).

Table III: Orbital Energy Levels for INDO Structures

Atom	Neutral HNCO			Linear doublet ion Coordinates, Å			Cyclic doublet ion ^a				
	X	Y	Z	X	Y	Z	X	Y	Z		
H	0.748	0.0	-0.748	0.0	0.0	-1.064	0.289	0.0	-1.068		
N	0.0	0.0	0.0	0.0	0.0	0.0	-0.638	0.0	1.134		
C	0.0	0.0	1.250	0.0	0.0	1.210	0.0	0.0	0.0		
O	0.0	0.0	2.493	0.0	0.0	2.499	0.669	0.0	1.188		
	Energy levels, atomic units			α spin		β spin		α spin		β spin	
	-1.5846			-2.0073		-1.9438		-2.4314		-2.3770	
	-1.4680			-1.8987		-1.8485		-1.5659		-1.5159	
	-0.8933			-1.3184		-1.3020		-1.4505		-1.4397	
	-0.7861			-1.2356		-1.1970		-1.3402		-1.1816	
	-0.7693			-1.2095		-1.0960		-1.1980		-1.1536	
	-0.6682			-1.1297		-1.0876		-1.1185		-1.0997	
	-0.4861			-0.9912		-0.9217		-0.9995		-0.9837	
	-0.4750			-0.9502		-0.3574		-0.9109		-0.3151	
	0.1384			-0.2178		-0.2067		-0.2817		-0.2305	
	0.2137			-0.1810		-0.1809		-0.1929		-0.1896	
	0.2562			-0.1797		-0.0789		-0.1332		-0.1234	
	0.3490			-0.0660		-0.0566		-0.1033		-0.0800	
	0.5652			0.1609		0.1713		0.0463		0.0517	
Binding energy	-1.504					-1.094				-1.217	

^a Structure d in Figure 1.

potentials are listed in Table II. The method was based on measurement of peak widths in TOF spectra,¹⁶ and yielded a value of kinetic energy released at onset, that is, at the appearance potential. The excess kinetic energy of HCO⁺ was 0.16 ± 0.03 eV, corresponding to a total kinetic energy release of 0.5 ± 0.1 eV for the fragmentation process (1); this is in agreement with the previously reported value.⁸

The results of INDO calculations are reported in Table III and Figure 1. An iterative procedure was used to find the optimum geometries for HNCO (1A'), open chain doublet HNCO⁺, and cyclic doublet HNCO⁺. In addition, calculations were made for open chain quartet HNCO⁺ and cyclic quartet HNCO⁺. The latter calculations were made using the same geometries as the respective doublet states, that is, no attempt was made to optimize the quartet geometries. Energies for several other structures were also calculated, using estimated structural parameters and no geometrical optimization.

Discussion

The energies, calculated by INDO for neutral HNCO and open chain doublet HNCO⁺, can be combined to give a value of 11.15 eV for the ionization potential of HNCO. The observed (12.15 eV) and calculated ionization potentials come into even closer agreement when one considers that the electron impact ionization is a vertical process, that is, a process occurring without change in bond lengths or angles. The open chain ion is linear whereas the neutral species has an equilibrium

HNC angle of approximately 130°, hence the ion will be formed with vibrational excitation of the HNC bend. The extent of this excitation is available from the INDO calculations, and is *ca.* 0.45 eV. Thus, the calculated vertical ionization potential is 11.6 eV.

From Figure 1 it is clear that the cyclic ion is considerably more stable than the open chain ion, and in view of the accuracy of the ionization potential calculation, the true energy difference between the open chain and cyclic structures is probably quite close to the calculated value of 80 kcal. The calculated energy difference of 160 kcal between the doublet and quartet states of the open chain ion is probably less reliable, since the width of the effective Franck-Condon region and the slope of the upper state curve are unknown. The calculated energies for the remaining structures in Figure 1 were sufficiently high that these structures were eliminated from consideration immediately, without calculation of optimum geometry.

The existence of the more stable cyclic structure leads us to conclude that the reaction scheme given in Table IV is preferable to the mechanism (2), (2a). The cyclic ion pathway serves to explain the experimental observations, as follows.

We found, as did previous workers, a comparatively large amount of HCO⁺ in the fragmentation pattern. This species can only be formed following extensive rearrangement of the open chain structure, and such

(16) J. L. Franklin, P. M. Hierl, and D. A. Whan, *J. Chem. Phys.*, **47**, 3148 (1967).

Table IV: Reaction Scheme for HNCO⁺ Fragmentation^a

	Ion	% abundance	A.P.
HNCO (¹ A')	HNCO ⁺ (linear) → NH ⁺	6.9	17.26
	HNCO ⁺ (linear) → NCO ⁺	21.7	16.66
	HNCO ⁺ (cyclic ^b) → CH ⁺	0.08	
	HNCO ⁺ (cyclic ^b) → NO ⁺	1.5	15.76
	HCO ⁺	13.8	15.76

^a HCN⁺ and CO⁺ are not assigned in the reaction scheme because their appearance potentials could not be determined accurately. See text for discussion. ^b Structure d in Figure 1.

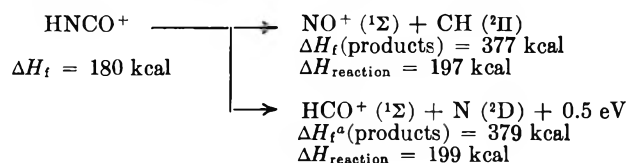
rearrangements are not observed at low ionizing voltages unless there is a lower energy state available in the rearranged configuration. On this basis, the mechanism (2,) (2a) seems an unlikely source of HCO⁺.

The transition from open chain to cyclic configuration is expected to be slow, since a considerable change in structure is involved. If the process is sufficiently slow, *i.e.*, on the order of 10⁻⁶ sec, metastable peaks corresponding to each of the subsequent fragmentation processes of the cyclic ion should be observed. Since ion rearrangements are known to give rise to metastable peaks in mass spectra,¹⁷ the reaction scheme in Table IV can explain the *m/e* 19.6 metastable peak without recourse to a spin-forbidden predissociation. Only the *m/e* 19.6 metastable peak has been reported in the mass spectrum of isocyanic acid, and we did not observe it, either with the conventional magnetic deflection instrument or with the TOF. It was marginally observed by Rowland, *et al.*,⁸ with a conventional instrument, then confirmed and characterized with the more sensitive double focusing instrument and the refocusing method of Barber and Elliott.¹⁸ Since the ion abundances of CH⁺ and NO⁺ are an order of magnitude lower than that of HCO⁺, it is not surprising that the corresponding metastable transitions have not been observed.

It is important to note that the relative magnitudes of the rate constants for the fragmentation of the linear ion and the slower rearrangement to the cyclic ion cannot be determined accurately. The quasiequilibrium theory of mass spectra developed by Rosenstock, Eyring, and coworkers¹⁹ predicts that the lifetimes of metastable ions will increase rapidly with increasing molecular complexity, but the theory does not work well for small molecules. Although Friedman, *et al.*,²⁰ applied the theory successfully to methanol, it cannot be expected that quantitative agreement with experiment can be achieved for a tetraatomic molecule. Qualitatively, the quasiequilibrium theory predicts

that the lifetimes of linear HNCO⁺ and cyclic HNCO⁺ will be of similar magnitude, although it is expected that fragmentation through the cyclic ion pathway will be somewhat slower than the linear ion pathway. Furthermore, the low intensity of the 19.6 metastable, observed by Rowland, *et al.*,⁸ indicates a relatively short lifetime for the metastable parent.

The energies required for two fragmentation processes of the cyclic ion can be calculated from tabulated heats of formation,^{21,22} the heat of formation of gaseous HNCO,²³ the appearance potential of HNCO⁺, and our calculated energy difference between the open chain and cyclic structures. The energies thus obtained are not exact, since the calculation assumes no stabilization or vibrational excitation of the fragments, and we wish merely to show that the resulting heats of reaction are quite reasonable for the breaking of two bonds. The results appear in Table V.

Table V: Thermochemistry of Fragmentation Reactions of Cyclic Doublet HNCO⁺

^a T. W. Shannon and A. G. Harrison, *Can. J. Chem.*, **39**, 1392 (1961), report ΔH_f(HCO) = -0.3 ± 3 kcal. Also, R. I. Reed and J. C. D. Brand, *Trans. Faraday Soc.*, **54**, 478 (1958), report an ionization potential of 9.88 ± 0.05 eV for HCO.

In conclusion, we feel that the slow rearrangement of the open chain ion to the more stable cyclic structure accounts for the observed features of the mass spectrum of isocyanic acid. The INDO calculations provide strong support for this mechanism.

Acknowledgment. We thank Dr. Lowell Kispert for his helpful suggestions.

(17) S. Meyerson and P. N. Rylander, *J. Chem. Phys.*, **27**, 901 (1957).

(18) M. Barber and R. M. Elliott, 12th Annual Meeting, ASTM, Committee E-14, Montreal, June 1964.

(19) (a) H. M. Rosenstock, M. B. Wallenstein, A. L. Wahrhaftig, and H. Eyring, *Proc. Natl. Acad. Sci. U. S.*, **38**, 667 (1952); (b) H. M. Rosenstock, A. L. Wahrhaftig, and H. Eyring, *J. Chem. Phys.*, **23**, 2200 (1955).

(20) L. Friedman, F. A. Long, and M. Wolfsberg, *ibid.*, **27**, 613 (1957).

(21) F. H. Field and J. L. Franklin, "Electron Impact Phenomena and the Properties of Gaseous Ions," Pure and Applied Physics Series, Vol. I, Academic Press, New York, N. Y., 1957, Appendix.

(22) (a) "Selected Values of Physical and Thermodynamic Properties of Hydrocarbons and Related Compounds," American Petroleum Institute, 1953; (b) F. D. Rossin, *et al.*, Ed., *Nat. Bur. Stand. (U. S.) Circ.*, No. 500 (1950).

(23) H. Okabe, *J. Chem. Phys.*, **53**, 3507 (1970).

Methylene Reaction Rates. Quantum Yields in the Diazomethane-Propane

Photolysis System: Effects of Photolysis Time, Reactant Ratios, and Added Gases

by Jerry A. Bell

Department of Chemistry, Simmons College, Boston, Massachusetts 02115 (Received January 25, 1971)

Publication costs assisted by the Petroleum Research Fund

Quantum yields have been measured for the production of the isomeric butanes in the photolysis of diazomethane-propane mixtures as functions of the C_3H_8/CH_2N_2 ratio, total pressure, photolysis time, and added competitor gases, CH_4 , N_2 , O_2 , Ar , and Xe . At C_3H_8/CH_2N_2 ratios above about 50, $\phi(C_4H_{10}) = 0.76$; at lower ratios $\phi(C_4H_{10})$ decreases. Added gases decrease $\phi(C_4H_{10})$ by reacting with 1CH_2 and/or causing intersystem crossing to 3CH_2 . The results are all consistent with the following set of reactions and rate constants ($cm^3 \text{ molecule}^{-1} \text{ sec}^{-1}$): $CH_2N_2 + h\nu (405 \text{ nm}) \rightarrow ^1CH_2 + N_2$, $\phi_1 = 1.0 \pm 0.4$ (1); $^1CH_2 + C_3H_8 \rightarrow C_4H_{10}$, $(6.3 \pm 1.7) \times 10^{-12}$ (2); $^1CH_2 + C_3H_8 \rightarrow ^3CH_2 + C_3H_8$, $(2.4 \pm 1.0) \times 10^{-12}$ (3); $^1CH_2 + CH_2N_2 \rightarrow C_2H_4 + N_2$, $(31 \pm 10) \times 10^{-12}$ (4); $^1CH_2 + CH_4 \rightarrow C_2H_6^*$, $(1.9 \pm 0.5) \times 10^{-12}$ (ref 4); $^1CH_2 + CH_4 \rightarrow ^3CH_2 + CH_4$, $(1.6 \pm 0.5) \times 10^{-12}$ (ref 4); $^1CH_2 + N_2 \rightarrow ^3CH_2 + N_2$, $(0.5 \pm 0.5) \times 10^{-12}$; $^1CH_2 + O_2 \rightarrow ^3CH_2 + O_2$ (or other products), $(4.0 \pm 1.0) \times 10^{-12}$; $^1CH_2 + Ar \rightarrow ^3CH_2 + Ar$, $(0.8 \pm 0.3) \times 10^{-12}$; $^1CH_2 + Xe \rightarrow ^3CH_2 + Xe$, $(1.8 \pm 0.6) \times 10^{-12}$. The results imply that the yield of 3CH_2 in CH_2N_2 - C_3H_8 systems is due to reaction 3. Analysis of the isomeric hexane yields gives the ratio of the reaction rates for $^3CH_2 + C_3H_8 \rightarrow CH_3 + C_3H_7$ (k_5) and $^3CH_2 + CH_2N_2 \rightarrow C_2H_4 + N_2$ (k_6); $k_6/k_5 = 400 \pm 100$, so 3CH_2 is efficiently scavenged by CH_2N_2 . Two reaction pathways are responsible for the isomeric pentane products: secondary $^1CH_2 + C_4H_{10}$ reactions and, probably, C_2H_5 -forming reactions followed by $C_2H_5 + C_3H_7$. Below 100 Torr total pressure the dissociation of $C_4H_{10}^*$, formed initially in reaction 2, adds significantly to the yields of the pentanes and hexanes, products associated with the radical reactions following reaction 5. Comparison of these results with other studies of CH_2 reactions indicates that great care must be taken in assessing relative 1CH_2 and 3CH_2 yields in the photodissociation of their precursors and the contributions of 1CH_2 and 3CH_2 reactions to overall product yields.

Introduction

Following the initial work of Frey and Kistiakowsky,¹ a number of other workers have studied systems in which they assume free methylene is produced in the presence of propane.² There appears to be substantial agreement among the various workers upon certain points: singlet methylene, 1CH_2 , inserts into the carbon-hydrogen bonds, favoring a secondary bond by a factor of 1.20 per bond; intersystem crossing from singlet to triplet methylene, 3CH_2 , can be collisionally induced; 3CH_2 abstracts hydrogen atoms to form methyl and propyl radicals, favoring secondary abstraction by a factor between 12 and 20; 3CH_2 is much less reactive than 1CH_2 ; both 1CH_2 and 3CH_2 are produced (in varying ratios) by dissociation of photolytically excited precursors. There is still, however, some question as to whether or not triplet methylene inserts into carbon-hydrogen bonds and about the details of the formation of minor products, for example, the C_5 hydrocarbons.^{2d,g,3}

This work on the diazomethane-propane system was begun to study some of these minor reactions. The serendipitous discovery that diazomethane was stable for relatively long periods (a few hours) in reaction vessels "seasoned" with diazirine led to an extensive investigation. The present analysis of the effects of

photolysis time, reactant ratios, and added gases on the quantum yields, combined with other recent results,^{2b,e,4} gives a detailed picture of the reaction mechanism and may serve to caution those of us trying to assess the relative yields of 1CH_2 and 3CH_2 from the photodissociation of its precursors.

Experimental Section

Materials. Fresh diazomethane (DM) was synthesized each day by mixing *in vacuo* about 1 g of *N*-methyl-*N*-nitroso-*p*-toluenesulfonamide, Eastman, with about 5 ml of degassed propylene glycol containing 4 or 5 KOH pellets. The product was trapped at -195°

(1) H. M. Frey and G. B. Kistiakowsky, *J. Amer. Chem. Soc.*, **79**, 6373 (1957).

(2) This is a leading, not an exhaustive, reference list of work to be referred to later in the paper: (a) G. Z. Whitten and B. S. Rabinovitch, *J. Phys. Chem.*, **69**, 4348 (1965); (b) M. L. Halberstadt and J. R. McNesby, *J. Amer. Chem. Soc.*, **89**, 3417 (1967); (c) S.-Y. Ho and W. A. Noyes, Jr., *ibid.*, **89**, 5091 (1967); (d) D. F. Ring and B. S. Rabinovitch, *Can. J. Chem.*, **46**, 2435 (1968); (e) T. W. Eder and R. W. Carr, Jr., *J. Chem. Phys.*, **53**, 2258 (1970); (f) A. K. Dhingra and R. D. Koob, *J. Phys. Chem.*, **74**, 4490 (1970); (g) C. J. Mischele, Ph.D. Thesis, University of California, Riverside, Calif., 1967.

(3) (a) D. C. Montagne and F. S. Rowland, *J. Phys. Chem.*, **72**, 3705 (1968); (b) T. W. Eder and R. W. Carr, Jr., *ibid.*, **73**, 2074 (1969).

(4) W. Braun, A. M. Bass, and M. Pilling, *J. Chem. Phys.*, **52**, 5131 (1970).

(liquid nitrogen), twice distilled from -80° (Dry Ice-trichloroethylene) to -195° , and held at -195° until use. Propane (Pr), Matheson instrument grade containing about 0.017% ethane and a slightly larger amount of propylene (indeterminate by our analytical techniques), and xenon, Matheson research grade containing no detectable hydrocarbon impurities, were put through several freeze-pump-thaw cycles to remove more volatile gases (O_2). Oxygen, Linde industrial grade, methane, Matheson research grade, and Matheson counting gas mixture P-10, 0.10 methane and 0.90 argon, were used directly from their cylinders.

Photolysis Procedure. All photolyses were carried out in 42.5-ml cylindrical, detachable quartz cells with greaseless stopcocks. One cell was used for most of the results reported here, in order to keep all optical parts of the system as constant as possible. This cell had about 7 Torr of diazirine, the cyclic isomer of DM, stored in it for 6 months prior to its use in these experiments. Under the conditions of the experiments reported here, cells without such pretreatment gave erratic and useless results ascribable to rapid, nonphotolytic decomposition of DM. (Two months storage of diazirine followed by addition of propane and photolysis of the diazirine at 320 nm for 1 hr produced the same conditioning effect. No shorter storage times were tried. Attempts to produce the same "poisoning" by using DM—100-Torr portions renewed every few hours—failed.)

The sample cell was filled on the conventional high-vacuum system used for DM synthesis and storage. To begin each experiment, the DM storage trap was warmed to -80° and pumped briefly; the appropriate pressure of DM, measured on a mercury manometer, was allowed to fill a small volume and expand into the evacuated photolysis cell to give the desired initial amount. Other reactant gases were then expanded into the cell and the final total pressure in the cell measured with a mercury manometer after each addition. Mixing was assumed to take place as the expanding gas rushed into the cell; the order of addition of reactants (other than DM which could not be tested) made no detectable differences in results.

The photolysis lamp was a 200-W PEK super-high-pressure mercury arc powered by a direct current supply. The light was passed through a Bausch and Lomb high-intensity monochromator, catalog no. 33-86-01 (entrance and exit slits, 3.3 and 2.0 mm; band pass, 6.6 nm), set at 405 nm and focused axially at the center of the photolysis cell. A selenium photocell and microammeter were used to monitor the light beam emerging from the cell to be sure the intensity remained constant within 5% during and between runs. Light fluxes were measured by ferrioxalate actinometry.⁵ In only a few cases were reactions carried beyond 20% depletion of the initial DM; 10–15% was more typical. No more than 2% of the Pr ever reacted, so its concentra-

tion was effectively constant for all runs. The light distribution was not uniform throughout the cell, but, due to the slit and cell geometries and focusing characteristics of the lens, probably was about twice as intense (per unit cross sectional area) on the axis in the center of the cell as at either end. Since almost no light is absorbed in the cell, less than 0.4% (Torr of DM)⁻¹, the nonuniform distribution probably does not lead to any severe mixing effects.

Analyses. All product analyses were done with a $1/8$ in. \times 5 ft gas chromatographic column of 20% SF-96 on Chromosorb, run at 0° with N_2 carrier gas, and a flame ionization detector and electrometer, Varian Aerograph Model 1200. The inlet system, stainless steel, Kovar, Teflon, and glass, caused the complete decomposition of the DM left in the product mixture to C_2H_4 and very small amounts of the C_4H_{10} isomers. The product yields and ratios from this decomposition were quite reproducible. Analyses of unphotolyzed blank runs for all sets of reaction conditions were used to correct the observed C_4H_{10} product yields for this extraneous source. Unfortunately, the large amount of C_2H_4 thus formed made it impossible reproducibly to determine the relatively small yields of CH_4 , C_2H_4 , and C_2H_6 from the photolysis. The chromatograph output was calibrated for almost all the identifiable products; those not calibrated directly were assumed to have the same sensitivity as their isomers. Calibrations were made with mixtures that reproduced typical reactant mixtures as nearly as possible, since the large excess of Pr in all product mixtures altered the detector response. The response was also slightly dependent on the total pressure of sample injected, so all data were empirically corrected to the same injection conditions. Analyses were done at least in duplicate for all runs. Absolute yields and ratios are estimated to be good to $\pm 5\%$. Yields of C_5 compounds, which are formed in small amounts and elute soon enough after Pr to make their analysis on its tail very imprecise, and *n*-hexane, *n*-H, which is formed in very small amounts, are known less precisely, only to within $\pm 20\%$.

Results

The major products of the reaction under all conditions were *n*-butane (*n*-B) and isobutane (*i*-B). CH_4 and C_2H_6 , which were not quantitatively determined, were formed in much smaller amounts. C_2H_4 was formed in moderate amount at low initial $[Pr]/[DM]_0$ ratios, but also could not be determined quantitatively. Other products, never present *in toto* in amounts greater than about 10% of the total C_4H_{10} product, were 2,3-dimethylbutane (2,3DMB), 2-methylpentane (2MP), *n*-hexane (*n*-H), C_4H_8 (isobutene and/or butene-1,

(5) J. G. Calvert and J. N. Pitts, Jr., "Photochemistry," Wiley, New York, N. Y., 1966, pp 783–786.

Table I: Yield Ratios in the DM-Pr System^e

[DM] ₀ Torr	[Pr]/[DM] ₀	<i>R</i> (<i>i</i> -B) ^a	<i>R</i> (2,3DMB) ^{b,c} × 10 ²	<i>R</i> (2MP) ^{b,c} × 10 ²	<i>R</i> (C ₄ H ₈) ^b × 10 ²	<i>R</i> (P1) ^b × 10 ²	<i>R</i> (4MP1) ^b × 10 ²
1.8	29	0.44	0.9	0.6	3.4	0.9	2.0
1.8	56	0.46	1.2	0.6	1.8	0.4	1.5
1.8	105	0.47	2.1	1.2	0.5	0.1	1.0
1.8 ^d	152	0.48	2.1	1.0			0.5
1.8 ^d	345	0.49	2.3	1.1			
3.3	9.1	0.42	0.5	0.4	7.2	2.0	1.9
3.3	53	0.46	1.1	0.6	1.6	0.3	1.2
10	5.0	0.42	0.21	0.18	7.0	1.8	1.3
10	8.8	0.43	0.30	0.25	4.5	1.4	1.1
20	5.0	0.42	0.11	0.09	5.5	1.6	1.0
19	8.6	0.43	0.18	0.16	4.5	1.3	1.1

^a Values are ±0.01. ^b Values are ±20% except for *R*'s less than 1 × 10⁻² where the error increases to about ±50%. ^c Averages for runs of 20 min or less. These yields are time dependent, Figure 5, but not enough data are available for all runs to extrapolate to zero time, so averages are used in all cases. ^d Results of a single run. ^e A blank space indicates the yield was not detectable.

which were not separated by our technique), isopentane (*i*-P), *n*-pentane (*n*-P), pentene-1 (P1), 4-methylpentene-1 (4MP1), and two unidentified, very minor, products that eluted between 2MP and *n*-H. In the longest runs a small amount of neopentane and traces of cyclopropane and 2-methylbutene-2 were also detected. All product yields are given as a ratio to [*n*-B], the yield of *n*-B, and labeled *R*(product) for ease in writing, *e.g.*, *R*(*i*-B) = [*i*-B]/[*n*-B].

DM-Pr: Butanes. In the pure DM-Pr system with [Pr]/[DM]₀ = 5 to 10, *R*(*i*-B) = 0.43 ± 0.01. Figure 1 shows that this product yield ratio is invariant with photolysis time as [*n*-B] is monotonically increasing; about 50% of [DM]₀ has been reacted at the longest time shown. Similar results in relation to time are obtained for all the DM-Pr systems; *R*(*i*-B) does increase slightly, Table I, as [Pr]/[DM]₀ increases. Addition of small amounts of O₂, less than 0.1[Pr], gives *R*(*i*-B) = 0.42 ± 0.01 in all cases and also eliminates all products except the butanes and pentanes (see below). The effect of the O₂ is presumably to intercept ³CH₂, or the radical products of its reactions,^{2e,6} leaving only the products of ¹CH₂ insertion reactions. The O₂ addition has no effect on [*n*-B], within analytical error. Assuming that the ratio of butanes formed as a result of ³CH₂ abstraction-recombination reactions (see mechanism below) in these systems is 4,^{2e} we can calculate the fraction of the observed [*n*-B] that would result from the ¹CH₂ reaction in the above systems. In all cases more than 98% of the [*n*-B] arises from ¹CH₂ reaction. In the DM-Pr systems, therefore, all [*n*-B] was assumed to be the result of ¹CH₂ insertion. In systems where ³CH₂ reactions contributed significantly to [*n*-B], the yield due to ¹CH₂ reaction was calculated as above. The [*i*-B] formed by ¹CH₂ insertion was taken to be 0.42[*n*-B] in these cases.

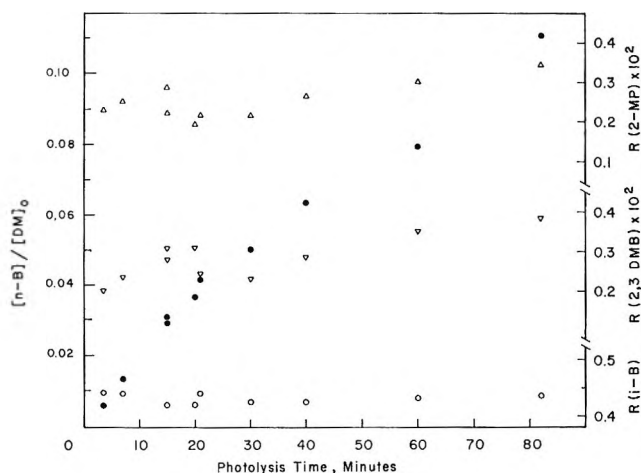


Figure 1. *n*-B yield, ●, and yield ratios, *R*(*i*-B), ○; *R*(2,3DMB), ▽; and *R*(2MP), △, as a function of 405 nm photolysis time for 10 Torr of DM with 88 Torr of Pr.

Figure 2 shows that [*n*-B]/[DM]₀ is a linear function of photolysis time for short times, *i.e.*, low conversions of DM. A large amount of data from other series at different [Pr]/[DM]₀ and total pressures has been omitted from this plot in order to simplify it; the results are the same in all cases, a linear initial increase in [*n*-B]/[DM]₀. With these initial rates of formation, the total photon flux through the cell (3.32 × 10¹⁶ photon sec⁻¹), and the amount of light absorbed per Torr DM initially present (with a decadic absorptivity = 3 l. mol⁻¹ cm⁻¹ for DM at 405 nm⁷), the quantum yield for formation of the C₄H₁₀ from ¹CH₂ may be calculated; φ(C₄H₁₀) = 0.59 ± 0.12 when [Pr]/[DM]₀

(6) (a) R. L. Russell and F. S. Rowland, *J. Amer. Chem. Soc.*, **90**, 1671 (1968); (b) F. S. Rowland, C. McKnight, and E. K. C. Lee *Ber. Bunsenges. Phys. Chem.*, **72**, 236 (1968).

(7) R. K. Brinton and D. H. Volman, *J. Chem. Phys.*, **19**, 1394 (1951).

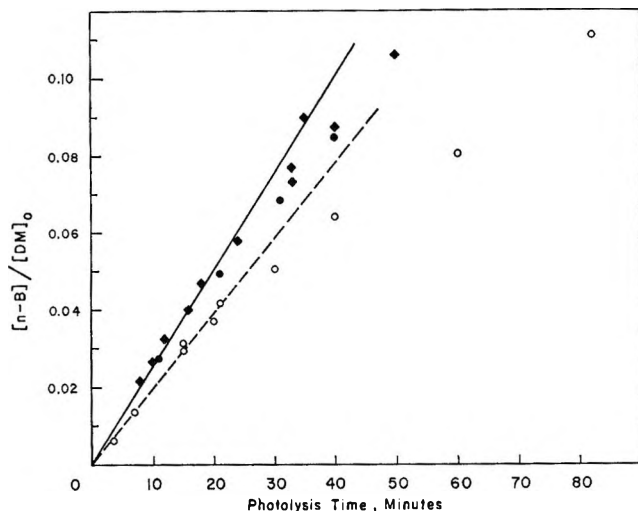


Figure 2. *n*-B yields as a function of 405 nm photolysis time: 10 Torr of DM, 88 Torr of Pr, \circ ; 1.8 Torr of DM, 101 Torr of Pr, \blacklozenge ; and 1.8 Torr of DM, 191 Torr of Pr, \bullet .

= 8.8 and $\phi(\text{C}_4\text{H}_{10}) = 0.76 \pm 0.15$ when $[\text{Pr}]/[\text{DM}]_0 \geq 50$. The large error estimate arises mainly from the estimated uncertainty in the absorptivity of DM, not from scatter in the experimental data. At intermediate values of $[\text{Pr}]:[\text{DM}]_0$, intermediate ϕ 's are obtained, but the experimental scatter is too large to tell exactly when the limit 0.76 is reached, although it is possible that a ratio of 30 is sufficient.

DM-Pr: Pentanes. Figure 3 shows that $R(i\text{-P})$ and $R(n\text{-P})$ increase linearly with photolysis time for $[\text{Pr}]/[\text{DM}]_0 = 8.8$ and total pressure about 100 Torr, and that extrapolation back to zero time yields finite intercepts. Addition of O_2 reduces the relative pentane yields substantially, but they again show an increase with photolysis time that may be extrapolated back to zero intercept at zero time. The rates of increase with time appear to be the same, within the considerable experimental error of these analyses, with or without O_2 .

Figure 4 shows that $R(i\text{-P})$ behaves similarly for all $[\text{Pr}]/[\text{DM}]_0$ ratios as a function of photolysis time in systems with a total pressure of 100 Torr or greater. All other factors being equal, however, when the total pressure of the system is reduced below 100 Torr, $R(i\text{-P})$ increases. Since the slope of the time dependence appears to be about the same at all total pressures, the increase must reflect a change in the mechanistic factor that gives rise to the nonzero intercept at zero time. The butane yields in these lower pressure series are those expected on the basis of the $[\text{Pr}]/[\text{DM}]_0$ ratios and Figure 2.

DM-Pr: Hexanes. Figure 1 shows $R(2,3\text{DMB})$ and $R(2\text{MP})$ as functions of photolysis time for $[\text{Pr}]/[\text{DM}]_0 = 8.8$ at a total pressure of about 100 Torr. $R(n\text{-H})$ is not shown because its small yield and the large scatter in the analyses make interpretation im-

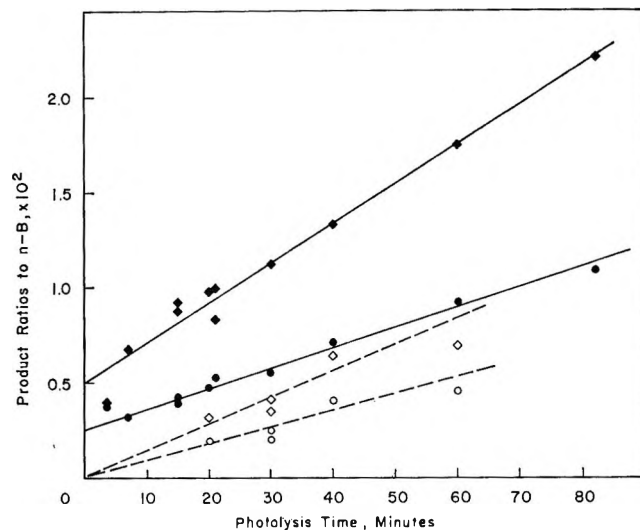


Figure 3. C_5H_{12} yield ratios as a function of 405 nm photolysis time and added O_2 , less than $0.1[\text{Pr}]$, for 10 Torr of DM with 88 Torr of Pr: $R(i\text{-P})$, \blacklozenge, \diamond , and $R(n\text{-P})$, \bullet, \circ . Open symbols are runs with added O_2 .

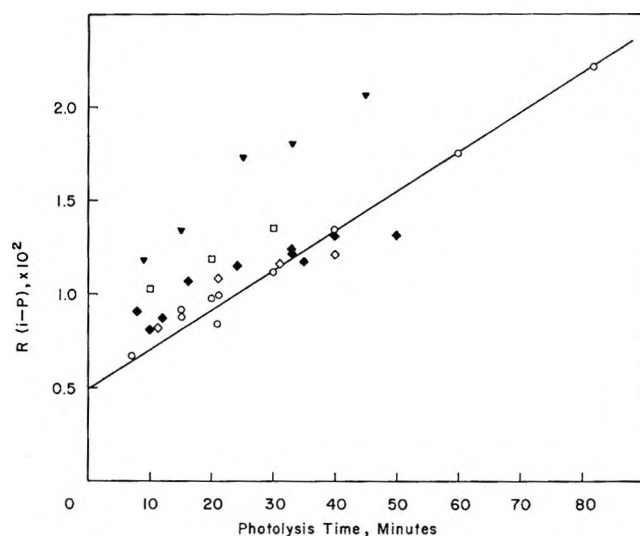


Figure 4. Yield ratios for *i*-P as a function of 405 nm photolysis time and mixture composition: 10 Torr of DM, 88 Torr of Pr, \circ ; 3.3 Torr of DM, 30 Torr of Pr, \blacktriangledown ; 1.8 Torr of DM, 52 Torr of Pr, \square ; 1.8 Torr of DM, 101 Torr of Pr, \blacklozenge ; and 1.8 Torr of DM, 191 Torr of Pr, \diamond . The line is the $R(i\text{-P})$ line from Figure 3 without added O_2 .

possible. At relatively short photolysis times the yield ratios for the isomeric hexanes remain constant, but as the time increases and a substantial fraction of DM is depleted, the ratios increase somewhat. Figure 5 illustrates the striking increase in this trend as $[\text{Pr}]/[\text{DM}]_0$ increases. Also we see that the initial values of $R(2,3\text{DMB})$ increase as $[\text{Pr}]/[\text{DM}]_0$ increases; a plot, Figure 6, of $R(2,3\text{DMB})_0$ (extrapolated to zero time) vs. $[\text{Pr}]/[\text{DM}]_0$ is linear. The points at total pressure below 100 Torr are neglected, because they again show larger yields relative to the $[\text{Pr}]/[\text{DM}]_0$ ratios. The addition of small amounts of O_2 eliminates all traces of

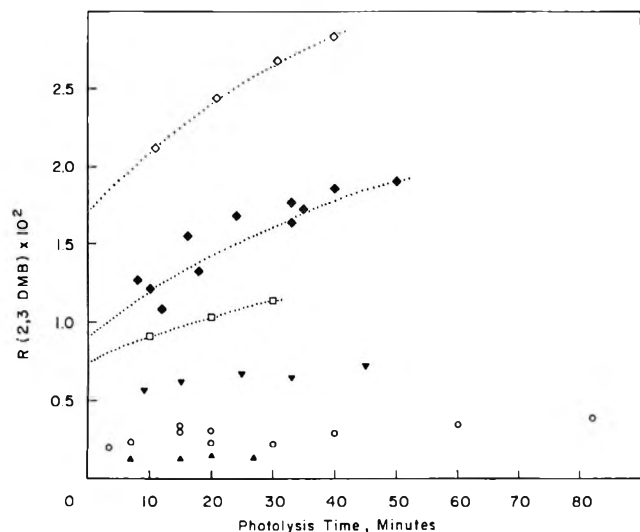


Figure 5. Yield ratios for 2,3DMB as a function of 405 nm photolysis time and mixture composition: 20 Torr of DM, 100 Torr of Pr, \blacktriangle ; 10 Torr of DM, 88 Torr of Pr, \circ ; 3.3 Torr of DM, 30 Torr of Pr, \blacktriangledown ; 1.8 Torr of DM, 52 Torr of Pr, \square ; 1.8 Torr of DM, 101 Torr of Pr, \blacklozenge ; and 1.8 Torr of DM, 191 Torr of Pr, \diamond . Dotted curves are the smooth extrapolations to zero photolysis time used in Figure 6.

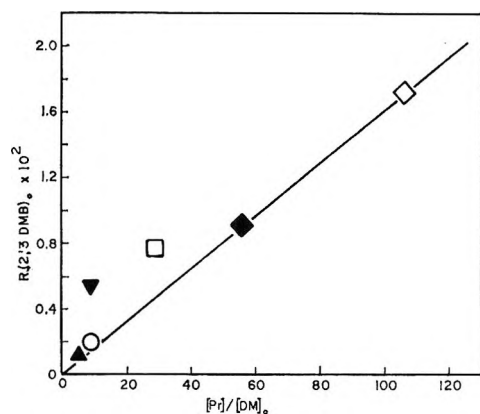


Figure 6. Yield ratios for 2,3DMB extrapolated to zero 405 nm photolysis time as a function of mixture composition. Symbols correspond to those in Figure 5. The points that lie above the line are for runs at a total pressure less than 100 Torr.

the isomeric hexanes, and we can conclude that they are formed by radical and/or $^3\text{CH}_2$ reactions. At pressures below about 100 Torr these radical and/or $^3\text{CH}_2$ reactions must be enhanced by some mechanism. The same mechanism is probably responsible for the similar increases in $R(\text{C}_5\text{H}_{12})$'s at lower total pressures.

Olefin Products. Table I presents product yield ratios for the three olefins formed in highest yield: C_4H_8 (isobutene and/or butene-1), P1, and 4MP1 (identified only by retention time and analogy with other work^{2d}). Addition of small amounts of O_2 eliminates all olefins. Yield ratios for olefin formation were somewhat erratic, so averages for runs with photolysis times less than 20 min were used in Table I. At long photol-

ysis times there is an apparent increase (10–20%) in the olefin yield ratios, but this may be an artifact resulting from the falloff of $[n\text{-B}]$ at long times. As $[\text{Pr}]/[\text{DM}]_0$ is increased the yield of olefins decreases markedly; at ratios above about 200 they are no longer formed in detectable amounts. At pressures below about 100 Torr, there is again, as with the pentanes and hexanes, an increase in olefin yield ratios. There is some evidence from those $[\text{Pr}]/[\text{DM}]_0$ series done at about 100 Torr and also at higher pressures that even at 100 Torr there may be slightly larger yield ratios than are expected. Unfortunately the analytical errors are too large to make an unequivocal assessment.

DM-Pr-Other Gases. Since at $[\text{Pr}]/[\text{DM}]_0 \geq 50$, $\phi(\text{C}_4\text{H}_{10})$ is constant and attributable to $^1\text{CH}_2$, it seemed reasonable to add other gases to the DM-Pr system as competitors with Pr for $^1\text{CH}_2$ and hence to determine relative rates of $^1\text{CH}_2$ reactions. CH_4 , Xe, and O_2 were studied in this way by adding them in increasing amounts to the system $[\text{DM}]_0 = 1.8$ Torr, $[\text{Pr}] = 100$ Torr. $[n\text{-B}]/[n\text{-B}]_M$, the ratio of $[n\text{-B}]$ with no added gas to that with added gas, M , is shown in Figure 7 for 20-min photolyses as a function of $[M]/[\text{Pr}]$.

Table II gives $R(i\text{-B})$ and yields, $Y(\text{products})$, for the hydrocarbons formed in largest amounts in the DM-Pr-Xe system. In this series there is an increase in $^3\text{CH}_2$ contribution to the C_4H_{10} yields, reflected in the increasing $R(i\text{-B})$ with increasing $[\text{Xe}]/[\text{Pr}]$. Using the assumptions cited previously, we can compute that the $^3\text{CH}_2$ reaction has contributed about 6% of the $[n\text{-B}]$ at the highest $[\text{Xe}]/[\text{Pr}]$ used. This amount, and the corresponding corrections for other runs, was subtracted from the observed yield before Figure 7 was plotted in order that the $[n\text{-B}]$ presented there should be wholly the result of $^1\text{CH}_2$ reactions.

For these competitive systems absolute yields (or quantities proportional thereto) are more meaningful than ratios to $[n\text{-B}]_M$, which is reduced due to the competition. The values in Table II are $Y(\text{product}) \equiv R(\text{product}) ([n\text{-B}]_M/[n\text{-B}])$. The yields of 2,3DMB (perhaps 2MP, but the results are ambiguous), C_4H_8 , and 4MP1 increase as $[\text{Xe}]/[\text{Pr}]$ is increased. Within the experimental error of these analyses the yields of $i\text{-P}$ and P1 appear unaffected by the addition of Xe.

The CH_4 series, Table II, presents different problems. More than half the reactions of $^1\text{CH}_2$ with CH_4 lead to the formation of C_2H_6^* , much of which dissociates before collisional stabilization to yield CH_3 ,^{4,8} upsetting the relative concentrations of radicals characteristic of $^3\text{CH}_2$ reactions with Pr. More of the propyl radicals combine with the increased CH_3 , yielding more C_4H_{10} by non- $^1\text{CH}_2$ reactions and reducing propyl-propyl reactions and, hence, the isomeric hexane yields, as Table II indicates. The ratio of isomeric C_4H_{10} 's thus

(8) J. A. Bell and G. B. Kistiakowsky, *J. Amer. Chem. Soc.*, **84**, 3417 (1962).

Table II: Yield Ratios and Yields for the Systems $[\text{Pr}]/[\text{DM}]_0 = 55$ with Added Gases^a

M	$[\text{M}]/[\text{Pr}]$	$R(i\text{-B})$	$Y(i\text{-P})^{b,c}$ $\times 10^2$	$Y(2,3\text{DMB})^{b,c}$ $\times 10^2$	$Y(2\text{MP})^{b,c}$ $\times 10^2$	$Y(\text{C}_4\text{H}_8)^{b,c}$ $\times 10^2$	$Y(\text{P1})^{b,d}$ $\times 10^2$	$Y(4\text{MP1})^{b,c}$ $\times 10^2$
Xe	0	0.46	1.0	1.6	1.0	1.8	0.4	1.5
	1.00	0.51	1.0	2.0	0.9	3.2	0.5	2.4
	1.56	0.52	0.9	2.5	1.2	3.2	0.4	2.7
	1.98	0.56	1.1	2.5	1.3	4.0	0.7	3.0
	3.20	0.57	1.0	2.5	1.1	4.3	0.5	3.3
CH ₄	0	0.46	1.0	1.6	1.0	1.8	0.4	1.5
	1.02	0.53	0.9	1.1	0.5	2.6	0.3	1.1
	1.91	0.56	0.8	1.1	0.4	2.1	0.3	0.8
	2.97	0.59	0.7	0.9	0.4	1.8	Trace	0.6
Ar + CH ₄ ^e	3.08	0.51	1.0	1.4	1.1	2.1		1.5
N ₂	0 ^f	0.42	1.5	0.5	0.4	7.2	2.0	2.0
	0 ^g	0.43	1.0	0.3	0.3	4.5	1.4	1.1
	10.9 ^h	0.44	0.8	0.5	0.2	12.2	1.3	2.6

^a $[\text{DM}]_0 = 1.8$ Torr; 20-min photolyses at 405 nm. ^b Yields, Y , are corrected values $Y = R_{\text{obsd}}([n\text{-B}]_{\text{M}}/[n\text{-B}])$, as explained in the text. ^c Values are $\pm 20\%$. ^d Values are $\pm 50\%$. ^e 0.10 CH₄; 0.90 Ar. ^f $[\text{Pr}]/[\text{DM}]_0 = 8.9$; $[\text{DM}]_0 = 3.3$ Torr. ^g $[\text{Pr}]/[\text{DM}]_0 = 8.8$; $[\text{DM}]_0 = 10$ Torr. ^h $[\text{Pr}]/[\text{DM}]_0 = 9.0$; $[\text{DM}]_0 = 3.3$ Torr.

formed will still, however, reflect the ratio of relative rates of ³CH₂ attack on primary and secondary bonds, so the technique for correcting observed $[n\text{-B}]$ for ³CH₂-reaction contributions should be valid; at $[\text{CH}_4]/[\text{Pr}] = 3$, the correction (reduction) is only 5%. Not only isomeric hexanes, but *i*-P, P1, and 4MP1 also decrease in yield as $[\text{CH}_4]/[\text{Pr}]$ increases, although the change is not large for *i*-P and may not be a real effect. In a blank photolysis run, DM-CH₄ (no Pr), at a total pressure of 200 Torr, the major analyzable product was C₄H₈ (C₁'s and C₂'s not analyzable). The yield was about 5 times the $[\text{C}_4\text{H}_8]$ in the DM-Pr-CH₄ system, total pressure 200 Torr, with $[\text{Pr}]/[\text{CH}_4] = 1$. [$R(\text{C}_4\text{H}_8) \approx 11$, but all the $n\text{-B}$ could be attributed to DM decomposition in the gas chromatographic inlet system.] The rapid rate of CH₃ and ³CH₂ formation in the DM-CH₄ system⁴ combined with their low reactivity toward CH₄ probably means that reactions with DM and, perhaps, radical-³CH₂ reactions^{9,10} account for the enhanced yield of C₄H₈. Time dependence studies on the $[\text{CH}_4]/[\text{Pr}] = 1$ system were carried out to test whether rapid depletion of $[\text{DM}]$ by such side reactions might cause lower yields of C₄H₁₀ that would lead to spurious values of $[n\text{-B}]/[n\text{-B}]_{\text{M}}$. The falloff in $[n\text{-B}]/[\text{DM}]_0$ in these runs exactly parallels that in the pure systems, so no significant amount of DM is being destroyed by the side reactions.

For the DM-Pr-O₂ series the only detectable products were C₂H₄, *i*-B, *n*-B, and traces of *i*-P.

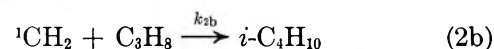
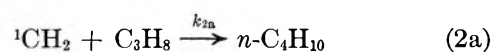
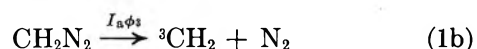
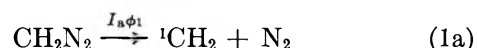
One run was done using a counting-gas mixture of CH₄ and Ar as the additive at a pressure of 313 Torr. The mixture contained 31 Torr of CH₄ and 282 Torr of Ar, and had the same effect on $[n\text{-B}]_{\text{M}}$ as the addition of 100 Torr of CH₄. Thus we can estimate that 69 Torr of CH₄ is as effective as 282 Torr of Ar in competi-

tion with Pr for ¹CH₂ or that the rate of the CH₄ reaction(s) is 4.1 times that of the Ar reaction.

The results of a single experiment done with 329 Torr of N₂ added to 3.4 Torr of DM and 30.2 Torr of Pr are given in Table II. As a comparison, the yields for both a low and high pressure system with $[\text{Pr}]/[\text{DM}]_0 = 9$ are also given. The changes observed with addition of N₂ compared to the higher pressure DM-Pr system are qualitatively similar to those in the DM-Pr-Xe system. For this run with $[\text{N}_2]/[\text{Pr}] = 10.9$, $[n\text{-B}]/[n\text{-B}]_{\text{M}} = 1.45$.

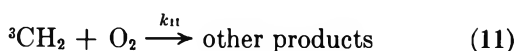
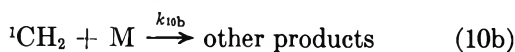
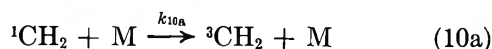
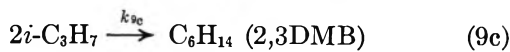
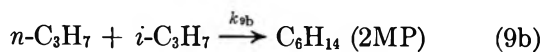
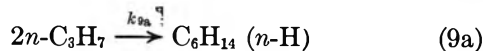
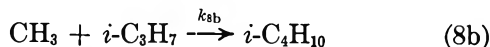
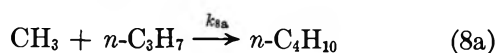
Discussion

Mechanism. A reaction mechanism consistent with previous work as well as this study is



(9) P. S. T. Lee, R. L. Russell, and F. S. Rowland, *Chem. Commun.*, 18 (1970).

(10) H. M. Frey and R. Walsh, *J. Chem. Soc.*, 2115 (1970).



I_a is the absorbed light intensity per unit concentration of DM per unit time and ϕ_1 and ϕ_3 are, respectively, the quantum yields for $^1\text{CH}_2$ and $^3\text{CH}_2$ production in the initial photodissociation.

The steady state concentration of $^1\text{CH}_2$ is

$$[^1\text{CH}_2]_{ss} = \frac{I_a \phi_1 [\text{DM}]}{(k_2 + k_3)[\text{Pr}] + k_4[\text{DM}] + k_{10}[\text{M}]} \quad (12)$$

The yield of $n\text{-B}$ is unaffected by the addition of small amounts of O_2 , less than $0.1[\text{Pr}]$, but all radical recombination products, reactions 7 and 9, are eliminated; $R(i\text{-B})$ is constant, 0.42, under these conditions. Thus, the contribution of reaction 5a, followed by 8a, to the $[n\text{-B}]$, in the absence of M, is negligible, and we have

$$\begin{aligned} d[n\text{-B}]/dt &= k_{2a}[^1\text{CH}_2]_{ss}[\text{Pr}] \\ \frac{d[n\text{-B}]/dt}{[\text{DM}]} &= \frac{k_{2a}I_a\phi_1[\text{Pr}]}{(k_2 + k_3)[\text{Pr}] + k_4[\text{DM}]} \end{aligned} \quad (13)$$

The slopes, λ , of the lines in Figure 2 are equal to $(d[n\text{-B}]/dt)/[\text{DM}]_0$; for two different sets of reaction conditions we can write

$$\frac{\lambda_A}{\lambda_B} = \frac{([\text{Pr}]/[\text{DM}]_0)_A \{ (k_2 + k_3)([\text{Pr}]/[\text{DM}]_0)_B + k_4 \}}{([\text{Pr}]/[\text{DM}]_0)_B \{ (k_2 + k_3)([\text{Pr}]/[\text{DM}]_0)_A + k_4 \}} \quad (14)$$

We can choose for condition (A), $[\text{Pr}]/[\text{DM}]_0 = 8.8$, but condition (B) is a problem, since the higher slope in Figure 2 is a limit that may be reached when $[\text{Pr}]/[\text{DM}]_0 \approx 30$. Using (14) with $\lambda_A/\lambda_B = 0.77$ and $([\text{Pr}]/[\text{DM}]_0)_B = 30$ gives $(k_2 + k_3)/k_4 = 0.25$; with $([\text{Pr}]/[\text{DM}]_0)_B = 50$, the rate constant ratio = 0.30. Thus the reactions of $^1\text{CH}_2$ with DM are about 3 to 4 times as fast as with Pr. At $[\text{Pr}]/[\text{DM}] \geq 50$, at least 94% of all $^1\text{CH}_2$ reacts with Pr, so (12) may be written approximately as

$$[^1\text{CH}_2]_{ss} = \frac{I_a \phi_1 [\text{DM}]}{(k_2 + k_3)[\text{Pr}]} \quad (12a)$$

and under these initial conditions, eq 13 reduces to

$$\frac{d[n\text{-B}]/dt}{[\text{DM}]_0} = \frac{k_{2a}I_a\phi_1}{k_2 + k_3} \quad (13a)$$

Since $[\text{C}_4\text{H}_{10}] = 1.42[n\text{-B}]$ and $k_2 = 1.42k_{2a}$, we have

$$\frac{d[\text{C}_4\text{H}_{10}]/dt}{[\text{DM}]_0 I_a} = \phi(\text{C}_4\text{H}_{10}) = \frac{k_2 \phi_1}{k_2 + k_3} = 0.76 \quad (15)$$

The ratio $k_2/(k_2 + k_3)$ may be estimated from information available in the literature. For reactions 10a and 10b with M = CH_4 , Braun, *et al.*,⁴ have measured $k_{10a} = (1.6 \pm 0.5) \times 10^{-12}$ and $k_{10b} = (1.9 \pm 0.5) \times 10^{-12}$ $\text{cm}^3 \text{ molecule}^{-1} \text{ sec}^{-1}$, where reaction 10b refers to



(C_2H_6^* may either be collisionally stabilized or dissociate to give 2CH_3 .) The ratios $k_{2a}/k_{10b} = 2.33$ and $k_{2b}/k_{10b} = 1.00$ were derived by Halberstadt and McNesby.^{2b} Thus $k_2 = k_{2a} + k_{2b} = (2.33 + 1.00) \cdot (1.9 \times 10^{-12}) = (6.3 \pm 1.7) \times 10^{-12}$ $\text{cm}^3 \text{ molecule}^{-1} \text{ sec}^{-1}$. Carr has suggested that the rate constants for the intersystem crossing reactions 3 and 10a are approximately proportional to the polarizabilities of the $^1\text{CH}_2$ collision partners.^{2e} In the range of polarizabilities for CH_4 , $\alpha = 27 \times 10^{-26}$ cm^3 , and Pr, 63×10^{-26} cm^3 , his intersystem crossing rate constants increase about a factor of 2 for a threefold change in polarizability. (Relative rather than absolute values are cited here, because our absolute values do not agree with Carr's.) Thus we can estimate that $k_3 = (2/3)(63/27)k_{10a} = (1.5)(1.6 \times 10^{-12}) = (2.4 \pm 1.0) \times 10^{-12}$ $\text{cm}^3 \text{ molecule}^{-1} \text{ sec}^{-1}$ and $k_2/(k_2 + k_3) = 6.3/(6.3 + 2.4) = 0.73 \pm 0.20$. Comparison with (15) indicates that $\phi_1 = 1.0 \pm 0.4$; we shall assume that ϕ_1 is unity in further data analyses.

Further evidence, but not unequivocal proof, of the validity of the assumptions made to obtain k_2 and k_3 is obtained from the competitive reaction systems, DM-Pr-M. The mechanism predicts that $[n\text{-B}]_M/[\text{DM}]_0$ for competitive systems, $[\text{Pr}]/[\text{DM}]_0 \geq 50$, will be related to $[n\text{-B}]/[\text{DM}]_0$, their pure counterparts, under constant, short-photolysis-time conditions, by the equation

$$\frac{[n\text{-B}]/[\text{DM}]_0}{[n\text{-B}]_M/[\text{DM}]_0} = 1 + \frac{k_{10}}{k_2 + k_3} \frac{[\text{M}]}{[\text{Pr}]} \quad (16)$$

where both $[n\text{-B}]$'s represent the yields due to reaction 2a. Figure 7 shows the straight-line relationships obtained and Table III gives values for $k_{10}/(k_2 + k_3)$ derived from the slopes of the lines. The rate constant ratio for CH_4 , 0.37 ± 0.08 , is⁴ $(k_{10a} + k_{10b})/(k_2 + k_3)$ and, using the rate constants above, we calculate this ratio to be 0.40 ± 0.16 , in excellent agreement with the measured value.

This agreement gives us confidence in the conclusion

Table III: Rate Constant Ratios Determined or Assumed in This Study

Ratio	Value	Notes
$k_2/(k_2 + k_3)$	0.76 ± 0.15	Assumes $\phi_1 = 1$
	0.73 ± 0.20	Assumes absolute values for k 's; see text
$k_3/(k_2 + k_3)$	0.39 ± 0.10	From $[n\text{-B}]/[\text{DM}]_0$ falloff
	0.28 ± 0.10	Assumes absolute values for k 's
k_{2a}/k_{2b}	2.33	Reference 2b
$k_4/(k_2 + k_3)$	3.6 ± 0.6	From relative $[n\text{-B}]$ at different $[\text{Pr}]/[\text{DM}]_0$
$k_{10}(\text{Xe})/(k_2 + k_3)$	0.21 ± 0.06	Figure 7
$k_{10}(\text{CH}_4)/(k_2 + k_3)$	0.37 ± 0.08	Figure 7
	0.40 ± 0.16	Assumes absolute values for k 's
$k_{10}(\text{O}_2)/(k_2 + k_3)$	0.46 ± 0.09	Figure 7
$k_{10}(\text{N}_2)/(k_2 + k_3)$	0.06 ± 0.06	See text
$k_{10}(\text{Ar})/(k_2 + k_3)$	0.09 ± 0.03	Ar is $1/4$ as effective as CH_4 ; see text
k_6/k_5	$(4.0 \pm 1.9) \times 10^2$	From 2,3DMB yields

Comparisons with Other Work

$k_{10}(\text{Ar})/k_{10}(\text{CH}_4)$	0.25 ± 0.05	This work
	0.18	Ratio of absolute rate constants measured by Braun, <i>et al.</i> , ref 4
$k_{10}(\text{Xe})/k_2$	0.29	This work
	0.047	Carr, ref 2e ^a
$k_{10}(\text{O}_2)/k_2$	0.63	This work
	0.46	Carr, ref 2e ^a
$k_{10}(\text{N}_2)/k_2$	0.08	This work
	0.048	Carr, ref 2e ^a
$k_{10}(\text{Ar})/k_2$	0.12	This work
	0.030	Carr, ref 2e ^a
	0.024, 0.033	Koob, ref 2f ^b

^a Ketene photolyzed at 313 nm. The data analysis used assumes $k_3 = k_{10}$. ^b Vacuum ultraviolet photolysis of Pr at 123.6 and 147 nm. The figures given assume that the quantum yield for CH_2 production is unity for $^1\text{CH}_2$. $k_{10}(\text{Ar})/(k_2 + k_3)$ is obtained directly and is 0.014 and 0.013 at the two wavelengths investigated.

that the photodissociation of DM yields $^1\text{CH}_2$, with a quantum yield of unity, which, at $[\text{Pr}]/[\text{DM}]_0 \geq 50$, all reacts with Pr either to form C_4H_{10} (70–80% of total CH_2) or to be deactivated to $^3\text{CH}_2$ (20–30% of total CH_2). At lower $[\text{Pr}]/[\text{DM}]_0$, reaction 4 with $k_4 = (3.6 \pm 0.5) (k_2 \pm k_3) = (3.1 \pm 1.0) \times 10^{-11} \text{ cm}^3 \text{ molecule}^{-1} \text{ sec}^{-1}$ has to be taken into account. Assuming $\phi_1 = 1$, we can use eq 12, revised to include all butanes, to calculate $\phi(\text{C}_4\text{H}_{10}) = 0.55 \pm 0.20$ for $[\text{Pr}]/[\text{DM}]_0 = 8.8$, which agrees very well with the experimental value 0.59 ± 0.12 .

To explain why the butane yield is not a function of $[\text{Pr}]/[\text{DM}]_0$ for ratios from 50 to 345, we must assume that reaction 6 is much faster than reaction 5, so that almost all the $^3\text{CH}_2$ is removed by reaction with DM. The data for C_6H_{14} yields confirm this assumption and

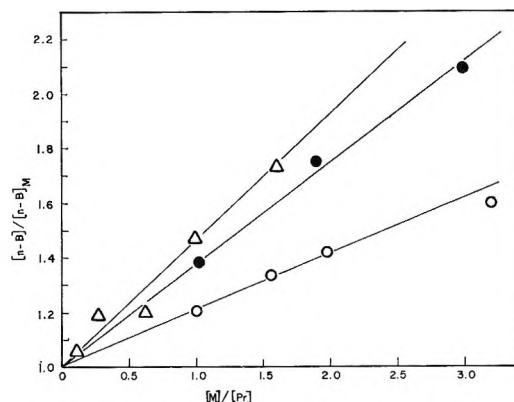


Figure 7. Relative $n\text{-B}$ yields as a function of added competitor gases for 20 min, 405 nm photolyses of 1.8 Torr of DM with 100 Torr of Pr: Xe, O; CH_4 , \bullet ; O_2 , Δ .

provide an estimate for k_6/k_5 . For pure DM–Pr systems the above mechanism predicts

$$\begin{aligned}
 [^3\text{CH}_2]_{\text{ss}} &= \frac{I_a \phi_3 [\text{DM}] + k_3 [^1\text{CH}_2]_{\text{ss}} [\text{Pr}]}{k_6 [\text{Pr}] + k_6 [\text{DM}]} \\
 &= \frac{k_3 [^1\text{CH}_2]_{\text{ss}} [\text{Pr}]}{k_6 [\text{DM}]} \\
 \frac{[^3\text{CH}_2]_{\text{ss}}}{[^1\text{CH}_2]_{\text{ss}}} &= \frac{k_3 [\text{Pr}]}{k_6 [\text{DM}]} \quad (17)
 \end{aligned}$$

where we have assumed $k_6 [\text{DM}] \gg k_5 [\text{Pr}]$ and, ϕ_3 , the quantum yield for $^3\text{CH}_2$ production, is equal to zero. The mechanism indicates that a constant ratio of CH_3 , $n\text{-C}_3\text{H}_7$, and $i\text{-C}_3\text{H}_7$ will be produced and, therefore, that a fixed fraction, f , of each of these radicals will disappear by each of the reactions 7–9. (That this assumption is not completely true is indicated by the $R(2,3\text{DMB})/R(2\text{MP})$ results from Table I, which show a variation with $[\text{Pr}]/[\text{DM}]_0$, presumably because of side reactions with DM and radicals derived therefrom.^{2d} This effect is small, however, and will be neglected.) Thus the rate of formation of any radical recombination product will be a fixed fraction of the rate of radical production, reaction 5, *e.g.*

$$f k_5 [^3\text{CH}_2]_{\text{ss}} [\text{Pr}] = k_{9c} [i\text{-C}_3\text{H}_7]^2 \quad (18)$$

Assuming that $k_{5b} = 4k_{5a}$ (secondary hydrogen abstraction favored by a factor of 12) and that the disproportionation–combination rate constant ratio is 0.6,^{2d} we get $f \approx 0.1$ in this case. (Disproportionation is not included in the mechanistic scheme explicitly since none of the disproportion products, CH_4 , C_3H_6 , and C_3H_8 , could be analyzed quantitatively in these experiments, but its effects have to be accounted for here.) We get, therefore

$$\frac{d[2,3\text{DMB}]/dt}{d[n\text{-B}]/dt} = R(2,3\text{DMB})_0 = \frac{f k_5 [^3\text{CH}_2]_{\text{ss}} [\text{Pr}]}{k_{2a} [^1\text{CH}_2]_{\text{ss}} [\text{Pr}]}$$

where $R(2,3\text{DMB})_0$ is the yield ratio at the initial reaction conditions, extrapolated for the higher $[\text{Pr}]/$

$[\text{DM}]_0$, as shown in Figure 5. Combining this expression with (17) yields

$$R(2,3\text{DMB})_0 = \frac{fk_5k_3[\text{Pr}]}{k_{2a}k_6[\text{DM}]} \quad (19)$$

Figure 6 is a plot of $R(2,3\text{DMB})_0$ vs. $[\text{Pr}]/[\text{DM}]_0$. The slope of the line, 1.6×10^{-4} , combined with $f = 0.1$ and $k_3/k_{2a} = 0.54$, gives $k_5/k_6 = 3.0 \times 10^{-3}$.

Another method of analyzing the 2,3DMB data is possible; at higher $[\text{Pr}]/[\text{DM}]_0$, combination of (12a) and (17) gives

$$[{}^3\text{CH}_2]_{ss} = \frac{k_3I_a}{k_6(k_2 + k_3)} \quad (20)$$

i.e., $[{}^3\text{CH}_2]_{ss}$ is constant at constant light intensity. Combining (20) with (18) and integrating, we obtain

$$[2,3\text{DMB}] = \frac{fk_5k_3I_a[\text{Pr}]}{k_6(k_2 + k_3)} t \quad (21)$$

assuming that $[\text{Pr}]$ is constant, an assumption valid within much better than 1%. A plot of $[2,3\text{DMB}]/[\text{DM}]_0$, the total number of molecules of 2,3DMB produced per Torr of DM initially present, vs. photolysis time is presented in Figure 8 for $[\text{Pr}] = 191$ Torr = 2.7×10^{20} molecules. I_a is 8.6×10^{-5} sec $^{-1}$ or 11.9×10^{13} photons sec $^{-1}$ (Torr of DM) $^{-1}$. The slope of the line in Figure 8 is 1.34×10^{12} molecules sec $^{-1}$ (Torr of DM) $_0^{-1}$ and, combining this value with the constants already calculated or assumed, we get $k_5/k_6 = 2.1 \times 10^{-3}$, which agrees satisfactorily with the results of the previous paragraph. Using all the data, we estimate $k_5/k_6 = (2.5 \times 1.2) \times 10^{-3}$.

At $[\text{Pr}]/[\text{DM}]_0 = 345$, only about $1/2$ the ${}^3\text{CH}_2$ reacts with Pr. Since about 20% of the total CH_2 is ${}^3\text{CH}_2$, approximately 10–15% of the products of $\text{CH}_2 + \text{Pr}$ reactions should be the result of ${}^3\text{CH}_2$ reactions. The yield of 2,3DMB in this system is about 1.6%

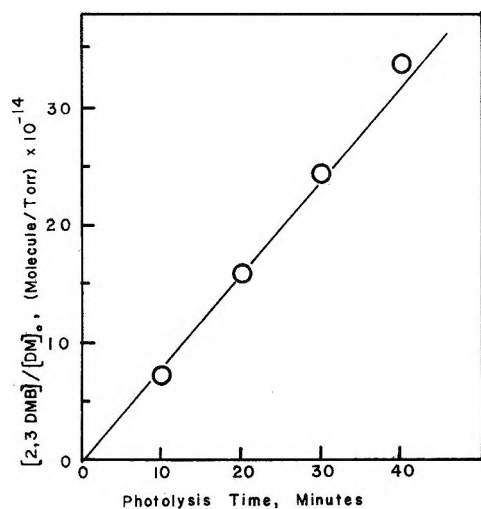


Figure 8. Absolute yields of 2,3DMB as a function of 405 nm photolysis time for 1.8 Torr of DM with 191 Torr of Pr.

that of the butanes formed by ${}^1\text{CH}_2$ insertion. If, as assumed previously, this yield represents about 10% of the overall yield of radical reactions following ${}^3\text{CH}_2$ attack on Pr, then the ${}^3\text{CH}_2$ reactions account for 16% of the products, in agreement with the prediction. Similar arguments can be made for systems with added gases, in which the $[{}^3\text{CH}_2]_{ss}/[{}^1\text{CH}_2]_{ss}$ ratio is increased; the results are consistent with the above relative reactivity of ${}^3\text{CH}_2$ toward DM and Pr.

Analysis of the $[n\text{-B}]/[\text{DM}]_0$ falloff shown in Figure 2 provides further evidence for the mechanism and rate constants derived above. The depletion of DM at $[\text{Pr}]/[\text{DM}] \geq 50$ is almost entirely a result of reactions 1a and 6

$$-d[\text{DM}]/dt = I_a[\text{DM}] + k_6[{}^3\text{CH}_2]_{ss}[\text{DM}] \quad (22)$$

Combining (20) and (22) and integrating gives

$$[\text{DM}]_t = [\text{DM}]_0 \exp(-It) \quad (23)$$

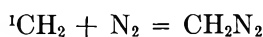
where

$$I = I_a \left(1 + \frac{k_3}{k_2 + k_3} \right) \quad (24)$$

By substituting (23) into (13a), integrating the resulting equation, and fitting the observed $[n\text{-B}]/[\text{DM}]_0$ vs. t data to the integrated equation, we can calculate I , $(1.2 \pm 0.2) \times 10^{-4}$ sec $^{-1}$; $I/I_a = (1.2 \times 10^{-4})/(8.6 \times 10^{-5}) = 1.39$. Thus $k_3/(k_2 + k_3) = 0.39 \pm 0.10$, which may be compared to the value 0.28 ± 0.10 derived from the rate constants themselves. In the runs with $[\text{Pr}]/[\text{DM}]_0 = 8.8$, the falloff in $[n\text{-B}]/[\text{DM}]_0$ is somewhat faster, reflecting the contribution of reaction 4 to the depletion of DM.

Competitive Systems. In the systems with added gases, the increased fraction of ${}^3\text{CH}_2$ reacts mainly with DM and depletes it faster than in pure systems, thus decreasing the rate of light absorption faster than in the pure systems. Since this means a lower rate of $n\text{-B}$ production, the effect could lead to spurious results for the competitive systems because the conclusions are based on analyses of the reductions in $n\text{-B}$ yields. In the DM-Pr- O_2 system, no trouble should arise since the ${}^3\text{CH}_2$ presumably reacts with O_2 , reaction 11, and is removed before it can react with DM.⁶ (If anything, the $[n\text{-B}]$ should be slightly enhanced, since DM is not being depleted as rapidly, but, at the largest $[\text{O}_2]/[\text{Pr}]$, the enhancement would be only about 2%.) For the highest $[\text{Xe}]/[\text{Pr}]$ used, we can use the rate constants already derived to calculate that 20% of the initial DM will have disappeared, compared with 13% in the absence of Xe under the same conditions. Very crudely, then, the average amount of DM present during the photolysis will be decreased from $0.93[\text{DM}]_0$ to $0.90[\text{DM}]_0$. Such an effect is within the experimental error of the technique and, therefore, was neglected in the data analyses. The special case of the CH_4 systems was treated in the Results section.

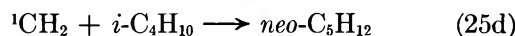
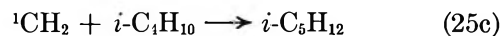
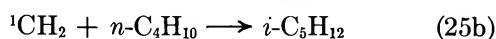
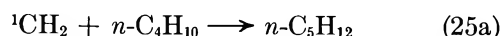
We can calculate k_{10} for N_2 by using an appropriate modification of eq 16 to include reaction 4, which makes a significant contribution under the reaction conditions used, $[Pr]/[DM]_0 = 8.9$. The result is $k_{10}(N_2)/(k_2 + k_3) = 0.06 \pm 0.06$ and $k_{10}(N_2) = (5 \pm 5) \times 10^{-13}$ cm^3 molecule $^{-1}$ sec $^{-1}$. (The large error limit reflects the great uncertainty involved in the analysis of only a single run.) 1CH_2 probably undergoes reaction 10b^{4,11}



In the analysis of short-photolysis-time runs we assume a constant $[DM]$, which is an average, but uncalculated, value. The reproduction of DM *via* reaction 10b will only make this average higher and hence could make the apparent effect of reaction 10 less than its true value. Time dependence studies need to be carried out in the DM-Pr- N_2 system to judge the relative size of k_{10a} and k_{10b} .

The results for other added gases have been previously discussed, and the results are given in Tables III and IV. The results for Ar relative to CH_4 are in moderately good agreement with those measured directly by Braun *et al.*⁴ Comparing our results with those of Carr,^{2e} in Table III, however, we note that, although the O_2 and N_2 results agree moderately well, for Ar and Xe our intersystem crossing rates relative to reactions with propane are 4–6 times as large. We see, Table IV, that our rate for N_2 is only about $1/2$ that obtained by Braun, *et al.* If the upper error limit for the N_2 run represents the correct value, then our result agrees with Braun's but is almost 3 times as high as Carr's. (The complications due to reaction 10b, reforming DM, probably make all N_2 data a bit suspect.) It is disturbing to see this almost systematic discrepancy between the two sets of results in steady-state, low-intensity systems. For his data analysis Carr assumes $k_3 \approx k_{10a}$, which is probably not a very good assumption, since $k_3 = 1.5k_{10a}$ for Xe, the most efficient gas, relative to Pr, that we used. Carr's technique involves reducing $[Pr]$ as $[M]$ is increased; removal of a more efficient 1CH_2 quencher tends to increase the contribution of 1CH_2 to the reaction and to make the apparent effect of M less than the equal-efficiency assumption suggests. However, if this were a major defect of his analysis, it is difficult to see how the data could yield the straight-line plots presented. (In a different system, vacuum ultraviolet photolysis of Pr-Ar- O_2 systems, Koob^{2f} finds $k_{10a}/k_2 = 0.024$ and 0.033, in agreement with Carr.) More experiments are necessary to resolve this discrepancy.¹²

Pentanes. Since $R(i-P)$ and $R(n-P)$ increase linearly with photolysis time, it is evident that one mode for their formation is



With $R(i-B) = 0.4$ and secondary insertion favored by 1.2 per bond over primary insertion, this scheme predicts $R(i-P)/R(n-P) = 1.4$. The observed ratio, Figure 3, with added O_2 , is about 1.6 ± 0.5 , which is reasonable agreement. The formation of *neo*- C_5H_{12} , detected at long photolysis times, is further confirma-

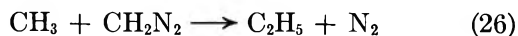
Table IV: 1CH_2 Reaction Rate Constants

Reaction	Rate constant, cm^3 molecule $^{-1}$ sec $^{-1} \times 10^{12}$
$^1CH_2 + CH_4 \rightarrow C_2H_6^*$ (10a)	1.9 ± 0.5^a
$^1CH_2 + CH_4 \rightarrow ^3CH_2 + CH_4$ (10b)	1.6 ± 0.5^a
$^1CH_2 + C_3H_8 \rightarrow n-C_4H_{10}$ (2a)	4.4 ± 1.2^b
$^1CH_2 + C_3H_8 \rightarrow i-C_4H_{10}$ (2b)	1.9 ± 0.5^b
$^1CH_2 + C_3H_8 \rightarrow ^3CH_2 + C_3H_8$ (3)	2.4 ± 1.0^b
$^1CH_2 + CH_2N_2 \rightarrow C_2H_4 + N_2$ (4)	31 ± 10^c
$^1CH_2 + O_2 \rightarrow ^3CH_2 + O_2$ (10)	4.0 ± 1.0^c
(or other products)	
$^1CH_2 + Xe \rightarrow ^3CH_2 + Xe$ (10a)	1.8 ± 0.6^c
$^1CH_2 + Ar \rightarrow ^3CH_2 + Ar$ (10a)	0.8 ± 0.3^c
	0.67 ± 0.13^a
$^1CH_2 + N_2 \rightarrow ^3CH_2 + N_2$ (10a)	$\geq 0.5 \pm 0.5^c$
	0.90 ± 0.20^a

^a Values of Braun, *et al.*, measured directly, ref 4. ^b These are the values assumed in our data analysis; they are internally consistent with all the experimental results with $\phi_1 = 1$. ^c These values are derived from our assumed rate constants and the experimental ratios of rate constants, Table III.

tion of this mechanism. When the yield of C_4H_{10} is about 1% of the starting amount of Pr, the yield of C_5H_{12} is about 0.5% of the C_4H_{10} , which is consistent with the very roughly equal rates of reaction of 1CH_2 with C_3H_8 and C_4H_{10} .

In the absence of O_2 there is obviously a second source of C_5H_{12} , which probably involves 3CH_2 or radicals, or both. As this source, Rabinovitch^{2d} has suggested the reactions



The present results offer little clear evidence regarding this mechanism, although it seems quite plausible.

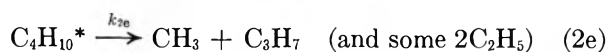
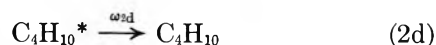
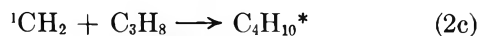
Any clear dependence of $R(i-P)$ on $[Pr]/[DM]_0$ is hard to discern from Figure 4, although total pressure, below 100 Torr, has a large effect which is discussed

(11) A. E. Shilov, A. A. Shteinman, and M. B. Tjabu, *Tetrahedron Lett.*, 4177 (1968).

(12) R. W. Carr, private communication, has suggested that 1CH_2 from diazomethane photolysis might be formed in a more highly energetic state than that from ketene. The density of final 3CH_2 states could then be sufficiently large to account for the higher intersystem crossing rates observed in the diazomethane system.

below. Reactions 2 and 25 together imply that $R(i\text{-P})$ should be inversely proportional to $[\text{Pr}]$ (as well as directly proportional to photolysis time when $[\text{Pr}]$ is constant). Assuming that reactions 1–10 determine the overall characteristics of the system and that (26) and (27) have little effect on radical steady-state concentrations, we see that the nearly constant $[\text{}^3\text{CH}_2]_{\text{ss}}$, eq 20, implies that $[\text{CH}_3]_{\text{ss}}$ and $[\text{C}_3\text{H}_7]_{\text{ss}}$ are proportional to $[\text{Pr}]^{1/2}$ and hence that $[\text{C}_2\text{H}_5]_{\text{ss}}$ is proportional to $[\text{DM}]$. The rates of production of C_5H_{12} and $n\text{-B}$ are then, respectively, functions of $[\text{DM}][\text{Pr}]^{1/2}$ and of $[\text{DM}]$, eq 13a, so that the contribution to the observed $R(i\text{-P})$ from reactions 26 and 27 should be proportional to $[\text{Pr}]^{1/2}$. The observed $R(i\text{-P})$ will, therefore, be a complex function of $[\text{Pr}]$ with decreasing and increasing terms whose contributions to the total vary as the photolysis proceeds. There is a slight bit of evidence from Figure 4 that the intercepts at zero time increase as $[\text{Pr}]$ increases and that at longer photolysis times $R(i\text{-P})$ decreases at higher $[\text{Pr}]$.

“Hot” Butane. At pressures below about 100 Torr the mechanism (1)–(10) still seems to work for C_4H_{10} production, but it has to be modified to account for the sharp increase in relative yields of radical recombination products, Figures 4 and 6 and Table I. Reaction 2 accounts quantitatively for the production of C_4H_{10} under all conditions studied. But it has been simplified and should be written



At lower pressures reaction 2e can begin to compete with 2d, collisional stabilization, to act as a second source of radicals added to those from reaction 5. Since k_6 is so much larger than k_5 , the yield of radicals from (5) is very small under most reaction conditions. Whitten and Rabinovitch^{2a} have found that $\omega_{2a}/k_{2e} = 1$ at 0.5 Torr and 1.5 Torr for $n\text{-B}^*$ and $i\text{-B}^*$, respectively. At 50 Torr, therefore, about 1% of the initially formed $\text{C}_4\text{H}_{10}^*$ would dissociate to produce radicals. The occurrence of 1% of (2e) relative to (2d) would be undetectable in the C_4H_{10} yield, but would add very significantly to the radical concentrations and hence to their reactions. This hot butane effect on radical product yields is also observed in other results below about 70 Torr.^{2c,g}

At higher $[\text{Pr}]/[\text{DM}]_0$ ratios, $R(2,3\text{DMB})/R(2\text{MP})$ approaches a constant value, 2.2 ± 0.5 , for systems with and without added gases, presumably reflecting reactions 5 and 7–9 plus disproportionation. At lower $[\text{Pr}]/[\text{DM}]_0$ ratios the $R(2,3\text{DMB})/R(2\text{MP})$ ratio decreases, probably because of side reactions with DM. At low pressures, reaction 2e should alter the ratio $[i\text{-C}_3\text{H}_7]/[n\text{-C}_3\text{H}_7]$ in favor of $n\text{-C}_3\text{H}_7$, but this

effect, if present, is masked by the side reactions, since the low pressure reactions were also carried out at relatively low $[\text{Pr}]/[\text{DM}]_0$.

There is some evidence from the data presented in Table I that even at 100 Torr the yields of hexanes and olefins are a bit higher than expected. The analytical error is too large to make this certain but, to be on the safe side, one should probably use pressures above 100 Torr to eliminate hot-molecule effects.

Olefin Production. Tables I and II show that olefin production is dependent on $[\text{Pr}]/[\text{DM}]_0$ and increases with decreasing total pressure below about 100 Torr. Olefin production is increased by the addition of “unreactive” gases, Xe and N_2 , which take part in reaction 10a; the behavior is more complex with added CH_4 because it reacts with ${}^1\text{CH}_2$ to give C_2H_6^* that dissociates to yield CH_3 in decreasing amounts as the total pressure increases. Clearly DM is involved directly in the olefin-forming reactions, but whether the reactions involve mainly ${}^1\text{CH}_2$, ${}^3\text{CH}_2$, or other radicals is very difficult to ascertain. Radicals must be involved at some stage, since, at low pressures where radical processes are enhanced by the small amount of $\text{C}_4\text{H}_{10}^*$ dissociation, the yield of olefins increases. The formation of C_4H_8 (butene-1 probably) in DM photolysis systems with hydrocarbons is universal and probably, Table II, involves ${}^3\text{CH}_2$, CH_3 , and DM. (It was the largest analyzable product in the blank photolysis run with CH_4 instead of Pr.) P1 production is little affected by increase in ${}^3\text{CH}_2$ and may be the result of ${}^1\text{CH}_2$, DM, and radical reactions. 4MP1 follows trends closely similar to C_4H_8 , except that its formation is definitely inhibited in the presence of CH_4 . Although the mechanisms for olefin formation remain obscure, their yields are low enough that they do not pose a major problem in interpreting the other results mechanistically.

Implications for Other Systems. It now appears well established that ϕ_3/ϕ_1 , reaction 1, varies with precursor, DM, ketene (K), or diazirine, and with photolysis wavelength for a given precursor. The conclusion reached here is that $\phi_3/\phi_1 = 0$ and $\phi_1 = 1$ for DM at 405 nm. A comparison of the results of this study with others in the literature indicates that a great deal of care in interpretation must be exercised as a result of differing rates for reactions 4 and 6 for the different precursors.

Carr finds $k_4(\text{K})/k_2 = 0.9$ and, thus, $k_4(\text{K}) = 5.7 \times 10^{-12} \text{ cm}^3 \text{ molecule}^{-1} \text{ sec}^{-1}$ for ketene at 313 nm and 760 Torr of total pressure,^{2e} compared with $k_4(\text{DM})/k_2 = 5$ from this work. Braun, *et al.*,⁴ suggest that the sum of the rate constants for CH_2 (multiplicity unspecified) + K reactions, not including intersystem crossing, lies between 1×10^{-12} and $5 \times 10^{-12} \text{ cm}^3 \text{ molecule}^{-1} \text{ sec}^{-1}$ which compares favorably with this estimate for $k_4(\text{K})$. Equation 12a should hold for K at a $[\text{Pr}]/[\text{K}]$ ratio $1/5$ as large as the $[\text{Pr}]/[\text{DM}]$

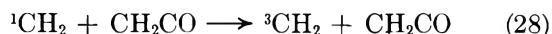
= 50 necessary for DM. If all CH_2 is initially formed as $^1\text{CH}_2$, then the maximum possible yield of C_4H_{10} from reaction 2 is $k_2/(k_2 + k_3) = 0.73 \pm 0.20$. Analysis of Noyes' data,^{2c} Table V, for K-Pr at 280 nm and 200 Torr of total pressure indicates a C_4H_{10} yield (corrected for $^3\text{CH}_2$ reaction) that is 0.66 of the total CH_2 (based on CO yield). It is conceivable, therefore, that a large fraction of all the $^3\text{CH}_2$ product in this system is a result of reactions 3 and 5-9 and that ϕ_3 is close to zero for K at 280 nm.¹³ Looking at "singlet" and "triplet" products without also doing relative quantum yield studies may, therefore, lead to spurious conclusions regarding ϕ_3/ϕ_1 .

Table V: Data for the K-Pr System at 280 nm. Yields Relative to CO^a

Total pressure, Torr	[Pr]/[K] ₀	[C ₄ H ₁₀]	R(i-B)	[C ₂ H ₄]	[C ₂ H ₆]	[CH ₄]
196	5	0.576	0.546	0.131	0.059	0.008
200	10	0.728	0.505	0.064	0.049	0.006

^a Ho and Noyes, ref 2c.

A further implication of the small $k_4(\text{K})/k_2$ is that the reaction



may be very important in K systems. We would expect, on the basis of Carr's polarizability correlation,^{2e} that this reaction would be relatively important compared with (3). K has $\alpha = 44 \times 10^{-25} \text{ cm}^3$, based on molar refractions, and a total polarizability $159 \times 10^{-25} \text{ cm}^3$ when its permanent dipole is taken into account;¹⁴ it should be at least as effective as Xe in inducing intersystem crossing in CH_2 . Disregarding reaction 28 might lead to serious errors in assessing ϕ_3/ϕ_1 . On a molecule-for-molecule basis, the reactivities of olefins and saturated hydrocarbons toward $^1\text{CH}_2$ are comparable,¹⁵ so reaction 28 may, under some conditions, be an important source of $^3\text{CH}_2$ in the K-olefin systems often used to assess ϕ_3/ϕ_1 .^{2c, 3b}

For DM we find $k_6/k_5 = 400$, but the corresponding ratio for K must be much lower. For [Pr]/[DM]₀ = 9, we find the $R(i-B) = 0.42 \pm 0.01$ characteristic of the $^1\text{CH}_2$ reaction. In systems with [Pr]/[K] = 10 photolyzed at 280 or 313 nm, the observed $R(i-B) = 0.53$,^{2c, 8} which implies a large $^3\text{CH}_2$ contribution *via* reactions 5 and 8. Using Noyes' results, Table V,^{2c} we can estimate $k_6(\text{K})/k_5$. The CO yield, corrected for the nonphotolytic production by reactions analogous to (4) and (6), is equal to the total amount of CH_2 produced upon photolysis. The sum of the yields of CH_4 , C_2H_4 , C_4H_{10} , and twice C_2H_6 should, given the mechanism we have been using, equal the CH_2 yield,

but in all cases the sum is slightly less. We assume that this "lost" CH_3 is lost *via* $^3\text{CH}_2$ reactions with K (an assumption that can only make the apparent reactivity with K larger than its true value). The amount of singlet product, $\text{C}_2\text{H}_4 + \text{C}_4\text{H}_{10}$, is calculated by using $R(i-B)$ to correct the observed C_4H_{10} yields for $^3\text{CH}_2$ reaction and then using $k_4(\text{K})/k_2$ to compute C_2H_4 from reaction 4. The yields of C_2H_4 and C_4H_{10} from $^3\text{CH}_2$ reactions are obtained by subtracting the amounts computed for $^1\text{CH}_2$ reactions from the totals. The yield of C_2H_4 from $^3\text{CH}_2$ plus the "lost" CH_2 is taken to be proportional to the rate of $^3\text{CH}_2$ reaction with K. The sum of the yields of CH_4 , twice C_2H_6 , and the C_4H_{10} from $^3\text{CH}_2$ is taken as proportional to the rate of $^3\text{CH}_2$ reaction with Pr. Combined with [Pr]/[K]₀, these relative rates give $k_6(\text{K})/k_5 = 6 \pm 2$ for a total pressure about 200 Torr in 280-nm photolyses. Thus the reaction of $^3\text{CH}_2$ with DM is about 60-70 times faster than with K.

Results for diazirine are qualitatively similar to K, *i.e.*, relatively low reactivity relative to Pr, but the experiments have not been completely analyzed as yet.¹⁶

A number of workers have studied systems with large proportions of inert to reactive gases to induce complete intersystem crossing of CH_2 and, hence, to study pure $^3\text{CH}_2$ reactions.^{2d, 17} The interpretation of these results has been questioned, because other work has suggested that a substantial fraction of $^1\text{CH}_2$ is still present under these conditions.^{3a, b, 10} The evidence from this study indicates that in DM-alkane systems there certainly could be a substantial contribution from $^1\text{CH}_2$ reactions; this would occur, not because there is a large proportion of $^1\text{CH}_2$ left in the system, but because the scavenging action of DM reduces the fraction of $^3\text{CH}_2$ that reacts with the substrate to only a small percentage of the total $^3\text{CH}_2$ formed. Thus a small amount of $^1\text{CH}_2$ would be responsible for a large percentage of the products observed as diagnostic for $^3\text{CH}_2$. In the system [DM]₀: [Pr]: [N₂] = 1:68:68 × 800, for example, Rabinovitch^{2d} found $R(i-B) = 1.47$. Assuming $\phi_1 = 1$ and the rate constants derived here, we can calculate that 1.5% of the CH_2 will react with Pr as $^1\text{CH}_2$ under these conditions. We have also assumed that all $^1\text{CH}_2$ reactions with N₂ lead to $^3\text{CH}_2$, which is not correct^{4, 11} but has the effect of increasing the predicted role of $^3\text{CH}_2$ in the reaction. Since $k_6/k_5 = 400$, only 14.5% of the $^3\text{CH}_2$ will react with Pr *via* reaction 5. On a statistical basis about 25% of the radicals so

(13) Recent work in G. B. Kistiakowsky's laboratory, private communication, suggests that $\phi_1 = 1$ for ketene photolysis at 260 nm.

(14) H. B. Hanney and C. P. Smyth, *J. Amer. Chem. Soc.*, **68**, 1357 (1946).

(15) J. A. Bell, *Progr. Phys. Org. Chem.*, **2**, 1 (1964).

(16) J. A. Bell, P. McIlvaine, and M. Ritchie, unpublished results.

(17) (a) H. M. Frey, *J. Amer. Chem. Soc.*, **82**, 5947 (1960); (b) R. F. W. Bader and J. I. Generosa, *Can. J. Chem.*, **43**, 1631 (1965); (c) R. A. Cox and K. F. Preston, *ibid.*, **47**, 3345 (1969).

formed will undergo reaction 8, *i.e.*, about 3.6% of the total CH_2 will react with Pr as $^3\text{CH}_2$ to yield C_4H_{10} . Combining the predicted contributions of $^1\text{CH}_2$ and $^3\text{CH}_2$ reactions, we calculate $R(i\text{-B}) = 1.8$, in reasonable agreement with experiment without the invocation of $^3\text{CH}_2$ insertion reactions. The reaction of $^1\text{CH}_2$ with N_2 to recycle CH_2 through DM will increase the contribution of $^1\text{CH}_2$ reactions to overall C_4H_{10} yields, while depletion of DM will increase the $^3\text{CH}_2$ component. (If information on the depletion of DM in these experiments was available, the relative sizes of these effects could be assessed and the relative rates of reactions 10a and 10b estimated.) At lower $[\text{Pr}]/[\text{DM}]_0$, Rab-inovitch finds a lower $R(i\text{-B})$, which is consistent with the decreased role of reaction 5 with the higher propor-

tion of scavenger. With $[\text{K}]_0:[\text{Pr}]:[\text{N}_2] = 1:6:6 \times 1110$, $R(i\text{-B}) = 1.55$, consistent with the lower reactivity of K toward $^3\text{CH}_2$. The suggestion here, that the large percentage of $^1\text{CH}_2$ reaction products in inert-gas-diluted systems is due to relative reactivities and not to large absolute amounts of $^1\text{CH}_2$, will presently be tested *via* absolute quantum yield measurements in DM-Pr-inert gas systems.

Acknowledgments. I am indebted to the Petroleum Research Fund, Grant 3275-B, administered by the American Chemical Society, for partial support of this research. Funds to purchase the gas chromatographic detector and electrometer were provided by the Simmons College Fund for Research.

Expressions for Multiple Perturbation Energies¹

by **D. P. Chong**

Department of Chemistry, University of British Columbia, Vancouver 8, B. C., Canada (Received September 15, 1970)

Publication costs assisted by the National Research Council of Canada

New expressions for multiple perturbation energies have been derived to complement the old. Possible applications in experimental as well as theoretical chemistry are discussed.

In double perturbation theory, the Hamiltonian for the perturbed system can be written as

$$\mathcal{H} = H_0 + \lambda H_1 + \mu H_2 \quad (1)$$

where H_0 is an unperturbed Hamiltonian. In this work, we consider only the case in which (a) the eigenvalue of H_0 for the state of interest is nondegenerate, and (b) H_0 , H_1 , and H_2 are all Hermitian. The eigenfunction and eigenvalue of \mathcal{H} are expanded in the usual² double power series

$$\Psi = \sum_{l=0}^{\infty} \sum_{m=0}^{\infty} \lambda^l \mu^m |l,m\rangle \quad (2)$$

$$E = \sum_{L=0}^{\infty} \sum_{M=0}^{\infty} \lambda^L \mu^M E^{(L,M)} \quad (3)$$

The calculation of $E^{(L,M)}$ requires knowledge of the perturbed wave function up to some $|l,m\rangle$. Great emphasis has been placed in keeping l as low as possible. For example, the well known Dalgarno's interchange theorem² gives

$$E^{(1,1)} = \langle 0,1|H_1|0,0\rangle + \langle 0,0|H_1|0,1\rangle \quad (4)$$

$$E^{(1,2)} = \langle 0,2|H_1|0,0\rangle + \langle 0,1|H_1|0,1\rangle + \langle 0,0|H_1|0,2\rangle \quad (5)$$

In a recent paper,³ Tuan extended Dalgarno's interchange theorem to higher orders. Two examples of her eq 12a are

$$E^{(2,1)} = \langle 0,0|H_1'|1,1\rangle + \langle 0,1|H_1'|1,0\rangle \quad (6)$$

$$E^{(2,2)} = \langle 0,0|H_1'|1,2\rangle + \langle 0,1|H_1'|1,1\rangle + \langle 0,2|H_1'|1,0\rangle \quad (7)$$

where $H_1' = H_1 - E^{(1,0)}$.

In this work, we (a) present an expression for $E^{(L,M)}$ which requires low $(l+m)$ in $|l,m\rangle$, (b) extend Tuan's work to triple perturbation, and (c) point out some possible applications of these new expressions for the perturbation energies.

Double Perturbation. In contrast to Tuan's two models,³ we consider both perturbations together. Instead of eq 1-3, we write

(1) Supported by grants from the National Research Council of Canada.

(2) J. O. Hirschfelder, W. B. Brown, and S. T. Epstein, *Advan. Quantum Chem.*, **1**, 255 (1964).

(3) D. F.-T. Tuan, *J. Chem. Phys.*, **46**, 2435 (1967). Her summation limits are all correct only if one regards all wave functions of negative orders as zero.

$$\mathcal{H} = H_0 + U \quad (8)$$

$$\Psi = \sum_{s=0}^{\infty} \Phi^{(s)} \quad (9)$$

$$E = \sum_{s=0}^{\infty} \epsilon^{(s)} \quad (10)$$

where

$$U = \lambda H_1 + \mu H_2 \quad (11)$$

$$\begin{aligned} \Phi^{(s)} &= \sum_{l=0}^s \lambda^l \mu^{s-l} |l, s-l\rangle \\ &= \sum_{m=0}^s \lambda^{s-m} \mu^m |s-m, m\rangle \end{aligned} \quad (12)$$

$$\begin{aligned} \epsilon^{(s)} &= \sum_{L=0}^s \lambda^L \mu^{s-L} E^{(L, s-L)} \\ &= \sum_{M=0}^s \lambda^{s-M} \mu^M E^{(s-M, M)} \end{aligned} \quad (13)$$

It is well known^{2,3} that

$$\begin{aligned} \epsilon^{(S)} &= \langle \Phi^{(A)} | U | \Phi^{(B)} \rangle - \\ &(1 - \delta_{S1}) \sum_{k=1}^B \epsilon^{(k)} \sum_{j=0}^{k-1} \langle \Phi^{(A+1+j-k)} | \Phi^{(B-j)} \rangle \end{aligned} \quad (14)$$

where $S > 0$; B is $S/2$ for even S and $(S-1)/2$ for odd S ; and $A = S - B - 1$. If we substitute eq 11-13 into eq 14, regroup terms, and match the coefficients of $\lambda^L \mu^M$, we get (after several pages of algebra)

$$\begin{aligned} E^{(L, M)} &= (1 - \delta_{L0}) \sum_l \langle l, A-l | H_1 | L-l - \\ &1, B-L+l+1 \rangle + (1 - \delta_{M0}) \sum_m \langle A - \\ &m, m | H_2 | B-M+m+1, M-m-1 \rangle - \\ &(1 - \delta_{S1}) \sum_k \sum_j \sum_p \sum_q E^{(L-p-q, k-L+p+q)} \times \\ &\langle p, A+1+j-k-p | q, B-j-q \rangle \end{aligned} \quad (15)$$

In eq 15, $S = (L+M) > 0$; A, B, k , and j have the same meaning as in eq 14. The new limits of summation are

$$\max(0, L-B-1) \leq l \leq \min(A, L-1) \quad (16)$$

$$\max(0, M-B-1) \leq m \leq \min(A, M-1) \quad (17)$$

$$\begin{aligned} \max(0, L-k-B+j) \leq p \leq \\ \min(L, A+1+j-k) \end{aligned} \quad (18)$$

$$\max(0, L-k-p) \leq q \leq \min(B-j, L-p) \quad (19)$$

If all the operators are real, a factor $(1 - \delta_{S2})$ can be inserted into the last term of eq 15, and simplifies the expressions for $E^{(L, M)}$ with $L+M=2$. For example

$$E^{(1,1)} = \langle 0,0 | H_1' | 0,1 \rangle + \langle 0,0 | H_2' | 1,0 \rangle \quad (20)$$

$$\begin{aligned} E^{(1,2)} &= \langle 0,1 | H_1' | 0,1 \rangle + \\ &\langle 1,0 | H_2' | 0,1 \rangle + \langle 0,1 | H_2' | 1,0 \rangle \end{aligned} \quad (21)$$

$$\begin{aligned} E^{(2,1)} &= \langle 0,1 | H_1' | 1,0 \rangle + \\ &\langle 1,0 | H_1' | 0,1 \rangle + \langle 1,0 | H_2' | 1,0 \rangle \end{aligned} \quad (22)$$

where $H_1' = H_1 - E^{(1,0)}$ and $H_2' = H_2 - E^{(0,1)}$. Equation 20 is just an example of eq IV.12 of Hirschfelder, *et al.*²

Triple Perturbation. Let us now consider the Hamiltonian

$$\mathcal{H} = H_0 + \lambda H_1 + \mu H_2 + \nu H_3 \quad (23)$$

where all the operators are Hermitian, and the triple power series expansions

$$\Psi = \sum_{l=0}^{\infty} \sum_{m=0}^{\infty} \sum_{n=0}^{\infty} \lambda^l \mu^m \nu^n |l, m, n\rangle \quad (24)$$

$$E = \sum_{L=0}^{\infty} \sum_{M=0}^{\infty} \sum_{N=0}^{\infty} \lambda^L \mu^M \nu^N E^{(L, M, N)} \quad (25)$$

It is easy to extend Tuan's eq 12a. The expression requiring low l in $|l, m, n\rangle$ becomes

$$\begin{aligned} E^{(L, M, N)} &= \sum_{m=0}^M \sum_{n=0}^N \{ \langle c, m, n | H_1 | d, M-m, N-n \rangle - \\ &(1 - \delta_{L1}) \sum_{k=1}^d E^{(k, m, n)} \sum_{j=0}^{k-1} \sum_{p=0}^{M-m} \sum_{q=0}^{N-n} \langle c+1 + \\ &j-k, p, q | d-j, M-m-p, N-n-q \rangle \} \end{aligned} \quad (26)$$

where d is $L/2$ for even L and $(L-1)/2$ for odd L , and $c = L - d - 1$. If H_1 is real, a factor $(1 - \delta_{L2})$ can be inserted into the second term of eq 26, and simplifies the expressions for $E^{(2, M, N)}$. For example

$$\begin{aligned} E^{(1,1,1)} &= \langle 0,0,0 | H_1 | 0,1,1 \rangle + \langle 0,0,1 | H_1 | 0,1,0 \rangle + \\ &\langle 0,1,0 | H_1 | 0,0,1 \rangle + \langle 0,1,1 | H_1 | 0,0,0 \rangle \end{aligned} \quad (27)$$

In contrast, the formula for $E^{(1,1,1)}$ which requires the lowest $(l+m+n)$ in $|l, m, n\rangle$ is

$$\begin{aligned} E^{(1,1,1)} &= \langle 0,0,1 | H_1' | 0,1,0 \rangle + \\ &\langle 0,1,0 | H_1' | 0,0,1 \rangle + \langle 0,0,1 | H_2' | 1,0,0 \rangle + \\ &\langle 1,0,0 | H_2' | 0,0,1 \rangle + \langle 0,1,0 | H_3' | 1,0,0 \rangle + \\ &\langle 1,0,0 | H_3' | 0,1,0 \rangle \end{aligned} \quad (28)$$

where $H_1' = H_1 - E^{(1,0,0)}$, $H_2' = H_2 - E^{(0,1,0)}$, and $H_3' = H_3 - E^{(0,0,1)}$.

Discussion

The new expressions in eq 15, 26, and 28 may be useful to experimental as well as theoretical chemists.

If finite basis sets are used and the matrix representations of H_0, H_1 , and H_2 can be regarded as known quantities, then the use of eq 15 is relatively simple. A computer program has been written for $E^{(L, M)}$ up to $(L+M) = 7$ and has been submitted to Quantum Chemistry Program Exchange.

Consider $H = H_0 + \lambda H_1$ as the true Hamiltonian of a system. Exact first-order properties are given by²

$$\langle W \rangle = E^{(0,1)} + \lambda E^{(1,1)} + \lambda^2 E^{(2,1)} + \dots \quad (29)$$

The first-order correction $E^{(1,1)}$ can be easily evaluated by Dalgarno's interchange theorem expressed in eq 4. To calculate the second-order correction $E^{(2,1)}$, Tuan's expression requires $|1,1\rangle$ in eq 6; our new formula in eq 22 needs only $|1,0\rangle$ and $|0,1\rangle$. If H_1 involves the usual two-electron operator, then it is still difficult to determine $|1,0\rangle$ exactly. However, we hope that eq 22 will stimulate some interest in the calculation of approximate second-order correction to first-order properties using approximate $|1,0\rangle$.⁴

For second-order properties such as electric polarizabilities, eq 15 does not lead to simple expressions. One has to use Dalgarno's interchange theorem expressed in eq 5 for the first-order correction and Tuan's formula expressed in eq 7 for the second-order correction (if the necessary perturbed wave functions are obtainable).

For second-order properties of a second type, such as chemical shifts and nuclear spin-spin coupling constants, eq 27 provides a simple way of calculating the first-order correction (if the necessary functions can be determined). One could, in principle, use eq 26 for higher order corrections; however, the perturbed wave functions required are extremely difficult to obtain.

Theoretical chemists interested in physical properties should see that our new expressions have been derived to complement Dalgarno's interchange theorem and Tuan's extension, not to replace them.

For some experimental chemists, the new expressions may be helpful in an entirely different manner. Unknown parameters in a Hamiltonian, such as force fields⁵ and spin parameters,^{6,7} are often extracted from spectroscopic data by least-squares analysis. The iterative procedure usually employed has been based on first-order multiple perturbation theory and multidimensional *simple* Newton-Raphson corrections. With the aid of eq 15 and 28, it becomes quite feasible to use *third-order* multiple perturbation theory with multidimensional *extended* Newton-Raphson corrections.⁸ One of the advantages of this new scheme is that it would reduce the chances of going from a safe initial set of parameter values to a set at which the sum of the squares is a local, but not true, minimum.

(4) D. M. Schrader has indicated an interest in this direction.

(5) J. Aldous and I. M. Mills, *Spectrochim. Acta*, **18**, 1073 (1962); **19**, 1567 (1963).

(6) S. Castellano and A. A. Bothner-By, *J. Chem. Phys.*, **41**, 3863 (1964).

(7) H. M. Gladney, IBM Research Report RJ-318 (1964); H. M. Gladney and J. D. Swalen, Quantum Chemistry Program Exchange, Program No. 134.

(8) J. A. Hebden, "An Electron Paramagnetic Resonance Study of Molecular Spin Multiplets with $S \geq 1$," Ph.D. Thesis, University of British Columbia, 1970. The fine-structure parameters for the ground-state triplet of *p*-nitrophenyl nitrene were successfully extracted in this manner.

The Nitrogen Afterglow and the Rate of Recombination of Nitrogen

Atoms in the Presence of Nitrogen, Argon, and Helium¹

by *W. Brennen** and Edward C. Shane

Department of Chemistry, University of Pennsylvania, Philadelphia, Pennsylvania 19104 (Received January 22, 1971)

Publication costs assisted by the Advanced Research Projects Agency

Pressure jump experiments in static samples of decaying active nitrogen are used to determine the pressure dependence of the yellow Lewis-Rayleigh afterglow specific emission intensity. The form of the dependence is $(I/[N]^2) = K[M](k\tau_B[M] + 1)^{-1}$. Values of the apparent quenching constant, k , are reported for N₂, Ar, and He diluents. Describing N atom recombination by the equation $-d[N]/dt = k_1[N]^2[M] + k_2[N]^2 + \tau^{-1}[N]$, analysis of afterglow decays in a static system has been used to evaluate the homogeneous and heterogeneous recombination rate coefficients. The effect of impurity oxygen on τ^{-1} is discussed. Our results on afterglow pressure dependence and atom recombination rate are combined with published measurements of the absolute afterglow intensity in pure nitrogen to evaluate the photon yield of recombination. The relative importance of the ⁵Σ and A³Σ afterglow mechanisms is discussed on the basis of existing evidence.

Introduction

The lack of adequate means for sufficiently precise and accurate measurement of low light intensity and absolute atomic concentration has created a distressing situation in research on the kinetics and mechanism of nitrogen atom recombination and its attendant Lewis-Rayleigh afterglow emission. After more than 50 years of effort it was not possible to write with confidence a tested rate law relating the relative (much less the absolute) intensity of a well defined portion of the afterglow spectrum to the atomic concentration and the concentration of diluent gas. In addition to that, the factor of 8 disagreement existing in the literature about the value of the homogenous termolecular overall recombination rate coefficient in pure nitrogen seemed a poor reward for the large effort that had been expended.^{2,3}

The important observation by Campbell and Thrush^{2d} that $[N]^2/I$, the reciprocal of the specific intensity of the yellow portion of the visible afterglow, increases linearly with $X(N_2)$, the mole fraction of nitrogen, in N₂-Ar and N₂-He mixtures above $X(N_2) \cong 0.2$ and at total pressures above 2 Torr led these workers to include in the afterglow mechanism strong quenching of the emitting N₂(B³Π_g, $v' = 10, 11, 12$) molecules by nitrogen. Lifetime studies⁴ of the B³Π_g state had previously given evidence of such a quenching process. This proposal has subsequently received support from the detailed work of Brown⁵ on the pressure and diluent composition dependence of the absolute intensity and spectral distribution of afterglow bands in the $\Delta v = 3$ sequence from levels $v' = 6$ to 12 of N₂(B³Π_g).

The introduction of quenching of N₂(B³Π_g) by diluent gas, M, into either the Berkowitz-Chupka-Kistiakowsky⁶ (⁵Σ) or Campbell-Thrush^{2d} (A³Σ) mechanisms

implies that the steady-state specific intensity of the afterglow from the highest populated levels of the B³Π_g state in pure diluent M should obey a rate law of the form

$$\frac{I}{[N]^2} = \frac{K[M]}{k\tau_B[M] + 1} \quad (1)$$

where K and k are constants for a particular diluent and τ_B is the radiative lifetime of the emitting state. Equation 1 shows that the specific intensity should be zero order with respect to diluent concentration, *i.e.*, independent of pressure, at sufficiently high pressure and first order at sufficiently low pressure. The characteristic parameter in eq 1 is the half-quenching pressure, $[M]_{1/2} = (k\tau_B)^{-1}$. We have reported preliminary results confirming eq 1 with M = N₂.⁷ We report here the details of that work and extensions to M = Ar, He. Jonathan and Petty,⁸ in an independent and simultaneous investigation of the afterglow pressure depen-

(1) Work supported by the Advanced Research Projects Agency in part under Contract DAHC15-67-C-0215 and in part under Contract F446320-67-C-0106 monitored by the Air Force Office of Scientific Research.

(2) (a) A. N. Wright and C. A. Winkler, "Active Nitrogen," Academic Press, New York, N. Y., 1968; (b) M. A. A. Clyne and D. H. Stedman, *J. Phys. Chem.*, **71**, 3071 (1967); (c) H. H. Brömer and W. Zwirner, *Z. Naturforsch. A*, **24**, 118 (1969); (d) I. M. Campbell and B. A. Thrush, *Proc. Roy. Soc., Ser. A*, **296**, 201 (1967).

(3) K. H. Becker, W. Groth, and D. Kley, *Z. Naturforsch. A*, **24**, 1840 (1969).

(4) M. Jeunehomme and A. B. F. Duncan, *J. Chem. Phys.*, **41**, 1692 (1964).

(5) R. L. Brown, *ibid.*, **52**, 4604 (1970).

(6) (a) J. Berkowitz, W. A. Chupka, and G. B. Kistiakowsky, *ibid.*, **25**, 457 (1956); (b) K. D. Bayes and G. B. Kistiakowsky, *ibid.*, **32**, 992 (1960).

(7) W. Brennen and E. Shane, *Chem. Phys. Lett.*, **2**, 143 (1968).

(8) N. Jonathan and R. Petty, *J. Chem. Phys.*, **50**, 3804 (1969).

dence by a technique quite different from ours, have obtained data for $M = N_2$ consistent with eq 1 which lead to a value of $[M]_{1/2}$ in fair agreement with ours. Becker, *et al.*,^{3,9} have also independently studied the pressure dependence of the visible nitrogen afterglow in the 7.5-m diameter stainless steel sphere in Bonn by a technique similar to ours, and these workers also confirm the form of eq 1 and agree with our values for the half-quenching pressure.

Knowing the pressure dependence of the specific afterglow intensity is important not only for understanding the afterglow mechanism but also for facilitating the study of total recombination rate by any method which relies on using the afterglow intensity to monitor the relative nitrogen atom concentration. We have used our findings on the pressure dependence of the afterglow in studying the total recombination rate of nitrogen atoms in nitrogen, argon, and helium diluents, and we have reported preliminary recombination results in the case of pure nitrogen.¹⁰ Our preliminary conclusions have been revised as will be seen below. The present paper gives the details of this work and includes results in Ar and He diluents.

One of the stimuli for our work was the surprising estimate made by Campbell and Thrush^{2d} that half of all homogeneous nitrogen atom recombination events in pure nitrogen proceed by way of the emitting $B^3\Pi_g$ state. Our results on afterglow pressure dependence and total recombination rate, when combined with existing knowledge about the absolute emission intensity, clarify further this matter of the photon yield of recombination. This question is dealt with in the discussion.

Experimental Section

Studies of the pressure dependence of the afterglow and the rate of nitrogen atom recombination were carried out with the apparatus shown schematically in Figure 1. Active nitrogen was produced in an air-cooled, electrodeless discharge in a fused silica tube using a 2450-MHz, 100-W Raytheon Model PGM-10 microwave power generator coupled to a Type 5,¹¹ $1/4$ wave cavity supplied by Ophthos Instruments. The per cent dissociation measured in the observation bulb was typically less than 0.25% in pure nitrogen and 1% for nitrogen diluted in He and Ar. A glass wool plug was inserted between the discharge and the light trap to remove vibrationally excited ground-state molecules formed in the discharge.¹² Stopcocks permitted capture of a static sample of active nitrogen in either a 3.1-l. or a 5 l. Pyrex observation bulb which was housed in a wooden, light-tight box painted dead black inside. Light emitted by the gas in the bulb passed through the bulb wall, a filter, and an 18 cm long 2.5-cm i.d. blackened brass tube, and was detected by an uncooled EMI 6256-SA photomultiplier tube operated at 1100 V from a Northeast Model RE-1602

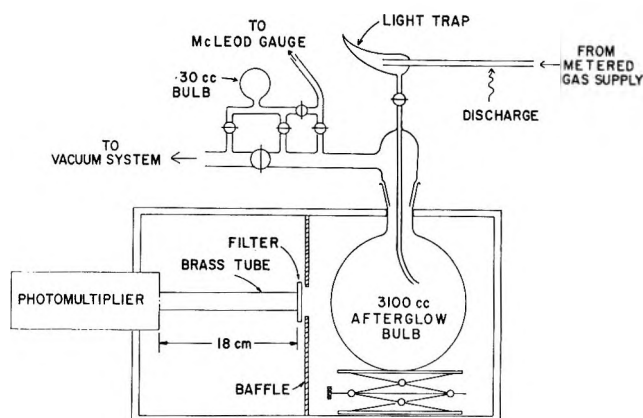


Figure 1. Schematic diagram of apparatus.

stabilized high-voltage power supply. The output of the photomultiplier tube was amplified by a Keithley Model 610-BR electrometer and displayed on a Leeds and Northrup Speedomax-G strip chart recorder. Experiments with nitrogen diluted in helium and argon employed a narrow-band interference filter (G-564-5800) from Oriel Optics Corp. which transmitted the nitrogen First Positive (11-7) and (10-6) bands. Some experiments with pure nitrogen employed a filter (G-564-5800) and some a two-filter set (600W-600B) from Optics Technology, Inc. Experiments with nitrogen containing added oxygen impurity employed the filter set (600W-600B). The two-filter set (550W-600B) was used for a number of preliminary experiments. Figure 2 shows the transmission curves of the filters obtained at normal incidence on a Cary Model 14 spectrophotometer.

All measurements were taken at room temperature, which was $21.0 \pm 1.5^\circ$.

The pressure dependence of the afterglow was studied using a pressure-increase technique. A steady flow of discharged gas was established through the observation bulb at the desired pressure. The bulb was then manually isolated by simultaneously closing stopcocks at the entrance and exit of the bulb. The initial pressure in the bulb after isolation was measured with a tilting McLeod gauge, and then after the afterglow had been allowed to decay for about 1 min the pressure was suddenly increased by opening a stopcock connecting the observation bulb to a 30-cc bulb containing gas at a higher pressure. For experiments with nitrogen diluted in argon or helium, pure diluent was added in the pressure increase. The afterglow intensity was re-

(9) K. H. Becker, A. Elzer, W. Groth, and D. Kley, SHA/2, Institute für Physikalische Chemie der Universität Bonn, 1968. We are grateful to Dr. Kley for making us aware of this work prior to publication.

(10) E. Shane and W. Brennen, *Chem. Phys. Lett.*, **4**, 31 (1969).

(11) F. C. Fehsenfeld, K. M. Evenson, and H. P. Broida, *Rev. Sci. Instrum.*, **36**, 294 (1965).

(12) J. E. Morgan, L. F. Phillips, and H. I. Schiff, *Discuss. Faraday Soc.*, **33**, 119 (1962).

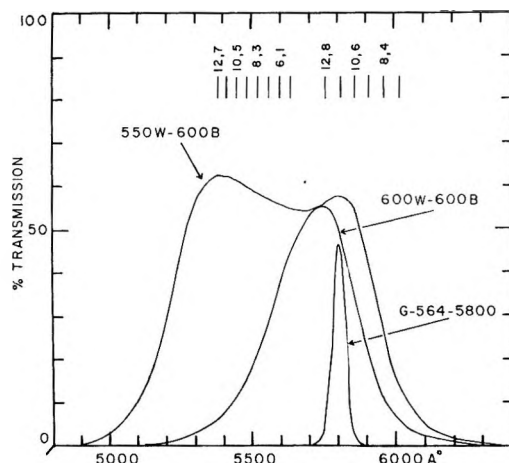


Figure 2. Filter transmission curves. Approximate positions of some afterglow bands [$B^3\Pi_g(v') \rightarrow A^3\Sigma_u^+(v'')$] are shown.

corded until several minutes after the pressure jump. The final pressure was also measured with the McLeod gauge.

Data on the rate of nitrogen atom recombination were extracted from static decay experiments. Discharged gas was passed through the observation bulb and the flow was adjusted to attain the desired conditions. The bulb was then isolated, and decay of the afterglow intensity in time was recorded. The pressure was measured at the end of each run. The initial absolute nitrogen atom concentration in the decay bulb, $[N]_0$, corresponding to I_0 , the afterglow intensity at the arbitrarily chosen zero of decay time—usually some seconds after the isolation of the bulb—was determined with the help of eq 1. If the signal current, i , is assumed to be proportional to I , eq 1 can be rearranged as follows.

$$[N] = \left\{ \frac{i(k\tau_B[M] + 1)}{K'[M]} \right\}^{1/2} \quad (2)$$

Knowing the value of $k\tau_B$ from measurements on the pressure dependence of $I/[N]^2$, we established a value for K' by carrying out a series of NO titrations at a known and experimentally convenient pressure. The value of K' of course depended on the filter used and on the nature of M. Once K' had been established, the absolute nitrogen atom concentration could be calculated from eq 2 at any pressure by measuring the signal current and the pressure. The reliability of this procedure was actually confirmed by doing NO titrations at several pressures and noting the constancy of K' and also by remeasuring K' from time to time to detect possible changes in the sensitivity of the photomultiplier. Our use of eq 2 to measure $[N]_0$ made it possible to study recombination at very low pressures where the direct use of the NO titration is difficult.

The NO titrations were carried out under steady-flow conditions in the exit tube leading from the observation bulb. The NO inlet was located about 2 cm

away from the bulb and the end point was detected with an auxiliary RCA 1P21 photomultiplier tube equipped with a filter transmitting from 5200 to 6100 Å and located 45 cm downstream of the NO inlet. Under the conditions prevailing during the NO titrations with the 3.1-l. bulb, the mean residence time of the active nitrogen in the observation bulb was about 10 sec, while the time of flow from the NO inlet to the end point detector was 0.3 sec. Also, under the same conditions, the time required for a nitrogen atom to diffuse a root mean square distance of one bulb diameter was 0.5 sec and the pseudo-first-order half-life for disappearance of atoms was about 40 sec. The observation bulb clearly satisfied the conditions for a stirred reactor,¹³ and the concentration of atoms in the efflux was the same as the uniform concentration of atoms in the bulb.

Prepurified nitrogen, ultrahigh purity helium, argon, oxygen, and hydrogen, and technical grade (98.5%) NO were obtained from the Matheson Co. For experiments with nitrogen diluted in argon and helium, mixtures containing 5% N_2 were prepared in a 12-l. bulb and flowed from there through the discharge. For experiments in which oxygen impurity was added after the discharge, a measured amount of oxygen was introduced into the observation bulb from the 30-cc appended bulb after the observation bulb had been isolated. All gas mixtures were passed through two spiral liquid nitrogen cooled traps before entering the discharge with the exception of N_2 -Ar mixtures, which were passed through the same traps cooled with Dry Ice in acetone. Gases were always conducted from the tanks in glass or copper tubing. Glass-metal connections were all made either with soldered Kovar seals or with epoxy adhesive. NO was purified by vacuum distillation from a trap maintained at 113°K to one cooled with liquid nitrogen, with initial and final fractions being discarded.

Diluent and NO flow rates had to be measured to carry out the NO titrations. Diluent flow rates were measured using a Poiseuille flowmeter¹⁴ made with a 29.70 ± 0.02 cm long piece of Fisher-Porter precision bore capillary tubing (0.500 mm nominal i.d.). The bore diameter was determined experimentally by repeated weighing of mercury threads of known length at a known temperature and found to be 0.5028 ± 0.0004 mm. The ends of the capillary were snapped off cleanly using a glass knife and sealed into larger tubes with epoxy adhesive. With this capillary under the flow conditions used, corrections for end effects and slip flow were negligible. Flows were calculated from the measured pressures at the ends of the capillary,

(13) K. G. Denbigh, "Chemical Reactor Theory," Cambridge University Press, New York, N. Y., 1966.

(14) H. Melville and B. G. Gowenlock, "Experimental Methods in Gas Reactions," MacMillan and Co., Ltd., London, 1964.

literature values for the gas viscosities,¹⁵ the capillary geometry, and the temperature. We estimate the accuracy of these flow rates to be $\pm 5\%$. Diluent flow rates were typically 10^{-5} mol/sec. For experiments in which oxygen impurity was added to the nitrogen before the discharge, flows were measured with less accuracy ($\pm 10\%$) ball float flowmeters.

Added NO flow rates were measured by timing a pressure drop in a calibrated volume¹⁶ using Dow-Corning DC-704 silicone oil ($\rho = 1.063$ g/cc at 25°) as the working fluid in the differential manometer.

The 3-l. observation bulb was ritually poisoned against wall recombination by rinsing with fuming red nitric acid, distilled water, 10% aqueous HF, and again with distilled water. N atom recombination studies with an N₂ buffer used both the 3-l. bulb and a 5-l. bulb whose walls were coated with syrupy phosphoric acid. The syrupy phosphoric acid was prepared by saturating 85% aqueous orthophosphoric acid with P₂O₅.

Results

Pressure Dependence of the Afterglow Intensity. Equation 1 is used as the starting point for the analysis of the pressure jump experiments. The main assumption on which this technique rests is that the sudden addition of diluent to a sample of afterglowing gas does not significantly alter the volume density of nitrogen atoms in the observation bulb in a time comparable to the mixing time. If this assumption is correct, the experiment measures the ratio of specific intensities at two pressures, which is to say it samples values of the function $[M](k\tau_B[M] + 1)^{-1}$ at two pressures as long as K (see eq 1) is not itself pressure dependent. Letting I_1 and I_2 be the intensities before and after the pressure increase, respectively, and $[M]_1$ and $[M]_2$ be the corresponding pressures, it follows from eq 1 that a single pressure increase experiment can be used to calculate a value for $k\tau_B$ from the equation

$$k\tau_B = \frac{[M]_2/[M]_1 - I_2/I_1}{[M]_2(I_2/I_1 - 1)} \quad (3)$$

For the most accurate results it is advantageous to choose the conditions of the experiment so that $[M]_1 < [M]_{1/2} < [M]_2$. If $[M]_1$ and $[M]_2$ are both smaller than $[M]_{1/2}$, then the numerator of eq 3 is small and inaccurately determined; if $[M]_1$ and $[M]_2$ are both much larger than $[M]_{1/2}$, then the denominator of eq 3 is small and inaccurately determined. Figure 3 shows the record of a typical pressure increase experiment in pure nitrogen.

A slight momentary overshoot in the intensity trace after the pressure jump, visible in Figure 3, was common, especially in runs with large pressure increases. This effect was not due to underdamping of the recording system. We attribute this effect to momentary enhancement of the rate of recombination of atoms resulting from the introduction of gas which has

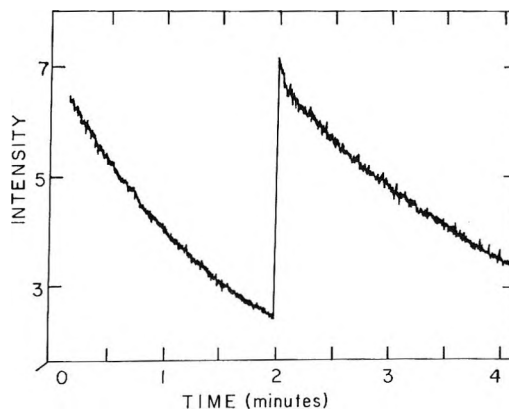


Figure 3. Typical pressure increase record. Nitrogen buffer with initial and final pressures of 0.046 and 0.48 Torr, respectively.

been cooled by sonic flow¹⁷ through the nozzle formed by the bore of the stopcock through which the gas is added. Since the amount of gas introduced in a typical pressure increase experiment is greater than the amount of afterglowing gas present in the bulb before the increase, the relaxation of the cooling effect ought to require a small multiple of the diffusional mixing time. This is consistent with the appearance of the effect on the traces. A rough calculation of the magnitude of the excess recombination resulting from momentary cooling revealed it to be sufficiently small so as not to invalidate the assumption that the concentration of atoms is the same before and after the pressure increase. To measure I_2/I_1 , the slow decay following the pressure increase was smoothly extrapolated back to the moment of mixing, effectively cutting the overshoot off the trace.

Results of the pressure increase experiments with $M = N_2$, Ar, and He are given in Table I.¹⁸ (See also footnote *e* in Table I.)

For the He and Ar experiments the gas composition changes during the pressure increase. The initial 5% N₂-He or 5% N₂-Ar mixture is diluted with pure He and Ar. If, using He to illustrate, the contributions of the third bodies are considered to be of the form, $k = k(\text{He})X(\text{He}) + k(\text{N}_2)X(\text{N}_2)$, where X is the mole fraction of the gas, then the apparent quenching constant for pure He, $k(\text{He})$, may be calculated from the equation

$$\tau_B k(\text{He}) = \frac{[M]_2/[M]_1 - I_2/I_1}{[M]_2 \{ (I_2/I_1)X_2(\text{He}) - X_1(\text{He}) \}} - \frac{\tau_B k(\text{N}_2) \{ X_2(\text{N}_2)(I_2/I_1) - X_1(\text{N}_2) \}}{\{ (I_2/I_1)X_2(\text{He}) - X_1(\text{He}) \}} \quad (3')$$

(15) J. Kestin and W. Leidenfrost, *Physica (Utrecht)*, **25**, 1033 (1959).

(16) W. R. Brennen and R. L. Brown, *Rev. Sci. Instrum.*, **39**, 608 (1968).

(17) L. D. Landau and E. M. Lifshitz, "Fluid Mechanics," Addison-Wesley, Reading, Mass., 1959.

(18) M. Jeunehomme, *J. Chem. Phys.*, **45**, 1805 (1966).

Table I: Recent Results of Studies on the Pressure Dependence of the Nitrogen Afterglow Intensity

M	$k\tau_B^a$	k^b	Comment	Ref
N ₂	8.6 ± 1.3	66	$v = 12, 11, 10$	This work
N ₂	7.7	60	v not given	3
N ₂	5.8 ^c	45	$v = 12, 11, 10$	8
N ₂	8.3	63	$v = 2$	8
N ₂		27	$v < 10$	e
N ₂	2.0	16	Determined from pressure dependence of the lifetime of the N ₂ (B) state; $v = 4-12$	4
He	0.6 ± 0.1	4.6 [2.4 ^d]	$v = 11, 10$	This work
He	0.5	4.0	v and gas composition not given	3
He		0.8	$v < 10$; gas composition not given	e
He		2.2	$v = 6-12$; 1% N ₂	5
Ar	1.5 ± 0.2	12 [1.8 ^d]	$v = 11, 10$	This work
Ar		1.1	$v = 6-12$; 1% N ₂	5
Ar	2.6	20	v and gas composition not given	3
Ar	1.5	12	$v = 12, 11, 10$; 11.5% N ₂	8
Ar	0.7	6	$v = 2$; 11.5% N ₂	8
Ar		1.6	$v < 10$; gas composition not given	e

^a In units of Torr⁻¹. ^b In units of 10⁻¹² cm³ molec⁻¹ sec⁻¹. When a value of $k\tau_B$ was reported, k was evaluated using $\tau_B = 4 \times 10^{-6}$ sec for $v = 12, 11,$ and 10 and $\tau_B = 9 \times 10^{-6}$ sec for $v = 2$.¹⁸ A temperature of 21° was assumed in making unit conversions. ^c Average of two sets of results, one observing the $\Delta v = 5$ sequence emission and one the $\Delta v = 4$ sequence emission. ^d Corrected using Brown's⁵ intensity distribution to represent quenching of levels $v = 6-12$. ^e R. A. Young, G. Black, and T. G. Slanger, *J. Chem. Phys.*, **50**, 303 (1969).

and likewise for Ar. The value of $\tau_B k(N_2)$ comes from the pure nitrogen experiments. Typically the second term amounts to a few per cent of the first term in our experiments. Equation 3' was derived using the assumption that K in eq 1 is independent of gas composition. This assumption is not really a good one as Brown's results show.⁵ Until we know more about the detailed mechanistic effects of third-body substitution, any procedure for dealing with the effects of composition on the afterglow intensity must needs be somewhat *ad hoc* and unsatisfactory.

Nitrogen Atom Recombination. Decay Experiments. The afterglow decays were analyzed in terms of the following differential equation, which was assumed to govern the rate of disappearance of nitrogen atoms

$$-d[N]/dt = \{k_r[M] + k_s\}[N]^2 + \tau^{-1}[N] \quad (4)$$

where k_r is the termolecular, homogeneous recombination rate coefficient, k_s is the sum of a homogeneous radiative recombination rate coefficient and a recently proposed second-order wall recombination rate coefficient,^{2d} and τ^{-1} is the apparent first-order wall recombination rate coefficient. Since eq 4 is taken to represent the disappearance of nitrogen atoms by all possible processes, it is important to recognize that k_r must be a composite rate coefficient which includes contributions of unknown relative magnitudes from recombination into the three bound states which correlate with normal atoms, *i.e.*, $^5\Sigma$, $A^3\Sigma_u^+$, and $X^1\Sigma_g^+$.

The solution of eq 4, when combined with eq 1, gives the following equation governing the decay of light intensity at constant pressure

$$z \equiv (I_0/I)^{1/2} = (1 + A) \exp(t/\tau) - A \quad (5)$$

where I_0 is the intensity at $t = 0$, $A = [N]_0\tau(k_r[M] + k_s)$, and $[N]_0$ is the atom concentration at $t = 0$. Two different methods can be used to extract values of the rate coefficients from the intensity-time relationship described by eq 5. One approach is to determine τ and A graphically by approximating dz/dt by $\Delta z/\Delta t$ and plotting $\ln(\Delta z/\Delta t)$ against t . The slope of such a graph is τ^{-1} and the intercept is $\ln\{[N]_0(k_r[M] + k_s) + \tau^{-1}\}$.

An alternative procedure is to graph z against t . Where only processes which are second order in $[N]$ are present such a graph is linear with a slope of $(k_r[M] + k_s)[N]_0$. The introduction of first-order N atom recombination causes a deviation from linearity in the z vs. t graph. It can be seen from eq 5 that such a graph will have a limiting initial slope equal to $\{(k_r[M] + k_s)[N]_0 + \tau^{-1}\}$.

Traditionally, in studies of N atom recombination the value for the k_r is derived from z vs. t graphs.^{2d,3,19-21} Decays in a 5-l. bulb coated with syrupy phosphoric acid were analyzed using z vs. t graphs for which the zero of time was taken to be a few seconds after isolation. These graphs deviated significantly from linearity after 20-30 sec.

Such a graph is shown in Figure 4b. The initial

(19) J. T. Herron, J. L. Franklin, P. Bradt, and V. H. Dibeler, *J. Chem. Phys.*, **30**, 879 (1959).

(20) P. Harteck, R. R. Reeves, and G. G. Mannella, *ibid.*, **29**, 608 (1958).

(21) K. M. Evenson and D. S. Burch, *ibid.*, **45**, 2450 (1966).

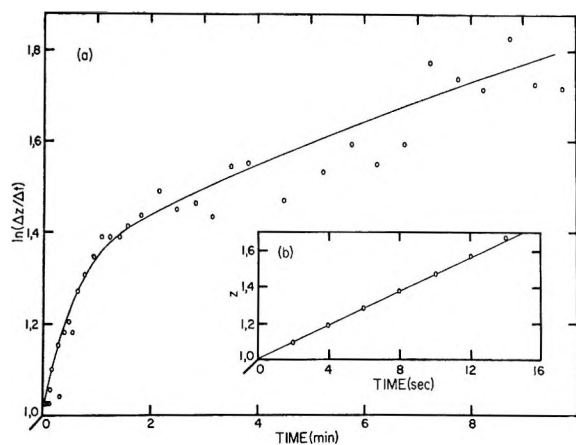


Figure 4. (a) $\ln(\Delta z/\Delta t)$ against time for a pure N_2 decay at 5 Torr. The bulb and inlet tube were coated with syrupy phosphoric acid. (b) z against time graph for the initial portion of the decay. The arbitrary time zero for both plots is about 3 sec after isolation of the bulb.

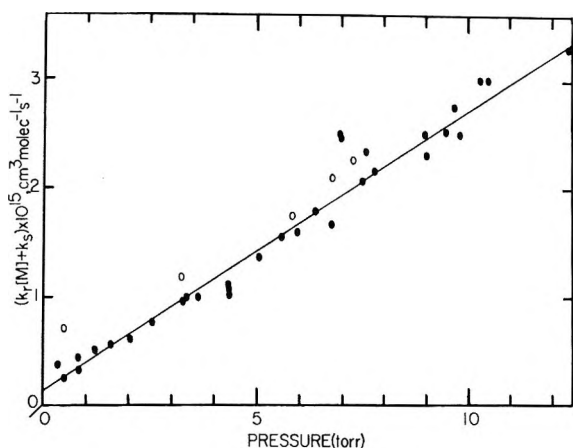


Figure 5. $(k_r[M] + k_s)$ against pressure for pure nitrogen. The filled-in circles represent runs in which the bulb was coated with syrupy phosphoric acid. The open circles represent runs in which the discharged gas passed through a trap containing syrupy phosphoric acid located just before the observation bulb; the observation bulb was not coated.

slope of the z vs. t graph was corrected for the τ^{-1} contribution to give a value of $(k_r[M] + k_s)[N]_0$. τ^{-1} was determined from the slope of a $\ln(\Delta z/\Delta t)$ graph of the initial decay data and amounted typically to a 20% correction. Using the absolute value of $[N]_0$ derived from I_0 , $(k_r[M] + k_s)$ was calculated. A graph of $(k_r[M] + k_s)$ against pressure is shown in Figure 5. The slope gives $k_r(N_2) = (0.79 \pm 0.10) \times 10^{-32}$ ($\text{cm}^6 \text{molec}^{-2} \text{sec}^{-1}$), and the intercept gives $k_s = (0.13 \pm 0.05) \times 10^{-15} \text{cm}^3 \text{molec}^{-1} \text{sec}^{-1}$.

The same information that is derived from z vs. t graphs of initial data should be available in $\ln(\Delta z/\Delta t)$ vs. t graphs for the duration of the decay. With syrupy phosphoric acid poisoning decays below 1.5 Torr gave identical results with both procedures. Above 1.5 Torr the $\ln(\Delta z/\Delta t)$ graph is not linear, as expected, but develops curvature. Such a graph is shown in Figure

4a. The same effect is present for all decays in a clean Pyrex bulb above 0.4 Torr.

In a preliminary report¹⁰ for the clean Pyrex system the initial curvature was overlooked and results were reported based on long-time decay data. It can be seen in Figure 4a that beyond the first minute of the decay the data, within scatter, follow a straight line. Typical decays were long enough (1-Torr decays lasted 1 hr) that 1-min time intervals were used in the $\ln(\Delta z/\Delta t)$ graphs. Thus long-time decay data were weighted most heavily and the initial curvature was obscured. The $(k_r[M] + k_s)$ against $[M]$ graph generated with long-time decay data is represented by the upper curve in Figure 6. Higher values of $(k_r[M] + k_s)$ were obtained and the k_r values were found to be pressure dependent. At this point the meaning of the results obtained from long-time decays with curved $\ln(\Delta z/\Delta t)$ graphs is not clear. Integration of eq 4 to give eq 5, which is used to derive the $\ln(\Delta z/\Delta t)$ relationship, assumed that the rate coefficients are constant. Figure 5 shows clearly that at least one of the terms is changing in time. This invalidates the integration of eq 4 and obscures the meaning of the $\ln(\Delta z/\Delta t)$ graph.

The cause of the curvature in the $\ln(\Delta z/\Delta t)$ graphs is unknown, but we think it is probably an impurity problem. Weak CN violet and $\text{NO}\beta$ emission is observed in our system. Experiments with added O_2 , to be discussed below, suggest that the small oxygen concentration responsible for $\text{NO}\beta$ emission does not produce curvature in the $\ln(\Delta z/\Delta t)$ graphs. The CN radical may be involved in reactions that are first and possibly second order in $[N]$. A change in $[\text{CN}]$ in the course of a run would then produce curvature in the $\ln(\Delta z/\Delta t)$ graph as the slope, reflecting first-order processes, and the intercept, reflecting second-order processes, change. The question of impurity contribution will be investigated in future experiments.

Limited initial decay data from our preliminary experiments¹⁰ with a clean Pyrex bulb were analyzed with z vs. t graphs. A graph of $(k_r[M] + k_s)$ against $[M]$ is shown in Figure 6. The results are significantly lower than those we previously obtained using long-time data from the same experiments and within scatter described a straight line. A least-squares fit of the data gave $k_r(N_2) = (1.1 \pm 0.4) \times 10^{-32} \text{cm}^6 \text{molec}^{-2} \text{sec}^{-1}$ and $k_s = (0.39 \pm 0.04) \times 10^{-15} \text{cm}^3 \text{molec}^{-1} \text{sec}^{-1}$. Within scatter the $k_r(N_2)$ value overlaps that obtained with phosphoric acid poisoning of the bulb.

Decays in which nitrogen was diluted in Ar and He buffers were not plagued with the difficulties just described for pure nitrogen; $\ln(\Delta z/\Delta t)$ graphs were linear for the duration of the decay. z vs. t graphs for the first 20–30 sec of the decay gave the same results as $\ln(\Delta z/\Delta t)$ graphs for long-time decay data. Graphs of $(k_r[M] + k_s)$ against $[M]$ are shown for Ar and He buffers in Figures 7a and 7b, respectively. Values for the slopes and intercepts gave $k_r(\text{Ar}) = (2.3 \pm 0.5) \times$

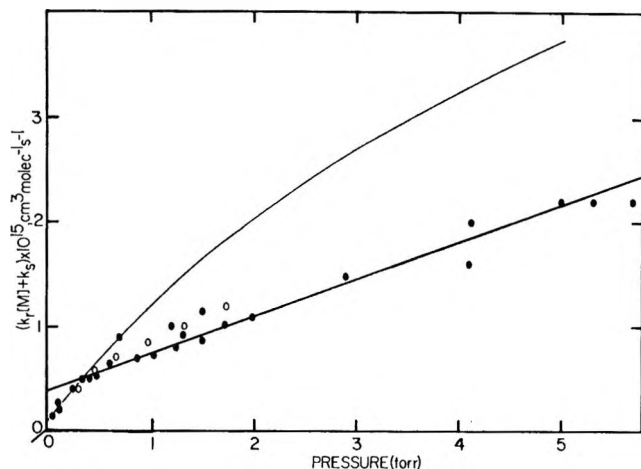


Figure 6. $(k_r[M] + k_s)$ against pressure for pure nitrogen in a clean Pyrex bulb. The filled-in circles represent the results of initial decay data analysis. The upper curve represents the results of long-time decay data analysis for the same experiments. For the open circles 0.07% O_2 was added to the decay bulb after isolation.

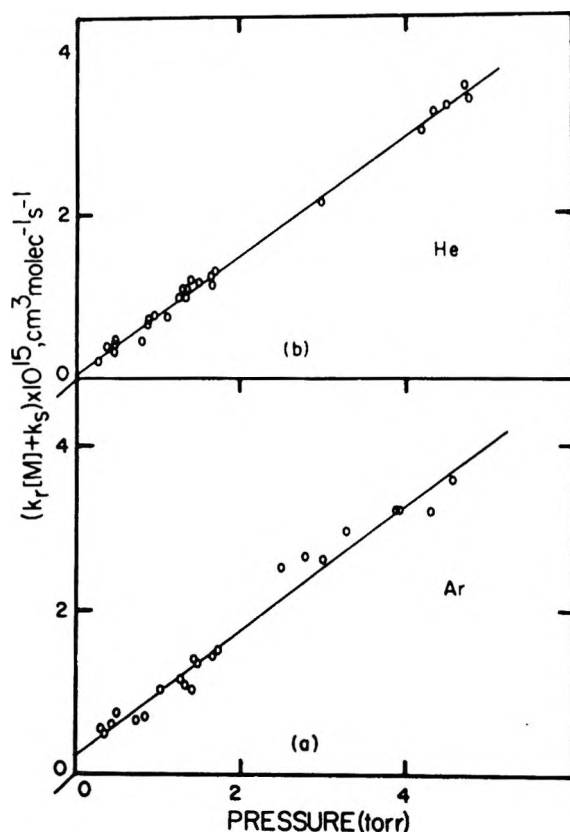


Figure 7. $(k_r[M] + k_s)$ against pressure for (a) Ar buffer and (b) He buffer in a clean Pyrex bulb.

10^{-32} and $k_r(\text{He}) = (2.22 \pm 0.12) \times 10^{-32} \text{ cm}^6 \text{ molec}^{-2} \text{ sec}^{-1}$ and $k_s(\text{Ar}) = (0.22 \pm 0.06) \times 10^{-15}$ and $k_s(\text{He}) = (0.65 \pm 0.13) \times 10^{-16} \text{ cm}^3 \text{ molec}^{-1} \text{ sec}^{-1}$. The results with Ar and He suggest that the difficulty with pure nitrogen decays may be an impurity that is present in the prepurified nitrogen. When the N_2 is sufficiently

diluted in Ar or He the impurity concentration is lowered enough so as to be ineffective.

Stirred Flow Reactor Experiments. A completely independent measurement of k_r is possible when the observation bulb is treated as a stirred flow reactor.^{13,22} Neglecting any contribution by k_s , stirred flow reactor theory gives the result

$$k_r = \frac{f_v}{V} \frac{[N]_a - [N]_b}{[N]_b^2[M]} - \frac{\tau^{-1}}{[N]_b[M]} \quad (6)$$

where τ^{-1} is the first-order rate coefficient, f_v is the volume flow rate of the gas at pressure $[M]$ in the bulb, V is the volume of the bulb, and $[N]_a$ and $[N]_b$ are the atomic concentrations at the entrance and exit of the bulb, respectively.

NO titrations were performed at the entrance and exit of the bulb under constant flow and discharge conditions to give $[N]_a$ and $[N]_b$. Titrations with $M = N_2$, Ar, and He performed at 0.8, 1.6, and 1.6 Torr, respectively, gave $k_r(N_2) = (1.2 \pm 0.4) \times 10^{-32} \text{ cm}^6 \text{ molec}^{-2} \text{ sec}^{-1}$, $k_r(\text{Ar}) = (2.7 \pm 1.0) \times 10^{-32} \text{ cm}^6 \text{ molec}^{-2} \text{ sec}^{-1}$, and $k_r(\text{He}) = (3.2 \pm 1.1) \times 10^{-32} \text{ cm}^6 \text{ molec}^{-2} \text{ sec}^{-1}$. These results are in reasonable agreement with the more accurate determination of k_r from decay experiments. The main reason the stirred flow reactor calculations are inherently less accurate than the decay results is that three different flow rates must be measured to evaluate k_r from eq 6. These flow rates enter eq 6 in such a way that we expect an error of 20–30% in a single k_r determination by this method.

For experiments with Ar and He buffer the term which is first order in $[N]$ reduces the calculated k_r by less than 5%. With a N_2 buffer the first-order correction is large, amounting to approximately 50%. The value of τ^{-1} was estimated from the data for the first 10 sec of a decay at the pressure at which the stirred flow reaction calculation was performed. For $M = N_2$ the inaccuracy in estimating the effective value of τ^{-1} introduces an additional 20% error in k_r .

Effect of Added Oxygen on k_r . Decays of N_2 with 0.07% O_2 added after the discharge did not show the peculiar features of pure nitrogen decays; $\ln(\Delta z/\Delta t)$ graphs were linear for the duration of the decay. k_r values derived from these graphs are represented by the open circles in Figure 6. Within experimental scatter they agree with the results of initial decay calculations for pure N_2 . Only lower pressure decays were taken with added oxygen because at higher pressures first-order removal of N atoms by atomic and molecular oxygen dominates the decay.

Real and Apparent First-Order Surface Recombination. Were the first-order recombination coefficient, τ^{-1} , due entirely to wall recombination, it should be independent

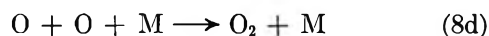
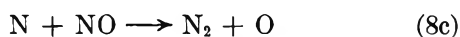
(22) (a) A. A. Frost and R. G. Pearson, "Kinetics and Mechanism," 2nd ed, Wiley, New York, N. Y., 1961, p 265; (b) G. B. Kistiakowsky and G. G. Volpi, *J. Chem. Phys.*, **27**, 1141 (1957).

of the total pressure and equal to $3\bar{c}\gamma/4R$, where \bar{c} is the average speed of the nitrogen atoms, γ is the wall recombination probability, and R is the radius of the spherical vessel. We observed, however, that τ^{-1} increased with increasing pressure as shown in Figure 8. These results forced us to consider the possibility that experimental τ^{-1} values arose partly from wall recombination and partly from homogeneous processes involving impurities, the latter appearing kinetically to be quasi-first order in $[N]$. The addition of only 0.07% oxygen impurity after the discharge, Figure 8, drastically increased the slope of the τ^{-1} vs. $[M]$ graph.²³

The quantity τ^{-1} may be decomposed as follows

$$\tau^{-1} = k_w + k_i[M] \quad (7)$$

where k_w is the true surface recombination rate coefficient and k_i contains the effects of impurity oxygen. We viewed the effect of added oxygen on the basis of the reaction scheme



Using this mechanism, the quantity k_i in eq 7 becomes

$$k_i = 2k_a X(O_2) + 2k_b [O] \quad (9)$$

where $X(O_2)$ is the mole fraction of molecular oxygen. The factors of 2 enter eq 9 because the removal of a nitrogen atom by reactions 8a or 8b guarantees the removal of another in each case by the subsequent very rapid reaction 8c. When molecular oxygen is added to afterglowing nitrogen the value of $[O]$ is initially zero. As reactions 8 proceed, $[O_2]$ decreases and $[O]$ increases. Using literature values of the rate constants²⁴ for reactions 8 and our results for the time dependence of $[N]$ we have made step-by-step calculations of the time dependence of k_i for our runs with 0.07% added O_2 . It appears that after 1-2 min of decay history, the value of k_i remains essentially constant for a long time. These limiting values of k_i were used to draw the upper curve in Figure 8. The agreement with experiment is good, which supports our interpretation of the effect of oxygen impurity. Very slight pressure dependence of τ^{-1} for the helium mixture is consistent with the low oxygen impurity level claimed for the helium we used. The results for the argon mixture lead us to conjecture that we did not exhaust the air from our mixing bulb with sufficient care prior to making the mixture.

From extrapolations to zero pressure we derived an average value of $k_w = 3 \times 10^{-1} \text{ sec}^{-1}$, which yields a value of $\gamma = 5.0 \times 10^{-8}$ for the wall recombination probability. This is the lowest value of γ for nitrogen atom recombination ever reported for any surface. The literature contains numerous reports of widely

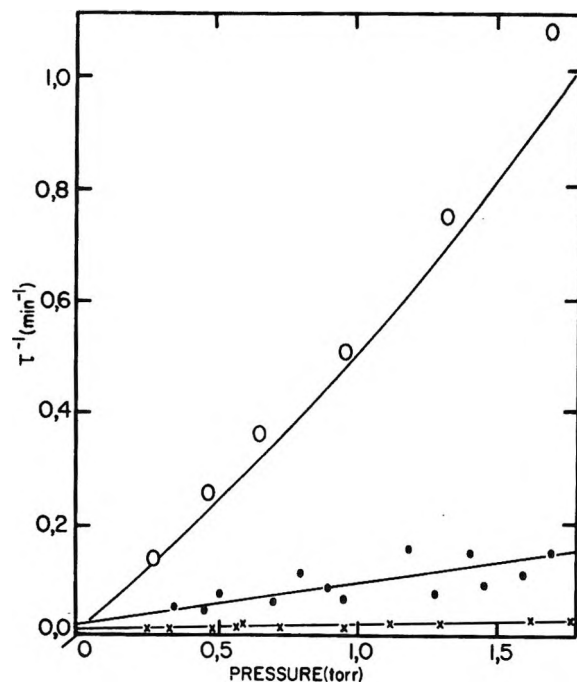


Figure 8. τ^{-1} against pressure for Ar buffer (filled-in circles), He buffer (\times), and pure nitrogen with 0.07% O_2 added after the discharge (open circles). The upper curve is a calculated curve based on eq 8 (see text).

varying γ values for nitrogen atom recombination at ostensibly similar surfaces (ref 2a and Table II); however, it is hard to assess the significance of these values because, with one exception,⁹ no τ^{-1} vs. $[M]$ data have previously been published. It is very likely that some published γ values are measures of gas impurity instead of effective surface characteristics. As far as our value of γ is concerned, we cannot confidently say this is a characteristic of clean Pyrex because of the possibility that tiny areas of stopcock grease or other material exposed to the afterglowing gas in our bulb may be very effective in destroying atoms. If such active regions of area S' have a wall recombination probability γ' , then it is sufficient that $\gamma'S' = 0.52 \times 10^{-4} \text{ cm}^2$ for our calculation of the apparent γ for the entire surface to come out as it did.

Obviously a very small active surface area could account for all the first-order heterogeneous recombination which, by calculating as we did, we attempt to attribute to the large interior surface area of the entire bulb. It is entirely possible that $\gamma = 0$ for clean Pyrex. Carefully designed experiments with pure gas in bulbs

(23) The value of τ^{-1} was taken from the slope of $\ln (\Delta z / \Delta t)$ graphs. Due to the ambiguity associated with $\ln (\Delta z / \Delta t)$ graphs for an N_2 buffer, only results for Ar and He buffers are reported. When N_2 was poisoned with 0.07% O_2 the $\ln (\Delta z / \Delta t)$ graphs were normal and τ^{-1} values obtained from the slopes could be used with confidence.

(24) (a) J. E. Morgan and H. I. Schiff, *J. Chem. Phys.*, **38**, 1495 (1963); (b) I. M. Campbell and B. A. Thrush, *Proc. Roy. Soc. Ser. A*, **296**, 222 (1967); (c) M. A. A. Clyne and B. A. Thrush, *ibid.*, **261**, 259 (1961); (d) K. Schofield, *Planet. Space Sci.*, **15**, 643 (1967); (e) W. E. Wilson, *J. Chem. Phys.*, **46**, 2017 (1967); (f) C. Mavroyannis and C. A. Winkler, *Can. J. Chem.*, **39**, 1601 (1961).

of different surface-to-volume ratios would help to clarify this point.

Discussion

Pressure Dependence of the Afterglow and the Afterglow Mechanism. Values of the apparent quenching constant, k , for pure N_2 are summarized in Table I. Pressure increase experiments reported here and by Becker, *et al.*,³ and an entirely independent experimental approach by Jonathan and Petty⁸ give similar values of k_{N_2} . Jeunehomme and Duncan's k_{τ_B} value is calculated from the pressure dependence of the lifetime of the $N_2(B)$ state. Later, Jeunehomme¹⁸ reported more accurate data on the lifetime, but new data on the pressure dependence of the lifetime in pure N_2 buffer were not reported, so a revised k_{τ_B} could not be calculated. The results of Young, *et al.* (see Table I, footnote *e*), are low but they are difficult to compare with our experiments due to their different method of formation of $N_2(B)$ and their observation of lower vibrational levels. For pure nitrogen the pressure dependence of the afterglow for the topmost emitting levels of the $B^3\Pi$ state seems firmly established with $k_{\tau_B} = (8.0 \pm 1.2) \text{ Torr}^{-1}$.

The pressure dependence of the afterglow varies with the third body. For an N_2 buffer the pressure at which the specific intensity, $I/[N]^2$, reaches 50% of its maximum value—the so-called half quenching pressure—is 0.12 Torr. Above 1 Torr little pressure dependence is detected, in agreement with higher pressure studies^{2d,5,25,26} which found the specific intensity to be pressure independent above about 2 Torr. With Ar and He buffers there is much less apparent quenching than in pure N_2 ; consequently the specific intensity depends significantly on pressure to higher pressures. The interpretation of pressure increase experiments in Ar and He is complicated by the fact that the vibrational distribution in $B^3\Pi$ is, especially in Ar, rather strongly dependent on pressure and gas composition as Brown⁵ has shown. Since we observe emission from levels 11 and 10 in the pressure increase experiments and the distribution shifts to lower levels at higher pressure, failure to correct for the distribution shift gives values of k_{τ_B} in Ar and He which are too high. We used Brown's vibrational distributions to correct our data for levels 11 and 10 to represent apparent quenching of the top seven vibrational levels of $N_2(B)$. In Table I we have shown both our uncorrected and corrected values of k_{τ_B} in Ar and He.

As can be seen in Table I there is only fair agreement on the value of k_{τ_B} for the inert gases. Becker, *et al.*,³ report a preliminary $k_{He\tau_B}$ value similar to ours, but since they did not report the gas composition it is not clear whether N_2 made a contribution to the observed value. An N_2 contribution will raise the observed k_{τ_B} value. In our experiments the nitrogen contribution was less than the scatter in the data, which amounted

to about 10%. Limited data by Young, *et al.*,²⁷ for a 1% N_2 -He mixture indicated the specific intensity was pressure dependent between 1 and 4 Torr. Our results indicate that the specific intensity has reached 71% of its maximum value at 4 Torr. Our value of k_{τ_B} for Ar and He, as corrected with Brown's⁵ intensity distribution, is in good agreement with Brown's apparent quenching constant for $v = 6$ -12. For an Ar buffer Becker, *et al.*,³ report a higher k_{τ_B} but again the N_2 contribution is unknown. Jonathan and Petty⁸ report an uncorrected k_{τ_B} value identical with ours but for an 11.5% N_2 -Ar mixture. This value is not influenced by the distribution shift because JP used a direct titration technique to measure atom concentrations, but it does include an N_2 contribution. Using the approximation the $k = k(\text{Ar})X(\text{Ar}) + k(\text{N}_2)X(\text{N}_2)$, JP's data suggest $k_{Ar\tau_B} = 0.23 \text{ Torr}^{-1}$. The contribution to k_{τ_B} of the small amounts of N_2 present in the inert gas mixtures need clarification.

Our experiments and other studies^{3,5,8} of the pressure dependence of the afterglow have determined the intensity-pressure relationship to be that represented in eq 1. The experiments of Jonathan and Petty⁸ suggest that the form of this equation is valid not only for the highest levels of $N_2(B)$, $v = 12, 11$, and 10, but also for lower levels, $v = 6, 5$, and 2. The pressure dependence of the afterglow is rooted in the mechanism of the afterglow. We will now consider the predictions of several proposed mechanisms and their agreement with experiment.

Berkowitz, Chupka, and Kistiakowsky^{6a} (BCK) have proposed that the mechanism for population of the topmost vibrational levels of $N_2(B)$ involves nitrogen atom recombination into the $N_2(^5\Sigma)$ state followed by collisionally induced transfer from $N_2(^5\Sigma)$ to N_2 -($B^3\Pi_g$). Introduction of the quenching reaction, $N_2(B) + M \xrightarrow{k_Q} \text{quench}$, into the BCK mechanism gives an intensity-pressure relationship of the form of eq 1 where $k = k_Q$. For the lower vibrational levels of $N_2(B)$ BCK suggest that $N_2(A^3\Sigma_u^+)$ is involved as an intermediate.

Campbell and Thrush^{2d} (CT) suggest that $N_2(A^3\Sigma_u^+)$ is the sole intermediate in the recombination. See Figure 9a. Steady-state analysis of the CT mechanism gives an intensity-pressure relationship of the form of eq 1 where $k = k_{-1}(k_{-} + k_v)(k_{-} + k_v + k_1)^{-1} + k_Q$. k is identified as a quenching constant plus a complex combination of rate constants. In the CT mechanism k no longer simply represents electronic quenching of the $N_2(B)$ state.

The model shown in Figure 9b schematically represents an obvious elaboration of the simple CT scheme,

(25) R. W. Gross, *J. Chem. Phys.*, **48**, 1302 (1968).

(26) R. A. Young and R. L. Sharpless, *ibid.*, **39**, 1071 (1963).

(27) R. A. Young, R. L. Sharpless, and R. Stringham, *ibid.*, **41**, 1497 (1964).

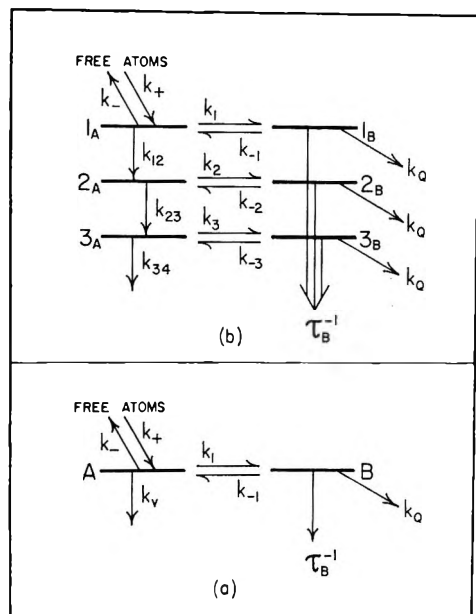


Figure 9. (a) Campbell-Thrush model and (b) expanded Campbell-Thrush model.

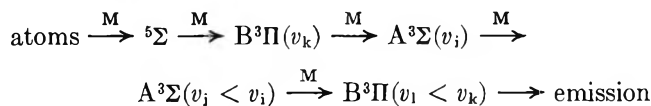
which shows the vibrational structure of the A and B states and suggests the possibility of crossover between A and B at various energies. If the quenching and radiative rate constants are assumed to be independent of level, the steady-state solution for the intensity of emission from level n of B, though algebraically messy, can be written down. The expression for the intensity from the top level of B is naturally identical with that from the CT mechanism. For lower levels the intensity-pressure relationship becomes more complicated in appearance, and it seems odd that eq 1 should apply to any but the topmost level. Simplifications are possible, however, when assumptions are made about the relative magnitudes of various rate constants. Consider two extreme examples. If quenching of $N_2(B)$ is always much more efficient than back-transfer to $N_2(A)$, *i.e.*, if $k_Q \gg k_{-n}$, for all n , then the intensity from each level of $N_2(B)$ obeys an equation of the form of eq 1, and the apparent quenching constant is k_Q . If, on the other hand, vibrational relaxation in $N_2(A)$ is always more efficient than crossing to $N_2(B)$, *i.e.*, $k_{n,n+1} \gg k_n$ for all n , then the intensity from each level of $N_2(B)$ is again of the form of eq 1, but the apparent quenching constant for each level is $k_Q + k_{-n}$. In this instance if $k_{-n} \gg k_Q$ for all n then k_{-n} would have to depend weakly on n for the same formula to apply to all levels.

Until more precise level-by-level measurements of the pressure dependence of the intensity are available, it will not be possible to make a firm decision about the mechanistic significance of the apparent quenching constant.

An important contribution to the evaluation of mechanistic models has been made by Brown.⁵ He mea-

sured the intensity distribution of the nitrogen first positive bands in the $\Delta v = 3$ sequence, coming from upper levels $v = 6-12$, in the range from 0.06 to 4.5 Torr with nitrogen, argon, and helium buffers. He attempted to fit the results for an Ar buffer to a model involving vibrational relaxation and electronic quenching in $N_2(B)$. The levels of $N_2(B)$ were assumed to be populated from an unidentified precursor. In order to obtain a reasonable fit to the observed $N_2(B)$ vibrational distributions it was necessary to use unreasonably high vibrational relaxation rate coefficients, corresponding to one transfer for every ten gas kinetic collisions. Brown concluded that vibrational relaxation in $N_2(B)$ was not adequate to explain the observed vibrational distributions. He suggested it was most likely that the vibrational relaxation occurs mainly in the precursor state.

Estimates of the depth of the ${}^5\Sigma$ potential well based on observed predissociations in other states²⁸ and on the effect of temperature on the vibrational distribution in the $B^3\Pi$ state^{6b} suggest that the ${}^5\Sigma$ state could be a direct precursor, if not the only one, of the $v = 12$ and possibly also the $v = 11$ and 10 levels of $N_2(B^3\Pi)$. For $N_2(B^3\Pi)$ levels below $v = 10$ the $A^3\Sigma$ state is a more reasonable direct precursor than ${}^5\Sigma$ on the grounds that amounts of electronic energy large compared to kT are unlikely to be dissipated into other degrees of freedom in simple collision events. Providing that molecules in the $B^3\Pi$ and $A^3\Pi$ states can be easily interconverted by collision, it is possible for the ${}^5\Sigma$ state to be the ultimate supplier of population in levels of the $B^3\Pi$ state well below the topmost emitting ones as indicated by the sequence



Our pressure dependence studies and those of others cannot be used to assess the relative importance of the several possible pathways by which molecules in various levels of $B^3\Pi$ are formed.

Nitrogen Atom Recombination. Values for the homogeneous termolecular rate coefficient for nitrogen atom recombination are summarized in Table II. Recent studies^{2a,b,2d,3} are in agreement that for $M = N_2$, $k_r = (1.0 \pm 0.2) \times 10^{-32} \text{ cm}^6 \text{ molec}^{-2} \text{ sec}^{-1}$ at room temperature. In our experiments the inconsistencies, apparently involving impurity reactions, that are associated with long time pure nitrogen decays have been avoided by using initial decay data. Initial decays on a clean Pyrex surface and on a surface coated with syrupy phosphoric acid give consistent results within experimental scatter. Experiments with added O_2 further suggested that impurity reactions are involved in N-atom removal and that O_2 is acting to quench

(28) P. K. Carroll, *J. Chem. Phys.*, **37**, 805 (1962).

Table II: Summary Results of Nitrogen Atom Recombination Studies

M	k_r^a	k_s^b	γ	Wall material or coating; method	Ref
N ₂	0.79 ± 0.1	0.13 ± 0.05		Syrupy phosphoric acid; static	This work
N ₂	1.1 ± 0.4	0.4 ± 0.1		Pyrex; static	This work
Ar	2.3 ± 0.5	0.22 ± 0.06	5 × 10 ⁻⁸	Pyrex; static	This work
He	2.2 ± 0.2	0.06 ± 0.01	5 × 10 ⁻⁸	Pyrex; static	This work
N ₂ , Ar	0.76 ± 0.06	1.44	Not detected	Pyrex; flow	2d
He	1.05 ± 0.2	1.44	Not detected	Pyrex; flow	2d
N ₂	0.96 ± 0.3	1.7	<10 ⁻⁶	Pyrex; flow	2b
N ₂	0.75 ± 0.05	<0.17	<10 ⁻⁶	Metaphosphoric acid; flow	2b
N ₂ , Ar	1.05	≤0.002	5 × 10 ⁻⁷	Stainless steel; static	3
He	0.91			Stainless steel; static	3
N ₂	1.4 ± 0.5	Not detected	2 × 10 ⁻⁶	Pyrex; flow	2c
N ₂	0.6 ± 0.3	2.7	7 × 10 ⁻⁶ ; 5.5 × 10 ^{-4c}	Fused silica; flow	21
N ₂	2.3 ± 0.9	2.8	5 × 10 ⁻⁷ ; 5 × 10 ^{-6c}	Teflon; flow	21
N ₂	2.25 ± 0.2	0.35	2 × 10 ⁻⁷ ; 2.5 × 10 ^{-6c}	Fused silica; static	21
N ₂	1.57 ± 0.2		1.5 × 10 ⁻⁶	Pyrex; flow	19
Ar	0.78 ± 0.08			Pyrex; flow	19
He	0.23			Pyrex; flow	19
N ₂	3.3 ± 0.8		3 × 10 ⁻⁵	Pyrex; flow	d
N ₂ , Ar	3.44 ± 0.4			Pyrex; flow	20
N ₂	2.9 ± 0.5		7.5 × 10 ⁻⁵	Pyrex; flow	e

^a In units of 10⁻³² cm⁶ molec⁻² sec⁻¹. Error limits for our results are calculated standard deviations based on least-squares fits and merely give a precision index for a particular set of experiments. ^b In units of 10⁻¹⁵ cm³ molec⁻¹ sec⁻¹. ^c Value of γ depended on source of nitrogen. ^d T. Wentink, J. O. Sullivan, and K. L. Wray, *J. Chem. Phys.*, **29**, 321 (1958). ^e C. Mavroyannis and C. A. Winkler, *Can. J. Chem.*, **39**, 1601 (1961).

the impurity. With added O₂, data from the entire decay can be used and give results consistent with initial decays of pure N₂. CN is a prime candidate for the impurity, and more experiments are needed to test this hypothesis.

The identity and value of the second-order coefficient, k_s , are still unresolved. Campbell and Thrush^{2d} originally proposed k_s as a second-order wall recombination coefficient. Clyne and Stedman^{2b} supported this opinion when they found that a tube coated with phosphoric acid gave a significantly lower k_s —equal to zero within their experimental error—than did a clean Pyrex tube. In our experiments decays in a clean Pyrex bulb with M = N₂, Ar, and He gave $k_s = (0.06-0.4) \times 10^{-15}$ cm³ molec⁻¹ sec⁻¹; our highest value is still a factor of 4 lower than that observed by Campbell and Thrush. Since experiments with the three buffers were performed in the same bulb the indication is that the range of values reflects our ability to determine k_s . An average result of $k_s = (0.2 \pm 0.2) \times 10^{-15}$ cm³ molec⁻¹ sec⁻¹ is reasonable. Within our experimental scatter, k_s for clean Pyrex may be zero. We did not observe the large decrease in k_s when using syrupy phosphoric acid that was observed by Clyne and Stedman. Two recent studies, one with a stainless steel surface³ and one with a Pyrex surface,^{2c} failed to detect k_s .

It can be seen from Table II that agreement is poor on the absolute and relative effects of different third bodies on k_r . We find that Ar and He increase the

observed k_r by about a factor of 3 relative to the pure nitrogen value. Campbell and Thrush report that Ar and N₂ have similar k_r values while He is 50% higher. Becker, *et al.*,³ report similar results for Ar, He, and N₂ third bodies. Herron, *et al.*,¹⁹ report results for He and Ar that are significantly lower than those for N₂. More careful experiments are required to clarify the third-body effect on k_r .

Luminous Efficiency of the Afterglow and the Vibrational Distribution in the B³Π_g State. Our results on the pressure dependence of the afterglow and the rate of homogeneous recombination when combined with absolute intensity measurements give the relationship between the rate at which molecules are formed and the rate at which photons are emitted. At pressures above 1 Torr in pure nitrogen eq 1 reduces to $I = K[N]^2/(k\tau_B)$; *i.e.*, the specific intensity is pressure independent. A value for the absolute intensity at a known atom concentration, when combined with our value for $k\tau_B$, gives an absolute value for K . Two absolute intensity measurements^{5,25} on First Positive bands in the afterglow with M = N₂ were corrected using the relative intensities of Bayes and Kistiakowsky^{6b} and Brown⁵ to give the total absolute intensity for the First Positive system. An average value of $K = 4 \times 10^{-33}$ cm⁶ sec⁻¹ was obtained. Combining eq 1 with $d[N_2]/dt = 1/2k_r[N]^2[M]$ gives the result

$$(\text{molecules formed/photons emitted}) = \frac{(1/2k_r/K)(k\tau_B[M] + 1)}{(1/2k_r/K)(k\tau_B[M] + 1)} \quad (10)$$

The ratio of the rate of molecule production to the rate of photon emission is directly proportional to pressure. Using our values for $k_r(\text{N}_2)$ and $k_{\text{N}_2\tau\text{B}}$ and the above estimate for K it may be seen that in the limit of zero pressure about 1.3 molecules per photon are formed. At 5 Torr this ratio has increased to about 55. At higher pressures the $\text{N}_2(\text{B})$ state or its precursor are significantly involved in nonradiative reactions.

In making our estimate of K we have not allowed for the possibility that one molecule might emit more than one photon in a $\text{B} \xrightarrow{\text{emission}} \text{A} \xrightarrow{\text{collision}} \text{B} \xrightarrow{\text{emission}} \text{A}$ cascade process. The levels $v = 7-13$ of the A state overlap the energy range of levels $v = 0-4$ of the B state. We estimate that 69% of all emission events from levels $v = 6-12$ in the B state terminate on levels $v = 7-13$ of the A state. On the other hand the total emission rate from levels $v = 6-12$ of the B state is about 36% of that from all levels of the B state. Therefore, if this cascade process were extremely efficient, it could account for at most 25% of the total emission from the B state. The correction to K does not seem justified at present in view of the probable inaccuracy of the absolute intensity and the lack of evidence about the efficiency of cascading.

The possibility of cascading may also be looked at from the standpoint of assessing the potential importance of the $^5\Sigma$ mechanism. The total emission from levels $v = 12, 11,$ and 10 of the $\text{B}^3\Pi$ state amounts to some 28% of all emission from the B state, and 87% of all the emission events from these top three levels could give rise to subsequent cascade emission. In other words, the potentiality for cascading is almost entirely the property of the top three emitting levels of the B state, just those levels which might be populated directly from the $^5\Sigma$ state. Therefore, on this basis alone the $^5\Sigma$ mechanism could account for over half of all the light emitted by the B state if cascading were very efficient. This, together with the possibility alluded to previously that the $^5\Sigma$ mechanism could populate lower levels of B through collisional interchange between B and A and vibrational relaxation in A, means that the $^5\Sigma$ mechanism cannot be lightly discarded or ignored as a minor contributor to the afterglow. Furthermore, it must be remembered that in all that has been said, the direct and indirect contributions to light production made by the $\text{B}'^3\Sigma_u^-$ state have not been taken explicitly into account, and insofar as this state may be populated by the $^5\Sigma$ mechanism, the importance of the $^5\Sigma$ mechanism may be enhanced.

Finally, the special role of the top three emitting levels of $\text{B}^3\Pi$ in the afterglow is apparent on a graph of the steady-state vibrational populations of this state as shown in Figure 10. The relative populations in this figure were estimated using the combined relative intensity data of Bayes and Kistiakowsky^{6b} and Brown,⁵ the lifetimes of Jeunehomme,¹⁸ and the Franck-Condon

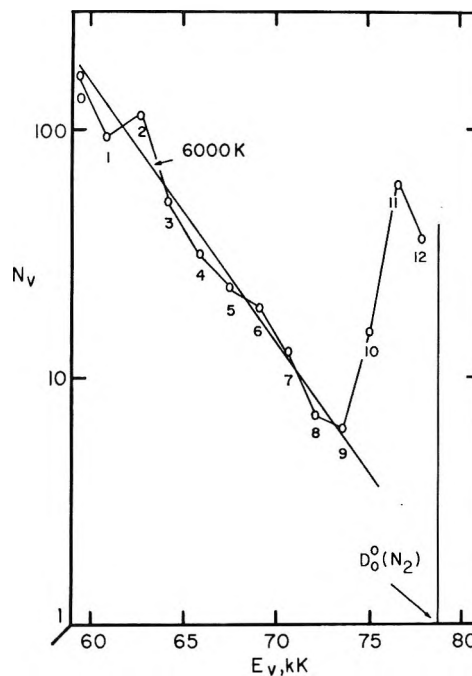


Figure 10. Vibrational distribution of the $\text{B}^3\Pi_g$ state in the pure nitrogen afterglow at room temperature. Vibrational level numbers are shown near the points. The energies of the levels are measured with respect to the lowest real level of the ground electronic state.

factors of Benesch, *et al.*²⁹ The results apply to pure nitrogen at pressures in the 1–10 Torr range at room temperature. It should be noted that the population peak at $v = 11$ is not the result of a peculiar pattern of transition probabilities but is preserved on a graph of relative total emission rates from the various levels. This means that if the rate constants of nonradiative processes which destroy $\text{B}^3\Pi$ molecules in various levels are comparable to one another—as the quenching results to date suggest—the actual rates of formation of molecules in the 11th and 12th levels must be considerably greater than those for all but the lowest three levels. If all levels of the B state were presumed to be populated from the A state, as in the CT mechanism, a rather special pattern of collisional transfer rate constants would have to be advanced to account for the observed population distribution. We are unaware of arguments which would make such a special pattern plausible, and the eventual quantitative assessment of the role played by the $^5\Sigma$ state may render the invention of such arguments unnecessary.

Acknowledgments. We are particularly grateful to Dr. R. L. Brown for participating in many stimulating, critical discussions of this work and for providing us with his results prior to publication. We wish to thank Pamela Schain, as she then was, for assisting with some

(29) W. Benesch, J. T. Vanderslice, S. G. Tilford, and P. G. Wilkinson, *Astrophys. J.*, **144**, 408 (1966).

of the early experimental work. Finally, one of us (W. B.) would like to thank Professor G. B. Kistiakowsky for kindling his interest in the baroque intricacies of

the nitrogen afterglow problem and for demonstrating the possibility of imposing order on manifest kinetic chaos.

The Absorption Spectrum of Benzene Vapor near 2537 Å^{1a}

by G. H. Atkinson^{1b} and C. S. Parmenter*

Department of Chemistry, Indiana University, Bloomington, Indiana 47401 (Received January 25, 1971)

Publication costs assisted by the National Science Foundation

The absorption spectrum of benzene vapor in the region of the Hg resonance line at 2536.52 Å has been re-examined. An absorption band not previously reported is seen to be nearly coincident with the position of the Hg line. Assignments of the five or six absorption bands overlapping the Hg line are considered. Specific assignments for three of these bands and possible assignments for the others are derived. These assignments are summarized in Table II.

Introduction

The vibrational levels excited in the first singlet (¹B_{2u}) state of benzene by absorption of light from the 2537-Å Hg line have been used by many workers as the starting point for investigations of excited-state relaxation processes. The majority of these studies probe electronic energy transfer and sensitized photochemical reactions.² Others use these levels for exploration of vibrational relaxation^{3a,b,4} and for experimental characterization of intersystem crossing.⁴⁻⁶ A few investigations have also used these levels as precursors to the photodecomposition of benzene itself.⁷

In view of such extensive study, it is remarkable that the identity of these levels has never been carefully worked out. Their assignments remain largely unknown.

In this and the following paper, efforts to provide that information are described. In the present paper, results from a general reexamination of the entire ¹B_{2u}-¹A_{1g} absorption system of benzene⁸ are used for a detailed analysis of the 2537-Å region. This provides a list of possible assignments for the absorption bands overlapping the position of the Hg line. In the following paper, some of those assignments are confirmed and others rejected by an analysis of the resonance fluorescence spectrum excited by the Hg line.

It is appropriate that these reports appear among papers dedicated to G. B. Kistiakowsky, for he was among the first to recognize the experimental virtues of benzene and the 2537-Å line. In 1932, he reported with Nelles⁹ the first really detailed characterization

of resonance fluorescence excited in benzene by absorption from that line. In 1936, he and Cuthbertson¹⁰ provided an analysis of that spectrum which correctly identified many of the progressions despite the fact that the vibrational frequencies and excited electronic states of benzene were then largely unknown. In 1937, Kistiakowsky and Solomon¹¹ further advanced the understanding of benzene by showing that the 160-cm⁻¹ band spacing seen throughout the 2600-Å spectrum was not a vibrational fundamental but rather a

(1) (a) Contribution No. 1912 from the Chemical Laboratories of Indiana University. We are grateful for a grant from the National Science Foundation which has made this work possible. (b) National Institutes of Health Predoctoral Fellow.

(2) Two reports particularly fundamental to subsequent energy transfer studies are H. Ishikawa and W. A. Noyes, Jr., *J. Chem. Phys.*, **37**, 583 (1962), and R. B. Cundall and T. F. Palmer, *Trans. Faraday Soc.*, **56**, 1211 (1960). For a review, see R. B. Cundall in "Transfer and Storage of Energy by Molecules," Vol. 1, G. M. Burnett and A. N. North, Ed., Wiley-Interscience, London, 1969, pp 1-63.

(3) (a) H. F. Kemper and M. Stockburger, *J. Chem. Phys.*, **53**, 268 (1970), and earlier references therein; (b) L. M. Logan, I. Buduls, and I. G. Ross, "Molecular Luminescence," E. C. Lim, Ed., W. A. Benjamin, New York, N. Y., 1969, p 53.

(4) C. S. Parmenter and A. H. White, *J. Chem. Phys.*, **50**, 1631 (1969).

(5) G. B. Kistiakowsky and C. S. Parmenter, *ibid.*, **42**, 2942 (1965); E. M. Anderson and G. B. Kistiakowsky, *ibid.*, **48**, 4787 (1968); E. M. Anderson and G. B. Kistiakowsky, *ibid.*, **51**, 182 (1969).

(6) C. W. Mathews and A. E. Douglas, *ibid.*, **48**, 4788 (1968).

(7) For example, see L. Kaplan and K. E. Wilzbach, *J. Amer. Chem. Soc.*, **90**, 3291 (1968).

(8) G. H. Atkinson and C. S. Parmenter, to be published.

(9) G. B. Kistiakowsky and M. Nelles, *Phys. Rev.*, **41**, 595 (1932).

(10) G. R. Cuthbertson and G. B. Kistiakowsky, *J. Chem. Phys.*, **4**, 9 (1936).

(11) G. B. Kistiakowsky and A. K. Solomon, *ibid.*, **5**, 609 (1937).

1-1, 2-2, ... sequence structure in a low-frequency vibration. Most recently, he has shown⁵ that excitation of benzene with the Hg line provides an ideal system with which to probe radiationless transitions in isolated molecules.

Notation

The scheme devised by Callomon, Dunn, and Mills¹² along with the vibrational mode numbering of Wilson¹³ is used to describe transitions. This notation can be illustrated by the example $6_1^2l_1^2l_0^1$. The large numbers indicate the vibrational modes that change quanta during the transition. The superscripts denote the quanta of a given mode in the upper (${}^1B_{2u}$) electronic state of the transition and the subscripts denote the quanta in the lower state (${}^1A_{1g}$). When a degenerate mode is multiply excited, the letter l is used to denote the specific angular momentum components associated with the transition, with super- and subscripts indicating the upper and lower states, respectively. Thus the transition given above is between the ${}^1B_{2u}$ state with $v_6' = 2$ ($l_6' = 2$), $v_1' = 1$ and the ground ${}^1A_{1g}$ state with $v_6'' = 1$ ($l_6'' = 1$), $v_1'' = 0$.

Assignment Criteria

The spectral region of interest for the present analysis is only a small (60 cm^{-1}) segment of an absorption system extending over almost $10,000\text{ cm}^{-1}$. Assignments of bands in that segment must obviously derive from a more general assignment of vibronic structure throughout the entire spectrum. An extension and refinement of those assignments has recently been made⁸ using new information on vibronic activity contained in fluorescence spectra from single vibronic levels of benzene.^{14,15} The extended assignments now form the basis for a more detailed examination of the $2537\text{-}\text{\AA}$ absorption region.

The new work on assignments has started with the results in three of the many papers concerned with the benzene problem. The first of these is that of Radle and Beck¹⁶ which provides the most complete compilation presently available of the positions and relative intensities of the benzene absorption bands. We use these positions and generally the intensities without modification. The second is the assignment of the more prominent features of the spectrum by Garforth and Ingold (GI)¹⁷ which provides an essentially correct fundamental interpretation of the spectrum. The last paper is that of Callomon, Dunn, and Mills (CDM).¹² It provides the rotational analysis necessary to relate vibronic band origins with band maxima and to unravel the nature of the spectrum where much overlapping structure exists. CDM have also presented helpful refinements, corrections, and extensions to the assignments of GI.

In the sections below, some general criteria governing assignments in the ${}^1B_{2u}\text{-}{}^1A_{1g}$ absorption spectrum are

given. Then in the following sections, the spectrum in the $2537\text{-}\text{\AA}$ region is described and assignments are proposed.

Vibronic Selection Rules. The symmetry selection rules governing vibronic activity in the ${}^1B_{2u}\text{-}{}^1A_{1g}$ transition are described in two excellent reviews¹⁸ and are set forth by CDM in a particularly useful form. The principal constraint is that vibrations must generate a component of e_{2g} symmetry in order to induce the otherwise forbidden transition. The most important single and binary combinations of active vibrational symmetries in benzene that can induce the transitions are given below.

Type of transition	Allowed vibrational species
X_0^1, X_1^0	e_{2g}
X_0^2, X_2^0, X_1^1	e_{1g}, e_{2g}, e_{2u}
$X_0^1Y_0^1, X_1^0Y_1^0, X_0^1Y_1^0$	$e_{2g} \times a_{1g}, e_{2g} \times e_{2g},$ $e_{2u} \times e_{2u}, e_{2u} \times a_{2u}$

The symmetries and selection rules for the specific angular momentum components of degenerate vibrations can be derived by simple procedures presented elsewhere.^{12,19}

In addition, quantum changes in other vibrations may combine with those changes above that induce the transition. These typically appear as $\Delta v_x = \pm 2$ or as 1-1, 2-2, ... sequence transitions. The totally symmetric vibrations ν_1 and ν_2 are active without restriction. The mode ν_1 is responsible for progressions seen throughout absorption and fluorescence.

Vibronic Activity in the ${}^1B_{2u}\text{-}{}^1A_{1g}$ Transition as Derived from Single Vibronic Level Fluorescence. The recent acquisition^{14,15,20} of fluorescence spectra from various single vibronic levels (SVL fluorescence) in the ${}^1B_{2u}$ state of benzene vapor has been helpful in assignment of the absorption spectrum. Analysis of SVL fluorescence is an easier task than absorption analysis because fluorescence transitions in general involve only ground-state vibrational frequencies, and these are well known from infrared and Raman studies. Because of this, many SVL fluorescence spectra have

(12) J. H. Callomon, T. M. Dunn, and I. M. Mills, *Phil. Trans. Roy. Soc. London, Ser. A*, **259**, 499 (1966).

(13) E. B. Wilson, Jr., *Phys. Rev.*, **45**, 706 (1934).

(14) C. S. Parmenter and M. W. Schuyler, *J. Chim. Phys.*, **92** (1970).

(15) C. S. Parmenter and M. W. Schuyler, *J. Chem. Phys.*, **52**, 5366 (1970).

(16) W. F. Radle and C. A. Beck, *ibid.*, **8**, 507 (1940).

(17) F. M. Garforth and C. K. Ingold, *J. Chem. Soc. (London)*, 417 (1948).

(18) T. M. Dunn, "Studies on Chemical Structure and Reactivity," J. H. Ridd, Ed., Methuen, London, 1966, p 103-132; G. Herzberg, "Electronic Spectra of Polyatomic Molecules," Van Nostrand, Princeton, N. J., 1966, pp 555-561.

(19) I. M. Mills, *Mol. Phys.*, **7**, 549 (1964).

(20) M. W. Schuyler, Ph.D. Thesis, Indiana University, Bloomington, Ind., 1970.

been analyzed, and examination of those assignments reveals an accurate picture of the activity of vibrations in the ${}^1B_{2u}-{}^1A_{1g}$ transition. This activity should be consistent in both fluorescence and absorption.

Vibronic transitions in fluorescence are entirely consistent with the selection rules developed from the absorption spectrum, but additional constraints on the activity of the various modes are also seen. Only eight vibrational frequencies are required to describe the significant structure in SVL fluorescence spectra. The other frequencies appear essentially inactive. Vibrational activity in fluorescence is limited to the modes ν_1 , ν_6 , ν_7 , ν_9 , ν_{10} , ν_{11} , ν_{16} , and ν_{17} .

To this list of modes active in the ${}^1B_{2u}-{}^1A_{1g}$ transition, one must add the mode ν_2 . Its activity can be seen in absorption where it is responsible for weak transitions. Observation of ν_2 in fluorescence is difficult because its high frequency ($\nu_2 = 3073 \text{ cm}^{-1}$) causes fluorescence bands with activity in ν_2 to fall in a region badly congested by members of many ν_1 progressions. This is probably the reason why the weak transitions in ν_2 are not identified in SVL fluorescence.

Thus a list of nine active vibrational frequencies is compiled from the complete set of 20.²¹ The active vibrations are listed with their best values in Table I. By using this set of vibrations in the simplest combinations allowed by the selection rules, plausible assignments of nearly all the significant bands in the absorption spectrum can be obtained.

Table I: Ground- and Excited-State Frequencies of Those Vibrations Known to Be Active in the Absorption and Fluorescence Spectra of Benzene

—Normal modes—		D_{3h} symmetry	—Fundamental frequencies—	
W.D.C. ^a	H. ^b		${}^1A_{1g}$ state ^c	${}^1B_{2u}$ state
1	2	a_{1g}	993.1 ^d	923
2	1		3073	3130
6	18	e_{2g}	608.0 ^e	522.4 ^e
7	15		3056	3077.2 ^e
9	17		1178	
10	11	e_{1g}	846	585 ^e
11	4	a_{2u}	674.0 ^e	514.8 ^e
16	20	e_{2u}	398.6 ^e	237.3 ^e
17	19		967	719 ^f

^a See ref 13. ^b G. Herzberg, "Infrared and Raman Spectra of Polyatomic Molecules," Van Nostrand, New York, N. Y., 1945. ^c Ground-state values from S. Broderson and A. Langseth, *Kgl. Dan. Vidensk. Selsk., Mat. Fys. Skr.*, **1**, No. 1 (1956), except where noted. ^d Correction to value listed by ref 12. ^e From ref 12. ^f From G. H. Atkinson, unpublished work.

Vibrational Frequencies. Most of the ground-state frequencies in Table I have been obtained from infrared and Raman work while most of the excited-state frequencies have been derived from analysis of the vibronic absorption spectrum. These frequencies form

the basis for the calculated positions of band maxima. It should be noted that the precise calculation of the position of a band maximum requires a complete anharmonic expression for the vibrational energy. Without a detailed understanding of the constants in such an expression (and in some cases also Coriolis coefficients), calculated positions for band maxima are only approximate. Unfortunately, the anharmonic constants are presently not available for most modes.

Additional Constraints on Assignments. A number of other criteria have been used to support or reject a proposed assignment that otherwise is in accord with selection rules and fits the position of a band maximum. These might be termed consistency checks. For example, many bands are easily identified as progression members. Other bands are recognized as members of sequences in ν_{16} (16_1^1) by the 160-cm^{-1} separation between a sequence band and its parent. The assignments must be consistent with this knowledge.

Intensities of bands also provide help with assignments. The relative intensities of progression members must be approximately that predicted by the Franck-Condon factors.²² For example, progressions from $\nu_1'' = 1$ are easily recognized by the unusually low intensity of the 1_1^1 member. The intensities must be consistent with Boltzmann factors for proposed assignments of hot bands. The relative intensities of various types of progression origins must correspond roughly with that seen for analogous progression origins in SVL fluorescence.

Further checks derive by searching for additional structure expected to be present as corollaries of proposed assignments. For example, the appearance of the hot band $6_1^0 11_0^2$ would also require the presence of the band $6_1^2 11_0^2$ with nearly equivalent intensity. In addition, the cold band $6_0^1 11_0^2$ and its sequence $6_0^1 11_0^2 16_1^1$ should be easily seen. Checks such as these will be used in the specific assignment discussed below.

The 2537-Å Region of Absorption

The absorption spectrum of benzene in the region of the 2537-Å Hg line is shown in Figure 1. The upper spectrum is from a sample of benzene containing Hg at its vapor pressure. The position of the Hg line is clearly marked by its intense absorption at $39,412 \text{ cm}^{-1}$. The lower spectrum is obtained by exciting a mercury-free sample of benzene with a xenon arc carefully selected to be free of Hg structure. The continuum from the lamp alone is shown at the bottom of Figure 1.

One should note that an absorption maximum at about $39,412 \text{ cm}^{-1}$ still appears in the lower benzene

(21) It should be emphasized that the classification of a vibration as active or inactive in the spectrum is one of degree. The principal optical activity is contained in the vibrational modes classified as "active." Other modes are probably also "active," but they contribute only to structure of very weak intensity.

(22) D. P. Craig, *J. Chem. Soc.*, 2146 (1950); W. L. Smith, *Proc. Phys. Soc. London (At. Mol. Phys.)*, 89 (1968).

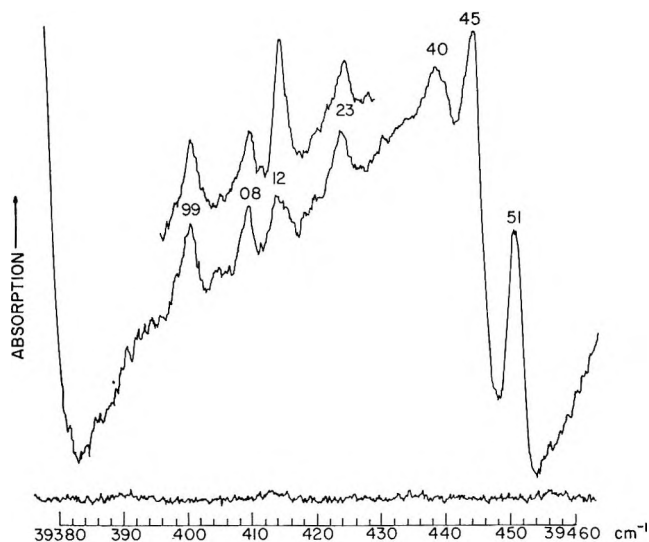


Figure 1. The absorption spectrum of benzene vapor near 2537 Å. The top spectrum is from benzene containing Hg at its room temperature vapor pressure. The sharp absorption near 39,412 cm^{-1} is that of Hg. The middle spectrum is from benzene vapor carefully handled to be free of Hg. The bottom spectrum is the xenon continuum used in obtaining the upper spectra. The precise positions of the absorption bands are given in Table II. The scale is cm^{-1} (vac).

spectrum even though Hg is completely absent. This absorption maximum has not been previously reported,¹⁶ presumably because it is obscured by mercury in the lamps and/or the sample. It must play a significant role in the absorption of 2537-Å excitation. This band is part of a ν_1' progression with related members elsewhere in the spectrum, so that the structure is not an artifact of residual Hg in the benzene sample.

A determination of which bands are pumped in absorption can be made from the rotational analysis provided by CDM. Their analysis of band contours in the absorption spectrum indicates that observable band contours fall into one of two general types which differ only in a relatively minor way. Both are characterized by a sharp high-energy edge whose onset is within about 2 cm^{-1} of the band maximum. The band degrades slowly to the low-energy side of the maximum so that each band has a long "rotational tail." This tail can be seen to extend in excess of 50 cm^{-1} for strong bands in relatively open areas of the spectrum. Examples are shown in Figure 2.

The known contours suggest that bands with maxima at higher energy than the Hg line at 39,412 cm^{-1} may overlap that position with their rotational tails. Bands more than a few cm^{-1} to lower energy will miss the Hg line.

The highest energy absorption bands that will overlap the Hg line with appreciable strength are the intense bands at 39,451 and 39,445 cm^{-1} . These are so strong relative to other bands in the 2537-Å region that they may be expected to be dominant in absorption. The band whose maximum at 39,412 cm^{-1} is nearly coinci-

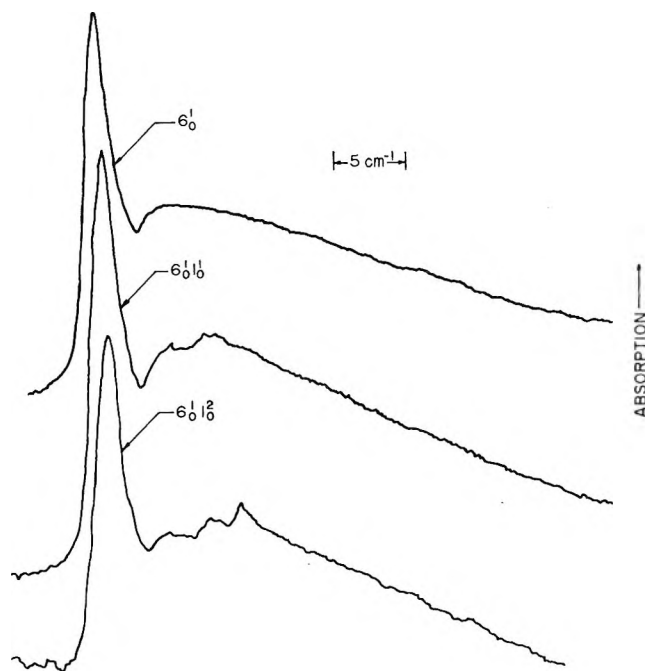


Figure 2. The A_0^0 , A_1^0 , and A_2^0 absorption bands¹⁶ (top to bottom) of benzene vapor. The transitions responsible for the sharp maxima are indicated. The positions of those maxima are 38,612.2, 39,534.2, and 40,456.0 cm^{-1} (vac), respectively. The small structure appearing on top of the subsidiary maxima in the lower two is from the transitions $17_0^2/0^2$ and $17_0^2/0^2 1_0^1$. Wave number decreases from left to right.

dent with the Hg line will also participate significantly in absorption even though it is very weak. The very weak bands with maxima at 39,440 and 39,423 cm^{-1} may also contribute to absorption, but because of the presence of the stronger bands, it is impossible to assess the strength of their rotational structure at the position of the mercury line.

Bands at lower energies seem less likely candidates for absorption of Hg radiation. The band with a maximum at 39,408 cm^{-1} is probably too far away from the Hg line for significant excitation (unless a pressure broadened Hg line is used), but one cannot discount 39,408 cm^{-1} absorption with certainty. Only a very minor departure from the contours most commonly seen among stronger bands will bring this band onto the Hg line. It does seem certain, however, that the band at 39,399 cm^{-1} and those lower in energy cannot be excited by the Hg line.

Assignment

The assignments of bands appearing in the 2537-Å region are summarized in Table II. The three high-energy maxima can be associated with specific transitions, but only a set of possibilities can be compiled for the remaining bands.

The absence of specific assignments for bands other than the high-energy maxima requires further comment. It stems from the fact that the bands are ex-

Table II: Absorption Bands and Assignments in the Benzene Spectrum near 2537 Å

Band maximum position, cm^{-1} vac	Assignment ^a
39,451.0	$6_1^2l_1^2l_0^1$
39,445.3	$6_1^2l_1^0l_0^1$
39,440.1	$6_1^0l_1^0l_0^1$
39,423.1	$\left\{ \begin{array}{l} 6_1^0l_0^2l_1^1l_0^1 \\ 16_0^2l_1^2 \\ 6_1^2l_1^0l_0^1l_1^1 \\ 6_0^1l_1^2l_0^1 \\ 6_0^1l_1^2l_0^1 \end{array} \right.$
39,412	
39,408.5	
39,398.9	

^a The positions of assignments within the bracket cannot be predicted with sufficient accuracy to associate them with a specific absorption band. They comprise a list of possibilities for those band maxima covered in the adjacent bracket. Each of the possible transitions may have sufficient intensity to be observed in absorption.

ceedingly weak.²³ They rank with the very minor structure of the ${}^1B_{2u} \rightarrow {}^1A_{1g}$ transition. Assignments of such structure usually involve either combinations of a number of different vibrations or high quantum levels in specific vibrations. As a result, the cumulative uncertainties in the anharmonic frequencies become important and preclude precise calculation of band portions. In such assignments, little confidence can be derived from close match of a calculated position with an observed position, nor can much significance be attached to a mismatch that may even exceed 10 cm^{-1} . In view of these uncertainties, heavy reliance is placed in this paper on criteria other than calculated positions for assignments of weak transitions.

The basis for each assignment in Table II is given in the following sections.

$6_1^2l_1^0l_0^1$ and $6_1^2l_1^2l_0^1$. The bands near $39,445 \text{ cm}^{-1}$ are members of the second most intense progression in the spectrum and hence have a considerable history of assignments. GI bracketed the maxima at 39,440, 39,445, and $39,451 \text{ cm}^{-1}$ with the assignment $6_1^2l_0^1$. CDM subsequently sought refinement by assigning the two components $6_1^2l_1^0$ and $6_1^2l_1^2$ of the progression origin to maxima at $38,518$ and $38,523 \text{ cm}^{-1}$, respectively. These are the bands C and D in the C_0^0 spectrum shown in Figure 3. This assignment requires (by adding $\nu_1' = 923 \text{ cm}^{-1}$) the components $6_1^2l_1^0l_0^1$ and $6_1^2l_1^2l_0^1$ to be the maxima at $39,440$ and $39,445 \text{ cm}^{-1}$, respectively (bands C and D of the C_1^0 spectrum in Figure 3). This selection leaves the strong maximum at $39,451 \text{ cm}^{-1}$ both unrelated and unassigned. There is a considerable body of evidence, however, to suggest that a close relationship between the maxima D and M throughout the C_n^0 progression does exist (Figure 3). In fact, this pair rather than the pair C–D chosen by CDM seems a better choice for the angular momentum components of the transition $6_1^2l_0^1$.

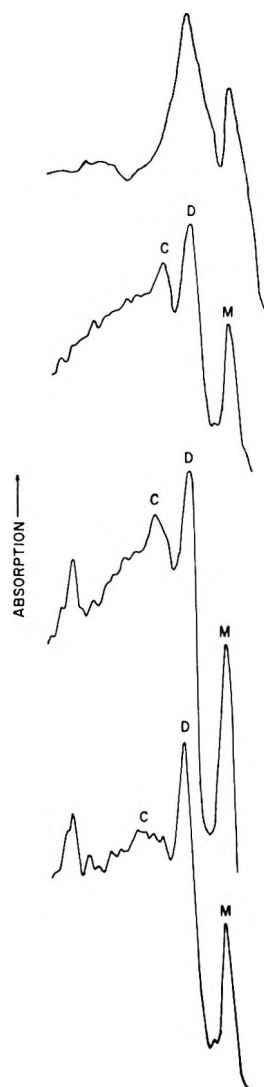


Figure 3. The upper spectrum is a synthesis made by overlapping the A_0^0 band (Figure 2) with itself, but with the vibronic origin of one displaced 6 cm^{-1} from the other. A tracing of the A_0^0 band given in CDM¹² was actually used for the construction. Wave number increases linearly from left to right. The remaining spectra are the C_0^0 , C_1^0 , and C_2^0 absorption bands,¹⁶ top to bottom. The positions of the maxima labeled D are $38,523.0$, $39,445.3$, and $40,366.4 \text{ cm}^{-1}$ (vac), respectively. The separation between D and M in the C_0^0 band is about 6 cm^{-1} .

Evidence comes from various sources. One may first consider the band contours associated with such transitions. Both of vibronically allowed l_1^0 and l_1^2 components are predicted to have CDM type I contours.¹² Such a contour is shown in Figure 2. To reproduce the appearance of the pair of angular momentum components, one must consider an overlapping composite of two type I bands with vibronic origins

(23) Radle and Beck¹⁶ list moderate intensity for some of these, but as can be seen in Figure 1, most of that intensity derives from the underlying rotational tails of the strong maxima at $39,445$ and $39,451 \text{ cm}^{-1}$. The actual intensities of those bands are probably less than a third of that indicated by Radle and Beck.

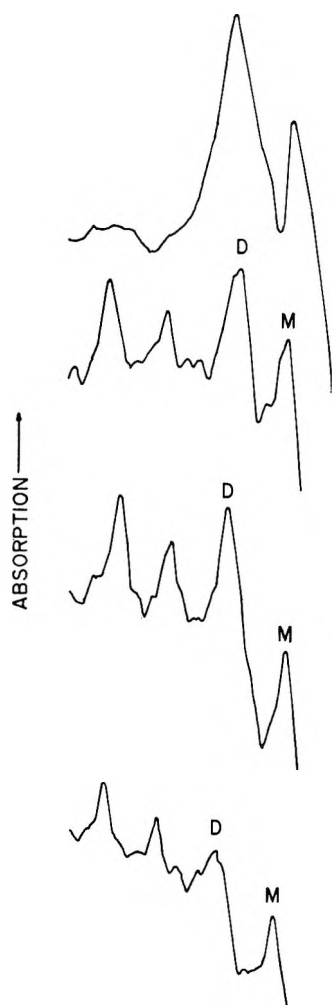


Figure 4. The upper spectrum is taken from the upper spectrum of Figure 3. The lower spectra are the C_0 , C_1 , and C_2 absorption bands¹⁶ (top to bottom) of benzene vapor. The maxima D are at 38,359.7, 39,281.4, and 40,202.5 cm^{-1} (vac). Wave number increases linearly from left to right and the separation from D to M is about 6 cm^{-1} .

separated by about 6 cm^{-1} . Such a construction is shown at the top of Figure 3. Distinctive double maxima appear which closely match the pair D–M at 39,451–39,445 cm^{-1} , but which bear only poor relationship to the pair C–D at 39,445–39,441 cm^{-1} .²⁴

The assignment of angular momentum components to the pair D–M also accounts for the consistent relationship of intensities and wave number separations shown by this pair in the progression members 1_0^0 , 1_0^1 , 1_0^2 appearing in Figure 3. In contrast, the relative intensity of the pair C–D is variable, particularly in the 1_0^2 progression member. The band C seems unrelated to D.

Similar correlations may be seen in the ν_{16} sequence of this progression. The progression $6_1^2 1_0^2 1_0^1$ is shown in Figure 4 with n running from 0 to 2. The high-energy pair D–M again maintains a consistent relationship, while structure at lower energies looks quite unrelated. Furthermore, the relative intensities of the bands D

and M match closely those seen in the parent progression in Figure 3. The structure at lower energies displays inconsistency between the two progressions, both in intensity and in displacement from the higher-energy band pair.

One must also consider the problem of assigning the 39,451- cm^{-1} maximum if it is to be excluded from the $6_1^2 1_0^1$ components. Its very strong intensity would almost demand that it be a member of a progression induced by an e_{2g} vibration appearing either by itself or in binary combination with another mode. However, it has not been possible to assign the band on this basis, nor has it been possible to assign it using any allowed binary combinations of active modes. It also seems most improbable that a band of such intensity could involve a tertiary or higher combination of active modes or involve modes not listed in Table I. Consequently, no alternate assignment of this band becomes apparent. This seems to be another compelling indication that it is one of the $6_1^2 1_0^1$ angular momentum components. (It should be remarked here that a similar dilemma does not exist for the rejected band at 39,440 cm^{-1} . A well supported assignment for it exists and is discussed later in the paper.)

There is thus a significant body of evidence (unfortunately none of it unique) to support the assignment of the bands at 39,445 and 39,451 cm^{-1} as the angular momentum components of the $6_1^2 1_0^1$ transition. On the other hand, little evidence can be found to support the assignment of the alternate pair of bands to this transition. Accordingly, the suggested assignments are

39,451.0 cm^{-1}	$6_1^2 l_1^2 1_0^1$
39,445.3 cm^{-1}	$6_1^2 l_1^0 1_0^1$

These assignments require revision of the vibrational constants for ν_6' . The new constants are most satisfactorily computed from the $6_1^2 l_1^2 \cdot 0_1^0$ progression origins. Therefore, with $6_1^2 l_1^2$ appearing at 38,529.3 cm^{-1} , $6_1^2 l_1^0$ appearing at 38,523.0 cm^{-1} , and 6_1^0 appearing¹² at 38,612.2 cm^{-1} , the vibrational constants for ν_6' become $\omega_6^{0'} = 520.9 \text{ cm}^{-1}$, $x_{6,6}^{0'} = -0.115 \text{ cm}^{-1}$ and $g_{6,6}^{0'} = 1.575 \text{ cm}^{-1}$.

$6_1^0 1_1^0 1_0^1$. The strongest transition involving ν_{11} is expected to be $6_0^1 1_1^0$, and the original assignment¹⁷ of this transition to the 39,638.2- cm^{-1} band appears firmly established.^{8,12} From the strong intensity of that band, it is expected that three other transitions in ν_{11} will appear with at least moderate intensity. These are the transitions $6_1^2 l_1^0 1_1^0$, $6_1^2 l_1^2 1_1^0$, and $6_1^0 1_1^0$. However, assignment of these transitions does not follow directly from the 1026- cm^{-1} value of $2\nu_{11}'$ de-

(24) This construction does not provide unique evidence for assignment of the higher energy pair because the reproduction of their structure depends on assuming that both components are of equal intensity. There is no evidence to deny this assumption, but little is known about the problem.

rived from the $6_0^111_0^2$ band. The calculated maxima for $6_1^2l_1^011_0^2$, $6_1^2l_1^211_0^2$, and $6_1^011_0^2$ with $2\nu_{11}' = 1026 \text{ cm}^{-1}$ all lie about $6\text{--}9 \text{ cm}^{-1}$ to the red of moderately strong, unassigned maxima. Alternate assignments for these maxima have been sought, but none were found to be as satisfactory as those involving ν_{11} . In view of their expected activity and the absence of other assignments, the assignments of the $6_1^2l_1^011_0^2$, $6_1^2l_1^211_0^2$, and $6_1^011_0^2$ transitions to the 39,460-, 39,468-, and 39,517- cm^{-1} bands appear to be correct.

The assignment of the $6_1^011_0^21_0^1$ progression member to a band in the Hg region is derived directly from the discussion above. When calculated with the value $2\nu_{11}' = 1026 \text{ cm}^{-1}$, it is predicted to have a maximum near $39,431 \text{ cm}^{-1}$. We have assigned it as the band maximum at $39,440 \text{ cm}^{-1}$ which exhibits the typical $6\text{--}9\text{-cm}^{-1}$ discrepancy in position. Two aspects of this require further comment. The variance between the observed and calculated positions may arise from rather strong coupling of ν_{11} with other modes. Its frequency calculated from seven progression origins is seen to vary between the limits 513.0 and 519.6 cm^{-1} (about a 1% variation). This is shown in Table III.

Table III: Transitions Related to $6_1^011_0^21_0^1$

Transition	Observed position, cm^{-1}	Relative intensity	Derived value ^a of ν_{11}' , cm^{-1}
$6_0^111_0^2$	39,638.2	335	513.0
$6_1^011_0^2$	38,517.4	210	517.8
$6_1^2l_1^011_0^2$	39,560.8	335	518.9
$6_1^2l_1^211_0^2$	39,568.7	250	519.6
$11_0^116_0^1$	38,839.7	35	515.7
$11_0^116_1^c$	38,204.3	55	514.8
$11_1^016_0^1$	37,651.4	10	516.2

^a The constants for $\nu_6' = 1$, $\nu_6'' = 1$, $\nu_{16}' = 1$, and $\nu_{16}'' = 1$, the value of the electronic origin, and the vibronic origin-to-peak separation is taken from CDM. The constants for $\nu_6' = 2$, $l' = 2$, and $\nu_6'' = 2$, $l = 0$ are calculated elsewhere in this work.

The second point concerns evidence that the maximum at $39,440 \text{ cm}^{-1}$ is a separate transition rather than solely rotational structure from the $6_1^21_0^1$ transition. It can be seen from Figure 3 that even though the rotational structure associated with the $6_1^2l_1^01_0^1$ and $6_1^2l_1^21_0^1$ transitions is still strong at $39,440 \text{ cm}^{-1}$, it cannot account for the rounded maximum that is seen. Hence, a transition of moderate intensity, such as $6_1^011_0^21_0^1$, seems to appear on top of the rotational structure at that position. Supporting evidence can be found in the progression member immediately above and below the $39,440\text{-cm}^{-1}$ positions in Figure 3. At the $6_1^011_0^2$ position, a maximum C, similar to the one at $39,440 \text{ cm}^{-1}$, is clearly visible. Analogous structure exists in the $6_1^011_0^21_0^2$ region as well. Furthermore, while the intensity of C relative to the pair D and M

Table IV: Transitions Related to $6_1^211_0^216_1^1$

Transition	Observed band maximum, cm^{-1}	Relative intensity
$6_1^2l_1^011_0^2$	39,560.8	335
$6_1^2l_1^211_0^2$	39,568.7	250
$6_0^111_0^2$	39,638.2	335
$6_0^111_0^216_1^1$	39,473	55

remains similar in the first two members of the progression, the intensity of C is significantly reduced in the third. Very obviously, the weak maxima C must include a transition unrelated to D and M.

$6_1^211_0^216_1^1$. Evidence from the absorption spectrum supporting the activity of this transition derives principally from related transitions assigned in Table IV. The transition above is a ν_{16} sequence of the $6_1^211_0^2$ transition that appears with significant intensity about 160 cm^{-1} to higher energy. One can see the effect of adding 16_1^1 to a transition in ν_{11} from the relative intensities of the pair of transitions $6_0^111_0^2$ and $6_0^111_0^216_1^1$ (Table IV). The latter is reduced by a factor of about 6. Such a reduction of the intensity of the $6_1^211_0^2$ parent when it is transformed into the $6_1^211_0^216_1^1$ sequence member discussed here will yield a transition whose intensity should be comparable with the minor structure in the 2537-\AA region. Another related transition, $6_1^011_0^2$, is discussed in the preceding section.

It should also be noted that like the 6_1^2 transitions, there are two vibronically allowed angular momentum components associated with this transition, *i.e.*, $6_1^2l_1^011_0^216_1^1$ and $6_1^2l_1^211_0^216_1^1$. Thus this transition might be expected to have two band maxima in the 2537-\AA region. However, band contours associated with these two components cannot presently be predicted with confidence so that at least one of the bands may be without an observable maximum.

One can specify which bands in the 2537-\AA region may be assigned to this transition. Since it is a progression origin, there should be no related transition 923 cm^{-1} to lower energies. By means of this restriction, the maximum at $39,413 \text{ cm}^{-1}$ can be eliminated as a possibility. The maxima at $39,399$, $39,408$, and $39,423 \text{ cm}^{-1}$ remain creditable.

$6_0^116_1^217_0^1$. This transition is simply the ν_{16} sequence (16_1^1) member of the $6_0^116_0^117_0^1$ transition, and as in the case of assignments above, its presence in the 2537-\AA region is suggested by transitions seen elsewhere. Both 6_0^1 and $16_0^117_0^1$ are separately capable of inducing transitions. Their assignment to bands in the spectrum are listed below.

Transition	Observed position, cm^{-1}	Intensity
6_0^1	38,612.2	7500
$16_0^117_0^1$	39,038.6	170
$6_0^116_0^117_0^1$	39,560.8	335

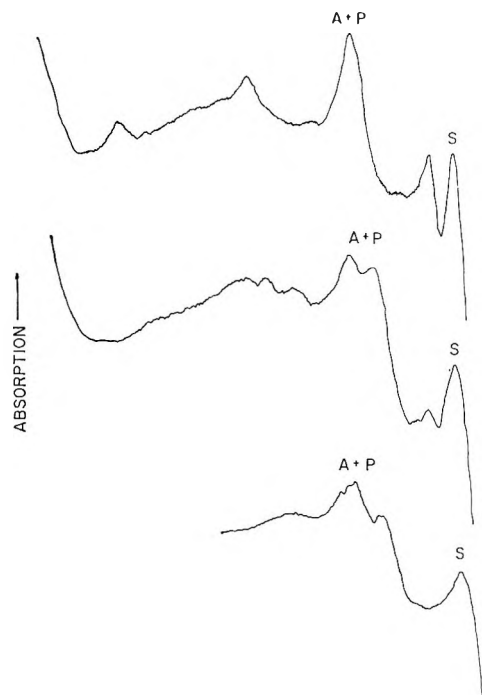


Figure 5. The E_0^0 , E_1^0 , and E_2^0 absorption regions¹⁶ of benzene vapor (top to bottom). The absorption maxima labeled S are 39,568.7, 40,489.4, and 41,409.9 cm^{-1} (vac), respectively. Wave number increases linearly to the right and the separation between S and (A + P) in the top spectrum is about 8 cm^{-1} .

Spectra of the "parent" progression $6_0^1 16_0^1 17_0^1 1_0^n$ are shown in Figure 5. It should be noted that the band at 39,560.8 cm^{-1} assigned as $6_0^1 16_0^1 17_0^1$ above has also been assigned to $6_1^2 11_0^2$ in previous discussion. There is strong evidence to suggest that one of these transitions is principally responsible for that band while the other produces a weaker band less than a wave number away. At the resolution in Figure 5, only one maximum is visible in the 39,560- cm^{-1} region (the maximum A + P, top spectrum). The relative positions of the two bands is more clearly demonstrated, however, by the bands in the $6_1^2 11_0^2 1_0^1$ and $6_0^1 16_0^1 17_0^1 1_0^1$ regions shown in the middle spectrum where two separated maxima are resolved. The splitting remains in the third progression members shown in the bottom spectra. It is not apparent which transition produces which maximum, but it does seem certain that both appear.

Although the parent transitions in Figure 5 seem fairly straightforward in assignment, one cannot easily translate this information when seeking to assign the sequence members in the 2537- \AA region. The difference in positions between the parent $6_0^1 16_0^1 17_0^1$ and the sequence member $6_0^1 16_1^2 17_0^1$ will be close to the 161 cm^{-1} predicted by the frequencies for $\nu_{16} = 1$ in the ground and upper states. However, anharmonicity in ν_{16} itself as well as coupling interactions with other modes alter both the expected position and intensity.

As a result of these uncertainties, it is not possible to reach a firm conclusion about the appearance of $6_0^1 16_1^2 17_0^1$ in the 2537- \AA region.

Additional complications arise if the two vibronically allowed angular momentum components associated with this transition are considered (*i.e.*, $6_0^1 16_1^2 l_1^0 17_0^1$ and $6_0^1 16_1^2 l_1^2 17_0^1$). As described in the preceding section, little is known about the splitting between these components, their relative intensities, and their band contours. It should be noted, however, that like the $6_1^2 11_0^2 16_1^1$ transition, $6_1^2 16_1^2 17_0^1$ is a progression origin and can be associated only with those maxima which do not have related bands 923 cm^{-1} to lower energy (*i.e.*, maxima at 39,399, 39,408, and 39,423 cm^{-1}).

$6_0^1 16_1^5$. This transition is formed by adding a ν_{16} sequence to $6_0^1 16_0^4$ which is expected to appear as a weak band in absorption.¹² Absence of precise vibrational constants for ν_{16}' prevents calculation of the positions of the three vibronically allowed angular momentum components associated with both $6_0^1 16_1^5$ and $6_0^1 16_0^4$ (*i.e.*, l_1^5 , l_1^3 , l_1^1 and l_0^4 , l_0^2 , l_0^0 , respectively). Little more can be said other than that the calculated position of the $6_0^1 16_1^5$ transition lies close to the Hg line. There are several maxima which can be assigned to the $6_0^1 16_0^4$ transitions and evidence exists in fluorescence experiments²⁰ to suggest their presence. However, their weak intensities also suggest that the even less intense transitions would not contribute significantly to the assignment of the 2537- \AA region.

$6_1^0 10_0^2 16_1^1 1_0^1$. Related transitions elsewhere in the spectrum are presented below along with their observed positions.

Transition	Observed position, cm^{-1}	Intensity
$6_1^0 10_0^2$	38,649.0	25
$6_0^1 10_0^2$	39,783.2	250
$6_0^1 10_0^2 16_1^1$	39,622.2	25

The activity of ν_{10} in the spectrum has been discussed by CDM, and though it appears that the position of the strongest band above ($6_0^1 10_0^2$) is involved in a perturbation, the value of $2\nu_{10}$ remains within several wave numbers of 1167 cm^{-1} in the assigned transitions. This value would place the sequence transition $6_1^0 10_0^2 16_1^1 1_0^1$ very close to the position of the Hg line, and it is therefore tempting to associate it with the absorption band at 39,412 cm^{-1} . However, the intensity of this transition should be low. It would be $1/5$ or less of that of its "parent" $6_0^1 10_0^2$. Such an exceedingly low intensity would be unlikely to be observed in the presence of the other structure in the 2537- \AA region.

$16_0^2 l_0^2 1_1^2$. The principal transition related to the $16_0^2 l_0^2 1_1^n$ progression is the cold band $16_0^2 l_0^2$. In both cases, only the l_0^2 angular momentum component is vibronically allowed and hence, each should produce a single band. The assignment of the $16_0^2 l_0^2 1_0^n$ progression is well established.^{12,17} It is weak and only two

Table V: Transitions Related to $16_0^2 1_1^2$

Transition	Observed band maximum, cm ⁻¹	Relative intensity
$16_0^2 1_0^2$	38,562.4	140
$16_0^2 1_0^2 1_0^1$	39,487.1	55
$16_0^2 1_0^2 1_1^0$	37,568.9	4
$X_m^n 1_0^0$ ^a	38,491.2	70
$X_m^n 1_0^1$	39,412	~90 ^b
$X_m^n 1_0^2$	40,333.2	55
$X_m^n 1_0^3$	41,253.9	25

^a New progression origin of unknown assignment. ^b Approximation made in this work based on the scale used in ref 16.

members can be seen. They are given with their intensities in Table V.

The assignment under discussion in this section is a member of a progression related to $16_0^2 1_0^2 1_1^n$ in that it originates from $\nu_1'' = 1$ rather than the zero-point level. Since the ground-state frequency $\nu_1 = 993$ cm⁻¹ is well known, the positions of $16_0^2 1_0^2 1_1^n$ are easily calculated from the observed maximum $16_0^2 1_0^2 1_1^n$. A progression

is found near those calculated positions and is listed in Table V. The assignment seems accurate when one considers only calculated positions.

Other consistency checks indicate a more complicated situation. One observes that the higher progression members seem much too intense for a transition from a ground state that is hot by almost 1000 cm⁻¹. The intensities are nearly equivalent in the two progressions, and this cannot be consistent with the proposed assignment $16_0^2 1_0^2 1_1^n$.

Another aspect of this progression should be noted. Franck-Condon restrictions²² predict that the 1_1^1 member of a progression will be much weaker than the 1_1^0 member. In the proposed $16_0^2 1_0^2 1_1^n$ assignment, a contradictory situation exists in that the first member is much weaker than the second. It seems that one is dealing with two progressions. The progression origin of one is at 37,569 cm⁻¹ and is very weak. It may well be the transition $16_0^2 1_0^2 1_1^0$. The progression origin of the other is at 38,491 cm⁻¹ and its greater intensity obscures the progression in ν_{16} . One would anticipate that the intensity of the member appearing in the Hg region derives almost entirely from this new progression.

Single Vibronic Level Fluorescence. IV. Its Application to the Analysis of Resonance Fluorescence from Benzene Excited by the 2537-Å Mercury Line^{1a}

by G. H. Atkinson,^{1b} C. S. Parmenter,* and M. W. Schuyler

Department of Chemistry, Indiana University, Bloomington, Indiana 47401 (Received January 25, 1971)

Publication costs assisted by the National Science Foundation

A partial analysis is given for the fluorescence spectrum excited in low pressures of benzene by absorption of light from the 2536.52-Å Hg line. The spectrum is shown to consist of emission from at least four excited states ($6^2 1^1$, $11^2 1^1$, $6^1 16^2 17^1$, plus another whose assignment is unknown, see Table III). By comparison with fluorescence from other known single vibronic levels in benzene, the contributions of each of these states to the fluorescence spectrum are identified (Table II).

The preceding paper identifies a number of absorption bands in the $^1B_{2u} \rightarrow ^1A_{1g}$ transition of benzene that may overlap the position of the 2537-Å Hg line. In this paper the assignment of the resonance fluorescence spectrum of benzene excited by absorption from that line is discussed. For convenience, this fluorescence

spectrum will be called the "2537-Å spectrum," or the "Hg spectrum" or "2537-Å fluorescence."

This work is motivated in part by anticipation that it

(1) (a) Contribution No. 1913 from the Chemical Laboratories of Indiana University. (b) National Institutes of Health Predoctoral Fellow.

will provide information concerning which excited states in benzene are actually pumped by absorption at 2537-Å. In addition, the resonance emission spectrum is among the few from large molecules that is sharply structured so that it provides an interesting problem in spectroscopy itself.

Although the contributions of this fluorescence to excited-state kinetics are widely recognized, its spectroscopic history is sparse. Only a few attempts at analysis exist and most of these were made prior to an understanding of the electronic states of benzene.

Pringsheim and Reimann^{2a} seem to be the first to distinguish between the fluorescence spectra observed at low and at high pressures with Hg excitation. Kistiakowsky and Nelles^{2b} described the resonance spectrum in detail in 1932 and correctly pointed out the necessity of working at pressures below 0.1 Torr to obtain emission that could be properly termed resonance emission—this is, emission truly from the states pumped in absorption. Recent studies³ indicate that some collisional redistribution of vibrational energy still occurs prior to emission in benzene until the pressure is reduced to less than 0.01 Torr, but the fluorescence spectra at 0.1 and 0.01 Torr differ only in very minor details.

An analysis of the 2537-Å spectrum published in 1936 by Cuthbertson and Kistiakowsky⁴ accurately identified the presence of many progressions in a 990-cm⁻¹ vibration and a number of progression origins as well. Ingold and Wilson⁵ also reported a study of this spectrum in 1936 and gave an extensive list of the positions of the band maxima. While that compilation remains the best available today, their analysis was based on the assumption of several excited electronic states and is not as satisfactory as that of Cuthbertson and Kistiakowsky. Aside from a recent and brief description of a few bands in the spectrum,⁶ these comprise the only attempts at analysis of this resonance fluorescence.

Since those efforts in 1936, the entire picture of the electronic states of benzene and of the nature of the electric dipole transitions between them has been developed. A large part of these advances is contained in the classic papers of Ingold and coworkers.⁷ As described elsewhere,^{8,9} this has led to a general understanding of much of the structure in the ¹B_{2u}-¹A_{1g} absorption spectrum. It now seems not a bold assumption that this knowledge combined with the new tool of single vibronic level (SVL) fluorescence spectroscopy can lead to considerable extension of assignments in the 2537-Å fluorescence spectrum.

Notation

The convenient scheme of Callomon, Dunn, and Mills¹⁰ (CDM) is used as described in the preceding paper, and the vibrational numbering scheme of Wilson¹¹ is adopted. This notation scheme is also used to refer to specific states in benzene. For example, the

notation 6²11²1¹ indicates a ¹B_{2u} benzene molecule with $v_6' = 2$, $v_{11}' = 2$, and $v_1' = 1$, whereas the notation

Table I: Observed Positions of the Progression Members in the 2537-Å Fluorescence Spectrum Shown in Figure 1^a

Band group notation	Displacement cm ⁻¹	Band group notation	Displacement, cm ⁻¹
a ₀	0	j ₀	1380
a ₁	992	j ₁	2350
a ₂	1995	j ₂	3360
a ₃	2965	j ₃	4356
a ₄	3963	j ₄	5373
a ₅	4930	p	1555
o	442	e ₀	1675
		e ₁	2690
		e ₂	3660
		e ₃	4656
b ₀	790	k ₀	1953
b ₁	1788	k ₁ + i ₀	2918
b ₂ + h ₀	2754	k ₂ + i ₁	3917
b ₃ + h ₁	3750	k ₃ + i ₂	4930
b ₄ + h ₂	4743		
b ₅ + h ₃	5747	l ₀	2145
		l ₁	3152
c ₀	1219	l ₂	4132
c ₁	2195	l ₃	5137
c ₂	3200		
c ₃	4182	m ₀	2437
c ₄	5184	m ₁	3422
c ₅	6167	m ₂	4420
		g ₀	2530
d ₀	1325	g ₁	3512
d ₁ + f ₀	2305	g ₂	4510
d ₂ + f ₁	3298		
d ₃ + f ₂	4280	n ₀	2570
		n ₁	3570
		n ₂	4584

^a The positions are approximately the centers of the band groups and are expressed as displacements from the exciting line at 39,412 cm⁻¹ (vac). The assignment of any band group can be found by setting n in the progression assignments in Table II equal to the subscript of the notation for the band group. For example, the assignment of a₃ is 6₁²1₃¹.

(2) (a) P. Pringsheim and A. Reimann, *Z. Phys.*, **29**, 115 (1924); A. Reimann, *Ann. Phys.*, **80**, 43 (1926); (b) G. B. Kistiakowsky and M. Nelles, *Phys. Rev.*, **41**, 595 (1932).

(3) C. S. Parmenter and A. H. White, *J. Chem. Phys.*, **50**, 1631 (1969).

(4) G. R. Cuthbertson and G. B. Kistiakowsky, *ibid.*, **4**, 9 (1936).

(5) C. K. Ingold and C. L. Wilson, *J. Chem. Soc.*, 955 (1936).

(6) H. F. Kemper and M. Stockburger, *J. Chem. Phys.*, **53**, 268 (1970).

(7) C. K. Ingold, *et al.*, *J. Chem. Soc.*, 222 (1946), and following papers; *ibid.*, 406 (1948), and following papers.

(8) T. M. Dunn, "Studies on Chemical Structure and Reactivity," J. H. Ridd, Ed., Methuen, London, 1966, pp 103-132.

(9) G. Herzberg, "Electronic Spectra of Polyatomic Molecules," Van Nostrand, Princeton, N. J., 1966, pp 555-561.

(10) J. H. Callomon, T. M. Dunn, and I. M. Mills, *Phil. Trans. Roy. Soc. London, Ser. A*, **259**, 499 (1966).

(11) E. B. Wilson, Jr., *Phys. Rev.*, **45**, 706 (1934).

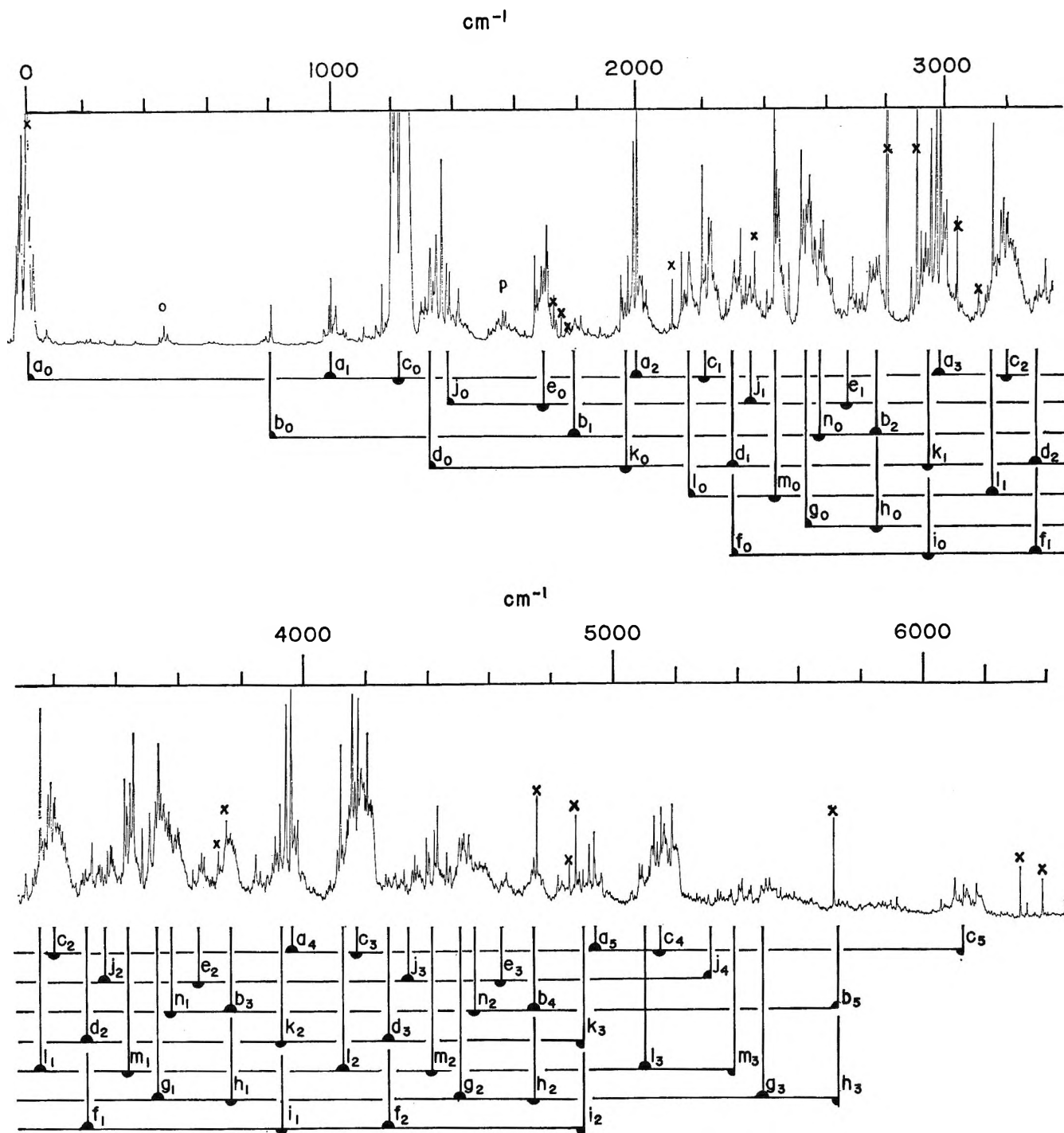


Figure 1. The resonance fluorescence spectrum from 0.05 Torr of benzene excited by absorption from a partially reversed Hg 2537-Å line whose width probably does not exceed 1 cm^{-1} .³ It is a photoelectric spectrum from apparatus described previously.³ The spectrum has not been corrected for the modest variation in sensitivity of the spectrometer-photomultiplier combination, and a few of the very sharp, intense maxima have been attenuated by the time constant of the photomultiplier amplifier. Those bands marked with an "X" are scattered Hg lines. The cm^{-1} scale indicates the displacement of structure from the exciting line at $39,412 \text{ cm}^{-1}$ (vac). The notation indicates the presence of a number of progressions in ν_1'' (990 cm^{-1}) with progression origins being those band groups with zero subscripts in the notation (a_0, b_0, c_0, \dots). See Table II for the displacements and assignments of the band groups.

$6_1 1_2$ indicates a molecule in the ground electronic state with $\nu_6'' = 1$ and $\nu_1'' = 2$.

The 2537-Å Resonance Fluorescence Spectrum of Benzene

A photographic spectrum of the fluorescence origi-

nating from the levels in the ${}^1B_{2u}$ state of benzene excited by absorption of the 2537-Å Hg line is described by Ingold and Wilson.⁵ They have published the positions and relative intensities of 621 maxima. It should be noted that the intensities are sometimes poor approximations of those observed photoelectrically.

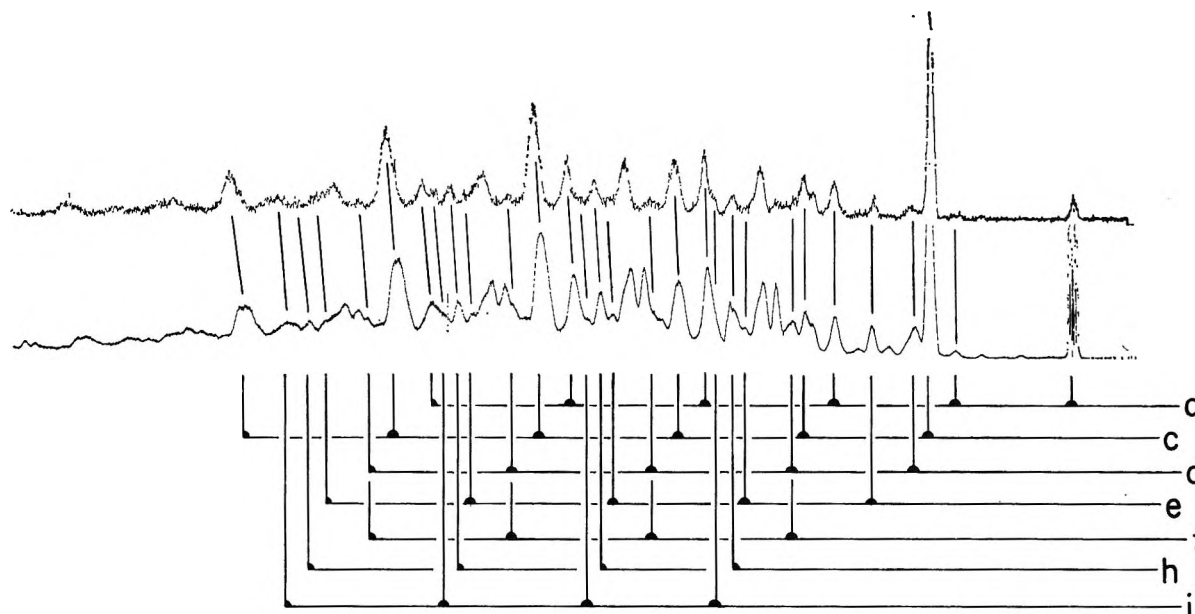


Figure 2. SVL fluorescence from the excited state 6^11^1 (upper spectrum) is compared with the 2537-Å resonance fluorescence spectrum. Both spectra were obtained with apparatus described elsewhere.¹³ The band pass of the fluorescence spectrometer is about 40 cm^{-1} for each spectrum. The position of the exciting light is the band at the extreme right, and fluorescence at that position is reduced by reabsorption. The exciting wavelengths have been aligned above one another for the purpose of comparing structure. Because the spectra are linear in wavelength rather than in wave number, and because the wavelength regions differ slightly, analogous features do not align precisely. Those progressions that originate from the level 6^11^1 in the SVL spectrum are connected with analogous progressions in the 2537-Å spectrum. Those features in the SVL spectrum left unmarked originate from the state 17^2 and, except by coincidence, have no analogous counterparts in the 2537-Å spectrum. The correspondence of the first member of the f progression (nearer the exciting line) seems poor in this figure, but the structure at that position can be seen more clearly in another 6^11^1 SVL spectrum shown in Figure 4.

Table II: Assignments of Progression Origins in the 2537-Å Fluorescence Spectrum in Figure 1^a

Observed displacement for $n = 0$	Progression notation	Assignments of progressions in $\nu_1'' = n$ (with calcd displacement for $n = 0$)				
		From excited state 6^21^1	From excited state 11^21^1	From excited state $6^116^217^1$	From excited state $6^111^216^1$	From excited state $10^216^11^1$
0	a_n	$6_1^21_n^1(990)$				
790	b_n			$6_0^116_3^217_0^11_n^0(798)$	$6_1^211_0^216_3^11_n^0(798)$	
1219	c_n	$6_3^21_n^1(1216)$				
1325	d_n	$6_1^211_2^01_n^1(1348)$	$6_1^011_2^21_n^1(1348)$		$6_1^211_2^216_1^11_n^0(1348)$	
1675	e_n	$6_2^211_1^016_0^01_n^1(1681)$ $6_1^210_2^01_n^1(1692)$				$6_1^010_2^216_1^11_n^1(1692)$
2305	f_n	$6_3^211_1^016_1^01_n^1(2289)$ $6_2^210_2^01_n^1(2300)$				
2530	g_n					
2754	h_n					
2918	i_n	$6_3^210_2^01_n^1(2908)$				
1380	j_n			$6_0^116_2^217_1^11_n^0(1367)$		
1953	k_n	$6_1^217_2^01_n^1(1934)$				
2145	l_n					
2437	m_n					
2570	n_n	$6_3^211_2^01_n^1(2564)$		$6_2^116_2^217_1^11_n^0(2583)$	$6_3^211_2^216_1^11_n^0(2583)$	
442	o		$11_1^216_1^01_n^1(465)$			
1555	p					

^a Assignment of any band group in the spectrum is obtained by setting n in the assignment notation (*i.e.*, $6_1^21_n^1$) equal to the subscript in the band group notation (*i.e.*, band group a_0 is the transition $6_1^21_0^1$).

To display the order that exists among those maxima, a photoelectric spectrum is shown in Figure 1 with resolution degraded to a resolvable line pair separation

of about 2 cm^{-1} . As the early workers commented,^{2b,5} the structure clusters into what might be called band groups.^{2b} To emphasize this clustering, a 2537-Å

fluorescence spectrum at even lower resolution is shown in Figure 2. In that spectrum, the clustering of the maxima into band groups remains as the only dominant feature of the spectrum.

Tables I and II list the positions and assignments of the band groups in Figure 1. Positions are expressed as displacements from the exciting line [at 39,412 cm^{-1} (vac)] and are taken as approximately the center of each band group.

Figure 1 and Table I define the spectrum for the purpose of the present analysis. The goal is to arrive at an analysis that will explain why the maxima cluster into band groups and that will identify both the excited state and the specific transition that accounts for the appearance of each group.

The analysis is summarized in Table II. It can be seen that even this limited endeavor is only partly realized. Further extension of the analysis to account for individual maxima is a problem of considerable difficulty. More information about the excited states and particularly about the rotational structure in the fluorescence bands is required before significant progress on that aspect of the analysis becomes possible.

Excited States Populated by Absorption at 2537 Å

The absorption spectrum in the 2537-Å region is shown in Figure 1 of the preceding paper. From a discussion of the rotational contours of the bands (rather sharp high energy heads with long rotational tails to low energy) it was shown that the bands whose maxima lie at 39,451, 39,445, 39,440, 39,423, and 39,412 cm^{-1} will overlap the position of the Hg line. The band at 39,408 cm^{-1} is less likely to participate in absorption from that line, and the band with a maximum at 39,399 cm^{-1} surely will not.

Specific assignments were given for the three bands at highest energy. A set of possible assignments was given for the remainder. From those assignments derives a list of excited levels in ${}^1B_{2u}$ benzene that might be populated by absorption from the Hg line. They are given in Table III.

From the discussion in the preceding paper, it is evident that the excited level 6^21^1 will be the dominant emissive state contributing to 2537-Å fluorescence. Other states must contribute as well but because of the uncertainties in their assignments and in the extent to which they are excited, one must look to analysis of the fluorescence itself for their identification.

Fluorescence from Single Vibronic Levels in Benzene

The preceding discussion indicates that the 2537-Å fluorescence spectrum is a superposition of emission from several vibronic levels in ${}^1B_{2u}$ benzene. In this section, the appearance of resonance fluorescence from a single vibronic level (SVL) in benzene is discussed, and such SVL fluorescence from a number of separate levels is compared. From these observations, one

Table III: Absorption Bands and Excited States Associated with 2537-Å Excitation in C_6H_6

Band maximum position, cm^{-1} (vac)	Assignment ^a	Present in fluorescence ^b	Vibrations excited in upper state	Vibrational energy in upper state, cm^{-1c}
39,451	$6_1^21_1^21_0^1$	Yes	$2\nu_6(l=2) + \nu_1$	1970
39,445	$6_1^21_1^01_0^1$	Yes	$2\nu_6(l=0) + \nu_1$	1964
39,440	$6_1^01_1^021_0^1$	Yes	$2\nu_{11} + \nu_1$	1953
39,423	$\left\{ \begin{array}{l} 6_1^01_0^21_61^11_0^1 \\ 16_0^21_1^2 \end{array} \right.$?	$2\nu_{10} + \nu_{16} + \nu_1$	2330
39,412		No	$2\nu_{16} + 2\nu_1$	2319
39,408 ^d	$\left\{ \begin{array}{l} 6_1^21_1^021_61^1 \\ 6_0^11_61^21_7^01 \end{array} \right.$?	$2\nu_6 + 2\nu_{11} + \nu_{16}$	2310
39,399 ^d		Yes	$\nu_6 + 2\nu_{16} + \nu_{17}$	1715
	$6_0^11_61^5$	No	$\nu_6 + 5\nu_{16}$	1707

^a The positions of assignments within the bracket cannot be predicted with sufficient accuracy to associate them with a specific absorption band. They comprise a list of possibilities for those band maxima covered in the adjacent bracket. Each of the possible transitions may have sufficient intensity to be observed in absorption. ^b These entries describe whether evidence for the absorption exists in the resonance fluorescence spectrum produced by absorption from the 2537-Å Hg line. "Yes" indicates that structure is observed in fluorescence that can be uniquely assigned to the upper state populated by absorption in this band. "No" indicates that structure expected in fluorescence following absorption in the given band is seen to be absent. "?" indicates that unique confirmation or refutation of absorption is not possible from analysis of fluorescence. ^c Except for the first two, these are only approximate values. The constants in the corresponding anharmonic expressions for the vibrational energies are not known with sufficient accuracy to warrant more precise calculations. ^d As described in text, this band probably does not absorb radiation from an unbroadened 2537-Å Hg line.

can then predict the most prominent features of emission expected from each of those levels that may be populated by absorption of Hg radiation. In following sections those predictions will be used for an analysis of the 2537-Å fluorescence spectrum.

SVL fluorescence spectra from each of seven levels in ${}^1B_{2u}$ benzene are shown in Figure 3. They were obtained by methods previously described.^{12,13} The exciting wavelengths for these spectra vary over about 3000 cm^{-1} (180 Å). In order to demonstrate a most significant characteristic, however, they are presented with their exciting wavelengths aligned above one another. When this is done, one can see that the spectra have common features. Specifically, the displacements of fluorescence bands from the exciting line are similar. For example, bands with displacements approximately 990 and 1215 cm^{-1} are prominent in these spectra. The displacements of numerous other bands also have common values.

(12) C. S. Parmenter and M. W. Schuyler, *J. Chim. Phys.*, 92 (1970).

(13) C. S. Parmenter and M. W. Schuyler, *J. Chem. Phys.*, 52, 5366 (1970).

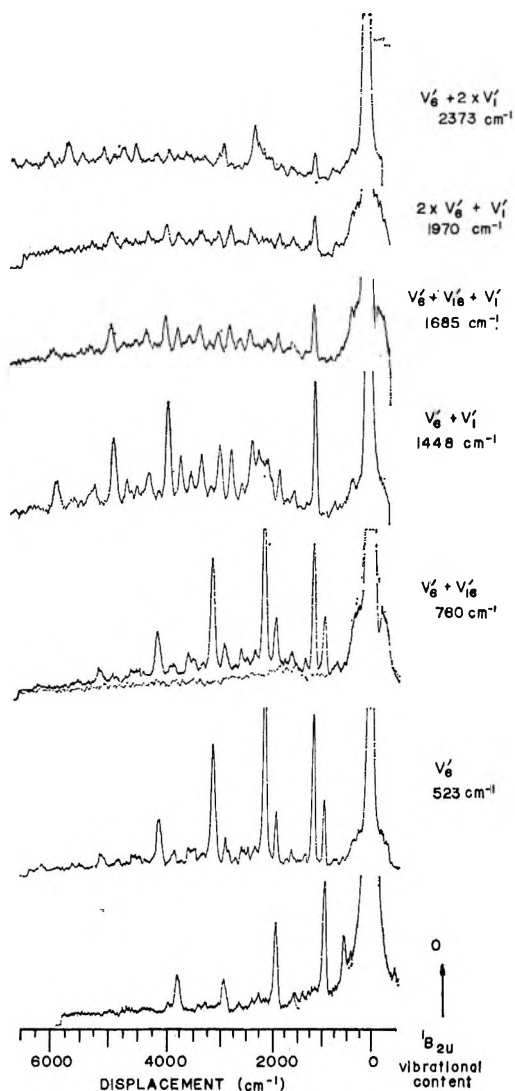


Figure 3. Fluorescence spectra from seven single vibronic levels in benzene at 0.2 Torr pressure are shown with exciting wavelengths aligned. The amount of vibrational energy and the particular vibrational modes excited in the ${}^1B_{2u}$ state are shown in the column to the right. Since these spectra are linear in wavelength, the scale shown for displacement in cm^{-1} from the exciting band (located at 0 cm^{-1} in each case) is approximate and fits well only the lowermost spectrum. Wavelength increases to the left in the spectra. The large band at 3800 cm^{-1} in the $\epsilon_{\text{vib}} = 0 \text{ cm}^{-1}$ spectrum only is present in the scattered exciting light.

Common displacements can be described by analogy between SVL fluorescence spectra and Raman spectra with respect to energy balance. In each case the molecules are pumped to an upper "state" by the incident radiation and then return to some excited vibrational level of the ground state with "emission" of radiation. With SVL fluorescence the upper state is of course a real excited state vibrational level rather than a virtual level, but the final state of the process in each case is an excited vibrational level of the ground electronic state. Thus as in the Raman effect, SVL fluorescence is an energy loss process for the incident radiation. Some of

the initial photon energy is converted into ground-state vibrational energy by the absorption-emission cycle. The energy displacements of the fluorescence bands are simply fundamentals, overtones, or combinations of ground-state vibrations. As a consequence, the displacements have values independent of the excited state producing the fluorescence.

The vibrations that can be left excited in the ground state are determined by the optical selection rules for the ${}^1B_{2u} \rightarrow {}^1A_{1g}$ transition in benzene. These have been well established by prior analysis of benzene absorption.^{8,9} We observe SVL emission spectra to be consistent with these rules from all levels we have investigated (now more than 20). Their application to analysis of SVL fluorescence spectra has been previously described.^{12,13}

An additional constraint on vibrational activity has been observed in the analysis of many SVL fluorescence spectra as well as in a reexamination of the vibrational assignments¹⁴ for the absorption spectrum. One observes that only nine of the 20 vibrational frequencies appear with appreciable activity in the ${}^1B_{2u} \rightarrow {}^1A_{1g}$ electric dipole transition. Assignments in both fluorescence and absorption appear to involve only these modes. They are listed in Table I of the preceding paper.

These principles are illustrated in the SVL fluorescence spectrum from the excited state 6^11^1 shown with specific assignments in Figure 4. The assignments are based on the active modes listed in Table I of the preceding paper and on the ${}^1B_{2u} \rightarrow {}^1A_{1g}$ selection rules. They are quite analogous to the assignments of SVL fluorescence from the zero-point level of the ${}^1B_{2u}$ state of C_6H_6 and of C_6D_6 published previously.¹³ Since that paper describes the basis of assignments in detail, only the most prominent features will be mentioned here.

Every SVL fluorescence spectrum consists of an assembly of progressions in the symmetric carbon ring breathing vibration ν_1 with a spacing of about 990 cm^{-1} between each progression member. Each ν_1 progression is built on a progression origin that induces the transition through a combination of vibrations containing an e_{2g} component. The most intense progression origins are those in which $\Delta\nu_6 = \pm 1$ while $\Delta\nu_x = 0$ for all other vibrations except ν_1 . Progression origins with $\Delta\nu_6 = \pm 1$ and $\Delta\nu_x = \pm 2$ also occur, but with much reduced intensity. In addition, some origins with $\Delta\nu_6 = 0$ occur, also with reduced intensity. The latter origins generally require quantum changes in other vibrations to produce the required e_{2g} component.

The spectrum in Figure 4 is typical. It has two prominent progressions seen to be the $\Delta\nu_6 = \pm 1$ transitions. Their assignments are $6_2^11_n^1$ and $6_0^11_n^1$, where n is a running index indicating excitation of ν_1 to form the progression. The progression origins are $6_2^11_0^1$ and

(14) G. H. Atkinson and C. S. Parmenter, to be published.

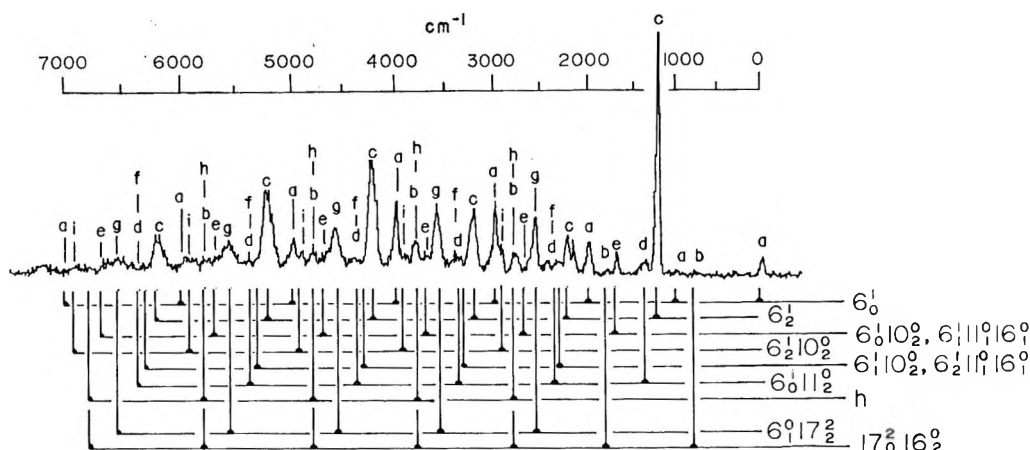


Figure 4. SVL fluorescence from the excited state $6^1 1^1$ produced by pumping the $6_0^1 1_0^1$ (A_1^0) absorption band with light isolated from a Xe arc by a monochromator with a 50-cm^{-1} band pass. The fluorescence spectrometer band pass is 25 cm^{-1} . The experimental details are similar to those described elsewhere.¹³ The cm^{-1} scale indicates displacement of structure to lower energy from the exciting light whose position is $38,600\text{ cm}^{-1}$. The letters identify progressions and either correspond or are analogous to those used in Table I and II, Figures 1 and 2. The assignments indicate the vibrations inducing the transition. To each assignment should be added the component 1_n^1 where n indicates the activity of $\nu_1'' = 0, 1, \dots$.

$6_0^1 1_0^1$, respectively. Other progression origins are greatly reduced in intensity relative to these.¹⁵

Another aspect of these spectra is important in their analysis. Notice of the relative intensities of members within a progression frequently allows identification of the quantum number of ν_1' in the emitting state. The intensities of progression members are principally governed by the Franck-Condon factors $|\langle \nu_1' = 0 | \nu_1'' = n \rangle|^2$, and $|\langle \nu_1' = 1 | \nu_1'' = n \rangle|^2$, depending upon whether the fluorescing state has $\nu_1' = 0$, or 1, etc. The $\nu_1' = 0$ intensity pattern differs grossly from that of $\nu_1' = 1$ so that recognition of each type of progression is easily made.

An indication of the Franck-Condon factors for a $\nu_1' = 0$ and a $\nu_1' = 1$ progression is shown in Figure 5.¹⁶ One can see that progressions from $\nu_1' = 0$ have maximum intensity with its second member (1_1^0) and then falls off smoothly with higher members. The progression from $\nu_1' = 1$, however, is exactly opposite. Its first member (1_0^1) is the most prominent and the second (1_1^1) is extremely weak. It then rises to a second maximum in higher members.¹⁷⁻¹⁹

Band Groups in the 2537-\AA Resonance Spectrum

The preceding characterization of absorption and of SVL resonance fluorescence now suggests an interpretation of some of the general features of the 2537-\AA resonance spectrum.

It should first be remarked that the list of excited states pumped by the Hg line indicates that resonance fluorescence will originate only from those states rather than from an additional set of states populated by subsequent intramolecular vibrational redistribution prior to emission. The highest level excited by 2537-\AA absorption would be one with about 2300 cm^{-1} of vibrational energy above zero point. The density of

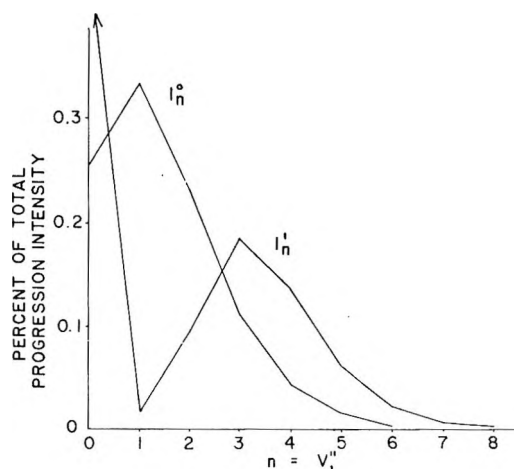


Figure 5. Calculated relative intensities for the progression members of $\nu_1' = 1 \rightarrow \nu_1'' = n$ and $\nu_1'' = 0 \rightarrow \nu_1'' = n$ progressions in benzene. The 1_0^1 transition has an amplitude of 0.46. These were calculated from Henderson's tables¹⁶ using parameters close but not matching exactly the known constants of benzene.

vibrational levels at that energy is less than 10 cm^{-1} , so that the level separation far exceeds their width.

(15) The absorption spectrum of benzene is analogous. Progressions in ν_1 dominate the spectrum, and $\Delta\nu_1 = \pm 1$ progression origins are the most intense.

(16) J. R. Henderson, *et al.*, "Tables of Harmonic Franck-Condon Overlap Integrals Including Displacement of Normal Coordinates," Douglas Report SM-45807, Jan 1964; *J. Chem. Phys.*, **41**, 580 (1964).

(17) These effects in benzene have been discussed by others.^{8,12,13,16,18,19} An experimental examination of intensities in nine different $\nu_1' = 0$ progressions is described in ref 13 and the appearance of $\nu_1' = 1$ progressions can be seen in Figure 4. The $6_2^1 1_n^1$ progression is the most easily seen example in that figure.

(18) D. P. Craig, *J. Chem. Soc. London*, 2146 (1950).

(19) W. L. Smith, *Proc. Phys. Soc. London (At. Mol. Phys.)*, **89** (1968).

Thus, from our present knowledge, there is no basis for considering emission from excited states other than those directly pumped in absorption. Consequently there is no basis to expect an underlying residue of unresolved structure in the 2537-Å resonance fluorescence other than that produced by accidental spectral congestion from the small set of initially excited states. At low resolution, this "congestion continuum" appears to be considerable as can be seen in Figure 2 where the 2537-Å spectrum is compared with that from a single vibronic level. As expected, the congestion continuum declines as resolution improves (see Figure 1) and it is apparently insignificant at even higher resolution.²

The most prominent aspect of the 2537-Å spectrum is clustering of structure into band groups. Since the 2537-Å spectrum is a superposition of spectra from several excited states, this clustering may seem anomalous in view of the complex structure expected from overlapping spectra. However, the cause of clustering becomes apparent upon examination of spectra in Figure 3. In that figure, it is shown that spectra from a variety of different excited states consist of transitions in a relatively small set of positions whose displacements from the exciting line are common. As discussed above, these displacements simply represent ground-state vibrational frequencies, and those are of course independent of the excited state from which fluorescence originates. The structure in the 2537-Å spectrum is analogous. While the fluorescence originates from at least several different excited states, the displacements of the fluorescence transitions from the exciting line are in each case constrained to a rather limited set of common positions.

Structure within a band group may be accounted for in principle but by no means in detail. It appears that three phenomena contribute to multiple maxima within band groups. The first is the near coincidence of two or more vibronic transitions. These transitions originate from the same excited state in some cases while several emitting states are involved in others. For example, it will be shown below that emission in the two adjacent band groups d_0 and j_0 (Figure 1) may include four transitions of rather comparable intensity from four excited states. On the other hand, the band group e_0 appears to consist of two nearly coincident transitions from a single excited state.

A more general contribution to multiple maxima arises from the rotational contour of individual vibronic transitions. The rotational structure appears to produce several maxima in a single vibronic transition, at least from some of the excited states. This can be seen in the very weak o band group in Figure 1, which as discussed below is a single transition from a single excited state. When examined at higher resolution, one observes three rotational maxima which clearly stand above subsidiary structure in that band group. A

more quantitative description would require rotational analysis of each absorption band and then a computation of the resulting fluorescence band contour from the known upper state rotational distribution. This could be approximated for the $6_1^2 1_0^1$ absorption bands from the work of Callomon, Dunn, and Mills,¹⁰ and seems a worthwhile project that needs to be undertaken.

A third cause of multiple structure must be the occurrence of nearly coincident vibronic transitions involving different angular momentum components of vibrational levels in the upper state or the lower state or both. These components have in some cases significant energy separations. Many examples exist in the absorption spectrum,¹⁰ and in fact this is seen in the absorption transitions at 39,451 and 39,445 cm^{-1} discussed in the preceding paper. Those maxima are vibronic transitions involving the two angular momentum components of the excited state $6^2 1^1$, separated by *ca.* 5 cm^{-1} .¹⁰ Similar situations will occur in fluorescence transitions from the excited states. For example, the $\Delta v_6 = +1$ fluorescence progression from that state will consist of three vibronically allowed components: $6_3^2 1_3^2 1_n^1$, $6_3^2 1_1^2 1_n^1$, and $6_3^2 1_1^0 1_n^1$. The band origins of the first two would be nearly coincident, but that of the latter would be separated from the pair by *ca.* 6 cm^{-1} .

Assignment of Structure in the 2537-Å Spectrum

The preceding discussion has accounted for some of the gross features of the 2537-Å spectrum. It has described in general terms both the causes of clustering of structure into band groups as well as the presence of so much structure within a band group. The discussion in the remainder of the paper now turns to the more specific problem of identifying the assignments for each band group. Since emission comes from several excited states, the task divides into two aspects. One must first identify which of the excited states contribute significantly to the intensity in a given band group, and then the transition from that state (or states) must be identified.

Identification of Emission from the Excited State $6^2 1^1$. As discussed above, the transition $6_1^2 1_0^1$ is expected to be the strongest absorber of the 2537-Å line. One therefore expects emission from the upper state $6^2 1^1$ to be responsible for the most intense structure as well as much of the subsidiary structure in the 2537-Å resonance fluorescence spectrum.

An ideal way to identify such structure would be to obtain an SVL fluorescence spectrum from the $6^2 1^1$ levels alone. This could be approximated with a properly placed exciting line whose width does not exceed *ca.* 5 cm^{-1} since the $6_1^2 1_0^1$ band heads do not appear to be significantly overlapped by other bands. However, there are presently no tunable excitation sources of sufficient intensity in such a narrow band spread to yield a useful SVL fluorescence spectrum.

Instead, the SVL fluorescence from the excited state 6^11^1 has been used to identify emission from the 6^21^1 state produced in 2537-Å excitation. The 6^11^1 state is reached by pumping the $6_0^11_0^1$ absorption band which is commonly designated as the A_1^0 band.²⁰ It is the most intense band in the entire ${}^1B_{2u}-{}^1A_{1g}$ absorption system and is among those shown in Figure 2 of the preceding paper. It is overlapped visibly by only one other absorption transition, the weak absorption 17_0^2 . With the exception of a few identifiable transitions from the 17^2 state, all emission following excitation of the A_1^0 band is from the state 6^11^1 .

The vibrational structure in SVL emission spectra from the states 6^21^1 and 6^11^1 is expected to be similar. The progression origins from the two states will have common displacements and roughly similar intensities. Examples of this are given in Table IV where a few of the more intense progression origins expected from each state are compared. Furthermore, the relative intensities of members within ν_1 progressions will also be similar, because in each case they are governed by the Franck-Condon factors for 1_n^1 transitions.

Table IV: A Comparison of the Positions of Analogous Progression Origins in SVL Fluorescence Spectra Produced by the Absorptions $6_1^21_0^1$ and $6_0^11_0^1$

Type of transition	Assignment	Displacement from the absorption band, cm^{-1} ^a
$\Delta\nu_6 = -1$	$6_1^21_0^1$	0
	$6_0^11_0^1$	0
	$6_1^211_2^01_0^1$	1348
$\Delta\nu_6 = +1$	$6_0^111_2^01_0^1$	1348
	$6_2^21_0^1$	1216
	$6_2^11_0^1$	1216
	$6_2^211_2^01_0^1$	2564
	$6_2^111_2^01_0^1$	2564
$\Delta\nu_6 = 0$	$6_2^211_1^016_1^01_0^1$	1681
	$6_1^111_1^016_1^01_0^1$	1681

^a To lower energy.

The SVL fluorescence spectrum from the excited state 6^11^1 is shown in Figure 4 with assignments of its principal structure. The fluorescence consists of ν_1 progressions built on about 10 prominent progression origins. Two of those progression origins come from the excited state 17_0^2 also pumped in absorption. (The relative intensities of the members in those progressions are characteristic of emission from an excited state with $\nu_1' = 0$. The more prominent progression ($6_1^017_2^21_n^0$) is the most intense transition expected from the upper state 17^2 . All other transitions from 17^2 are expected to be much weaker—not more than 10% of that intensity. The progression $17_0^216_2^0$ is seen only

because it falls in an area of the spectrum devoid of strong transitions from the state 6^11^1 .)

A comparison of 6^11^1 SVL fluorescence and the 2537-Å fluorescence spectrum is given in Figure 2. The correspondence of structure is striking, and from this comparison the contributions to the 2537-Å fluorescence spectrum that come from the excited state 6^21^1 can be identified.

One first observes that there is no structure in emission from 6^11^1 that is not also seen in the Hg spectrum. This is consistent with the assumption that the Hg spectrum originates in part from the excited state 6^21^1 and hence should contain counterparts to all structure in the 6^11^1 spectrum. In addition, the Hg spectrum contains progressions not present in the SVL fluorescence. This is the expected result of emission from states in addition to 6^21^1 . The congestion appearing in the low resolution Hg spectrum in Figure 2 is a further consequence of multiple emitting states. That congestion is entirely absent in the SVL fluorescence from 6^11^1 shown at similar resolution in that figure.

Corresponding progressions in those spectra are labeled with lower case letters. They can be identified easily on the separate spectra (SVL fluorescence in Figure 4 and a higher resolution Hg spectrum in Figure 1) where we have labeled progressions with the same scheme used in Figure 2. The progressions a, c, d, f, e, i, and h correspond closely in position and in relative intensities on the two spectra. These are thus the progressions in the Hg spectrum whose principal intensity derives from the excited states 6^21^1 .

Assignment of Emission from the Excited State 6^21^1 . Assignments of the above progressions from 6^21^1 in the 2537-Å spectrum are given in Table II under the heading appropriate for that state. A few comments about them are made below.

$6_1^21_n^1$ and $6_3^21_n^1$. These $\Delta\nu_6 = \pm 1$ transitions are the strongest type of progression origins seen in both emission and absorption. It should be noted that the progression origin of $6_1^21_n^1$ is coincident with the exciting line and is thereby somewhat altered in appearance.²¹ The low intensity of its member a_1 at 990 cm^{-1} is due to the fact that this is the $6_1^21_1^1$ progression member for which a severe Franck-Condon restriction exists (see Figure 5).

A progression origin (l_0) seems to be on the shoulder of band group c_1 in the 2537-Å spectrum and the resulting progression causes the c band groups at larger displacements to have widths in excess of 100 cm^{-1} . This progression also occurs in the SVL fluorescence spectrum so that it is probably associated with the

(20) H. Sponer, G. Nordheim, A. L. Sklar, and E. Teller, *J. Chem. Phys.*, **7**, 207 (1939); W. F. Radle and C. A. Beck, *ibid.*, **8**, 507 (1940); F. M. Garforth and C. K. Ingold, *J. Chem. Soc.*, 417 (1948).

(21) In Figure 1, scattered exciting light obscures much of this transition. In Figure 2, scattered light is reduced to a low value, but reabsorption of fluorescence at that position has attenuated the $6_1^21_0^1$ fluorescence transition.

excited states 6^{11} and 6^{21} in the SVL and 2537-Å spectra, respectively. However, a satisfactory assignment for it has not been found.

$6_1^{21}1_2^0$ and $6_3^{21}1_2^0$. One of the consistency checks for an assignment of a transition induced by $\Delta v_6 = -1$ is that the companion transition $\Delta v_6 = +1$ must also be present with at least equal if not greater intensity.¹² Accordingly, since the $6_0^{11}1_2^0 1_n^1$ progression origin was assigned in the 6^{11} SVL fluorescence of Figure 4, its partner $6_2^{11}1_2^0 1_n^1$ should also be observed. It is hidden, however, by the much stronger transition $6_1^0 17_2^2$. By coincidence, the corresponding transition $6_3^{21}1_2^0 1_0^1$ in the low resolution Hg spectrum in Figure 2 is also obscured due to emission from an excited state other than 6^{21} . However, this transition becomes clearly visible in the higher resolution Hg spectrum of Figure 1. It is the progression origin n_0 in Figure 1. As discussed below, progression origins from two other excited states may also contribute significant intensity at this position, and in addition, they are both from excited states with $v_1' = 0$ so that their second members at n_1 are strong. If that emission was absent, the band group n_1 would be of low intensity since it is the $n = 1$ member of the $6_3^{21}1_2^0 1_n^1$ progression.

$6_3^{21}1_1^0 16_1^0 1_n^1$ and $6_2^{21}10_2^0 1_n^1$. These progressions have calculated displacements separated by only 11 cm^{-1} so that they could not be resolved separately in our spectra. They are indicated by the series f in Figure 1, and the progression origins are coincident with band group d_1 . The presence of one or both of the progression origins is evident from the equivalent intensities of band groups d_0 and d_1 in the SVL and Hg spectra. Without these new progression origins, the intensity of the d_1 band group would be vanishingly low, since then it would derive only from the 1_1^1 member of the progression $6_1^{21}1_2^0 1_n^1$.

Further support for these progressions derives from analogous transitions. The strong companion transitions to $6_2^{21}10_2^0$ are discussed in the next section. One also expects to observe the companion progression origin $6_2^{11}1_1^0 16_1^0 1_0^1$ with an intensity diminished from that of $6_3^{21}1_1^0 16_1^0 1_0^1$. This would appear at a displacement of 1073 cm^{-1} . No transition appears above noise in this region, suggesting that the progression origin $6_3^{21}1_1^0 16_1^0 1_0^1$ may be the weaker of the two contributing to the f series of bands.

$6_2^{21}1_1^0 16_1^0 1_n^1$ and the Pair $6_1^{21}10_2^0 1_n^1$ and $6_3^{21}10_2^0 1_n^1$. The cross sequence $11_1^0 16_1^0$ is rather effective in inducing a transition between the two electronic states. It is among the absorption bands of modest intensity and it is seen prominently in SVL fluorescence from a number of excited states. In fact, it is actually stronger when it appears alone rather than in combination with $\Delta v_6 = \pm 1$.¹² Thus although the transitions $6_1^{21}1_1^0 16_1^0 1_n^1$ and $6_2^{21}1_1^0 16_1^0 1_n^1$ may be weak, the progression origin $6_2^{21}1_1^0 16_1^0 1_n^1$ with $\Delta v_6 = 0$ is expected to be moderately strong among the lesser structure from

6^{21} . Also the transition $6_1^{21}10_2^0 1_0^1$ probably contributes appreciably to the intensity of the e_0 band group, since its companion, $6_2^{21}10_2^0 1_0^1$, forms a rather strong progression origin i_0 that is clearly evident in the 2537-Å spectrum in Figure 1.

$6_1^{21}17_2^0 1_n^1$. This appears close to a member of the strong $6_1^{21} 1_n^1$ progression and its analogous partner $6_0^{11}17_2^0 1_n^1$ in the SVL fluorescence spectrum is for this reason neither seen nor assigned. The principal support for this assignment lies in its expected presence. Analogous transitions are important in the absorption spectrum¹⁴ and in some SVL fluorescence spectra.¹³

The Progression Origin h_0 . This appears as a very sudden enhancement of the b progression at b_2 in both the 6^{11} SVL fluorescence and in the 2537-Å spectrum. It thus seems associated with the excited state 6^{21} in the latter. A problem exists with this assumption, however, in that the next progression member h_1 is of even greater intensity in both spectra. This is inconsistent with the Franck-Condon factors for emission from an upper state with $v_1' = 1$ and matches the factors for a state with $v_1' = 0$. However, a satisfactory assignment from the state 17^2 in the SVL fluorescence spectrum is not apparent, nor can it be satisfactorily assigned in the 2537-Å spectrum. An alternate possibility is that h_0 and h_1 each form progression origins from the $v_1' = 1$ excited states in both spectra, but again no assignments are apparent on this basis either.

Identification of Emission from States Other Than 6^{21} . There remain prominent features in the 2537-Å spectrum that either have no counterparts in the 6^{11} SVL spectrum or which appear in both spectra but originate from the state 17^2 in the SVL spectrum. These features in the 2537-Å spectrum are most reasonably attributed to emission from states other than 6^{21} . They are enumerated below in order of decreasing intensity.

Progression g. This is present in both the A_1^0 SVL spectrum and the 2537-Å spectrum. In the former, it originates from the excited state 17^2 , and accordingly, it has no analogous assignment from the state 6^{21} in the 2537-Å spectrum. It must be due to emission from other states. The progression intensity pattern in the 2537-Å spectrum is that of emission from an excited state with $v_1' = 0$.

Progression m. This progression is unique to the 2537-Å spectrum.

Progression d. The band groups d_0 and d_1 have marked intensity enhancement in the 2537-Å spectrum. States in addition to 6^{21} must make a significant contribution to their intensity.

Progression b. This came from the excited state 17^2 in the 6^{11} SVL spectrum and thus it must come from states other than 6^{21} in the 2537-Å spectrum. Its intensity envelope suggests that these states have $v_1' = 0$.

Progression Origin o. This is weak in the 2537-Å

spectrum and is visible only because it lies in a region free of other structure. Its higher members are obscured by other stronger progressions.

Progression Origin p. The corresponding region in the SVL spectrum is completely vacant and this feature is thus clearly associated with some excited state unique to 2537-Å excitation. Its higher members are obscured by the g and n progressions.

Assignment of Emission from States Other Than 6²1¹. We now consider whether fluorescence from other excited states can account for the structure whose principal intensity cannot be attributed to 6²1¹ fluorescence. The other states are listed in Table III. Experience with SVL fluorescence indicates that the dominant fluorescence transitions from each state are those in which $\Delta v_6 = \pm 1$ while all other vibrations except ν_1 have $\Delta v_x = 0$. Those transitions are listed in Table V. They comprise the minimum list of transitions expected to be seen from a given state if it is to contribute to the 2537-Å spectrum. The new features in the 2537-Å spectrum described above should be contained in this list if it correctly includes all of the possible excited states.

Table V: The Most Intense Transitions Expected in Fluorescence from Some Single Vibronic Levels in ¹B_{2u} Benzene

Absorption transition leading to excited state	Excited state	Most intense ^a fluorescence transition(s)	Displacement ^b from absorption band, cm ⁻¹
6 ₁ ⁰ 11 ₀ ² 1 ₀ ¹	11 ² 1 ¹	6 ₁ ⁰ 11 ₂ ² 1 ₀ ¹	1348
16 ₀ ² 1 ₁ ²	16 ² 1 ²	6 ₁ ⁰ 16 ₂ ² 1 ₀ ²	414
		6 ₁ ⁰ 16 ₀ ² 1 ₀ ²	+384 ^c
		16 ₀ ² 1 ₀ ²	+992 ^c
		16 ₂ ² 1 ₀ ²	+195 ^c
6 ₂ ² 11 ₀ ² 16 ₁ ¹	6 ² 11 ² 16 ¹	6 ₂ ² 11 ₂ ² 16 ₁ ¹	2564
		6 ₂ ² 11 ₂ ² 16 ₁ ¹	1348
6 ₀ ¹ 17 ₀ ¹ 16 ₁ ²	6 ¹ 17 ¹ 16 ²	6 ₀ ¹ 17 ₁ ¹ 16 ₂ ²	2582
		6 ₀ ¹ 17 ₁ ¹ 16 ₂ ²	1366
6 ₀ ¹ 16 ₁ ⁵	6 ¹ 16 ⁵	6 ₂ ¹ 16 ₅ ⁵	2812
		6 ₀ ¹ 16 ₅ ⁵	1596
6 ₁ ⁰ 10 ₂ ² 16 ₁ ¹ 1 ₀ ¹	10 ² 16 ¹ 1 ¹	6 ₁ ⁰ 10 ₂ ² 16 ₁ ¹ 1 ₀ ¹	1692

^a Listed in decreasing order of expected intensity. ^b All displacements except those marked (+) are measured to lower energy from the absorption band. ^c Expected to be low in intensity relative to the transition at 414 cm⁻¹.

Fluorescence Excited by 16₀²1₁² Absorption. It is fairly certain that emission from the state 16²1² is not present in 2537-Å fluorescence, and hence this excited state is not populated by absorption of the 2537-Å line. Its most intense emission would occur at a displacement of 414 cm⁻¹. The only structure near that position is the very weak o band group at 440 cm⁻¹ which seems perhaps too far away. The 440-cm⁻¹ group can also be ascribed to emission from another state. However,

more convincing evidence for lack of emission from 16²1¹ is the absence of bands at 195, 384, and 992 cm⁻¹ to higher energies from the exciting line. Although these transitions would be weak relative to that at 414 cm⁻¹ to lower energy, they should be observable. No emission whatsoever can be found anywhere at energies appreciably higher than the exciting line.

Fluorescence Excited by 6₀¹16₁⁵ Absorption. Convincing evidence for emission from the state 6¹16⁵ following 6₀¹16₁⁵ absorption cannot be found. The most intense transition will be that at 2812 cm⁻¹, and that position is the valley between the h₀ and i₀ band groups. The transition at 1596 cm⁻¹ should also be strong and that position is in the valley between the p and e₀ band groups. It is possible that rotational excitation could cause both of these transitions to appear displaced from their predicted positions. If these transitions were each displaced 40 cm⁻¹ toward the exciting line from their calculated positions, they would then coincide with the p and e₀ bands group. Each of these bands are progression origins, but, as discussed above, e₀ appears to be an origin associated with the excited state 6²1¹. Thus, although the structure in the 2537-Å spectrum could conceivably accommodate emission from the excited state 6¹16⁵, it seems rather improbable.

Fluorescence Excited by 6₁⁰11₀²1₀¹ Absorption. A minor transition from the state 11²1¹ provides the best evidence that this excitation occurs with the 2537-Å line.

The o band group is weak but clearly visible at 445 cm⁻¹ in the 2537-Å spectrum. The displacement is close to that predicted for a fluorescence transition which leaves the molecule with one quantum less of ν_6'' and one quantum more each of ν_{11}'' and ν_{16}'' than it had prior to absorption. It is consistent with the fluorescence transition 11₁²16₁⁰1₀¹ with a calculated displacement of 465 cm⁻¹ from the absorption 6₁⁰11₀²1₀¹. Since it is difficult to otherwise account for this observed band group and since the suggested cross sequence will be prominent among the minor transitions from 11²1¹ (see, for example, the intensity of the analogous transition 11₁⁰16₁⁰ in the zero point SVL fluorescence spectrum¹²), it seems good evidence for participation of 6₁⁰11₀²1₀¹ in the absorption act.

The SVL spectrum from the 11²1¹ level is expected to consist of a single strong progression 6₁⁰11₂²1_n¹ plus the regular array of minor structure such as the transition discussed above. There is no opportunity for $\Delta v_6 = -1$ to occur. The strong progression origin is at 1348 cm⁻¹. It is coincident with a transition also seen to occur from the excited states 6²1¹, and in part accounts for the enhancement of this progression in the 2537-Å spectrum.

Fluorescence Excited by 6₀¹16₁²17₀¹ Absorption. The positions of the two intense $\Delta v_6 = \pm 1$ transitions from the state 6¹16²17¹ are each coincident with new pro-

gression origins in the 2537-Å spectrum. The more intense of these, that at 2583 cm⁻¹, describes the progression origin n_0 which is coincident with another progression origin from the state $6^2 1^1$. It can be seen in Figure 1 that the first two members of this progression are of approximately equal intensity so that a progression from an excited state with $v_1' = 0$ contributes to this structure. However, it will be shown below that another excited state can also account for this progression, so that it does not provide unique evidence for the excitation of $6_0^1 16_1^2 17_0^1$ with 2537-Å radiation.

On the other hand, the transition $6_0^1 16_2^2 17_1^1$ at a calculated displacement of 1367 cm⁻¹ provides an assignment of the j_0 progression origin that cannot be assigned from any other excited state. The j progression also has an intensity pattern characteristic of emission from a state with $v_1' = 0$, so that the evidence for the presence of an emitting excited state $6^1 16^2 17^1$ looks satisfactory.

Among the minor structure expected in emission from this state is the transition $6_0^1 16_3^2 17_0^1$ with a calculated displacement of 798 cm⁻¹. This coincides with the b progression not yet assigned and seen to be from some excited state with $v_1' = 0$ in the 2537-Å spectrum. The observed intensity of that progression is consistent with this assignment, but there is also the possibility that a minor transition from another $v_1' = 0$ state (discussed below) contributes as well.

Fluorescence Excited by $6_1^2 11_0^2 16_1^1$ Absorption. The $\Delta v_6 = \pm 1$ transitions from the excited state $6^2 11^2 16^1$ populated by this absorption are at 1348 and 2564 cm⁻¹ and each coincide with progression origins that can be reasonably assigned as having significant intensity from other excited states. Thus there is no feature that provides unique evidence for the presence of this absorption. This state, if present, may also contribute to the b progression by the minor transition $6_1^2 11_0^2 16_3^1$ with a calculated displacement of 798 cm⁻¹ for the progression origin.

Fluorescence Excited by $6_1^0 10_0^2 16_1^1 1_0^1$ Absorption. Unique structure from the upper level $10^2 16^1 1^1$ cannot be seen in the 2537-Å spectrum. The single prominent fluorescence band has a displacement of 1692 cm⁻¹ which is essentially coincident with the e_0 band group. This group is assigned from the excited states $6^2 1^1$, and since it is the same relative intensity in both the Hg and SVL fluorescence spectra, there seems little evidence for major contributions from other states.

Fluorescence Excited by Absorption into an Unassigned Band. The discussion above has described transitions from a variety of excited states that can account for major contributions to the intensity in various band groups. There remains, however, prominent structure in the 2537-Å spectrum for which assignment of the principal contributor has not been made. One of these is the progression beginning at band group h_0 discussed previously. The deficiency in assignment

of other structure is more severe. One has yet to account for the prominent g and m progressions which are both unique to the 2537-Å spectrum. The progression origin p is also unassigned.

In each of the progressions g and m , the first two members are of equivalent intensity, so that they are transitions from an excited state with $v_1' = 0$. The progressions g and m are more intense than any of the other structure in the 2537-Å spectrum that could be attributed to the excited states with $v_1' = 0$ so far considered. It is therefore apparent that these progressions are transitions from an excited state that is pumped efficiently by the 2537-Å line, but which is not accounted for by assignments of absorption bands suggested in the preceding paper. The assignment remains unknown.

Summary

The fluorescence analysis indicates that at least four states are excited by absorption from the Hg line (Table II). The state $6^2 1^1$ (with $l_6 = 2$ and 0) has the greatest population. The states $11^2 1^1$, $6^1 17^1 16^1$ plus some other state with $v_1' = 0$ but whose assignment is otherwise unknown are also excited. The vibrational energies of the known excited states fall within the range 1715 to 1970 cm⁻¹ above zero-point energy. One can be fairly certain that the vibrational energy of the unknown state does not exceed at 2330 cm⁻¹, which corresponds to excitation from a level with 1000 cm⁻¹ of vibrational energy above the ground-state zero-point level. The lowest possible vibrational energy excited by absorption of the Hg line would be about 1325 cm⁻¹.

The fluorescence spectrum appears consistent with a proposed construction of overlapping SVL spectra. Table II can be considered a summary of all known or expected contributions of significance to the band groups from the identified excited states. Other transitions from those excited states will be too weak to contribute more than perhaps a rather structureless background in certain regions. The resulting fluorescence spectrum thus consists of a modest set of band groups, and the intensity of a band group in most cases derives from only a few vibronic transitions. The large amount of sharp structure within a band group is generated in part from the near coincidence of several vibronic transitions and in part from close lying angular momentum components of a single transition. However, the most common contributor to the wealth of sharp structure may be the possibility of multiple maxima in the rotational contours of individual transitions.

The fluorescence analysis has not provided the key to definitive assignments of absorption bands in the 2537-Å region. It appears that either the absorption maximum at 39,423 cm⁻¹ or the maximum at 39,408 cm⁻¹ is from the transition $6_0^1 16_1^2 17_0^1$ seen to be active in absorption of the Hg line. Both maxima are known to belong to sequence transitions in ν_{16} , and both are

transitions with $\nu_1' = 0$. A choice between the two cannot be made on any basis other than the fact that the $39,408\text{ cm}^{-1}$ band seems less likely to be excited by the Hg line.

A dilemma arises in establishing the position of the unassigned absorption band whose excitation is responsible for the intense g and m progressions in fluorescence. Several facts suggest that it is the maximum at $39,412\text{ cm}^{-1}$. The prominent intensity of emission from this state is consistent with pumping a weak band almost in exact coincidence with the exciting line. Also the progression m seems absent or at least very weak in fluorescence generated by broad band¹⁸ excitation of the region $39,400\text{--}39,450\text{ cm}^{-1}$ with light isolated from

a Xe arc. This is evidence that the presence of the progression m in the 2537-\AA excited spectrum is due to the great emphasis that the narrow Hg line puts on weak absorption bands close to $39,412\text{ cm}^{-1}$. However, the requirements that $\nu_1' = 0$ for the unassigned upper state is hard to reconcile with the $39,412\text{ cm}^{-1}$ absorption maximum. As discussed in the preceding paper, that maximum appears to be the 1_0^1 member of an absorption progression. An alternate explanation for this absorption is not apparent.

Acknowledgment. This work was made possible by a grant from the National Science Foundation. The spectrum in Figure 1 was kindly provided by A. H. White.

Absolute Rate Constants for the Reactions of Hydrogen Atoms with Olefins

by J. A. Cowfer, D. G. Keil, J. V. Michael,* and C. Yeh

Department of Chemistry, Carnegie-Mellon University, Pittsburgh, Pennsylvania 15213 (Received December 24, 1970)

Publication costs assisted by the U. S. Atomic Energy Commission

The reaction rate constants for the reactions of hydrogen atoms with various olefins were measured at room temperature. Two fundamentally different techniques were used. In the first method, a discharge-flow system was coupled to a time-of-flight mass spectrometer, and the rate constants under excess hydrogen atoms were determined for the reactions of hydrogen atoms with propene, 1-butene, *cis*-2-butene, *trans*-2-butene, and 1-pentene. The second method is a newly devised technique in which the rate constants can be measured relative to the well characterized hydrogen atom-acetylene reaction. This method is based on the observation of the steady-state hydrogen atom concentration in the presence and absence of reactant. Hydrogen atom concentration is produced by mercury photosensitization and is observed by means of Lyman α photometry. The relative results obtained are compared with other relative determinations, and the absolute rate constants (inferred from a knowledge of the $\text{H} + \text{C}_2\text{H}_2$ rate constant) are compared with the absolute determinations reported here as well as with other reported work.

Introduction

The reactions of hydrogen atoms with olefins have been of continuing interest for many years.¹ This interest results from the importance of these reactions in complex reactive systems. Thus, radiation chemists, photochemists, and thermal kineticists have inferred the importance of these reactions in a wide variety of experimental systems which range from radiation induced polymerization to flame or shock tube studies.

Most of the work which has been done to specifically characterize these reactions in the gas phase has been carried out at room temperature. This work has generally been directed toward obtaining rate constants of these reactions relative to that of some common reaction.² The most important contributions in this area have been due to Cvetanović and coworkers.³⁻⁵ Sev-

eral absolute determinations on reaction systems of this type have also been reported.⁶⁻¹⁰ In general, the

(1) For an early review see E. W. R. Steacie, "Atomic and Free Radical Reactions," 2nd ed, Reinhold, New York, N. Y., 1954. More recent reviews are R. J. Cvetanović, *Advan. Photochem.*, **1**, 115 (1963) and B. A. Thrush, *Progr. React. Kinet.*, **3**, 65 (1965).

(2) K. Yang, *J. Amer. Chem. Soc.*, **84**, 3795 (1962).

(3) K. R. Jennings and R. J. Cvetanović, *J. Chem. Phys.*, **35**, 1233 (1961).

(4) G. R. Woolley and R. J. Cvetanović, *ibid.*, **50**, 4697 (1969).

(5) R. J. Cvetanović and L. C. Doyle, *ibid.*, **50**, 4705 (1969).

(6) W. Braun and M. Lenzi, *Discuss. Faraday Soc.*, **44**, 252 (1967).

(7) J. H. Knox and D. G. Dalgleish, *Int. J. Chem. Kinet.*, **1**, 69 (1969).

(8) J. A. Eyre, T. Hikida, and L. M. Dorfman, *J. Chem. Phys.*, **53**, 1281 (1970).

(9) M. J. Kurylo, N. C. Peterson, and W. Braun, *ibid.*, **53**, 2776 (1970).

correlations between the relative and absolute determinations have not been altogether satisfactory. The present investigation was therefore undertaken in order to examine certain apparent discrepancies which have previously existed between these two types of studies.

In this work, both absolute and relative rate constants have been obtained for reactions of hydrogen atoms with olefins. The absolute rate constants were determined with a discharge flow system coupled to a time-of-flight mass spectrometer,¹¹⁻¹³ and the relative rate constants were determined with a steady-state photolytic technique.¹⁴ The photolytic technique was used to measure the rates of these reactions relative to the reaction of hydrogen atoms with acetylene. This method is based on the Lyman α photometric detection of hydrogen atoms.^{15,16} The absolute rate constant for hydrogen atoms with acetylene has been measured in this laboratory by means of time-resolved Lyman α photometry¹⁷ with an apparatus of similar design to that used for the relative determinations.^{13,18} Therefore, absolute rate constants can be inferred from the relative determinations. The relative rate constants are compared to those of other workers, and the inferred absolute rate constants are compared to those reported here and to those of other workers.

Experimental Section

Experiment A. Discharge Flow Apparatus with Time-of-Flight Mass Spectrometric Detection. The apparatus and experimental procedure used in the present study is essentially the same as that described previously.¹³ The details of the apparatus have been discussed, and its use in kinetic studies has been demonstrated. Therefore, only a general description will be given here.

The apparatus consists of a discharge-flow system coupled to a Bendix Model 14 time-of-flight mass spectrometer. Tank He is used as the carrier gas in the flow reactor, and the flow rate is determined with a calibrated flow meter. Molecular hydrogen is introduced into the carrier gas upstream from a microwave discharge. Molecular hydrogen is dissociated into atomic hydrogen to the extent of 20-50% by an electrodeless microwave discharge. In this study the absolute rate constants are measured for a variety of olefin molecules with atomic hydrogen at room temperature. A particular olefin is introduced downstream from the discharge through a sliding probe, and the distance between the probe outlet and a pinhole leak into the mass spectrometer determines the dwell time in which the olefin is in the presence of hydrogen atoms.

The spectrum of each olefin was recorded with 70-eV ionizing electrons and was compared with the reported spectrum from the API mass spectral tables.¹⁹ The spectrum was repeated at 18.6 eV. This was the normal condition under which the kinetic studies were carried out. Hydrogen atoms were then allowed to react

with the olefin and the spectrum of reactants and products was recorded. After completing this preliminary study, the reaction rate constants were determined as described previously.¹³ A plot of the logarithm of the peak height of olefin against dwell time in the presence of a large concentration of hydrogen atoms ($[H] \approx 20-50[O_1]$) gave a straight line with a slope of $k_{app}[H]$. The hydrogen atom concentration was determined by measurement of the percentage change in the molecular hydrogen peak height (proportional to concentration) with the discharge turned on and then off. Thus, the per cent dissociation of an accurately metered amount of molecular hydrogen was used to calculate the sensitivity (concentration/peak height) for atomic hydrogen before and after each run. In general the sensitivity factors before and after were constant to $\pm 5\%$. The average peak height of m/e 1 during the run was used to calculate the atomic hydrogen concentration with the averaged sensitivity factors. $k_{app}[H]$ was determined as a function of atomic hydrogen concentration, and $k_{app}[H]$ was then plotted against $[H]$. The best straight line was drawn, and the slope of this line yielded k_{app} .

Experiment B. Steady-State Photolysis Apparatus with Lyman α Detection of Hydrogen Atoms. The apparatus used in this study has also been described previously,¹⁴ so no detailed description will be given here. The experiment utilizes Lyman α photometry to monitor hydrogen atom concentration in a steady-state photolytic system. The hydrogen atoms are produced by the photosensitized decomposition of molecular hydrogen with the resonance line, 2537 Å, of mercury. The intensities of both 2537 and 1216 Å (Lyman α) are observed experimentally, and therefore, transmittances for both resonance transitions can be measured concurrently. The transmittance of 2537 Å radiation, and therefore, the absorbed intensity can be varied systematically by the adjustment of mercury concentration in the reaction cell with cold traps. Under a given set of experimental conditions the transmittance of Lyman α can be obtained as a function of absorbed 2537 Å intensity. By the utilization of a

(10) M. P. Halstead, D. A. Leathard, R. M. Marshall, and J. H. Furnell, *Proc. Roy. Soc. Ser. A*, **316**, 575 (1970).

(11) C. A. Arrington, W. Brennen, G. P. Glass, J. V. Michael, and H. Niki, *J. Chem. Phys.*, **43**, 525 (1965).

(12) J. V. Michael and H. Niki, *ibid.*, **46**, 4969 (1967).

(13) J. R. Barker, D. G. Keil, J. V. Michael, and D. T. Osborne, *ibid.*, **52**, 2079 (1970).

(14) J. V. Michael and C. Yeh, *ibid.*, **53**, 59 (1970).

(15) J. V. Michael and R. E. Weston, Jr., *ibid.*, **45**, 3632 (1966).

(16) J. R. Barker and J. V. Michael, *J. Opt. Soc. Amer.*, **58**, 1615 (1968).

(17) D. T. Osborne, Ph.D. Thesis, Carnegie-Mellon University, 1970.

(18) J. V. Michael and D. T. Osborne, *Chem. Phys. Lett.*, **3**, 402 (1969).

(19) Catalog of Mass Spectral Data, American Petroleum Institute Research Project 44, 1956.

previous calibration from this laboratory for a Lyman α photometer of similar design,¹⁶ accurate relative hydrogen atom concentrations can then be deduced as a function of absorbed mercury resonance intensity.

In the present work, known mixtures of molecular hydrogen and olefin were introduced into the photolysis cell. Incident intensities of Lyman α and 2537 Å radiations were measured. Small concentrations of mercury were then introduced. The steady-state hydrogen atom concentration at a known absorbed intensity of mercury resonance radiation was then measured during photolysis. The photolysis time necessary to reach a steady state was typically 0.5–3 sec. The measurements were then repeated on a newly prepared sample of exactly the same hydrogen to olefin concentration ratio at the same total pressure. Only the mercury concentration, and therefore the absorbed intensity, was varied. A new sample was necessary since some depletion of olefin was noted even for these short photolysis times. However, since the olefin to atom concentration ratio in all experiments was large (typical values for [Ol] and [H] are 3×10^{13} molecules/cc and 2×10^{11} atoms/cc, respectively), the depletion during photolysis never exceeded 30%. The end result of a series of these experiments was a plot of absorbed intensity of 2537 Å radiation, I_a , against hydrogen atom concentration, [H], at essentially constant olefin concentration. A typical result is shown in Figure 1. I_a is expressed in arbitrary units and [H] is given in relative units based

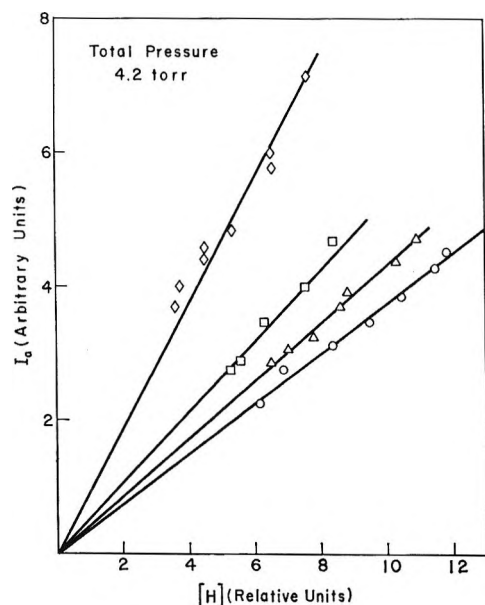


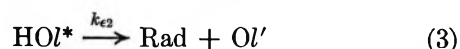
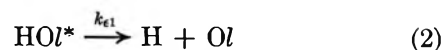
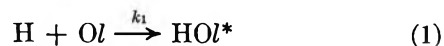
Figure 1. Plot of I_a (arbitrary units) against measured steady-state hydrogen atom concentration. The relative values of atom concentration are based on a calibration on a photometer of similar design. This point is discussed in the text: \circ , pure H_2 , $P = 4.2$ Torr; \triangle , H_2 with $[C_2H_2]_0 = 3.7 \times 10^{13}$ molecules/cc, $P = 4.2$ Torr; \square , H_2 with $[C_2H_2]_0 = 10.0 \times 10^{13}$ molecules/cc, $P = 4.2$ Torr; \diamond , H_2 with $[C_2H_2]_0 = 30.0 \times 10^{13}$ molecules/cc, $P = 4.2$ Torr.

on the previously cited calibration. The rationale for the use of these results in obtaining relative rate constants will be described in a later section.

In both experiments A and B, chemically pure grades of ethylene, propene, 1-butene, and isobutene were obtained from Matheson Compressed Gases, Inc., and were used without further purification. Research grade hydrogen and *trans*-2-butene were obtained from Air Products, Inc., and research grade *cis*-2-butene was obtained from Phillips Petroleum Co. These substances were also used without further purification. Acetylene from the Linde Division of the Union Carbide Corp. and 1-pentene from the American Petroleum Institute Research Project 6 were purified by bulb to bulb distillation, the middle third being used in sample preparation. Helium was obtained from Airco and was used as the carrier gas in experiment A without further purification. Neon and argon (research grades) were obtained from Air Products, Inc., and were used without further purification in the Lyman α and mercury resonance lamps of experiment B, respectively. Nitric oxide for use in the Lyman α photoionization detector of experiment B was obtained from Matheson Compressed Gases, Inc. and was purified by bulb to bulb distillation.

Results and Discussion

The addition of a hydrogen atom to an olefin results in the formation of a vibrationally excited radical which can do one of three things. It can dissociate back into a hydrogen atom and the original olefin, it can dissociate into a radical plus an olefin, or it can undergo collisional stabilization. These reaction channels are illustrated by the general mechanism



ω represents the rate of collisional deactivation for the excited radical. With the steady-state assumption for HOL^* , the above mechanism predicts, for the two level model

$$\frac{-d[H]}{dt} = \frac{-d[Ol]}{dt} =$$

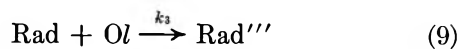
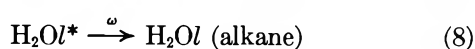
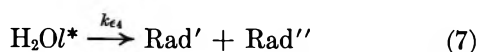
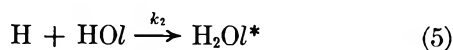
$$k_1[H][Ol] \left(\frac{k_{e2} + \omega}{k_{e1} + k_{e2} + \omega} \right) = k_{a1}[H][Ol] \quad (I)$$

The overall rate constant is k_{a1} . In the limit of zero pressure k_{a1} reduces to

$$k_{a1} = k_1 \left(\frac{k_{e2}}{k_{e1} + k_{e2}} \right) \quad (II)$$

k_{a_1} is k_1 times the fraction of radicals which dissociate by the path different from that by which they were formed. If k_{e_2} is zero, the overall reaction rate constant becomes zero. In the case of high pressure [$\omega \gg (k_{e_1} + k_{e_2})$], k_{a_1} becomes equal to k_1 . This relation also holds at any pressure if $k_{e_1} = 0$. If $k_{e_1} \neq 0$, the overall rate constant for this mechanism will increase with pressure from a minimum value at zero pressure to a maximum value of k_1 .

The mechanism illustrated by reactions 1-4 is often complicated by secondary reactions which can become important under certain experimental conditions. These include



Alkane* may further react in a parallel manner to the excited alkane, H_2Ol^* .

In experiment A, $[\text{H}] \gg [\text{Ol}]$, and the pseudo-first-order decay of $[\text{Ol}]$ at constant $[\text{H}]$ was observed.

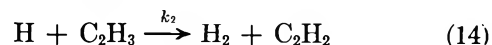
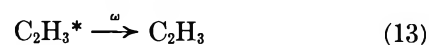
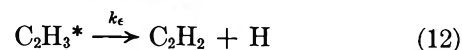
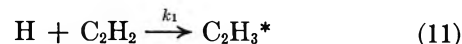
$$\frac{-d[\text{Ol}]}{dt} = k_{1st}[\text{Ol}] \quad (\text{III})$$

where $k_{1st} = k_{app}[\text{H}] = \text{constant}$. k_{app} becomes equal to k_{a_1} in eq I if reaction 9 is negligible. In all of the reactions studied in this work with experiment A the $[\text{Ol}]$ was kept low relative to $[\text{H}]$, and no products were observed in significant amounts which contained more carbon atoms than the initial reactant olefin. On the basis of this observation, reaction 9 is concluded to be negligible. Thus, k_{app} at infinite pressure can be equated with k_1 . Moreover, if $k_{e_1} \ll k_{e_2}$, k_{app} becomes k_1 at any pressure.

In experiment B, secondary reactions become important in the interpretation since the steady state $[\text{H}]$ is observed under olefin excess conditions. In order to instrumentally observe the steady-state concentration of atomic hydrogen, the reaction mixture must be photolyzed for at least 0.5 sec. This results in the build-up of radicals which either react with atomic hydrogen by reaction 5, react with olefin by a reaction of type 9, or recombine. In general the atom-olefin and radical recombination rates are much faster than the radical-olefin rates at comparable concentrations, and therefore the radical-olefin reactions are neglected with respect to the atom-olefin and recombination reactions. A steady state of $[\text{HOl}]$ is ultimately

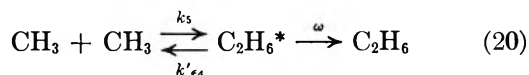
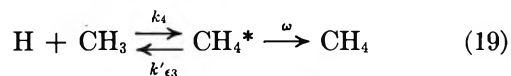
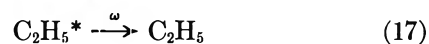
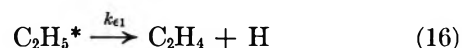
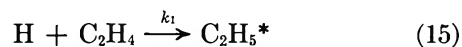
established, and the apparent rate constant is increased to $2k_1[(k_{e_2} + \omega)/(k_{e_1} + k_{e_2} + \omega)]$.

A simple example of this behavior can be seen in the reaction of atomic hydrogen with the alkyne, acetylene. The mechanism proposed by a number of workers^{12, 15, 20, 21} is



The terminology used for reactions 11-14 nearly conforms with the general mechanism of reactions 1-10. Reaction 14 may proceed by the chemical activation mechanism denoted by reactions 5 and 7. On the other hand, this reaction may be analogous to a disproportionation reaction and would then be pressure independent. Initially $[\text{C}_2\text{H}_3]$ is small and $k_{a_1}[\text{H}] \cdot [\text{C}_2\text{H}_2] > k_2[\text{H}][\text{C}_2\text{H}_3]$, but photolysis in experiment B over long periods of time (seconds), even with low $[\text{H}]$, will result in the build-up of $[\text{C}_2\text{H}_3]$ until a steady-state concentration of vinyl radical is reached. Under these conditions, $k_{app} = 2k_1[\omega/(k_e + \omega)]$, where the factor of 2 is the stoichiometry factor for the reaction.

A mechanism based on the general mechanism, shown in reactions 1-10, has been proposed for the reaction of atomic hydrogen and ethylene.¹³ For this case reaction



18 is associated with reaction 5 followed by fast decomposition by reaction 7. Stabilization by reaction 8 only occurs at much larger pressures than those used in the earlier work¹³ and in the present work. Reaction 19 is associated with reaction 10 followed by the subsequent decomposition or stabilization processes for excited alkanes. Reaction 20 represents the radical recombination mode of chemical activation and is not included in the general mechanism.

Prolonged photolysis in experiment B results in the development of steady-state concentrations of both

(20) G. G. Volpi and F. Zocchi, *J. Chem. Phys.*, **44**, 4010 (1966).

(21) K. Hoyermann, H. Gg. Wagner, and J. Wolfrum, *Ber. Bunsenges. Phys. Chem.*, **72**, 1004 (1968).

ethyl and methyl radicals. Calculations by Rabinovitch and Setser²² predict a much longer lifetime for $C_2H_6^*$ (3×10^{-8} to 2×10^{-7} sec) than for CH_4^* (5×10^{-10} sec), and unpublished results from this laboratory²³ indicate that the overall rate constant for reaction 20, at the pressures in the present study, is about six times as great as the overall rate constant for reaction 19. Calculations show that atomic hydrogen is removed almost entirely by reactions 15 to 18 after the steady-state concentrations of C_2H_5 and CH_3 are reached at the pressures and hydrogen atom concentrations employed here. The apparent rate constant for hydrogen atom removal therefore reduces to $2k_{a1}$, and the same stoichiometry factor is inferred for this case as in the $H + C_2H_2$ study.

The reaction of hydrogen atoms with propene again follows the mechanism given by reactions 1–10. In this case, however, two modes of addition have been documented.²⁴ Thus 94% isopropyl radicals and 6% *n*-propyl radicals result from the initial reaction of hydrogen atoms with propene.

Unstabilized *n*-propyl radicals dissociate according to reactions 2 and 3, and it has been found that 99% of these dissociations proceed into methyl plus ethylene ($k_{e2} \gg k_{e1}$).²² Under the present experimental conditions, the resulting methyl and ethylene concentrations are low and do not compete for atomic hydrogen. Therefore, the stoichiometry factor for this minor mode of decomposition is taken to be unity.

On the other hand, isopropyl radicals (about 94% of the initial radicals formed) dissociate mainly to propene and atomic hydrogen ($k_{e1} \gg k_{e2}$). Thus a pressure falloff in the apparent rate constant should be expected in the present work if k_{e1} is comparable in magnitude to ω . Rabinovitch and Setser calculate $\langle k_{e1} \rangle$ for isopropyl radical to be approximately 10^5 sec^{-1} .²² In both experiments A and B, the collision rates ranged from 10^7 to 10^8 sec^{-1} . Therefore, no pressure dependence should be observed under the present experimental conditions. However, as noted in the following section, a pressure dependence was observed for this mode of decomposition between zero and 3–5 Torr. This may indicate that the value given by Rabinovitch and Setser, $\langle k_{e1} \rangle \approx 10^5 \text{ sec}^{-1}$, is underestimated.

Stabilized isopropyl radicals formed from reaction 4 may react with hydrogen atoms by reaction 5 to form vibrationally excited propane. At sufficiently high pressures the excited propane will be deactivated, in which case the overall stoichiometry factor is 2. At lower pressures, however, the vibrationally excited propane dissociates into methyl and ethyl radicals (reaction 7). The ethyl radicals can then react with hydrogen atoms to produce methyl radicals (reaction 18). In this case, reaction 19 should be negligible in comparison with reaction 20 (as in the ethylene case), and the overall stoichiometry factor in experiment B should approach 3. In experiment A, where propene

decay is observed, the stoichiometry factor should be unity at any pressure.

The mechanism related to the reaction systems of atomic hydrogen with C_4 and C_5 olefins is described by reactions 1–10 also. Since the critical energy for breaking a C–H bond is ~ 10 kcal greater than the critical energy to break a C–C bond, k_{e1} (reaction 2) $\ll k_{e2}$ (reaction 3). Furthermore, Rabinovitch and Setser²² calculate $\langle k_{e2} \rangle$ to be on the order of 10^7 sec^{-1} . In the present work, however, the collision rate is always greater than this value. Therefore, the stabilization process (reaction 4) predominates, and the experimentally determined k_{ePP} in experiment A is equal to k_1 as previously described.

Experiment B was performed at 10–15 Torr, where the third-body collision rate is greater than 10^8 sec^{-1} , and therefore, ω (reaction 4) $\gg k_{e1} + k_{e2}$ (reactions 2 and 3). This also implies that all butyl radicals are stabilized at the experimental pressures used. Secondary reactions yield excited butanes by reaction 5; however, Rabinovitch and Setser did not calculate the rate constants for the dissociation of these species. Because of the greater number of degrees of freedom in excited butanes, one expects these rate constants to be less than those for $C_3H_8^*$ (from $H + C_3H_7$) even if the excited butanes have slightly higher excess energy.²² Therefore, it is estimated that the rate constants for dissociation of the excited butanes produced by reaction 5 are less than 10^7 sec^{-1} . It then follows that the above arguments which hold for excited butyl radicals also hold for excited butanes ($\omega_2 \gg k_{e1} + k_{e2}$). Since butyl radicals are in a steady state, the apparent rate constants determined in experiment B are equal to $2k_1$ for these systems. Extrapolation of the above reasoning to higher massed olefins leads to the same conclusions for the reaction of 1-pentene and atomic hydrogen.

It is therefore concluded that the stoichiometry factors for the reactions of atomic hydrogen with all of the olefins considered in the present work are unity for experiment A and are two for experiment B. This conclusion may be incorrect for the $H + C_3H_6$ reaction at lower pressures as already discussed. If the stoichiometry factors are constant then the relative rate constants determined in experiment B will be in the ratio of rate constants determined for unit stoichiometry, and therefore valid comparisons can be made between the absolute and the relative determinations. This will be attempted in the following sections.

Experiment A. The apparent bimolecular rate constants under hydrogen atom excess conditions were determined for 1-butene, *cis*-2-butene, *trans*-2-butene,

(22) B. S. Rabinovitch and D. W. Setser, *Advan. Photochem.*, **3**, 1 (1964).

(23) J. V. Michael and G. N. Suess, private communication, 1970.

(24) W. E. Falconer, B. S. Rabinovitch, and R. J. Cvetanović, *J. Chem. Phys.*, **39**, 40 (1963).

and 1-pentene each at one pressure of 2–3 Torr. The rate constants for the hydrogen atom–propene reaction at five pressures from 1 to 5 Torr were also determined under atom excess conditions. The resultant rate constants and corresponding pressures are given in Table I. As discussed above, the apparent rate constants should be identical with k_1 for all reactions, with the exception of propene. The propene reaction exhibits a slight pressure dependence, and the implications of this have already been discussed. The propene results are also shown in Figure 6.

Table I: Absolute Rate Constant Determinations (Experiment A)

Olefin	Total pressure, Torr	$k_{app} \times 10^{11}$, cc/molecule sec
Propene	0.96	6.6 ± 0.6
Propene	1.92	6.6 ± 0.6
Propene	2.66	8.5 ± 0.8
Propene	3.57	8.0 ± 1.0
Propene	4.91	8.0 ± 0.8
1-Butene	2.86	11.3 ± 0.8
<i>cis</i> -2-Butene	3.24	6.4 ± 0.5
<i>trans</i> -2-Butene	1.79	7.1 ± 0.4
1-Pentene	2.96	10.6 ± 0.8

The present results may be compared to those of Daby, Niki, and Weinstock,²⁵ who have made similar measurements on these reactions. This comparison is made in Table III.

Experiment B. In an earlier publication¹⁴ it was shown that hydrogen atoms, produced from the mercury photosensitized decomposition of molecular hydrogen, could be observed in small concentrations ($\sim 5 \times 10^{10}$ atoms/cc) by means of Lyman α photometry. A mechanism was adopted to explain the molecular H_2 quenching of $Hg(^3P_1)$, and eq IV was derived to indicate the relation between absorbed intensity of 2537-Å radiation, I_a , and steady-state hydrogen atom concentration, $[H]_{\infty}$.

$$[H]_{\infty} = \frac{nI_a\phi}{k_w} \quad (IV)$$

n is either 1 or 2 depending on the number of atoms which are produced per quenching event, k_w is the first-order rate constant for wall termination of hydrogen atoms, and ϕ is the primary quantum yield.

In Figure 1 plots are shown of I_a (arbitrary units) against $[H]_{\infty}$ and the slope, s_0 , of the line without added reactant can be correlated through eq IV to

$$s_0 = \frac{k_w}{n\phi} \quad (V)$$

If reactant is added to the system the steady-state hydrogen atom concentration decreases, all other things

remaining constant, in a predictable way which depends only on the overall rate of the reaction of atoms with reactant. Thus, the reactant competes for hydrogen atoms with removal by wall termination and the steady-state hydrogen atom concentration then becomes

$$[H]_{\infty} = \frac{nI_a\phi}{k_w + k_{app}[R]} \quad (VI)$$

If $[R] \gg [H]$ (an easily obtainable condition since the measured $[H]$ is generally less than 4×10^{11} atoms/cc) then the denominator in eq VI is a constant for a particular observation and can be varied systematically from experiment to experiment. Equation VI predicts linearity in plots of I_a against $[H]_{\infty}$, but the slopes, s , of these lines should be greater than the slopes without added reactant since

$$s = \frac{k_w + k_{app}[R]_0}{n\phi} \quad (VII)$$

That such behavior exists can be seen in Figure 1. If the slopes obtained with reactant present are divided by that obtained with no reactant present, eq VII and V predict the correlation

$$\frac{s}{s_0} = 1 + \frac{k_{app}[R]_0}{k_w} \quad (VIII)$$

This equation is the basis for the relative reaction rate constants obtained in this work and is tested in Figure 2 for the reaction of hydrogen atoms and acetylene at different total pressures.

As stated previously the reaction of hydrogen atoms with acetylene has been well characterized.^{12,15,20,21} The absolute reaction rate constant is known accurately at room temperature and the overall reaction mechanism is also known. The pressure dependence of this reaction has been studied in detail, and with the present technique a relative falloff curve can be obtained by means of eq VIII. The results are shown in Figure 3 where slopes of lines such as those presented in Figure 2 are plotted against total pressure. These slopes according to eq VIII should be in the ratio of k_{app} to k_w where k_{app} is the apparent rate constant for the hydrogen atom–acetylene reaction. As already discussed in the previous section, k_{app} is equal to $2k_{a1}$ for experiment B. Thus, k_{app}/k_w is proportional to k_{a1} , and if k_w is constant the relative falloff curve may be correlated with the absolute rate constant falloff curve. Also shown in Figure 3 is an absolute scale. This scale is deduced from absolute data for this reaction obtained in this laboratory from a time resolved Lyman α photometric study.¹⁷ Points obtained from this absolute study are also shown in Figure 3 along with data obtained by Hoyermann,

(25) E. E. Daby, H. Niki, and B. Weinstock, private communication, reported by H. Niki at 158th National Meeting of the American Chemical Society, New York, N. Y., Sept 1969.

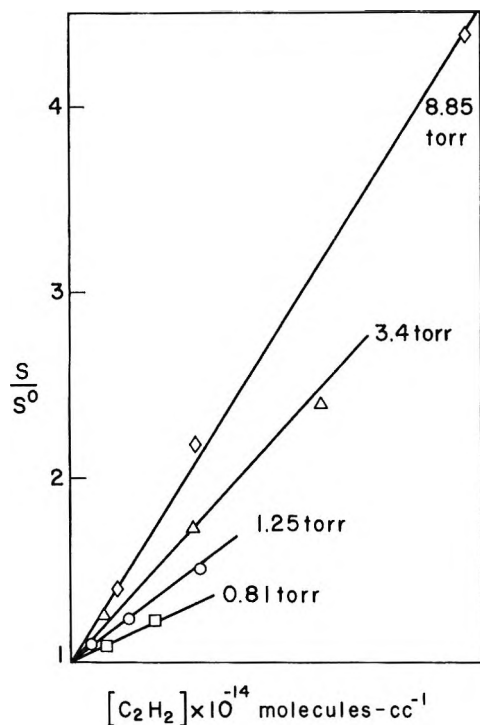


Figure 2. Plots of s/s_0 (defined in text) against $[C_2H_2]_0$.

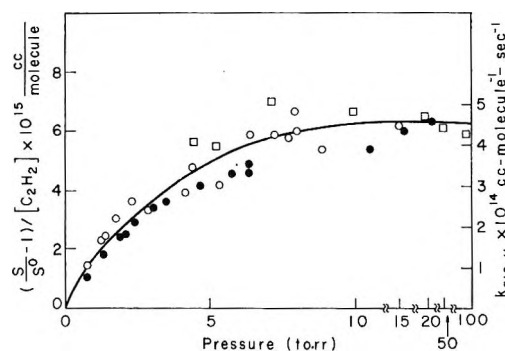


Figure 3. Relative and absolute falloff curve for the $H + C_2H_2$ reaction: O, experiment B (relative scale); □, absolute determination from ref 17; ●, absolute determination from ref 21.

Wagner, and Wolfrum in their excellent paper.²¹ The data of these latter workers have been divided by a uniform stoichiometry factor of 2. The consistency between the two absolute studies is apparent and the agreement is well within the errors of both studies. Thus, the relative data obtained in this study can be fitted to the absolute determinations and a value for the wall termination constant, k_w , can be calculated. For the results shown in Figure 3, k_w is $14.6 \pm 1.4 \text{ sec}^{-1}$. This value compares quite favorably with an absolute determination in a similar system from this laboratory.¹⁸

Results have also been obtained for the hydrogen atom-ethylene reaction, and a relative falloff curve is shown in Figure 4. In order to establish the absolute scale also shown in Figure 4, it is necessary to develop procedures so that the rate constant of $H + C_2H_4$ can

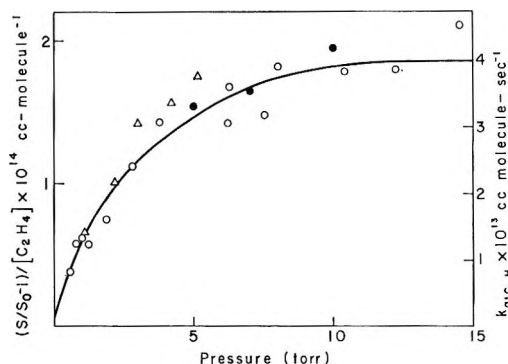


Figure 4. Relative and absolute falloff curve for the $H + C_2H_4$ reaction: O, experiment B (relative scale); Δ, absolute determination from ref 13; ●, absolute determination from ref 9.

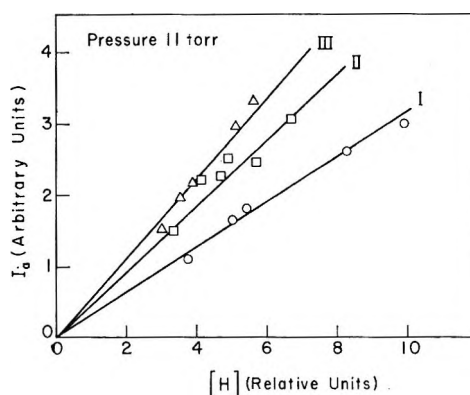


Figure 5. Plots of I_n (arbitrary units) against relative $[H]$ (see caption to Figure 1): O, pure H_2 , $P = 11 \text{ Torr}$; □, H_2 with $[C_2H_4]_0 = 1.79 \times 10^{13} \text{ molecules/cc}$, $P = 11 \text{ Torr}$; Δ, H_2 with $[C_2H_4]_0 = 2.10 \times 10^{14} \text{ molecules/cc}$, $P = 11 \text{ Torr}$.

be measured relative to $H + C_2H_2$. Since the major component present in the system is always molecular hydrogen and small concentrations of reactant are not expected to change the wall activity appreciably, k_w , the wall termination rate constant in eq VIII, should be expected to remain invariant for rather long periods of time. If this assumption is made, then eq IX can be derived

$$\left(\frac{s}{s_0} - 1\right)_{C_2H_4} / \left(\frac{s}{s_0} - 1\right)_{C_2H_2} = \frac{k_{app-C_2H_4}[C_2H_4]_0 / k_{app-C_2H_2}[C_2H_2]_0}{k_{app-C_2H_4}[C_2H_4]_0 / k_{app-C_2H_2}[C_2H_2]_0} \quad (\text{IX})$$

$[(s/s_0) - 1]_{C_2H_4}$ and $[(s/s_0) - 1]_{C_2H_2}$ are experimentally determined from data similar to those shown in Figure 1 for the $H + C_2H_4$ and $H + C_2H_2$ reactions, respectively. These determinations are made at constant reactant concentrations and constant pressure, and a typical result is shown in Figure 5. The slopes, s_0 (no reactant) and s (with constant concentrations of C_2H_4 and C_2H_2 , respectively), are determined and the corresponding quantities $[(s/s_0) - 1]_R$ are calculated. Since the ratio $[C_2H_4]_0/[C_2H_2]_0$ is known, $k_{app-C_2H_4}/k_{app-C_2H_2}$ can

Table II: Relative and Inferred Absolute Rate Constants

Reaction	Number of determinations	$k_{\text{app-alkane}}^a$ $k_{\text{app-C}_2\text{H}_2}$	$k_{\text{a1R}}^b \times 10^{13}$, cc/molecule sec	Cvetanović and coworkers, ^c $k_{\text{a1R}} \times 10^{13}$, cc/molecule sec
H + ethylene	9	8.6 ± 1.3	3.9 ± 1.0	$8.9^{d,e,f}$
H + propene	5	20.8 ± 0.9	9.4 ± 1.4	$14^{d,e,f}$
H + 1-butene	10	29.6 ± 5.8	13 ± 4	$14^{d,f}$
H + <i>trans</i> -2-butene	6	11.9 ± 1.4	5.4 ± 1.4	8.0^f
H + <i>cis</i> -2-butene	6	9.1 ± 0.9	4.1 ± 1.0	6.5^f
H + isobutene	10	74.5 ± 14.9	34 ± 10	$34^{d,e,f}$
H + 1-pentene	4	28.6 ± 4.8	12.9 ± 4	12^e

^a Total pressure, 10–15 Torr. ^b Values obtained from relative rate data multiplied by $k_{\text{C}_2\text{H}_2} = (4.5 \pm 0.5) \times 10^{-14}$ cc/molecule sec. ^c $k_{1\text{-butene}}$ is assumed to be 14×10^{-13} cc/molecule sec. ^d Total pressure ~ 750 Torr CO_2^d . ^e Total pressure ~ 600 Torr H_2^e . ^f Total pressure ~ 435 Torr $\text{C}_4\text{H}_{10}^f$.

be computed from eq IX. One complete relative rate constant determination can be made in about 0.5 hr; however, the exposure time per sample is typically 0.5–3 sec. Since the determinations are rapid and involve small depletion of olefin, the assumption that k_w is in fact invariant over the determination time is probably good.

Nine determinations for the ratio of $k_{\text{app-C}_3\text{H}_6}/k_{\text{app-C}_2\text{H}_2}$ have been made between 10 and 15 Torr of pressure and the results are presented in Table II. The value obtained is 8.6 ± 1.3 . The absolute value of the rate constant for the H + C_2H_2 reaction from the previously mentioned studies in this pressure range is $(4.5 \pm 0.5) \times 10^{-14}$ cc/molecule sec, and this implies a value of k_{a1} for the ethylene reaction rate constant between 10 and 15 Torr of $(3.9 \pm 1.0) \times 10^{-13}$ cc/molecule sec if the stoichiometry factors for both reactions are the same. Arguments have been given in the previous section which indicate stoichiometry factors of two for both cases. This value of 3.9×10^{-13} cc/molecule sec has therefore been used to scale the relative results of Figure 4 into absolute units. As an internal consistency check, results from recent absolute determinations are included in Figure 4,^{9,13} and the agreement is seen to be quite satisfactory.

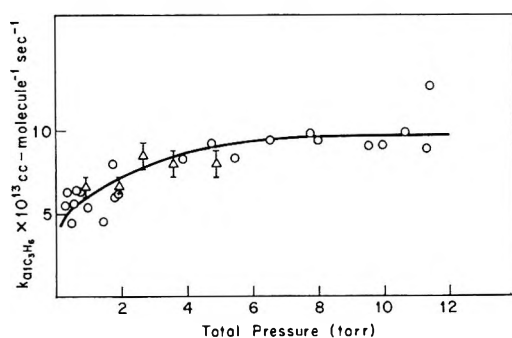


Figure 6. Absolute falloff curve for the H + C_3H_6 reaction: O, experiment B (normalized to H + C_2H_2 reaction, see text); Δ , experiment A.

The relative rate technique described above has been applied to the reaction of hydrogen atoms with propene. The relative rate constant data obtained as a function of pressure are presented in Figure 6. The absolute scale shown in this figure is made to conform with the value for the hydrogen–acetylene reaction in exactly the same way as described for the hydrogen atom–ethylene reaction. Between 10 and 15 Torr of pressure, the relative ratio, $k_{\text{app-C}_3\text{H}_6}/k_{\text{app-C}_2\text{H}_2}$, is 20.8 ± 0.9 (Table II). In this

Table III: Absolute Rate Constant Determinations for Comparison with Present Work

Reaction	Rate constant, cc/molecule sec $\times 10^{13}$	Pressure, Torr
H + ethylene	1.7 ± 1.0	2 (Ar) ^a
	1.7 ± 0.1	2.4 (He) ^b
	3.8 ± 0.4	5 (He) ^c
	3.3 ± 0.1	5 (He) ^d
	2	8 (Ar) ^e
	8.5 ± 3.0	10 (He) ^f
	4.2 ± 0.1	10 (He) ^d
	12 ± 1.0	500 (He) ^g
	12 ± 1.0	500 (He) ^d
	9.1 ± 0.9	700–1500 (He) ^h
H + propene	7.6 ± 0.4	2 (Ar) ⁱ
	13.0 ± 4.0	6.7 (He) ^f
H + 1-butene	13.8 ± 0.8	2 (He) ⁱ
	15.0 ± 4.5	6.7 (He) ^f
H + <i>trans</i> -2-butene	8.9 ± 0.7	2 (He) ⁱ
	10.0 ± 1.5	5.5–50 (He) ^f
H + <i>cis</i> -2-butene	7.9 ± 0.6	2 (He) ⁱ
	55 ± 22	2 (He) ^a
H + isobutene	38 ± 6	~ 8 –50 (He) ^j

^a Knox and Dalglish.⁷ ^b Westenberg and DeHaas;²⁷ the stoichiometric factor is assumed to be 2.5. ^c Barker, Keil, Michael, and Osborne.¹³ ^d Kurylo, Peterson, and Braun.⁹ ^e Halstead, Leathard, Marshall, and Purnell.¹⁰ ^f A. F. Dodonov, G. K. Lavrovskaya, and V. L. Talfoze, *Kinet. Katal.*, **10**, 14 (1969). ^g Ahumada, Michael, and Osborne.²⁶ ^h Eyre, Hikida, and Dorfman.⁸ ⁱ Daby, Niki, and Weinstock.²⁵ ^j Braun and Lenzi.⁶

pressure range the stoichiometry factors for both reactions are identical and will cancel as discussed previously. Therefore, the inferred absolute rate constant should be identified with $k_{a,i}$ and is equal to $(9.4 \pm 1.4) \times 10^{-13}$ cc/molecule sec. A slight pressure dependence may be indicated, and the implications have already been discussed. As an internal consistency check, the results from experiment A are also plotted in Figure 6, and the agreement between the inferred absolute rate constants from this experiment with the absolute determinations of experiment A is satisfactory.

The relative rate technique has been applied to a variety of other hydrogen atom-olefin reactions, and the results are also given in Table II. In all cases the relative rate constants were determined with respect to the hydrogen atom-acetylene reaction. The inferred absolute rate constants, as in the previous cases, should be identified with $k_{a,i}$. As discussed previously, the rate constants should be at the high-pressure limit, and comparisons with the absolute determinations from experiment A (Table I) are valid.

A comparison of the results obtained in this work (Tables I and II) can be made with those determined absolutely by others, and Table III presents the comparison. Also for comparison, the relative results of Cvetanović and coworkers at pressures approaching 1 atm are shown in Table II as inferred absolute rate constants. These were calculated with an assumed value of 1.4×10^{-12} cc/molecule sec for the 1-butene reaction. This rate constant was chosen for normalization since it is in good agreement with the present work (1.1×10^{-12} and 1.3×10^{-12} cc/molecule sec). Also in agreement is the value obtained by Daby, Niki, and Weinstock²⁵ in the absolute flow reactor study at 2 Torr.

With regard to the ethylene reaction, comparison of all results given in Tables I, II, and III shows that the apparent discrepancies which have existed for this reac-

tion are primarily due to a rather strong pressure effect on the reaction rate. The value inferred from the high-pressure work of Cvetanović and coworkers is in excellent agreement with that of Eyre, Hikida, and Dorfman,⁸ Braun and coworkers,^{6,9} and Michael and coworkers.²⁶ The combined uncertainties in all these studies probably overlap. The low-pressure comparison of Figure 4 and Table III is also in substantial agreement with other absolute determinations.^{7,9,13,27}

Apparent discrepancies seem to exist with regard to the propene reaction, but these discrepancies might also be attributed to a pressure effect on the reaction. The present study at the lowest pressure indicates a value of about 0.5 the highest pressure value of Cvetanović and coworkers. The present work in the low to intermediate pressure range indicates some pressure dependence, and, as pressure increases, this value might increase to the value of Cvetanović and coworkers.

Excellent agreement is noted in all studies of the isobutene and 1-butene reactions. Moderate agreement is noted for the *trans*-2-butene and the *cis*-2-butene reactions, and it is questionable whether or not the combined uncertainties in all work indicate a real discrepancy from study to study for these reactions.

Acknowledgment. The authors acknowledge the support of the Atomic Energy Commission under Contract AT(30-1)-3794 for this work. We also wish to thank Drs. E. E. Daby, H. Niki, and B. Weinstock for communicating their results in advance of publication. We are also indebted to Mr. A. J. Streiff of the American Petroleum Institute Research Project 6, who supplied the sample of 1-pentene for this study.

(26) J. J. Ahumada, J. V. Michael, and D. T. Osborne, private communication, 1970.

(27) A. A. Westenberg and N. DeHaas, *J. Chem. Phys.*, **50**, 707 (1969).

The Use of Tubular Flow Reactors for Kinetic Studies over Extended Pressure Ranges^{1a,b}

by Robert V. Poirier and Robert W. Carr, Jr.*

*Department of Chemical Engineering and Materials Science, University of Minnesota, Minneapolis, Minnesota 55455
(Received January 22, 1971)*

Publication costs assisted by the U. S. Atomic Energy Commission

The continuity equations for first- and second-order chemical reactions, coupled with radial diffusion, were solved numerically for isothermal, incompressible, viscous-flow tubular reactors. Radial concentration profiles were averaged by integrating over reactor geometries closely approximating the experimental arrangements for some techniques commonly used in tubular flow reactor experiments. The applications of the results to gas-phase systems were explored, and a comparison with experiments on hydroxyl radical kinetics was made. The calculated and experimental results are in accord with one another. A simple method is described in which plots of average concentration *vs.* axial distance can be used to extend the useful pressure range of tubular flow reactors for fundamental rate studies from the low-pressure regime where rapid radial diffusion rates allow use of a uniform residence time assumption to higher pressures where parabolic concentration profiles exist.

Introduction

When using steady-flow tubular reactors for kinetic studies, one encounters the problem of relating axial distance along the reactor with reaction time. In the case of gas phase reactions, the experimental conditions are most frequently such that laminar flow occurs. The resulting parabolic velocity profile gives rise to a distribution of residence times for the reactive species in which those traveling near the wall remain in the reactor longer and experience larger extents of reaction than those traveling nearer the center of the reactor. This difficulty may be circumvented by operating at sufficiently low pressure and concentration that diffusional dispersion becomes extremely rapid. One can then assume, to a close approximation, that the radial concentration profile is flat. The concentration of reactive species is therefore independent of radial distance, and reaction time is equal to axial distance divided by average velocity. In apparatus of the type and dimensions commonly used for kinetic studies it is usually a good assumption at pressures of approximately 1 Torr or less.

The necessity of operating tubular reactors under conditions where the radial concentration profile is uniform has imposed severe limitations upon a widely used and otherwise versatile technique. With diffusion rates great enough to maintain a flat profile, the rapid transport to the reactor walls may allow heterogeneous reactions to occur at rapid rates and thus complicate the kinetic analysis. This difficulty will, of course, become more severe as operating pressure decreases. In addition to heterogeneous effects, limitations imposed by detector sensitivity and increasing importance of viscous pressure drop impose restrictions upon operation at the lower pressures. Experiments are thus

limited to a narrow range of pressures which handicaps the kinetic investigation. For example, the formation of chemically activated intermediates may go undetected, or the possible importance of a termolecular combination reaction may not be adequately tested experimentally.

In the operation of a tubular flow reactor at higher pressures it is necessary to know the concentrations of reacting species as a function of both radial and axial distance in order to extract accurate values of reaction rate coefficients from the data. The required information can be obtained by solution of the continuity equation for diffusive and convective flow in the presence of chemical reaction. Bosworth^{2a} obtained approximate solutions for a viscous-flow tubular reactor and discussed the effects of reactor size upon extent of reaction compared to the plug-flow situation. He also discussed conditions where the effects of either axial or radial diffusion can be neglected. Walker^{2b} obtained asymptotic solutions to the continuity equation for concurrent first-order homogeneous and heterogeneous reactions in Poiseuille flow with both radial and axial diffusion. The results were used as a guide for estimating the error introduced through using a one-dimensional model. Numerical integration techniques have been used to treat the case of first-order³ and second-order⁴ homogeneous reactions in order to determine the effects of a

(1) (a) Work supported by U. S. Atomic Energy Commission, Contract No. AT(11-1) 2026. This is AEC document No. COO-2026-5; (b) paper presented in part at the 160th National meeting of the American Chemical Society, Chicago, Ill., Sept 1970.

(2) (a) R. C. L. Bosworth, *Phil. Mag.*, **39**, 847 (1948); (b) R. E. Walker, *Phys. Fluids*, **4**, 1211 (1961).

(3) F. A. Cleland and R. H. Wilhelm, *A.I.Ch.E. J.*, **2**, 489 (1956).

(4) J. P. Vignes and P. J. Trambouze, *Chem. Eng. Sci.*, **17**, 73 (1962).

nonuniform concentration profile upon extent of reaction (*i.e.*, reactor productivity). Krongelb and Strandberg⁵ also used numerical methods to examine mass transport with second-order homogeneous and first-order heterogeneous reactions, and discussed conditions for minimizing the wall reaction. The effects of termolecular combination reactions and convective flow on measurements of atom removal by catalytic surfaces in "side-arm diffusion" apparatus have been examined by Wise and Ablow.⁶ The results were also applied to evaluation of homogeneous atom combination kinetics. The problem of diffusion and chemical reaction also arises in investigations of ion-molecule reactions in flowing afterglow apparatus, and approximate treatments in which the highly efficient removal of ions at the reactor surface are taken into account have recently been published.⁷

In spite of the published work on solutions of the continuity equation in tubular flow reactors, to our knowledge there is not yet a general scheme for obtaining kinetic parameters from experiments where a parabolic concentration profile exists. The earlier approximate treatments^{2a,b} and the later precise numerical results^{3,4} were concerned almost solely with the qualitative and quantitative effects of a nonuniform residence time distribution upon the extent of a chemical reaction, which is the important chemical engineering question. The other investigations⁵⁻⁷ have treated special cases having the factor of a catalytic surface in common.

The objective of this research was to solve the continuity equation for some simple kinetic cases and to present the results in such a form as to be useful to kineticists for extracting reasonably accurate values of rate constants for elementary reactions from data obtained with a tubular reactor over a wide pressure range. Accordingly, numerical solutions for first- and second-order kinetics were obtained. The theoretical model was verified by comparison with experimental results for some hydroxyl radical reactions.

Theory

The conditions under which many flow experiments are done may be modeled by laminar, incompressible flow. Also, a system composed of a diluent plus several components at low concentration can be treated as a binary system composed of the diluent and the component of interest.⁸ Under these conditions the continuity equation for a binary system of constant density with chemical reaction is

$$V_0 \left[1 - \left(\frac{r}{R} \right)^2 \right] \frac{\partial c}{\partial z} = D \left[\frac{1}{r} \frac{\partial}{\partial r} r \frac{\partial c}{\partial r} + \frac{\partial^2 c}{\partial z^2} \right] + kc^n \quad (1)$$

with the boundary and initial conditions $c = c_0$ at $z = 0$, $\partial c / \partial t = 0$ at $r = 0$, and $-D\partial c / \partial r = k_w C$ at $r = R$. The form of the chemical rate law used in eq 1, kc^n , arises since this work is solely concerned with elemen-

tary chemical reactions. The only cases of importance will be $n = 1$ and $n = 2$ since termolecular combination reactions, where the third body is an inert heat bath molecule, will follow a pseudo-second-order rate law. Bimolecular reactions between different chemical species can be made to follow pseudo-first-order kinetics by adding one reactant to large excess. The case of second-order reaction between different species present in similar concentrations was not treated in this investigation.

Assuming that axial diffusion is negligible in comparison to bulk flow in the axial direction, the dimensionless form of the continuity equation is

$$(1 - u)^2 \frac{\partial \theta}{\partial \lambda} = \alpha \frac{1}{u} \frac{\partial}{\partial u} u \frac{\partial \theta}{\partial u} - \theta^n \quad (2)$$

with $\theta = 1$ at $\lambda = 0$, $\partial \theta / \partial \lambda = 0$ at $u = 0$, and $-\alpha \partial \theta / \partial u = \beta \theta$ at $u = 1$; where $u = r/R$, $\theta = c/c_0$, and $n =$ kinetic order of the chemical reaction. For $n = 1$, $\lambda = kz/v_0$, $\alpha = D/kR^2$, and $\beta = k_w/kR$, while for $n = 2$, $\lambda = kC_0z/v_0$, $\alpha = D/kc_0R^2$, and $\beta = k_w/kc_0R$. Equation 2 was solved for θ as a function of u and λ in an isothermal system by the method of finite differences for $n = 1$ and $n = 2$ on the University of Minnesota CDC 6600 digital computer. The case of homogeneous first- or second-order reaction with concurrent first-order wall reaction was handled by letting the parameter β in the boundary condition $-\alpha \partial \theta / \partial u = \beta \theta$ have positive values. For homogeneous reaction only, β was set equal to zero. For first-order kinetics, the treatment followed Cleland and Wilhelm.³ The treatment of the second-order case is outlined in the Appendix. In each case the size of the increments was decreased until no significant gain in accuracy resulted.

Concentrations were averaged over radial direction by three different methods

$$\bar{c}_1 = \int_0^1 \theta \, du \quad (3)$$

$$\bar{c}_2 = 2 \int_0^1 \theta \, u \, du \quad (4)$$

$$\bar{c}_3 = 4 \int_0^1 [1 - u^2] \theta \, u \, du \quad (5)$$

Equation 3 is the average along a principal diameter of the reactor, and is the average measured by the apparatus used for the experiments described below. Equation 4 averages over a cross section, such as might be

(5) S. Krongelb and M. W. P. Strandberg, *J. Chem. Phys.*, **31**, 1196 (1959).

(6) H. Wise and C. M. Ablow, *ibid.*, **35**, 10 (1961).

(7) R. W. Huggins and J. H. Cahn, *J. Appl. Phys.*, **38**, 180 (1967); E. E. Ferguson, F. C. Fehsenfeld, and A. L. Schmeltekopf, *Advan. At. Mol. Phys.*, **5**, 1 (1969); R. C. Bolden, R. S. Hemsworth, M. J. Shaw, and N. D. Twiddy, *J. Phys. B*, **3**, 45 (1970); A. L. Farragher, *Trans. Faraday Soc.*, **66**, 1411 (1970).

(8) R. B. Bird, W. E. Stewart, and E. N. Lightfoot, "Transport Phenomena," Wiley, New York, N. Y., 1960, p 570.

approximated by an esr detection system, and (5) is the "cup mixing" average. The concentration that would be measured by mass spectrometric detection with a pinhole leak on the reactor axis would be obtained by calculating θ vs. λ at $u = 0$, and no averaging procedure need be done.

Experimental Section

The apparatus was similar to that used by Kaufman and Del Greco.⁹ The reactor was a quartz tube 3 cm in diameter by 150 cm long. Reactants diluted by helium could achieve flow velocities of up to 6×10^3 cm sec⁻¹ with a Kinney KDH 130 high-capacity vacuum pump. At the upstream end a 2-cm diameter glass ring formed from 3-mm o.d. Pyrex tubing and pierced with 30 small holes appropriately spaced around the inner and outer circumference served as a dispersing inlet for NO₂. The effectiveness of mixing was tested by observing chemiluminescence from the reaction of atomic oxygen with nitric oxide.¹⁰ The emission was of uniform intensity at the inlet, and no striations were observable downstream. Also, an experiment was done in which helium was added to the nitrogen dioxide before the inlet ring. This increased the velocity of the gas emerging from the ring, thus increasing the effectiveness of mixing. No change in the hydroxyl decay characteristics were observed, which was taken as evidence in favor of good mixing without added helium.

Hydroxyl radical concentrations were determined by the line absorption technique. The light source consisted of 0.6% by volume of water vapor in argon at 18 Torr flowing in a 13-mm o.d. quartz tube through a Fehsenfeld, Evenson, and Broida¹¹ designed microwave cavity. The cavity was powered by a Raytheon PGM-10 generator operating at 10% of power, and was tuned such that a hydroxyl rotational temperature of approximately 500°K was maintained. A narrow beam of light from the source passed through the reactor three times within a 3-mm axial distance before entering the 0.5-m grating spectrometer which isolated either the P₁₂ or the Q₁₄ line, which were interchangeably used as absorption sources with no difference in results. The IP28 photomultiplier output was displayed on a 1-mV strip chart recorder. The light source and monochromator traversed the axial reactor direction on their lathe-bed carriage mounting.

Flow rates were measured with Brooks rotameters which were calibrated, with the exception of NO₂, with a "wet test meter." The NO₂ rotameter was calibrated by a weighing technique. Nitrogen dioxide was supplied from a Pyrex reservoir of liquid maintained at 0°. All other gases were taken directly from cylinders. The 99.9% helium and argon were from Air Reduction Co., 99.9% hydrogen from National Cylinder Gas, while 99.9% carbon monoxide, 99.5% nitrogen dioxide, and CP ethylene were from Matheson.

Atomic hydrogen was generated by passing molecular

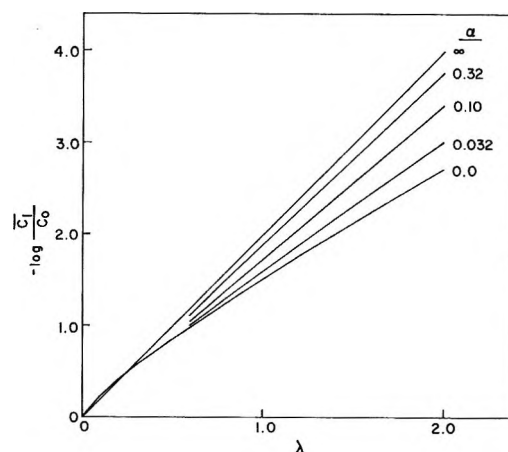


Figure 1. Solutions of the continuity equation for a first-order reaction. Average concentration = C_1 , $\beta = 0$.

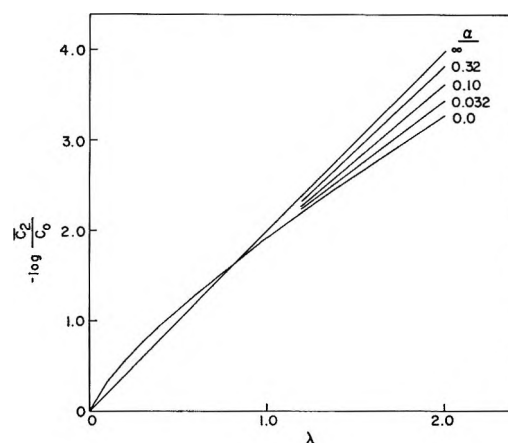


Figure 2. Solutions of the continuity equation for a first-order reaction. Average concentration = C_2 , $\beta = 0$.

hydrogen containing 3% water vapor through a water-cooled Fehsenfeld, Evenson, and Broida¹¹ microwave cavity coupled to a PGM-10 generator. The cavity was on a quartz side arm located 10 cm upstream from the nitrogen dioxide inlet. The yield of atomic hydrogen was measured by a tandem platinum calorimetric probe technique.¹² Complete dissociation of hydrogen was obtained for the flow rates most commonly used in this work.

The temperature in the reaction zone was measured by a glass-enclosed copper-constantan thermocouple which was inserted through a close fitting rubber sleeve at the downstream end of the reactor. Under typical operating conditions the temperature variation in the reaction zone varied as much as 20–30°K in the axial

(9) F. P. Del Greco and F. Kaufman, *Discuss. Faraday Soc.*, **33**, 128 (1962).

(10) P. Harteck, R. R. Reeves, and G. Mannella, *J. Chem. Phys.*, **29**, 1333 (1958).

(11) F. C. Fehsenfeld, K. M. Evenson, and H. P. Broida, *Nat. Bur. Stand. Rept.*, No. 8701 (1964).

(12) R. V. Poirier, Ph.D. Dissertation, University of Minnesota, Minneapolis, Minn., 1970.

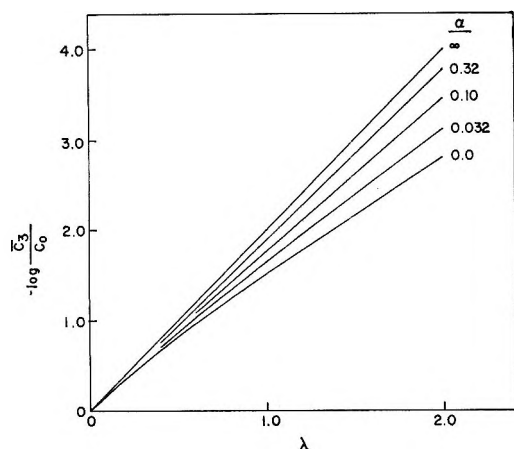


Figure 3. Solutions of the continuity equation for a first-order reaction. Average concentration = C_3 , $\beta = 0$.

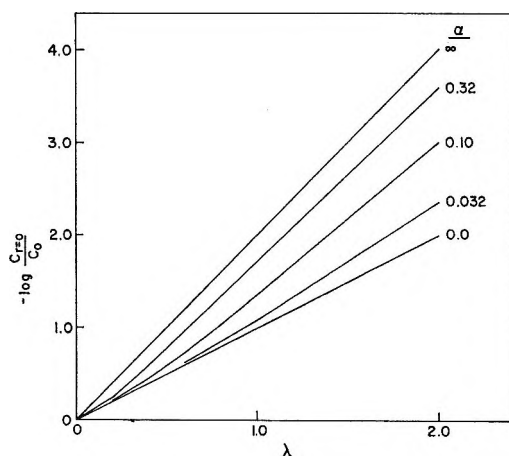


Figure 4. Solutions of the continuity equation for a first-order reaction. $C_{r=0}$ is concentration evaluated along the reactor axis, $\beta = 0$.

direction. The reactor walls were coated with G.E. "Drifilm," a mixture of silanes, to retard wall reactions.

For the range of flow conditions used in these experiments, the Reynolds numbers varied from $Re = 0.1$ to 1.0. The maximum reactor entrance length (calculated from $L_e = 0.035 d Re$, ref 8 p 47) was 0.2 cm.

Results

Computer solutions of the continuity equation are displayed in Figures 1-9. For the first-order homogeneous reaction, Figures 1-3 are the solutions for the different average concentrations given by eq 3-5, respectively, and Figure 4 is the computer result for concentration along the reactor axis. Figures 5-8 are the corresponding solutions for a second-order homogeneous reaction, while Figure 9 displays the theoretical results for \bar{c}_1 with a second-order homogeneous reaction and a first-order wall reaction. In each of these plots the ordinate was deliberately chosen as the functional form of concentration ($\ln c$ and $1/c$) commonly plotted vs.

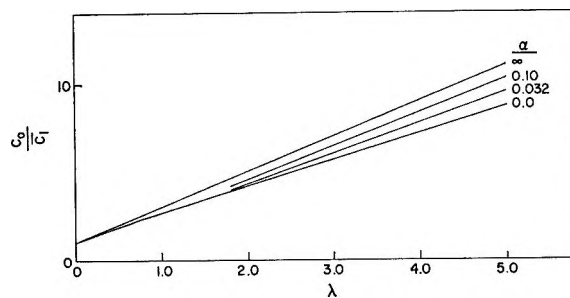


Figure 5. Solutions of the continuity equation for a second-order reaction. Average concentration = C_1 , $\beta = 0$.

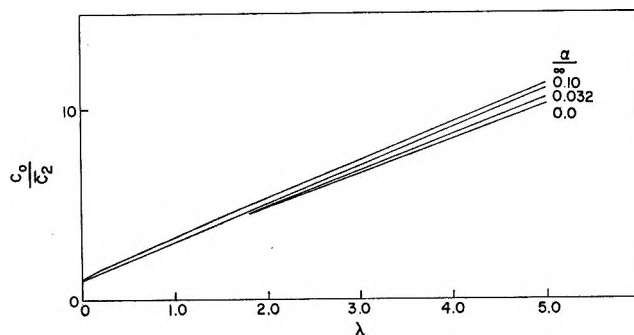


Figure 6. Solutions of the continuity equation for a second-order reaction. Average concentration = C_2 , $\beta = 0$.

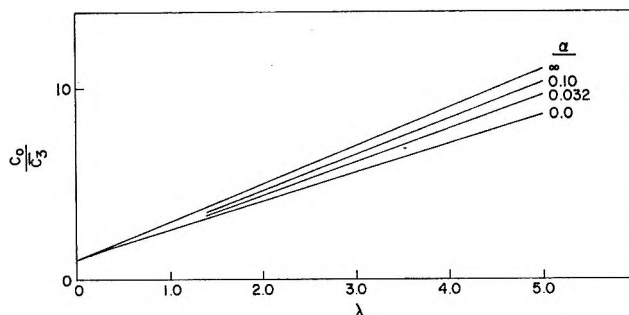


Figure 7. Solutions of the continuity equation for a second-order reaction. Average concentration = C_3 , $\beta = 0$.

time for first- or second-order reactions. The abscissa is a dimensionless distance which may be converted to time if the concentration profile is assumed to be uniform. The figures are therefore in a conventional form used by kineticists. The concentration profile is flat only when $\alpha = \infty$, and for this condition the slopes of Figures 1-8 are related to the true value of the reaction rate constant. For $\alpha < \infty$ the plots for both first- and second-order reactions show slight curvature near the origin, and a nearly linear region of lower slope than at $\alpha = \infty$.

The concentration of hydroxyl is related to optical density by Beer's law when $I_0/I < 1.5$.¹³

$$[\text{OH}] = \frac{1}{x} \log \frac{I_0}{I} \quad (6)$$

(13) A. G. C. Mitchell and M. W. Zemansky, "Resonance Radiation and Excited Atoms," Cambridge and New York, 1961.

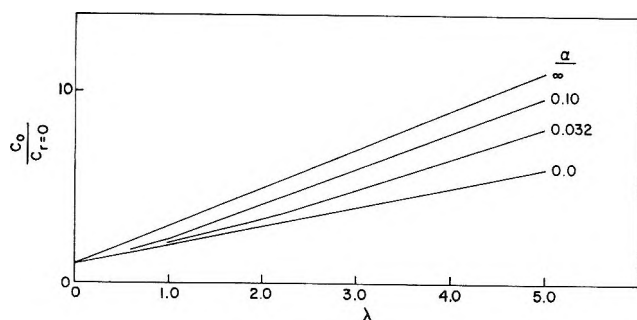


Figure 8. Solutions of the continuity equation for a second-order reaction. $C_{T=0}$ is concentration evaluated along the reactor axis, $\beta = 0$.

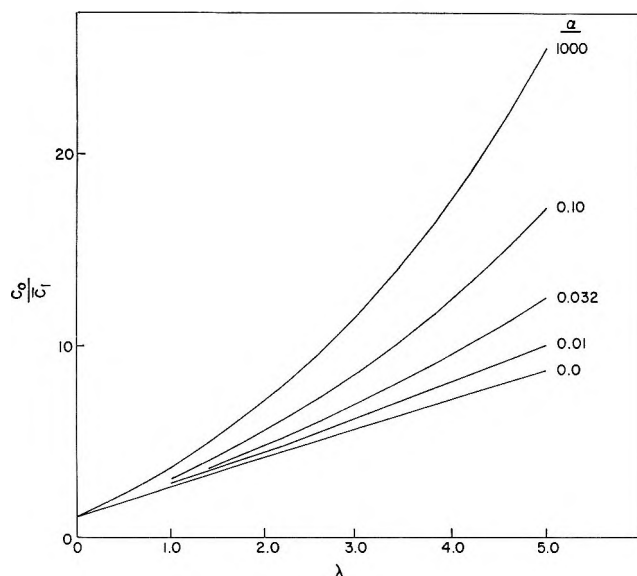


Figure 9. Solutions of the continuity equation for a second-order reaction and wall reaction. Average concentration = C_1 , $\beta = 0.07$.

and a plot of $\log (I_0/I)^{-1}$ vs. time should be linear if hydroxyl decays by a second-order rate law. Figure 10 shows such a plot obtained under typical experimental conditions and at "low pressure," *e.g.*, 1.05 Torr. The value of the extinction coefficient, κ , for the P₁₂ line was empirically determined. Its value was $4.55 \pm 0.25 \times 10^8$ cc mol⁻¹ at 340°K, which is in satisfactory agreement with the value 4.3×10^8 cc mol⁻¹ which was calculated from the P₁₂ line oscillator strength measured by Golden, Del Greco, and Kaufman.¹⁴ The linearity of Figure 10 and other similar plots obtained during this investigation supports the use of hydroxyl decay data to test the theoretical model. Accordingly, experiments were done over the pressure range 1–15 Torr. Work at higher pressures was not possible owing to the pump capacity limitation. Representative data are given in Figure 11. In this series of experiments, all flow rates except the helium diluent were kept constant, and all other experimental conditions were the same.

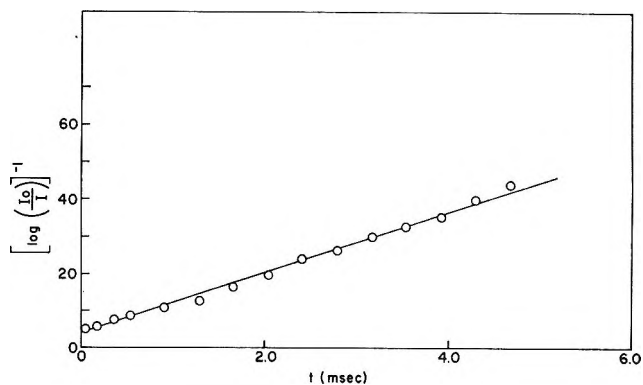


Figure 10. Second-order hydroxyl decay plot. Least-squares slope = 8.2 msec^{-1} . Experimental conditions: $w_{\text{NO}_2} = 0.0180$ m mol sec⁻¹, $w_{\text{H}_2} = 0.0675$ m mol sec⁻¹, $w_{\text{total}} = 1.76$ m mol sec⁻¹; $(\text{OH})_0 = 8.7 \times 10^{-3}$ Torr; $\bar{v} = 61.1$ m sec⁻¹; $T = 336^\circ\text{K}$.

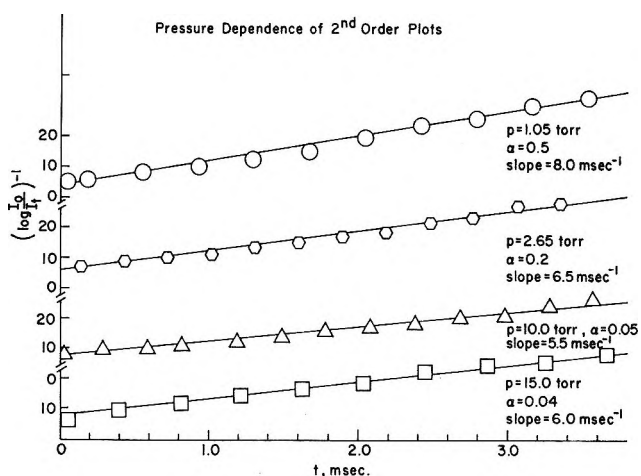


Figure 11. Pressure dependence of second-order hydroxyl decay plots; $w_{\text{NO}_2} = 0.0231$ m mol sec⁻¹, $w_{\text{H}_2} = 0.068$ m mol sec⁻¹.

The reproducibility of the slopes of the second-order plots was tested by doing a number of experiments at the same initial conditions. The conditions chosen were those of low $[\text{OH}]$, where, owing to the low light absorbance, the greatest error is to be expected. The slopes were reproduced to within 10%. At higher $[\text{OH}]$, such as in the experiments of Figure 11, the reproducibility was considerably better.

Discussion

The computer results clearly show that experimental data taken at pressures where $\alpha < \infty$, and plotted in the conventional way, may appear to yield satisfactorily linear first- or second-order plots for homogeneous reactions. The expected curvature in the vicinity of the origin may be obscured by random experimental error, or by effects caused by inefficient mixing of the reactants. Thus the uncritical use of the relationship

(14) D. M. Golden, F. P. Del Greco, and F. Kaufman, *J. Chem. Phys.*, **39**, 3034 (1963).

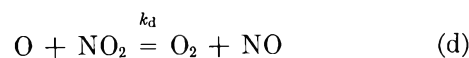
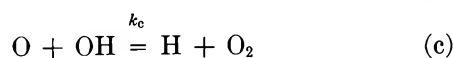
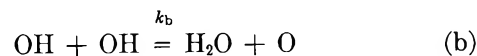
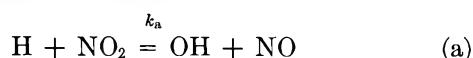
$t = z/\bar{v}$ to calculate reaction time in flow regimes where it is no longer warranted leads to rate constants which are *smaller* than the true value. The deviation may be as much as a factor of 2 in unfavorable cases. In practice, however, the calculation of reaction time by use of the uniform concentration profile approximation is probably satisfactory for $0.5 \lesssim \alpha < \infty$, or for even smaller values of α if accuracy is not necessary.

It is apparent from Figures 1–8 that to obtain accurate values of rate constants in tubular reactors one must obtain data with experimental conditions such that α is large, or operate at other conditions and estimate the deviation of the apparent rate constant from the true value with the aid of theoretical results such as presented in Figures 1–9. The latter case may be necessary if it is not experimentally feasible to do the experiments with suitably large values of α . For example, in the second-order homogeneous case, if wall reactions are not negligible the behavior illustrated in Figure 9 is predicted, where the wall reaction is most pronounced at large values of α . In the first-order homogeneous case with competing first-order wall reaction it is apparent that the first-order plots will remain linear, but will yield a larger spread of slopes between $\alpha = 0$ and $\alpha = \infty$ than those predicted by the first-order homogeneous case alone. An experimental procedure would be to operate at conditions such that the effect of diffusion is small (α small) and estimate a correction factor to the apparent rate constant based on Figures 1–8, where the wall reaction is not included.

To estimate such a correction one must have values for D and k . If an experimental value for D is not available, it can be estimated by the methods described in the literature.¹⁵ The experimentally obtained apparent rate constant can be used as an estimate for the required rate constant when initially calculating α . At the extremes of α large and α small in the case of no wall reaction, and α small when wall reactions are important, the slopes of the theoretical curves are relatively insensitive to α and hence to estimated values of D and k . Thus, only a rough estimate of D is required if the experiments can be conducted under such conditions. The calculation of α and λ can then be done and an estimate made of the deviation of the apparent rate constant from the true rate constant. The corrected value can then be used to obtain an improved correction factor if this becomes necessary.

The theoretical model was tested with the bimolecular disproportionation of hydroxyl radicals. Also, a limited test was achieved in the reaction of hydroxyl with ethylene, which followed a pseudo-first-order rate law under the experimental conditions used.

According to previous investigations,^{9,16–20} the atomic hydrogen–nitrogen dioxide reaction system can be described by reactions a–d



Since reaction a is very fast,¹⁷ and since the experiments reported here were done with the initial conditions $[\text{H}]_0/[\text{NO}_2]_0 = 10$, nitrogen dioxide is nearly completely consumed (98%) in the first centimeter of the approximately 20-cm reaction zone. Since $k_c \simeq 10k_b$, a steady-state assumption on atomic oxygen has been made in the past, leading to the following rate law for the downstream region where the rates of reactions a and d are negligible.

$$\frac{-d(\text{OH})}{dt} = 3k_b(\text{OH})^2 \quad (7)$$

The validity of eq 7 was tested by solving the four simultaneous rate equations for reactions a–d on the CDC 6600 digital computer using the Runge-Kutta method. Using the cited values for the rate constants, and an initial excess of atomic hydrogen over nitrogen dioxide, the results of Figure 12 were obtained. Also plotted on Figure 12 is the solution of eq 7 assuming the same k_b as used in the computer simulation. It is apparent that eq 7 is an adequate representation of the rate of disappearance of hydroxyl.

A wall removal of hydroxyl was considered, and it was concluded that while a wall reaction may be occur-

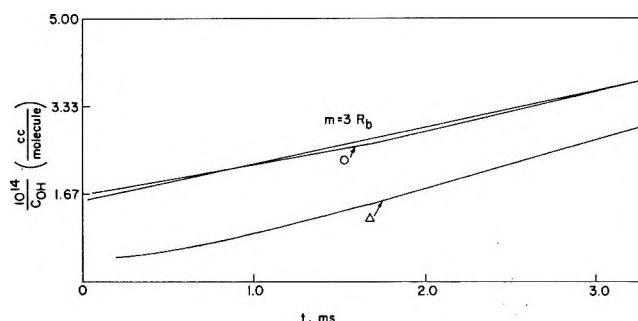


Figure 12. Computer simulation of hydroxyl decay for reactions a–d. Parameters chosen: $k_a = 5 \times 10^{-11}$ cc molecule⁻¹ sec⁻¹, $k_b = 2.5 \times 10^{-12}$ cc molecule⁻¹ sec⁻¹, $k_c = 1.7 \times 10^{-11}$ cc molecule⁻¹ sec⁻¹, $k_d = 5.3 \times 10^{-12}$ cc molecule⁻¹ sec⁻¹; O, $C_{0,\text{NO}_2} = 6 \times 10^{13}$ molecules cc⁻¹, $C_{0,\text{H}} = 6 \times 10^{14}$ molecules cc⁻¹; Δ, $C_{0,\text{NO}_2} = 3 \times 10^{14}$ molecules cc⁻¹, $C_{0,\text{H}} = 4.0 \times 10^{14}$ molecules cc⁻¹.

(15) J. O. Hirschfelder, C. F. Curtiss, and R. B. Bird, "Molecular Theory of Gases and Liquids," Wiley, New York, N. Y., 1954.

(16) F. Kaufman and F. P. Del Greco, *Symp. (Int.) Combust. [Proc.]*, 9th, 659 (1963).

(17) L. F. Phillips and H. I. Schiff, *J. Chem. Phys.*, 37, 1233 (1962).

(18) G. Dixon-Lewis, W. E. Wilson, and A. A. Westenberg, *ibid.*, 44, 2877 (1966).

(19) A. A. Westenberg and N. De Haas, *ibid.*, 43, 1550 (1965).

(20) J. E. Breen and G. P. Glass, *ibid.*, 52, 1082 (1970).

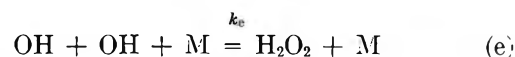
ring it is not necessary for an adequate explanation of the qualitative experimental observations. During the early stages of experimentation slight curvature of the inverse hydroxyl concentration *vs.* time curves, obtained with a large excess of H, was noticed. Consequently, the walls of the reactor were coated with "Drifilm," a solution of silanes. No appreciable changes in the curves were apparent. It was concluded that some curvature should be expected as indicated by an exact solution of the proposed mechanism of reactions a-d, Figure 12. Computer simulation revealed that the curvature is greatly increased when there is only a slight excess of atomic hydrogen, and this was experimentally verified.

The value of k_b obtained by setting the slope of Figure 10 equal to $3k_b/\alpha$ was 2.04×10^{-12} cc molecule⁻¹ sec⁻¹. This is between the values 2.65×10^{-12} cc molecule⁻¹ sec⁻¹ reported by Dixon-Lewis, Wilson, and Westenberg,¹⁸ and 1.4×10^{-12} cc molecule⁻¹ sec⁻¹ reported by Kaufman.²¹ Although it was not possible to ascertain whether wall reactions involving hydroxyl occurred in these experiments, a correction for a possible first-order wall removal of hydroxyl, having a rate constant $k_w = 80$ sec⁻¹, obtained from independent experiments,²² reduced k_b to 0.68×10^{-12} cc molecule⁻¹ sec⁻¹. This is close to the value 0.84×10^{-12} cc molecule⁻¹ sec⁻¹ reported by Breen and Glass,²⁰ who are the only others to have made such a correction. Furthermore, values of k_b obtained from plots similar to Figure 10 showed a previously unreported dependence upon nitrogen dioxide flow rate; k_b decreased with increasing nitrogen dioxide flow rate, all other conditions being held constant. The range of rate constants obtained, assuming eq 7, was from 4.65×10^{-12} cc molecule⁻¹ sec⁻¹ to 0.91×10^{-12} cc molecule⁻¹ sec⁻¹ which encompasses the range of previously reported values. Rate constants at the lower end of the range were obtained under conditions close to those used by Kaufman, *et al.*,¹⁶ while those at the upper end of the range were obtained at conditions approaching those of Westenberg, *et al.*^{18,19} Equations a-d are incapable of accounting for this effect even if removal of hydroxyl at the wall is included.

Regardless of the correct value of k_b , the apparent linearity of Figure 10 as well as other similar plots supports the use of hydroxyl decay data as a test of the theoretical model for a second-order reaction. Experimental data were obtained at constant flow rates of nitrogen dioxide and atomic hydrogen but at varying pressures, Figure 11. The slopes of these plots decrease with increasing pressure as is predicted by theory, except at 15 Torr, where a slight increase over the slope at 10 Torr was observed. The binary diffusion coefficient for hydroxyl in helium was calculated¹⁵ to be $D = 830/P$ cm² sec⁻¹, from which the parameter α was calculated to be 0.5 at 1.05 Torr, 0.2 at 2.65 Torr, and 0.05 at 10.0 Torr. The slope of the experimental

curves decreased by a factor of 1.45 over the 10 Torr pressure range involved, while inspection of Figure 5 indicates that a decrease in slope, due to the change in the radial concentration profile, of a factor of about 1.2 would be expected for the range of α covered. At 10 Torr, the apparent second-order rate constant is 1.40×10^{-12} cc molecule⁻¹ sec⁻¹. Correction by the theoretical factor of 1.2 yields $k_b = 1.68 \times 10^{-12}$ cc molecule⁻¹ sec⁻¹, compared with the experimental value, 2.0×10^{-12} cc molecule⁻¹ sec⁻¹, obtained at 1.05 Torr. The approximately 20% discrepancy may be due in part to experimental error, and in part to the effects of wall removal of hydroxyl which makes a greater contribution to the rate of hydroxyl decay at 1 Torr than at 15 Torr.

The increase in the apparent value of k_b observed at 15 Torr may be due to the occurrence of



Caldwell and Back²³ have reported $k_e = 0.85 \times 10^{-33}$ cm⁶ molecule⁻² sec⁻¹. Using this value along with $k_b = 2.0 \times 10^{-12}$ cm³ molecule⁻¹ sec⁻¹, $R_e/R_b = 1.3 \times 10^{-2}$ at 1 Torr and 0.19 at 15 Torr, where P stands for differential reaction rate. Thus at 15 Torr the rate of termolecular hydroxyl combination becomes an important additional path for hydroxyl decay, whereas at 1 Torr it is negligible.

In view of the preceding considerations a precise, quantitative test of the second-order case was not attempted. The general agreement between theory and experiment, however, was considered satisfactory.

A pseudo-first-order reaction, the addition of hydroxyl to ethylene in excess ethylene, was briefly studied over the narrower pressure range 1-5 Torr. The apparent first-order rate constant changed by approximately the amount predicted in Figure 1 over the range of the parameter α spanned by the experiments.

The *maximum* effect of increasing pressure predicted by the results of this work is to cause the apparent rate constants to be about 50% smaller than their true value. The most deviation is predicted for axial sampling, *i.e.*, mass spectrometry, while other experimental methods predict lesser deviations. We feel that the approximations made in solving eq 1 are not severe, since experiments can usually be designed to approximate isothermal and isobaric conditions. If these experimental conditions are attained, then the analysis presented here can be reliably used to estimate rate constants of elementary chemical reactions where data have been taken at "high" pressures in tubular flow reactors.

(21) F. Kaufman, *Ann. Geophys.*, **20**, 106 (1964).

(22) A. Pastrana, unpublished results, University of Minnesota.

(23) J. Caldwell and R. A. Back, *Trans. Faraday Soc.*, **61**, 1939 (1965).

Symbols

C	concentration
C_0	initial concentration
D	diffusion coefficient
d	reactor diameter
I	transmitted intensity of light from source
I_0	incident intensity of light from source
k	homogeneous rate constant
k_w	heterogeneous rate constant
P	pressure
R	radius of reactor
r	radial distance
T	temperature
t	time
V_0	axial velocity at $r = 0$
w	flow rate
z	axial distance
α	D/kC_0R^2
β	k_w/kC_0R
κ	extinction coefficient
λ	kC_0z/V_0

Appendix

In difference form, eq 2 for $n = 2$ becomes

$$(1 - u_j^2) \left[\frac{C_j^{\kappa+1} - C_j^{\kappa}}{\Delta\lambda} \right] = \alpha \left[\frac{C_{j+1}^{\kappa+1} + C_{j-1}^{\kappa+1} - 2C_j^{\kappa+1} + C_{j+1}^{\kappa} + C_{j-1}^{\kappa} - 2C_j^{\kappa}}{2(\Delta u)^2} \right] + \left[\frac{C_{j+1}^{\kappa+1} - C_{j-1}^{\kappa+1} + C_{j+1}^{\kappa} - C_{j-1}^{\kappa}}{4u_j\Delta u} \right] - \left[\frac{C_j^{\kappa+1} + C_j^{\kappa}}{2} \right]^2$$

where the subscript refers to the increment in the radial direction and the superscript to the increment in the axial direction. The boundary conditions become

$$\frac{C_0^{\kappa} - C_1^{\kappa} + C_0^{\kappa+1} - C_1^{\kappa+1}}{2\Delta u} = 0 \text{ at } u = 0$$

$$\alpha \left[\frac{C_{N-1}^{\kappa} - C_N^{\kappa} + C_{N-1}^{\kappa+1} - C_N^{\kappa+1}}{2\Delta u} \right] = \beta C_N^{\kappa+1} \text{ at } u = 1$$

Thus, one has $N + 1$ simultaneous nonlinear partial differential equations. Using a method similar to that used by Bruce, Peaceman, Rachford, and Rice,²⁴ the equations are linearized

$$C_0^{\kappa+1} - C_1^{\kappa+1} = -C_0^{\kappa} + C_1^{\kappa}$$

$$-\alpha \left[\frac{2u_j}{(\Delta u)^2} - \frac{1}{\Delta u} \right] C_{j-1}^{\kappa+1} + u_j \left[\frac{4(1 - u_j^2)}{\Delta\lambda} + \right.$$

$$\left. \frac{4\alpha}{(\Delta u)^2} + 2C_j^{\kappa} + P_j^{\kappa+1} \right] C_j^{\kappa+1} - \alpha \left[\frac{2u_j}{(\Delta u)^2} + \frac{1}{\Delta u} \right] C_{j+1}^{\kappa+1} = \alpha \left[\frac{2u_j}{(\Delta u)^2} - \frac{1}{\Delta u} \right] C_{j-1}^{\kappa} + u_j \left[\frac{4(1 - u_j^2)}{\Delta\lambda} - \frac{4\alpha}{(\Delta u)^2} - C_j^{\kappa} \right] C_j^{\kappa} + \alpha \left[\frac{2u_j}{(\Delta u)^2} + \frac{1}{\Delta u} \right] C_{j+1}^{\kappa} - \left[\frac{\alpha}{2\Delta u} \right] C_{N-1}^{\kappa+1} + \left[\frac{\alpha}{2\Delta u} + \beta \right] C_N^{\kappa+1} = \left[\frac{\alpha}{2\Delta u} \right] C_{N-1}^{\kappa} - \left[\frac{\alpha}{2\Delta u} \right] C_N^{\kappa}$$

The predictive equation

$$(1 - u_j^2) \left[\frac{C_j^{\kappa+1} - C_j^{\kappa}}{\Delta\lambda} \right] = \alpha \left[\frac{C_{j+1}^{\kappa} + C_{j-1}^{\kappa} - 2C_j^{\kappa}}{(\Delta u)^2} + \frac{1}{u_j} \frac{C_{j+1}^{\kappa} - C_{j-1}^{\kappa}}{2\Delta u} \right] - \left[\frac{C_j^{\kappa+1} + C_j^{\kappa}}{2} \right]^2$$

is used to predict a value for $C_j^{\kappa+1} = P_j^{\kappa+1}$. Writing the equations in linear form

$$B_0 C_0^{\kappa+1} + D_0 C_1^{\kappa+1} = -E_0 C_0^{\kappa} - D_0 C_1^{\kappa} \quad j = 0$$

$$A_j C_{j-1}^{\kappa+1} + B_j C_j^{\kappa+1} + D_j C_{j+1}^{\kappa+1} = -A_j C_{j-1}^{\kappa} + E_j C_j^{\kappa} - D_j C_{j+1}^{\kappa} \quad 1 \leq j \leq N - 1$$

$$A_N C_{N-1}^{\kappa+1} + B_N C_N^{\kappa+1} = -A_N C_{N-1}^{\kappa} + E_N C_N^{\kappa} \quad j = N$$

or

$$B_0 C_0^{\kappa+1} + D_0 C_1^{\kappa+1} = W_0^{\kappa}$$

$$A_j C_{j-1}^{\kappa+1} + B_j C_j^{\kappa+1} + D_j C_{j+1}^{\kappa+1} = W_j^{\kappa}$$

$$A_N C_{N-1}^{\kappa+1} + B_N C_N^{\kappa+1} = W_N^{\kappa}$$

Writing the equations in matrix form

$$\begin{bmatrix} B_0 & D_0 & 0 & 0 & \dots \\ A_1 & B_1 & D_1 & 0 & \dots \\ 0 & A_1 & B_2 & D_2 & \dots \\ \vdots & & & & \end{bmatrix} [C_j^{\kappa+1}] = [W_j^{\kappa}]$$

Applying the appropriate operations to this equation, it becomes

$$\begin{bmatrix} 1 & f_0 & 0 & 0 & \dots \\ 0 & 0 & f_1 & 0 & \dots \\ 0 & 0 & 1 & f_2 & \dots \\ \vdots & & & & \end{bmatrix} [C_j^{\kappa+1}] = [g_j]$$

(24) G. H. Bruce, D. W. Peaceman, H. H. Rachford, and J. D. Rice, *Trans. AIME*, 198, 79 (1953).

where

$$f_0 = \frac{D_0}{B_0} \quad f_N = 0$$

$$f_j = \frac{D_j}{B_j - A_j f_{j-1}} \quad 1 \leq j \leq N - 1$$

$$g_0 = \frac{W_0}{B_0}$$

$$g_j = \frac{A_j^{\kappa} - A_j g_{j-1}}{B_j - A_j f_{j-1}} \quad 1 \leq j \leq N$$

From this equation the concentration is easily calculated.

$$C_j^{\kappa+1} = g_j - f_j C_{j+1}^{\kappa+1}$$

The procedure is to obtain a value of $P_j^{\kappa+1}$ from the predictive equation, calculate g_j , f_j , and then $C_j^{\kappa+1}$, compare these values with the predicted values, and if they are not within the required error repeat the procedure using the calculated $C_j^{\kappa+1}$ values as the predictive values. Repeat this procedure until the required accuracy is attained.

A computer program has been written to solve these equations for first- and second-order reactions.¹²

Mass Spectrometric Studies of Rate Constants for Addition Reactions of Hydrogen and of Deuterium Atoms with Olefins in a Discharge-Flow System at 300°K

by E. E. Daby, H. Niki,* and B. Weinstock

Scientific Research Staff, Ford Motor Company, Dearborn, Michigan 48121 (Received December 29, 1970)

Publication costs assisted by the Ford Motor Company

Absolute rate constants for the addition reaction of H and of D atoms with a number of olefinic hydrocarbons have been determined directly at 25° using mass spectrometric detection in a fast discharge-flow system. The rate constants obtained range from 0.7 to 9×10^{-12} cm³ molecule⁻¹ sec⁻¹, and their ratios agree well with relative values reported by Cvetanović and coworkers. The relevant reaction scheme is $\text{H} + (\text{olefin})_1 \xrightleftharpoons[k'_e]{k_{t(e)}}$

R_1^* ; $\text{R}_1^* \xrightarrow{k_e} \text{R}_2 + (\text{olefin})_{II}$; $\text{R}_1^* \xrightarrow{\omega} \text{R}_1$. Under the experimental conditions used, the observed bimolecular rate constants yield $k_{t(e)}$ directly in most cases. The systematic variations of rate constant with molecular structure of the olefins are discussed.

Introduction

When atomic hydrogen reacts with olefinic hydrocarbons, chemically activated alkyl radicals are formed. The subsequent unimolecular dissociation of these adducts has been the subject of extensive experimental and theoretical studies.¹ The absolute rate constants for the initial addition reactions are known to a much lesser degree² with the exception of ethylene. Values of the absolute rate constant for the addition of atomic hydrogen to ethylene have been determined by a variety of experimental techniques, but show an order of magnitude spread and a critical choice of the most reliable value is difficult to make.³ Several measurements of relative rates for olefins also lack consistency, with the exception of three independent photochemical studies by Cvetanović and coworkers.⁴⁻⁶ In Table I, mean

values of the relative addition rates obtained by Cvetanović's group are compared with those of other systematic studies.^{7,8}

In a previous note from this laboratory, mass spec-

- (1) B. S. Rabinovitch and D. W. Setser, *Advan. Photochem.*, **3**, 1 (1964).
- (2) For reviews prior to 1964: R. J. Cvetanović, *ibid.*, **1**, 115 (1963); B. A. Thrush, *Progr. React. Kinet.*, **3**, 65 (1965).
- (3) See, for example, Table I of ref 6.
- (4) K. R. Jennings and R. J. Cvetanović, *J. Chem. Phys.*, **35**, 1233 (1961).
- (5) G. R. Woolley and R. J. Cvetanović, *ibid.*, **50**, 4697 (1969).
- (6) R. J. Cvetanović and L. C. Doyle, *ibid.*, **50**, 4705 (1969).
- (7) (a) P. E. M. Allen, H. W. Melville, and J. C. Robb, *Proc. Roy. Soc., Ser. A*, **218**, 311 (1953); (b) J. N. Bradley, H. W. Melville, and J. C. Robb, *ibid.*, **236**, 318 (1956).
- (8) K. Yang, *J. Amer. Chem. Soc.*, **84**, 719, 3795 (1962).

Table I: Literature Values of the Relative Rates for H + Olefins at 25°

Olefins	Allen Melville, and Robb ⁷	Yang ⁸	Cvetanović, et al. ⁹
<chem>C=C</chem>	1.0	1.0	1.00
<chem>C=C-C</chem>	0.32 (1.6)	1.3	1.53
<chem>C=C-C-C</chem>			1.58
<chem>C=C</chem> <chem>C</chem>	0.76	13.3	3.85
<chem>C</chem> <chem>C=C</chem> <chem>C</chem>	1.06	0.49	0.72
<chem>C=C</chem> <chem>C</chem>	0.83	0.52	0.90
<chem>C</chem> <chem>C=C</chem> <chem>C</chem>	0.98	2.05	1.28
<chem>C=C-C=C</chem>		23.5	7.5

trometric determinations of absolute rate constants were reported for the reaction of H and of D atoms with *cis*- and *trans*-butene-2 in a discharge-flow system at 300°K.⁹ For these reactions, the absolute rate constants obtained by this technique agreed well with those of other workers, who used entirely different experimental methods.^{7,10} This paper describes an extension of the mass spectrometric studies to a large variety of olefins.

Experimental Section

Reactions of H and of D atoms with olefins have been studied in a fast discharge-flow reactor coupled to a Bendix Type 14 time-of-flight mass spectrometer.¹¹ A schematic diagram of the apparatus is shown in Figure 1. The flow reactor was fitted to a Bendix fast-reaction chamber. The reaction was monitored directly by sampling the reacting gas into the mass spectrometer through a pinhole (~200- μ diam) drilled in a Teflon sheet or through a miniature nozzle (~3-mm length) formed in a Teflon sheet. The olefins were introduced into the reactor through a multiholed outlet probe, whose position was adjustable by means of a sliding rubber vacuum seal, lubricated with silicone grease. Exposure of the greased section of the probe to the atomic hydrogen was prevented by using a long side arm (~20 cm), which was flushed with a small fraction of the diluent helium. The olefin was diluted with a carrier gas, which helped to prevent back diffusion of atomic hydrogen into the probe and also to provide a fast response to flow adjustment of the olefin. The reactor pressure was monitored through this probe with an Octoil oil manometer, which was read with a cathetometer to ± 0.01 Torr. The axial pressure gradient in the reactor was at most 2% of the total

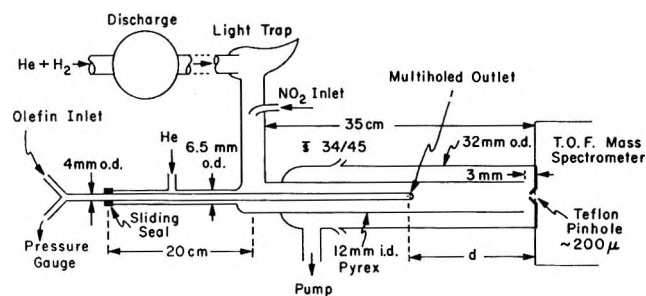


Figure 1. Schematic diagram of the discharge-flow apparatus coupled to a time-of-flight mass spectrometer.

pressure. The average of all pressure readings during a run was used to calculate the linear flow velocity. The reaction temperature was measured to be $300 \pm 2^\circ\text{K}$ with a thermocouple attached externally to the reactor wall. Heat generation by the reaction was assumed to be negligible, since the olefin concentration was generally maintained at an extremely small fraction (~0.01%) of the diluent gas. The reactor walls were coated with G.E. Drifilm to minimize heterogeneous recombination of atomic hydrogen. The extent of the wall recombination was determined by generating H atoms free of H₂ as a product in the reaction of O atoms with C₂H₂ in the presence of an excess of O atoms.¹² The results showed that less than 5% of the total H atoms were recombined under all the experimental conditions used.

Atomic hydrogen was generated by dissociating molecular hydrogen in a microwave discharge. In most runs, molecular hydrogen was highly diluted with He carrier gas, and a large fraction (~50%) of H₂ could be converted to H atoms. The H-atom concentration was determined directly from the extent of the H₂-to-H conversion, and also by the NOCl titration method.¹³ Results obtained by the two methods agreed within 5% for H-atom concentrations of the order of 10¹⁴ atoms per cm³. The impurity O-atom concentration was determined to be always less than 1% of the H-atom concentration. The mass spectral signals for H and H₂ varied linearly with concentration in the range of 10¹² to 10¹⁴ particles per cm³. The mass spectral sensitivities for H and H₂ remained constant to $\pm 5\%$ over the period of half a day, after an initial 1-hr con-

(9) E. E. Daby and H. Niki, *J. Chem. Phys.*, **51**, 1255 (1969).

(10) W. Braun and M. Lenzi, *Discuss. Faraday Soc.*, **44**, 252 (1967).

(11) See, for example, J. V. Michael and H. Niki, *J. Chem. Phys.*, **46**, 4969 (1967); H. Niki, E. E. Daby, and B. Weinstock, *Symp. (Int.) Combust. [Proc.]*, **12th**, 277 (1969).

(12) J. M. Brown and B. A. Thrush, *Trans. Faraday Soc.*, **63**, 630 (1967).

(13) L. F. Phillips and H. I. Schiff, *J. Chem. Phys.*, **37**, 1233 (1962); F. Kaufman and F. P. Del Greco, *Symp. (Int.) Combust. [Proc.]*, **9th**, 659 (1963); M. A. A. Clyne and B. A. Thrush, *Proc. Roy. Soc., Ser. A*, **275**, 544 (1963); A. A. Westenberg and N. deHass, *J. Chem. Phys.*, **43**, 1550 (1965).

(14) R. E. Harrington, B. S. Rabinovitch, and R. D. Diesen, *ibid.*, **32**, 1245 (1960).

ditioning of the microwave discharge, the flow system, and the mass spectrometer. The experiments with D atoms were done similarly. The energy of the ionizing electron beam was kept below 25 eV to obtain an optimum signal-to-noise ratio and minimum interference from cracking patterns of other species present. Four analog outputs were used to monitor reactants and products simultaneously during the course of the reaction.

Flow rates of the diluent He (~ 100 NTP $\text{cm}^3 \text{min}^{-1}$) were measured with calibrated Matheson flow meters. The lowest gas flow rates (< 1 NTP $\text{cm}^3 \text{min}^{-1}$) were determined by the PV method with either an Octoil manometer or a Pace Type-P7D differential pressure transducer. Each flow rate was measured at least three times and the standard deviations generally were within 3%.

Phillips Research grade olefins were used as received. Isomeric impurities in these samples were determined to be less than 3% by gas chromatographic analysis. Ultrahigh purity He and H_2 (Matheson) and CP grade D_2 (Air Products and Chemicals, Inc.) were passed through liquid N_2 traps located in the flow system. Research grade NO_2 (Matheson) was treated with O_2 and was purified by trap-to-trap distillation *in vacuo*.

Experimental Results

Bimolecular rate constants for the reaction of H and of D atoms with a variety of olefins have been determined at 300°K from the exponential decay of the olefin in the presence of a 100-fold excess of atoms, using the integrated pseudo-first-order rate equation

$$k_{\text{exptl}} = \frac{\ln [(\text{olefin})_{t_1}/(\text{olefin})_{t_2}]}{\langle \text{H} \rangle_{\text{av}}(t_2 - t_1)} \quad (1)$$

where $(\text{olefin})_t$ is the concentration of the olefin at reaction time, t , and $\langle \text{H} \rangle_{\text{av}}$ is the average hydrogen atom concentration during the time interval, $(t_2 - t_1)$. The approximation used for the denominator did not differ from the more precise integrated form, since the H-atom concentration did not generally vary by more than 2% during each run.

The reaction time, t , was calculated from the distance, d , between the mixing point of the reactants and the mass spectrometer pinhole, and the linear flow velocity, v , with the plug-flow relation $t = d/v$. Although only the relative olefin concentrations are required to evaluate k_{exptl} , absolute concentrations of the reactant olefin were routinely measured. According to eq 1 the exponential decay slope is proportional to the atom concentration and is independent of the initial olefin concentration. This behavior has been verified for all the olefins studied. Typical runs for the reaction of H + *trans*-butene-2 are shown in Figures 2 and 3. In Figure 2, the decay slopes of *trans*- C_4H_8 -2 are shown to be unaffected by a fivefold variation in the initial *trans*- C_4H_8 -2 concentration. For these three runs, the

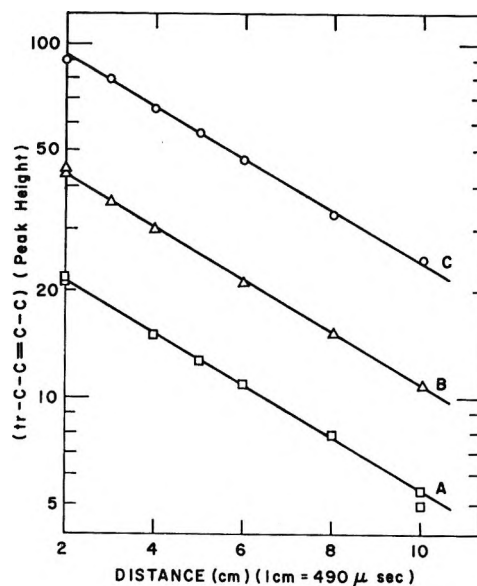


Figure 2. First-order decays of *trans*-butene-2 in an H-atom rich system as a function of reaction distance, d , between the olefin inlet and the mass spectrometer pinhole. Experimental flow parameters: He diluent pressure = 1.20 Torr; velocity = 2063 cm sec^{-1} ; $\langle \text{H} \rangle_{\text{av}}/(\text{trans-}\text{C}_4\text{H}_8) \simeq 100$. $(\text{trans-}\text{C}_4\text{H}_8)_0$ was varied by a factor of 4 in these runs. Line A: $\langle \text{H} \rangle_{\text{av}} = 3.69 \times 10^{14}$ atom cm^{-3} ; $k_{\text{exptl}} = 9.5 \times 10^{-13}$ $\text{cm}^3 \text{molecule}^{-1} \text{sec}^{-1}$. Line B: $\langle \text{H} \rangle_{\text{av}} = 3.54 \times 10^{14}$; $k_{\text{exptl}} = 9.8 \times 10^{-13}$. Line C: $\langle \text{H} \rangle_{\text{av}} = 3.50 \times 10^{14}$; $k_{\text{exptl}} = 9.6 \times 10^{-13}$.

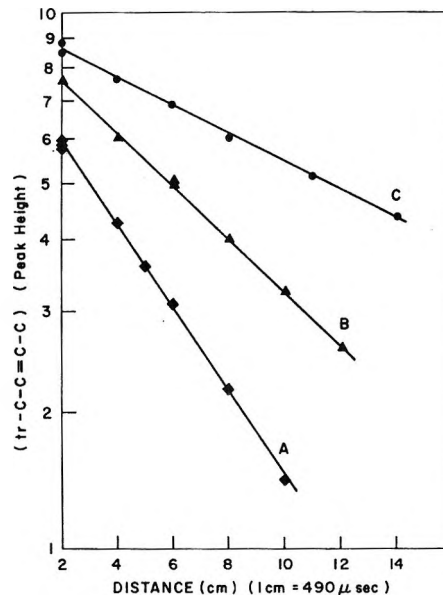


Figure 3. First-order decays of *trans*-butene-2 as a function of H-atom concentration. Same flow conditions as Figure 2. Line A: $\langle \text{H} \rangle_{\text{av}} = 3.69 \times 10^{14}$; $k_{\text{exptl}} = 9.5 \times 10^{-13}$; Line B: $\langle \text{H} \rangle_{\text{av}} = 2.41 \times 10^{14}$; $k_{\text{exptl}} = 9.0 \times 10^{-13}$. Line C: $\langle \text{H} \rangle_{\text{av}} = 1.20 \times 10^{14}$; $k_{\text{exptl}} = 9.8 \times 10^{-13}$ in units of $\text{cm}^3 \text{molecule}^{-1} \text{sec}^{-1}$.

maximum initial *trans*- C_4H_8 -2 concentration was kept less than 2% of the H-atom concentration. In Figure 3, the decay slopes of *trans*- C_4H_8 -2 are shown to be proportional to $\langle \text{H} \rangle_{\text{av}}$ in the range of 1.2 to 3.5×10^{14} atoms

Table II: Absolute Rate Constants for H + Olefins at 25°^a

(He), Torr	Flow velocity, cm sec ⁻¹	(H) _{av} × 10 ¹⁴ atoms cm ⁻³	k _{exptl} × 10 ⁻¹³ cm ² molecule ⁻¹ sec ⁻¹	(He), Torr	Flow velocity, cm sec ⁻¹	(H) _{av} × 10 ¹⁴ atoms cm ⁻³	k _{exptl} × 10 ⁻¹³ cm ² molecule ⁻¹ sec ⁻¹
<i>trans</i> -Butene-2				Butene-1 (continued)			
0.41	1717	1.40	8.95	1.20	2063	2.41	14.3
1.01	3105	3.31	7.60	1.20	2063	3.69	13.6
1.15	1200	1.90	8.86	1.49	2090	2.44	14.9
1.18	1840	3.10	9.25	0.74	1563	(2.7)	13.3
1.20	2063	1.20	9.8	0.74	1563	(2.1)	14.6
1.20	2063	2.41	8.98	0.74	1563	(2.0)	13.6
1.20	2063	3.50	9.62	0.75	1651	(2.0)	14.2
1.20	2063	3.54	10.00	0.78	1651	(2.0)	14.6
1.20	2063	3.69	9.45	0.78	1651	(1.9)	13.6
1.24	2019	4.26	8.31	1.06	1283	(5.0)	14.1
1.24	2019	4.18	8.31	2.41	1569	(3.3)	13.2
1.32	1988	2.24	9.06	2.62	1600	(1.3)	13.2
1.49	2090	2.44	8.80	2.64	1600	(1.3)	13.0
1.90	2381	4.07	8.00	2.65	1606	(2.1)	12.3
				2.76	1710	(1.9)	14.6
				2.76	1710	(1.4)	11.8
				2.76	1710	(1.7)	13.2
			Av				Av
			8.93 ± 0.69				13.8 ± 0.8
<i>cis</i> -Butene-2				3-Methylbutene-1			
1.13	1325	1.03	8.35				
1.20	2063	1.20	7.48				
1.20	2063	2.50	7.60				
1.20	2063	3.78	8.53	0.63	1635	(2.0)	13.8
1.22	1370	2.71	8.77	0.63	1635	(2.0)	12.1
1.22	1370	2.71	8.81	0.69	1723	2.00	12.2
1.33	1370	4.91	7.32	0.70	1583	(2.03)	10.6
0.674	1910	(3.5)	7.25	1.09	1253	(1.47)	13.9
0.689	1824	(2.1)	8.41	1.28	1878	3.78	13.0
0.689	1824	(2.1)	7.52	2.67	1601	(2.12)	12.0
0.80	1400	(2.6)	7.34	2.68	1601	(2.23)	11.2
2.66	1839	(2.1)	7.97	2.69	1610	(1.15)	11.0
2.66	1839	(2.0)	7.28	2.72	1589	(2.37)	11.7
2.76	1710	(2.1)	7.37				
2.76	1710	(1.9)	8.23				
			Av				Av
			7.88 ± 0.58				12.2 ± 1.0
Tetramethylethylene				Trimethylethylene			
0.69	1723	2.00	11.1	0.69	1635	(2.0)	12.1
0.87	~1500	(~1.7)	12.4	0.69	1723	2.00	13.5
1.24	1800	1.98	11.3	0.87	~1500	(~1.7)	16.1
1.24	1800	1.80	11.6	0.87	~1500	(~1.7)	15.3
1.27	1745	1.83	11.8	1.27	1745	1.83	12.3
				1.28	1878	3.78	12.5
			Av				Av
			11.6 ± 0.51				13.6 ± 1.7
Propene				2-Methylbutene-1			
1.06	1283	(1.63)	7.63	0.69	1723	2.00	17.1
1.06	1283	(1.63)	7.26	0.87	~1500	(~1.7)	15.0
1.06	1283	(1.63)	7.17	0.87	~1500	(~1.7)	16.1
2.4	1569	(4.02)	7.50	1.27	1745	1.83	14.4
2.4	1569	(4.02)	8.22	1.28	1878	3.78	12.9
			Av				Av
			7.56 ± 0.41				15.1 ± 1.6
Butene-1				1,3-Butadiene			
0.41	1717	1.40	14.3	1.26	1765	0.52	79.2
0.85	1927	2.85	14.6	1.26	1765	0.59	71.0
1.01	3105	3.31	14.0	1.26	1725	0.27	96.1
1.03	1325	1.03	14.4	1.26	1725	0.27	87.3
1.20	2063	1.20	14.7				
							Av
							83.4 ± 10.8

^a The H atom concentrations given in parentheses have been estimated from the decay slopes for *trans*-C₄H₆-2. Thus, the corresponding rates have been determined relative to that of *trans*-C₄H₆-2, i.e., 8.93 × 10⁻¹³ cm² molecule⁻¹ sec⁻¹.

Table III: Rate Constants for D + Olefins at 25°^a

(He), Torr	Flow velocity, cm sec ⁻¹	(D) _{av} × 10 ¹⁴ atom cm ⁻³	k _{exptl} × 10 ⁻¹³ cm ³ molecule ⁻¹ sec ⁻¹	(He), Torr	Flow velocity, cm sec ⁻¹	(D) _{av} × 10 ¹⁴ atom cm ⁻³	k _{exptl} × 10 ⁻¹³ cm ³ molecule ⁻¹ sec ⁻¹
<i>trans</i> -Butene-2				3-Methylbutene-1			
0.69	1870	1.15	7.93	0.57	1698	1.44	13.3
0.97	2066	2.80	7.75	0.57	1644	1.43	13.1
0.98	2024	1.96	7.86	1.06	1603	(1.93)	13.5
1.24	1470	1.83	7.99	1.23	1635	0.92	11.4
1.24	1470	1.97	7.64	1.23	1635	0.94	11.5
1.53	1700	3.36	7.90	1.23	1635	0.96	11.9
2.17	1720	1.72	7.25	1.30	1725	1.18	12.3
2.23	1660	5.16	7.60	1.58	1492	(1.10)	14.5
			Av 7.74 ± 0.24	2.62	1569	0.80	12.2
				2.62	1569	1.69	12.9
<i>cis</i> -Butene-2				2-Methylbutene-2			
0.62	1730	2.49	6.75				Av 12.7 ± 1.0
0.98	2024	1.92	7.54				
1.24	1470	1.86	6.76	0.57	1644	(1.43)	16.0
1.24	1470	1.97	6.71	0.62	1730	(2.39)	14.1
1.53	1700	3.08	6.92	1.06	1603	(2.04)	16.3
2.17	1720	1.72	6.69	1.23	1635	0.80	14.3
2.23	1660	5.23	6.31	1.23	1635	0.83	14.7
2.57	1568	3.56	6.31	1.23	1635	0.85	15.0
			Av 6.75 ± 0.37	1.30	1725	1.04	15.1
				2.62	1569	1.77	16.6
Tetramethylethylene				Isobutene			
0.62	1730	2.40	12.0				Av 15.3 ± 0.9
0.69	1851	(1.69)	15.4				
0.69	1851	(1.64)	14.3	0.98	2024	2.02	34.6
0.69	1851	(1.63)	14.2	1.24	1470	1.76	34.7
2.04	1616	(2.80)	15.4	1.24	1470	1.93	33.0
2.62	1569	(1.77)	13.6	2.17	1720	1.60	31.5
			Av 14.2 ± 1.3				Av 33.5 ± 1.5
Propene				2-Methylbutene-1			
0.62	1730	2.42	9.4	1.23	1635	0.41	35.5
0.98	2024	2.04	12.3	1.23	1635	0.44	35.8
1.24	1470	1.78	10.4	1.23	1635	0.45	33.6
1.24	1470	2.02	10.6	1.30	1725	1.02	33.7
2.17	1720	1.62	10.2	2.62	1569	0.78	31.8
2.21	1683	3.72	9.0				Av 34.1 ± 1.6
			Av 10.3 ± 1.1				
Butene-1				1,3-Butadiene			
0.60	1697	1.04	14.4	1.58	1492	(0.78)	52.4
0.60			12.8	2.62	1569	0.39	52.0
0.69	1870	1.18	11.1	2.62	1569	0.60	53.6
0.69	1851	(1.63)	14.9				Av 52.7 ± 0.8
0.97	2066	2.80	13.6				
0.98	2024	1.85	15.5				
1.06	1603	(1.85)	13.4				
1.24	1470	1.76	14.6				
1.24	1470	1.92	14.3				
1.53	1700	3.14	14.4				
2.04	1616	(2.80)	13.2				
2.17	1720	1.66	13.4				
2.30	1442	1.11	13.7				
2.57	1568	3.56	13.2				
2.62	1569	0.91	13.4				
2.62	1569	1.67	13.7				
			Av 13.7 ± 1.0				

^a The D atom concentrations given in parentheses have been calculated from the decay slopes for *trans*-C₄H₈-2. Thus, the corresponding rates have been determined relative to that of *trans*-C₄H₈-2, i.e., 7.74 × 10⁻¹³ cm³ molecule⁻¹ sec⁻¹.

cm⁻³. These results further indicate that heterogeneous and diffusional corrections for k_{exptl} are unimportant under these conditions.

In addition to the absolute determinations, a number of rate constants were also determined relative to *trans*-C₄H₈-2. In these determinations, *trans*-C₄H₈-2 and the other olefin were alternately introduced into the reactor without other changes in experimental conditions. The rate constant is then given as the ratio of decay slopes times the absolute *trans*-C₄H₈-2 rate. This procedure served as a check against possible systematic errors in the absolute determinations.

The experimental data for the H and D atom reactions are given in Tables II and III. Table IV summarizes the rate constants and also gives the ratio of the H-atom rate to the D-atom rate. The assigned uncertainties are standard deviations, which generally remain within 10% of the absolute rate constants. For the reaction of H + *trans*-butene-2, the experimental rate constants are constant over the pressure range of 0.4 to 1.9 Torr He and are not affected by variation in other experimental parameters. The value of k_{exptl} for H + *trans*-C₄H₈-2, $(8.93 \pm 0.09) \times 10^{-13}$ cm³ molecule⁻¹ sec⁻¹, was used as the reference standard to calculate the absolute rate constants for other olefins from the relative decay slopes. Those rate constants that were determined by the relative method are dif-

ferentiated in Table II by the $\langle H \rangle_{\text{av}}$ value given in parentheses. Similarly in Table III, the $\langle D \rangle_{\text{av}}$ value is given in parentheses when the rate constant was evaluated relative to that of k_{exptl} for D + *trans*-C₄H₈-2, $(7.74 \pm 0.24) \times 10^{-13}$.

For the reaction of H + *cis*-butene-2, several absolute measurements were made at about 1.2 Torr of He to check the reproducibility; the relative method was used to obtain k_{exptl} over a much wider pressure range up to 2.8 Torr. Agreement between both methods is well within the experimental uncertainty. The reactions of H atoms with propene, isobutene, and 2-methylbutene-2 yield k_{exptl} which are markedly reduced from the true addition rates, as is discussed in the following section. No extensive data were, therefore, obtained for these reactions. Ethylene was not included in the present study since its apparent reaction rate is greatly affected by the total pressure. Detailed knowledge of the reaction mechanism is required to determine the rate constant for the addition step in such a reaction system. The rate constants listed for the highly substituted or extremely reactive olefins are considered to be more uncertain than the standard deviations indicate.

A semiquantitative analysis of the reaction products has been made in order to obtain information on the reaction mechanisms. The lower olefins and methyl radicals are common products in all these reactions. In the reaction of H + butene-2, the primary yield of propene has been found to be dependent on the diluent pressure. The propene yield is close to 50% of the butene-2 consumed at about 2 Torr of He, which is in qualitative agreement with the previous observations by Rabinovitch, *et al.*¹⁴

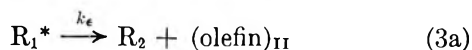
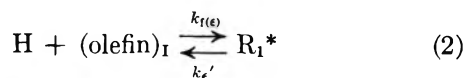
In the D-atom reactions, isotopic scrambling in the reactant olefins has been examined. In the case of propene, isobutene, and 2-methylbutene-2 isotopic scrambling is very extensive under the conditions given in Table III. *cis*- and *trans*-butene-2 and butene-1 do not yield deuterium-substituted reactants. For the other olefins, the extent of scrambling was found to be slight. Formation of HD also occurs in reactions of isobutene and 2-methylbutene-2, although a quantitative estimate of the HD yield was uncertain due to interference from the large HD background from the discharged D₂ compared with the minute quantities of reactants used. The molecular HD was shown to be produced mostly in the gas phase rather than on the reactor walls. Atomic hydrogen was observed in all the D-atom reactions, but was not measured quantitatively. The reactant olefins were monitored by their parent peaks for the rate measurements. Accordingly, necessary cracking pattern corrections were routinely made in the reaction systems which yielded high mass products.

Discussion

The reaction of H atoms with olefins is described by the following equations

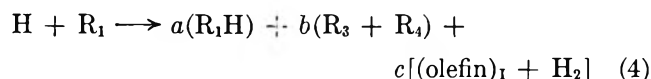
Table IV: Summary of k_{exptl} for H and D + Olefins at 25°

Olefin	$k_{\text{H}} \times 10^{-13}$ cm ³ molecule ⁻¹ sec ⁻¹	$k_{\text{D}} \times 10^{-13}$ cm ³ molecule ⁻¹ sec ⁻¹	$k_{\text{H}}/k_{\text{D}}$
	8.9 ± 0.7	7.7 ± 0.2	1.15
	7.9 ± 0.6	6.8 ± 0.4	1.17
	11.6 ± 0.5	14.2 ± 1.3	0.82
	(7.6 ± 0.4)	10.3 ± 1.1	0.73
	13.8 ± 0.8	13.7 ± 1.0	1.00
	12.3 ± 1.0	12.7 ± 1.0	0.97
	13.6 ± 1.7	15.3 ± 0.9	0.89
	(~7)	33.5 ± 1.5	0.2
	(15.1 ± 1.6)	34.1 ± 1.6	0.44
	(83.0 ± 11)	53.0 ± 11	1.58



where the symbols follow the usual notations of Rice-Ramsperger-Kassel-Marcus (RRKM) theory of unimolecular reactions.¹ The hydrogen abstraction reaction is not included in the primary step because its rate constant is less than 10% of $k_{f(\epsilon)}$.⁶ In the case of asymmetrically substituted olefins, the H atom may add to either olefinic carbon. Previous studies show that the addition to the least substituted carbon is the predominant process.^{1,2,15}

Subsequent reactions of collisionally stabilized alkyl radicals, R_1 , with H atoms become important at high H-atom concentration and lead to a variety of products

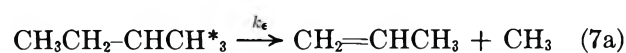
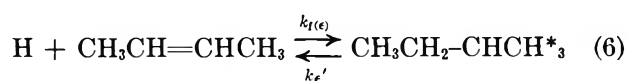


where a , b , and c are the fractional yields of the several components. In addition, secondary reactions of the alkyl radicals, R_1 and R_2 , with the initial and product olefins are too slow to be important in these systems, *i.e.*, $\sim 10^{-3}k_{f(\epsilon)}$.¹⁶ Thus, the experimentally observed rate constant, k_{exptl} , is related to the individual rate constants (eq 2-4) by the following expression

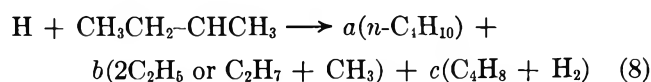
$$k_{\text{exptl}} = \frac{k_{f(\epsilon)}[k_{\epsilon} + (1 - c)\omega]}{k_{\epsilon'} + k_{\epsilon} + \omega} \quad (5)$$

Equation 5 is more correctly written as an integral over the energy states, ϵ , of R_1^* , but this is omitted here for simplicity. For most of the compounds reported here, forward dissociation of the chemically activated alkyl radical, R_1^* , by C-C splitting is greatly favored over the competitive backward dissociation by C-H splitting, *i.e.*, $k_{\epsilon} \gg k_{\epsilon'}$.¹ In addition, the fraction of events, c , that result in a regeneration of the original olefin is very small. Consequently, eq 5 reduces to $k_{\text{exptl}} = k_{f(\epsilon)}$ and the observed rate of decay of the olefin gives the correct value for the rate of hydrogen addition.

This situation can be best illustrated by the reaction of H with butene-2, *i.e.*



and



For chemically activated *sec*-butyl radicals,¹ k_{ϵ} has been shown to be approximately 10^7 sec^{-1} , and $k_{\epsilon'}$ less than 10^4 sec^{-1} , *i.e.*, $k_{\epsilon} \gg k_{\epsilon'}$. This was confirmed in this work by the observation that isotopically scrambled butenes were not an important product in the reaction system D + butene-2. In addition, regeneration of the butene-2 or its isomeric species, eq 8, would also be ruled out on the basis of this observation. This conclusion is further substantiated by the absence of a pressure effect on k_{exptl} for this reaction. It is worth noting that at the diluent He pressure used, 0.4-2 Torr, only a fraction of the activated *sec*-butyl radicals are collisionally stabilized, *i.e.*, $k_{\epsilon} \geq \omega$.

These considerations do not apply to four compounds studied here, propene, isobutene, 2-methylbutene-2, and butadiene-1,4. In the reactions of D atoms with these compounds, extensive isotopic scrambling of the reactant was observed. Thus, in these systems the reactant olefin must be regenerated either by redissociation of the corresponding activated radicals and/or by the secondary reaction of the stabilized radicals with atomic hydrogen. Therefore, the approximation, $k_{\text{exptl}} = k_{f(\epsilon)}$, is not valid for these compounds and values for k_{ϵ} , $k_{\epsilon'}$, ω , and c would be required to evaluate $k_{f(\epsilon)}$ from k_{exptl} for the system H + olefin, *i.e.*, k_{H} . This difficulty has been circumvented by measuring k_{exptl} using D atoms, *i.e.*, k_{D} . Then, the decay of the completely protonated olefin gives a good approximation of $k_{f(\epsilon)}$; because very little of the completely protonated olefin is regenerated, most of the regenerated olefin contains deuterium.

An estimate of the uncertainty introduced by using this approximation can be made by considering the statistical scrambling that occurs in the regeneration of the parent olefin. For example, in the case of isobutene the activated complex is completely symmetrical and contains eight equivalent H atoms and one D atom. In the previous notation, $k_{\epsilon'}$ corresponds to the dissociation of a D atom and k_{ϵ} to that of an H atom. In this case k_{ϵ} is equal to or greater than $8k_{\epsilon'}$. It is probably much greater because of the kinetic isotope effect for breaking a C-H bond compared with a C-D bond. Similar considerations show that regeneration of the protonated parent olefin by reaction of the stabilized complex with D atoms is also not significant. Therefore, $k_{\text{D}} = k_{\text{exptl}}$ is a valid approximation.

The values of k_{H} and k_{D} obtained in this study are summarized in Table IV and their ratios are given in the last column of that table. For six of the compounds listed, there is no isotope effect within the experimental uncertainty. The ratios are apparently less than unity for propene, isobutene, and 2-methylbutene-2 because k_{H} , which is given in parentheses, is too large for reasons

(15) R. D. Kelley, R. Klein, and M. D. Scheer, *J. Phys. Chem.*, **69**, 905 (1965); **74**, 4301 (1970).

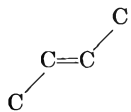
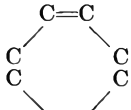
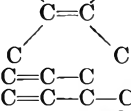
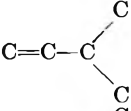
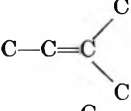
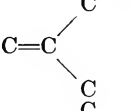
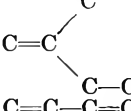
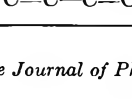

(16) R. J. Cvetanović and R. S. Irwin, *J. Chem. Phys.*, **46**, 1694 (1967).

discussed previously. For butadiene, the same arguments apply, although the observed ratio is greater than unity. In this case, the experimental uncertainty is probably greater than indicated by the standard deviation because it is a very rapid reaction.

Comparison with Previous Measurements. Extensive studies of the rate constants for the reactions of H atoms with olefins have been reported by Cvetanović and coworkers.⁴⁻⁶ In their work they did not measure absolute rate constants, but rather obtained relative rates. Photochemical methods were used to generate hydrogen atoms and the reactions were studied under high pressure conditions where the addition complex is generally collisionally stabilized. Their rate constants, k_H' , relative to k_H for *trans*-butene-2 taken as unity are summarized in the last column of Table V. Our results for k_H' and k_D' are also included in this table for comparison. The agreement between the two sets of data is seen to be excellent. For the four molecules for which k_D' (and not k_H') should be taken for comparison, the agreement is also good. The only disagreement in the table is our apparent value for k_H' of butadiene, which we stated earlier to be relatively inaccurate.

Absolute rate constants have been reported by Melville and coworkers,⁷ who derived their values from H-atom decay rates rather than olefin decays. In their

Table V: Comparison of Relative Rates for H and for D + Olefin at 25°

Olefin	This work		Cvetanović, <i>et al.</i> k_H'
	k_H'	k_D'	
	1.00	1.00	1.00
	0.88	0.87	0.80
	1.30	1.83	1.42
	(0.85)	1.33 (1.60)	1.70
	1.55	1.77	1.76
	1.38	1.64	
	1.52	1.98	1.74
	(~0.8)	4.33	4.28
	(1.69)	4.40	
	(9.34)	6.81	8.35

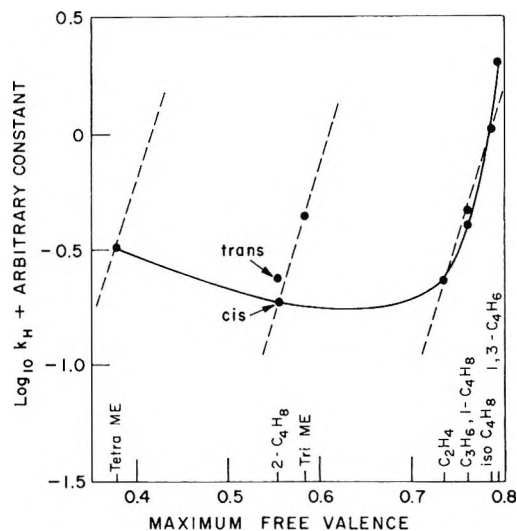


Figure 4. Correlation of experimental rate constants for addition of H atom to olefins with the maximum free valence energies of the olefins. The solid curve is that of Jennings and Cvetanović (ref 4). See text for discussion of dashed lines.

work, the H atoms were generated photochemically and were monitored by the MoO₃ bluing technique at a reactant pressure of 6~7 Torr in the absence of an inert gas. Their results are summarized in Table I relative to their value for ethylene of 12×10^{-13} and are seen to be in agreement with the relative values of Cvetanović. There are two exceptions, propene and isobutene, although a redetermination by them of the rate constant for propene^{7b} now gives agreement.

Also shown in Table I are reactivities obtained by Yang.⁸ His values are seen to deviate from the others, although the reason is not immediately clear. Yang's competitive method is similar to one used by Cvetanović with the exception of the method of generation of H atoms. A possible explanation is that γ radiolysis of propene does not provide a clean source of H atoms under the experimental conditions used by Yang. It is unfortunate that Yang's work appears to be unreliable because it provides the only experimental determination of activation energies for these reactions.

More recently, Braun and Lenzi¹⁰ have determined k_H for *trans*-butene-2 and isobutene to be $(10.0 \pm 15\%) \times 10^{-13}$ and $(38 \pm 15\%) \times 10^{-13}$, respectively, at high pressures using vacuum uv flash-photolysis. In their work the first-order H-atom decay was monitored by Lyman- α -fluorescence. The absolute rate constants determined by this method agree well with those of this work. Under their experimental conditions, the H-atom concentrations were apparently low enough to minimize secondary reactions of H atoms with the radical products. Knox and Dalglish¹⁷ have obtained the rate expression for H + isobutene to be $(5.6 \pm 2.3) \times 10^{-11} \exp[-1360 \pm 200]/RT$ in the tempera-

(17) J. H. Knox and D. G. Dalglish, *Int. J. Chem. Kinet.*, **1**, 69 (1969).

ture range 12 to 132°. The H-atom decay was monitored by a Pt foil probe in a conventional discharge-flow reactor at 2 Torr of Ar in this work. These authors found that the H-atom decay could be substantially accounted for in terms of the catalytic recombination of H atoms by isobutene, *i.e.*, $2\text{H} + i\text{-C}_4\text{H}_8 \rightarrow \text{H}_2 + i\text{-C}_4\text{H}_8$, and used this stoichiometry to derive their rate constant. Our own studies with H- and D-atom reactions with isobutene confirm the reasonableness of their overall mechanism. Most recently, Tal'rose and co-workers¹⁸ have reported rate constants for propene and for butene-1 to be $(1.3 \pm 0.4) \times 10^{-12}$ and $(1.5 \pm 0.45) \times 10^{-12}$, respectively, at $293 \pm 3^\circ\text{K}$ in agreement with our values. The olefin decay was monitored mass spectrometrically in the presence of an excess of H atoms at 6.7 Torr of He under "diffusional-cloud-in-flux" flow conditions.

Reactivity Systematics. The good agreement between the rate constants at 300°K reported here with those of Cvetanović and coworkers gives some additional confidence to the reliability of the present values. It is therefore of interest to see if any correlation exists between the rate constants and olefinic structure. The compounds studied have been arranged in Table V in such a systematic order. Namely, for monoolefins, the reactivity varies systematically with the degree of structural asymmetry in alkyl substitution, and not with the total number or type of alkyl groups on the olefinic carbons.

For example, butene-2, butene-1, and isobutene are the three possible isomeric C₄ olefins, and their reactivity ratios are approximately 1:2:4. Butene-2 is the symmetrically substituted isomer with zero degree of asymmetry. Likewise, butene-1 and isobutene possess 1 and 2 degrees of asymmetry, respectively. Furthermore, both mono- and trisubstituted olefins belong to the same class of asymmetry, and their reactivities are nearly identical. An apparent exception to this systematics is tetramethylethylene (TME) which has a slightly greater reactivity than other olefins with zero degree of asymmetry.

The observed reactivity systematics may be taken to reflect the effect of olefinic structure on either the *A* factors or activation energies of the rate constants for these addition reactions. However, the present data were obtained only at 300°K and do not provide an adequate basis to distinguish which parameter is affected. Nevertheless, it is worth noting that the reactivity associated with each symmetry class of olefin substitution is not affected by the type of alkyl substituents. This suggests that the *A* factors are less susceptible to the olefinic structure and that the difference in activation energies among these olefins is at most 1 kcal/mol. An upper limit for the activation energy is 4 kcal/mol, if the *A* factor is identical with the hard-sphere collision frequency. However, this appears to be substantially greater than the actual value,

since the reasonable *A* factor for the atom addition reaction is generally smaller than the collision frequency by more than a factor of 10. Indeed, Knox and Dalglish have obtained an *A* factor of 5×10^{-11} for the reaction of H atoms with isobutene.

Theoretical basis for the reactivity systematics has been discussed by several previous workers.² Commonly, free valency (*f_r*) and atom localization energy (*E_{loc}*) have been used as indices for classifying atom and radical reagents to "electrophilic" and "radical" types.¹⁹ In the present case, *E_{loc}* is an energy required to localize π electrons at a reaction center; *f_r* is a quantity related to the energy change in π electronic system as a result of a small perturbation at a reaction center. Hence, *f_r* relates to the initial stage of a reaction, while *E_{loc}* stresses the importance of the final stage. Fair success in such correlations has been obtained for several olefinic systems, particularly by Szwarc's²⁰ and by Cvetanović's groups.^{4,21} For example, Jennings and Cvetanović⁴ found a linearity between the H-atom reactivities and *E_{loc}* (but not *f_r*) of monoolefins, which led these authors to infer that H atoms are a radical-type reagent.

With the additional data obtained for trimethylethylene (tri-ME) in this work as well as in the most recent study by Cvetanović's group,⁶ it is now possible to examine this suggestion further. The new datum

Table VI: Relative Rate Constants for H + Olefin and CF₃ + Olefin at 25°

Olefin	H ^a	CF ₃ ^b
	1.0	1.0
	0.72	1.1
	0.90	1.3
	1.28	1.8
	1.53	1.4
	1.58	1.5
	4.28	4.7
	8.35	13.4
<i>E_{C2B0}</i> , kcal mol ⁻¹	~3.2	~2.4

^a Reference 6. ^b Reference 21, calculated by extrapolation from the data obtained at high temperatures.

(18) A. F. Dodonof, G. K. Lavroskoya, and B. L. Tal'rose, *Kinet. Katal.*, **10**, 22 (1969).

(19) S. Sato and R. J. Cvetanović, *J. Amer. Chem. Soc.*, **81**, 3223 (1959).

(20) M. Szwarc and J. H. Binks, "Theoretical Organic Chemistry," Butterworths, London, 1959.

(21) R. J. Cvetanović, *Advan. Photochem.*, **1**, 115 (1963).

point for tri-ME does not alter the previous correlation of the reactivity with E_{100} . However, as shown in Figure 4, the reactivity of tri-ME does not lie on the original curve in the plot of reactivity as a function of f_r . On the other hand, a systematic correlation can be represented by the dashed parallel lines indicated. Namely, the terminal olefins have high values of maximum free valence and their reactivities lie on a single line, whereas the internal olefins are in the medium range on this scale and are related linearly by another line parallel to that for the terminal olefins. A third parallel line was drawn through the single point of TME, because it can be considered as a class by itself. A constant displacement of the intercept for each olefinic group may be justified on the basis of the theoretical argument made by Yang.⁸ A further support for the correlation with f_r comes from the remarkably similar reactivities of H atoms and of CF_3 radicals, although the A factors for the two sets of reagents differ by roughly three orders of magnitude (Table VI). The CF_3 radical is known to be an "electrophilic" reagent.²²

The absolute values of addition rate constants are also useful in evaluating the rate constants for the thermal dissociation of alkyl radicals in terms of the principle of microscopic reversibility. Recently, Frey and Walsh have reviewed the thermochemical kinetic analysis of these systems.²³ On the basis of equilibrium constants and previous estimates of the Arrhenius parameters for the addition rates, Arrhenius parameters for the decomposition rates were calculated and compared with experimental data. The agreement obtained was poor. However, these authors have assigned an order of magnitude uncertainty to the calculated dissociation rates. The values for k_H adopted by these authors disagree significantly with those of the present work. Thus, such a comparison of the experimental and calculated dissociation rates does not warrant a definitive conclusion.

(22) J. M. Pearson and M. Szwarc, *Trans. Faraday Soc.*, **60**, 553 (1964); G. E. Owen, Jr., J. M. Pearson, and M. Szwarc, *ibid.*, **60**, 564 (1964); **61**, 1722 (1965).

(23) H. M. Frey and R. Walsh, *Chem. Rev.*, **69**, 103 (1969).

Numerical Quadrature Methods in the Analysis of Reaction

Kinetic Experiments

by Ian D. Gay

Department of Chemistry, Simon Fraser University, Burnaby 2, British Columbia, Canada (Received January 7, 1971)

Publication costs assisted by the National Research Council of Canada

Methods of analyzing reaction kinetic data are presented which involve numerical integration (quadrature) of experimental data. The application of such methods to homogeneous, heterogeneous, and temperature-programmed kinetic experiments is discussed. Advantages of the proposed methods relative to alternative procedures are pointed out.

Introduction

The differential equations describing a kinetic mechanism of only moderate complexity are frequently incapable of analytic solution in terms of elementary functions. Indeed, it is only for first-order and a very restricted range of higher-order systems that such solution is possible. Nevertheless, it is necessary to be able to test general mechanisms against experimental data and to determine values of the rate constants involved.

The most commonly used procedure for such problems is numerical solution of the differential equations

by Runge-Kutta or predictor-corrector methods, with adjustment of rate constants to make the solutions agree with experimental data.¹⁻⁴ While this procedure is undoubtedly effective, the adjustment of rate constants amounts to a nonlinear least-squares problem, which must be solved iteratively, and is in general of a

(1) M. Berman, E. Šol, and M. F. Weiss, *Biophys. J.*, **2**, 275 (1962).

(2) I. D. Gay, *J. Amer. Chem. Soc.*, **86**, 2747 (1964).

(3) W. E. Ball and L. C. D. Groenweghe, *Ind. Eng. Chem., Fundam.*, **5**, 181 (1960).

(4) M. Kubin, *Coll. Czech. Chem. Comm.*, **34**, 1254 (1969).

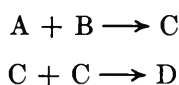
magnitude to require at least a medium-sized digital computer.

In this paper we discuss methods which reduce the above problem to one of linear least squares, by the use of numerical quadrature. In many cases the calculations are simple enough for solution by hand.

Homogeneous Isothermal Systems

If the rates of reactions are expressible as sums of mass action terms, the system is simplified by introducing as new variables the time integrals of the various concentrations. This method has been discussed by Himmelblau, Jones, and Bischoff.⁵ Since its potentialities do not appear to be widely realized, we present an example of its use and report the results of some statistical experiments.

As an example, we consider the consecutive second-order system



This system leads to the differential equations

$$\frac{dA}{dt} = \frac{dB}{dt} = -k_1AB \quad (1)$$

$$\frac{dC}{dt} = k_1AB - k_2C^2 \quad (2)$$

$$\frac{dD}{dt} = k_2C^2 \quad (3)$$

Equations 1 to 3 do in fact have a solution in terms of Legendre functions,⁶ but this is not particularly useful in evaluation of experimental data.

If eq 1 to 3 are multiplied by dt and integrated from 0 to arbitrary time t , one obtains

$$A - A^0 = B - B^0 = -k_1 \int_0^t AB dt \quad (4)$$

$$C = k_1 \int_0^t AB dt - k_2 \int_0^t C^2 dt \quad (5)$$

$$D = k_2 \int_0^t C^2 dt \quad (6)$$

where A^0 and B^0 indicate the initial concentrations of A and B, those of C and D being assumed zero. The integrals in (4) to (6) can be evaluated for every experimental point by a graphical or numerical method, and hence constitute new variables which may be used to determine the rate constants.

Thus if we put

$$X = \int_0^t AB dt$$

$$Y = \int_0^t C^2 dt$$

eq 4-6 become

$$A - A^0 = B - B^0 = -k_1X \quad (7)$$

$$C = k_1X - k_2Y \quad (8)$$

$$D = k_2Y \quad (9)$$

In a hand calculation, one could determine k_1 by standard methods for a second-order reaction, evaluate Y by graphical integration of C^2 , and determine k_2 by a plot of D against Y .

If a computer is available, it is preferable to use all available experimental data. If concentrations of A, B, C, and D are available at n experimental points, X and Y can be evaluated numerically, and application of (7)-(9) at all experimental points produces $4n$ equations for k_1 and k_2 which can be solved in the least-squares sense by standard linear regression methods.⁷

It is clear that this general method can be applied to a mechanism of arbitrary complexity, provided sufficient experimental data are available. If the nature of the experiment is such that initial concentrations are unreliable, there is no reason why the integrals in (4)-(6) should not begin at some experimental point, say the i th, rather than the first, producing

$$A - A_i = B - B_i = -k_1 \int_{t_i}^t AB dt \quad (10)$$

and similar variants of (5) and (6), where A_i , B_i represent concentrations of A and B at time t_i .

Determination of Unknown Calibration Constants

A situation which can readily occur is that one cannot measure one of the relevant concentrations, but only some parameter proportional to it. An example might be the spectroscopic observation of an intermediate whose extinction coefficient is unknown, and which is too unstable for isolation.

For example, in the above mechanism, suppose we measure Q where Q is related to C by an unknown constant α

$$Q = \alpha C \quad (11)$$

then $dQ/dt = \alpha dC/dt$, $C = Q/\alpha$, and (2) can be rewritten

$$\frac{dQ}{dt} = \alpha k_1AB - \frac{k_2}{\alpha} Q^2 \quad (12)$$

Since Q is an experimentally available quantity, we can define

$$Z = \int_0^t Q^2 dt$$

and rewrite (12) as

(5) D. M. Himmelblau, C. R. Jones, and K. B. Bischoff, *Ind. Eng. Chem., Fundam.*, **6**, 539 (1967).

(6) T. Kelen, *Z. Phys. Chem. (Frankfurt am Main)*, **60**, 191 (1968).

(7) These methods are described in many textbooks; for example, N. R. Draper and H. Smith, "Applied Regression Analysis," Wiley, New York, N. Y., 1966.

$$Q = \alpha k_1 X - \frac{k_2 Z}{\alpha} \quad (13)$$

The combined quantities αk_1 and k_2/α can then be obtained from linear regression using (13), and since k_1 is obtainable from (1) or (7) the three parameters k_1 , k_2 , and α may be separately obtained.

Statistical Tests

The above procedures can readily be carried out, but there is some doubt as to the validity of using standard least-squares methods, since both dependent and independent variables in the final linearized equations can be functions of the same experimental quantities. As a test of the performance of the method, we have generated various sets of artificial data for the consecutive second-order system and solved sufficient of these to draw some statistical conclusions about the results obtained.

Test data were generated by numerical solution of eq 1 to 3, and normally distributed errors were introduced using a random number generator. Rate constants were then determined by simultaneous least-squares fitting of eq 7 to 9. These fits were weighted on the basis of the errors in the dependent variables. The results were compared with the known exact values, and with results obtained from an iterative least-squares method based on the "spiral" algorithm described by Jones.⁸ Data were generated for initial A:B ratios of 1:1 to 10:1 and $k_1:k_2$ ratios of 0.1:1 to 10:1. For each choice of initial concentrations and rate constants, sev-

eral sets of data were generated using different random perturbations, so that a statistical study of the results could be made. Some typical results are given in Table I.

The general conclusions of this study were as follows. (a) The present method and the iterative least-squares method retrieve values of the rate constants which are in agreement with each other and with the known correct values. This was confirmed by the application of *t*-tests. (b) Standard deviations for the rate constants calculated from the variance-covariance matrix of the linear regression are consistently too small. They are typically a factor of 2 to 3 lower than those found by direct computation from the results of several runs. The relative magnitudes of these standard deviations were, however, approximately correct. (c) From the above results it would appear that the overall fit of the transformed equations is too good with the present method, due to correlations between the dependent and independent variables. Valid rate constants are obtained by the present method, but standard deviations estimated in the usual way should be interpreted with caution. If reliable standard deviations are required, it would seem advisable to perturb the experimental data with several sets of random numbers of the appropriate magnitude and derive standard deviations directly from the results.

Surface Kinetics with Langmuir Adsorption

The simplest model for the kinetics of a system undergoing heterogeneous catalysis is one in which rates are assumed proportional to surface concentrations, which are assumed to be related to bulk concentrations by the Langmuir isotherm. Thus for gas reactions

$$\theta_A = \frac{k_A P_A}{1 + \sum_i k_i P_i} \quad (14)$$

where θ_A and P_A are the fraction of surface covered with A and the pressure of A, respectively. The *k*'s are referred to as the adsorption constants for the respective species. For unimolecular steps, rates are taken as proportional to θ , and for bimolecular steps to either the product of two surface coverages (Langmuir-Hinshelwood mechanisms) or to a surface coverage times a pressure (Rideal mechanisms). The kinetics of surface reactions will thus in general contain all the adsorption constants, as well as the various rate constants.

It is clear that for a mechanism containing *n* independent reaction steps, it will be impossible to determine more than *n* adsorption constants from the kinetics of a single run, since a linear relationship between the $k_i P_i$ terms is established by the stoichiometry of the reaction. Indeed, it is well known that determination

Table I: Results^a of Rate Constant Determination for Consecutive Second-Order System

Exact constants	Av found ^b constants	Std dev ^c	Calcd ^d std dev
$k_1 = 1.000$	1.009	0.038	0.019
$k_2 = 0.100$	0.101	0.010	0.012
$k_1 = 1.000$	1.004	0.040	0.018
$k_2 = 0.200$	0.200	0.024	0.015
$k_1 = 1.000$	0.997	0.053	0.018
$k_2 = 0.500$	0.509	0.031	0.024
$k_1 = 1.000$	1.013	0.032	0.019
$k_2 = 1.000$	1.002	0.059	0.040
$k_1 = 1.000$	0.013	0.041	0.019
$k_2 = 2.000$	1.981	0.106	0.065
$k_1 = 1.000$	1.012	0.052	0.018
$k_2 = 5.000$	4.971	0.247	0.125
$k_1 = 1.000$	0.991	0.057	0.021
$k_2 = 10.000$	9.622	0.815	0.266

^a Data were generated for *k* values as specified, with $A^0 = B^0 = 1.000$ for 10 points at a time interval of 0.200. Normally distributed random errors were applied to each point, the standard deviation of these errors being $0.005 + 5\%$ of the concentration value. ^b Average of 10 runs with differing generated errors. ^c Calculated directly from the results of 10 runs. ^d Average of values calculated in each run from the variance-covariance matrix of the linear regression.

(8) A. Jones, *Computer J.*, **13**, 301 (1970).

of adsorption constants from kinetic results will only be satisfactory when the $k_i P_i$ terms are of the order of unity, since if $k_i P_i$ is small in comparison with unity, it has no effect, and if $k_B P_B$, say, is large compared with unity, one can rewrite (14) as

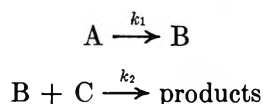
$$\theta_A = \frac{\frac{k_A}{k_B} P_A}{\sum_i \frac{k_i}{k_B} P_i} \quad (15)$$

which amounts effectively to the disappearance of one constant.

For the above reasons, solution of surface kinetic mechanisms is often attempted only in cases where adsorption constants are known independently or can be estimated. If this is the case, the denominator of (14) is calculable at all experimental points, and the system can be solved by the methods described above.

If adsorption constants are not known but are of a reasonable magnitude, numerical integration methods can be used to solve systems in which they enter linearly (*i.e.*, systems in which any bimolecular steps proceed by Rideal mechanisms).

As an example, we consider the system



in which it is assumed that A and B adsorb according to the Langmuir isotherm, that the second reaction proceeds *via* collision of gaseous C with adsorbed B, and that neither C nor the products are strongly adsorbed. Putting

$$k_1^1 = k_1 k_A; \quad k_2^1 = k_2 k_B$$

the rate equations can be written

$$\frac{-dP_A}{dt} = \frac{k_1^1 P_A}{1 + k_A P_A + k_B P_B} \quad (16)$$

$$\frac{dP_B}{dt} = \frac{k_1^1 P_A - k_2^1 P_B P_C}{1 + k_A P_A + k_B P_B} \quad (17)$$

$$\frac{-dP_C}{dt} = \frac{k_2^1 P_B P_C}{1 + k_A P_A + k_B P_B} \quad (18)$$

rearranging and integrating, one obtains

$$A_0 - A = k_1^1 \int_0^t A dt + k_A \frac{A^2 - A_0^2}{2} + k_B \int_{A_0}^A B dA \quad (19)$$

$$B - B_0 = k_1^1 \int_0^t A dt - k_2^1 \int_0^t BC dt - k_A \int_{B_0}^B A dB - k_B \frac{B^2 - B_0^2}{2} \quad (20)$$

$$C - C_0 = -k_2^1 \int_0^t BC dt - k_A \int_{C_0}^C A dC - k_B \int_{C_0}^C B dC \quad (21)$$

where for simplicity A, B, C have been written for P_A , P_B , P_C and A_0 , B_0 , C_0 for their initial values.

If one has measurements of A, B, C as functions of time, these also define A, B, C as functions of each other, and hence integrals such as $\int_{A_0}^A B dA$ may be numerically evaluated for all experimental points. Equations 19–21 thus comprise a system in which k_1^1 , k_2^1 , k_A , and k_B are unknown, and all other quantities are calculable at each point from experimental data. They are therefore a system which may be solved by linear least squares, again with some reservations about the effect of correlations on the results.

As a test, we have solved eq 16–18 by the proposed method, again using artificial data with randomly generated perturbations. In general, it was found that the method worked satisfactorily provided that the constants assumed were such that $k_A P_A$ and $k_B P_B$ were of the order of magnitude of unity during at least part of the reaction, and that P_A and P_B varied significantly during the reaction. If these conditions did not hold, the system became very ill-conditioned, as would be expected from the form of eq 16–18. When the above conditions did hold, it was found that the rate constants obtained were again correct, and that standard deviations from the linear regression were again too small.

It can be concluded, then, that the proposed method can be used to solve a certain class of heterogeneous systems, provided that the experimental data adequately define the constants involved. It should be noted that equations of the form of (19) to (21) arising from several experimental runs at different reactant pressures could be simultaneously least-square fitted, which would be preferable when k_A and k_B are not of the same order of magnitude.

Temperature-Scanned Reactions

It is becoming increasingly common in some types of research (*e.g.*, desorption spectroscopy, differential thermal analysis) to observe the rate of reaction while the temperature is varied, often linearly, with time. The kinetics of such a reaction may be written as

$$r = -\frac{dC}{dt} = AC^n \exp(-E/RT(t)) \quad (22)$$

where r is the rate of reaction, C is the concentration of reactant, A is the preexponential factor, E is the activation energy, and n is the order of reaction. The experimental data consist of a peak when rate is plotted against time or temperature, since the rate initially in-

creases due to increase of the temperature, and then falls due to depletion of reactant.

Methods for obtaining kinetic parameters from such experiments are available in the literature^{9,10} and usually involve the requirement of some specific temperature-time relationship (*e.g.*, linear) together with data from several runs at different temperature sweep rates. Equation 22 can, however, be solved directly if rate data are integrated numerically to produce concentration data. Thus in the normal experiment, heating is continued until the reactant is completely consumed, and one has

$$C(t) = \int_t^{\infty} r dt \quad (23)$$

one can then rewrite (22) as

$$\ln r = \ln A + n \ln C - \frac{E}{R} \frac{1}{T(t)} \quad (24)$$

so that $\ln A$, n , and E may be obtained by least-squares fit, since r and T are experimentally available, and C is obtained from (23). It should be noted that r and C enter logarithmically, and hence E and n may still be obtained even if the experiment is such that r cannot be obtained in absolute units. In this case $\ln A$ will contain a term involving the unknown calibration factor, if n is other than 1.

It should be noted that equations of the form of (24) arising from runs under various conditions (*e.g.*, differing temperature-time programs) may be combined in the least-squares fit to obtain optimum values of all parameters. The method will still apply if E is a

simple function of C . For example, if $E = E_0 - \alpha C$, which is a model of interest in desorption studies, (24) becomes

$$\ln r = \ln A + n \ln C - \frac{E_0}{R} \frac{1}{T(t)} + \frac{\alpha}{R} \frac{C}{T(t)} \quad (25)$$

and given sufficient data, a least-squares fit can be used to determine all parameters. These methods have been tested with some experimental desorption data¹¹ previously analyzed by iterative techniques and found to yield the same results within reasonable uncertainty. Unfortunately, the method is not applicable to the resolution of overlapping peaks resulting from two or more rate processes.

Summary

The methods discussed provide a simple and direct way of analyzing kinetic data for complex mechanisms. For systems in which they are applicable they are much quicker than iterative least-squares techniques and more reliable than alternative traditional methods involving such processes as graphical or numerical differentiation.

Acknowledgment. The author thanks the National Research Council for an operating grant under which this work was carried out, and the Simon Fraser Computing Centre for provision of computing resources.

(9) H. E. Kissinger, *Anal. Chem.*, **29**, 1703 (1957).

(10) R. J. Cvetanović and Y. Amenomiya, *Advan. Catal.*, **17**, 103 (1967).

(11) I. D. Gay, *J. Catal.*, **17**, 245 (1970).

The Rate of Exchange of Hydrogen and Deuterium behind Reflected Shock Waves. Dynamic Analysis by Time-of-Flight Mass Spectrometry¹

by R. D. Kern* and G. G. Nika²

Department of Chemistry, Louisiana State University in New Orleans, New Orleans, Louisiana (Received November 25, 1970)

Publication costs assisted by the National Science Foundation

The reaction of equimolar mixtures of hydrogen and deuterium diluted by neon has been studied over the temperature range 1800–3000°K. The gas in the reflected shock zone was analyzed at 20- μ sec intervals by a time-of-flight mass spectrometer during a typical reaction time of 500 μ sec. Equilibrium was attained during the observation period in several of the experiments at temperatures exceeding 2600°K. The time dependence of the mole fraction f_{HD} was determined to be quadratic. The reaction profiles were fit to the equation $[1 - 2f_{\text{HD}}] = \exp(-k[M]t^2)$, where $k = 10^{16.93 \pm 0.24} \exp(-44,370 \pm 2,510/RT)$, $\text{cm}^3 \text{mol}^{-1} \text{sec}^{-2}$. The rate constants from a single-pulse shock tube study of this reaction were recalculated using a quadratic time dependence for product formation. The agreement was within one standard deviation. The Arrhenius parameters determined from both the single-pulse data and this work, which together cover a temperature range of 1000–3000°K, are $\log A = 16.55 \pm 0.05$ and $E^* = 40.44 \pm 0.34 \text{ kcal mol}^{-1}$. The units of A are $\text{cm}^3 \text{mol}^{-1} \text{sec}^{-2}$. The validity of the dynamic sampling process is supported by agreement of the kinetic results from two other reactions, $\text{D}_2\text{-HCl}$ and $\text{D}_2\text{-HCN}$, which were obtained by employing the independent technique of infrared emission. Several mechanisms for the exchange and their relation to the experimental results are discussed.

Introduction

The coupling of a shock tube to a time-of-flight mass spectrometer (TOF) by Bradley and Kistiakowsky³ is recognized as a significant step in the study of chemical kinetics. The status of both the shock tube and the TOF with regard to rate studies was fledgling in 1959. From the beginning there was an effort to compare the kinetic results from this new experimental technique with other independent sources of data. There was an awareness of the difficulties of extracting a sample of gas from the reflected shock zone which was representative of the reacting gases and which did not contain substantial amounts of the boundary layer that was forming on the end wall during the observation period. These pioneering experiments convinced many people of the authenticity of the sample but also produced critics, many of whom resided in Gibbs Laboratory.

The next set of workers under Professor Kistiakowsky's guidance completely rebuilt the apparatus.⁴ Many important changes were made: the shock tube diameter was increased from 0.5 to 1 in. i.d.; the rotating drum camera was replaced by a series of gating circuits which enabled a number of successive mass spectra to be photographed by open-shutter cameras loaded with Polaroid film;⁵ the driver section was shortened to a 13-in. length, large diameter cylinder designed by Dr. Paul Kydd; a four-way rotary valve was positioned in the test section which allowed the diaphragm to be replaced while the majority of the test section and the mass spectrometer remained at high vacuum.

A miniature divergent nozzle constructed to minimize boundary layer effects replaced a pinhole at the end wall. A high particle transmission, positively biased grid placed in the TOF ion source close to the gas inlet prevented the entry of chemi-ions formed during oxidation reactions. The grid was also used to focus chemi-ions. The focusing was achieved by reversing the polarity of the bias and applying positive pulses that were synchronized with the negative ion focus pulses.⁶

A continuing effort has been the collection of kinetic data on the same reaction system by a number of independent analytical techniques. Notable examples are the agreement of the induction periods and exponential time constants for the oxidation of acetylene measured in both incident and reflected waves.⁶ Two shock tubes were employed. One tube used a Langmuir probe to monitor gas conductivity and visible emission spectroscopy to detect CH^* chemiluminescence. The observations of the reflected shock zone were of a gas

(1) Support of this work by the National Science Foundation under grant GP-23137 and also funds for equipment from NSF Departmental Science Development Program GU-2632 are gratefully acknowledged.

(2) NDEA Fellow.

(3) J. N. Bradley and G. B. Kistiakowsky, *J. Chem. Phys.*, **35**, 256 (1961).

(4) J. E. Dove and D. Mc L. Moulton, *Proc. Roy. Soc., Ser. A*, **283**, 216 (1965).

(5) D. Mc L. Moulton and J. V. Michael, *Rev. Sci. Instrum.*, **36**, 226 (1965).

(6) G. P. Glass, G. B. Kistiakowsky, J. V. Michael, and H. Niki, *J. Chem. Phys.*, **42**, 608 (1965).

at rest which differs from the TOF experiments (the second tube) in which the gas is flowing from the reflected shock zone, through the pinhole nozzle, and into the ion source before the analysis process begins. The recording of exponential growth of the oxidation products and chemi-ions demonstrates the validity of the TOF results. Additional support is provided by the comparison of pseudo-first-order rate constants for decomposition reactions. Examples are the agreement of TOF data with results of infrared emission experiments for the pyrolyses of C_2H_4 ^{7,8} and N_2O .^{9,10} A quadratic time dependence for product formation was observed in TOF experiments on the following systems: $C_2H_2 + C_2D_2$,⁹ $^{18}O_2 + ^{16}O_2$, CO ,^{11a} and $^{18}O_2 + SO_2$, CO_2 .^{11b}

The exchange of HCl and D_2 was studied behind reflected waves by infrared emission and time-of-flight mass spectrometry.¹² The rate constants determined from the reaction profiles of the infrared emissions from HCl and DCl agree with those calculated from the TOF recording of m/e 36 and 37. The growth of the product concentration was observed to have a quadratic time dependence. In this paper, the rate constants for the HCl- D_2 exchange have been measured by TOF monitoring of m/e 3 and 4. Similar experiments were performed on the HCN- D_2 reaction to support the determination of rate constants by TOF low-mass analysis. This demonstration is important because there exists no other practical, independent technique for the dynamic analysis of the H_2 - D_2 homogeneous exchange other than the TOF.

Single pulse shock tube results for the H_2 - D_2 reaction and the HD self-exchange have been reported previously.¹³ It will be shown in the Discussion section that the single-pulse rate constants are in remarkable agreement with those calculated from the TOF experiments when allowance is made for a quadratic time dependence.

The energetics of the exchange have been the subject of several theoretical calculations.¹⁴ The mechanism for the exchange has also received considerable attention.^{13a, 15, 16} The relationship of this work to the experimental results will be presented in the Discussion section.

Experimental Section

The infrared emission and the TOF shock tubes which comprise the complementary shock tube technique have been described previously.¹² The basic idea is to gather data on the same reaction system by two independent analytical techniques. In one tube, the infrared emission from two different species is recorded simultaneously in the reflected zone at a position 3.2 mm from the end wall which is a sample of gas somewhat similar to that analyzed in the TOF shock tube.

The gas in the TOF shock tube flows from the reflected zone, through a nozzle 1 mm in length and 0.101

mm in diameter, and into the ion source. Mass spectra are displayed at 20- or 30- μ sec intervals. To increase the sensitivity of the TOF for m/e 2, 3, and 4, an additional compensating magnet was placed in front of the multiplier magnets. Subsequent optimization of deflection voltages and compensating magnets' position and orientation produced a tenfold increase in the low-mass signals. For an equimolar mixture of H_2 and D_2 in neon, the signals for m/e 2 and 4 measured as analog output were equal within 2%. The ionizing voltage was 35 eV.

The gas mixtures which were shocked were allowed to reside in the TOF shock tube no longer than 45 sec before diaphragm rupture. During this time, the analog signal for O_2 was recorded and compared with background which was monitored prior to introduction of the mixture. Calibrated mixtures of known ppm O_2 were prepared and the comparison of the respective m/e 32 signals is the basis for saying that no experiment was performed with an oxygen content greater than 25 ppm. Outgassing rates in the TOF shock tube were less than 0.01 μ /min. Typical ultimate vacuums were 1×10^{-6} Torr in the shock tube, 5×10^{-7} Torr in the ion source ballast volume, and 2×10^{-7} Torr in the TOF main chamber.

Reacting mixtures were prepared by addition of equal amounts of Matheson research grade hydrogen (99.999%) and Matheson CP deuterium (99.5%). Matheson research grade neon (99.995%) was used as the diluent. These gases were used without further purification. Mass spectrometric analysis of each gas indicated oxygen levels below 25 ppm. Calibration mixtures of H_2 and of D_2 were prepared with appropriate amounts (usually 1%) of Liquid Carbonic argon (99.998%) added to H_2 or D_2 with neon as the diluent. The reacting mixture of HCl and D_2 was made by addition of Matheson hydrogen chloride (99.0%) purified by two liquid nitrogen bulb-to-bulb distillations; the middle fraction was accepted at each stage. Mass spectrometric analysis revealed oxygen and chlorine impurities at a level indistinguishable from background.

(7) I. D. Gay, R. D. Kern, G. B. Kistiakowsky, and H. Niki, *J. Chem. Phys.*, **45**, 2371 (1966).

(8) J. B. Homer and G. B. Kistiakowsky, *ibid.*, **47**, 5290 (1967).

(9) I. D. Gay, G. B. Kistiakowsky, J. V. Michael, and H. Niki, *ibid.*, **43**, 1720 (1965).

(10) E. S. Fishburne and R. Edse, *ibid.*, **41**, 1297 (1964).

(11) (a) S. H. Garnett, G. B. Kistiakowsky, and B. V. O'Grady, *ibid.*, **51**, 84 (1969); (b) T. C. Clark, S. H. Garnett, and G. B. Kistiakowsky, *ibid.*, **52**, 4692 (1970).

(12) R. D. Kern and G. G. Nika, *J. Phys. Chem.*, **75**, 171 (1971).

(13) (a) S. H. Bauer and E. Ossa, *J. Chem. Phys.*, **45**, 434 (1966); (b) A. Burcat and A. Lifshitz, *ibid.*, **47**, 3079 (1967); (c) D. Lewis and S. H. Bauer, *J. Amer. Chem. Soc.*, **90**, 5390 (1968).

(14) (a) C. W. Wilson, Jr., and W. A. Goddard III, *J. Chem. Phys.*, **51**, 716 (1969); (b) M. Rubenstein and I. Shavitt, *ibid.*, **51**, 2014 (1969); (c) B. M. Gimarc, *ibid.*, **53**, 1623 (1970).

(15) K. Morokuma, L. Pedersen, and M. Karplus, *J. Amer. Chem. Soc.*, **89**, 5064 (1967).

(16) L. Poulsen, *J. Chem. Phys.*, **53**, 1987 (1970).

HCN was prepared by addition of 50% H_2SO_4 to KCN. The evolved gas was collected and then distilled several times before its placement in the gas handling system. The reacting mixture of HCN and D_2 was made and analyzed as described above. Impurity levels were less than background. Partial pressures for the various components of the mixtures were measured with Wallace-Tiernan differential pressure gauges, 0–10 and 0–400 in. of water range. All mixtures were allowed to stand for 24 hr in 5-l. storage bulbs prior to use.

The infrared emission experiments performed on the HCN– D_2 mixtures were accomplished in a shock tube described previously.¹² Interference filters at 3.0 and 3.8 μ , 0.1- μ band pass, were selected to monitor the emission intensity of HCN and DCN, respectively. Additional details not pertinent here will be presented at a later time.¹⁷

The calculation of the temperature from measurements of the shock velocity at four equally spaced stations and the extrapolation of the slightly decelerating velocity to the end wall were performed as reported earlier.¹²

Results

The reaction profile for bimolecular isotope exchange in an equimolar mixture of H_2 and D_2 reacting to equilibrium at temperatures where $K = 4$ is represented by the equation

$$[1 - 2f_{\text{HD}}] = \exp(-k_1[\text{H}_2]_0 t) \quad (1)$$

where

$$f_{\text{HD}} = \frac{[\text{HD}]}{2[\text{H}_2]_0}$$

The initial concentration is given by $[\text{H}_2]_0$ and the rate constant for the forward reaction is k_1 . The rate of product formation is defined by

$$\text{rate} = \frac{1}{2} \frac{d[\text{HD}]}{dt}$$

Equation 1 may be cast into a general form to test experimentally by setting $k_1 = k[\text{M}]^y$ to allow for any inert gas dependence of order y and writing $[\text{H}_2]_0^x$ and t^z to discover any values of x and z other than unity.

$$[1 - 2f_{\text{HD}}] = \exp(-k[\text{H}_2]_0^x [\text{M}]^y t^z) \quad (2)$$

At early times, eq 2 reduces to a form that neglects the

$$[\text{HD}]_t = k'[\text{H}_2]_0^x [\text{D}_2]_0^{x'} [\text{M}]^y t^z \quad (3)$$

back reaction. Equation 3 is similar to that used in single-pulse tube studies¹³ if $x + x' \simeq 1$, $y \simeq 1$, and $z = 1$. Hence

$$\frac{\Delta \text{HD}}{\Delta t} = k'[\text{H}_2]_0 [\text{M}] \quad (4)$$

where Δt is the residence time.

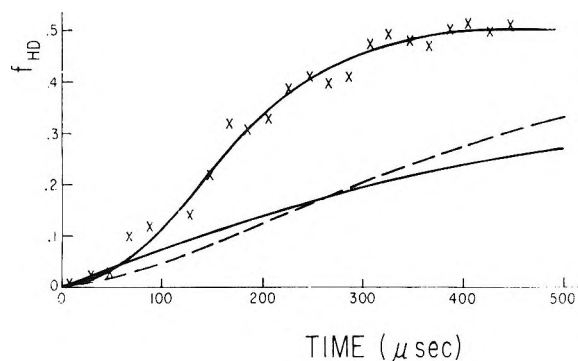


Figure 1. TOF profiles calculated using different time dependencies for an equimolar 2% mixture, $P_1 = 7.5$ Torr, at 2525°K: \times , experimental points; — (uppermost), t^2 plot; ---, $t^{1.5}$; — (lower), t^1 .

In the TOF experiments, the mole fraction of the product was calculated by measuring the peak height of m/e 3 and dividing by the sum of the peak heights of m/e 2, 3, and 4. A typical reaction profile is shown in Figure 1; f_{HD} was observed to increase with a nonlinear dependence on reaction time.

Equation 2 was transformed into an early times form

$$2f_{\text{HD}} = k[\text{H}_2]_0^x [\text{M}]^y t^z \quad (5)$$

from which a preliminary value of z was determined by plotting $\log f_{\text{HD}}$ vs. $\log t$. An initial estimate for k_{obsd} ($=k[\text{H}_2]_0^x [\text{M}]^y$) was obtained by plotting f_{HD} vs. t raised to various powers; 1, $3/2$, and 2. Profiles calculated according to this procedure are depicted in Figure 1 along with the experimental points.

The value of z was also derived from plots of the $\log(-\log)$ of the left-hand side of eq 2 vs. $\log t$. The graphical value for z was about 1.7 although the individual reaction profiles were fit satisfactorily by z equal to two. There was no experimental evidence for an induction period.

The initial estimate for k_{obsd} was used as input for the computer. The computer searched for the value of k_{obsd} which reproduced the entire experimental reaction profile with the lowest standard deviation. The equation for the profile was in the form

$$[1 - 2f_{\text{HD}}] = \exp(-k_{\text{obsd}} t^2) \quad (6)$$

The reaction was studied at different initial concentrations of H_2 and D_2 to determine x and at a different starting pressure to determine y . The value of x was zero, while the value of y was not clearly determined. It was not possible to work at starting pressures greater than 7.5 Torr. Hence, the variance in $[\text{M}]$ was only 50% which perhaps is not enough to determine y . In order to make a comparison with the single-pulse data, the profiles were fit with $y = 1$. The value of $x = 0$ is consistent with the single-pulse work.^{13a}

(17) J. M. Brupbacher and R. D. Kern, work in progress.

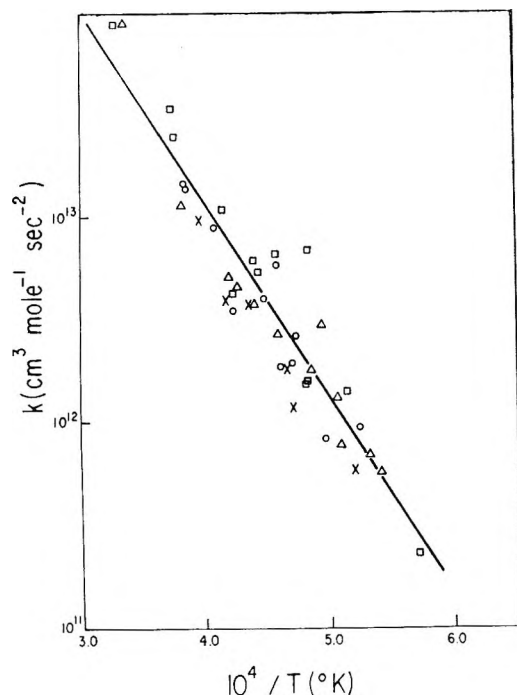


Figure 2. Arrhenius plot of data in Table I: O, mixture A; Δ , B; \times , C; \square , D.

All of the TOF experiments were fit to the equation

$$[1 - 2f_{\text{HD}}] = \exp(-k[M]t^2) \quad (7)$$

The results are listed in Table I for the various mixtures and starting pressures. An Arrhenius plot of the data is shown in Figure 2. Least-squares treatment of the rate constants yielded values of $\log A = 16.93 \pm 0.24$ and $E^* = 44.37 \pm 2.51$ kcal mol⁻¹. The units of A are centimeter³/mol sec².

The rate constants for the single-pulse experiments were recalculated on the basis of eq 2 with $x = 0$, $y = 1$, and $z = 2$. The residence time Δt was held constant within 3% for all of the runs listed in Table II of ref 13a. The Arrhenius parameters for the recalculated rate constants are $\log A = 17.10 \pm 0.15$ (cm³ mol⁻¹ sec⁻²) and $E^* = 43.50 \pm 0.89$ kcal mol⁻¹. Compared with the TOF results reported here, the data agree within one standard deviation with respect to both $\log A$ and E^* . A least-squares treatment of both sets of data yielded the values $\log A = 16.55 \pm 0.05$ and $E^* = 40.44 \pm 0.34$ kcal mol⁻¹. The rate constants cover a temperature range of 1000–3000°K. The Arrhenius plot is displayed in Figure 3.

A series of experiments was performed to support the validity of the TOF analysis of low masses. The rate constants for the D₂-HCl exchange were calculated three different ways: TOF analysis of m/e 36 and 37; infrared emission of HCl and DCl; and TOF analysis of m/e 3 and 4. The rate constants for the D₂-HCN exchange were also determined in a like manner: TOF analysis of m/e 27 and 28; infrared emission of HCN and DCN; and TOF analysis of m/e 3 and 4. The data

Table I: Rate Constants for the Homogeneous Exchange of Hydrogen and Deuterium

Mixture	T_0 , °K	$\rho_0 \times 10^6$, mol cm ⁻³	$k \times 10^{-11}$, cc mol ⁻¹ sec ⁻²	
Neon Diluent				
A. 3% H ₂ -3% D ₂ $P_1 = 5$ Torr	1909	1.82	9.60	
	2010	1.92	8.25	
	2110	1.86	25.7	
	2121	1.83	19.0	
	2171	2.00	18.3	
	2183	1.86	56.8	
	2230	2.04	39.5	
	2361	1.95	34.8	
	2441	1.93	87.6	
	2585	1.94	139	
	2600	2.14	143	
	2677	1.99	339	
B. 2% H ₂ -2% D ₂ $P_1 = 5$ Torr	1845	1.67	5.62	
	1885	1.72	6.82	
	1964	1.75	7.79	
	1974	1.77	13.0	
	2019	1.78	29.7	
	2054	1.75	17.6	
	2182	1.80	26.7	
	2267	1.83	37.1	
	2342	1.84	44.8	
	2374	1.87	51.3	
	2621	1.93	115	
	2965	2.03	913	
C. 2% H ₂ -2% D ₂ $P_1 = 7.5$ Torr	1926	2.68	5.76	
	2129	2.76	11.4	
	2151	2.76	17.8	
	2157	2.80	18.0	
	2292	2.91	36.4	
	2394	2.93	38.9	
	2525	2.94	94.2	
	D. 1.5% H ₂ -1.5% D ₂ $P_1 = 5$ Torr	1749	1.63	2.26
		1949	1.72	13.7
		2064	1.77	15.8
2069		1.81	67.8	
2079		1.79	15.6	
2194		1.83	65.5	
2253		1.81	52.9	
2271		1.85	60.0	
2365		1.89	42.5	
2411		1.89	107	
2662	1.93	241		
3052	2.03	890		

for both reaction systems were internally consistent with respect to quadratic time dependence of product formation and E^* . The value of E^* was different: $E^* = 34$ kcal mol⁻¹ for D₂-HCl and $E^* = 57$ kcal mol⁻¹ for D₂-HCN. The former exchange has been studied with respect to reactant and inert gas order dependence.¹² Work on D₂-HCN is not complete with respect to order determination.¹⁷ Experiments were performed with a 2% D₂-HCN mixture at 5 Torr initial pressure and were analyzed with an equation similar in form to (6). Arrhenius plots for these two reactions appear in Figures 4 and 5, respectively. It is pertinent to note that low-mass data were treated in the same fash-

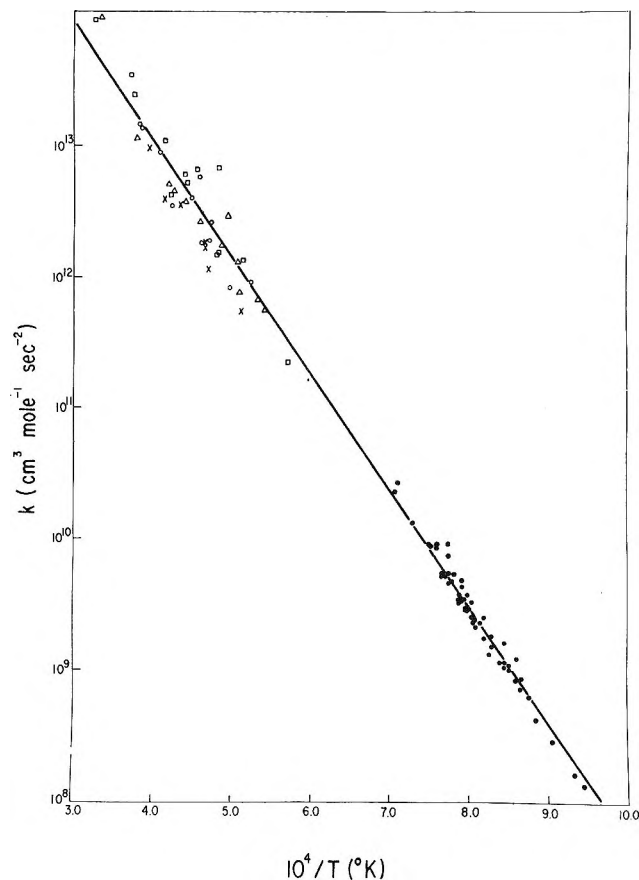


Figure 3. Arrhenius plot of TOF (same symbols as Figure 2) and single pulse data ●.

ion as the data for the $\text{H}_2\text{-D}_2$ exchange. The mole fraction of the product was obtained by dividing the peak height for m/e 3 by the sum of the peak heights for m/e 3 and 4.

Previous work on the $\text{H}_2\text{-D}_2$ exchange using a TOF-shock tube apparatus in connection with the pyrolysis of ethylene⁷ and on the exchange itself¹⁸ revealed that the sum of the peak heights of H_2 , HD, and D_2 increased during the observation period for the reaction. A series of experiments was conducted with the $\text{D}_2\text{-HCl}$ exchange reported herein to assess quantitatively the magnitude of the sum increase at low masses.

During the first 50–100 μsec after shock arrival at the end wall, there is a steady pressure increase in the TOF ion source region. Small amounts of argon ($\sim 1\%$) have been used as an internal standard and reacting concentrations have been expressed as a ratio of peak heights. Hence, in a nonreacting mixture of 2% HCl, 1% Ar, and 97% Ne, the peak heights of m/e 36 and 40 increase during the initial portion of the observation period and then show a constancy for 500 or more microseconds while the ratio of 36:40 is constant throughout the observation period.

With the magnets aligned for low-mass optimization, the following experiments were conducted. The first two recording scopes were triggered in parallel which

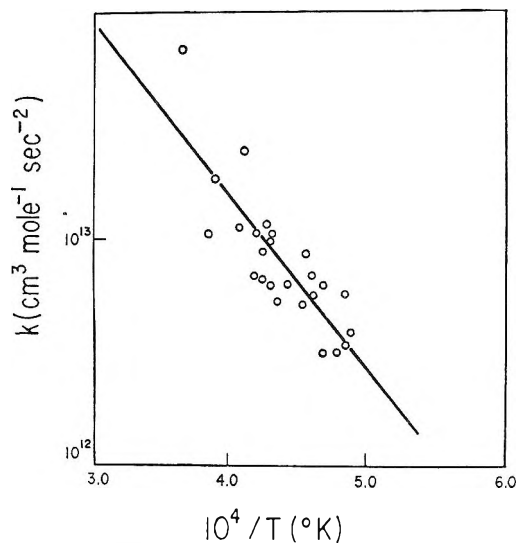


Figure 4. Arrhenius plot of low-mass data for $\text{HCl} + \text{D}_2$ exchange. $\log A = 16.23 \pm 0.45$ (16.12 ± 0.30), $E^* = 34.70 \pm 4.69$ (34.34 ± 3.13). Values in parentheses reported in ref 12.

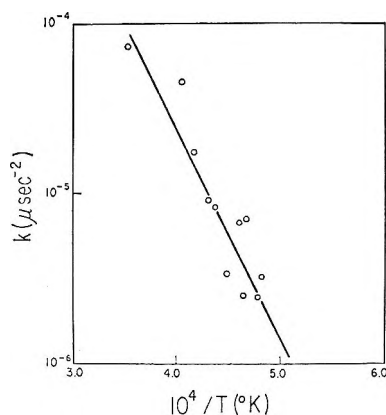


Figure 5. Rate constants calculated for the exchange of HCN plus D_2 from low-mass data: O, compared to solid line established by ir and TOF m/e 27, 28 experiments.

permitted simultaneous observation of m/e 2, 3, and 4 on the first scope and m/e 36, 37, and 40 on the second scope. A second pair of scopes was triggered after the first two. Spectra were recorded at 30- μsec intervals for a total observation time of 300 μsec .

The sums of the ratios $36/40 + 37/40$ and $3/40 + 4/40$ were fit to the equation

$$\Sigma = mt + b$$

The values of m and b for $\Sigma(3/40 + 4/40)$ and $\Sigma(36/40 + 37/40)$ were $17.0 \times 10^{-4} \mu\text{sec}^{-1}$ and 1.81, $8.0 \times 10^{-4} \mu\text{sec}^{-1}$ and 1.52, respectively. Experiments performed on this gas mixture with the four scopes triggered in series, TOF frequency 50 kHz, yielded $m = 0.6 \times 10^{-4} \mu\text{sec}^{-1}$, $b = 1.91$ for $\Sigma(36/40 + 37/40)$.

(18) R. D. Kern, G. B. Kistiakowsky, and B. V. O'Grady, unpublished work.

These values contrast with those obtained at the same TOF frequency but magnet optimization for m/e 36 and 37; namely, $m = -0.7 \times 10^{-4} \mu\text{sec}^{-1}$ and $b = 2.05$. It is observed that the sums depend upon instrumental factors to some extent, but the important point is that the rate constants derived from these various configurations are not affected to any great extent. The agreement is shown in Figure 4. Most encouraging is the agreement of the rate constants obtained by monitoring m/e 3 and 4 at 20- μsec intervals without an argon internal standard. The pressure increase is allowed for by calculating mole fractions; m/e 3 divided by the sum of m/e 3 + 4.

Similar agreement of the rate constants for the D_2 -HCN reaction derived from low-mass, high-mass, and infrared emission experiments is displayed in Figure 5.

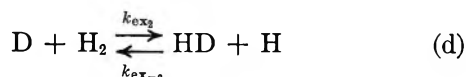
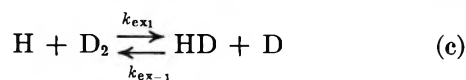
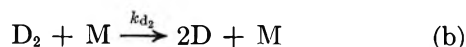
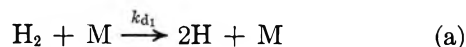
Another encouraging aspect is the experimental value of f_{HD} at equilibrium. In all three exchange reactions, the observed value was in agreement with the calculated value.

Discussion

The TOF and the single-pulse data for the exchange of H_2 and D_2 agree with respect to the activation energy. The data also agree with respect to $\log A$ if the same order dependence for reactants and inert gas is used and if the time dependence is taken to be quadratic. The value of z in eq 4 is a constant in the single-pulse experiments and is assumed to have a value of one. In the TOF experiments, z is an observable.

All of the experimental work rules out the direct four-center mechanism because of the magnitude of the calculated activation energy ($\geq 148 \text{ kcal mol}^{-1}$).^{14a} The observed inert gas dependence reported by the single-pulse workers¹³ and the nonlinear time dependence reported here also argue against the four-center molecular mechanism.

An atomic mechanism provides an explanation for the quadratic time dependence but requires an activation energy on the order of 110 kcal mol^{-1} .



Neglecting the back reactions

$$\frac{d[\text{HD}]}{dt} = k_{ex1}[\text{H}][\text{D}_2] + k_{ex2}[\text{D}][\text{H}_2] \quad (8)$$

Considering an equimolar mixture and setting $k_{d1} \simeq k_{d2}$ ¹⁹ and $k_{ex1} \simeq k_{ex2}$,²⁰ the resulting equalities are

$$\left(\frac{1}{2}\right) \frac{d[\text{HD}]}{dt} = k_{ex1}[\text{H}][\text{D}_2] \quad (9)$$

$[\text{H}] = [\text{D}]$ and $[\text{H}_2] = [\text{D}_2]$. Approximating $[\text{H}_2]_t \simeq [\text{H}_2]_0$, and substituting into eq 10 and integrating

$$\left(\frac{1}{2}\right) \frac{d[\text{H}]}{dt} = k_{d1}[\text{H}_2][\text{M}] \quad (10)$$

$$[\text{H}]_t = 2k_{d1}[\text{H}_2]_0[\text{M}]t \quad (11)$$

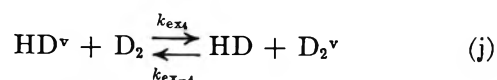
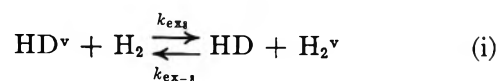
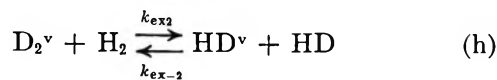
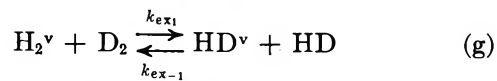
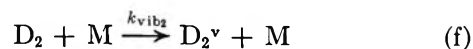
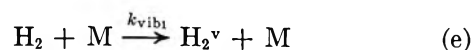
The rate constant k_{d1} has been measured¹⁹ and it can be shown that the reaction time required to produce equilibrium concentrations of hydrogen atoms at the temperatures achieved in the TOF experiments is much longer than the observed time for the H_2 - D_2 exchange reaction to make equilibrium amounts of HD. Substituting for $[\text{H}]$ in eq 9 with (11) and integrating

$$[\text{HD}]_t = 2k_{d1}k_{ex1}[\text{H}_2]_0[\text{D}_2]_0[\text{M}]t^2 \quad (12)$$

$$f_{\text{HD}} = k_{d1}k_{ex1}[\text{H}_2]_0[\text{M}]t^2 \quad (13)$$

The atomic mechanism predicts $x = 1$, $y = 1$, and $z = 2$ for eq 2. The activation energy is the sum of the activation energies of reactions a and c which is on the order of 110 kcal mol^{-1} . Extending the approximations used here to include the back reactions along with $K = 4$ and $[\text{H}_2]_0 + [\text{D}_2]_0 = [\text{H}_2]_t + [\text{D}_2]_t + [\text{HD}]_t$, eq 2 may be derived with the values of x , y , and z mentioned above. A predicted activation energy of 110 kcal mol^{-1} is far in excess of the experimental value of 40 kcal mol^{-1} . The quadratic time dependence is consistent with the TOF results but the value of x is not consistent with either the single pulse or the TOF experiments.

A vibrational energy chain mechanism may be written in which vibrational energy is transferred in straight chains.



The superscript v represents one or more quanta of vi-

(19) R. L. Belford and R. A. Strehlow, *Ann. Rev. Phys. Chem.*, **20**, 260 (1969).

(20) A. A. Westenberg and N. de Haas, *J. Chem. Phys.*, **47**, 1393 (1967).

brational energy. Reactions e and f represent a sequence of steps in which the vibrational energy is added in a stepwise fashion. Equations g and h represent reaction while i and j replenish the straight chain with H_2^v and D_2^v .

A derivation similar to the atomic mechanism yields the result

$$f_{HD} = k_{vib_1} k_{ex_1} [H_2]_0 [M] t^2 \quad (14)$$

The assumptions involved are that $k_{vib_1} \simeq k_{vib_2}$, which for the discussion here is approximately correct,²¹ and that the back reactions for (e) and (f) may be neglected which is incorrect. The time predicted to reach equilibrium concentrations of H_2 and D_2 in the first vibrational level using the experimental vibrational relaxation data²¹ is much less than the observation time for the exchange reaction. If the back reactions for (e) and (f) are included, the time dependence of product formation is no longer quadratic; it is linear.

Admittedly, the treatment of the reaction scheme (e)-(j) presented here is far from rigorous. A more proper approach would be the solution of the master equation for this mechanism.^{13a} This problem has been considered recently and some of the difficulties involved in a numerical solution without some approximations are discussed.¹⁶ A similar problem arose in the D_2 -HCl exchange¹² and it is hoped that more calculational

effort in this area will be forthcoming.²² However, mechanistic schemes that invoke the steady-state approximation are not consistent with the nonlinear time dependence reported here.

The preceding discussion states what the mechanism is not and in that sense is a negative contribution to the overall problem. The positive aspects of this investigation are the extension of the temperature range to a 2000° interval, the recording of the extent of conversion from zero to equilibrium, and the deduction of a nonlinear time dependence for product formation. The agreement of data obtained from shock tubes where the absence of gas flow does not complicate the analysis with TOF data is encouraging.

Acknowledgments. The authors wish to remember the patience and skill of the late Mr. Joseph McPherson, who made a major contribution to the construction of the apparatus. Mr. Darryl Olivier provided able assistance in the operation and maintenance of the equipment. R. D. K. wishes to express his appreciation to Professor G. B. Kistiakowsky for the opportunity to work as a Research Fellow in his laboratory.

(21) (a) J. H. Kiefer and R. W. Lutz, *J. Chem. Phys.*, **44**, 658 (1966); (b) J. H. Kiefer and R. W. Lutz, *ibid.*, **44**, 668 (1966).

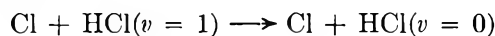
(22) S. H. Bauer, private communication.

COMMUNICATIONS TO THE EDITOR

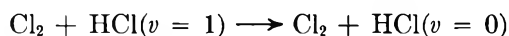
Vibrational Relaxation of Hydrogen Chloride by Chlorine Atoms and Chlorine Molecules

Publication costs assisted by the Advanced Research Projects Agency

Sir: Chemical affinity is thought to explain exceptionally rapid deactivation of vibrationally excited molecules.¹ Such processes involving strong attractive intermolecular forces are of importance in chemical lasers where highly reactive species are necessarily present. In this communication we describe a method for direct measurement of the rate of



and report a preliminary value for the rate constant for this process, which is indeed large. A value for the rate of



is also reported.

The principal experiment consisted of exciting HCl vibrationally in an HCl-Cl₂-Ar mixture with a pulse from an HCl laser and then, after partial decay of the vibrational fluorescence from HCl[†], photodissociating Cl₂ with a pulse of 3471-Å doubled ruby light. The construction of the HCl laser source and the detection of fluorescence from the R-branch of the HCl fundamental were essentially the same as described previously.² The HCl laser was initiated by a 15-kV, 17-μF discharge through a xenon flashlamp. Infrared pulses were about 10 μsec in duration and about 10 mJ in energy. Ultraviolet light from the Q-switched ruby laser system,³ located about 8 m away from the fluorescence cell and filtered free of red light, was a pulse of 4.2 × 10¹⁵ photons/cm² in 15 nsec. For both laser sources energies were measured with an Eppley 16-junction thermopile. The two lasers were fired directly at one another through opposite windows of the 3-cm long, 3-cm diameter fused-silica fluorescence cell. The infrared beam, which was stopped down to 1-cm diameter and which was coaxial with the 2-cm diameter ultraviolet beam, defined a fluorescence zone smaller than that in which chlorine atoms were produced. Gas mixtures were prepared from research grade argon (J. T. Baker) and chlorine (Matheson) and from distilled, electronic grade hydrogen chloride (Matheson). Pressures were measured with the aid of a stainless steel transducer (Pace-Whitaker), and Krytox grease⁴ was used for all critical stopcocks.

Figure 1, photographed on a Tektronix 7704 oscilloscope, shows a sharp increase in the fluorescence decay

rate at the instant of the ultraviolet pulse. The downward blip on the lower trace is a marker from the Pockels cell Q-switch circuit and is coincident with the ruby laser pulse. For the run shown in Figure 1 the simultaneous triggering of the oscilloscope sweep and the flashlamp for the HCl laser was delayed until 500 μsec after the start of the pumping flash in the ruby system. As in previous HCl fluorescence experiments, semilogarithmic graphs were linear (over more than three lifetimes) for the decays of mixtures excited with infrared light alone. Figure 2 is a corresponding decay curve following chlorine atom production. The upward curvature in the latter third of the graph is characteristic of the runs with chlorine atoms present.

From the results in Table I, we calculate $k_{\text{Cl}_2} = 180 \pm 30 \text{ sec}^{-1} \text{ Torr}^{-1}$.⁵ From the observed ultraviolet

Table I: Observed Fluorescence Lifetimes for Various Gas Mixtures

	Pressure, Torr			τ, μsec
	HCl	Cl ₂	Ar	
No uv	1.6		147	600
No uv	1.4	21	127	195
With uv	1.4	21	127	62 ^a

^a A value of 160 μsec was used for the rate in absence of uv; the background rate increased somewhat during uv experiments.

photon flux, the published absorption coefficient of 2.0 × 10⁻¹⁹ cm²/molecule for Cl₂ at 3470 Å,⁶ a 1.5-cm average depth in the fluorescence cell, and the data in Table I we calculate a chlorine atom pressure of 0.028 Torr (0.07% dissociation of Cl₂). k_{Cl} is then (3.5 ± 2) × 10⁵ sec⁻¹ Torr⁻¹, which implies a 1.2-Å² cross section for deactivation of vibrationally excited HCl by Cl atoms. The relaxation rate constant is comparable to that for HCl by H₂O, for which a hydrogen bonding (as well as a V → V) mechanism is probably important.

(1) A. B. Callear and G. J. Williams, *Trans. Faraday Soc.*, **62**, 2030 (1966); J. H. Kiefer and R. W. Lutz, *Symp. (Int.) Combust. [Proc.]*, **11th**, 67 (1967); W. D. Breshears and P. F. Bird, *J. Chem. Phys.*, **48**, 4768 (1968); R. J. Donovan, D. Husain, and C. D. Stevenson, *Trans. Faraday Soc.*, **66**, 2148 (1970).

(2) H.-L. Chen and C. B. Moore, *J. Chem. Phys.*, in press.

(3) E. S. Yeung and C. B. Moore, *J. Amer. Chem. Soc.*, **93**, 2059 (1971).

(4) Krytox is a DuPont product. It is a polymer of perfluoropropylene oxide thickened with Teflon.

(5) R. L. Johnson, M. J. Perone, and D. W. Setser, *J. Chem. Phys.*, **52**, 6372 (1970). That our value is about a factor of 10 smaller than the previously reported value of 2200 sec⁻¹ Torr⁻¹ is presumably attributable to more rigorous exclusion of impurities.

(6) D. J. Seery and D. Britton, *J. Phys. Chem.*, **68**, 2263 (1964).

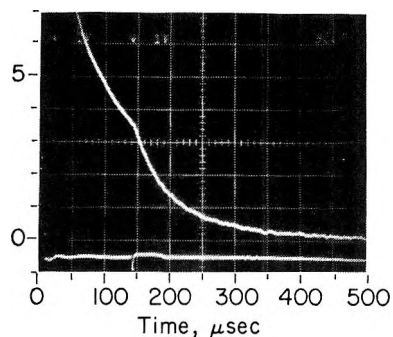


Figure 1. Decay of HCl infrared fluorescence. HCl laser pulse near 30 μsec ; ruby laser pulse at 140 μsec . Vertical scale: 1 V/div.

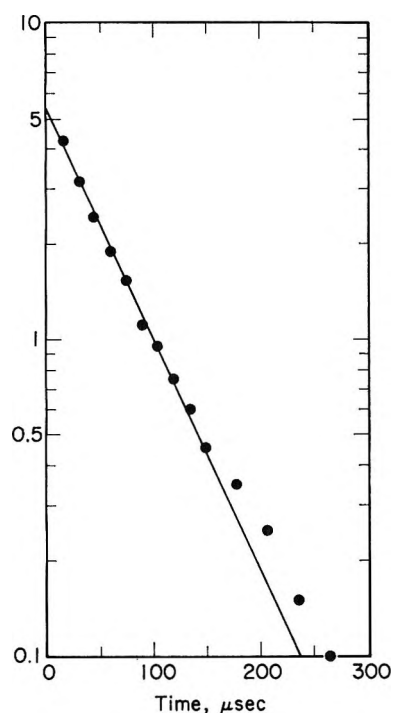


Figure 2. Analysis of HCl fluorescence decay in the presence of chlorine atoms. Chlorine atom production at $t = 0$, $\tau = 60 \mu\text{sec}$.

Thirty per cent (24 kcal/mol) of the energy of the 3471- \AA photons used to dissociate Cl_2 goes into heating the gas mixture.⁷ For a C_v of 3 cal/deg-mol and a chlorine atom production of 0.03 Torr, the temperature of 150 Torr of gas will rise only 1° . Thus, thermal effects should not be important in this argon moderated system. From the published values for Cl_2 molecule [$k_{\text{Cl},\text{Cl}_2} = 7.9 \times 10^{-32} (\text{cm}^3/\text{molecule})^2 \text{sec}^{-1}$] and Ar atom [$k_{\text{Cl},\text{Ar}} = 1.1 \times 10^{-32} (\text{cm}^3/\text{molecule})^2 \text{sec}^{-1}$]

mediated recombination of chlorine atoms,⁸ one calculates only 0.15 msec^{-1} for $(1/[\text{Cl}])/(d[\text{Cl}]/dt)$. Thus, if partial recombination of chlorine atoms is the cause of the upward curvature in the decay line as in Figure 2, HCl-mediated recombination must be rapid with $k_{\text{Cl},\text{HCl}} \approx 300k_{\text{Cl},\text{Cl}_2}$. It is also possible that some trace impurity acts as a scavenger for chlorine atoms. Diffusion of chlorine atoms out of the active zone is another possible explanation but is one which requires an unrealistically high diffusion coefficient for these atoms.

Chlorine atoms are about 2000 times more efficient than chlorine molecules in relaxing vibrationally excited HCl. The large cross section for chlorine atom deactivation is consistent with Pacey and Polanyi's estimate of a 0.1 to 0.01 probability based on infrared chemiluminescence studies of the $\text{H} + \text{Cl}_2$ reaction.⁹ Chen, Stephenson, and Moore also came to the tentative conclusion that chlorine atoms were an effective agent in quenching the $\text{Cl} + \text{HI}$ chemical laser.⁷ That a strong attractive potential is involved in the collinear attack of Cl on the H end of HCl is shown by Noble and Pimentel's trapping of linear ClHCl radicals in an argon matrix.¹⁰ This reaction is also favored by considerations of orbital symmetry.¹¹

We expect to examine the details of the chlorine atom deactivation process and to study related chemically potent deactivation systems.

Acknowledgments. We wish to thank P. F. Zittel and E. S. Yeung for assistance in setting up the experimental apparatus. We are grateful to the Advanced Research Projects Agency of the Department of Defense (monitored by the U.S. Army Research Office, Durham, N. C., under Contract No. DAHC04 68 C 0044) and to the National Science Foundation for financial support.

(7) H.-L. Chen, J. C. Stephenson, and C. B. Moore, *Chem. Phys. Lett.*, **2**, 593 (1968).

(8) M. A. A. Clyne and D. H. Stedman, *Trans. Faraday Soc.*, **64**, 2693 (1968).

(9) P. D. Pacey and J. C. Polanyi, *J. Appl. Opt.* in press.

(10) P. N. Noble and G. C. Pimentel, *J. Chem. Phys.*, **49**, 3165 (1968); V. Bondybey, G. C. Pimentel, and P. N. Noble, *ibid.*, in press.

(11) C. Maltz, *Chem. Phys. Lett.*, in press.

(12) National Science Foundation Science Faculty Fellow; on leave from Oberlin College, Oberlin, Ohio 44074.

DEPARTMENT OF CHEMISTRY
UNIVERSITY OF CALIFORNIA
BERKELEY, CALIFORNIA 94720

Norman C. Craig*¹²
C. BRADLEY MOORE

RECEIVED MARCH 26, 1971

Platinum Group Metals and Compounds

ADVANCES IN CHEMISTRY SERIES
NO. 98



Eleven papers from a symposium by the Division of Inorganic Chemistry of the American Chemical Society chaired by U. V. Rao.

What new complexes of the platinum group metals have been synthesized? Here is a collection of papers presenting data on chalcogenides, oxides, nitrido and hydrido complexes, as well as the catalytic properties of these metals and their alloys. Information is included on

- synthesis
- structure
- magnetic susceptibility
- double bond migration

The platinum group metals are considered from the viewpoints of both industry and research. Their magnetic and thermodynamic properties are explored, as well as recent chemistry of σ - and π -bonded complexes. Crystal structure is discussed by several authors, with data presented in the form of

- x-ray scattering data
- absorption spectra
- crystal spectra
- infrared spectra
- Mossbauer spectra
- vibrational spectra

165 pages with index. Cloth bound (1971) \$9.00 Postpaid in U.S. and Canada; plus 35 cents elsewhere.

Set of L. C. cards with library orders upon request.

Other books in the ADVANCES IN CHEMISTRY SERIES of interest to inorganic chemists include:

No. 89 Isotope Effects in Chemical Processes
278 pages Cloth bound (1969) \$13.00

No. 82 Radiation Chemistry — II
558 pages Cloth bound (1968) \$16.00

No. 81 Radiation Chemistry — I
616 pages Cloth bound (1968) \$16.00

No. 81 and No. 82 ordered together \$30.00

No. 78 Literature of Chemical Technology
732 pages Cloth bound (1968) \$17.50

No. 73 Trace Inorganics in Water
396 pages Cloth bound (1968) \$12.50

No. 72 Mass Spectrometry in Inorganic Chemistry
329 pages Cloth bound (1968) \$12.00

Order from:
Special Issues Sales
American Chemical Society
1155 16th St., N. W.
Washington, D. C. 20036

ISOTOPE EFFECTS IN CHEMICAL PROCESSES

ADVANCES IN CHEMISTRY SERIES NO. 89

Thirteen papers from a symposium by the Division of Nuclear Chemistry and Technology of the American Chemical Society, chaired by William Spindel. Includes:

- Separating isotopes by chemical exchange, distillation, gas chromatography, electromigration, and photochemical processes
- Methods for fractionating isotopes of hydrogen, lithium, boron, carbon, and nitrogen
- Thermotransport in monatomic and ionic liquids
- Statistical-mechanical theory determining isotope effects

278 pages with index

Clothbound (1969)

\$13.00

Set of L.C. cards free with library orders upon request

Other books in the ADVANCES IN CHEMISTRY SERIES in physical and colloid chemistry include:

No. 87 Interaction of Liquids at Solid Substrates. Twelve papers survey recent research on solid/liquid interaction, including work on "coupling agents," adhesion of polymers, organic/inorganic interfaces, ultrasonic impedometry. Four more papers are concerned with heparinized surfaces at the blood/material interface. 212 pages
Cloth (1968) \$9.50

No. 84 Molecular Association in Biological and Related Systems. Nineteen articles survey and report new work on molecular association in fat digestion, in soap systems, in membrane constituents, and in mixed monolayers. Other topics include bile salt micelles, lipid monolayers and membranes, and a definitive review of biological membrane structure. 308 pages
Cloth (1968) \$10.50

No. 82 Radiation Chemistry—II. Thirty-six papers and 17 abstracts on radiation chemistry in gases, solids, and organic liquids. Includes three plenary lectures. 558 pages
Cloth (1968) \$16.00

No. 81 Radiation Chemistry—I. Forty-one papers and 17 abstracts on radiation chemistry in aqueous media, biology, and dosimetry. From the international conference at Argonne National Laboratory. 616 pages
Cloth (1968) \$16.00

No. 81 and No. 82 ordered together \$30.00.

No. 79 Adsorption from Aqueous Solution. Fifteen papers discuss thermodynamic and kinetic aspects of adsorption phenomena and the results of studies on a variety of adsorbate-adsorbent systems. 212 pages
Cloth (1968) \$10.00

No. 68 Mössbauer Effect and its Application in Chemistry. Ten papers that will familiarize chemists with Mössbauer spectroscopy as an analytical tool, for studying chemical bonding, crystal structure, electron density, magnetism, and other properties. 178 pages
Cloth (1967) \$8.00

No. 67 Equilibrium Concepts in Natural Water Systems. Sixteen papers represent the collaboration of aquatic chemists, analytical chemists, geologists, oceanographers, limnologists, and sanitary engineers, working with simplified models to produce fruitful generalizations and valuable insights into the factors that control the chemistry of natural systems. 344 pages
Cloth (1967) \$11.00

No. 64 Regenerative EMF Cells. Seventeen papers survey current progress and research on regenerative systems for converting and storing electrical energy. Principal emphasis is on thermally regenerative systems, but chemical and photochemical systems are considered. 309 pages
Cloth (1967) \$11.00

No. 63 Ordered Fluids and Liquid Crystals. Twenty-two studies on characterization, properties, and occurrence of these phenomena in many substances such as tristearin, p-azoxyanisole, mono- and di-hydric alcohols, phospholipids and polypeptides. 332 pages
Cloth (1967) \$11.50

No. 58 Ion-Molecule Reactions in the Gas Phase. Eighteen papers survey spectrometric and other methods for producing and studying ion-molecule reactions, such as pulsed sources for studying thermal ions, reactions in flames and electrical discharges. 336 pages
Cloth (1966) \$10.50

No. 54 Advanced Propellant Chemistry. Primarily directed to the search for new oxidizers; 26 papers survey oxygen-containing oxidizers, fuels and binders, fluorine systems including oxygen difluoride and difluoramines and liquid systems. 290 pages
Cloth (1966) \$10.50

No. 50 Solvated Electron. Reviews of theory, structure, reactions of solvated and hydrated electrons; detailed papers on electrical transport properties, photochemistry, theory of electron transfer reactions, structure of solvated electrons, hydrated electron research. 304 pages
Cloth (1965) \$10.50

No. 47 Fuel Cell Systems. Developments in theory, performance, construction, and new systems for the energy converter that is proving itself in military and space uses. 360 pages
Cloth (1965) \$10.50

No. 43 Contact Angle, Wettability, and Adhesion. Twenty-six papers on theoretical and practical approaches to wettability and adhesion; with summary of the surface chemical studies of W. A. Zisman, the 1963 Kendall Award winner. 389 pages
Cloth (1964) \$10.50

No. 40 Mass Spectral Correlations. By Fred W. McLafferty. Over 4000 spectra listed by mass/charge ratios of fragment ions with the most probable original structures for each. 117 pages
Paper (1963) \$6.00

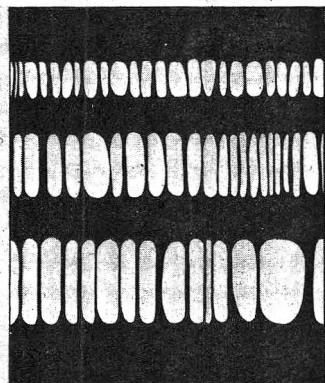
No. 33 Solid Surfaces and the Gas-Solid Interface. Thirty-seven papers from the Kendall Award Symposium honoring Stephen Brunauer. Theory and techniques for studying surface phenomena. 389 pages
Cloth (1961) \$12.00

No. 31 Critical Solution Temperatures. By Alfred W. Francis. CST answers the question, "Do two liquids mix?" and is widely used for screening solvents. Over 6000 systems are included, 70% with a hydrocarbon as one component; nearly 1100 non-hydrocarbon solvents are listed. 246 pages
Cloth (1961) \$8.00

All books postpaid in U.S. and Canada; plus 30 cents in PUAS and elsewhere.

Order from: **SPECIAL ISSUES SALES**
AMERICAN CHEMICAL SOCIETY
1155 SIXTEENTH ST., N.W.
WASHINGTON, D.C. 20036

Interaction of Liquids at Solid Substrates



ADVANCES IN CHEMISTRY SERIES **87**

INTERACTION OF LIQUIDS AT SOLID SUBSTRATES

ADVANCES IN CHEMISTRY SERIES NO. 87

Papers from two symposia by the Division of Organic Coatings and Plastics Chemistry of the American Chemical Society.

This volume includes twelve papers comprising the symposium on "The Interaction of Liquids at Solid Substrates," chaired by Allen L. Alexander. These papers include work on "coupling agents," adhesion of polymers, organic/inorganic interfaces, and ultrasonic impedometry. Also included are four papers concerned with heparinized surfaces at the blood/material interface which were part of the symposium on "The Medical Applications of Plastics," chaired by R. I. Leininger.

212 pages with index Cloth (1968) \$9.50

Free set of L. C. cards with library orders upon request.

Other books in the **ADVANCES IN CHEMISTRY SERIES** in colloid chemistry include:

No. 86 Pesticidal Formulations Research: Physical and Colloidal Chemicals Aspects. Fifteen papers survey contact angle of surface active agents, transport through a membrane, vapor pressure of pesticides, role of surfactants in sprays, biological activity, evaporation, spray formation and drift, and several studies on specific pests and pesticides.
212 pages Cloth (1969) \$9.50

No. 84 Molecular Association in Biological and Related Systems. Nineteen articles survey and report new work on molecular association in fat digestion, in soap systems, in membrane constituents, and in mixed monolayers and membranes, include bile salt micelles, lipid monolayers and membranes, and a definitive review of biological membrane structure.
308 pages Cloth (1968) \$10.50

No. 79 Adsorption from Aqueous Solution. Fifteen papers discuss thermodynamic and kinetic aspects of adsorption phenomena and the results of studies on a variety of adsorbate-adsorbent systems.
212 pages Cloth (1968) \$10.00

No. 63 Ordered Fluids and Liquid Crystals. Twenty-two studies on characterization, properties, and occurrence of these phenomena in many substances such as tristearin, p-azoxyanisole, mono- and di-hydric alcohols, phospholipids, and polypeptides.
332 pages Cloth (1967) \$11.50

No. 43 Contact Angle, Wettability, and Adhesion. Surface chemistry studies. Relation of equilibrium contact angle to liquid and solid construction, contact angle as a thermodynamic property, surface energy estimation from contact angle. Contact angle hysteresis, relationship between wetting and adhesion.
389 pages Cloth (1964) \$10.50

No. 33 Solid Surfaces and the Gas-Solid Interface. Thirty-seven papers from the Kendall Award Symposium honoring Stephen Brunauer. Theory and techniques for studying surface phenomena.
381 pages Cloth (1961) \$12.00

No. 25 Physical Functions of Hydrocolloids. Treats six broad physical functions—production of viscosity or body, gelatin, stabilization of emulsions, stabilization of suspensions, stabilization of foams, control of crystal growth—with emphasis on food applications.
103 pages Paper (1960) \$5.00

No. 11 Natural Plant Hydrocolloids. The protective colloids or stabilizers, including calcium pectinate, agar, gum arabic, gum karaya, tragacanth, locust bean gum, alginates, Irish moss, and red seaweed.
103 pages Paper (1954) \$5.00

All books postpaid in U.S. and Canada; plus 30 cents in PUAS and elsewhere.

Order from:

**SPECIAL ISSUES SALES
AMERICAN CHEMICAL SOCIETY
1155 SIXTEENTH ST., N.W.
WASHINGTON, D.C. 20036**